TECHNICAL DIGEST

MPLP-2016

The VII International Symposium
and Young Scientists School

"MODERN PROBLEMS OF LASER PHYSICS"

Novosibirsk, Russia, August 22 – 28, 2016

mplp2016.laser.nsc.ru

Organized by:

Institute of Laser Physics, SB RAS, Novosibirsk, Russia

Novosibirsk State University, Novosibirsk, Russia

Institute of Spectroscopy, RAS, Troitsk, Moscow Region, Russia

International Laser Center, M.V. Lomonosov Moscow State University, Moscow, Russia

Federal State Unitary Enterprise "VNIIFTRI", Mendeleevo, Moscow region, Russia

Supprted and Sponsored bu:

Federal Agency for Scientific Organizations

Russian Foundation for Basic Research

Novosibirsk Regional Fund of Support of Science and Innovative Activities

The Nauchnoe Oborudovanie group of companies

INTERNATIONAL ADVISORY COMMITTEE

Sergei Arakelian	*Vladimir State University, Vladimir, Russia*
Viktor Balykin	*Institute of Spectroscopy RAS, Troitsk, Russia*
Nicolò Beverini	*Dipartimento di Fisica, Universita' di Pisa, Italy*
Razvan Dabu	*National Institute for Nuclear Physics and Engineering, Bucharest-Magurele, Romania*
Evgueni Dianov	*Fiber Optics Research Center at GPI RAS, Russia*
Martial Ducloy	*Laboratoire de Physique des Lasers, Universite Paris-Nord, France*
Elisabeth Giacobino	*Laboratoire Kastler Brossel, Université Paris 6, France*
Hidetoshi Katori	*University of Tokyo, Science and Technology Agency, Japan*
Sergei Kilin	*B.I. Stepanov Institute of Physics NASB*
John Kitching	*National Institute of Standards and Technology (NIST), Boulder, USA*
Vasiliy Klimov	*P.N. Lebedev Physics Institute RAS, Moscow, Russia*
Nikolai Kolachevsky	*P.N. Lebedev Physics Institute RAS, Moscow, Russia*
Leong Chuan Kwek	*Centre for Quantum Technologies, National University of Singapore*
Gerhard Leuchs	*Universität Erlangen-Nürnberg, Institut für Optik, Germany*
Filippo Levi	*INRIM, Optic Division, Torino, Italy*
Helen Margolis	*National Physical Laboratory, Teddington, Middlesex, UK*
Vitaly Pal'chikov	*Scientific Research Institute "VNIIFTRI", Moscow region, Mendeleevo, Russia*
Kyung Hyun Park	*THz Photonics Creative Research Center, Electronics and Telecommunications Research Institute, Korea*
Ekkehard Peik	*Physikalisch-Technische Bundesanstalt (PTB), Braunschweig, Germany*
Hélène Perrin	*Université Paris 13, Villetaneuse, France*
Ernst Rasel	*Institute of Quantum Optics, Hanover, Germany*
Philip Russell	*Max Planck Institute for the Science of Light (MPL), Erlangen, Germany*
Aleksandr Sergeev	*Institute of Applied Physics RAS, Nizhny Novgorod, Russia*
Anatoly Shalagin	*Institute of Automation and Electrometry SB RAS, Novosibirsk, Russia*
Feng Song	*Nankai University, Tianjin, China*
Aleksey Taichenachev	*Institute of Laser Physics SB RAS, Novosibirsk, Russia*
Sergei Turitsyn	*Aston University, Birmingham, UK*
Antoine Weis	*University of Fribourg, Fribourg, Switzerland*
Jun Ye	*JILA, NIST and University of Colorado, Boulder, USA*
Victor Zadkov	*Institute of Spectroscopy RAS, Troitsk, Russia*

Symposium Chair: Prof. Sergei N. Bagayev, *Institute of Laser Physics, SB RAS*

Symposium Secretary: Dr. Denis V. Brazhnikov, *Institute of Laser Physics, SB RAS*

Table of Contents

Oral Presentations

(Authors are listed in the alphabetical order within each chapter)

1. New trends in laser physics

2. High-resolution spectroscopy and fundamental metrology

3. Physics of ultracold atoms, ions, and molecules

4. Quantum and atom optics and quantum information

5. Ultrahigh laser fields and attoscience

6. Nonlinear optics and novel phenomena

7. Nano- and femto- photonics: Foundations and applications

8. Fiber optics and fiber lasers

9. Applications of laser radiation from THz to UV in biomedicine, geophysics and other fields

Poster Sessions

New schemes and regimes of Raman fiber lasers

S.A. Babin
Institute of Automation and Electrometry, SB RAS, Novosibirsk 630090, Russia
Novosibirsk State University, Novosibirsk 630090, Russia
E-mail: babin@iae.nsk.su

It is known that laser generation is possible in not only in active fibers, but also in passive fibers owing to stimulated Raman scattering (SRS) of pump radiation providing amplification of the Stokes-shifted scattered light (by ~13 THz and ~40 THz for Si02/GeO2 and P_2O_5, correspondingly), see [1] for a review. In Raman fiber lasers (RFLs), cavity is usually formed by fiber Bragg gratings (FBGs) which reflect the Stokes waves (of the first, as well as of higher orders). As a result, a cascaded generation in a broad spectral range with continuous tuning within Raman gain spectrum is possible. However, a relatively low Raman gain requires rather long (0.1-1 km) passive fibers with high-power pumping into the fiber core, e.g. by efficient single-mode Yb-doped fiber lasers (YDFLs).

In the report, a review of recent results on new schemes and regimes of Raman fiber lasers will be presented.

First, implementation of polarization-maintaining (PM) passive fibers and linearly polarized pumping in new RFL scheme with random distributed feedback [2] results in great improvements in RFL efficiency [3]. Such random RFL made of 500-m PM fiber with PM fiber loop mirror at one fiber end generates a linearly polarized radiation at 1.11 μm with polarization extinction ratio as high as 25 dB at the output power of up to 9.4 W. The absolute optical efficiency of pump-to-Stokes wave conversion reaches 87% (corresponding to quantum efficiency of 92%) that is a record value for Raman fiber lasers. In the same scheme with longer PM fiber (1 km), efficient cascaded generation up to 4th Stokes order (1.3 μm) has been demonstrated, at the polarization extinction ratio > 22 dB for all orders [4]. At that, record values of quantum efficiency (around 80% relative to pump photons) have been obtained for the generation of 2nd (1.17 μm) and 3rd (1.23 μm) Stokes orders. The laser bandwidth grows with increasing order, but it is almost independent of power in the 1-10 W range, amounting to ~1,~2 and ~3 nm for orders 1–3, respectively. So, the random Raman fiber laser exhibits no degradation of output characteristics with increasing Stokes order. A theory adequately describing the unique laser features has been developed. Thus, a full picture of the cascaded random Raman lasing in fibers is shown.

Second, a further nonlinear conversion of 1.3-μm radiation generated in phosphosilicate RFL is demonstrated to longer wavelengths (>1.4 μm) using active Bi fiber as a nonlinear medium [5], as well as to shorter wavelengths (0.65 μm) using PPLN nonlinear crystal for second harmonic generation (SHG) [6]. It has been shown that the SHG efficiency for random RFL is higher than that for conventional RFL with linear cavity in the same fiber.

Third, pulsed operation in various RFL configurations is also explored. It has been shown that active Q-switching (closing of fiber loop mirror by acousto-optic modulator) in RFL configuration with RDFB provides generation of nanosecond pulses which energy and period proportional to the fiber length [7]. In the proposed scheme, the pump energy distributed along the passive fiber is directly converted to the Stokes pulse, which reaches 30 μJ energy in case of 1-km long PM fiber. This RFL configuration being converted to a ring PM-fiber cavity with loss modulation synchronously with round trip provides actively mode locked RFL operation [8]. As a result, one or several sub-ns pulses are formed within the modulator window. It has been found that the formation of such stable multi-pulse structure is defined by the single-pulse energy limit (~20 nJ) set by the second-order Raman generation. Adding a NPE-based saturable absorber in the actively mode locked

cavity, results in sufficient shortening of the generated pulses both in single- and multi-pulse regimes (down to 50 ps). A model is developed adequately describing these regimes. Femtosecond Raman pulses of the first and second Stokes orders have been also generated in the scheme with synchronous pumping in a specially designed PM-fiber cavity of dissipative-soliton YDFL [9]. The pulses at different wavelengths have similar duration (40 ps) and are externally compressed to 200–300 fs. Their coherent combination is also demonstrated. This technique offers a way for generation of high-energy pico- and femtosecond pulses at new wavelengths.

Finally, principally new approach in RFL design based on direct pumping of a gradient-index (GRIN) fiber by multimode LDs has been developed, demonstrating lasing at <1 μm with high beam quality and conversion efficiency. Based on this concept, CW Raman fiber with direct pumping by a high-power multimode laser diode at 915 nm enables generation of high-quality 954-nm output beam with power ~10 W [10].

References

[1] E.M. Dianov and A.M. Prokhorov, IEEE J. of Sel. Topics in Quant. Electronics **6**, 1022 (2000).
[2] S.K. Turitsyn, S.A. Babin, A.E. El-Taher, P. Harper, D.V. Churkin, S.I. Kablukov, J.D. Ania-Castañón, V. Karalekas, E.V. Podivilov, Nature Photonics **4**, 231 (2010).
[3] E.A. Zlobina, S.I. Kablukov, S.A. Babin, Opt. Lett. **40,** 4074 (2015).
[4] S.A. Babin, E.A. Zlobina, S.I. Kablukov, E.V. Podivilov, Scientific Reports **6**, 22625 (2016).
[5] I.A. Lobach, S.I. Kablukov, M.I. Skvortsov, E.V. Podivilov, M.A. Melkumov, S.A. Babin, E.M. Dianov, Scientific Reports **6**, 30083 (2016).
[6] E.I. Dontsova, S.I. Kablukov, I.D. Vatnik, S.A. Babin. Opt. Lett. **41**, 1439 (2016).
[7] A.G. Kuznetsov, E.V. Podivilov, S.A. Babin, Laser Phys. Lett. **12**, 035102 (2015).
[8] A.G. Kuznetsov, D.S. Kharenko, E.V. Podivilov, S.A. Babin, Opt. Express **24**, 16280 (2016).
[9] D.S. Kharenko, A.E. Bednyakova, E.V. Podivilov, M.P. Fedoruk, A. Apolonski, S.A. Babin, Opt. Lett. **41**, 175 (2016).
[10] E.A. Zlobina, S.I. Kablukov, M.I. Skvortsov, I.N. Nemov, S.A. Babin, Las. Phys. Lett. **13**, 035102 (2016).

The quantum vacuum as a dielectric

G. Leuchs[1,2,3], M. Hawton[4], and L.L. Sanchez-Soto[2,5]
[1]*Department Physik, Universität Erlangen-Nürnberg, Staudtstr. 7 B2, 91058 Erlangen, Germany*
[2]*Max Planck Institut for the Science of Light, Günther-Scharowsky-Str. 1 Bau 24 , 91058 Erlangen, Germany*
[3]*Department of Physics, University of Ottawa, 25 Templeton Street, Ottawa, ON, K1N 6N5, Canada*
[4]*Department of Physics, Lakehead University, 955 Oliver Road, Thunder Bay, ON, P7B 5E1, Canada*
[5] *Departamento de Óptica, Facultad de Física, Universidad Complutense, 28040 Madrid, Spain*
E-mail: gerd.leuchs@fau.de

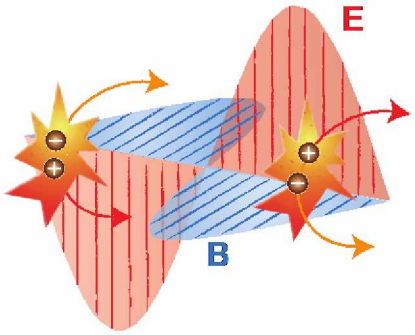

Theory predicts that the quantum vacuum has nonlinear optical properties. High intensity laser systems are under construction in order to search for light-light scattering, for magnetic field induced birefringence and for pair creation – all in the vacuum [1,2]. One might ask about the underlying linear optical response of the vacuum and it is obvious that Maxwell must have already taken any linear response into account when formulating the equations named after him – hence their success. This set of equations puts the laws found by others into context but to make the set consistent Maxwell had to add a new term the vacuum displacement current driving the magnetic field in addition to the current of free or bound charges. It is this first term on the right hand side in Maxwell's displacement field $\vec{D} = \varepsilon_0 \vec{E} + \vec{P}$, so we postulate, that contains information about the quantum vacuum [3]. Understanding this linear response will hopefully help planning for measurements of the nonlinear response. Urban et al. published a related approach [4].

When treating the quantum vacuum as a dielectric full of virtual and polarizable particle – anti-particle pairs, one finds that the permittivity of the vacuum ε_0 is related to the sum over the squared charges of all the different types of elementary particles [3,5]. Incidentally, summing over different types of elementary particles in the context of charge renormalization is well known [6,7]. In our model the vacuum permittivity becomes energy dependent [5], which is related to the sum over different types of elementary particles. This is equivalent to charge renormalization, or the running of the fine structure constant [8]. The special situation in our case is that the dielectric model seems to provide us with information about all types of particles existing in nature, because the model gives the sum over the squared charges of all these particles in nature. We are currently trying to confirm this more rigorously. In any case, the dielectric model of the vacuum provides insight into the zero point energy, relates the coefficients in Maxwell's equations to the properties of the quantum vacuum and provides information about high-energy particles via low energy observations.

References

[1] https://eli-laser.eu/the-eli-project/
[2] http://www.xcels.iapras.ru/img/XCELS-Project-english-version.pdf
[3] G. Leuchs, A.S. Villar and L.L. Sanchez-Soto, Appl. Phys. B **100**, 9 (2010).
[4] M. Urban, F. Couchot, X. Sarazin and A. Djannati-Atai, Eur. Phys. J. D **67**, 58 (2013).
[5] G. Leuchs, L.L. Sanchez-Soto, Eur. Phys. J. D **67**, 57 (2013).
[6] L. Landau and I. Pomeranchuk, Dokl. Akad. Nauk SSSR **102**, 489 (1955).
[7] A.D. Sakharov, Teoret. Math. Fizika **23**, 178 (1975).
[8] C.J. Hogan, Rev. Mod. Phys. **72**, 1149 (2000).

Recent advances in high-precision spectroscopy of ultracold atoms and ions

Alexey Taichenachev[1,2], Valeriy Yudin[1,2,3], and Sergey Bagayev[1,2]
[1]*Institute of Laser Physics, Novosibirsk, Russia*
[2]*Novosibirsk State University, Novosibirk, Russia*
[3]*Novosibirsk State Technical University, Novosibirsk, Russia*
E-mail: taich.alex@gmail.com

Presently, laser spectroscopy and fundamental metrology are among the most important and actively developed directions in modern physics. Frequency and time are the most precisely measured physical quantities, which, apart from practical applications (in navigation and information systems), play critical roles in tests of fundamental physical theories (such as QED, QCD, unification theories, and cosmology) [1,2]. Now, laser metrology is confronting the challenging task of creating an optical clock with fractional inaccuracy and instability at the level of 10^{-17} to 10^{-18}. Indeed, considerable progress has already been achieved along this path for both ion-trap- [3,4] and atomic-lattice-based [5,6] clocks.

Work in this direction has stimulated the development of novel spectroscopic methods such as spectroscopy using quantum logic [7], magnetically induced spectroscopy [8], hyper-Ramsey spectroscopy [9], spectroscopy of "synthetic" frequency [10] and others [11]. Part of these methods was developed in order to excite and detect strongly forbidden optical transitions. The other part fights with frequency shifts of various origins. In the present talk we will review both parts with a special emphasis on methods developed and studied in Institute of Laser Physics SB RAS, Novosibirsk. The history and present status of experimental works devoted to the optical frequency standards will be discussed.

Our work is supported by Russian Foundation for Basic Research (grants nos. 14-02-00712, 14-02-00806, 14-02-00939, 15-02-08377, 15-32-20330), Ministry of Education and Science of Russian Federation (State Assignment № 2014/139 project № 825), Russian Academy of Sciences, and by a grant of President of RF (NSH-4096.2014.2).

References

[1] S. N. Bagayev *et al.*, Appl. Phys. B **70**, 375 (2000).
[2] S. A. Diddams *et al.*, Science **306**, 1318 (2004).
[3] T. Rosenband *et al.*, Science **319**, 1808 (2008); C.W. Chou *et al.*, Phys. Rev. Lett. **104**, 070802 (2010).
[4] N. Huntemann *et al.*, Phys. Rev. Lett. **116**, 063001 (2016).
[5] T. Akatsuka,M. Takamoto, and H. Katori, Nature Physics **4**, 954 (2008).
[6] N. Hinkley *et al.*, Science **341**, 1215 (2013); B.J. Bloom *et al.*, Nature **506**, 71 (2014).
[7] P. O. Schmidt *et al.*, Science **309**, 749 (2005).
[8] A. Taichenachev *et al.*, Phys. Rev. Lett. **96**, 083001 (2006); Z. Barber *et al.*, Phys. Rev. Lett. **96**, 083002 (2006).
[9] V. Yudin *et al.*, Phys. Rev. A **82**, 011804(R) (2010); N. Huntemann *et al.*, Phys. Rev. Lett. **109**, 213002 (2012).
[10] V. Yudin *et al.*, Phys. Rev. Lett. **107**, 030801 (2011).
[11] V. Yudin *et al.*, Phys. Rev. Lett. **113**, 233003 (2014).

Challenge for thermal-lens-free ceramic lasers

Ken-ichi Ueda
Institute for Laser Science, Univ. of Electro-Communications, Tokyo, Japan
Institute of Laser Engineering, Osaka University, Osaka, Japan
Central Research Institute, Hamamatsu Photonics K.K., Shizuoka, Japan
TOYOTA Physical & Chemical Institute, Aichi, Japan
JST PREST, Tokyo, Japan
Institute of Applied Physics, Russian Academy of Sciences, Nizhny Novgorod, Russia
E-mail: ueda@ils.uec.ac.jp

Today we need an unlimited power scaling technology, that is, a coherent beam combining. This is a long time dream since 1960, the first laser demonstration. ICFA-ICUIL joint task force recommended fiber laser array for the laser driver of the TeV-class laser-plasma accelerator because it was unique solution to generate real plane wave in 2011. Joint task force asked us to develop alternative way using ceramic lasers. How to solve the thermal lens effect in a solid state laser? We made effort to create new scheme for thermal-lens-free solid state lasers last five years. In this paper I talk about the new approach towards thermal-lens-free solid state lasers.

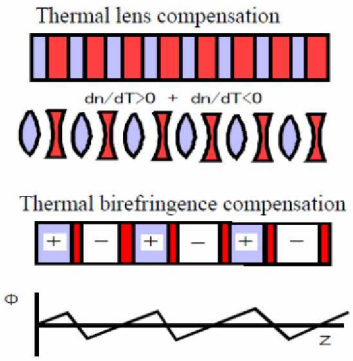

Fig. 1 Thermal lens compensation by combined active media.

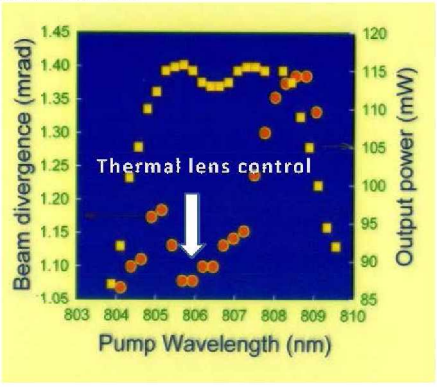

Fig. 2 Beam quality control by thermal lens compensation of Nd:YVO_4/Nd:SVAP.

The mechanism of thermal lens effect is the temperature gradient across the beam diameter. This is attributed to the thermal flow for cooling the gain volume. Simple solution is the end-cooling under the full aperture pumping. One dimensional cooling along the longitudinal direction does not induce thermal lens effect. However, full-aperture pumping is not so efficient in a typical case because the outer edge area pumping is not deleted by laser amplification. Ring heater method is partially available to expand the area of full flat wavefront amplification. Efficient cooling relaxes the thermal lens effect in a thin disk geometry. The cooling power of high speed rotary disk with 120 Hz rotation is more than 1600 times larger than static disk. High efficiency cooling is effective for stational thermal lens effect. However, the transit thermal lens during pumping is not so easy to solve. Fundamental solution of thermal lens problem is the development of athermal laser material. If the laser material is athermal, that means the refractive index is constant and independent to the temperature, the thermal lens effect disappears even under the lateral thermal flow cooling. This is an ideal solution.

We tried to develop a hybrid laser system for the thermal lens compensation for the first step. As shown in Fig.1, thermal lens and birefringence compensation by multi-thin-disk amplifier is possible. Quasi-phase-matching of nonlinear crystals is also similar in principle. Combined active media with *dn/dT* positive Nd:YVO_4 and *dn/dT* positive Nd:SVAP crystals. These crystals have slightly shifted absorption and emission spectra. As a result, we can control the pumping materials by tuning the operation temperature of pumping LD. Shorter wavelength pumping is effective to Nd:YVO_4 and longer wavelength is good for Nd:SVAP. Thermal lens compensation was demonstrated as shown in Fig.2.

There exists an athermal optical glass for high precision optics. In the case of glasses, material tuning by mixing is relatively easy, because glass is a kind of liquid. However, we can not make an intermediated properties of crystals by mixing sapphire and diamond. This is the reason why we developed a hybrid crystal system for the tuning of material parameters of crystal. It has been a common sense until today. I investigated laser ceramics more than 20 years. We succeeded to develop full transparent, high power laser ceramics comparable or better than single crystals. However, all laser ceramics developed were oxide ceramics. Yb:CaF_2 ceramics is attractive for high power and ultrashort pulse generation. But it has not been easy to fabricate full transparent Yb:CaF_2 until recently. In 2015, there were three reports on the laser performance of Yb:CaF_2 ceramic lasers.

We made effort to develop highly transparent CaF_2 ceramics last 10 years. One of the difficulties of CaF_2 ceramics is the rare earth (Re) doping, because there is an mismatching of doping ion Re^{3+} and Ca^{2+} site. The charge state of doping ion changed at 0.3% and >1% in Eu doping case. We needed high and stable Yb^{3+} doping. Yb^{2+} induces absorption loss and scattering. We solved this problem by using solid solution of CaF_2-LaF_3 ceramics. Optically transparent Yb:CaF_2-LaF_3 ceramics have been fabricated for various concentration of Yb and La covering 1% to 6% respectively as shown in Fig.3. Fabrication technique is hot press and reactive sintering. These are the first successful

Yb:CaF_2-LaF_3 ceramics. We understand Yb:CaF_2-LaF_3 ceramics is stable and high optical quality. The emission lifetime of Yb is 2.1-2.2 ms for 1-3% Yb-doping. The absorption and emission spectra have no difference between these ceramics and single crystal Yb:CaF_2. We demonstrated the laser experiments by simple LD pumping.

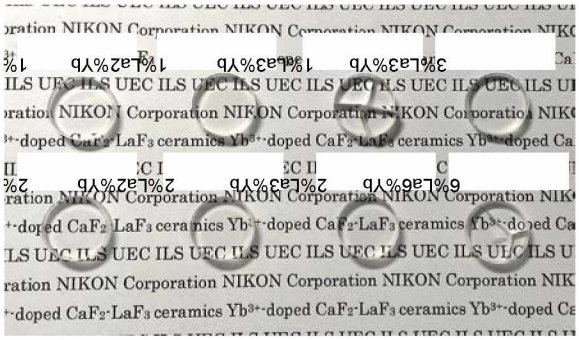

Fig. 3 Yb:CaF_2-LaF_3 ceramics.

Material	dn/dT x10^{-6}	α x10^{-6}	n	dn/dT+α(n-1) x10^{-6}
ZnSe	61	7.8	2.7	74.26
Al2O3	13	8.4	1.772	19.4848
YAG	9.1	7.8	1.815	15.457
Silica	10	0.52	1.45	10.234
MgF2	2.3	13.7	1.3836	7.55532
N-PSK53a	-4.3	9.6	1.53	0.788
CaF2	-10.6	18.85	1.428	-2.5322
SrF2	-12	19.2	1.433	-3.6864
LHG8	-5.3	0.6	1.5201	-4.98794
BaF2	-15.2	18.1	1.45	-7.055
LaF3	n/a			n/a

Table 1 Thermal lens effect of optical materials.

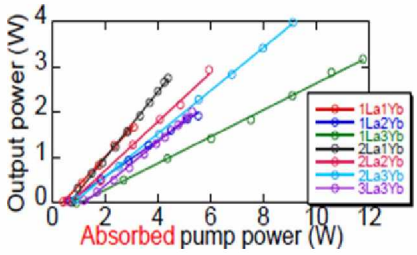

Slope efficiency (%)

La (at.%) \ Yb (at.%)	1	2	3
1	63.2	39.9	27.7
2	73.1	54.0	47.5
3	-	-	48.1

Fig. 4 Laser demonstration of 4 W output and 73 % efficiency.

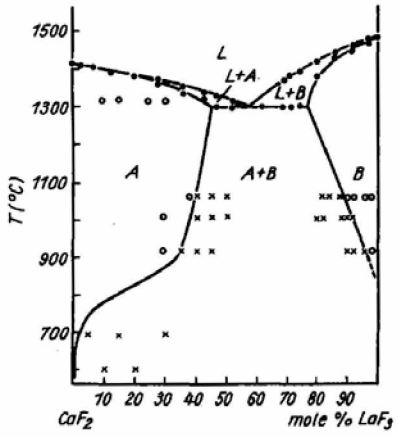

Fig. 1. The phase diagram of CaF_2-LaF_3 system. A - $Ca_{1-x}La_xF_{2+x}$ solid solution with fluorite-like structure; B - Solid solution with tysonit-like structure; L - melt. • - DTA data, o - single-phase samplex, x - two phase sample

Fig. 5 Phase diagram of CaF_2-LaF_3.

As shown in Fig.4, laser oscillation was observed by all samples of Yb 1-3% doping. There was no saturation in this experimental condition. The results were good enough. Output power of 4 W and slope efficiency of 73% was highest ever measured in fluoride ceramics, respectively. These results show the quality of Yb:CaF_2-LaF_3 is excellent. Output power is limited by pump power and 73% slope efficiency is comparable or better than a single crystal Yb:CaF_2.

Thermal lens effect dS/dT is defined as follows: $dS/dT = l\left[dn/dT + \alpha(n-1)\right]$, where l is the active length, n is the refractive index, T is the temperature, α is the thermal expansion coefficient. First term and second term of the thermal lens effect is positive in the typical laser materials. However, fluoride materials have negative dn/dT. As shown in Table 1, CaF_2 and SrF_2 are the best materials for thermal lens issue. Is it possible to develop an athermal fluoride ceramics? It has been a long time dream. In Table 1, N-PSK53a is an athermal glass for high precision optics. The thermal lens effect of CaF_2 is 3 times larger in this table. Is it possibel to tune these value by changing the LaF_3 concentration. In this case we have to check the phase diagram of CaF_2-LaF_3 matrix. The phase diagram of CaF_2-LaF_3 was investigated in 1979 as shown in Fig.5 [1]. From this data, CaF_2-LaF_3 is stable below 700 C in any concentration of LaF_3. This means the refractive index and thermal lens constant should be modified by the mixing ratio of CaF_2 and LaF_3. This is a new channel to develop athermal fluoride laser ceramics in near future.

We acknowledge the collaboration of Prof. Shirakawa (ILS/UEC), Dr. Ishizawa (NIKON) and Mega Grant program of Russia (14.B25.31.0024).

References

[1] M. Svantner et al, Kristall und Technik **14**, 365 (1979).

Nonlinear optics in the mid-infrared: new morning

A.M. Zheltikov
Physics Department, International Laser Center, M.V. Lomonosov Moscow State University, Moscow 119992, Russia
Department of Physics and Astronomy, Texas A&M University, College Station, TX 77843, USA
Russian Quantum Center, ul. Novaya 100, Skolkovo, Moscow Region, 143025 Russia
Kurchatov Institute National Research Center, pl. akad. Kurchatova 1, Moscow 123182, Russia
E-mail: zheltikov@physics.msu.ru

The mid-infrared spectral range is unique in many ways. Within this region, electromagnetic radiation can resonate with the most intense signature molecular bands, thus drastically enhancing the coupling between the field and molecular motions. Electrons driven by intense ultrashort mid-IR field waveforms acquire unusually high pondermotive energies within a fraction of the field cycle, giving rise to new regimes of high-field nonlinear optics. The λ^2 scaling of phase-space mode volume with radiation wavelength λ translates into the λ^2 dependence of the self-focusing threshold, allowing much higher peak powers to be transmitted in a single laser filament in the mid-IR range without losing beam continuity and spatial coherence. Recent breakthroughs in ultrafast photonics in mid-IR help understand complex interactions of high-intensity ultrashort mid-IR pulses with matter, offer new approaches for x-ray generation, enable mid-IR laser filamentation in the atmosphere, facilitate lasing in filaments, give rise to unique regimes of laser–matter interactions, and reveal unexpected properties of materials in the mid-IR range. Motivated and driven by numerous applications and long-standing challenges in strong-field physics, molecular spectroscopy, semiconductor electronics, and standoff detection, ultrafast optical science is rapidly expanding toward longer wavelengths. Experiments reveal unique properties of filaments induced by ultrashort laser pulses in the mid-infrared, where the generation of powerful supercontinuum radiation is accompanied by unusual scenarios of optical harmonic generation, giving rise to remarkably broad radiation spectra, stretching from the visible to the mid-infrared. Generation of few- and even single-cycle mid-infrared field waveforms has been demonstrated within a broad range of peak powers and central wavelengths. Below-the-bandgap high-order harmonics generated by ultrashort mid-infrared laser pulses are shown to be ideally suited to probe the nonlinearities of electron bands, enabling an all-optical mapping of the electron band structure in bulk solids.

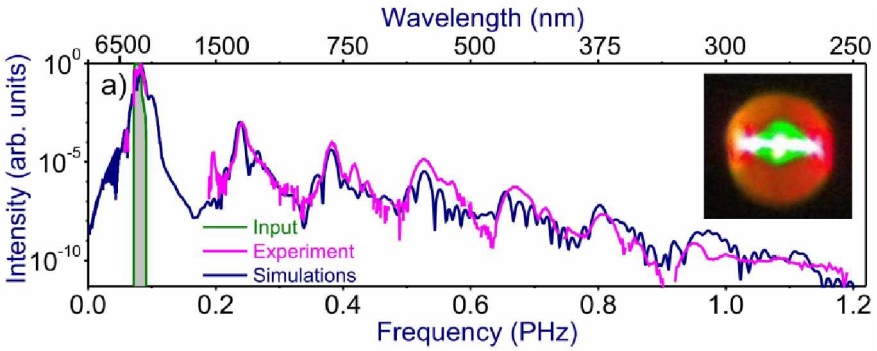

Fig. 1. The on-axis spectrum of supercontinuum radiation generated in a filament induced by the mid-IR OPCPA output in the air: (red) experiment, (blue) simulations. The spectrum of the mid-IR driver inducing the filament is shown by grey shading. The supercontinuum beam behind the filament is shown in the inset.

References

[1] A.V. Mitrofanov, D.A. Sidorov-Biryukov, A.A. Voronin, A. Pugžlys, G. Andriukaitis, E.A. Stepanov, S. Ališauskas, T. Flöri, A.B. Fedotov, V.Ya. Panchenko, A. Baltuška, and A.M. Zheltikov, Phys. Usp. **58**, 89 (2015).
[2] A. A. Lanin, A. A. Voronin, E. A. Stepanov, A. B. Fedotov, and A. M. Zheltikov, Opt. Lett. **39**, 6430 (2014).
[3] P.A. Zhokhov, A.M. Zheltikov "Attosecond Shock Waves," Phys. Rev. Lett. **110**, 183903 (2013).
[4] A.V. Mitrofanov, A.A. Voronin, D.A. Sidorov-Biryukov, A. Pugžlys, E.A. Stepanov, G. Andriukaitis, T. Flöry, S. Ališauskas, A.B. Fedotov, A. Baltuška, and A.M. Zheltikov, Scientific Reports **5,** 8368 (2015).
[5] E. A. Stepanov, A. A. Lanin, A. A. Voronin, A. B. Fedotov, and A. M. Zheltikov, Phys. Rev. Lett (2106).
[6] E.E. Serebryannikov and A. M. Zheltikov, Phys. Rev. Lett. **113,** 043901 (2014).
[7] A. V. Mitrofanov, A. A. Voronin, S. I. Mitryukovskiy, D. A. Sidorov-Biryukov, A. Pugžlys, G. Andriukaitis, T. Flöry, E. A. Stepanov, A. B. Fedotov, A. Baltuška, and A. M. Zheltikov, Opt. Lett. **40,** 2068 (2015).
[8] A.V. Mitrofanov, A.A. Voronin, D.A. Sidorov-Biryukov, S.I. Mitryukovsky, A.B. Fedotov, E.E. Serebryannikov, V. Shumakova, S. Ališauskas, A. Pugžlys, V. Ya. Panchenko, A. Baltuška, and A. M. Zheltikov, Optica **3**, 299 (2016).

Double-resonance spectroscopy in Rubidium vapour-cells for high performance and miniature atomic clocks

C. Affolderbach, M. Gharavipour, and G. Mileti
Laboratoire Temps – Fréquence (LTF), Institut de Physique, Université de Neuchâtel, Avenue de Bellevaux 51, 2000 Neuchâtel, Switzerland
E-mail: Gaetano.mileti@unine.ch

Microwave-optical double resonance spectroscopy in alkali vapour cells constitutes simultaneously a field of basic research and of more application-oriented developments of precision instruments such as frequency standards and magnetometers [1].

The first investigations were realized with alkali plasma discharge lamps as optical source while the radio-frequency (rf) or microwave field was applied using different techniques such as simple metallic loops, antennas, horns or resonant cavities. The various types of optical pumping processes [2] and the AC Stark shift induced on the rf or microwave atomic transitions by the resonant optical field were investigated in great details from both the experimental and the theoretical points of view [3, 4]. Different techniques inspired by the Nuclear Magnetic Resonance (NMR) methods were also developed in order to study the sources of relaxations (in particular the collisions) [5] and frequency shifts. In the case of Rubidium atomic vapour cells, the presence of two isotopes with partially overlapping optical transitions allowed to improve the efficiency of the hyperfine optical pumping, thanks to the so-called "isotopic filtering", and resulted in the realization of commercial atomic frequency standards that were required in many applications such as network synchronization, secure telecommunication and satellite positioning and navigation systems. These devices are still in use nowadays. Their volume range typically from 0.2 to 5 Liters and their fractional frequency instability lies at the 10^{-12}-10^{-10} level for one second averaging time and 10^{-11}-10^{-14} for averaging times ranging between several hours to one day. Their accuracy and their medium to long term frequency stability are ultimately limited by the fact that the atoms are stored in a thermal vapour cell with unavoidable collisions which effects are very sensitive to the environmental changes and other aging processes.

Since the advent of tunable laser sources, a few decades ago, the research in this area has greatly evolved, while the impact on commercial devices is only in its initial phase. On one hand, the use of laser diodes has allowed to enhance the accuracy of the spectroscopic studies, thanks to their much narrower and widely tunable optical spectrum. On the other hand, new effects (such as Coherent Population Trapping, CPT) and new schemes (based in particular on pulsed operation) have paved the way to a new generation of atomic frequency standards with either better frequency stability and/or improved specifications such as reduced size and consumption.

Our research in this field [6] has included the development of compact frequency-stabilized laser sources [7] for future high performance atomic clocks [8]. A relatively small size microwave cavity [9] has allowed us to achieve short term frequency stabilities in the 10^{-13} range with both the continuous [10] and the pulsed [11] mode. In parallel, we have conducted several studies towards further miniaturization [12], including the demonstration of double-resonance with a micro-fabricated discharge lamp [13]. We have also shown that microwave-optical double resonance in a micro-fabricated cell [14, 15] constitutes a very promising alternative to CPT for future chip-scale atomic clocks. More recently, we have been investigating pulsed techniques to determine experimentally the spatial distribution of important physical quantities in micro-fabricated [16] and glass-blown [17] Rubidium vapour cells: the microwave field strength, the DC magnetic field amplitude, the longitudinal and the transverse relaxation times.

As mentioned above, the performances of vapour cell atomic clocks are ultimately limited by the collision-related effects that may affect the short-term stability (due to their direct impact on the resonance linewidth) as well as their medium and long term drift (due to their influence on frequency

shifts). Usually, one or more "buffer gases" such as Argon, Nitrogen and Neon are introduced in the vapour cell in order to significantly suppress the collisions between the alkali atom and the glass walls. However, the right pressure and mixing ratio have to be used so as to minimize other sources of instability such as the temperature coefficient of the cell [18]. In addition, aging effects related to very tiny variations in the buffer gas have to be taken into account [19]. A potential alternative consists in covering the inner walls of the alkali vapour cell with an "anti-relaxation" coating. We have performed preliminary studies on the application of this technique in both glass-blown [20] and micro-fabricated cells [21] that show the present limits of this approach, especially concerning the medium and long-term frequency stability.

The AC Stark shift (or "light-shift") may be strongly enhanced when using a tunable laser diode instead of a spectral discharge lamp. This enhancement constitutes an advantage for detailed studies on this basic phenomena [22, 23] but may also become a strong drawback in view of the use of laser diodes in commercial devices, especially if one takes into account the unavoidable aging processes occurring in the laser diode itself [24]. For this reason, several techniques are being developed in order to suppress the light-shift in laser-pumped Rubidium clocks [25]. We will present our latest results also in this line of research.

Acknowledgements. The authors acknowledge the contributions to this research of the colleagues and partners listed as co-authors in ref. [6-25]. This work was supported by the Swiss National Science Foundation and the European Metrology Research Programme (EMRP project IND55-Mclocks). The EMRP is jointly funded by the EMRP participating countries within EURAMET and the European Union. We also acknowledge previous support from the European Union, the European Space Agency (ESA) and the Swiss Space Office (Swiss Confederation).

References

[1] J. Camparo, Physics Today **60**, 33 (2007).
[2] A. Kastler , J. Phys. Radium **11**, 255 (1950).
[3] C. Cohen-Tannoudji and J. Barrat, J. Phys. Radium **22**, 329 (1961).
[4] B. S. Mathur, H. Tang and W. Happer, Phys. Rev. **171**, 11 (1968).
[5] W. Franzen, Phys. Rev. **115**, 850 (1959).
[6] M. Gharavipour, C. Affolderbach, S. Kang, T. Bandi, F. Gruet, M. Pellaton and G. Mileti, Journal of Physics: Conference Series **723**, 012006 (2016).
[7] C. Affolderbach, G. Mileti, Review of Scientific Instruments, **76** 073108 (2005).
[8] C. Affolderbach, F. Droz, G. Mileti, IEEE Transactions on Instrumentation and Measurements **55** (2), 429 (2006).
[9] C. Stefanucci, T. Bandi, F. Merli, M. Pellaton, C. Affolderbach, G. Mileti, and A. K. Skrivervik, Review of Scientific Instruments **83**, 104706 (2012).
[10] T. Bandi, C. Affolderbach, C. E. Calosso, and G. Mileti, Electronics Letters, **47** (12), 698 (2011).
[11] S. Kang, M. Gharavipour, C. Affolderbach, F. Gruet, G. Mileti, Journal of Applied Physics **117**, 104510 (2015).
[12] Y. Pétremand, C. Affolderbach, R, Straessle, M. Pellaton, D. Briand, G. Mileti and N. F. de Rooij, Journal of Micromechanics and Microengineering **22**, 025013 (2012).
[13] V. Venkatraman, S. Kang, C. Affolderbach, H. Shea and G. Mileti, Applied Physics Letters **104**, 054104 (2014).
[14] M. Violetti, M. Pellaton, F. Merli, J.–F. Zürcher, C. Affolderbach, G. Mileti, A. K. Skrivervik, IEEE Journal of Sensors, **14**, 9 (2014).
[15] M. L. Pellaton, C. Affolderbach, Y. Petremand , N. de Rooij , G. Mileti, Physica Scripta **T149**, 014013 (2012).
[16] A. Horsley, G.-X. Du, M. Pellaton, C. Affolderbach, G. Mileti, P. Treutlein, Physical Review A **88**, 063407, (2013).
[17] C. Affolderbach, G.-X. Du, T. Bandi, A. Horsley, P. Treutlein, G. Mileti, IEEE Transactions on Instrumentation and Measurement **64**, 3629 (2015).
[18] D. Miletic, P. Dziuban, R. Boudot, M. Hasegawa, R. K. Chutani, G. Mileti, V. Giordano and C. Gorecki, Electronics Letters **46**, (15) 1069 (2010).
[19] S. Abdullah, C. Affolderbach, F. Gruet, and G. Mileti, Applied Physics Letters **106**, 163505 (2015).
[20] T. Bandi, C. Affolderbach, G. Mileti, Journal of Applied Physics **111** (12), 124906 (2012).
[21] R. Straessle, M. Pellaton, C. Affolderbach, Y. Pétremand, D. Briand, G. Mileti, N. F. de Rooij, Applied Physics Letters **105**, 043502 (2014).
[22] D. Miletic, T. Bandi, C. Affolderbach, G. Mileti, Physica Scripta **T149**, 014012 (2012).
[23] D. Miletic, C. Affolderbach, M. Hasegawa, R. Boudot, C. Gorecki, G. Mileti, Applied Physics B **109**, 89 (2012).
[24] R. Matthey, C. Affolderbach, G. Mileti, Optics Letters **36** (17), 3311 (2011).
[25] C. Affolderbach, C. Andreeva, S. Cartaleva, T. Karaulanov, G. Mileti, D. Slavov, Applied Physics B **80**(7), 841 (2005).

Antirelaxation organic coating for optical resonant experiments

S. Atutov
Institution or Organization: Institute of Automation and Electrometry SB RAS, Novosibirsk, Russia
E-mail: atutovsn@mail.ru

We present recent results of study of polydimethylsiloxane and paraffin antirelaxation organic coatings used in various optical experiments. The implementation of a resonant cell without "reservoir effect" (that is constructed in order to maximized relaxation time of polarization of the ground state rubidium atoms) is discussed as well.

Optical frequency standard with ytterbium single ion

S.V. Chepurov[1], A.A. Lugovoy[1], S.N. Kuznetsov[1,2], K.M. Rumynin[1,2], M.V. Okhapkin[1,3], A.V. Taichenachev[1,2], V.I. Yudin[1,2] and S.N. Bagayev[1]
[1]*Institute of Laser Physics SB RAS, Novosibirsk, Russia*
[2]*Novosibirsk State University, Novosibirsk, Russia*
[3]*Physikalisch Technische Bundesanstalt, Braunschweig, Germany*
E-mail: svc04@ngs.ru

Frequency standards play very important role in both fundamental research and various applications. This is primarily related to the fact that the accuracy of modern frequency standards, which implement a reference for one of the basic units of measure of the SI system (second) is several orders of magnitude higher than the accuracy of references for other physical values. Development of a new generation of highly accurate optical frequency standards is a fundamental problem of laser spectroscopy. Currently, the standards based on atoms or ions localized in space are considered to be the most stable ones.

The largest frequency shift that contributes to the systematic uncertainty of many atomic frequency standards is the interaction of the thermal blackbody radiation with the atomic eigenstates. Presence of two ultra narrow optical transitions in the same thermodynamic environment makes possible implementation of so called "synthetic" frequency standard with suppressed blackbody radiation (BBR) frequency shift [1]. In ^{171}Yb ion at room temperature the residual BBR shift is estimated to be on the order of 10^{-18} for the "synthetic" frequency which is a combination of the octupole (467 nm) and the quadrupole (436 nm) optical transition frequencies. Thus, the "synthetic" frequency standard based on $^{171}Yb^{+}$ can be practically immune to the blackbody radiation shift. We report on the progress in development of a highly accurate optical frequency standard based on the single ion of ytterbium-171 at the Institute of Laser Physics, Novosibirsk.

Miniature endcap trap is used for capturing and retaining the single ion by means of a quadrupole radio frequency potential.

The quasicycling $^2S_{1/2}$ (F=1) → $^2P_{1/2}$ (F=0) electric dipole transition with natural linewidth of 23 MHz at 370 nm is used for Doppler cooling and detection of the ion. Doppler cooling of the ion is performed with the help of a frequency modulated radiation of the diode laser resonantly frequency doubled in a nonlinear crystal [2].

Narrow line probe laser is constructed to excite the ion clock transition. The linewidth of the free-running laser is decreased to ~ 1 Hz by the Pound-Drever-Hall frequency stabilization to a high-finesse Fabry-Perot etalon made of ultralow expansion (ULE) glass.

Using compact commercially available diode lasers for the ion energy state handling and optical fibers for laser radiation delivery enables the development of a transportable Yb single ion standard.

References

[1] V. I. Yudin et al, Phys. Rev. Lett. **107**, 030801 (2011).
[2] S V Chepurov, A A Lugovoy, S N Kuznetsov, Quantum Electron. **44**, 527 (2014).

Optical frequency standard based on cold strontium atoms

S.I. Donchenko, I.Yu. Blinov, S.N. Slyusarev
Federal State Unitary Enterprise "AllRussia Research Institute for Physicotechnical and Radio Engineering Measurements" (VNIIFTRI), Mendeleevo, Moscow oblast, 141570 Russia
E-mail: serslyu@mail.ru

The unsurpassed stability and high accuracy of optical clocks based on cold alkaline earth atoms make them the most attractive candidate for use in modern metrological laboratories that provide the construction of national time scales. We report on our results of realization of a strontium optical lattice clock, which is under development at VNIIFTRI as a part of GLONASS program.

Vertical-cavity surface-emitting lasers for chip-scale atomic clocks

V.A. Haisler
A. V. Rzhanov Institute of Semiconductor Physics SB RAS, 630090, Novosibirsk, Russia
Institute of Laser Physics SB RAS, 630090, Novosibirsk, Russia
Novosibirsk State Technical University, 630092, Novosibirsk, Russia
Novosibirsk State University, 630090, Novosibirsk, Russia
E-mail: vahvah55@mail.ru

Available atomic clocks are based on resonant lamps emitting at the frequency of optical transitions in Rb and Cs atoms and on absorbing cells in the microwave resonator tuned to the frequency of the transition between sublevels of the superfine structure of these atoms ground state. Such devices are rather heavy (several kilograms), large (several cubic decimeters), inefficient energy (with energy consumption of tens of watts), and expensive; therefore, they did not find numerous applications in standard devices and instruments.

In chip-scale atomic clocks (CSACs), resonant lamps are replaced by low-power high-stability vertical-cavity surface-emitting lasers (VCSELs). The reference signal is obtained with the use of a small-scale absorbing cell in the magnetic screen, while the microwave resonator is not used at all. The injection current of the laser diode emitting at an optical frequency ω_L is modulated by a microwave generator at a frequency f; as a result, lateral frequencies $\omega_L - f$ and $\omega_L + f$ arise in the laser spectrum. These frequencies initiate optical transitions from two superfine sublevels of the ground state of atoms to the global excited state. During reconstruction of the generator frequency, a narrow interference resonance of coherent population trapping appears, and it can be used to stabilize the frequency of the microwave generator with relative accuracy from 10^{-10} to 10^{-12}. This offers prospects for creating a new class of atomic clocks with a low weight (tens of grams), small size (several cubic centimeters), and low energy consumption (tens of milliwatts). Such devices can substantially improve the performance of a large number of telecommunication and navigation systems.

Here we present a numerical simulation and investigation of the generation characteristics of single-mode VCSELs with the wavelengths of 795 nm and 894.6 nm for Rb and Cs based CSACs. The details of VCSELs design, growth condition of VCSELs structures, post-growth techniques of lasers fabrication and performance of VCSELs for CSACs will be presented and discussed in this contribution.

Yb:YAG/I_2 optical frequency standard at 515 nm with instability at the level 10^{-15}

S.M. Ignatovich[1], M.N. Skvortsov[1], V.I. Vishnyakov[1], D.V. Brazhnikov[1,2], N.L. Kvashnin[1]
[1] *Institute of Laser Physics SB RAS, Novosibirsk, Russia*
[2] *Novosibirsk State University, Novosibirsk, Russia*
E-mail: sign@laser.nsc.ru

We present the results of development of optical frequency standard based on Yb:YAG laser with second harmonic at 515 nm. The laser frequency is locked to the saturated-absorption resonance in a gas cell filled with molecular iodine. Final instability of the standard is 1.3×10^{-15} at 10^4 s.

Optical frequency standards, involved saturated-absorption resonance in molecular iodine as a reference, have been developing many years [1, 2]. The best value of instability, which was reached previously, is equaled to ~ 6×10^{-15} at 10^4 s. We developed optical standard of frequency based on Yb:YAG laser with intracavity second harmonic at 515 nm. As reference for stabilization resonance of iodine R(66)44-0 was chosen. It resonance has biggest ratio amplitude to width inside frequency tuning range of laser. Width of resonance was Γ = 310 kHz. For achieving of maximum stability optical scheme with detection of resonance in luminescent light was developed (Fig.1). Such scheme produce better signal/noise ratio relatively schemes with detection in transmitting light due to reducing short noise of photo detector from background light. Also luminescent detection make possible use for receiving of signal bigger photosensitive area, what allowing to use massive of photodiodes with next adding all signals together. So as every photodiode produce shot noise signal/noise ratio increased in $\sqrt{N}$ times, where N – quantity of photodiodes in massive. We are using 24 FDS10X10 Thorlabs photodetectors in every standard, it produce of signal/noise in 5 times higher in comparison with one photodiode and allow to observe resonance with signal/noise >10^4 in bandwidth 10 Hz.

Conventional locking scheme based on the third harmonic detection of a signal [3] has been used in our case. Functional diagram of the optical frequency standard is presented at Fig.1.

We have quantitatively estimated the influence of various destabilizing factors on performance of optical frequency standard and, as the result, made several key modifications:

1. Electronic digital systems for precise laser beam modulation and for detecting of reference resonance have been developed and implemented. Modulation was produced by acoustooptic modulator (AOM) with signal from direct digital synthesizer (DDS). For achieving high stability we apply OCXO quartz with instability 10^{-10} in 1s as clock signal for DDS. It allow tune frequency of laser with accuracy $4\cdot10^{-3}$ Hz. Also this clock signal was used in digital lock-in amplifier (DLock) for detection of resonance. Digital lock-in was built at FPGA chip. Main advantage of digital lock-in is absence of output drifts of zero level, but for realization of this property we needed to program PID regulator inside of FPGA.

2. Stabilization of residual amplitude noises in modulated laser beam has been ensured up to 10^{-8} from total power. It was done due to mixing irregularity distribution of noises over the beam diameter in the polarization maintaining optical fiber and suppression of noises by PID which controlled power of signal at AOM [4].

3. Two-stage system of iodine cell thermostabilization has been designed for accurate stabilization of iodine vapors pressure. So as vapors pressure shift is ~ -800 Hz/°C instability in temperature should be better than 1 mK. It was achieved with two stages. External stage was built around all cell and has accuracy 20 mK. Internal stabilize temperature only finger of cell with instability <1mK.

4. High-quality beam profile has been provided, allowing us to avoide relevant frequency shift due to wave-front curvature. It was done due to polarization maintaining optical fiber with high quality collimator.

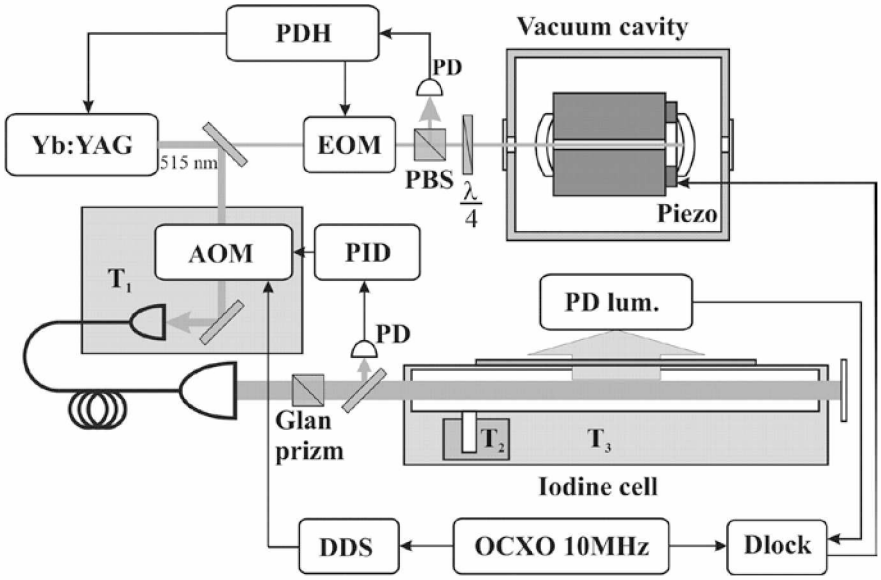

Fig. 1 Functional diagram of optical frequency standard.

Stability of the constructed optical frequency standard has been retrieved from stability of the beat signal of two identical setups. So, instability equals to 1.3×10^{-15} at 10^4 s (Fig.2).

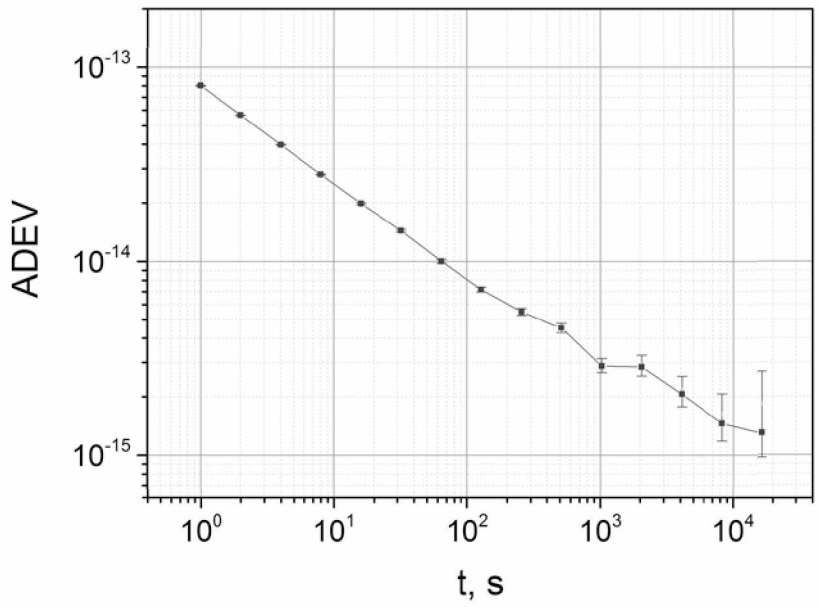

Fig. 2 Allan deviation.

This work was supported by the Russian Foundation for Basic Research (grant no. 15-32-20330, 16-32-00159).

References

[1] M.N. Skvortsov, M.V. Okhapkin, A.Yu. Nevsky, S.N. Bagaev, Quantum Electron. **34**(12), p. 1101 (2004).

[2] J.L. Hal, L.-S. Ma, M. Taubman, B. Tiemann, F.L. Hong, O. Pfister and J. Ye, "Stabilization and frequency measurement of the I_2-stabilized Nd:YAG laser", IEEE Trans. Instrum. Meas. **48**(2), pp. 583–586 (1999).

[3] K. Nyholm, M. Merimaa, T. Ahola and A. Lassila, "Frequency stabilization of a diode-pumped Nd:YAG laser at 532 nm to iodine by using third-harmonic technique", IEEE Trans. Instrum. Meas. **52**(2), pp. 284–287 (2003).

[4] V I Denisov, S M Ignatovich, N L Kvashnin, M N Skvortsov, S A Farnosov, "Precise modulation of laser radiation by an acousto-optic modulator for stabilisation of the Nd : YAG laser on optical resonances in molecular iodine", Quantum Electron, **46** (5), p. 464(2016).

Atomic magnetometry for the neutron EDM experiment at PSI

H.-C. Koch[1] on behalf of the nEDM collaboration at PSI
[1]*Paul Scherrer Institut, 5232 Villigen PSI, Switzerland*
E-mail: hans-christian.koch@psi.ch

An international collaboration at Paul Scherrer Institut, Switzerland, is searching for a possible electric dipole moment of the neutron (nEDM). The current most sensitive measurement [1] constrains the nEDM to $d_n \leq 3.0 \times 10^{-26}\,\mathrm{e\,cm}\,(90\%\,\mathrm{CL})$ and is compatible with zero. The (non)existence of an nEDM is closely linked to a number of persisting problems of cosmology, such as the baryon asymmetry of the universe [2] and is furthermore a sensitive probe for physics beyond the standard model.

The measurements are performed on stored ultracold neutrons using Ramsey's technique of separated oscillating magnetic fields [3]. This is achieved by measuring the neutron's precession frequency in applied homogeneous parallel and antiparallel electric and magnetic fields. An nEDM would lead to different precession frequencies in these two configurations and from the frequency difference the magnitude of the nEDM can be inferred. Since the magnetic contribution to the neutron's precession frequency is many orders of magnitude larger than that of a (possible) nEDM, the applied $1\,\mu\mathrm{T}$ magnetic field has to be precisely monitored and controlled during the precession time of typically 200 seconds in order to avoid systematic measurement errors. The spatial homogeneity of the field is of similar importance in this respect. To this aim a ^{199}Hg magnetometer and an array of cesium magnetometers are currently employed in the apparatus. In a future stage of the experiment they will be complemented by an array of ^{3}He-Cs magnetometers. The three types of magnetometers (will) fulfill different tasks in the nEDM experiment, yet they all exploit the proportionality of the respective species' Larmor frequency ω_i and the magnetic field, $\omega_i = \gamma_i \cdot B$.

The volume averaged magnetic field in the neutron precession chamber is measured by the ^{199}Hg co-magnetometer. Polarized Hg atoms are precessing simultaneously with the neutrons in the same volume. Their Larmor frequency is assessed by monitoring the transmission of a polarized resonant UV-light beam traversing the neutron precession chamber. These measurements are extremely important to correct the neutron data for cycle-to-cycle fluctuations of the magnetic field.

The Cs array consists of 16 laser driven double resonance M_x magnetometers [4] placed in a grid at strategic positions above and below the neutron precession chamber. They offer a high sensitivity and bandwidth and are used to survey the temporal stability and spatial homogeneity of the applied field in the whole apparatus. Based on their measurements, currents are applied to a set of dedicated correction coils in order to homogenize the field in the region of the precession chamber.

The ^{3}He/Cs magnetometers envisioned for the next stage of the experiment will acquire the field at their positions by measuring the precession frequency of a polarized ^{3}He gas sample. This is achieved through detection of the oscillating magnetic field associated with the nuclei's precession using a set of dedicated Cs magnetometers of the type mentioned above [5]. The absence of a number of systematic effects that may affect other magnetometers and the sensitivity of the ^{3}He's depolarization time to magnetic field gradients will make this magnetometer a powerful tool for homogenizing the applied magnetic field.

In this talk the different magnetometric schemes will be detailed and their significance for the nEDM measurement explained.

References

[1] J.M. Pendlebury et al., Phys. Rev. D **92**, 092003 (2015).
[2] A.Riotto, N.Trodden, Ann.Rev.Nucl.Part.Sci. **49**, 35 (1999).
[3] N.F.Ramsey, Phys. Rev. **78**, 695 (1950).
[4] S.Groeger, G.Bison et al., Eur. Phys. J. D **38**, 239 (2006).
[5] H.-C.Koch, G.Bison et al., Eur. Phys. J. D **69**, 202 (2015).

Progress in optical frequency standards: ultracold Thulium, ions, and passive resonators

Nikolay Kolachevsky
P.N. Lebedev Physical Institute, Leninsky prospect 53, 119991 Moscow, Russia
E-mail: kolachevsky@lebedev.ru

This talk summarises current research at P.N. LebedevInstitute aimed for development of stable optical frequency references based on laser cooled lanthanide element Thulium, single Aluminum ion and passive optical cavitites.

The inner-shell transition [Xe]4f136s2 (J = 7/2, F = 4, m = 0) → [Xe]4f136s2 (J= 5/2, F= 3, m = 0) in the Tm atom at λ = 1.14 μm is considered as a candidate for an optical lattice clock. The transition wavelengths and probabilities for two clock levels J = 7/2 and J = 5/2 in the spectral range 250 – 1200 nm are calculated using the COWAN package which allows deducing of the differential dynamic polarizability and suggests that the magic wavelength is at around 807 nm with an attractive optical potential.The suggested clock transition demonstrates a low sensitivity to the BBR shift which provides a clock frequency instability at the low 10^{-18} level competing with the best known optical clocks. We also evaluated other feasible contributions to clock performance (magnetic interactions, light shifts, van der Waals, and quadrupole shifts) which, after reasonable assumptions, can be lowered to the 10^{-18} level. Together with the relative simplicity of laser cooling and trapping Tm atoms, our results demonstrate that Tm is a promising candidate for optical clock applications [1].. Experiments with direct excitation of the clock transition by spectrally narrow laser radiation at λ=1.14 μm set a lower limit for the upper clock level lifetime of 112 ms which corresponds to the natural linewidth of < 1.4 Hz. Modulating the trap depth and analyzing the corresponding parametric resonances frequencies, we deduced the scalar polarizability of the Tm ground state at 532 nm which shows reasonable agreement with our calculations.

Also, current progress in trapping and laser cooling of Mg^+ ions in a linear Paul trap for sympathetic cooling of Al^+ clock ion is discussed. Theoretical and experimental study of trap losses for hot atoms give understanding of the trapping process and set initial conditions for laser cooling. Laser cooled clouds of Mg^+ ions show life time in the trap approaching 10 min. In the near future we are aiming for trapping of short chains and single ions as well as for sympathetic cooling of Al^+ ions. Together with ground state cooling of Mg^+ ion it will be an important step to realization of the Al^+ ion standard.

Progress in development of optical standards is tightly connected with development of frequency stabilized lasers. Our former research allowed to set up a family of diode lasers stabilized to ULE cavities which show the fractional frequency instability of 1.5×10^{-15} in 1-100 s time interval approaching the thermal noise limit. Lasers are currently used in Sr, Tm and Al optical clocks at VNIIFTRI and P.N. Lebedev Institute. To reach better performance we are currently working at cryogenic Si cavities with GaAs/InGaAs mirrors for λ=1.5 μm. The thermal noise will be lowered to 10^{-16} level which opens new perspectives both for applications in current optical frequency standards, and for relatively compact and simple ultrastable passive frequency references.

References

[1] D. Sukachev et al., arXiv:1605.09032F

Ultrastable, 10 mHz linewidth lasers based on cryogenic silicon resonators

T. Legero[1], D.G. Matei[1], S. Häfner[1], C. Grebing[1], R. Weyrich[1], F. Riehle[1], and U. Sterr[1]
W. Zhang[2], J. Robinson[2], L. Sonderhouse[2], and J. Ye[2]
[1]*Physikalisch-Technische Bundesanstalt (PTB), Bundesallee 100, 38116 Braunschweig, Germany*
[2]*JILA, National Institute of Standards and Technology and University of Colorado, 440 UCB, Boulder, CO 80309-0440, USA*
E-mail: Thomas.Legero@ptb.de

Laser can emit polarized light with high intensity and superior spatial and temporal coherence. The corresponding spectral purity and high frequency stability revolutionized optical spectroscopy and allowed for the study and control of internal states of atoms and molecules. Today's most stable and spectrally narrow laser sources are essential for probing ultra narrow optical clock transitions [1,2], precision tests of relativity [3] and the detection of gravitational waves [4].

The most common concept for ultrahigh frequency stability and narrow linewidth relies on stabilization of a laser system to a passive Fabry-Pérot resonator [5] with the Pound-Drever-Hall (PDH) stabilization technique [6]. The fractional frequency stability of the laser is then identical to the fractional optical-length stability of the resonator. This sets the highest requirements on the isolation of the resonator from temperature and pressure fluctuations, as well as from seismic and acoustic vibrations. In addition to technical noise, inevitable Brownian thermal noise fundamentally limits the resonators length stability [7]. During the last years there has been a remarkable progress in reducing the resonators thermal noise limit [8-10].

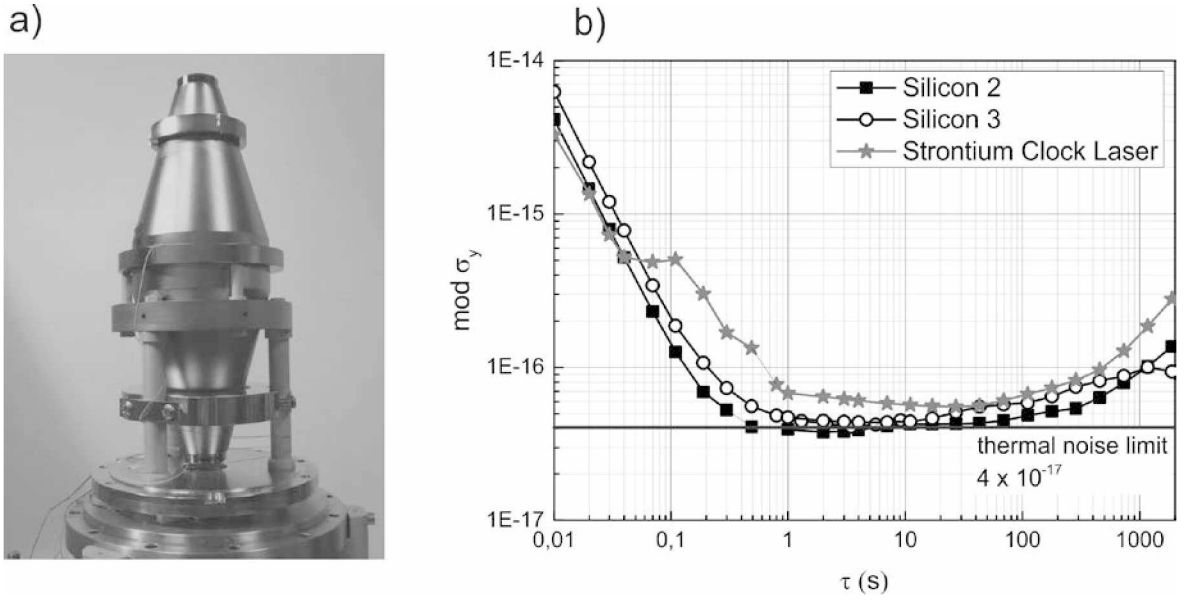

Fig. 6 Photograph of one of the silicon resonators resting on a stiff tripod support (a). Individual frequency instability determined from a three-cornered hat comparison of the two silicon based laser systems (Silicon 2 and 3) working at 1.5 μm [8] and a 698 nm laser stabilized on a 48 cm long ULE resonator [9].

We follow this approach by stabilizing a commercial DFB fiber laser to a Fabry-Pérot resonator made of single-crystal silicon cooled to 124 K [11]. Both the cavity spacer and the mirror substrates are made out of the same crystal. The low temperature and the high mechanical Q-factor of silicon result in an exceptional low level of thermal noise. Setting up two independent laser systems

employing individual silicon resonators we demonstrate an unprecedented fractional frequency instability of 4×10^{-17}. The linewidth of the emitted light at 1.5 μm is 10 mHz, corresponding to a coherence time of 100s.

Each resonator employs a 212 mm long conical shaped silicon spacer optically contacted to silicon mirrors with high-reflectivity Ta_2O_5/SiO_2-coatings (Fig 1 a). Both resonators show a finesse close to 500 000. The resonators' thermal noise is dominated by the contribution of the mirror coatings. The expected fractional frequency instability is calculated to be 4×10^{-17}. Each resonator is placed in a vacuum chamber with residual pressure of 10^{-9} mbar. They are actively cooled to the cross-over temperature of silicon's coefficient of thermal expansion at around 124 K. Additional thermal shielding further suppresses the impact of residual temperature fluctuations. All other technical noise sources, such as seismic and acoustic vibrations as well as residual amplitude modulation [12], have been carefully studied and suppressed to levels well below the expected thermal noise limit.

We confirmed the individual frequency stabilities of the two silicon laser systems by a three-cornered hat comparison [13] with a third ultra-stable laser at 698 nm [14]. This additional laser serves as interrogation laser in PTB's strontium-lattice clock. Stabilized on a 48 cm long resonator, made from ultra low expansion glass, this laser shows a thermal noise limited frequency instability of mod $\sigma_y \approx 7\times10^{-17}$. A femtosecond frequency comb is used to bridge the wavelength gap between the 1.5 μm systems and the 698 nm laser [10]. The necessary optical fiber links between the lasers and the frequency comb are stabilized by active fiber noise cancelation [15]. The modified Allan deviations of both silicon-based laser systems show a thermal-noise-limited flicker floor at mod $\sigma_y = 4\times10^{-17}$ for averaging times between 1s and 100s.

The direct beat signal between the two 1.5 μm laser systems was recorded over periods of 200 s and spectrally analyzed by Fast-Fourier-Transform. On average the width of the beat signal is as narrow as 13 mHz, indicating an individual linewidth of the lasers at around 10 mHz.

References

[1] B.J. Bloom, T.L. Nicholson, J.R. Williams et al., Nature **506**, 71 (2014).
[2] N. Huntemann, C. Sanner, B. Lipphardt et al., Phys. Rev. Lett. **116**, 063001 (2016).
[3] C. Eisele, A. Y. Nevsky, and S. Schiller, Phys. Rev. Lett. **103**, 090401 (2009).
[4] B. P. Abbott et al., Phys. Rev. Lett. **116**, 061102 (2016).
[5] B.C. Young, F.C. Cruz, W.M. Itano and J.C. Bergquist, Phys. Rev. Lett. **82**, 3799 (1999).
[6] R.W.P. Drever, J.L. Hall, F.V. Kowalski et al., Appl. Phys. B **31**, 97 (1983).
[7] K. Numata,A. Kemery, J. Camp, Phys. Rev. Lett. **93**, 250602 (2004).
[8] Y.Y. Jiang, A.D. Ludlow, N.D. Lemke et al., Nature Phot.**5**, 158 (2011).
[9] T. Kessler, C. Hagemann, C. Grebing, et al., Nat. Phot. **6**, 687 (2012).
[10] S. Häfner, S. Falke, C. Grebing, et al., Opt. Lett. **40**, 2112 (2015).
[11] D.G. Matei, T. Legero, C. Grebing, et al., J. Phys.: Conf. Ser. **723**, 012031 (2016).
[12] W. Zhang, M.J. Martin, C. Benko et al., Opt. Lett. **39**, 1980 (2014).
[13] J.E.Gray, D.W. Allan, Proc. of the 28th Ann. Symp. on Freq. Contr., 243 (1974).
[14] H.R. Telle, B. Lipphardt, J. Stenger, Appl. Phys. B **74**, 1 (2002).
[15] L.S. Ma, P. Jungner, J. Ye and J.L. Hall, Opt. Lett. **19**, 1777 (1994).

An ultra-stable silicon cryogenic optical resonator

A. Nevsky, E. Wiens, S. Schiller
Institut für Experimentalphysik, Heinrich-Heine Universität Düsseldorf, Germany
E-mail: alexander.nevsky@uni-duesseldorf.de

We report on the characterization of a silicon optical resonator operating in the deep cryogenic regime at temperatures down to 1.5 K. The measured expansion coefficient, frequency drift and the sensitivities of the resonator to external perturbations indicate that this system should enable frequency stabilization of lasers at the low-10^{-17} level.

Search for the low-energy isomer in ^{229}Th

M. Okhapkin, D.-M. Meier, J. Thielking, P. Glowacki, E. Peik
Physikalisch-Technische Bundesanstalt, Bundesallee 100, 38116 Braunschweig, Germany
E-mail: Maksim.Okhapkin@ptb.de

The existence of a nuclear isomeric state in ^{229}Th at about 8 eV excitation energy has stimulated the development of novel ideas in an unexplored domain of atomic and nuclear physics where the nuclear excitation energy is in the same range as transition energies of valence electrons [1]. An optical nuclear clock, using a γ- transition as a reference offers advantages like an insensitivity against field-induced systematic frequency shifts and the opportunity to obtain high stability from interrogating many nuclei in the solid state (see [2] for a recent review). A direct optical detection of the ^{229}Th isomer's excitation or decay is still missing. While the expected natural linewidth is 1 mHz or less, the transition wavelength in the VUV range is presently determined with a large uncertainty as 160(10) nm.

Our approach to achieve an excitation of the isomer is to use two-photon laser excitation via electronic bridge processes in trapped $^{229}Th^{+}$ [3,4] and Th^{2+} ions. The high density of electronic states of Th^{+} in the energy range of the isomer promises a strong enhancement of the excitation rate. Presently, the experimental search for the laser excitation of the isomeric state in singly charged thorium is ongoing. Doubly charged thorium has some advantages over Th^{+} notwithstanding the lower density of the electronic states. It has the *5f8s* electronic configurations in the range of the isomer energy which can provide an efficient isomer excitation because the wave function of the *s*-electron has the greatest overlap with the nucleus [6,7]. We study a possible two-photon excitation scheme in Th^{2+} for energies higher than 8.3 eV, since this range is hardly accessible in Th^{+} with our excitation scheme due to resonantly enhanced three-photon ionization.

We also discuss an experiment started in the collaboration with the Ludwig-Maximilians-University of Munich for the laser spectroscopy of trapped ^{229}Th recoil ions, where the isomeric state is populated with about 2% probability in α- decay from ^{233}U [8,9]. The main goal of this experiment is to observe a hyperfine structure of electronic transitions of the isomer.

This work is supported by EU FET-Open project 664732–nuClock.

References

[1] E.V. Tkalya, Physics Uspekhi **46**, 315 (2003).
[2] E. Peik, M. Okhapkin, C.R. Physique **16**, 516 (2015); arXiv:1502.07322
[3] S.G. Porsev et. al., Phys. Rev. Lett. **105**, 182501 (2010)
[4] O.A. Herrera-Sancho, et. al., Phys. Rev. A **88**, 012512 (2013)
[5] M.V. Okhapkin et. al., Phys. Rev. A, **92**, 020503(R) (2015)
[6] F.F. Karpeshin et al., Phys. Lett. B 372, 1 (1996).
[7] F.F. Karpeshin et al., Nucl. Phys. A **654**, 579 (1999).
[8] L. v.d. Wense et al., EPJ A **51**, 29 (2015).
[9] L. v. d. Wense et. al. Nature **533**, 47 (2016).

Higher-order effects on uncertainties of clocks of Mg atoms in an optical lattice

V.D. Ovsiannikov[1], S.I. Marmo[1], S.N. Mokhnenko[1] and V.G. Palchikov[2,3]
[1]*Voronezh State University, 394006 Voronezh, Russia*
[2]*FGUP "VNIIFTRI", 141570 Mendeleevo, Moscow Region,Russia*
[3]*National Research Nuclear University "MEPhI", Moscow, Russia*
E-mail: ovd@phys.vsu.ru

The recent progress in detecting experimentally the $^3P_0 - {}^1S_0$ clock transition in neutral Mg atoms and determination of corresponding magic wavelength (MWL) 468.46 nm [1] paves the way to the development of a new time-frequency standard of Mg atoms in an optical lattice. To ensure the Mg clock fractional uncertainties below 10^{-17}, the role of higher-order nonlinear and non-dipole effects of interaction between trapped atoms and the magic-frequency lattice should be evaluated.

In this paper we present theoretical considerations of the most appropriate operational conditions based on results of numerical calculations of higher-order susceptibilities of the clock states in Mg atoms. The single-electron Fues' model-potential (FMP) approach was used with modifications introduced for the most efficient account of contributions from the valence electrons and from their interaction with the inner-electron shells [2,3]. The modifications of the FMP parameters were based on comparison of the calculated MWL 472.6 nm and static polarizabilities 61 and 109 a.u. of clock states with the above-presented result of experimental measurements and evaluations of polarizabilities 71 and 101 a.u. correspondingly, in the many-body perturbation theory with account of configuration interactions [1].

The frequencies of clock transitions between the ground $3s^2(^1S_0)$ and metastable $3s3p(^3P_0)$ states of all atoms confined to an oscillatory motion in a Stark-effect energy wells of an optical lattice will be equal exactly to those of free atoms (taken for the frequency standard) if the vibration energies of each atom in its normal E_g^{vib} and excited E_e^{vib} states will coincide with one another [3]. To this end, the difference $\Delta\nu_{clock}^{latt} = E_e^{vib} - E_g^{vib}$, the most important contributions to which may be determined from a few lowest orders of the perturbation theory (PT) for interaction of an atom with the lattice-radiation field, should be reduced to its minimal value, independent of the trapped atom position along the optical lattice (every atom in its personal well). With account of the second- and fourth-order PT for the atom-lattice interaction, the dependence of the clock-frequency shift on the lattice-laser intensity I may be presented, as follows [3]

$$\Delta\nu_{clock}^{latt}(n,\delta,\xi,I) = c_{1/2}(n,\delta)I^{1/2} + c_1(n,\delta,\xi)I + c_{3/2}(n,\xi)I^{3/2} + c_2(\xi)I^2. \qquad (1)$$

The intensity-independent coefficients in this resolution depend on the oscillator quantum number n of the trapped-atom state in the lattice well, assumed independent of the atomic clock state (normal or metastable). The shift (1) depends also on the deviation $\delta = \omega_{latt}^{op} - \omega_{mag}^{E1}$ of the lattice-laser operational frequency ω_{latt}^{op} from the exact magic frequency ω_{mag}^{E1} (determined from the equality $\alpha_e^{E1}(\omega_{mag}^{E1}) = \alpha_g^{E1}(\omega_{mag}^{E1})$ of the electric dipole (E1) polarizabilities of the clock states) and on the degree of the lattice-laser circular polarization ξ, which appears in the fourth-order PT from the ξ-dependence of the clock-transition hyperpolarizabilities [2,3]:

$$\Delta\beta(\xi,\omega) = \beta_e(\xi,\omega) - \beta_g(\xi,\omega) = \Delta\beta^l(\omega) + \xi^2\left(\Delta\beta^c(\omega) - \Delta\beta^l(\omega)\right), \qquad (2)$$

where $\Delta\beta^{l(c)}(\omega)$ is the frequency-dependent component of the susceptibility determining the hyperpolarizability of the clock transition in the field of linearly (circularly) polarized radiation. Also the dependence appears on the recoil energy of the lattice photons $\mathcal{E}^{rec} = k^2/(2\mathcal{M})$ ($\mathcal{M}$ is the mass of the atom, $k = \omega/c$ is the lattice-photon momentum equal to the wave number related with the wavelength $\lambda = 2\pi/k$, determining the principal geometric characteristics of the lattice, e.g. the distance $\lambda/2$ between the lattice potential wells and the separation $\lambda/4$ between tops and bottoms

of the lattice wells) arising from the higher-order multipolar (first of all, the electric quadrupole E2 and magnetic dipole M1) interaction of atoms with the optical lattice field.

With account of the E1, E2 and M1 contributions to the Stark-effect energy, three different definitions of the magic frequency may be proposed on the basis of different conditions for equalization of the upper and lower-level Stark shifts in the traveling and standing waves. The traditionally used condition of the shift equality written in terms of the E1 polarizabilities as $\alpha_e^{E1}(\omega_{mag}^{E1}) = \alpha_g^{E1}(\omega_{mag}^{E1}) \equiv \alpha_m^{E1}$, modifies for a traveling wave to $\alpha_e^{\Sigma}(\omega_{mag}^{t}) = \alpha_g^{\Sigma}(\omega_{mag}^{t})$, where the E2-M1 interactions are synchronous to the E1 interaction, therefore $\alpha_{e(g)}^{E1}(\omega)$ is replaced by the sum $\alpha_{g(e)}^{\Sigma}(\omega) = \alpha_{g(e)}^{E1}(\omega) + \alpha_{g(e)}^{qm}(\omega)$ of $\alpha_{e(g)}^{E1}(\omega)$ and the sum of E2-M1 polarizabilities $\alpha_{e(g)}^{qm}(\omega) = \alpha_{e(g)}^{E2}(\omega) + \alpha_{e(g)}^{M1}(\omega)$.

On the contrary, in a standing wave the E2-M1 interactions are a quarter period off-phase to the E1 interaction and E2-M1 polarizabilities are subtracted from the dipole polarizability $\alpha_{e(g)}^{dqm}(\omega) = \alpha_{e(g)}^{E1}(\omega) - \alpha_{e(g)}^{qm}(\omega)$, the difference of the E1 and, giving the standing-wave magic-frequency condition $\alpha_e^{dqm}(\omega_{mag}^{s}) = \alpha_g^{dqm}(\omega_{mag}^{s})$. The absolute value of $\alpha_{g(e)}^{E1}(\omega_{mag}^{E1})$ is 6 to 7 orders greater than $\left|\alpha^{qm}(\omega_{mag}^{s(t)})\right|$, so the difference between ω_{mag}^{E1} and $\omega_{mag}^{s(t)}$ appears only in the 6th or 7th decimal place. Nevertheless, small deviations of the lattice-laser frequency may cause significant variations of the shift (1) confining the precision of the atomic clocks.

The deviations $\delta^s = \omega_{mag}^{s} - \omega_{mag}^{E1}$ and $\delta^t = \omega_{mag}^{t} - \omega_{mag}^{E1}$ are approximately opposite to one another, $\delta^s \approx -\delta^t$. Assuming the operational frequency of the lattice laser $\omega_{latt}^{op} = \omega_{mag}^{E1} + \delta$, the coefficients of the resolution (1) may be presented, as follows

$$c_{1/2}^{E1}(n) = \left(\frac{\partial \Delta\alpha_m^{E1}}{\partial \nu}\delta - \Delta\alpha_{E1}^{qm}\right)\sqrt{\frac{\mathcal{E}_{E1}^{rec}}{\alpha_m^{E1}}}\left(n+\frac{1}{2}\right), \quad c_1^{E1}(\xi,n) = -\frac{\partial \Delta\alpha_m^{E1}}{\partial \nu}\delta - \frac{3\mathcal{E}_{E1}^{rec}}{2\alpha_m^{E1}}\Delta\beta_{E1}(\xi)\left(n^2+n+\frac{1}{2}\right),$$

$$c_{3/2}^{E1}(\xi,n) = 2\Delta\beta_{E1}(\xi)\sqrt{\frac{\mathcal{E}_{E1}^{rec}}{\alpha_m^{E1}}}\left(n+\frac{1}{2}\right), \quad c_2^{E1}(\xi) = -\Delta\beta_{E1}(\xi). \qquad (3)$$

It is evident, that the atoms should be cooled to the ground-state vibrations of the oscillator quantum number $n=0$. The calculated data for susceptibilities and recoil energy confirm the most important contributions to the shift (1) from the first two terms. The deviation of the magic frequency δ may be used to reduce $\Delta\nu_{clock}^{latt}(n,\delta,\xi,I)$ to a minimal value, which depends on the degree of circular polarization ξ and the intensity of the lattice laser I. For example, at the intensity $I = 75$ kW/cm^2 of the linearly polarized lattice laser beam (which corresponds to the lattice trap depth of $35\,\mathcal{E}^{rec}$) the real part of the shift (1) $\mathrm{Re}\left\{\Delta\nu_{clock}^{latt}(n,\delta,\xi,I)\right\} \approx 0$ for the frequency deviation $\delta = -19.65$ MHz, while the imaginary part, which determines the clock-frequency broadening and comes from the imaginary part of the clock-transition hyperpolarizability $\Delta\beta_{E1}$, is $\mathrm{Im}\left\{\Delta\nu_{clock}^{latt}(n,\delta,\xi,I)\right\} \approx 28.3$ mHz; this value also determines the rate of the two-photon ionization of the excited clock state.

References

[1] A.P. Kulosa, D. Fim, K.H. Zipfel, et al, Phys.Rev.Lett. **115**, 240801 (2015).
[2] N.L. Manakov, V.D. Ovsiannikov and L.P. Rapoport, Phys. Rep. **141**, p.319 (1986).
[3] V.D. Ovsiannikov, S.I. Marmo and V.G. Pal'chikov and H. Katori, Phys. Rev. A **93**, 043420 (2016).

Optical spectroscopy of atomic Bloch bands

E.M. Rasel[1], A. Kulosa[1], D. Fim[1], K. Zipfel[1], N. Jha[1], S. Rühmann[1], S. Sauer[1], M. Safranova[2], K. Gibble[3]
[1]*Institut für Quantenoptik, Leibniz Universität Hannover, Welfengarten 1, 30167 Hannover, Germany*
[2]*Department of Physics and Astronomy, University of Delware, 217 Sharp Lab , Newark, DE 19716,USA*
[3]*Department of Physics, 104 Davey Laboratory, Penn State University, University Park, PA 16802, USA*
E-mail: rasel@iqo.uni-hannover.de

We report on optical spectroscopy of atomic Bloch bands of laser cooled magnesium atoms tunneling in an optical lattice. We show that this allows us even for shallow lattices to accurately determine the magic wavelength of the lattice, for which the energy bands of the ground and excited electronic states become identical. Beyond atomic physics and metrology, Bloch band spectroscopy of atoms with ultra-narrow optical transitions is of interest for quantum simulations of condensed matter phenomena.

Cryogenic optical lattice clocks towards an uncertainty of sub-10^{-18} level

I. Ushijima[1], M. Das[2], M. Takamoto[1,2] and H. Katori[1,2,3]
[1]*RIKEN Center for Advanced Photonics, Japan*
[2]*Quantum Metrology Laboratory, RIKEN, Japan*
[3]*Department of Applied Physics, the University of Tokyo, Japan*
E-mail: ushijima@riken.jp

Optical atomic frequency standards made remarkable progress during the last decade and are expected to redefine the SI second as well as find applications in testing of fundamental physics [1, 2] and chronometric geodesy [3]. Recently, uncertainties of 10^{-18} have been reported using neutral strontium (Sr) optical lattice clocks [4, 5].

Cryogenic Sr optical lattice clocks [4], where the atoms are interrogated in a cryogenic environment, have achieved both the uncertainty and the agreement of two clocks at 10^{-18} by reducing one of the major sources of systematic uncertainties due to blackbody radiation impinging on to the atoms. As progress of cryogenic clock continues towards the total uncertainty of 10^{-19} level, the cryogenic clock reveals that the next major uncertainty arises from higher-order lattice light shifts. To tackle this, an operational magic frequency [6] has been proposed recently, which has been shown to reduce the lattice light shifts to low 10^{-19}. So far, optical lattice clocks have been operated with lattice laser tuned to a frequency, where the lattice light shift is thought to be proportional to the intensity of lattice laser I in the intensity range used for the experiments. The proposed operational magic frequency also includes the contributions from higher-order terms like magnetic-dipole and electric-quadrupole polarizabilities and hyperpolarizability. The light shift then consists of terms proportional not only to I but also to $I^{1/2}$, $I^{3/2}$ and I^2. We have evaluated the higher order terms of lattice light shift by employing a cavity for the 1D lattice and measuring the dependence of light shift on intensity of lattice laser and vibrational levels of atoms.

Further an accurate clock enables many applications for example in chronometric geodesy, monitoring movement of the Earth's crust and searching underground resources as well as topological dark matter [2]. To demonstrate the chronometric geodesy, we have measured the frequency difference between two cryogenic Sr optical lattice clocks located at RIKEN and the University of Tokyo.

In this talk, we will discuss the latest results of these experiments.

References

[1] J. P. Uzan, Rev. Mod. Phys. **75**, 403 (2003).
[2] A. Derevianko and M. Pospelov, Nature Phys. **10**, 933 (2014).
[3] M. Vermeer, Rep. Finnish Geodetic Inst. **83**, 1 (1983).
[4] I. Ushijima, M. Takamoto, M. Das, T. Ohkubo and H. Katori, Nature Photon. **9**, 185 (2015).
[5] T. Nicholson et al., Nature Commun. **6**, 6896 (2015).
[6] H. Katori, V. D. Ovsiannikov, S. I. Marmo, V. G Palchikov, Phys. Rev. A **91**, 052503 (2015).

Collisions in ultra-cold thulium atoms

A.V. Akimov[1,2,3], I.S. Cojocaru[2,4], S. Pyatchenkov[2], S. Snigirev[2,3], I. Luchnikov[2,4], E. Davletov[2,3,4],V. Tsyganok[2,4], D.N. Kublikova[2,4], V. Bushmakin[2,4], D. Sukachev[2,4], E. Kalganova[2,3], G. Vishnyakova[2,3], V.N. Sorokin[2,3]

[1] *Texas A&M University, Department of Physics, 4242 TAMU, College Station, TX, 77843, USA*
[2] *Russian Quantum Center, 100, Novaya st., Skolkovo, Moscow Reg., 143025, Russia*
[3] *P. N. Lebedev Institute of Russian Academy of Sciences, 53 Leninsky prospect, Moscow, 119991, Russia*
[4] *Moscow Institute of Physics and Technology, 9 Institutskiy per., Dolgoprudny, Moscow Region, 141700, Russia.*
[5] *Harvard University, Department of Physics, 17 Oxford Street, Cambridge, MA 02138, USA*
E-mail: akimov@physics.tamu.edu

Recently laser cooled rare earth elements attracted considerable attention due to the high orbital and magnetic moments. Such a systems allow low-field Feshabach resonances enabling tunable in wide range interactions. In particular, thulium atom has one hole in 4f shell therefore having orbital moment of 3 in the ground state, magnetic moment of 4 Bohr magnetons in ground state. While magnetic moment of the thulium atom is less than that of Erbium or Dysprosium simpler level structure, possibility to capture thulium atoms and the dipole trap at 532 nm make thulium atom an extremely attractive subject for quantum simulations.

Collisional properties play important role in physics of ultracold atoms and quantum simulations with such an atoms. In particular inelastic light assisted collisions limit considerably number of atoms one could achieve with magneto-optical trap. To the contrarily Feshabash resonances could be very helpful for control of interaction strength in ultracold atoms. In this contribution, we present our study of the both light assisted collisions and low field Feshabach resonances for Thulium atom.

In our effort toward deep laser cooling of Thulium atom we realized its laser cooling at narrow 0.36 MHz wide transition with wavelength of 530.7 nm and achieved around 10^7 atoms with temperature of about 30 μK. We performed studies of light assisted collisions near in Magneto optical trap operating near this transition. We found, that light assisted inelastic binary collisions losses rate $\beta \sim 10^{-9}\,\mathrm{cm}^3/\mathrm{s}$. In order to study Feshbach resonances we loaded thulium atoms into crossed dipole trap formed by 10W of 532 nm laser radiation. With short evaporative cooling step, we were able to low temperature of the thulium atoms down to 3 μK and record low-field spectra of the Feshbach resonances.

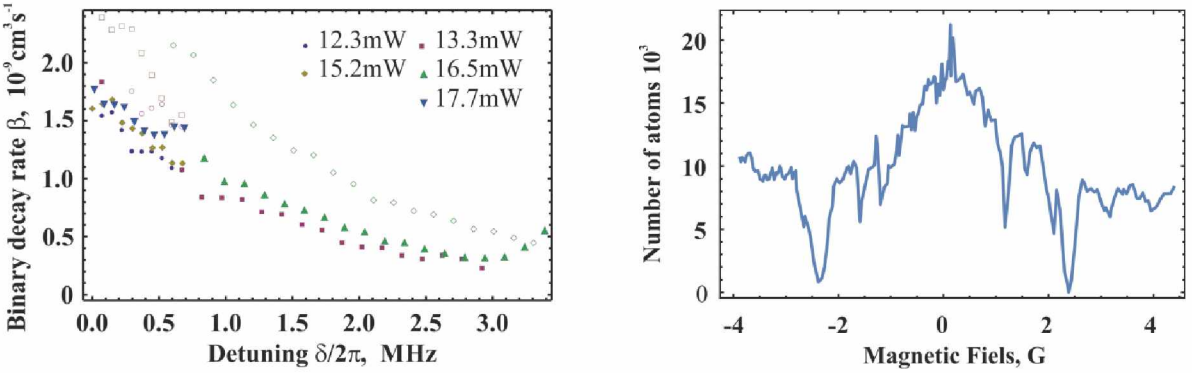

Fig. 1 Left: binary collision loss coefficient near 530.7 nm transition versus detuning. Right – spectrum of low-field Feshbach resonances (preliminary data).

Atom interferometers' phases at the presence of heavy masses; their use to measure Newtonian gravitational constant; optimization, error model, perspectives

Boris Dubetsky
1849 S Ocean D, Apt 207, Hallandale, Florida 33009, USA
Email: bdubetsky@gmail.com

Among the fundamental physical constants c, ℕ, G, the Newtonian gravity constant G=6.67408(31)×10^{-11} m^3kg^{-1} s^{-2} (CODATA, 2015) is measured with the lowest accuracy of only 46ppm. In this talk we consider the possibility of increasing this accuracy by using the atom interferometry technique [1]. This technique was first applied [2] by using a test mass moving vertically around the trajectories of atom clouds. For this talk, we assume [3] that the test mass has a cuboid shape with a small cuboid hole for atoms to go through, and this cuboid shape consists of 2 parts moving horizontally to and from atom clouds (see Fig. 1). We calculated the phase double difference

$$\Delta^2\varphi = \Delta\varphi_a - \Delta\varphi_b, \Delta\varphi = \varphi(z_1, v_{1z}) - \varphi(z_2, v_{2z}),$$

where ϕ(z,v) is a phase of the atom interferometer in which atoms are launched from point z with velocity v. Since both atom clouds are irradiated by the same field and stay on the same platform, the vibration contributes equally to the phases and that contribution is excluded in the 1st order phase difference $\triangleq\phi$. When test mass halves are joined or separated (see Fig. 1a and b), phase differences are equal to $\triangleq\phi_{a,b}$. The part of the phase difference caused by Earth's gravitational field is evidently the same for both differences, and this part is eliminated in the phase double difference. Therefore, $\triangleq^2\phi$ depends only on the gravitational field of the test mass, which is linear in G. In contrast to [3] (where the calculation was made for the parameters' modest values), we calculated the phases for ^{87}Rb and the maximal value of the parameters achieved at the current state of the art in atom interferometry, i.e. for the time delay between pulses T=1.15 s [5], the effective wave vector k=7.248×10^8 m^{-1}, the test mass M=1080 kg of Pb [6], and the phase noise ϕ_{err}=10^{-4} rad. The chosen value of k vector can be obtained by using multiphoton processes, first considered in [1]. This value is 45 times greater than the wave vector associated with 2-quantum Raman process in ^{87}Rb. It was achieved [7] using a sequential technique.

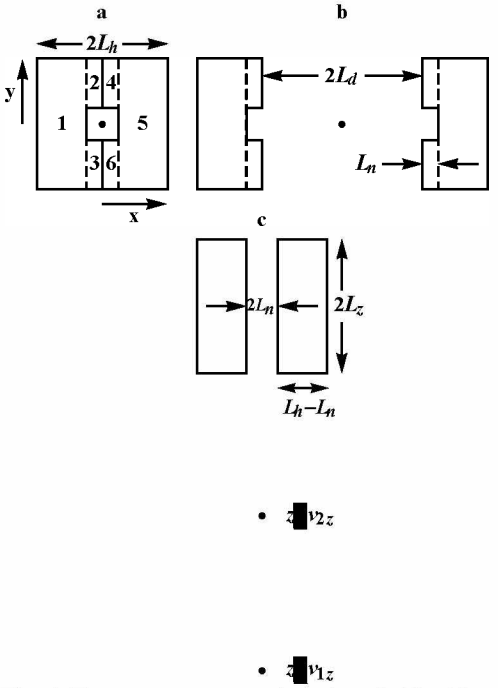

Fig. 1 The test mass as a whole is cuboid with a narrow hole for Raman fields and atom trajectories. Atoms are launched from the points z_1 and z_2 with velocities v_{1z} and v_{2z}. Test mass consists of 2 halves. (a) Top view. Joined halves. (b) Top view. Halves separated on the distance $2L_d$. (c) Side view, cross section x=0 for joined halves.

The contribution to the phase caused by the test mass δϕ was studied in detail in review [8]. We obtained a response linear in the test mass gravity δ**g** assuming that [9] the magnitude is δg<<g, where g is Earth's gravitational field magnitude. The ratio δg/g is a small parameter of our theory. Evidently, only this part contributes to the double difference, $\triangleq^2\phi$=$\triangleq^2\delta\phi$. Using the Wigner representation of the atomic density matrix (first applied for atom interferometry in [10]), we showed that δϕ consists of 3 parts, the classical part, the recoil term and the Q-term. The recoil term was obtained without expanding over recoil velocity ℚ**k**/M_a, M_a is the atomic mass, while for the Q-term, we used perturbation over gravity curvature tensor. Calculations performed in [8] showed that for the chosen value of the wave vector, the recoil term will overcome the classical part, while the Q-term is 2-3 orders of magnitude smaller and we did not include it in the calculations presented here. From the Eqs. (62, 66, 73) in [8], the following expression is obtained for the sum of the classical part and the recoil term:

$$\delta\phi(z,v) = \mathbf{k}\cdot\int_0^T d\theta\left\{(T-\theta)\delta\mathbf{g}\left[\mathbf{X}^{(0)}(\mathbf{x},\mathbf{v},T+t_1+\theta)+\frac{\hbar\mathbf{k}}{2M_a}(T+\theta)\right]+\theta\delta\mathbf{g}\left[\mathbf{X}^{(0)}(\mathbf{x},\mathbf{v},t_1+\theta)+\frac{\hbar\mathbf{k}}{2M_a}\theta\right]\right\},$$

where $\mathbf{x}=\{0,0,z\}$ and $\mathbf{v}=\{0.0.v\}$ are the initial atom cloud's position and velocity, $\mathbf{X}^{(0)}(\mathbf{x},\mathbf{v},t)$ is the atom trajectory, t_1 is the time delay between the moment of the atoms' launching and 1st Raman pulse.

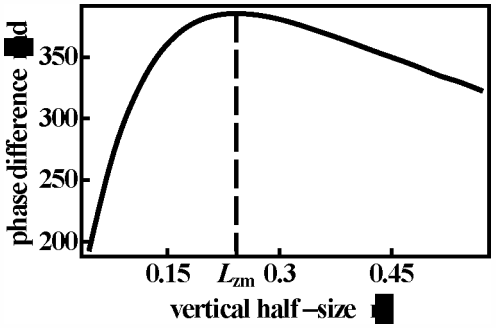

Fig. 2 Dependence of the maximum of phase difference on cuboid half-size.

phase difference	$\Delta^2\delta\phi$ = 386.52738
vertical half–size	L_{zm} = 0.24219097m
horizontal half–size	L_{hm} = 0.22162188m
1st cloud position	z_{1m} = –6.8517823m
1st cloud velocity	v_{1m} = 11.158930m/
2nd cloud position	z_{1m} = –6.2983410m
2nd cloud velocity	v_{1m} = 11.172994m/

Table 1. Maximal value of the phase double difference and optimal values of the test mass and atom clouds variables.

Evidently, $\Delta^2\delta\varphi$ achieves the maximum when $\{z_1,v_{1z}\}$ is the point of absolute maximum, and$\{z_2,v_{2z}\}$ is the point of absolute minimum. We found these extrema iteratively using a reasonably wide area and reasonably small steps in z and v. The sizes of the area and steps were restricted by my PC's speed and power. For the given test mass M and density ρ, we found extrema as a function of cuboid vertical halfsize L_z, see Fig. 2. To get a maximum signal, we recommend choosing L_{zm} shown in Fig. 2 as vertical halfsize of test mass. Values of the other optimum parameters of the system are presented in Table 1. One can estimate the accuracy of measurement as

$$\frac{\delta G}{G} = \frac{\phi_{err} \approx 10^{-4} rad}{\Delta^2\delta\phi \approx 386 rad} \approx 200\, ppb.$$

This accuracy is more than 200 times better than that claimed in CODATA 2015. To achieve this accuracy one needs to precisely position the atoms [11] and assign the velocities. To get the requirements for the precisions we determine the phase dependence on the small variations of the atomic variables. It brings us to atomic radii and temperatures presented in Table 2. Even though it is challenging to cool to those temperatures and focus on to the radii, temperatures and radii are higher than those achieved in article [12].

1st cloud vertical radius [m]	0.00017297989
1st cloud vertical velocity [m/s]	0.00014838628
1st cloud vertical temperature [K]	$1.1519682 \times 10^{-10}$
1st cloud horizontal radius [m]	0.00024463051
1st cloud horizontal velocity [m/s]	0.00020984989
1st cloud horizontal temperature[K]	$2.3039364 \times 10^{-10}$
2nd cloud vertical radius [m]	0.00037028943
2nd cloud vertical velocity [m/s]	0.00031717019
2nd cloud vertical temperature [K]	$5.2630531 \times 10^{-10}$
2nd cloud horizontal radius [m]	0.00052366833
2nd cloud horizontal velocity [m/s]	0.00044854639
2nd cloud horizontal temperature[K]	1.0526106×10^{-9}

Table 2. Atom interferometers' parameters one has to hold to achieve measurements of 200 ppb error.

Conclusion. We showed that using the atom interferometry technique, for the chosen geometry of the test body, at the positions and velocities of the atom clouds determined by the optimization, can give the double difference of the atomic interferometers phases as large as 387 rad at the phase noise level 10^{-4} rad. This should allow one to measure the Newtonian gravitational constant G with an accuracy of 200ppb, which is 2 to 3 orders of magnitude better than that currently achieved using conventional methods. To achieve this result one has to realize SIMULTANEOUSLY (a) sequential technique to increase the effective wave vector, (b) small radii and (c) low temperatures of the atom clouds, determined by using the built error model. Each of the parameters is within the current state of the art in atomic interferometry.

References

[1] B. Dubetsky, A. P. Kazantsev, V. P. Chebotayev, V. P. Yakovlev, Pis'ma Zh. Eksp. Teor. Fiz. **39**, 531 (1984)].
[2] J. B. Fixler, G. T. Foster, J. M. McGuirk, M. A. Kasevich1, Science **315**, 74 (2007).
[3] B. Dubetsky, arXiv: 1407.7287 (2014).
[4] M. J. Snadden, J. M. McGuirk, P. Bouyer, K. G. Haritos, and M. A. Kasevich, Phys. Rev. Lett. **81,** 971 (1998).
[5] S. M. Dickerson, Jason M. Hogan, Alex Sugarbaker, David M. S. Johnson, and Mark A. Kasevich, Phys. Rev. Lett. **111**, 083001(2013).
[6] G. W. Biedermann, X. Wu, L. Deslauriers, S. Roy, C. Mahadeswaraswamy, and M. A. Kasevich, Phys. Rev. A **91**, 033629 (2015).
[7] T. Kovachy et al., Nature **528,** 530 (2015).
[8] B. Dubetsky, S. B. Libby and P. Berman, Atoms **4**, 14 (2016).
[9] B. Dubetsky, unpublished work (2008).
[10] B. Dubetsky, M. A. Kasevich, Phys. Rev. A **74**, 023615 (2006).
[11] G. Rosi, F. Sorrentino, L. Cacciapuoti, M. Prevedelli & G. M. Tino, Nature, **510**, 518 (2014).
[12] T. Kovachy et al., Phys. Rev. Lett. **114**, 143004 (2015).

Continuous cold-atom inertial sensor with 1 nrad·s^{-1} rotation stability

B. Fang, I. Dutta, D. Savoie, N. Miélec, R. Sapam, B. Venon, C. L. Garrido Alzar, R. Geiger, and A. Landragin
LNE-SYRTE, Observatoire de Paris, PSL Research University, CNRS, Sorbonne Universités, UPMC Univ. Paris 06, 61 avenue de l'Observatoire, 75014 Paris, France
Email: bess.fang@obspm.fr

We report the operation of a cold-atom inertial sensor in a joint interrogation scheme, where we simultaneously prepare a cold-atom source and operate an atom interferometer (AI) in order to eliminate dead times [1]. This is illustrated in Fig. 1. Dead times and noise aliasing are consequences of the sequential operation which is intrinsic to cold-atom AIs. Both phenomena have deleterious effects on the performance of these sensors. We show that our continuous operation improves the short-term sensitivity of AIs, by demonstrating a record rotation sensitivity of 90 nrad.s-1/√Hz in a cold-atom gyroscope of 11 cm2 Sagnac area. We also demonstrate a rotation stability of 0.9 nrad.s-1 after 104 s of integration, improving previous results by an order of magnitude [2-4]. We expect that the continuous operation will allow cold-atom inertial sensors with long interrogation time to reach their full sensitivity, determined by the quantum noise limit.

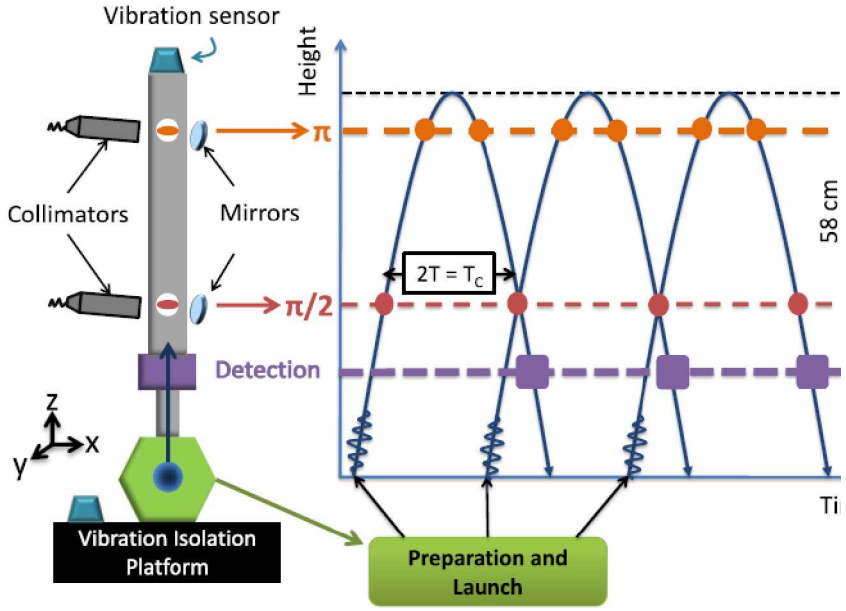

Fig. 1 Schematic and operation principle of the continuous cold-atom gyroscope. Continuous measurement is performed with a joint interrogation sequence where the bottom π/2 pulse is shared between the atomic clouds entering and exiting the interrogation zone.

References

[1] I. Dutta, D. Savoie, B. Fang, B. Venon, C. L. Garrido Alzar, R. Geiger, and A. Landragin, Phys. Rev. Lett. **116**, 183003 (2016).
[2] D. S. Durfee, Y. K. Shaham, and M. A. Kasevich, Phys. Rev. Lett. **97**, 240801 (2006).
[3] A. Gauguet, B. Canuel, T. Lévèque, W. Chaibi, and A. Landragin, Phys. Rev. A **80**, 063604 (2009).
[4] P. Berg, S. Abend, G. Tackmann, C. Schubert, E. Giese, W. Schleich, F. Narducci, W. Ertmer, and E. Rasel, Phys. Rev. Lett. **114**, 063002 (2015).

An optical frequency standard based on ultracold magnesium atoms

A.N. Goncharov[1,2,3], A.E. Bonert[1], D.V. Brazhnikov[1,2], O.N. Prudnikov[1,2], M.A. Tropnikov[1],A.V. Taichenachev[1,2], S.N. Bagayev[1,2]

[1]*Institute of Laser Physics SB RAS, 13/3 Lavrent'eva ave., 630090 Novosibirsk, Russia*

[2]*Novosibirsk State University, 2 Pirogova str., 630090 Novosibirsk, Russia*

[3]*Novosibirsk State Technical University, 20 Karla Marksa ave., 630073 Novosibirsk, Russia*

E-mail: gonchar@laser.nsc.ru

This paper presents the recent experimental and theoretical results and perspectives on development of an optical frequency standard based on ultra cold magnesium atoms with relative frequency uncertainty and long term stability at the level of $\Delta\nu/\nu<10^{-16}$.

Ultracold atoms for simulation of many body quantum systems

D.A.W. Hutchinson
Dodd-Walls Centre, Department of Physics, University of Otago, Dunedin, New Zealand
E-mail: David.Hutchinson@otago.ac.nz

It took 70 years from the prediction of Bose-Einstein condensation (BEC) in 1925 to the experimental realization[1] in 1995 in ultracold atomic gases. Whilst phenomena such as superfluidity in liquid helium, superconductivity of Cooper Pairs and even the macroscopic occupation of an individual cavity mode in the laser are all related to BEC, the experiments in 1995 where the first to directly show this condensation directly. In time of flight images – where the trapped cloud of atoms are allowed to expand and are then detected via an absorption image – the momentum distribution of the atoms is directly inferred showing the macroscopic occupation of the lowest momentum state.

The first experiments were then an exercise in characterization and developing an understanding of wave interference in these new systems. We were involved in a large part in the characterization of collective excitations at finite temperatures in these early systems, with the key characteristic being the demonstration of precision control both over internal and external degrees of freedom.

The ultracold gases were saved from being a purely demonstration experiment by the advent of further control over the inter-particle interactions through the use of so-called Feshbach[2] resonances. These resonances vary the relative energy between open and closed channels in two-particle scattering by the imposition of a uniform magnetic field. The differing Zeeman shift for the different levels then leads to a change in the position of the last bound state, varying the effective *s*-wave scattering length. Interactions could therefore be tuned from attractive through zero (non-interacting) to repulsive, including also the divergent scattering length in the unitary regime.

Optical lattices[3] were then introduced in to the experimentalist's arsenal of techniques. This uses two counter-propagating laser beams to create a standing wave. The ac Stark shift then leads to an effective harmonic potential for the atoms. One, two and three dimensional lattices can be formed in this manner together with more exotic potentials through the use of spatial light modulation techniques. By making one or more of these lattices very strong, with tight confinement in that direction, even the dimension of the system can be manipulated to create two-dimensional sheets, one dimensional wires of dot-like structures.

Beautiful experiments by the group of Jean Dalibard in Paris then used optical lattices to produce two-dimensional sheets[4] of degenerate Bose gases. Theory of the non-interacting Bose gas shows that there is no BEC transition in the uniform two-dimensional Bose gas, but predicts a finite degeneracy temperature for a harmonically trapped gas – like those in the Dalibard experiments. The interacting two-dimensional gas can however undergo a superfluid phase transition to the so-called Berezinskii-Kosterlitz-Thouless (BKT) Phase. In this state fluctuations in the form of thermally activated vortices are bound in to vortex-antivortex pairs. Whilst global phase coherence – the characteristic of BEC – is destroyed, the systems retains a local order that leads to a superfluid phase. The superfluid phase is then destroyed at higher temperatures by the vortex-antivortex pairs unbinding. The critical temperature is therefore related to the interparticle interactions. Cross over from the BEC to BKT phase and through to the thermal phase was investigated and characterized in these experiments and supporting theoretical work from ourselves and others.

The next piece in the quantum simulation jigsaw was the introduction of disorder. Disorder can be introduced in to a cold atom system via either a new, weak optical lattice incommensurate[5] with the

primary optical lattice or through laser speckle[6]. The former, while not strictly disorder, provides an effectively random shift to the bottoms of the primary lattice potential. Laser speckle consists of a light shone through a diffusive plate to provide a random optical potential shift. Both mechanisms have been used to demonstrate localization and effective superfluid to insulating phase transitions in ultracold gas systems. Work is now ongoing investigating the effects of disorder in ultracold gases with the hope of shedding light on the role of disorder in more complicated solid state systems.

The final element to be introduced to our world of ultracold atomic emulation of solid state systems are gauge fields. These ultracold atomic systems are by definition uncharged. They therefore do not couple to electric or magnetic fields in the sense of, say, electrons in solids. We need to introduce effective potentials in to the system Hamiltonian via other means. For example rotating the system introduces a term in the kinetic energy which mirrors the effects of a magnetic field. Quantised vortices and vortex lattices have been observed using rotation. Analogues of the integer and fractional quantum Hall effect based upon rotation have been proposed but are limited. Rotation also introduces an effective centripetal force which, at a rotation frequency equal to that of the harmonic trap confinement leads to instability of the gas through failure of the trapping.

A scheme first implemented by Ian Spielman's group at NIST used a Raman scheme to couple hyperfine states[7] in a spatially dependent manner. This lead to a minimum in the kinetic energy term centred at a momentum $\boldsymbol{p}\neq 0$. Effectively this introduces a spatially dependent vector potential $\boldsymbol{A}$ and hence a synthetic magnetic field. Spielman was able to demonstrate that implementing this coupling lead to vortices in his condensate analogous to rotation. This scheme has since been extended to other gauge fields[8] including non-abelian fields and also spin-orbit coupling. We have used a synthetic magnetic field to demonstrate theoretically how a magnetic field can suppress localization by disorder – so-called negative magnetoresistance.

Ultracold atoms therefore offer a platform for studying many phenomena from solid state physics with excellent control, through precision laser and atomic physics, over all system parameters. Model Hamiltonians can really be engineered[9] in the spirit of Richard Feynman's vision of quantum simulation from the 1980s.

References

[1] E. A. Cornell and C. E. Wieman, Rev. Mod. Phys., **74**, 875 (2002).
[2] J. M. Vogels *et al.*, Phys. Rev. A **56**, R1067 (1997).
[3] O. Morsch and M. Oberthaler, Rev. Mod. Phys. **78**, 179 (2006).
[4] Z. Hadzibabic *et al.*, Nature **441**, 1118 (2006).
[5] G. Roati, *et al.*, Nature **453**, 895 (2008).
[6] J. Billy, *et al.*, Nature **453**, 891 (2008).
[7] Y.-J Lin, *et al.*, Nature **462**, 628 (2009).
[8] J. Dalibard, F. Gerbier, G. Juzeliunas and P. Ohberg, Rev. Mod. Phys. **83**, 1523 (2011).
[9] I. Bloch, J. Dalibard and S. Nascimbene, Nat. Phys. **8**, 267 (2012).

Wave-packet dynamics of cold atoms in 2D lattices subject to synthetic magnetic and electric fields

A. Kolovsky
L.V.Kirensky Institute of Physics SB RAS, Krasnoyarsk, Russia
E-mail: andrey.r.kolovsky@gmail.com

We discuss theoretical expects of the recent experiment on dynamics of cold neutral atoms in the square optical lattice subject to synthetic magnetic and electric fields. This setup mimics the Hall physics in solids yet requires a special consideration because of extremely high values of the fields, inaccessible in the solid-state physics.

Rydberg atom mediated non-destructive readout of rotational states of polar molecules and indirect molecular interactions

Elena Kuznetsova[1,2] , **Seth T. Rittenhouse**[3] , **Hossein R. Sadeghpour**[4], **Susanne F. Yelin**[4,5,6]
[1]*Institute of Applied Physics, 46 Ulyanov Street, Nizhny Novgorod, 603950, Russia*
[2]*Rzhanov Institute of Semiconductor Physics SB RAS, 630090 Novosibirsk, Rusia*
[3]*Department of Physics, United States Naval Academy, Annapolis, MD 21402, USA*
[4]*ITAMP, Harvard-Smithsonian Center for Astrophysics, 60 Garden Street, Cambridge, MA 02138, USA*
[5]*Department of Physics, University of Connecticut, 2152 Hillside Road, Storrs, CT 06269*
[6]*Department of Physics, Harvard University, 17 Oxford Street, Cambridge, MA 02138, USA*
E-mail: lena.kuznetsova@gmail.com

Ultracold polar molecules placed in a periodic array represent an attractive setup for quantum computation and simulation of strongly correlated many-body systems due to the ability to interact via anisotropic and long-range electric dipole-dipole interaction. Polar molecules in optical lattices can be used to simulate quantum magnetism, exotic topological states and complex many-body entanglement. Typically a spin-1/2 particle or a qubit is encoded in two rotational molecular states and an initial many-body state becomes strongly entangled due to the interaction. The state of such entanglement will need to be read out to extract useful information about the system. Most current methods for molecular state readout, such as inverse STIRAP combined with Feshbach dissociation for alkali dimers and REMPI, are destructive.

We propose a non-destructive approach to reading out populations of rotational molecular states relying on charge-dipole interaction between molecular dipoles and a nearby Rydberg atom. This interaction shifts the states of the combined molecule-Rydberg atom system depending on the rotational state, which allows to measure its population by conditionally exciting the atom to a Rydberg state and measuring atomic fluorescence intensity. The readout, therefore, does not require the molecule to be destroyed or lost. We give a detailed analysis of measurement of rotational states populations of a single molecule and extend it further to measure populations of collective rotational states in a mesoscopic molecular system. More specifically, we study the interaction between a 1D array of polar molecules and an array or a cloud of atoms in a Rydberg superatom (blockaded) state and calculate the resolved energy shifts of Rb(60s) with KRb and RbYb molecules, with N=3, 5 molecules. We show that collective molecular rotational states can be read out using the conditioned Rydberg energy shifts.

We also analyze indirect interaction between polar molecules mediated by their interaction with Rydberg atoms. We again consider the interaction between a 1D array of molecules and an array of atoms in a Rydberg superatom state and show that the XXZ and Heisenberg types of indirect molecular interactions can be realized by using a Forster resonance between Rydberg atomic and molecular rotational transitions such as $|ns\rangle|J=1,m_J=0\rangle \rightarrow |np,m=0\rangle|J=0,m_J=0\rangle$, $|ns\rangle|J=1,m_J=0\rangle \rightarrow |(n-1)p,m=0\rangle|J=0,m_J=0\rangle$.

Deep sub-Doppler cooling of Mg in MOT formed by light waves with elliptical polarization

O.N. Prudnikov[1,2], D.V. Brazhnikov[1,2], A.V. Taichenachev[1,2], V.I. Yudin[1,2,3], and A.N. Goncharov[1,2,3]
[1]*Novosibirsk State University, Novosibirsk, Russia*
[2]*Institute of Laser Physics SB RAS, Novosibirsk, Russia*
[3]*Novosibirsk State Technical University, Novosibirsk, Russia*
E-mail: oleg.nsu@gmail.com

We consider possibility of deep sub-Doppler cooling of Mg atoms on ${}^1S_0 \rightarrow {}^1P_1$ optical transition. Mg atom is one of perspective candidates for realization of new-generation of atomic clock, based on optical lattices. These atoms have the narrow spectroscopic lines due to forbidden optical transition from the ground state ${}^1S_0$ to the lowest excited states ${}^3P_{0,1,2}$ (see Fig.1).

First of all we note the sub-Doppler laser cooling of neutral atoms require light fields with nonuniform spatial polarizations and atoms with energy levels degenerated over angular momentum. Sub-Doppler cooling effects originate from polarization gradient contribution to force on slow atoms [1]. These effects are well studded in semiclassical approaches [1] and quantum approaches [2] that uses reduced equation for atomic density matrix in ground state only with adiabatic illumination of non-diagonal and excited elements of density matrix.

$$\frac{\partial}{\partial t}\hat{\rho}^{gg} = -\frac{i}{\hbar}\left[\hat{H}_{eff}, \hat{\rho}^{gg}\right] - \hat{\gamma}\left\{\hat{\rho}^{gg}\right\} \tag{1}$$

with effective Hamiltonian $\hat{H}_{eff}$. In our previous work [3] we clearly show that approaches based on equation (1) and describing sub-Doppler cooling are valid in the limit of extremely low semiclassical parameter $\varepsilon_R = \hbar k^2 / 2\gamma M << 1$ even the consideration is done with taken into account quantum recoil effects and the atoms with optical transitions characterized $\varepsilon_R > 0.01$ temperature characteristics of cooled atoms differ significantly from sub-Doppler cooling temperatures predicted in models based on reduced equation (1).

In particular for Mg atoms on ${}^1S_0 \rightarrow {}^1P_1$ optical transition the recoil parameter is not extremely low $\varepsilon_R \approx 0.002$. The results of our analysis based on general quantum equation for atomic density matrix demonstrate limitation of laser cooling temperature in $\sigma_+ - \sigma_-$ light filed configuration slightly bellow Doppler temperature [4]. The experimental realization of laser cooling operating on ${}^3P_2 \rightarrow {}^3D_3$ in $\sigma_+ - \sigma_-$ MOT [5] also demonstrate temperature about *1mK*, that above the Doppler limit for this optical transition $T_D = 425\ \mu K$.

In the following work we consider the MOT for ${}^{24}Mg$ atoms operating on the closed triplet ${}^3P_2 \rightarrow {}^3D_3$ transition, formed by the light waves with elliptical polarization ($\varepsilon - \theta - \bar{\varepsilon}$ configuration). In the frame of 1D model we study magneto-optical potential, temperature and the fraction of extremely cooled atoms with momentum bellow $p = 3\hbar k$ (12.9 cm/s) as function of intensity, detuning, and polarization of light waves forming MOT. For our simulations we use recently suggested method [3,6] that allows to take into account quantum recoil effects of interaction of atoms with light field and correctly takes into consideration the slow atoms localized in the optical potential wells as well the atoms moving above the potential wells.

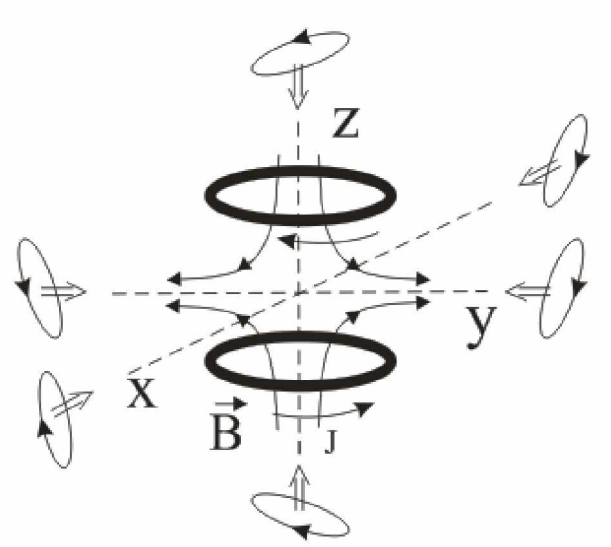

Fig. 1: Magneto-optical trap formed by waves with elliptical polarization $\varepsilon - \theta - \bar{\varepsilon}$ configuration.

We find the $\varepsilon - \theta - \bar{\varepsilon}$ light field configuration formed by the waves with elliptical polarization and orientation angle $\theta = -\pi/4$ with parameters ellipticity are close to linear polarization can offer the lowest cooling temperatures $T \approx 100\,\mu K$ together with enough depth magneto-optical potential. Compare to conventional MOT, formed by waves with $\sigma_+ - \sigma_-$ polarizations, the suggested $\varepsilon - \theta - \bar{\varepsilon}$ MOT should operate with lower gradient of magnetic field. Really, compare to conventional $\sigma_+ - \sigma_-$ MOT, the $\varepsilon - \theta - \bar{\varepsilon}$ MOT is more exacting to field parameters, because of strong magnetic field may reverse magneto-optical trap force for slow atoms in $\varepsilon - \theta - \bar{\varepsilon}$ configuration that limit the numbers of atoms captured in MOT. Parameters of critical magnetic field were also found.

The work was supported by the Ministry of Education and Science of the Russian Federation (State Assignment No. 2014/139, Project No. 825), by the Russian Foundation for Basic Research (Grants No. 14-02-00806, 14-02-00712, 14-02-00939, 15-02-08377, 15-32-20330).

References

[1] J.Dalibard and C.Cohen-Tannoudji, J. Opt. Soc. Am. B **6**, 2023 (1989).
[2] Y. Castin and J. Dalibard, Europhys. Lett. **14**, 761 (1991).
[3] O. N. Prudnikov, R.Ya. Ilenkov, A. V. Taichenachev, A. M. Tumaikin, and V. I. Yudin "Steady state of a low-density ensemble of atoms in a monochromatic field taking into account recoil effects", JETP **112**, 939 (2011).
[4] O. N. Prudnikov, D. V. Brazhnikov, A. V. Taichenachev, V. I. Yudin, A. E. Bonert, R. Ya. Il'enkov, and A. N. Goncharov, Phys. Rev. A **92**, 063413 (2015).
[5] M. Riedmann, H. Kelkar, T. Wubbena, A. Pape, A. Kulosa, K. Zipfel, D. Fim, S. Ruhmann, J. Friebe, W. Ertmer, and E. Rasel, Physical Review A **86**, 043416 (2012).
[6] O.N. Prudnikov, A.V. Taichenachev, A.V. Tumaikin, V.I. Yudin, JETP **104**, 839 (2007).

Probing superfluidity in a quasi two-dimensional Bose gas through its local dynamics

C. De Rossi[1,2], R. Dubessy[1,2], K. Merloti[1,2], M. de Goër de Herve[1,2], T. Badr[2,1], A. Perrin[2,1], L. Longchambon[1,2], and H. Perrin[2,1]

[1]*Université Paris 13, Sorbonne Paris Cité, Laboratoire de physique des lasers, F-93430, Villetaneuse, France*

[2]*CNRS, UMR 7538, F-93430, Villetaneuse, France*

E-mail: helene.perrin@univ-paris13.fr

Superfluidity is an intriguing property of certain quantum fluids, which is characterized by a few manifestations in its dynamics: absence of viscosity, existence of a critical velocity for the appearance of excitations, vanishing moment of inertia, hydrodynamic behavior including irrotational flow, quantum vortices and collective oscillations. Widely studied in the context of liquid helium, it has been extended to three-dimensional quantum degenerate weakly interacting Bose gases which appear to present a superfluid character as Bose-Einstein condensation (BEC) is reached.

The case of two-dimensional quantum gases is very different in this respect. In homogeneous gases, BEC is absent while a superfluid transition still occurs at low temperature when local phase fluctuations are reduced by vortex-antivortex pairing, as described by Berezinskii, Kosterlitz and Thouless (BKT) [1,2]. Superfluidity then exists even in the absence of long range order. In trapped Bose gases, BEC is recovered but the BKT superfluidity mechanism still holds and is responsible for the superfluid character of the sample. As the density is inhomogeneous in a trapped gas, the central core is expected to present a superfluid dynamics while the outer region of the sample is still normal. At equilibrium at a given temperature, the gas properties (density, chemical potential) can be defined locally, which is know as the local density approximation (LDA). The criterion for the BKT transition could then be applied locally, giving rise to the existence of a boundary in the sample between a normal component and a superfluid component.

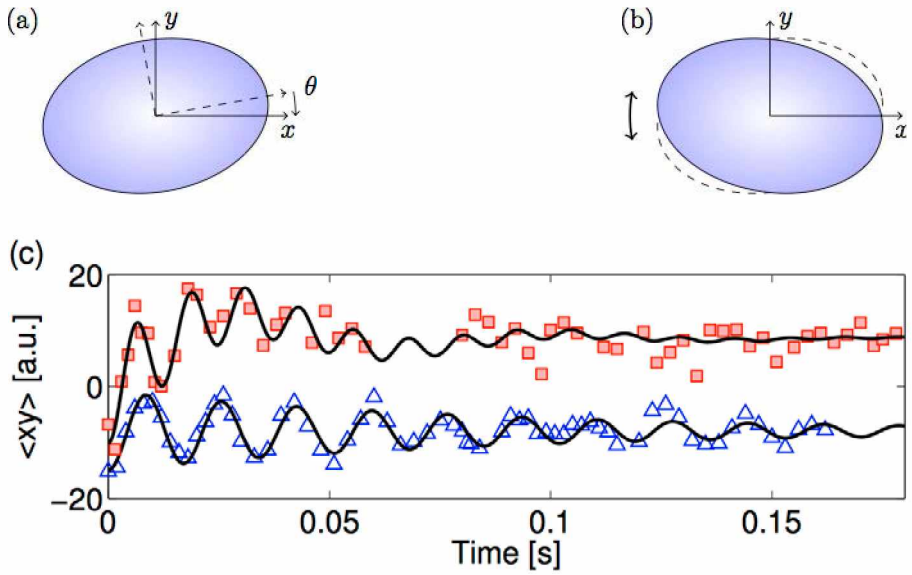

Fig. 1 Excitation of the scissors mode: (a) the trap axes are suddenly rotated by an angle θ and (b) the gas starts oscillating around the new long trap axis. (c) Typical evolution of the observable $\langle xy \rangle$ (average value of xy), which is characteristic of the scissors mode. Red squares: thermal gas, two damped frequencies are present but no superfluid mode; blue triangles: superfluid oscillation of a well defined scissors mode.

However, as explained above, superfluidity is a dynamical property and should be tested in a dynamics experiment. In particular, the scissors mode, which is a collective mode describing the oscillation of an anisotropic superfluid around one of the trap axes [3], is characteristic of the superfluid behavior of a dilute gas, and has already been used in the past to identify the superfluid

character of a three-dimensional Bose gas [4]. In this talk, I will present experiments performed at LPL in which we use the scissors mode to characterize the superfluid nature of a trapped two-dimensional Bose gas, for various values of the temperature and chemical potential at the center [5]. Some of the samples are purely superfluid and evolve at the scissors frequency, other are purely normal and present beat notes between the two trap frequencies (Fig. 1). On the other hands, we also observe samples which present a clear bimodal behavior. Thanks to a local average analysis of the gas oscillation frequency (Fig. 2(c)), we are able to isolate the superfluid phase from the normal phase in these samples. It is evidenced by a sudden change in the mode frequency as a function of the distance to its center, located at a well-determined boundary corresponding to the normal to superfluid threshold (see Fig. 2(a)).

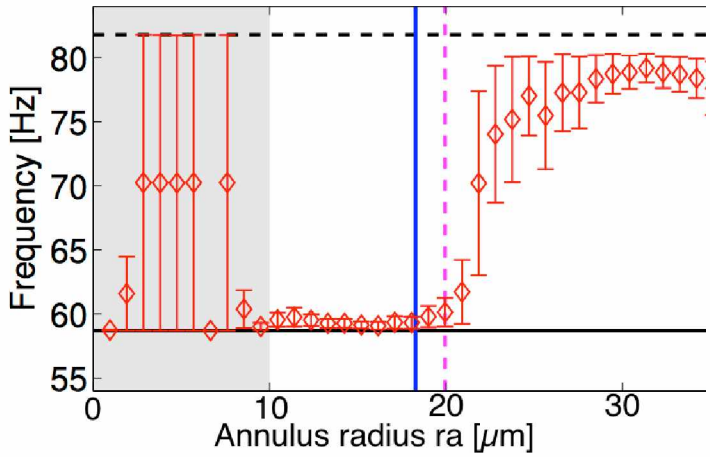

(a)

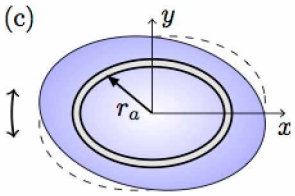

Fig. 2 (c) Region of local average analysis: the average <*xy*> is computed in a thin annulus of radius r_a. (a) Frequency of the scissors mode as a function of the analysis annulus radius r_a. A transition from the superfluid frequency near the center (small r_a) to a normal frequency near the edges (large r_a) is clearly visible. The blue vertical line corresponds to the expected BKT threshold computed for a homogeneous gas within the LDA.

References

[1] V. L. Berezinskii, J. Exp. Theor. Phys. **34**, 610 (1971).
[2] J. M. Kosterlitz and D. J. Thouless, J. Phys. C Solid State Phys. **6**, 1181 (1973).
[3] D. Guéry-Odelin and S. Stringari, Phys. Rev. Lett. **83**, 4452 (1999).
[4] O. M. Marago, S. A. Hopkins, J. Arlt, E. Hodby, G. Hechenblaikner, and C. J. Foot, Phys. Rev. Lett. **84**, 2056 (2000).
[5] C. De Rossi et al., New J. Phys. **18**, 062001 (2016)

Light localization in cold and dense atomic ensemble

I.M. Sokolov
Peter the Great St. Petersburg Polytechnic University, 195251, St. Petersburg, Russia
E-mail: ims@is12093.spb.edu

We report on results of theoretical analysis of possibilities of light strong (Andersen) localization in a cold atomic ensemble. The analysis is based on the consistent quantum-posed theoretical approach developed previously in [1]. In the frame of this approach we solve nonstationary Schrodinger equation for the wave function of the joint system consisting of N motionless atoms and the weak electromagnetic field. We take into account the vector nature of the field and do not introduce any model of continuous media. Restriction of the total number of states taken into account by the states with no more than one photon in the field allows us to obtain finite set of equation for Fourier component of amplitudes of states with one excited atom. This set of equation is solved numerically and amplitudes of the other states are calculated through found ones. The procedure gives us opportunity to find approximately the wave function of the system and consequently analyze both the properties of atomic system and the light.

To analyze the possibilities of strong localization at first we studied the fulfillment of Ioffe-Regel criterion. For this purpose we calculate the dispersion of dielectric susceptibility of cold atomic gases. We show that there is a spectral region where the photon mean free path is less than its wave length, i.e. where the criterion is satisfied. The fulfillment of the Ioffe-Regel criterion is likely a necessary, but not sufficient, condition for strong localization. A clearer answer to the question about light localization in cold gases can be obtained by means of analysis of the incoherent radiation transfer in such gases. We studied the light transport and trapping in cold dense atomic clouds by several ways [2,3]. Particularly we have analyzed:

1. Afterglow dynamics of clouds excited by pulse radiation;
2. Spatial distribution of atomic excitation in quasi homogeneous ensemble caused by monochromatic coherent light;
3. Transmission coefficient of the cloud for different conditions;
4. Statistical properties of atomic excitation and light transmission.

This analysis shows no noticeable signs of light strong localization effects, even in those parameter regions where the Ioffe-Regel criterion of strong localization is satisfied. However, a comparative calculation performed in the framework of the often-used scalar approximation to the dipole-dipole interaction displays explicit manifestation of strong localization for some conditions.

This result was confirmed in the frame of scaling theory of localization [4]. Analysis of the Thouless number based on calculation of collective eigenstates of cold atomic ensemble, as well as analysis of their spatial localization based on calculation of inverse participation ratio showed that strong localization of light cannot be achieved in a random three-dimensional ensemble of atomic scattering [5]. Localization is reclaimed if the vector character of light is neglected.

Performed calculations demonstrate the importance of the vector character of electromagnetic waves in the context of the Anderson localization problem and elucidate the role of resonant dipole-dipole interactions in multiple light scattering. At the same time they cause to anticipate that suppressing this interaction can open the way to localization.

Our analysis shows that static magnetic field giving rise to Zeeman splitting changes the nature of atomic exchange of photons in the ensemble and essentially modifies resonant dipole-dipole interatomic interaction [6] (see also [7]). This effect influences strongly on light trapping. The

efficiency of magnetic field depends on specific type of optically excited atomic transition, particularly on magnetic quantum numbers of quasi resonant states. We found out appearance of long lived polyatomic collective states which lifetimes essentially exceed those take place in the absence of magnetic field. Calculation of inverse participation ration shows that these states are localized. Scaling analysis of collective eigenstates distribution revealed that, in many aspects, this distribution exhibits the behavior expected for the Anderson transition driven by disorder [7].

On the basis of our approach we analyze also the possibility to observe manifestation of these long-lived localized states in experiment. We study the dynamics of fluorescence of atomic clouds initiated by pulse radiation. For an appropriate choice of frequency and polarization of the exciting pulse, the field is expected to speed up the fluorescence of a dilute atomic system. In a dense ensemble, the field does not affect the early-time superradiant signal but amplifies intensity fluctuations at intermediate times and induces a very slow, nonexponential long-time decay [8]. We analyze as well the influence of magnetic field on the steady-state transmission of plain layer of motionless atomic scatterers.

References

[1] I. M. Sokolov, D. V. Kupriyanov, and M. D. Havey, J. Exp. Theor. Phys. **112**, 246 (2011).
[2] I. M. Sokolov, D. V. Kupriyanov, R. G. Olave and M. D. Havey, J. Mod. Opt. **57**, 1833 (2010).
[3] Ya. A. Fofanov, A. S. Kuraptsev, I. M. Sokolov and M. D. Havey, Phys. Rev. A **87**, 063839 (2013).
[4] E. Abrahams, P.W. Anderson, D. C. Licciardello, and T. V.Ramakrishnan, Phys. Rev. Lett. **42**, 673 (1979).
[5] S. E. Skipetrov and I. M. Sokolov, Phys. Rev. Lett. **112**, 023905 (2014).
[6] S. E. Skipetrov and I. M. Sokolov, Phys. Rev. Lett. **114**, 053902 (2015).
[7] K. Afrousheh, P. Bohlouli-Zanjani, J. D. Carter, A. Mugford, and J. D. D. Martin, Phys. Rev. A **73**, 063403 (2006).
[8] S. E. Skipetrov, I. M. Sokolov and M.D. Havey, Phys. Rev. A **94**, 013825 (2016).

Near-field interference in a chain of fluctuating Bose condensates

A. Turlapov
Institute of Applied Physics, Russian Academy of Sciences, ul. Ulyanova 46, Nizhniy Novgorod, 603000, Russia
E-mail: turlapov@appl.sci-nnov.ru

Chain of interfering elements is a paradigmatic model in several areas of physics. The relative phases of the field in each element determine the stationary state and the dynamics of the chain. The evolution of a chain with equal phases was studied in optics back in 1836 [1]: In the free space, the electromagnetic field from a chain of identical sources reassumes its initial form after certain propagation distance, which is presently referred to as the Talbot effect. Similar effects are observed in vacuum electronics, acoustics, plasmonics, and matter-wave optics. For matter fields the effect may be seen in the time domain, without propagation.

Solid state physics offers a variety of situations, where the phase of each element fluctuates either due to thermal effects or purely quantum reasons. In the Josephson junction chains such fluctuations drive phase transitions between superconducting and isolating states [2, 3]. Phase slips and the resulting negative interference may prevent the electric current from flowing through the chains. Another example of a chain is high-temperature superconductors, which are composed of layered structures. In systems composed of thin layers, the phase may also fluctuate in the layer plane. The amount of in-plane fluctuations signals transitions between Bose-condensed state, non-condensed Berezinskii-Kosterlitz-Thouless superfluid, and the normal state.

The most direct information about the phases in the chain elements is obtained in interference experiments. In solids, where most interesting problems are encountered, the ability to observe interference is far below that in optics. Experiments with ultracold atoms combine reach physics borrowed from the stolid state and the possibility to directly observe interference of the matter waves. The Talbot effect has been observed in the near-field interference of phased matter waves.

Here, in experiment, we show that for a chain of randomly phased fields, the spatial quasi-order appears shortly after the onset of the free evolution. Within a simple model, we show that the spatial periodicity is the direct consequence of disordered phases. The spatial period differs from that of the original Talbot effect. Therefore, from the spatial period of the interference one may distinguish whether the initial state of the chain was ordered or not. Moreover, for partially disordered phases two effects combine: One may see the Talbot effect on top of the disordered-phase interference. From the relative strength of the two effects one may judge the degree of the phase disorder.

In experiments we use a chain of molecular Bose-Einstein condensates (BECs) trapped in a one-dimensional optical lattice as shown in Fig. 1. Each cloud is a kinematically two-dimensional (2D) system, where most of the molecules occupy the lowest state of motion along the lattice and many states of motion along the layers. In uniform 2D systems the Bose condensation is prohibited at $T > 0$. However, in a harmonic potential a noninteracting Bose gas may condense at finite temperatures. In a repulsive BEC, a molecule locally sees a flat potential, which is the sum of the harmonic trap and the repulsive mean field. From the straight interference fringes we judge that the gas condenses at relatively high temperatures.

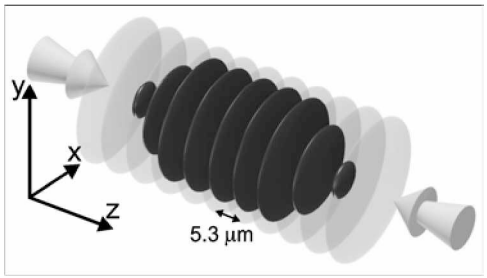

Fig. 1 Trapping ultracold atoms in antinodes of a standing optical wave. The isolated clouds of atoms shown in dark grey, the standing-wave intensity shown in light grey.

The experimental setup is similar to that of Ref. [4] and references therein. The bosons are weakly-bound Li_2 molecules in a long-lived excited vibrational state, each composed of two fermionic ^{6}Li atoms. A series of BECs is prepared in an optical lattice potential formed by two counter-propagating laser beams of wavelength 10.6 μm. The maxima of the standing-wave intensity are the minima of the potential. Weak transverse confinement appears due to the Gaussian shape of the mode. In the z direction, the period of the potential is d = 5.3 μm. A sequence of about 30 wells is populated by condensates containing about N = 1200–1300 molecules each. The gas is nearly kinematically 2D which may be found from the chemical potential and temperature.

To observe the interference, the trapping potential is turned off nearly instantaneously at $t = 0$. The condensates start to expand and interfere in free space. Dynamics in the z direction is most notable, while the expansion in the orthogonal directions is slow and unimportant here.

If the initial state were a BEC with identical phases φ_j, the evolution would show the Talbot effect: The initial periodic density distribution would reappear at the integer multiples of the Talbot time $T_d = Md^2/\pi h = 1.693$ ms, where M is the molecular boson mass.

The observed interference, as shown in Figs. 2(b)–(e), differs from the Talbot effect dramatically. At $t = T_d/2$ the period of the interference fringes equals to the initial one in agreement with the temporal Talbot effect. At $t = T_d$, however, the prime spatial period is $2d$, which is twice larger than the biggest period possible within the Talbot effect. Snapshots taken after larger evolutions time also show that the density modulation is periodic with the period growing linearly with time. In particular, the period is $4d$ at $t = 2T_d$ and $8d$ at $t = 4T_d$ as seen in Fig. 2(c) and Fig. 2(d) respectively. The presence of spatial order and increase in periodicity are also seen in the Fourier transforms of the density distribution along z. We display the respective Fourier transforms in Figs. 2(a′)–(d′). The increase of the spatial periodicity is seen as the peaks at the fractional spatial frequencies.

We interpret the observation as the interference of molecular BECs whose phases φ_j are random relative to each other. The relative phases of the BECs establish due to the competition between the tunneling, which tends to lock the phases and dephasing, which may happen either due to quantum fluctuations or the temperature.

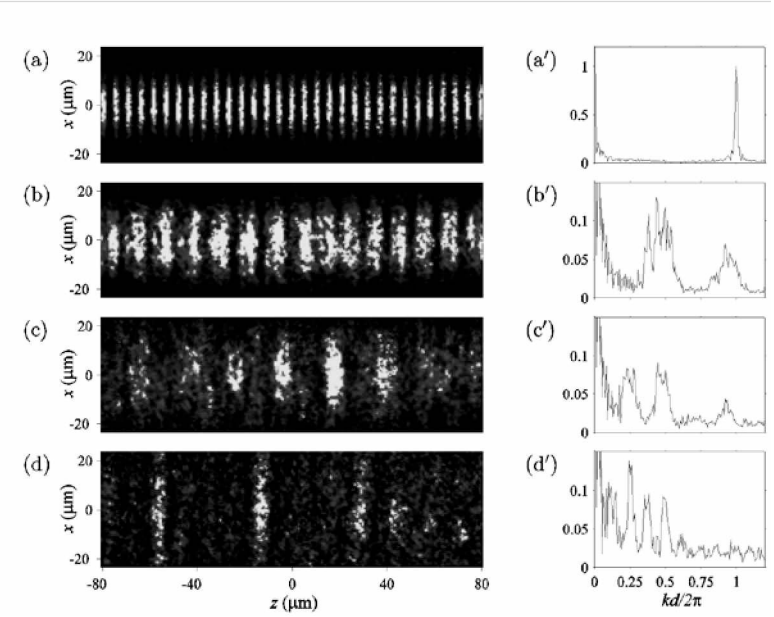

Fig. 2 The interference of BECs prepared at $t = 0$ with random phases relative to each other. (a)–(d): Images taken at $t = 0$, $t = T_d$, $t = 2T_d$, and $t = 4T_d$ respectively. In each image one may see periodic density distribution. (a′)–(d′) are Fourier transforms of density distribution along z for the respective times. Increase of the spatial period is seen as peaks at fractional spatial frequencies.

References

[1] H. F. Talbot, Philosophical Magazine **6**, 401 (1836).
[2] R. M. Bradley and S. Doniach, Phys. Rev. B **30**, 1138 (1984).
[3] L. I. Glazman and A. I. Larkin, Phys. Rev. Lett. **79**, 3736 (1997).
[4] V. Makhalov, K. Martiyanov, and A. Turlapov, Phys. Rev. Lett. **112**, 045301 (2014).

An experimental toolbox for the generation of cold and ultracold polar molecules

M. Zeppenfeld, T. Gantner, R. Glöckner, M. Ibrügger, M. Koller, A. Prehn, X. Wu, S. Chervenkov, and G. Rempe
MPI for Quantum Optics, Hans Kopfermann Str. 1, 85748 Garching, Germany
E-mail: martin.zeppenfeld@mpq.mpg.de

Molecules cooled to very low temperatures offer an exciting platform to investigate quantum phenomena. Thus, precision measurements on molecules allow the investigation of fundamental symmetries of nature [1]. Investigation of chemical reactions at low temperatures provides insight into chemical processes in interstellar space [2]. Moreover, the long-range dipole-dipole interactions between polar molecules and the variety of internal molecular states would be ideal for quantum information processing [3], and for investigation of many body physics in quantum degenerate gases [4].

In this summary, we present our multistep approach for generating internal state controlled molecular ensembles at cold (~<1 K) and ultracold (~<1 mK) temperatures. First, an initial sample of cold molecules is generated via velocity filtering [5] or buffergas cooling [6]. Second, molecules are decelerated via a centrifuge decelerator [7]. Third, molecules are trapped in a microstructured electric trap [8]. Fourth, cooling to sub-millikelvin temperatures is achieved via optoelectrical Sisyphus cooling [9–11]. Control of the internal molecular state is achieved either by buffergas cooling [6, 12], or by optical pumping via a vibrational transition [13].

For all our experiments, we make use of the strong interaction between polar molecules and static electric fields. For laboratory fields of up to 100 kV/cm, interaction energies on the order of 1 K$\times k_B$ are possible, allowing for guiding and trapping of low-field-seeking states. As a first application, filtering of the low-velocity tail of the Maxwell-Boltzmann velocity distribution emerging from an effusive molecule source using a quadrupole electric guide provides a robust high-flux source of cold polar molecules [5]. Alternatively, pre-cooling via a Helium buffergas at ~5 K in a buffergas cell is possible [6].

For velocity filtering and buffergas cooling, the slowest molecules are reduced or eliminated, respectively, due to collisions with faster molecules and/or Helium atoms at the source [14]. To provide a large flux of slow molecules, we have developed a centrifuge decelerator for molecules [7], allowing for deceleration of continuous beams of molecules. Molecules in a lab-fixed quadrupole guide are injected into a quadrupole guide at the periphery of a rotating disk. A quadrupole guide on the rotating disk guides the molecule to the center of the disk where they are transferred back to a lab-fixed guide along the axis of rotation. Due to the centrifugal potential in the rotating frame, molecules are thereby decelerated. Molecules with initial velocities >150 m/s can be decelerated almost to a standstill. A clever design of the transition from the lab-fixed quadrupole guide to the rotating quadrupole guide allows for deceleration of continuous rather than pulsed molecular beams.

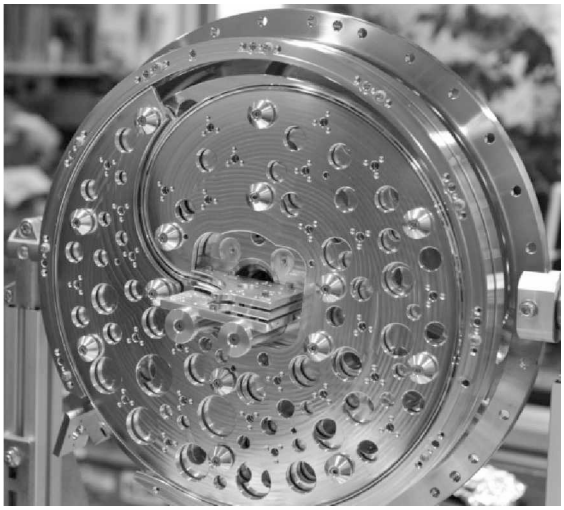

Fig. 1 Centrifuge decelerator for polar molecules. Molecules enter the centrifuge in the lower left and exit along the axis in the center.

Molecules with a kinetic energy below roughly 1 K$\times k_B$ can be loaded into an electrostatic trap. In our experiments, we make use of a relatively unique trap design, with molecules trapped between a pair of microstructured capacitor plates, with an additional perimeter electrode for transverse

confinement [8, 9]. In addition to providing record trap lifetimes of up to a minute [11], this trap design provides homogeneous electric fields in a large fraction of the trap volume. This is ideal for spectroscopic applications and to selectively address individual molecular rotational states via microwave and infrared radiation.

Most applications of cold molecules require temperatures substantially below the ~1 K achievable with the previously mentioned techniques. For this purpose, we have developed optoelectrical Sisyphus cooling [9]. The operation principle of this generally applicable cooling scheme is shown in Fig. 2. Molecules move from weaker to stronger electric fields in a strongly trapped state $|s_1\rangle$ and are transferred to a more weakly trapped state $|s_2\rangle$ in high electric fields via an RF field. Moving back to weaker electric fields, the molecules regain less kinetic energy than they lost when moving to stronger electric fields. Optical pumping back to the strongly trapped state via excitation to an excited state $|e\rangle$ closes the cycle in a one-way process, thus providing the necessary entropy dissipation. We have demonstrated this cooling scheme in a proof of principle experiment by reducing the temperature of about a million methyl fluoride (CH_3F) molecules by more than an order of magnitude to 29 mK [10]. More recently, we have applied optoelectrical cooling to formaldehyde (H_2CO) producing an ensemble of 300,000 molecules at 420 μK [11]. This represents the largest ensemble of ultracold molecules in any experiment worldwide.

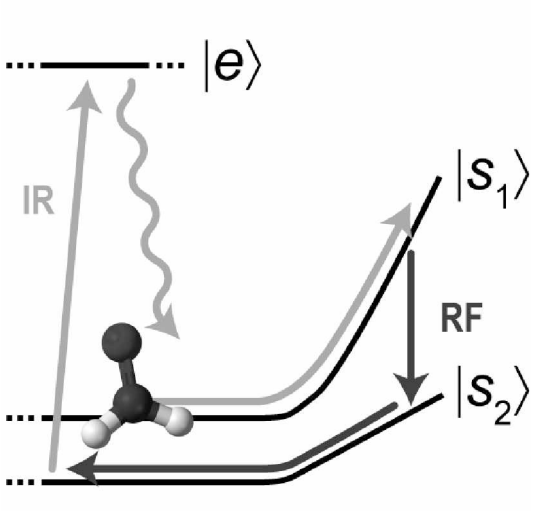

Fig. 2 Operation principle of optoelectrical Sisyphus cooling, as explained in the text.

A final requirement for many applications of cold molecules is gaining and maintaining control of the internal molecular state. Here, buffergas cooling plays a key role by providing internal state cooling already at the molecule source [6]. In this way, we obtain molecule beams with over 90 % of molecules in a single rotational state [12]. As an alternative, we have demonstrated internal state cooling in combination with optoelectrical Sisyphus cooling via optical pumping inside our electric trap [13]. In this way, we achieve ultracold molecules with over 80 % of molecules in a single rotational state [11].

The presented techniques enable a wide range of exciting measurements. The long lifetimes inside our electric trap, combined with internal state purity and sufficiently high densities enable state-resolved collision studies for molecules in a new temperature regime. Temperatures below 1 mK allow the realization of a molecular fountain, enabling greatly improved precision measurements on molecules. Finally, investigation of sympathetic or evaporative cooling offers a promising route to a quantum degenerate gas of polar molecules.

References

[1] J. Baron, *et al.*, Science **343**, 269 (2014).
[2] I.W.M. Smith and B.R. Rowe, Acc. Chem. Res. **33**, 261 (2000).
[3] D. DeMille, Phys. Rev. Lett. **88**, 067901 (2002).
[4] M.A. Baranov, *et al.*, Chem. Rev. **112**, 5012 (2012).
[5] S.A. Rangwala, *et al.*, Phys. Rev. A **67**, 043406 (2003).
[6] L.D. van Buuren *et al.*, Phys. Rev. Lett. **102**, 033001 (2009).
[7] S. Chervenkov *et al.*, Phys. Rev. Lett. **112**, 013001 (2014).
[8] B.G.U Englert *et al.*, Phys. Rev. Lett. **107**, 263003 (2011).
[9] M. Zeppenfeld *et al.*, Phys. Rev. A **80**, 041401(R) (2009).
[10] M. Zeppenfeld *et al.*, Nature **491**, 570 (2012).
[11] A. Prehn *et al.*, Phys. Rev. Lett. **116**, 063005 (2016).
[12] X. Wu *et al.*, accepted in ChemPhysChem, arXiv 1605.08723 (2016).
[13] R. Glöckner *et al.*, Phys. Rev. Lett. **115** 233001 (2015).
[14] M. Motsch *et al.*, New J. Phys. **11**, 055030 (2009).

Quantum-enhanced protocols with mixed states using cold atoms in dipole traps

K. Krzyzanowska, M. Copley-May, R. Romain, C. MacCormick and S. Bergamini
Department of Physical Science, The Open University, Milton Keynes, United Kingdom
E-mail: Silvia.Bergamini@open.ac.uk

Entanglement is widely recognised as a key resource in quantum technology, however an advantage over classical computing can be achieved without it in the presence of non-classical correlations, also known as *discord* [1]. Experiments using few photonic qubits have shown that specific computational tasks can be efficiently solved even with no entanglement [2].

In the past years, there has been outstanding progress in the demonstration of quantum processing based on pure states with a limited number of qubits. However scalability remains an issue, mainly because of decoherence. In pure-states quantum computation (QC) this problem can possibly be solved by error correction. Nevertheless, scaling up to a significant number of qubits and being able to perform a classically intractable calculation has been impossible so far. As entanglement is extremely vulnerable to decoherence, the investigation of protocols that are more robust against it is a promising route for progressing the field.

One of such protocols is called Deterministic Quantum computation with 1 clean qubit (or DQC1). This protocol relies on one pure state control qubit together with a register of completely mixed state qubits, where non-classical correlations are created between the control and the register. DQC1 is a non-universal model of computation (essentially a phase estimation protocol) that can speed up some computational tasks for which no efficient classical algorithms are known. Whilst requiring only a single qubit with coherence, its power scales up with the number of mixed state register qubits.

To date, experiments based on photonic implementation of DQC1 have evaluated the normalised trace of a two-by-two unitary matrix [2] and using an NMR implementation, performed the approximation to the Jones polynomial with a system of four qubits, thus demonstrating the principle of mixed state computation.

In this work we present theoretical models of a cold-atoms based platform for the benchmarking of the protocol with a large number of qubits, thus extending the implementation to large Hilbert space. In comparison to the photonic or NMR experiments, a cold atoms approach offers scalability. A single pure qubit is to be prepared in a microscopic dipole trap and a register of N qubits are prepared in a mixed state in a nearby trap, as shown in Fig.1. Rydberg interactions between the control and the ensembles of cold atoms in mixed state can activate the implementation of DQC1. An appropriate sequence of lasers pulses individually addressing the two traps will implement an algorithm to calculate the trace of a $2^N \times 2^N$ matrix.

We show that the protocol can be operated with many qubits using a cold atoms setting, and we explore the possibility of tackling non-trivial problems [3], such as many-body physics. The same scheme enables the preparation of quantum enhanced probes for phase estimation and promises high-precision measurement, without relying on quantum entanglement and using highly mixed states [4]. Modelling of this scheme, using cold atoms in dipole traps, demonstrates that the register of partly mixed qubits becomes a powerful resource for phase estimation when supplied with the coherence from the control qubit. A concrete mixed-state model for quantum sensing is also proposed. The scheme can achieve quantum-enhanced precision scaling with the size of the atomic register ensemble

[5]. We will finally present the full design for this test and our progress in the experimental setup and implementation.

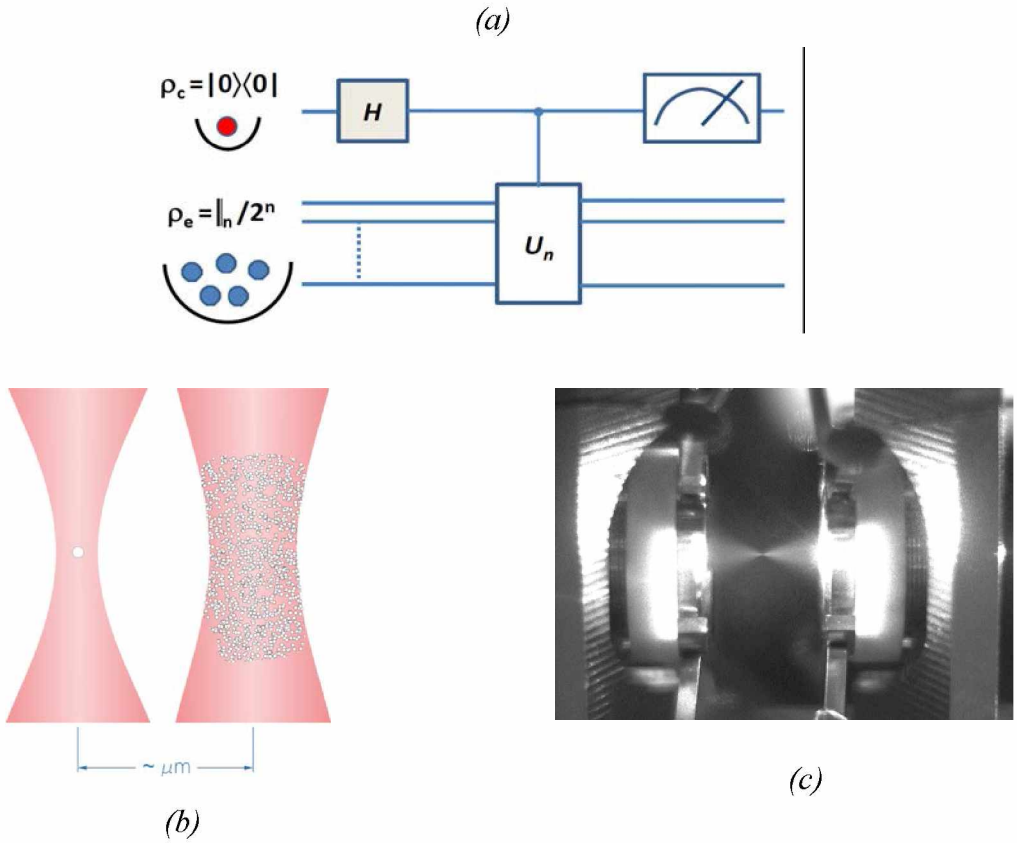

Fig. 1 (a) The DQC1 circuit scheme to be implemented by a control atom and mixed state register in two independent traps (b) and (c) represent the dipole traps design and experimental implementation.

References

[1] Knill E and Laflamme R, Phys. Rev. Lett. **81**, 5672 (1998).
[2] Lanyon B P, Barbieri M, Almeida M P and White A G, Phys. Rev. Lett. **101**, 200501 (2008).
[3] C W Mansell, S Bergamini, New J. Phys. **16**, 053045 (2014).
[4] Modi K, Cable H, Williamson M and Vedral V, Phys. Rev. X **1**, 021022 (2011).
[5] C MacCormick, S Bergamini, C Mansell, H Cable, K. Modi, Phys. Rev. A **93**, 023805 (2016).

Hybrid quantum system: superconducting resonator-Rydberg system

L. C. Kwek
Centre for Quantum Technologies, National University of Singapore, Singapore 117543
Institute of Advanced Studies (IAS), Nanyang Technological University, Singapore 639673
National Institute of Education, Nanyang Technological University, Singapore 637616
MajuLab, CNRS-UNS-NUS-NTU International Joint Research Unit, UMI 3654, Singapore
E-mail: kwekleongchuan@nus.edu.sg

By considering two eigenstates near an avoided-level crossing in the DC Stark map of Rydberg atom, we proposed a feasible hybrid quantum system of a highly-excited Rydberg atom coupled strongly to a superconducting LC oscillator. We also show that different universal two-qubit logic gates can be implemented on the hybrid system.

Controlling the interactions between cold Rydberg atoms by a time-varying electric field

I.I. Ryabtsev[1, 2], D.B. Tretyakov[1, 2], V.M. Entin[1, 2], I.I. Beterov[1, 2], E.A. Yakshina[1, 2], and C. Andreeva[3]
[1]*Rzhanov Institute of Semiconductor Physics SB RAS, 630090 Novosibirsk, Russia*
[2]*Novosibirsk State University, 630090 Novosibirsk, Russia*
[3]*Institute of Electronics, Bulgarian Academy of Sciences, Sofia, 1784, Bulgaria*
E-mail: ryabtsev@isp.nsc.ru

Long-range interactions between cold Rydberg atoms are being investigated for neutral-atom quantum computing, quantum simulations, phase transitions in cold Rydberg gases and other applications [1]. Fine tuning of the interaction strength can be implemented using Förster resonances between Rydberg atoms controlled by an electric field. Observation of the Stark-tuned Förster resonances between Rydberg atoms excited by narrowband cw laser radiation requires the use of a Stark-switching technique to excite the atoms first in a constant electric field and then to induce the interactions in a varied electric field, which is scanned across the Förster resonance.

In our experiments with cold Rb Rydberg atoms we have found that the transients at the edges of the electric pulses strongly affect the line shapes of the Förster resonances, since the resonance occurs on a time scale of ~100 ns being comparable with the duration of the transients. For example, a short-term ringing at certain frequency causes additional radio-frequency (rf) assisted Förster resonances, while non-sharp edges lead to an asymmetry. An intentional application of the radio-frequency field induces transitions between collective states whose line shape depends on the interaction strengths and time. In this report we present the experimental and theoretical analysis of the line shapes of the Förster resonances $\mathrm{Rb}(nP_{3/2}) + \mathrm{Rb}(nP_{3/2}) \rightarrow \mathrm{Rb}(nS_{1/2}) + \mathrm{Rb}((n+1)S_{1/2})$ for a few cold Rb Rydberg atoms in a time-varying electric field [2]. In particular, we studied the rf-assisted Förster resonances between N=2-5 cold Rb Rydberg atoms [3] (Fig.1). We have shown that they can be induced both for the "accessible" Förster resonances which can be tuned by the dc field alone [Fig.1(a)] and for those which cannot be tuned and are "inaccessible" [Fig.1(b)]. The van der Waals interaction of almost arbitrary high Rydberg states can thus be tuned to resonant dipole-dipole interaction.

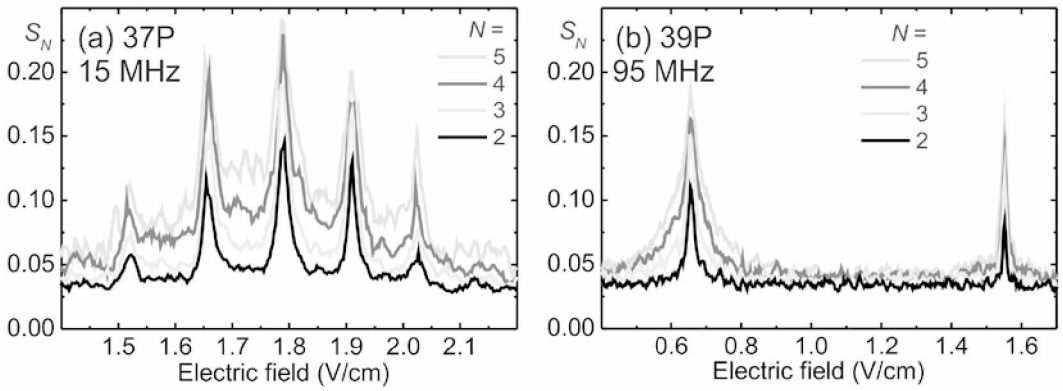

Fig. 1. Radio-frequency (rf) assisted Förster resonances for N=2-5 detected cold Rb Rydberg atoms: (a) "accessible" resonance in Rb(37P) atoms can be tuned by dc field alone at 1.79 V/cm, while rf-field induces additional resonances; (b) "inaccessible" resonance in Rb(39P) atoms can be induced only by the rf field.

This work was supported by the RSF Grant No. 16-12-00028, RFBR Grants No. 14-02-00680 and 16-02-00383, Novosibirsk State University and Russian Academy of Sciences.

References

[1] I.I.Ryabtsev, I.I.Beterov, D.B.Tretyakov, V.M.Entin, and E.A.Yakshina, Physics − Uspekhi **59**, 196 (2016).
[2] E.A.Yakshina, D.B.Tretyakov, I.I.Beterov, V.M.Entin, C.Andreeva, A.Cinins, A.Markovski, Z.Iftikhar, A.Ekers, and I.I.Ryabtsev, arXiv: 1606.06016 (2016).
[3] D.B.Tretyakov, V.M.Entin, E.A.Yakshina, I.I.Beterov, C.Andreeva, and I.I.Ryabtsev, Phys. Rev. A **90**, 041403(R) (2014).

Laser-driven proton acceleration experiments at PW-class PEARL facility

K. Burdonov[1], A. Eremeev[1], J. Fuchs[1,2], V. Ginzburg[1], E. Khazanov[1], A. Kuzmin[1], R. Osmanov[1], S. Pikuz[3], G. Revet[1,2], A. Shaykin[1], I. Shaykin[1], A. Sladkov[1], A. Soloviev[1], M. Starodubtsev[1], and I. Yakovlev[1]

[1]*Institute of Applied Physics of the Russian Academy of Sciences, 603950 Nizhny Novgorod, Ul'yanov street, 46, Russia*
[2]*Laboratoire d'Utilisation des Lasers Intenses (LULI), Palaiseau, Ecole Polytechnique, F-91128 France*
[3]*Joint Institute for High Temperatures Russian Academy of Sciences, 125412 Moscow, Izhorskaya street, 13, Russia*
E-mail: kfb.iap@gmail.com

We present the results of laser-driven proton acceleration experiments in TNSA regime [1] at the PW-level PEARL facility (IAP RAS, Nizhny Novgorod, Russia) [2]. In experiments a *p*-polarised laser pulse with wavelength 910 nm, duration 60 fs and energy up to 10 J was focused by means of f/4.2 parabolic mirror on the aluminum foil targets with thicknesses from 10 μm to 0.2 μm in the vacuum chamber (Fig. 1). The use of adaptive wavefront correction system provided a Strehl ratio 0.36, resulting in a maximum intensity about 3×10^{20} W/cm^2 on the target surface. Targets were set at an angle of 45° to the incident radiation. The accuracy of the target positioning was provided by original method of fine alignment.

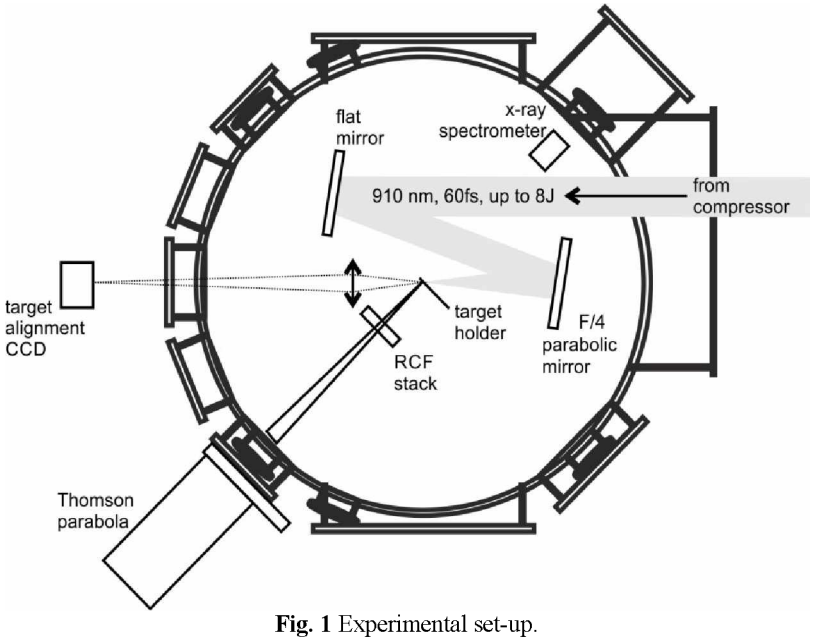

Fig. 1 Experimental set-up.

The energy and angular spectrum of the protons emitted from the rear surface of the target was measured simultaneously by means of a radiochromic films (RCF) assembled in stack with a hole in the middle to let a small beam of protons go through and Thomson parabola spectrometer, both positioned along the target surface normal. The RCF stack can analyze the beam in its entirety, but with coarse steps in energy, while the Thomson parabola can resolve much more finely the spectrum, but only over a small solid angle. The amplitudes of the co-orientated magnetic and electric fields in the Thomson parabola were 0.4 T and 6.5 kV/cm, respectively. Its input pinhole of 0.3 mm diameter was situated at a distance of 80 cm from the proton source. The protons were detected using Image Plates scanned by a commercial IP-scanner procured from Dürr-NDT.

Laser-plasma coupling at the front surface of the target was characterized through X-ray emission measured with a high-resolution FSSR spectrometer (Focusing Spectrometer with Spatial Resolution)

equipped with a spherically bent mica (K2O-3Al2O3-6SiO2-2H2O) crystal. The measured X-ray spectrum provides clear evidence that the target remains at solid density by the time the main laser pulse arrives. Indeed, although the diagnostic is not capable of temporal resolution, we diagnose that the x-ray emission induced by the intense laser pulse irradiation is void of the signature of a significant preplasma at the target front.

Maximum energies of accelerated protons measured by the radiochromic film (RCF) stack detector were in the range of 43.3 to 44.1 MeV and generated by 7.5 J, 60 fs laser pulse focused on the 0.8 μm aluminum foil (Fig. 2 (a)). The total conversion efficiency to the protons from the laser energy is above 0.1%. To the best of our knowledge, this is a world record for laser pulse with energy less than 10 J. Thomson parabola also registered the signs of accelerated with protons carbon ions C^{1+} - C^{6+} and oxygen ions O^{1+} and O^{6+} (Fig. 2 (b)). The proton energy spectra are in a good agreement with the data from Thomson parabola data and temperature estimations made with help of X-ray diagnostics.

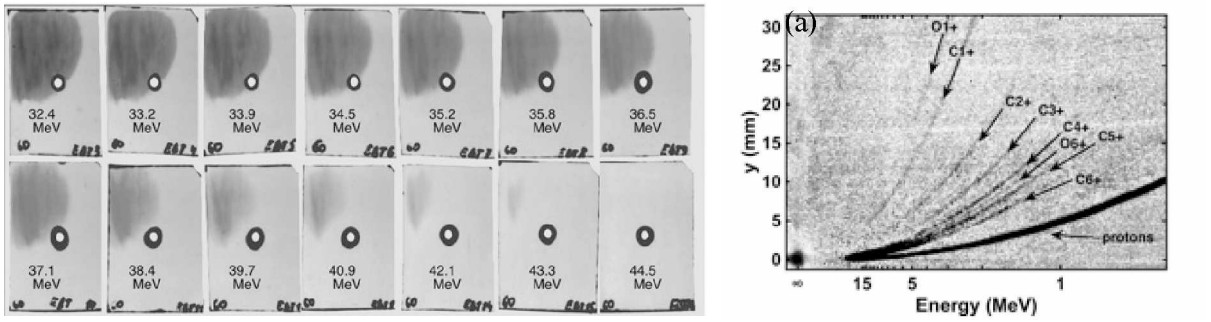

Fig. 2 RCF stack with 43.3 MeV record proton energies (a), Thomson parabola with traces of H^{+}, C^{1+}– C^{6+}, O^{1+} and O^{6+} ions (b).

The temporal contrast of the laser beam, which supposed to be very high for OPCPA systems, is a crucial factor to obtain high-energy protons. It was estimated by measuring the laser parametric luminescence as follows: (i) we measured the contrast in energy between the parametric luminescence and the main pulse of the compressed laser, which was equal to 5×10^{-4}, i.e. 5 mJ compared to 10 J, (ii) we also measured that there is a factor 4 difference between the Strehl ratio of the main pulse and that of the parametric luminescence, and (iii) finally we also measured the temporal profile of the luminescence using a fast photodiode on a nanosecond timescale. As a result, the contrast between the 1-ns duration parametric luminescence and the PEARL 60-fs main pulse was estimated to be $1/(2\times10^{8})$.

References

[1] S. Wilks, A. Langdon, T. Covan et al., Phys. Plasmas **8**, 542 (2001)
[2] V. Lozhkarev, G. Freidman, V. Ginzburg et al., Laser Phys. Lett. **4** 421 (2007)

The interaction of intensive femtosecond radiation with atmospheric media

G.G. Matvienko, A.A. Zemlyanov
V.E. Zuev Institute of Atmospheric Optics SB RAS, 1 Academician Zuev Square Tomsk, 634055, Russia,
E-mail: mgg@iao.ru

Forecast of propagation of high-power laser radiation of femto- and picosecond duration requires new knowledge of fundamental physics of interaction between radiation and substance in the atmosphere and development of new concepts of the phenomena. Such investigations are carried out at the Institute of Atmospheric Optics. The results of these investigations will be demonstrated in this report for the following problems: a) control of the domain of multiple filamentation of terawatt laser pulses along a hundred-meter air path; b) post-filamentation high-intensive light channels formation upon ultrashort laser pulses self-focusing in air.

Filamentation of laser radiation is the main regime of highpower ultrashort pulse propagation through a transparent medium. Filamentation in air may stem from the spatial decay of the beam transverse profile to localised domains of high intensity – filaments, lengthy shining plasma channels arising along the propagation path, and generation of extremely wideband radiation – a supercontinuum.

After the termination of pulse filamentation and plasma generation the laser pulse maintains its spatial localization as elongated light structures, which are named the post-filament channels (PFCs). These light channels possess sufficiently high intensity (~1 TW/cm^2) and lowered angular divergence in comparison with the whole laser beam.

Our work presents results of experimental investigations on control of the position of the filamentation domain for ultrashort pulses of a Ti:sapphire laser on a 150-meter long air path under varied initial spatial focusing and laser output power. We have realised a complete control over the cross-section structure of the laser beam along the propagation path, which made it possible to observe the spatial evolution of high-intensity light channels formed due to the beam filamentation.

Facility of experiments was the following. The driving generator was a Ti : sapphire laser with the passive mode locking based on the Kerr effect. The laser source generated pulsed radiation at a centre wavelength λ_0 = 800 nm, with the pulse HWHM duration t_p = 50 fs, the energy $E_0 \le 82$ mJ and the peak power $P_0 \le 1.5$ TW. The pulse repetition rate was 10 Hz. A variable-base Galileo telescope was used as a focusing element. The focal distance for the defocusing mirror was f_1 =–50 cm, and for the focusing mirror it was f_2 = +100 cm. The beam diameter d_0 at the output of the amplifying stage was 2.5 cm and after the telescope it was d_0 = 5 cm.

We have analyzed the longitudinal position of the filamentation domain and the transverse structure of the radiation channel in this domain. We were interested in the number of fixed plasma channels N and its variation along the path. The number of plasma channels in the laser beam cross section was found by calculating the number of contrast burns left on a photographic paper placed at various distances along the optical path. One such result is shown in Fig. 1*a* for the collimated beam at the maximal realised pulse energy. One can see that the parameter N is nonmonotonic along the filamentation domain. At first, only several burns are observed, then its number increases to approximately twenty for initial energy 82 mJ near the geometrical centre of the filamentation zone, and finally the number of burns again reduces to the end of the zone.

For focused laser beams (Fig.1*b*), variation in the focal length F shifts the start of the filamentation domain: the focusing makes it closer to the beginning of the path and defocusing makes it farther.

Thus the results of conducted experiments show the real possibility to control the spatial position of the domain of multiple filamentation and plasma initiation of a high-power ultrashort pulse propagating along a 150-metre air path. The control was realised both by varying the initial spatial focusing of the beam and by changing the energy of the initial radiation pulse. In the first case, at a stronger focusing the domain of filamentation starts closer to the beginning of the optical path and simultaneously its length becomes shorter. In the case of increasing the pulse energy at constant

focusing, the earlier start of filamentation/plasma initiation is observed, and the length of the filamentation domain increases.

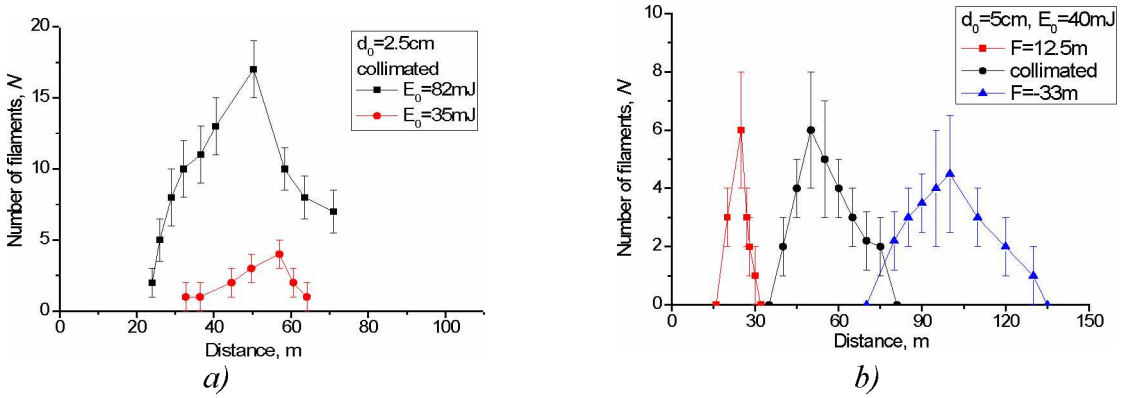

Fig. 1 Distribution of the number of filaments inside area filamentation at different focusing (defocusing) beam diameter: a) 2.5 cm b) 5 cm

In the experiments, the quantitative data on PFC's angular divergence were obtained from the measured transverse energy profiles analyzed by means of software module. Fig. 2*a* show the experimental data on the dependence of effective radius of the channel and of the whole beam on the distance. Fig. 2*b* depicts the spectrum of radiation from the post-filamentation channel.

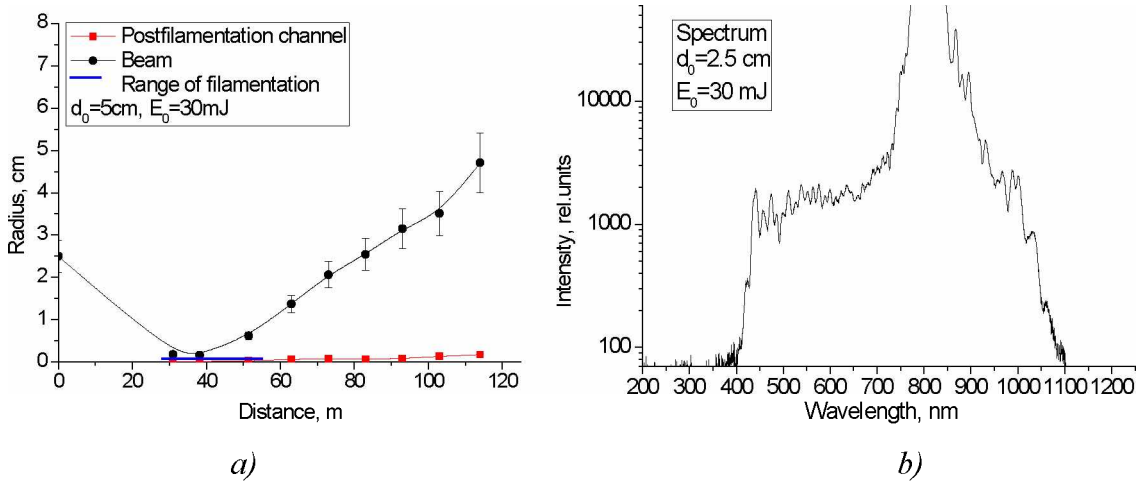

Fig. 2 Change of the radius of the beam and the radius postfilamentation channel (a) the distance distribution of the laser pulses. b) spectrum of the postfilamentation channel.

As a main conclusion from the presented data one can notice the opposite trends of radii for laser beam and PFC. The increase in the divergence of the whole beam after the filamentation area is originated from the developing aberrations of initially smooth beam profile in course of ring structures formation around the filaments. The lowered angular divergence of PFC as compared to the whole beam is provided by self-focusing via Kerr nonlinearity in the PFC area and is sustained by a specific spatial beam energy profile exhibiting a system of concentric rings around each post-filament channel. The minimum PFC angular divergence obtained in our experiments is approximately 0.03 mrad for a collimated beam.

New trends in ultrahigh intensity coherent beam combining

V.I. Trunov[1], **S.A. Frolov**[1], **E.V. Pestryakov**[1,2],**S.N. Bagayev**[1,2]
[1]*Institute of Laser Physics SB RAS, Novosibirsk, Russia*
[2]*Novosibirsk State National Research University, Novosibirsk, Russia*
E-mail: trunov@laser.nsc.ru

The new trends in coherent beam combining using parametrically amplified femtosecond pulses are discussed. The futures of multipump parametric amplifications and precise time synchronization of the set of independent pump lasers are analyzed. The optimal conditions of multibeam tight focusing for achieving extremely high intensities are investigated.

Polychromatic optical field generation in two-photon excited Rb vapour

A. Akulshin[1], D. Budker[2,3], and R. McLean[1]
[1]*Centre for Quantum and Atom Optical Science, Swinburne University of Technology, PO Box218, Melbourne 3122, Australia*
[2]*Department of Physics, University of California,Berkeley,CA94720-7300,USA*
[3]*Johannes Gutenberg University, Helmholtz Institute, D-55128 Mainz, Germany*
E-mail: aakoulchine@swin.edu.au

Laser-induced coherence is a key element of various parametric and non-parametric processes in alkali vapours resulting in generation of new optical fields with wavelength varying from the mid-IR to visible spectral region [1-4]. Here we present an experimental study of spectral and spatial characteristics of the frequency down-converted radiation at 5.23 μm generated on the $5D_{5/2} \rightarrow 6P_{3/2}$ transition in Rb vapour excited with low-power cw resonant light (Fig. 1a).

To date, studies of the new field generation in alkali atoms have focused almost exclusively on detecting the coherent blue light (CBL). The mid-IR emission has not been widely studied; however, it is a crucial component of the nonlinear process. Furthermore, the backward-directed mid-IR radiation is of particular interest because of possible applications in remote atmospheric sensing [5].

We find that over a wide range of the experimental parameters the counter-propagating excitation is more efficient, as more atoms are involved in the atom-light interaction due to nearly complete Doppler shift cancelation resulting in more intense amplified spontaneous emission (ASE) directed both backwards and forwards. It is also found that velocity-selective and quasi Doppler-free two-photon excitation could produce two spectrally and spatially distinguishable mid-IR fields, as shown in Fig. 1b.

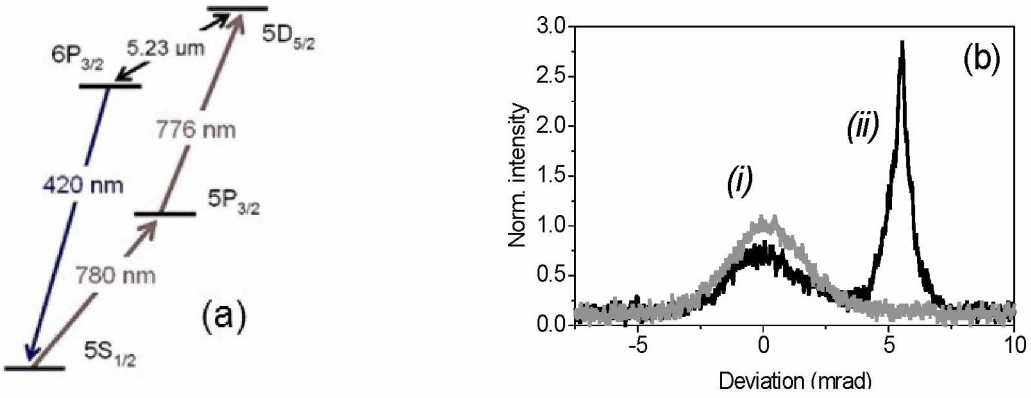

Fig. 1.(a) Rb energy level diagram. (b) Spatial profiles of ASE generated by co-propagating two-colour laser (*i*) without and (*ii*) with involvement of Doppler-free two-photon excitation produced by back-reflection.

Spectral profiles of ASE for both the velocity-selective and quasi Doppler-free are narrower than the corresponding resonances of isotropic blue fluorescence, which we attribute to the amplification effect. We alsofind and explain why two-colour laser light focused inside the cell results in spatial broadening of the CBL, leaving the divergence of ASE almost unchanged.

In conclusion, a new way of detecting two-photon excitation in atomic vapours using ASE is suggested. The link between properties of the mid-IR emission and frequency up-converted directional radiation at 420 nm is discussed.

References

[1] A. S. Zibrov, M. D. Lukin, L. Hollberg, and M. O. Scully, Phys. Rev. A **65**, 051801 (2002).
[2] A. M. Akulshin, R. J. McLean, A. I. Sidorov, and P. Hannaford, Opt. Express **17**, 22861 (2009).
[3] J. F. Sell, M. A. Gearba, B. D. DePaola, and R. J. Knize, Opt. Lett. **39**, 528 (2014).
[4] A. Akulshin, D. Budker, and R. McLean, Opt. Lett. **39**, 845 (2014).
[5] J. Kasparian and J.-P. Wolf, Opt. Express, **16**, 466 (2008).

Mid-infrared tunable, narrow-linewidth difference-frequency laser based on orientation-patterned gallium phosphide

G. Insero[1], C. Clivati[2], D. D'Ambrosio[2], P. de Natale[1,3], G. Santambroglio[1,2], P. G. Schunemann[4], S. Borri[1,3] and J.-J. Zondy[5]

[1]*European Laboratory for Nonlinear Spectroscopy,LENS, Via Nello Carrara 1, 50019 Sesto Fiorentino, Italy*
[2]*Istituto Nazionale di Ricerca Metrologica, INRIM, Strada delle Cacce 91, 10135 Torino, Italy*
[3]*Istituto Nazionale di Ottica, INO-CNR, Via Nello Carrara 1, 50019 Sesto Fiorentino, Italy*
[4]*BAE Systems, Inc., MER15-1813, P.O. Box 868, Nashua, NH, USA 03061-0868, Address, Country*
[5]*Nazarbaev University, School of Science and Technolog (Phys. Dep.), Kabanbay Batyr 53, 010000 Astana, Kazakhstan*
E-mail: jeanjacques.zondy@nu.edu.kz

We report on the first characterization of orientation-patterned gallium phosphide (OP-GaP) crystals used to generate narrow-linewidth, coherent mid-infrared (MIR) radiation at 5.85 μm by difference frequency generation (DFG) of continuous-wave (cw) Nd:YAG laser at 1064 nm and tunable diode-laser at 1301 nm. By comparison of the experimental MIR efficiency versus focusing to Gaussian beam DFG theory, we derive an effective nonlinear coefficient d_{14} = 17 pm/V (±15%) for first-order quasi-phase-matched OP-GaP. The temperature and signal-wave tuning curves are also in qualitative agreement with a recently proposed temperature-dependent Sellmeier equation for OP-GaP [1].

Narrow-linewidth (<100 kHz), single-frequency and powerful laser sources are needed for precision molecular spectroscopy in the mid-IR range above 5μm. The 6μm range is particularly interesting for cold CO molecules high-precision spectroscopy [2], and the only available sources, with linewidths in the few MHz to tens of MHz range and ~ 0.1 W maximum power, are quantum cascade lasers (QCL's). For precision spectroscopy, μW-level of narrow-band coherent radiation must be produced to either phase-lock or injection-lock such QCL lasers. Among possible down-conversion processes, the simplest alternative to cover the 5 – 6 μm range with μW to mW power range from convenient ~1μm lasers is to use difference frequency generation (DFG) with a ~ 1.3 μm diode laser in a high-nonlinearity mid-IR crystal. For cw DFG in which the pump lasers need to be strongly focused, most birefringent phase-matched mid-IR nonlinear chalcogenide materials ($AgGaS(e)_2$, $LiInS(e)_2$, $CdSiP_2$) suffer from spatial walkoff limitations. The use of novel quasi-phase-matched (QPM) III-V semiconductors – the so-called *orientation-patterned* (OP) semiconductors (OP-GaAs, OP-GaP) for which periodic polarization domain reversal is performed during growth [3,4] – is then particularly interesting because they are intrinsically walkoff-free and possess large second-order $\chi^{(2)}$ nonlinear coefficients. In this talk, we provide the first characterization of the linear and nonlinear properties of OP-GaP via cw DFG of a single-frequency Nd:YAG laser (λ_p=1064 nm, Mephisto MOPA, Coherent Inc, short-term linewidth $\Delta\nu \approx$10 kHz) and an extended-cavity tunable diode laser (λ_s= =1301.1 nm, DL100, Toptica Photonics AG, $\Delta\nu \approx$100 kHz).

Up to 65 μW of single-frequency idler at λ_i=5.85 μm have been generated from ~10 W of Nd:YAG laser and ~ 45 mW of diode laser in a l_c = 24.5 mm of QPM structure, limited by thermal dephasing effects arising from the non-negligible absorption at the pump and signal lasers's wavelengths, despite the larger bandgap of GaP as compared with GaAs. From the absolute measurement of DFG conversion efficiency versus focusing and comparison with cw Gaussian beam DFG theory [5] an effective first-order QPM nonlinear coefficient $d = (2/\pi)d_{14}$ =17 pm/V (±15%) has been evaluated, in agreement with recent absolute measurements of the nonlinear coefficient $d_{14} \approx$ 40pm/V of GaP performed using non phase-matched methods [6-7]. From the experimental spectral and temperature tuning curve bandwidths, we could also validate a recently proposed temperature-dependent Sellmeier equation for GaP [1].

Figure 1(a) shows the absolute DFG output power as function of the incident pump power at 1064 nm (the signal extended-cavity diode laser power was maintained at its maximum output of P_s=40 mW), for various lenses focusing the overlapped parallel pump and signal lasers. As examples the f=150 mm focal length corresponds to pump and signal waists w_p = 67.5 μm and w_s = 82.5 μm.

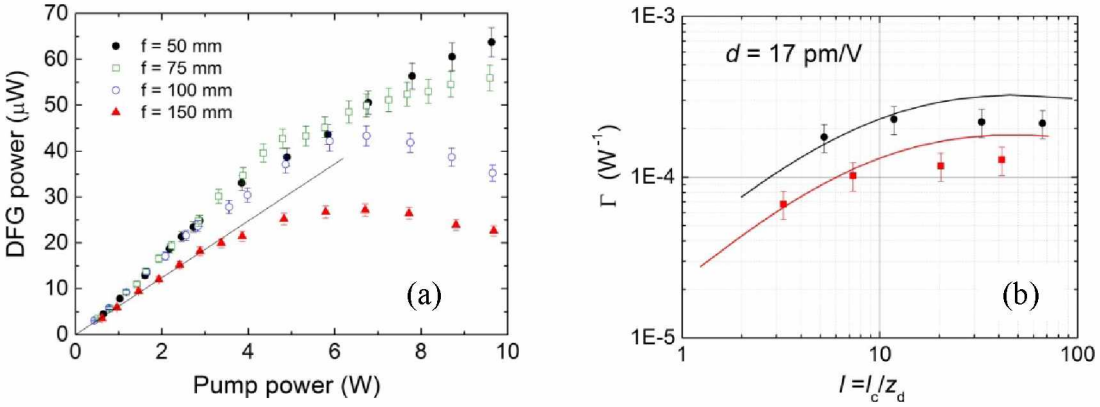

Fig. 1 (a) Cw idler power versus pump laser power for fixed signal laser power, for various focusing parameters $l = l_c/z_d$ where z_d is the idler Rayleigh range $z_d = (1/2)k_i w_d^2$, $k_i = 2\pi n_i/\lambda_i$ and $w_d = w_p w_s/[w_p^2 + w_s^2]^{1/2}$; (b) Conversion efficiency Γ versus focusing parameter. The solid lines are theoretical Gaussian beam DFG conversion efficiencies.

The strongest focusing (f=50 mm) corresponds to w_p = 19 μm and w_s = 23 μm. Because of the non-negligible absorption at 1064 nm ($\alpha_p \approx 0.17$ cm^{-1}) and 1301 nm ($\alpha_s \approx 0.12$ cm^{-1}), thermal dephasing effects lead to mid-IR power saturation. In order to retrieve the absolute value of the nonlinear coefficient for the Gaussian beam DFG theory [5], only the linear part of each curve (shown as straight line in Fig.1(a) was used to derive the conversion efficiency $\Gamma = P_i/P_p P_s$ shown as function of the focusing parameter in Fig. 1(b).

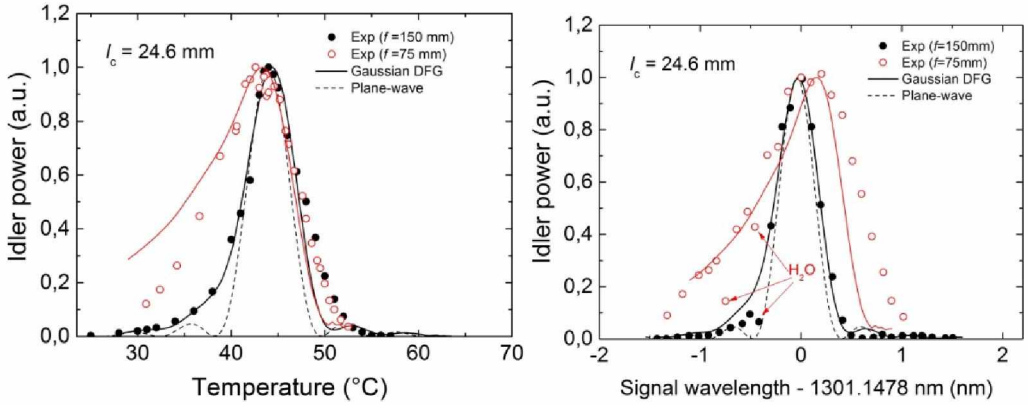

Fig. 2 (a) Temperature tuning curve for the loosest and strongest focusing case; (b) Corresponding spectral tuning curves when the diode laser wavelength is tuned around optimal phase-matching conditions (fixed T=43°C).

Finally the temperature and spectral acceptance curves are shown in Figure 2, where again the solid curves are theoretical ones computed from Gaussian beam DFG theory.

References

[1] L. A. Pomeranz, P. G. Schunemann, D. J. Magarrell, J. C. McCarthy, Kevin T. Zawilski, and D. E. Zelmon, Proc. SPIE **9347**, 93470K (2015).
[2] S. Marx, D. Adu Smith, G. Insero, S. A. Meek, B. G. Sartakov, G. Meijer, and G. Santambrogio, Phys. Rev. A **92**, 063408 (2015).
[3] V. Tassev, M. Snurea , R. Petersona , K. L. Scheplera , R. Bedforda , M. Manna , S. Vangalab , W. Goodhuec , A. Lind , J. Harrisd , M. Fejerd , Peter Schunemann, Proc. of SPIE **8604**, 86040V (2013).
[4] L. A. Pomeranz, P. G. Schunemann, D. J. Magarrell, J. C. McCarthy, Kevin T. Zawilski, and D. E. Zelmon, Proc. SPIE **9347**, 93470K (2015).
[5] J.-J. Zondy, Opt. Commun. **149**, 181 (1998).
[6] Z. H. Levine, Phys. Rev. B **49**, 4532 (1994).
[7] I. Shoji, T. Kondo, A. Kitamoto, M. Shirane, and R. Ito,J. Opt. Soc. Am. B **14**(9), 2268 (1997).

Wide tunable OPO at MID-IR spectral region pumped by Q-switch Nd:YAG laser

L. Isaenko, D. Kolker, V. Vedenyapin, A. Elisseev, S. Lobanov, A. Boyko, N. Kostyukova, V. Petrov
Novosibirsk State University, Novosibirsk, Russia
Institute of Laser Physics SB RAS, Novosibirsk, Russia
E-mail: dkolker@mail.ru

LiGaSe2 (LGSe) optical parametric oscillator (OPO) pumped by compact nanosecond Nd:YAG laser was demonstrated. Wide tuning range from 4.8 up m is shown for the first time of our knowledge. The OPOμto 9.9 m was demonstrated byμspectral tuning range from 4.8 up to 9.90 f-rotation of LGSe element at the OPO cavity.

Influence of energy transfer upconversion on high power Nd:YAG laser by calculating the population distributions

D.D. Ju [1], S.J. Liu [2], W.J. Cui[1], F.F. Song[1] and F. Song[1]
[1] *School of Physics, Nankai University, Tianjin 300071, China*
[2] *School of Biomedical Engineering, Tianjin Medical University, Tianjin 300070,China*
E-mail: fsong@nankai.edu.cn

The 1064 nm Nd:YAG lasers have been widely used for many applications such as the laser ranging, signal interference, laser printer, biological, medical diagnostics and so on. Recently, it was used as fundamental source to generate deep ultraviolet laser by sixth harmonic, the laser power of fundamental laser source (1064 nm) is up to 250 W level [1], even higher energy. But, the high and good quality output laser is limited by thermal issues and a major challenge is how to decrease the heat load in high-power diode end-pumped solid-state lasers. The energy levels of Nd^{3+} are complicated, an energy-level diagram for Nd:YAG is shown in Fig.1.

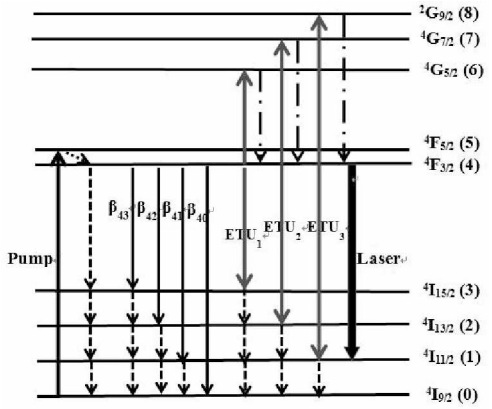

Fig. 1. The energy-level scheme for Nd:YAG crystal. Dash line represents cascaded nonradiative processes. Four thin solid lines which are down to lower levels represent fluorescence processes. There are three ETU processes in figure.

The involved processes in a stable laser system are described by the following rate equations:

$$\frac{dN_8(r,z)}{dt}=W_3N_4^2(r,z)-\frac{N_8(r,z)}{\tau_8} \quad (1) \qquad \frac{dN_7(r,z)}{dt}=W_2N_4^2(r,z)+\frac{N_8(r,z)}{\tau_8}-\frac{N_7(r,z)}{\tau_7} \quad (2)$$

$$\frac{dN_6(r,z)}{dt}=W_1N_4^2(r,z)+\frac{N_7(r,z)}{\tau_7}-\frac{N_6(r,z)}{\tau_6} \quad (3) \qquad \frac{dN_5(r,z)}{dt}=R_{05}(r,z)+\frac{N_6(r,z)}{\tau_6}-\frac{N_5(r,z)}{\tau_5} \quad (4)$$

$$\frac{dN_4(r,z)}{dt}=\frac{N_5(r,z)}{\tau_5}-\frac{N_4(r,z)}{\tau_4}-2(W_1+W_2+W_3)N_4^2(r,z)-S(r,z) \quad (5) \qquad \frac{dN_3(r,z)}{dt}=W_1N_4^2(r,z)+\beta_{43}\frac{N_4(r,z)}{\tau_4}-\frac{N_3(r,z)}{\tau_3} \quad (6)$$

$$\frac{dN_2(r,z)}{dt}=W_2N_4^2(r,z)+\beta_{42}\frac{N_4(r,z)}{\tau_4}+\frac{N_3(r,z)}{\tau_3}-\frac{N_2(r,z)}{\tau_2} \quad (7) \qquad \frac{dN_1(r,z)}{dt}=W_3N_4^2(r,z)+\beta_{41}\frac{N_4(r,z)}{\tau_4}+\frac{N_2(r,z)}{\tau_2}-\frac{N_1(r,z)}{\tau_1}+S(r,z) \quad (8)$$

$$N_d(r,z)=\sum_{i=0}^{8}N_i(r,z) \quad (9) \qquad \frac{d\Phi(r,z)}{dt}=\sigma\frac{c_0}{n}\iint(N_4(r,z)-N_1(r,z))\phi_p(r,z)drdz-\frac{\Phi}{\tau_c}=0 \quad (10)$$

where N_i, τ_i (i=1- 8) denote the population distribution and lifetime in different levels respectively. W_i (i=1-3) is the upconversion rate. β_{4j} (j=3,2,1)are the branching radios from $^4F_{3/2}$ level to $^4I_{15/2}$, $^4I_{13/2}$, $^4I_{11/2}$ levels respectively. τ_c is the photon lifetime. N_d is the total of Nd^{3+} ions. Φ is the total of photons.

Under 808 nm CW laser operation, we assume that the pump and laser beams are TME_{00} Gaussian beams [1]. From Eq. (1)-(10) and the values of all parameters [2, 3-6], the population profiles of $^2G_{9/2}$, $^4G_{7/2}$, $^4G_{5/2}$ levels at the pump power of 20 W are obtained, the number of ions distribution indirectly expresses the heat distribution caused by ETU effects.

For studying the influence of ETU effects on heat generation further, the relationship between thermal power and pump power is:

$$Q(r,z)=\sum_{i=0}^{8}\Delta E_i \vartheta_i(r,z) vor(r,z) \qquad (11)$$

where the ΔE_i is energy gaps that have to be bridged among different energy levels, $\vartheta_i(r, z)$ is the rate equations term of nine individual multiphonon processes that lead to heat generation.

We calculate thermal power in the whole crystal versus absorbed pump power which is generated by ETU processes respectively,the result is shown in Fig. 2(a). The proportion distribution of heat generation due to ETU effects under the steady-state condition is shown in Fig. 2(b).

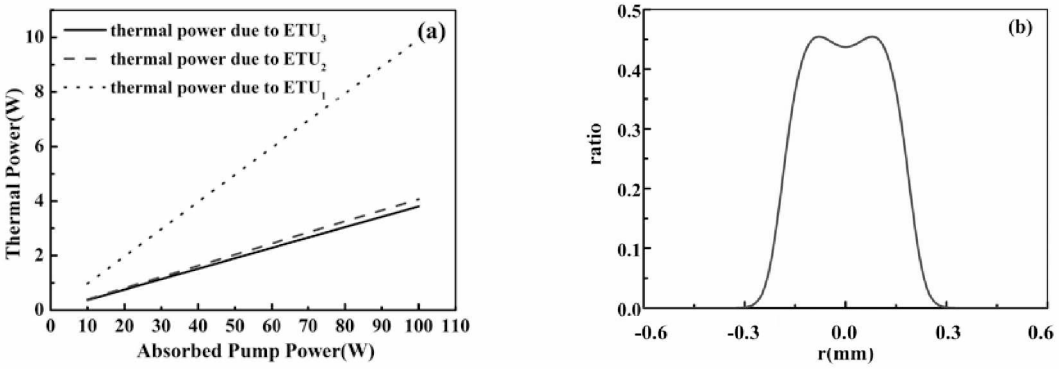

Fig. 2 (a) The thermal power versus absorbed pump power. (b) The proportion distribution value of heat load due to ETU effects The value of the proportion of ETU is about 0.48 at the center of the rod. So it is essential and useful to take into account the higher laser levels when we study the laser performance.

In following section, the influence of round-trip dissipative loss and waist of pump beam on population in higher levels are analyzed when considering ETU effects, see figure 3.

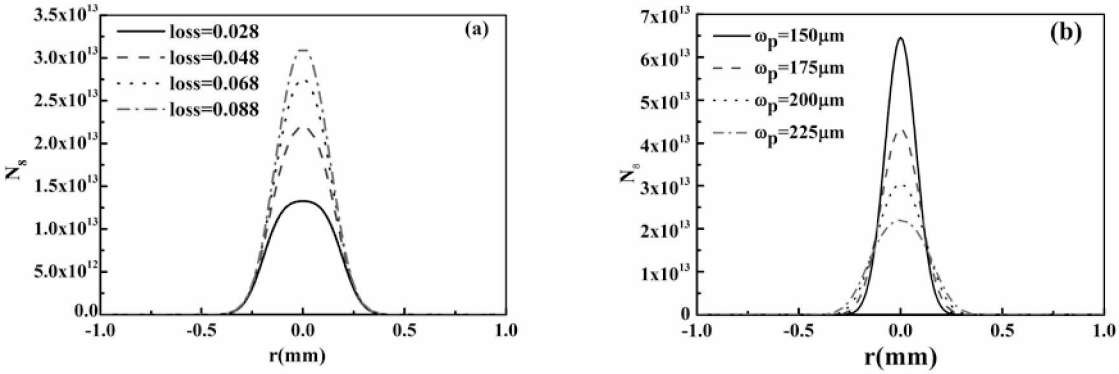

Fig. 3 (a) (b) The population distribution in $^2G_{9/2}$ level for four values of cavity loss and pump beam waist at incident surface respectively. It is clear that the influence of upconversion on heat load increases with the round-trip dissipative loss, (b) shows the population increases with the waist of pump beam nonlinearly, the influence of ETU effects drops when the output laser beam waist matches to the pump laser beam.

A theoretical model of the influence of ETU effects based on population dynamics on higher energy level in laser diode end-pump Nd:YAG crystal laser to study has been developed. We find that the ETU effects lead to a strong thermal loading under higher excitation density. According to the simulation results of population distribution of $^2G_{9/2}$ level in different round-trip dissipative loss and the waist of pump beam, the heat generation and the laser cavity optimization are investigated in detail. We believe that the theoretical model including nine energy levels can provide a useful guideline to optimize high-power Nd-doped crystal lasers.

References

[1] M. Frede, R. Wilhelm, D. Kracht., Opt. Lett. **31**, 3618 (2006).
[2]Y. T. Wang, R. H. Zhang, J. Phys. B **44**, 1350401(2011).
[3] X. D. Li, X. Yu, J. Gao et al., Laser Phys. Lett. **6**, 125 (2009).
[4] D. C. Brown, IEEE J. Quantum Electron. **34**, 560 (1998).
[5] M. Pollnau, P. J. Hardman, M. A. Kern et al., Phys. Rev. B **58**,16076 (1998).
[6] R. P. Yan, S. J. Yoon, S. J. Beecher et al., IEEE J. Sel. Top. Quantum Electron. **21**, 1601208 (2015).

Single photon transport by a moving atom

A.E. Afanasiev[1], P.N. Melentiev[1], A.A. Kuzin[1,2], A.Yu. Kalatskiy[1,2], V.I. Balykin[1]
[1] *Institute of Spectroscopy Russian Academy of Sciences, Fizicheskaya Str., 5, Moscow, Troitsk, 108840, Russia*
[2] *Moscow Institute of Physics and Technology, 9 Institutskiy per., Dolgoprudny, Moscow Region, 141700, Russia*
E-mail:afanasiev.isan@gmail.com

It follows from basic principles of wave physics that the passage of a wave through a hole that is considerably smaller than the wavelength can be neglected. In the classical work by Bethe [1] on transmission of light by a nanohole in an infinitely thin and perfectly conducting screen, a simple expression for the transmission efficiency of light has been obtained, which is scaled in relation to the hole size as $(r/\lambda)^4$, where r is the radius of the hole, and λ is the wavelength. Under assumptions made on the screen, the transmission efficiency falls rapidly when the wavelength becomes greater than the hole radius. Ebbesen and collaborators [2] discovered the Extraordinary Optical Transmission (EOT) through sub-λ periodic hole array. The EOT is mediated by the aid of electromagnetic surface modes supported by the holey surfaces [3]. The majority of researchers agree that the central role in this phenomenon is played by surface waves, such as *surface plasmons*.

Here we demonstrate a new physical approach for an effective light transmission through nanohole. It is based on the photon transport that involves the participation of a particle other than a plasmon, namely, a *neutral atom*. In this scheme, a *single atom* transfers a *single photon* through a nanohole. The proposed scheme is an another mechanism of photon's transport through the nanohole which supplement existing [1,2]. Besides the using of a new particle for photon transport it opens up a new possibilities for surface science. It is possible to use such scheme for investigation of van der Waals interaction because of atom-surface interaction [4]. Another application is for atom - plasmon interaction investigation. Indeed the subwavelength hole is a highly nonlinear plasmonic element. So the interaction of excited atom with such structure opens a new way for tailoring the spectral properties of materials [5].

The basic idea of the photon transport by a moving atom is presented in Figure 1 [6]. An atom moving toward a metal screen with a hole absorbs a photon of laser radiation immediately in front of the hole. If the lifetime of the excited atom is substantially larger than the time of flight of the atom through the nanohole (in a real experiment, the nanochannel), the transition of the atom from the excited state to the ground state with emission of a photon can occur on the other side of the screen, which means the transfer of the energy of the photon through the nanohole.

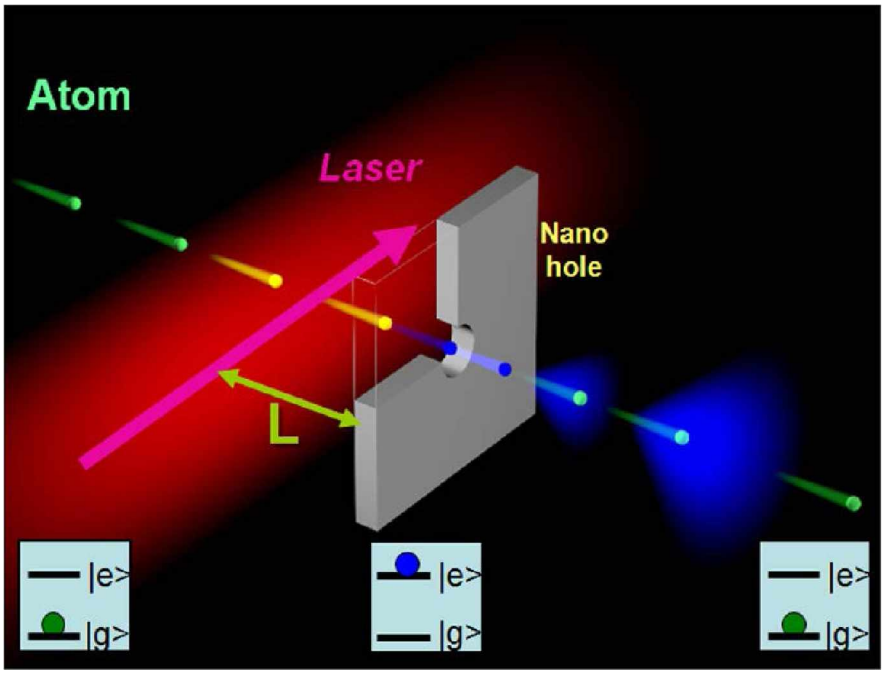

Fig. 1 Scheme of a photon transport by atom through nanohole.

At the wavelength λ=800 nm and the nanohole radius r = 50 nm, the ratio of the probability of passage of a photon involving the participation of an atom to the probability of passage of a photon alone is $\eta \sim 2\times10^4$. The physical reason for such high photon transfer efficiency is the reduction of the "single photon wave packet" due to its absorption by the atom and, as a result, its localization in a volume less than the wavelength and the nanohole size. In principle this scheme allows to transform "single-photon in single-mode wave packet" of the laser light into a "single-photon but multimode wave packet" in free space.

The experiment was performed with *Rb* atoms. A beam of *Rb* atoms is directed to the sample with nanoholes. Atoms were excited into a long-lived excite state $5D_{5/2}$ at the transitions $5S_{1/2}\rightarrow5P_{3/2}$ and $5P_{3/2}\rightarrow5D_{5/2}$. The decay of the $5D_{5/2}$ state via the channel $5D_{5/2}\rightarrow6P_{3/2}\rightarrow5S_{1/2}$ with the emission of a photon at a wavelength of 420 nm takes place with a characteristic lifetime of 500 ns. Such a long lifetime makes it possible for the atom to transfer the photon energy over a distance of about 150 μm. This value suffices to ensure the flight of the atom in the excited state through the nanohole. The probability of emission of a blue photon by the atom is about 2%. The detection of blue photon gives an evidence of atom passage through the hole in the excited $5D$ state. As a consequence, this fact gives an evidence of photons transfer at 776 nm and 780 nm wavelengths (through the $5D_{5/2}\rightarrow5P_{3/2}\rightarrow5S_{1/2}$ decay channel). Our calculations show that for one detected blue photon there are about 20 photons at 776 nm and 780 nm.

The photon transfer efficiency depends on the nanohole size, the material of the screen, and the velocity and the scheme of energy levels of the atom. At small sizes of the nanohole, the photon transfer efficiency decreases substantially because of the interaction of the excited atom with the surface. As a result the surface of the nanohole in the screen causes deexcitation of the atomic state. The described scheme of the atom interaction with the surface offers opportunities to study quantum friction [7] and strength of atom-surface interaction [8].

This work was supported by the Russian Science Foundation (project No. 14-12-00729).

Refrences

[1] H.A. Bethe, "Theory of diffraction by small holes", Phys.Rev. **66**, 163 (1944).
[2] Ebbesen T.W., Lezec H.J., Ghaemi H.F., Thio T. and Wolff P.A., "Extraordinary optical transmission through sub-wavelength hole arrays", Nature **391**, 667 (1998).
[3] García-Vidal F. J., Martín-Moreno L., Ebbesen T. W. and Kuipers L. "Light passing through subwavelength apertures", Rev. Mod. Phys. **82**, 729 (2010).
[4] Bloch D and Ducloy M, "Atom-wall interaction" Advances In Atomic, Molecular, and Optical Physics **50**, 91–154 (2005).
[5] S. A. Aljunid, E. A. Chan, G. Adamo, M. Ducloy, D. Wilkowski, and N. I. Zheludev, "Atomic response in the near-field of nanostructured plasmonic metamaterial", Nano Lett. **16**, 3137 (2016).
[6] A.E. Afanasiev, P.N. Melentiev, A.A. Kuzin, A.Yu. Kalatskiy and V.I. Balykin, "Photon transport through a nanohole by a moving atom", New J. Phys. **18**, 053015 (2016).
[7] Scheel S and Buhmann S Y "Casimir-Polder forces on moving atoms", Phys. Rev. A **80**, 042902 (2009).
[8] Persson B N J and Lang N D, "Electron-hole-pair quenching of excited states near a metal", Phys. Rev. B **26**, 5409–5415 (1982).

Laser-induced semiconductor fractal structures with topological quantum effects

S.M. Arakelian[1], S.V. Kutrovskaya[1], A.O. Kucherik[1], S.P. Zimin[2]
[1]*Stoletovs Vladimir State University, Vladimir, Russia*
[2]*Demidov Yaroslavl State University, Yaroslavl, Russia*
Email: arak@vlsu.ru

In experimental aspect, the laser synthesis technique to produce the nanoparticles (NPs) of different composition in both semiconductor samples (PbTe): direct laser modification of thin films and laser evaporation of substance from target in liquid to produce the colloidal systems and subsequent deposition of particles from colloidal system on solid substrate (glass). Under a cw-laser radiation a bimodal distribution on PbTe particle size takes place. For such laser-induced nanostructures we demonstrated the superconductivity tendency to increase the electrical conductivity by several times for our case at room temperature in comparison with a homogenous monolithic sample. By drop deposition technique it has been obtained the cluster structures with various topology, and the nanoparticles become quantum dots under some conditions. Such structures with controlled electro-physical properties are very principal to construct the elements and devices of optoelectronics and photonics in hybrid circuits on new physical principles.

We present the topology controlled laser synthesis of nanoparticles/the semiconductor PbTe nanoparticles by direct laser modification of thin films and by deposition of clusters and so, macroscopic quantum effects for a spatially inhomogeneous/modulated/periodic micro/nano structures occur. In such systems we studied, in particular, the electrical transport properties (electroresistance behavior vs the cluster parameters variation, and also the current Volt-Amper characteristics vs conditions of the experiment), and quantum tunneling effect (for a spatially periodic nanocluster structure) and/or jump conductivity (in frames of shell-model cluster presentations) have been obtained (cf. [2]).

Fig. 1 shows the direct laser modification of a PbTe-target surface due to the termolization equilibrium process only by the laser ablation technique (cw-laser radiation: λ=1.06 μm, the intensity – up to 106 W/cm^2). Real time scale observation of laser-induced processes has been carried out. The observed effect of the surface self-organization structuring in particle size, is achievable only in a fixed laser intensity range and for a certain scan-velocity of the laser beam on the sample surface.

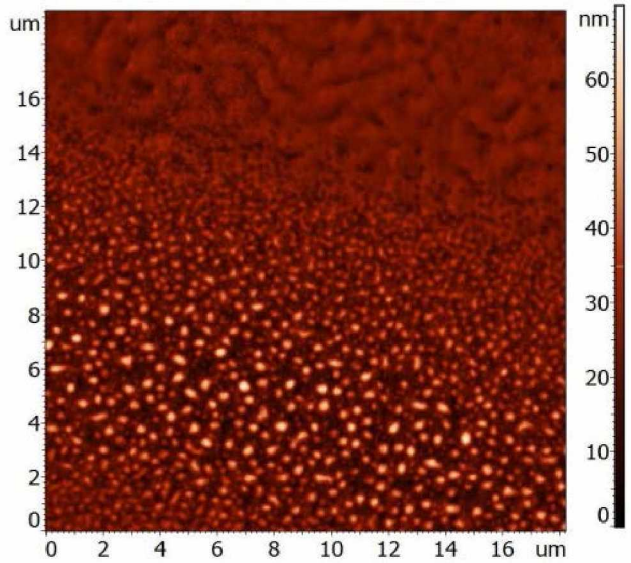

Fig.1 The picture of the target surface structure under laser irradiation: it looks as a bimodal distribution.

Fig. 2 show the results obtained by measuring current Amper-Voltage characteristics for different experimental conditions using a preliminary prepared sample with a bimodal distribution of nanoparticles on the surface discussed above. We give present the results on the detection of the jump-conductivity for different surface density of NPs on the films (shown by figures at the dependences). Moreover, its occurrence is universal – there have been shown two types measurements of the electrical resistance in both longitudinal and transverse one directions; the fact depending only on the topology of the conducting layer (constant for a given sample). So, the implementation of transition of the electrons from the bound state to a free state can be taken into account in the frames of shell model clusters.

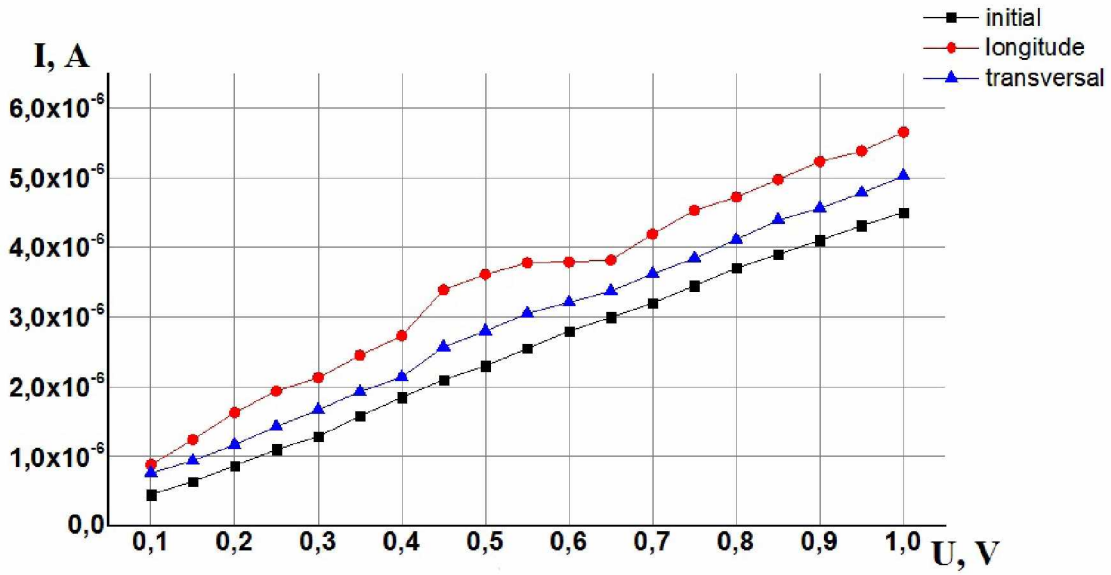

Fig. 2 Jump-conductivity dependences for different surface density of NPs on the PbTe films. All measurements have been carried out by averaging the results of 10 experiments.

In progress, it is expected to carry out a more detailed study of the correlation between the topology of a nanostructure of different composition and its functional and dynamic properties, and also of optical properties for fabricated nanocluster structures under the conditions when macroscopic quantum effects occur, including e.g. the tendency of high-temperature superconductivity, and multiple quantum transitions resulting in modification of the optical spectra in layer structures.

When solving the existing problems we should address modern challenges for the creation of new and also, on new physical principles, the hybrid (optics/photonics + electronics) elements and devices with given properties (both functional and design). The main stream of the problem includes in particular the units for quantum information processing, based on advantages of modern femto-nanophotonic technologies by laser synthesis of nano- and microstructures with variable topology and size/form parameters on the surface of various solid state materials.

This work was in part supported by the Russian Foundation for Basic Research, project № 13-02-97513, and the project component of the state contract of Vladimir State University №16.440.2014/K to perform public works in the field of scientific activity.

References

[1] S.M. Arakelian, A.O. Kucheruk, V.G. Prokoshev, V.G. Rau, A.G. Sergeev, "Introduction to femto-nanophotonics:fundamentals and laser methods of controled fabrication and diagnostics of nanostructured materials". Monograph, 744 p., Logos Publ., Moscow (2015).

[2] S. Arakelian, V. Emel'yanov, S Kutrovskaya., A. Kucherik, S. Zimin, "Laser-induced semiconductor nanocluster structures on the solid surface: new physical principles to construct the hybrid elements for photonics", Journal Optical and Quantum Electronics **48**(6), 1 (2016).

Random lasing based on doped nanocrystals

G. Feng, S. Zhou
Sichuan University,Chengd 610064, China
E-mail: guoing_feng@scu.edu.cn

By using femtosecond laser pulses to ablate microsized targets that are dispersed in liquid media, doped nanocrystals have been successfully fabricated. The nature of the nanocrystals was characterized by SEM, TEM, EDS-Mapping, and XRD. By using the doped nanocrystals as the gain medium, random lasing has been established at room temperature.

Optical refrigerator for charged nanocrystals doped by Yb^{3+} ions

A. Ivanov, A. Kovalev, V. Polyakov, Yu. Rozhdestvensky, and S. Rudyi
ITMO University, Birzhevaya liniya, 14, Saint Petersburg, 199034, Russia
E-mail: avivanov@mail.ifmo.ru

Laser cooling of matter has become a separate area of the physics in the last few decades. A great success in this area has been especially achieved for translational cooling of gaseous matter. At present, methods for cooling of atoms make it possible to reach the nanokelvin temperature range [1]. In contrast of gaseous medium, laser cooling of internal energy of solid materials has more modest results. The record cooling of 110 K has been achieved to date for the bulk YLF crystal doped by Yb^{3+} ions [2]. The main cause of such a situation is the difference in the cooling mechanisms of external and internal degrees of matter freedom. The internal cooling of doped systems is based on the anti-Stokes fluorescence from Stark split sublevels of the excited level of rare-earth (RE) ions which are optically pumped. The anti-Stokes fluorescence is a result in the interaction of optically excited electrons of an RE ion with vibrational modes of a crystal system. Thus, thermalization of the electrons at sublevels leads to the situation in which the average energy of the spontaneously emitted photons exceeds the energy of the absorbed photons. Since the optical cooling occurs at the electron transitions between the Stark split sublevels, the minimum temperature of cooling for doped solids is limited and cannot be lower than 50 K [3]. Laser cooling of nanocrystals presents a more complicated problem because such nanoobjects have both external and internal degrees of freedom simultaneously. As a result, even a localized nanocrystal has considerable internal temperature that can prevent a variety of high-precision experiments.

In this work, we propose the model of an optical refrigerator for the charged CaF_2 nanocrystals doped by Yb^{3+} ions. The refrigerator is composed of the RF Paul trap to capture and the optical module to cool the doped nanocrystal. The feature of the proposed model is the combination of the translational and vibrational cooling of the nanocrystal in one process of laser-matter interaction (Fig. 1).

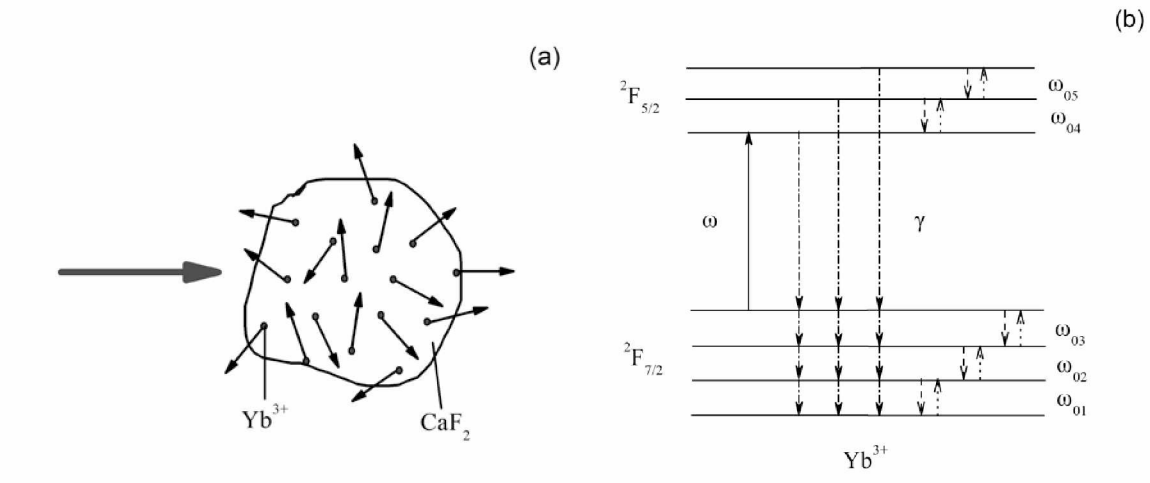

Fig. 1 Laser cooling scheme: (a) translational cooling of the doped nanocrystal; (b) anti-Stokes fluorescence cooling of the Yb ion, solid arrow shows optical transition at the frequency ω; dotted arrows show vibronic-interaction-induced transitions at the frequencies ω_{0i}; downward dashed arrows refer to nonradiative relaxation; dash-dotted arrows show the radiative relaxation of rate γ.

We show the possibility of translational cooling of doped nanocrystals, taking into account the effects of photon recoil. Laser cooling of the translational motion of a nanocrystal (as well as an ion or atom) is based on momentum exchange between the field of optical radiation and the nanoobject. The peculiarity of the manifestation of such kind of exchange for doped nanocrystals is that the recoil

momentum exists due to the reemission of resonant photons of RE ions as a result in the vibrational cooling. At the same time, the recoil rate is ensured by the all RE ions in nanocrystal. Thus, the average acceleration, which transfers to the nanocrystal, depends on the characteristics of the sample and atomic transition: the weights of matrix atoms, the content of Yb ions, the wave vector of the optical radiation, the natural linewidth of the transition, and the intensity of radiation. The estimates for Yb^{3+}:CaF_2 (5 mol % Yb content) nanocrystal show that the average acceleration of the nanocrystal (100 nm diameter) is 3.3 cm s^{-2}. Additionally, the magnitude and sign of the frequency detuning for efficient internal cooling should be determined by the magnitude of the Doppler shift.

For cooling of vibrational energy of the nanocrystal, we compare two approaches of optical pumping: direct $4f - 4f$ pumping [3] and coherent pumping through the $5d$ level [4]. Our calculations show that the net cooling power for direct pumping between forbidden $4f - 4f$ optical transitions is not enough to cool the nanocrystal because of the large thermal load of environment. In contrast of the direct pumping, the pumping through the $5d$ level gives rise to the deep and fast cooling and allows to refrigerate the nanocrystal up to 60 K.

Since the average acceleration of the nanocrystal is slow in comparison with the ionic case, the successful deceleration can only take place when the spatial localization of the nanocrystal occurs. The most universal method of spatial localization is the localization of a nanocrystal in radio field (RF) ion trap. In recent years, the localization of nanoobjects in a line RF trap has been studied most intensively. For instance, nanodiamonds [5], graphene nanoparticles [6], and biomolecules [7], were localized in a quadrupole ion trap. The ion trap provides the means to control both the dynamics and temperature of a nanoobject.

The nanocrystal dynamics in the ion trap throughout the translational cooling is nonlinear. In this work, we obtain the dependence of the dynamics of the doped nanocrystal in a nonlinear RF trap on the orientation of the traveling light waves used in the cooling process. We consider two types of RF traps, namely, quadrupole (four electrodes) and sextupole (six electrodes) ones. It is shown that the both RF ion traps are efficient for three-dimensional cooling and all of three components of the nanocrystal speed decrease equally over time.

Obtained results can be helpful in constructing logic elements of quantum computers and performing high-precision experiments. Additionally, cooled nanocrystals are the promising contenders for using in the ultrasensitive metrology.

References

[1] A. Aspect, E. Arimondo, R. Kaiser et al., Phys. Rev. Lett. **61**, 826 (1988).
[2] M. Ghasemkhani, A. R. Albrecht, S. D. Melgaard et al., Proc. SPIE **9380**, 938003 (2015).
[3] D. V. Seletskiy, M. P. Hehlen, R. I. Epstein et al., Adv. Opt. Phot. **4**, 78 (2012).
[4] A. Ivanov, Y. Rozhdestvensky, E. Perlin, J. Opt. Soc. Am. B **33**, 1673 (2015).
[5] A. Kuhlicke, A. W. Schell, J. Zoll et al., Appl. Phys. Lett. **105**, 073101 (2014).
[6] P. Nagornykh, J. E. Coppock, Appl. Phys. Lett. **106**, 244102 (2015).
[7] X. Zhao, P. S. Krstic, Nanotechnology **19**, 195702 (2008).

Laser-induced synthesis of nanostructured metal-carbon clusters and complexes for optical application

A. Kucherik[1], S. Arakelian[1], S. Kutrovskaya[1], A. Osipov[1], T. Vartanyan[2], A. Povolotckaia[3], A. Povolotskiy[3], A. Manshina[3]

[1]*Stoletov Vladimir State University, Vladimir, Russia*

[2]*St.Petersburg National Research University of Information Technologies, Mechanics and Optics, St. Petersburg, Russia*

[3]*Saint-Petersburg State University, St.Petersburg, Russia*

E-mail: kucherik@vlsu.ru

Metal-carbon complexes consisting of noble metal nanoparticles and carbon matrix is a prospective material for photonics applications. One application of these objects is to provide materials for the implementation of Surface Enhanced Raman Scattering (SERS) [1,2]. Carbon stabilizes the metal particles and increases SERS. The control of size and morphology of formed metal-complexes allows to vary its properties. The application of laser ablation materials in a liquid allows to create nanoparticles and clusters with various optical properties [3-5]. A very perspective carbon material with structural sensitive optical properties is carbyne [6].

In this work we present the investigation of metal-carbyne clusters formation under the laser radiation of colloidal systems. Colloidal solutions were consisted of carbon and noble metals nanoparticles As a result, there was shown that clusters are forming during the irradiation process. The Raman spectra of those systems depends on the concentration of the particles in the solution and on the laser radiation conditions.

The gold and silver particles were obtained during the cw-irradiation of the targets placed in liquid media. [3]. The power of radiation was 35-50 W, laser beam diameter equaled 30 μm. A target was scanned by the laser beam with the speed of 10-30 μm/s. The irradiation time was 30 min. The average particle size after laser irradiation was 10-30 nm. The size of particles in colloidal system was measured by the Horiba LB-550 (dynamical light scattering particle size analyzer).

Carbon nanoparticles were obtained using the pulse-periodical laser radiation (pulse 2 ms), energy in pulse was from 1 J up to 20 J, pulse frequency – 20 Hz, on the shungite targets placed in water. [7]. This kind of method allows to obtain carbon particles with diameters about 100 nm - 2 μm.

The carbon, gold and silver particle colloidal solution was prepared by the intense mixing with concentratration C:Au:Ag 10:1:1 in water (5cl), then the ultrasonic bath was used for about 10 minutes for particle decoagulation. The fiber Yb-laser setup (pulse - 100 ns, repetition rate - 20 kHz, the pulse energy up to 1mJ) was used for the metal-carbyne clusters obtaining [5]. This kind of laser system can realize the particle absorption on the wavelength of 1.06 μm, with short pulse. The colloidal system irradiation was carried out by the scanning of the cuvette volume by focused beam (spot diameter - 50 μm, irradiation time - 15 minutes).

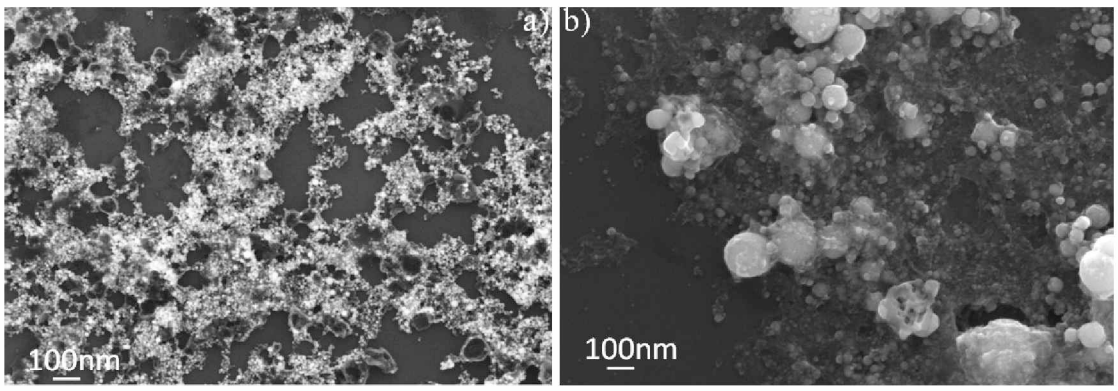

Fig. 1 SEM-images of synthesis metal-carbyne clusters for the different laser pulse energy 1mJ (a) and 0.5mJ (b).

The morphological properties of deposited nano-clusters were investigated using atomic force microscopy (AFM) and scanning electron microscopy (SEM). It was found that the transmission spectra of the resulting structures depend on the concentration of gold and silver nanoparticles in the colloidal solution.

The SERS research by deposited films was performed using Senterra spectrometer (Bruker), with the pump laser wavelength of 532 nm, the power of 0.1 mW and the focal spot diameter of 2 microns (Center for laser and optical materials research, SPbSU).

The standard dye Rhodamine 6G was used as a test molecule (Raman spectrum of the solution is shown in Fig. 2a). The dye solution in ethanol (10^{-6} M) was placed on a metal-carbon structures using a micropipette. The metal-carbon surfaces are formed on an oxide glass substrates with different composition of metal nanoparticle. The Raman spectra of molecules of Rhodamine 6G on various substrates are shown on Figure 2b.

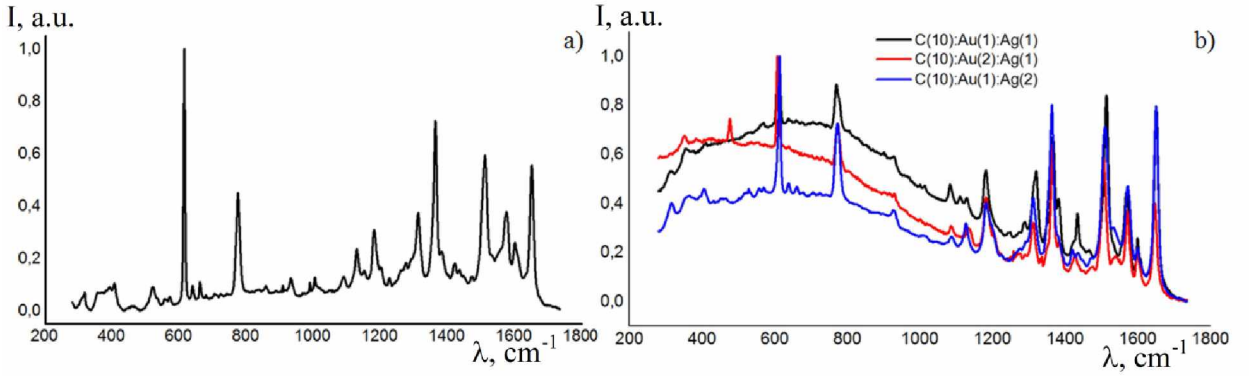

Fig. 2 Raman spectra: initial due (a) and test by deposited metal-carbon films (b).

If the oxide glass or carbon film are used as a substrates – the bands corresponding to Rhodamine 6G with a concentration of 10^{-6}M are not detected. At the same time, the use of films as a substrate of metal-carbon nanostructures under the same measurement conditions allow to detect and identify the dye on the Raman spectra with sureness in Figure 5b. The changing of the gold and silver nanoparticles ratio results in varying of the amplification degree of different bands in the spectrum of the dye. The peaks of plasmon resonances for silver and gold are in the range of 410 and 540 nm, thus, various vibration modes are amplified at gold and silver particles with different gain.

References

[1] A Povolotskiy., A.Povolotckaia, Y.Petrov, A. Manshina, S. Tunik: Laser-induced synthesis of metallic silver-gold nanoparticles encapsulated in carbon nanospheres for surface-enhanced Raman spectroscopy and toxins detection. Applied Physics Letters (2013).

[2] A. A. Manshina, E. V. Grachova, A. V. Povolotskiy, A. V. Povolotckaia,Y. V. Petrov, I. O. Koshevoy, A. A. Makarova, D. V. Vyalikh, S. P.Tunik: Laser-induced transformation of supramolecular complexes: Approach to controlled formation of hybrid multi-yolk-shell Au-Ag@a-C:H nanostructures. Source of the Scientific Reports (2015).

[3] S. M. Arakelyan, V. P. Veiko, S. V. Kutrovskaya, A. O. Kucherik, A. V. Osipov, T. A Vartanyan., T. E. Itina Reliable and well-controlled synthesis of noble metal nanoparticles by continuous wave laser ablation in different liquids for deposition of thin films with variable optical properties. J Nanopart Res (2016) 18:155.

[4] A. A.Antipov, S.M. Arakelyan, T. A. Vartanyan, T.E. Itina, S.V. Kutrovskaya, A.O. Kucherik, I.V. Sapegina: Optical properties of nanostructured gold–silver films formed by precipitation of small colloid drops. Optics and Spectroscopy (2015).

[5] A.A. Antipov, S.M. Arakelyan, S.V. Garnov, S.V. Kutrovskaya, A.O. Kucherik, D.S. Nogtev, A.V. Osipov: Laser ablation of carbon targets placed in a liquid. Quantum Electronics (2015).

[6] K.Akagi, M. Nishiguchi, H. Shirakawa, Y. Furukawa, I. Furukawa One-dimensional conjugated carbyne – synthesis and properties// Synthetic Metals Volume 17, Issues 1-3 (1987), p. 557-562.

[7] S. Arakelian, S. Kutrovskaya, A. Kucherik, A. Osipov, A. Povolotckaia, A. Povolotskiy, A. Manshina Laser-induced synthesis of a nanostructured polymer-like metal-carbon complexes// Proc. of SPIE Vol. 9884, 988425 (2016).

Investigation of single defects created in crystals by laser emission and hard radiation

E.F. Martynovich[1,2], V.P. Dresvyanskiy[1], S.V. Boychenko[1], A.L.Rakevich[1], S.A. Zilov[1], S.N.Bagayev[3]
[1]*Irkutsk Branch of the Institute of Laser Physics SB RAS, 130A Lermontov str, Irkutsk, 664033, Russia*
[2]*Irkutsk State University, 20 Gagarin blvd, Irkutsk, 664033, Russia*
[3]*Institute of Laser Physics SB RAS, 13/3 Ac. Lavrentyev's prosp., Novosibirsk, 630090 Russia*
E-mail: filial@ilph.irk.ru

Exciton mechanism of radiation-induced defects formation is implemented to a large part of the known inorganic crystalline media. Exposure to particles and hard radiation quanta on the crystals leads to the formation of stable electron excitations: electrons, holes and excitons after a series of quick intermediate energy transfer processes. Then started the processes of interaction of electronic and nuclear subsystems of the crystals. Structural defects result from this interaction. The basic process of this kind is the decay of the excitons on the primary structural defects, ie Frenkel pairs with subsequent recharging, migration and aggregation.

Intense femtosecond laser light excites the electron subsystem of crystalline media effectively without affecting in the first stage the nuclear subsystem, ie, not warming up the crystal. Therefore, the use of laser radiation is preferable in practical terms for the creation of radiation defects. Femtosecond lasers with low power may well replace electron accelerators and gamma settings in some applications, with the aim of radiation modifying of the properties of the class of crystals above.

Optical properties of ensembles of the main radiation-induced defects, such as color centers, are relatively well studied. However, many different types of defects occur in crystals during irradiation. There are intrinsic defects and the intrinsic-impurity defects, which are formed by impurities which are always present in the crystals. Therefore, relevant task is the spectroscopic differentiation and identification of defects. This problem can not be solved by conventional absorption and luminescence spectroscopy. This is a huge homogeneous broadening and overlap of the spectral lines of radiation defects caused by electron-phonon interaction.

In this paper, we study the possibility of identifying radiation-created quantum systems via the characteristics of quantum trajectories of the intensity of their luminescence measured on individual centers by confocal scanning fluorescence microscopy with the time-correlated single photon counting [1].

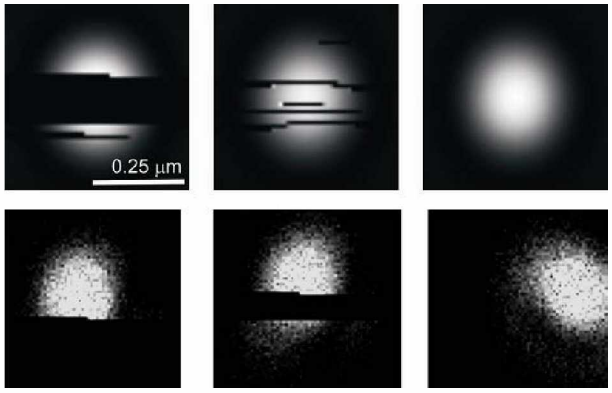

Fig. 1 Confocal scanned fluorescent images of single color centers with different characteristics of quantum trajectories. Above - theoretically calculated, at the bottom - experimental.

Experimental studies were carried out using a confocal microscope MicroTime 200 of PicoQuant Gmbh. Quantum trajectories calculations were carried out by the density matrix method. Calculations of confocal scanned images of single centers conducted by diffraction method developed by B.Richards and E.Volf based on the Huygens-Fresnel principle.

In Fig. 1 the images of study single F_2 color centers in LiF crystal displays. Gaps in the images correspond to centers transitions in the non-emitting state during the scanning. One experimental trajectories presented in Fig. 2. In the process of recording this trajectory increased the intensity of the exciting radiation abruptly. Therefore, the trajectory consists of two parts: linear and non-linear.

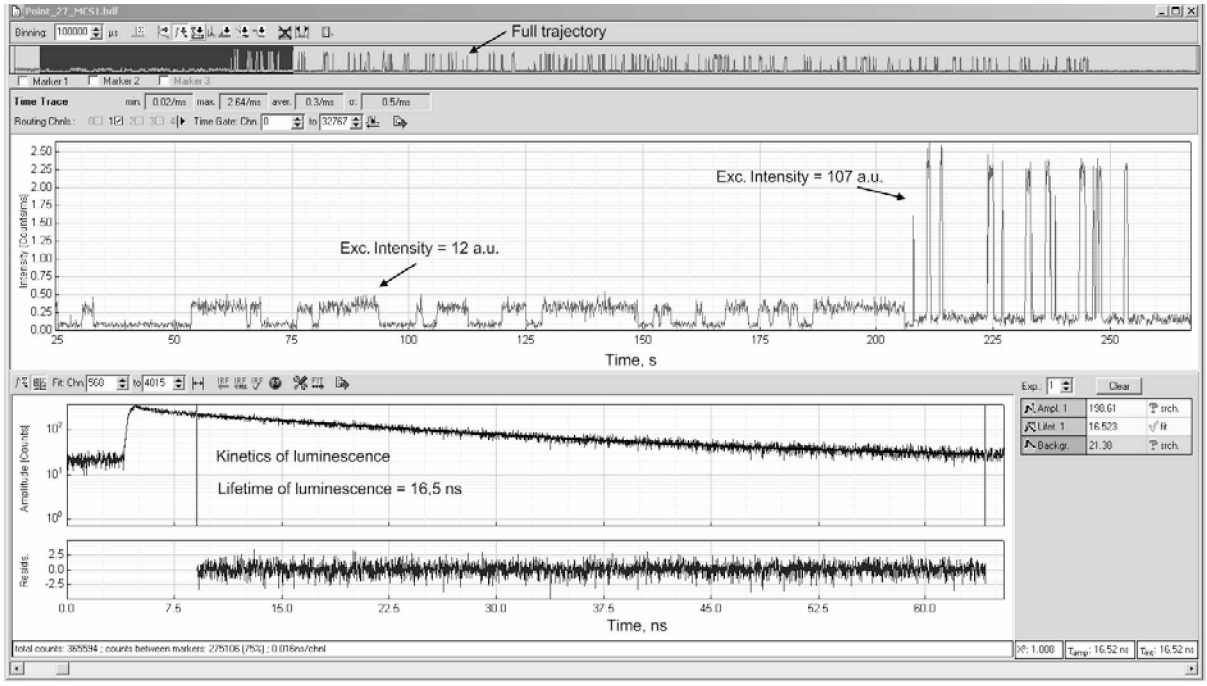

Fig. 2 Linear and non-linear parts of the trajectory of the intensity of the same center when excited by continuous sequence of picosecond pulses. Switching the excitation intensity is on 208 seconds. Below - the kinetics of the rise and decay of the luminescence intensity of the center.

Trajectories can be called linear, if the processes occurring during excitation centers are limited to the scheme shown in Fig. 3. There are no induced transitions down under the influence of the exciting radiation. They should not be taken into account because the F_2 centers have a large Stokes shift and the cross section of stimulated emission in the spectral line of the pump is very little. In addition, in the diagram are no stimulated transitions under the influence of the spontaneous emission, i.e. are no superluminescence. In our experiments, it is confirmed by the fact that luminescence decay time does not depend on the intensity. Also on the scheme shown in Fig. 3, does not take into account the possible transitions on higher levels of singlet and triplet systems. For linear trajectories, the luminescence intensity increases with excitation intensity. Accordingly, the intervals of stay of the center in the radiating state S_0 decreases as increasing the probability σI.

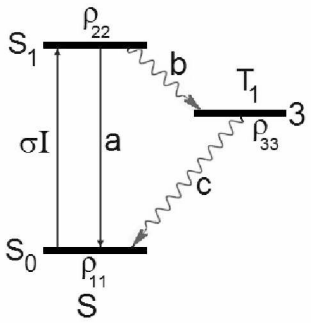

Fig. 3

With a substantial increase in the intensity of the exciting radiation observed decrease in the average time of stay in the center of a non-emitting state T_1. This is due to the transition to the nonlinear regime, due to the excitation overlying states and triplet-singlet conversion.

As a new individual "spectroscopic" characteristic of the centers, can be used ratio of lifetimes in the emitting and non-emitting states at a fixed intensity of the exciting radiation.

This work was supported by the project II.10.1.6 of Fundamental Research Programs of state academies of RF, project number 3833 of ISU State Task and RFBR grant № 16-52-44056.

References

[1] E. F. Martynovich, V. P. Dresvyansky, S. A. Zilov, A. L. Rakevich, S. V. Boychenko, and S. N. Bagayev, *In* Advanced Photonics 2015, OSA, 2015, paper SeW2B.5.

Spaser as novel versatile biomedical tool

A. Plekhanov
Institute of Automation and Electrometry SB RAS, Novosibirsk, Russia
E-mail: fractal@iae.nsk.su

Nanoplasmonics deals with collective electron excitations at the surfaces of metal nanostructures, called surface plasmons, and has numerous applications in science, technology, biomedicine. We will present recent breakthrough in application of the spaser as an ultrabright nanolabel and an efficient theranostic agent in biomedicine.

Fiber-based femtosecond optical frequency comb stabilized to iodine frequency standard

S. Bagayev, V. Denisov, A. Dychkov, N. Koliada, B. Nyushkov, V. Pivtsov, and S. Farnosov
Institute of laser physics, SB RAS, 630090 Novosibirsk, Russia
E-mail: clock@laser.nsc.ru

Here we report an experimental study aimed at precise stabilization of a fiber-based octave-spanning optical frequency comb to Nd(Yb):YAG/I_2 optical standards. The comb was generated by means of a home-made femtosecond erbium fiber laser and a hybrid highly-nonlinear fiber [1, 2]. Optical phase-locked loops (OPLLs) were applied to stabilize the comb teeth to the optical standard as depicted in Fig.1. The corresponding short-wavelength (λ_1~1 μm) and frequency-doubled long-wavelength (λ_2~2 μm) teeth were locked to the fundamental laser wavelength (λ_{os}~1 μm) of the optical standard.

To ensure reliable and tight locking of the relatively noisy optical frequency comb to the optical standard, the used OPLLs have to be fast enough and feature large-bandwidth noise suppression. On this basis we designed feedback loops which incorporate a miniature intracavity electro-optic phase modulator [3] and a fiber-coupled acousto-optic frequency modulator (Brimrose). These elements allowed fast frequency control and implementation of OPPLs with bandwidths of ~200 kHz and ~100 kHz for the short-wavelength and long-wavelength sides of the optical frequency comb, respectively. In order to extend the effective dynamic range of the OPPLs and provide continuous long-term stabilization of the comb, the fast frequency controls were assisted by the relatively slow controls: PZT-based cavity length control, pump power control, and temperature control.

To the best of our knowledge, such combination of controls including a fiber-coupled acousto-optic frequency modulator was not yet used for stabilization in the early experimental and commercial frequency combs generated by femtosecond erbium fiber laser systems. Therefore, stabilization performance in those systems was limited by the relatively slow pump power control of erbium fiber lasers. The millisecond life time of the upper laser level limits the bandwidth of the corresponding laser frequency control via population inversion variation to a value less than 10 kHz [4].

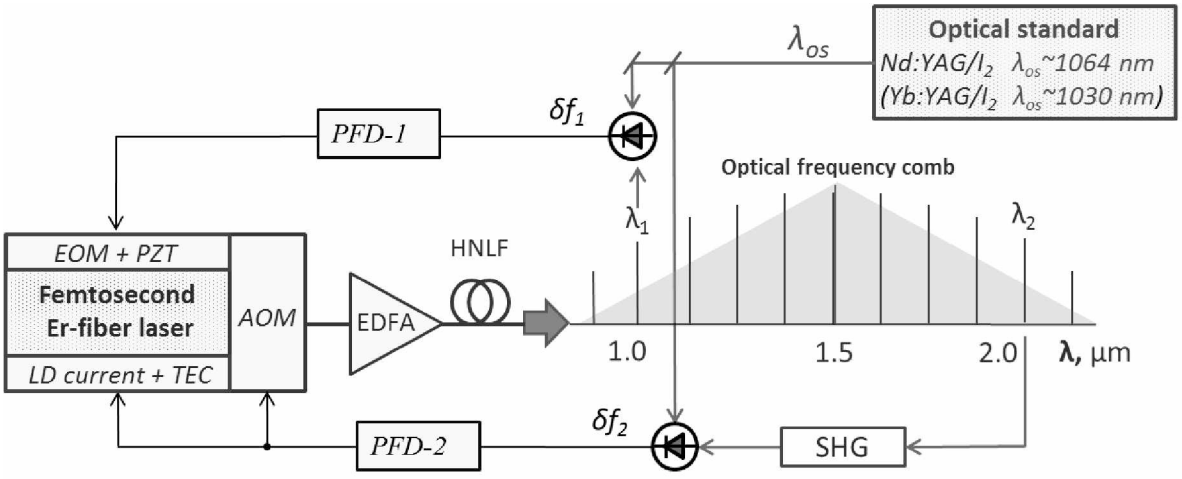

Fig. 1 Implemented scheme of precise stabilization of a fiber-based optical frequency comb to an iodine optical frequency standard: EOM – electro-optic phase modulator, PZT – piezoelectric translator, AOM – acusto-optic frequency modulator, LD – laser diode, TEC - thermoelectric converter, EDFA- erbium-doped fiber amplifier, HNLF – highly-nonlinear fiber, PFD-1,2 – phase-frequency detectors, SHG – second harmonic generation.

The implemented OPPL design has ensured tight locking of the optical frequency comb to the reference optical standard. It features millihertz-scale residual random deviations of the corresponding comb teeth against the optical standard frequency (Fig.2).

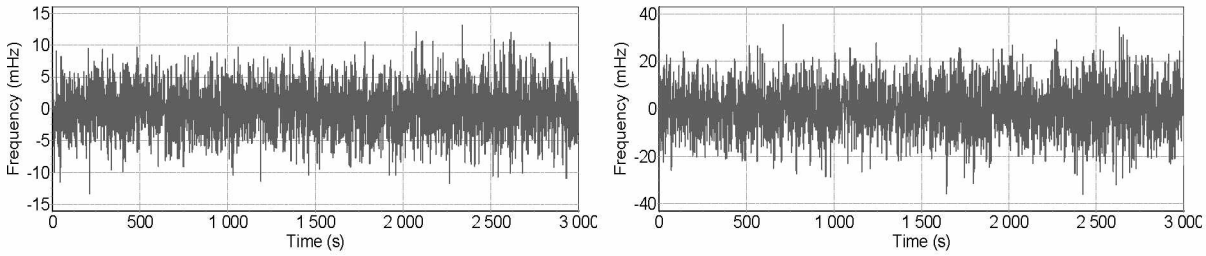

Fig. 2 Residual random frequency deviations of the corresponding comb teeth against the optical standard frequency. The left graph represents measurements of the beat frequency (δf_1=20 MHz) obtained with the short-wavelength comb tooth at λ_1~1 μm. The right graph represents measurements of the beat frequency (δf_2=10 MHz) obtained with the frequency-doubled long-wavelength comb tooth at λ_2~2μm.

The reference standard is based on a frequency-doubled Nd:YAG (Yb:YAG) laser stabilized to a narrow nonlinear saturated absorption resonance in the hyperfine structure of molecular iodine. Its long-term frequency instability was measured to be as low as ~10^{-15} [5]. Fig.3 represents an added instability which is additive to the instability of the optical standard. It characterizes performance of the achieved locking of the frequency comb to the frequency standard. Data for the Allan deviation calculation were obtained using an original experimental arrangement which allows direct measurement of a radio frequency f_{rf} defined as:

$$f_{rf} = 2\Delta f_{comb} - f_{Nd:YAG},$$

where $\Delta f_{comb} = f_{\lambda 1} - f_{\lambda 2} \approx 1{,}4 \cdot 10^{14}$ *Hz* is the octave width of the optical frequency comb, and $f_{Nd:YAG} \approx 2{,}8 \cdot 10^{14}$ *Hz* is the fundamental frequency of the optical standard. Thus instability of the measured frequency f_{rf} was attributed to the residual random deviations of the doubled comb width ($2\Delta f_{comb}$) against the optical standard frequency ($f_{Nd:YAG}$).

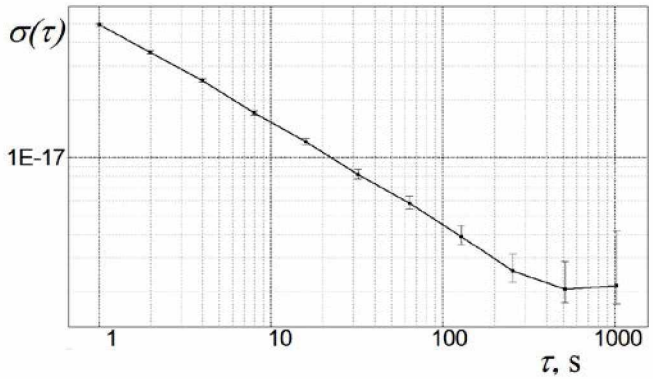

Fig. 3 Allan deviation calculated for residual random deviations of the doubled comb width ($2\Delta f_{comb}$) against the optical standard frequency ($f_{Nd:YAG}$).

Thus measurement-based evaluation of the instability added by residual phase errors of the OPPLs proves the capability of the implemented optical frequency comb to transfer the stability of the iodine-based optical frequency standards across a huge wavelength range (~0.5 to 2.1 μm) without serious degradation. The strict equidistance of the comb optical frequencies, whose spacing is equal to a certain radio frequency, allows also transfer of the optical frequency stability to a radio-frequency band and implementation of optical clocks. Important advantages of the presented fiber-based frequency comb over classical solid-state femtosecond systems are compactness and low power consumption that makes possible implementation of mobile metrological devices on the comb basis.

References

[1] I.I. Korel, B.N. Nyushkov, V.I. Denisov et al, Laser Phys. **24**, 074012 (2014).
[2] V.S. Pivtsov, B.N. Nyushkov, I.I. Korel et al., Quantum Electron. **44**, 507 (2014).
[3] B.N. Nyushkov, V.S. Pivtsov, N.A. Koliada et al., Quantum Electron. **45**, 486 (2015).
[4] N. Haverkamp, H. Hundertmark, C. Fallnich et al., Appl. Phys. B **78,** 321 (2004).
[5] V.I. Denisov, S.M. Ignatovich, N.L. Kvashnin et al., Quantum Electron.**46**, 464 (2016).

Recent developments in femtosecond fibre lasers

J.D. Harvey[1,2], P. G. Bowen[1], J. Kho[1], N. G. R. Broderick[1], M. Erkintalo[1] and R. Provo[2]
[1]*Dodd-Walls Centre for Photonic and Quantum Technologies, Department of Physics, The University of Auckland, Private Bag 92019 Auckland New Zealand*
[2]*Southern Photonics, Level 4, 49 Symonds St Auckland 1010 New Zealand*
E-mail: j.harvey@auckland.ac.nz

In the last decade, research in high energy, short duration, pulsed fibre laser systems has yielded significant advances that have allowed fibre laser systems to compete with more established solid state lasers in a range of applications[1,2]. Important features of femtosecond lasers in all applications include high pulse energy and ultrashort pulse duration. Other design objectives concern beam quality, wall plug efficiency, thermal stability and long term reliability. Early ultrafast fibre laser systems took advantage of the propagation of solitons in optical fibres in the anomalous dispersion regime using Erbium doped fibres, but the energy of a fundamental soliton is fixed by the dispersion and nonlinearity of the fibre, and generally limited to sub nanojoule level. These pulses can however, be stretched using linear propagation in a fibre or by using a grating, and then further amplified using chirped pulse amplification.

More recently it has been possible to take advantage of the greater efficiency of Ytterbium doped optical fibre amplifiers, which operate in the normal dispersion regime, where soliton formation is precluded. These "all normal dispersion" (ANDi) fibre lasers produce linearly chirped pulses which are ideally suited to further amplification using Ytterbium doped chirped fibre amplifiers. In addition these lasers can operate at low repetition rates (a few MHz) and produce pulses with tens of nanojoules of pulse energy, thus simplifying the subsequent amplification stages.

Most ANDi lasers are mode locked using one of two mechanisms: either by the use of a semiconductor saturable absorber mirror (SESAM) or using the phenomenon of nonlinear polarization evolution in a section of optical fibre. Both of these techniques can exhibit long term stability issues, and for industrial application a totally reliable seed oscillator is needed.

We have recently demonstrated robust, passively mode-locked fibre laser designs using nonlinear amplifying loop mirrors (NALMs) for mode-locking, which allows for integrated all-fibre, all-polarisation maintaining (PM) cavity configurations, which are inherently stable against environmental perturbations. This laser system is self starting, producing linearly chirped pulses with an operating bandwidth of several nanometers.

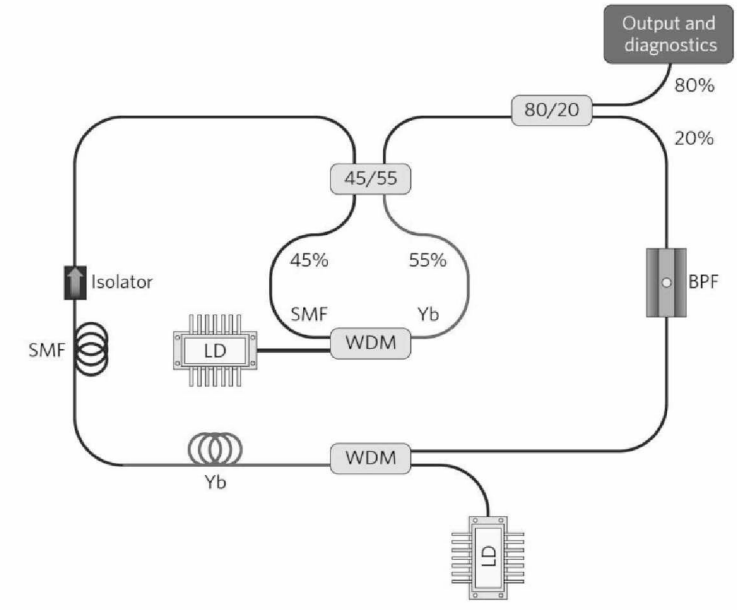

Fig. 1 Schematic diagram of laser cavity using a nonlinear amplifying loop mirror

We report on our latest achievements in this area focussing on the excellent long term stability and adaptability of these sources. Fig.1 shows our basic design fabricated using all-normal dispersion fibres and all-PM fibres making for an environmentally robust system. These laser systems have been operated at a range of wavelengths between 1030nm and 1060nm, and at a range of repetition rates from as low as 500kHz to 15MHz. The fundamental property of these lasers is that the NALM preferentially transmits rectangular pulses with a constant intensity, which develop within the laser with a linear chirp. Thus the energy of the output pulses scales inversely with the repetition rate. The low repetition rate systems operate at over 10nJ per pulse, producing pulses with an excellent linear chirp which can be readily compressed after further amplification using a grating compressor.

Using a short length of normal dispersion erbium doped gain fibre and dispersion shifted fibres, it is even possible to operate this laser in the C band, and this result emphasises the flexibility of the design and highlights what can be achieved using an all-fibre approach. Progress in amplifying these pulses to multi Watt levels will also be discussed.

References

[1] W. Shiner, Nature Photonics **4**, 29 (2010).
[2] M.E. Fermann and I. Hartl ,Nature Photonics **7**, 868 (2013).
[3] C. Aguergaray, R. Hawker, A. Runge, and M. Erkintalo, and N.G.R. Broderick, Applied Phys. Lett. **103**, 121111 (2013).

21st century mid-infrared biomedical spectroscopy: conventional FTIR vs Field Resolved

A. Apolonski and BIRD Project[1,2]

[1]*Ludwig Maximilian University of Munich, Germany*
[2]*Max Planck Institute of Quantum Optics, Garching, Germany*

E-mail: apolonskiy@lmu.de

The status of BIRD (Broadband infrared medical diagnostics) project will be presented. It includes a) protocols (sample collection and storage), b) results with a conventional Fourier spectrometer (FTIR, [1]) in the *fingerprint* range 6-11 μm for blood serum and exhaled air as well as tests of a laser spectrometer based on Field Resolved Spectroscopy (FRS). A mid-infrared range is chosen because of fundamental vibrational absorption bands of biological probes.

Broadband mid-infrared laser oscillators in the range 3-20 μm do not exist. Therefore, several nonlinear schemes based on fibers [2], solids [3] as well OPOs [4] were recently developed to cover this range. Nevertheless, up to date none of them exceeds the spectrum bandwidth of a thermal source (globar) used in mid-infrared FTIR conventional spectrometers.

Our FRS spectrometer is based on a thin-disk Kerr-lens Yb:YAG oscillator centered at 1,03 μm [5] and a difference generation conversion scheme that transfers infrared to mid-infrared supercontinuum centered at 10 μm [6]. 20-fs infrared pulses after the broadening-compression stage become transferred into 70-fs pulses (coherent supercontinuum 7 to 18 μm) in a nonlinear crystal [6]. An essential part of the spectrometer is a FRS scheme used before in THz spectroscopy that allowed us to achieve both high sensitivity and high dynamic range. The FRS detection approach leads to the dynamic range at least 10^7 versus 10^4 achieved for FTIR, and the *detection sensitivity* for exhaled air and blood serum at least 10 ppb (part-per-billion of relative volume concentration) approaching that of FTIR. In general, laser-based spectrometers hold the promise for higher *detection sensitivity* because of higher flux of mid-infrared radiation. It is worth mentioning that chromatography and mass spectroscopy demonstrate comparable sensitivity suffering in the same time from well-known limitations.

High *detection sensitivity* is an essential part of a concept of early disease diagnosis. The concept relies on effective therapy modifying metabolic processes in the body in the direction of the norm specific for each individual. The concept implies that the earlier the deviation from the norm is found the higher the chance for successful treatment. The targeting *detection sensitivity* lies in the ppt range. Other critical statistical parameters of the concept are *sensitivity of the technique* (SeT) defining the proportion of correctly identified sick individuals and *specificity of the technique* (SpT) defining the ability of the technique to correctly identify individuals without the disease.

For FTIR spectrometer, we started with the protocol development for blood serum probes, continued then with the development of pre- and post-processing data analysis. As the next step we used the protocols and analysis software package for experiments with probes of three groups of individuals: healthy, bronchitis and lung cancer. For these statistically limited groups (up to 30 individuals per group), SeT and SpT approached 85 and 90%, respectively. First FRS calibration tests of the same probes as we used for FTIR will be presented and discussed.

References

[1] "Fourier transform infrared spectrometry", ed.: P. R. Griffiths and J. A. de Haseth, 2nd edition, Wiley (2007).
[2] C. R. Petersen et al., Nat. Phot. **8**, 830 (2014); Yi Yu et al., Opt. Lett. **40**, 1081 (2015).
[3] A. A. Lanin et al., Opt. Lett., **40**, 974 (2015).
[4] N. Leindecker et al., Opt. Exp. **20**, 7046 (2012).
[5] O. Pronin et al., Nat. Com. **6**, 6998 (2015).
[6] I. Pupeza et al. Nat. Phot. **9**, 721 (2015).

Laser gyroscopes and their applications in fundamental physics, metrology and seismology

J. Belfi
INFN section of Pisa, largo Pontecorvo 3, Pisa, Italy
E-mail: belfi@pi.infn.it

He-Ne ring lasers are extremely sensitive devices for inertial rotation measurements. Such devices find applications in different fields of technology and science [1], from inertial navigation to structural engineering, from metrology to geophysics and seismology. Their resolution depends on the optical cavity size and its geometrical stability. The state of the art is represented by the large frame "G" ring-laser operating at the Geodetic Observatory of Wettzell (Germany). It is a square monolithic zerodur cavity with a side length of 4m. In the last years "G" performed a continuous monitoring of the Earth rotation obtaining very exciting results in the field of geophysics and geodesy [2]. The resolution of "G" is approaching the requirements for the detection of the small shift on the Earth's rotation given by its gravito-magnetic field. According to the Einstein's General Relativity, this effect, also known as Lense Thirring effect, is about 1 part in 10^9 the Earth rotation rate itself.

I will report about the experiments conducted by the Italian Institute of Nuclear Physics (INFN) aiming to demonstrate the feasibility of a large frame detector for ground-based measurement of the Earth's gravito-magnetic field by means of actively controlled ring laser arrays [3]. Presently, three square-cavity ring laser gyroscopes are under development: GINGERino, GP2 and G-LAS.

GINGERino is shown in Fig. 1. It is 3.6 m in side and is located inside the deep underground INFN laboratories of the GranSasso; its aim is to characterize the underground rotational seismic noise in view of the installation of a larger gyroscope array for fundamental Physics tests. The present measured resolution is 30 prad/s in 500 s of integration time. This corresponds to a precision of 0.6 ppm on the Earth rotation rate. GINGERino has been able to detect the tiny ground rotations (around the vertical direction) induced by the passage of several teleseismic waves in the frequency range between (1 mHz and 1 Hz) [4]. Standard seismometric equipment has been installed on the laser cavity frame by INGV (Italian National institute of Geophysics and Volcanology). This allows us to perform comparative analysis of rotations and translations and to have an insight on the surface wave propagation properties.

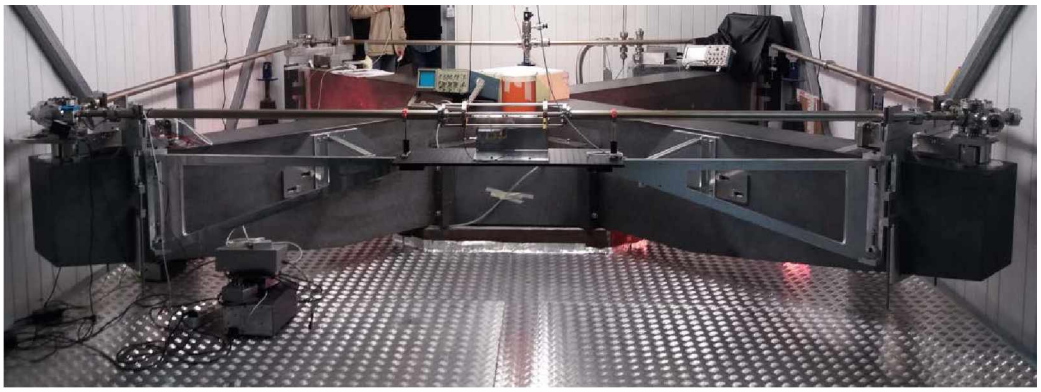

Fig. 1 GINGERino ring laser gyroscope inside the deep underground laboratory of LNGS. Two broadband seismometers and a nano-tiltmeter are installed on top of the central structure of the granite frame supporting the optical cavity.

GP2 is shown in Fig. 2. It is 1.6 m in side and is located in Pisa, by the INFN laboratories. Its plane is oriented perpendicularly to the Earth rotation axis, in order to have a maximum bias for the Sagnac effect. The aim of this setup is to study and optimize the control of the ring laser cavity geometry. GP2 optical cavity is equipped with a dedicated diagnostic system, based on laser interferometry, for the control of the cavity deformations down to the sub-nanometric level. Since the effects of the environmental parameters on the ring laser beam path stability are strongly reduced if the two diagonals length are constrained to a constant value, we decided to exploit the two Fabry-

Pérot resonators formed by the opposite mirrors of the ring cavity. In this way one can determine very precisely the distances between opposite mirrors (diagonal lengths) of the square and lock them to the frequency of a common externally-injected reference laser. The experimental technique [5], based on a triple phase- modulation scheme, and the present status of the stabilization system will be presented.

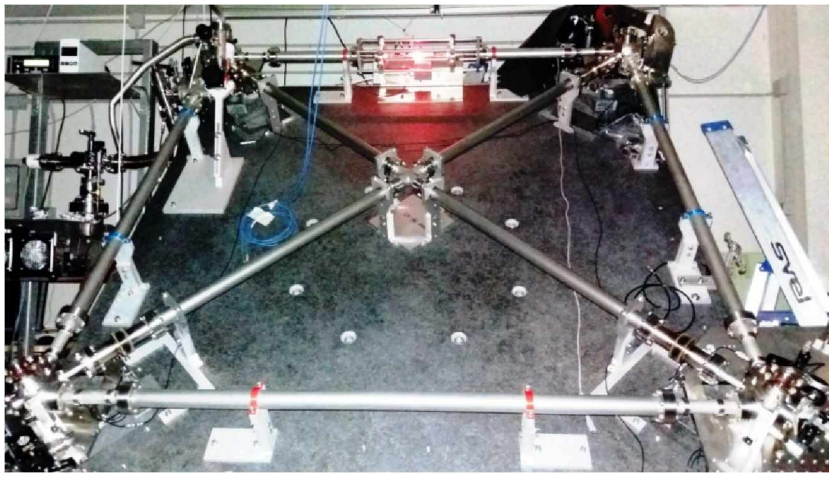

Fig. 2 GP2 setup. Laser excitation is obtained with a He-Ne plasma produced with a RF discharge in a small region in the middle of one side. The vacuum chamber contains the optical path of the ring and of the two diagonal linear resonators.

G-LAS (Fig. 3) is a new kind of dynamic laser goniometer [6], being developed by a collaboration between INRIM (Italian Institute of Metrology) and INFN. The main purpose of this project is the implementation of an extremely accurate transportable rotational standard. Further applications of this device are connected also to the measurements of seismic rotational effects and to the demonstration of a self-calibration concept of the gyroscope for geodetic and relativistic experiments. The target accuracy is 10 nrad, being the accuracy of the most precise angular encoders at the level of some 100 nrad. Our key idea is to setup a rotating square non-monolithic cavity of about 0.5 m in side making use of the last generation dielectric super-mirrors employed in the much larger gyroscopes for geodetic and geophysical applications. I will discuss the main issues and proposed strategies.

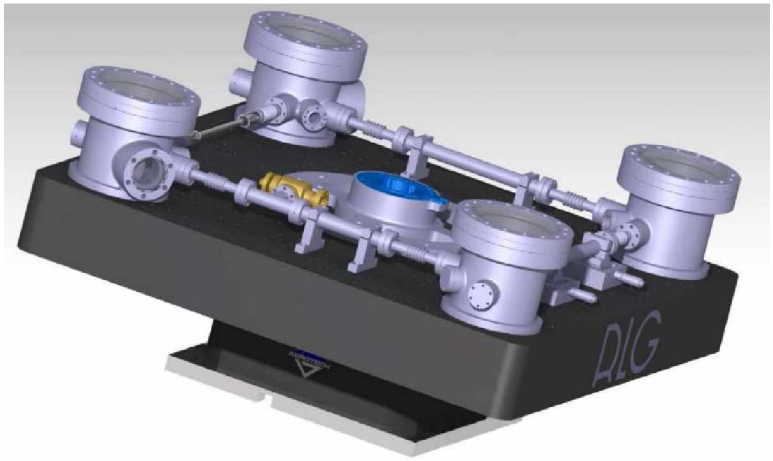

Fig. 3 G-LAS prototype design. The supporting frame is in carbon fiber and the four corner boxes composing the ring laser in aluminum. The ring laser goniometer is attached onto a rotating platform.

References

[1] K.U. Schreiber and J.-P.R. Wells, Rev. Sci. Instrum. **84**, 041101 (2013)
[2] K.U. Schreiber et al., Phys. Rev. Lett. **107**, 173904 (2011)
[3] F. Bosi et al., Phys. Rev. D **84**, 122002 (2011)
[4] A. Simonelli, Annals of Geophysics, **59**, Fast Track 4, (2016)
[5] J. Belfi et al., Classical and Quantum Gravity **31**, 225003 (2014)
[6] Yu. Filatov, D.P. Loukianov, R. Probst, Metrologia **34**, 343 (1997).

LECTURE
Sagnac effect and gyroscopes

Nicolò Beverini
Dipartimento di Fisica, Università di Pisa and INFN, sezione di Pisa, Italy
Email: beverini@df.unipi.it

George Sagnac in 1913 showed that light traveling along a closed-ring path in opposite directions allows one to detect the rotational speed of the ring structure with respect to inertial space. Michelson was able a few years later to measure the Earth rotation rate with a very large interferometer with some hundredth meter of size. Using classical optical source, however, the observation of the effect was a quite hard experimental task.

The invention of laser changed completely the perspective. First demonstration of laser gyroscopes based on Sagnac effect was published yet in 1963. This was the beginning of a strong technological effort. Since a laser gyroscope has no moving mechanical part and, differently from mechanical gyroscopes, is in principles completely not sensitive to translational motion. It was then the ideal solution for inertial navigation.

Starting with the last years of 20th century, thanks to the great improvement in mirror manufactory, large frame ring lasers with very high sensitivity has been built. Presently, the best performing one is the "G-ring" in Wettzell (Bavaria, Germany). It is currently able to measure the Earth rotation rate with a resolution approaching 10^{-9}, paving the way to application in geodesy, in geophysics and seismology.

The lecture will review the present state of the art of ring laser technology and its applications. In particular, I will discuss the INFN GINGER project, which has the aim to build in the underground Gran Sasso laboratories a ring apparatus able to attain the sensitivity necessary to observe of very thin effect drag effect on the metric foreseen by General Relativity that is generated by the rotating Earth mass.

Properties of aqueous solutions in THz frequency range

O. Cherkasova[1], M. Nazarov[2,3], A. Shkurinov[2,4]
[1]*Institute of Laser Physics of SB RAS, Novosibirsk, 630090 Russia*
[2]*Crystallography and Photonics Federal Research Center, RAS, Moscow, Russia*
[3]*Kurchatov Institute National Research Center, pl. akad. Kurchatova 1, Moscow 123182, Russia*
[4]*Lomonosov Moscow State University, Moscow, 119991, Russia*
E-mail: o.p.cherkasova@gmail.com

THz spectroscopy is a unique tool that can be used for analysis of solutions because changes in relative proportions of free and bound water and in relaxation times for either of these states can all be observed in THz range. The THz time-domain spectroscopy (THz-TDS) has been used for measuring of bovine serum albumin (BSA) and glucose solutions. We also analyzed the change in the THz absorption during incubation of BSA with glucose. This is a model experiment for the study of the process of protein glycation. Protein glycation is accelerated under hyperglycemic conditions resulting in loss of the structure and biological functions of proteins.

To detect small-scale changes in solutions we have performed measurements using both transmission in 0.5 mm cell and attenuated total internal reflection (ATR). By combining the results obtained in both configurations, the reliable range of the obtained complex dielectric function spectrum can be considerably broadened (0.07-2.7 THz).

The THz time-domain spectrometer used in the study was described previously [1]. It is known that the biological solutions spectral shape is mainly determined by Debye gamma-relaxation (or "slow" relaxation) of water molecules [2, 3], thus we should move to as low frequencies as possible. We analyzed the reasons for the THz transmission changes of studied solutions comparing experimental spectra to the model dielectric function of water. The insertion of glucose into water leads only to an increase of relaxation time τ_1 of the slow Debye process of this solution. This simple approach describes observed spectral changes in a broad frequency range and for a number of concentrations from 10 mM to saturated solution. The obtained experimental and model spectra of the dielectric function for the aqueous solution of glucose at a concentration of 4.7 M are shown in Fig. 1.

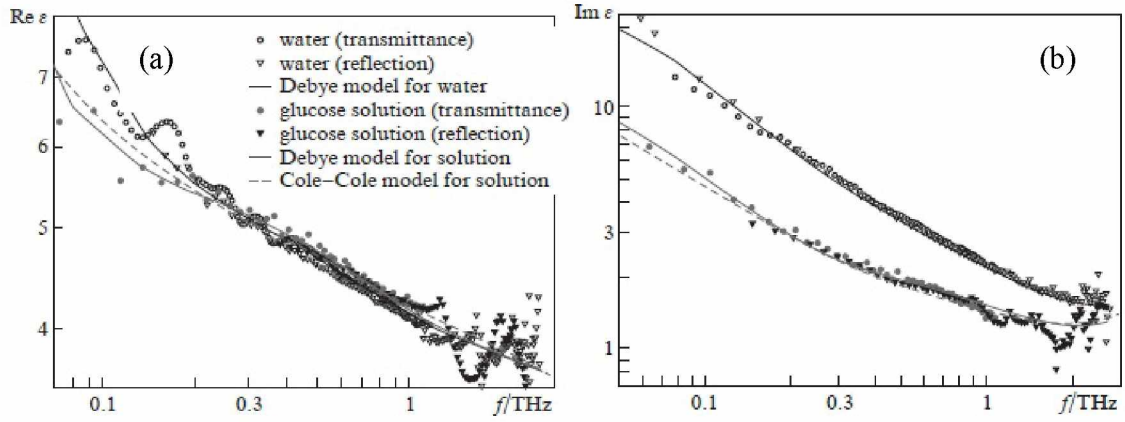

Fig. 1 Spectra of (a) real and (b) imaginary parts of the dielectric function ε(f) for a saturated aqueous solution of D-glucose and water at T = 22 °C. Points show combined experimental data on the transmittance and reflectance spectroscopy, solid curves are the Debye models, and the dashed curve is the Cole – Cole model.

Of course, the real and imaginary parts of ε(f) can be accurately approximated in the case of several varying parameters. However, we perform fitting simultaneously for both parts of ε(f), which complicates obtaining an exact agreement between the model and experimental results in a wide

frequency range. Thus, in the case of the glucose solution, the calculation results for both models (the Cole – Cole model and the two-component Debye model) are equally consistent with the measurement results. We believe that, instead of complicating the models used for the analysis of experimental data, it is necessary to improve the accuracy and repeatability of experiments and to expand the spectral range of a measurement.

We have found that increasing of BSA concentration in the solution results in a decrease of the amplitude $\Delta\varepsilon_1$ of the slow Debye relaxation process (Fig. 2). It can be seen that the dependence of $\Delta\varepsilon_1$ from concentration of BSA in solution is not linear and has a bend at 30 mg/ml. We have not confirmed anomalous changes observed in papers [4, 5] at low concentrations and at low frequencies.

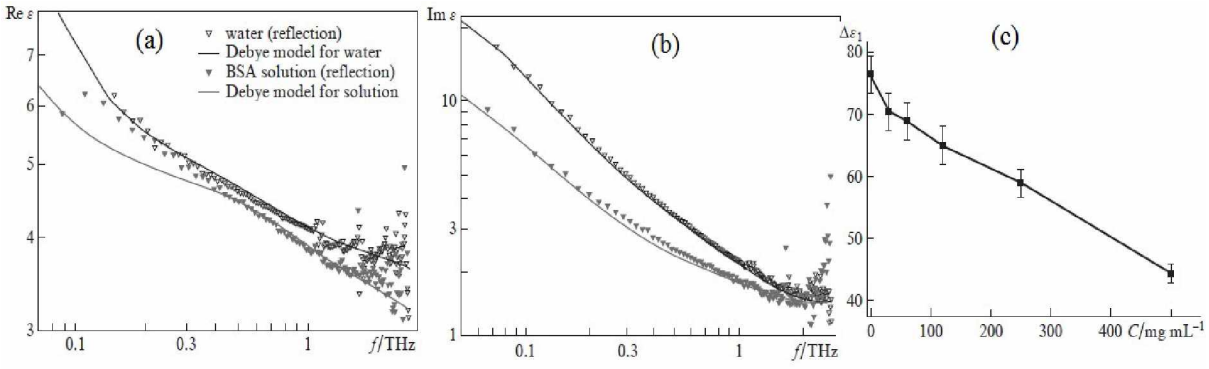

Fig. 2 Spectra of (a) real and (b) imaginary parts of the dielectric function ε(f) for an aqueous solution of BSA and water at T = 22 °C. Points show the ATR experimental data and solid curves are the Debye model; (c) the dependence of the parameter $\Delta\varepsilon_1$, found as a result of approximation from BSA concentration in water.

Of practical interest is not a study of aqueous solutions of proteins or sugars separately, but a study of their mixtures. It is known that a high glucose level in human blood leads to glycation of proteins. The BSA (50 mg·mL^{-1}) was incubated in a phosphate buffer (50 mM, pH 7.4) in the presence of glucose (0.5 M) for 96 hours at T = 47 °C. It was found that value of THz absorption coefficient of glycated albumin solution varies considerably during incubation. At the early stage of incubation, the amplitude of the first Debye term $\Delta\varepsilon_1$ was 88% relative to the value for pure water. After 96 hours of incubation BSA with sugar the amplitude of the first Debye term $\Delta\varepsilon_1$ was 92% relative to that for pure water [6].

So, dielectric properties of BSA and glucose solutions were thoroughly measured at 0.07-2.7 THz. It was found that the most significant is the reduction $\Delta\varepsilon_1$ (or increase τ_1) of the slow Debye relaxation process with increasing concentrations of solute. Glycation of BSA results in a change the parameters of slow Debye relaxation. During incubation of BSA with sugars the incubation mixture contains a significantly smaller part of sugar molecules bound with water molecules and the amount of free water molecules is increased at the final stage of incubation.

This work has been supported by RFBR (grant № 14-02-00846, № 14-02-00979 and № 16-52-00222).

References

[1] M.M. Nazarov, A.P. Shkurinov, E.A. Kuleshov, V.V. Tuchin, Quantum Electronics, **38**, 647 (2008).
[2] O.P. Cherkasova, M.M. Nazarov, A.A. Angeluts, A.P. Shkurinov, Optics and Spectroscopy, **120** (1), 50 (2016).
[3] M.M. Nazarov, O.P. Cherkasova, A.P. Shkurinov, Quantum Electronics, **46** (6), 488 (2016).
[4] J.W. Bye, S. Meliga., D. Ferachou et al., J. Phys. Chem. A, **118** (1), 883 (2014).
[5] O. Sushko, R. Dubrovka, R.S. Donnan, The Journal of Chemical Physics, **142**, 055101-1 (2015).
[6] O.P. Cherkasova, M.M. Nazarov, A.P. Shkurinov, Proc. SPIE **9917**, 991706 (2016).

Characterizing and imaging magnetic nanoparticles by optical magnetometry

S. Colombo[1], V. Dolgovskiy[1], Z. D. Grujić[1], V. Lebedev[1], A. Weis[1], J. Zhang[1]
[1]*Physics Department, University of Fribourg, Chemin du Musée 3, 1700 Fribourg, Switzerland*
E-mail: antoine.weis@unifr.ch

The deployment of magnetic nanoparticles (MNPs) for biomedical applications has steadily increased in the past decade [1]. The use of MNPs as MRI contrast agents and for hyperthermia is well investigated. More importantly, functionalized MNPs injected into the blood stream have a high potential for targeted drug delivery to biological entities, such as tumors or organs. In view of clinical applications, most MNP-based methods require quantitative methods for monitoring the spatial MNP distribution in the biological tissue. Magnetorelaxation (MRX, [7]) imaging and Magnetic Particle Imaging (MPI, [8]) are two imaging modalities that are actively being developed towards this goal. There is also an evident need for measuring and optimizing the MNP properties, in particular their size distribution, in view of obtaining the highest possible MNP detection sensitivity with the lowest possible quantity of injected MNPs.

Imaging and characterization both rely on the MNPs' superparamagnetic character which relates to the fact that MNPs of sufficiently small size are single ferromagnetic domains. As such, the *M(H)* dependence of an ensemble of MNPs can be represented by a Langevin function

$$L\left(x=\frac{H}{H_k}\right)=M(x)/M_s=\coth x-\frac{1}{x} \qquad \text{with the saturation field} \qquad H_k=\frac{k_B T}{\mu_0 M_S V}, \tag{1}$$

where M_s is the saturation magnetization, and V the MNP's core volume. The characteristic features of this magnetization behavior are (a) the absence of hysteresis and (b) the relatively modest value (few mT) of the saturation field $B_k=\mu_0 H_k$.

All applications mentioned above rely on magnetizing the MNP located, say at $\vec{r}=0$, by a magnetic excitation field $\vec{H}(0)$, and detecting the magnetic flux density $\vec{B}(\vec{r}) \propto \vec{M}(0)$ produced by the sample magnetization $\vec{M}(0)$ with a magnetometer located at $\vec{r}$. In most conventional magnetic MNP experiments one deploys excitation fields $\vec{H}(\vec{r}=0,t)$ that harmonically oscillate at ω_{exc}, in combination with detection of $\vec{B}(\vec{r},t)$, or rather $d\vec{B}(\vec{r},t)/dt$ by a pick-up loop based on Faraday's induction law. Because of the time-derivative, the efficiency of pick-up detection decreases at low frequencies like ω_{exc}^{-1}. We strongly believe that atomic magnetometers (AM) present an interesting alternative to the pick-up loop detection of MNP signals, since their performance does not degrade with decreasing frequency, thus allowing efficient low-frequency, and even DC detection. Here we review several proof-of-principle experiments that we have performed along these lines.

Magneto-relaxation (MRX): Magnetized MNPs, when immobilized (e.g., attached to a cell surface, or embedded in a matrix/tissue) have Néel relaxation times in the seconds to minutes range, depending on the particles' size. This property is used to discriminate signals from blocked MNPs against signals produced by MNPs in body fluids. MRX consists in magnetizing the particles by a field $\vec{H}$ of several mT for a given amount of time, and then monitoring the decaying magnetic flux density's magnitude $B(t)$, after $\vec{H}$ has been switched off. In [2] we have shown that two AMs (operated as a gradiometer) can be used to monitor $B(t)$ decaying from a few nT down to a few pT over two minutes. In that paper we have also revised the functional dependence of the MRX-decay, which in a simplified form is given by $B(t) \propto \ln(1+\tau/t)$, to compare relaxation curves from various samples having average MNP particle radii ranging from 14 to 21 nm. Fits of the results have further allowed us extracting the saturation magnetization M_s and the so-called magnetic anisotropy constant K, and to study the dependence of M_s and K on particle size.

Magnetic source imaging camera (MSIC): Conventional MRX does not yield direct information about the MNP's spatial distribution. The latter can be assessed by simultaneously recording MRX signals with an AM array. Based on the methods described by Fescenko and Weis [3], we are in the process of developing a magnetic source imaging camera (MSIC), i.e., a device yielding a direct

visualization of the two-dimensional spatial distribution of a specific component of the magnetic field vector. The MSIC principle is sketched in Fig. 1.a. A sheet of circularly-polarized resonant laser light pumps a layer of Cs atoms (contained with a buffer gas in a cubic vapor cell) into a dark state that is stabilized by a magnetic field $\vec{B}_0$. A CCD camera records fluorescence from that layer. Any field $\delta\vec{B}_{MNP}(\vec{r})$ produced by the object of interest (here a magnetized MNP sample) adds to $\vec{B}_0$, thereby changing the total field – and hence the spin polarization by virtue of the ground state Hanle effect – at each position $(\vec{r})$ in the sheet. Since the fluorescence yield depends on the local degree and orientation of the spin polarization, the fluorescence from each point changes in a specific manner as discussed in [3]. Figure 1.b shows CCD frames that represents the fluorescence changes (proportional do δB_H) induced by magnetized MNPs [4] and the sample magnetization's decay (MRX signal).

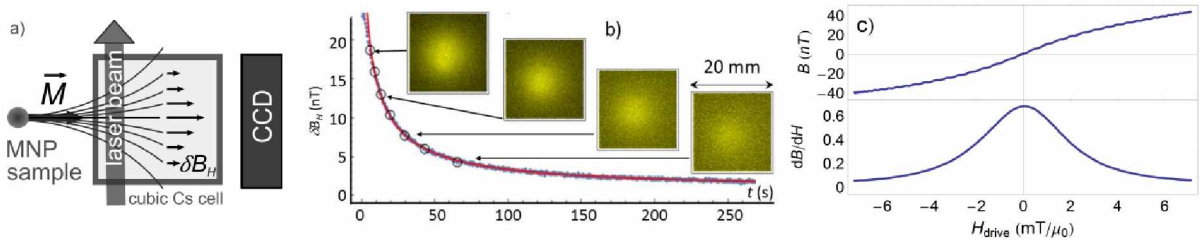

Fig. 1 a): MSIC principle; b) CCD frame representing fluorescence induced by dried MNPs and MRX decay of integrated signal; c) Magnetization curve and its derivative of water-suspended MNP sample.

AC susceptometry (ACS) and Magnetic Particle Imaging (MPI): In contrast to blocked MNPs, the magnetization of MNPs suspended in a fluid undergoes a very fast (microsecond or less) Brown relaxation through rotational diffusion. This fact prevents their detection by MRX, but allows the particles to react quasi-instantaneously to oscillating drive fields $\vec{H}_{drive}(t)$ producing a related response $\vec{B}_{MNP}(t)$. Because of the nonlinear $B_{MNP}(H_{drive}) \propto M_{MNP}(H_{drive})$ relation given by Eq. (1), a monochromatic drive produces odd overtones in the Fourier spectrum of the $B_{MNP}(t)$ response. We have developed AM-based methods [5] allowing the direct recording (Fig. 1.c) of the $B_{MNP}(H_{drive})$ dependence and its derivative $dB_{MNP}/dH_{drive}(H_{drive})$. The method can be applied to MNP samples containing down to 1 μg of iron and can be used to extract MNP size distributions [6]. The fact that the dB_{MNP}/dH_{drive} signal peaks at H_{drive}=0 can be used for measuring spatial MNP distributions. Suppose that a bulk sample containing an inhomogeneous MNP distribution is exposed to an inhomogeneous drive field, such that H_{drive}=0 (Fig. 1.c) at one specific point (zero field point, ZFP) in the sample. Suppose further that the H_{drive} field in other parts of the sample is sufficiently strong to saturate the MNP magnetization at those points. The magnetometer will then detect dB_{MNP}/dH_{drive} signals only from MNPs located at or near the ZFP. A record of the magnetometer signal while scanning the ZFP position through the bulk will thus yield information of the spatial MNP distribution. The method, deployed so far only with pick-up coil detection is known as X-space variant [7] of MPI. MPI was invented a decade ago by researchers at Philips [8]. Currently, both X-space and frequency-space implementations of MPI deploy drive fields oscillating at 25 kHz, together with pick-up coil detection. The high frequency at which the high power drive field oscillates leads to concerns regarding heating and peripheral nerve stimulation of the patients. We believe that AM-detection offers a promising perspective for developing a low-frequency MPI-scanner that may circumvent those issues.

Work funded by grants 200021/160128 and 200021/149542 of Swiss National Science Foundation.

References

[1] S.-H. Huang and R.-S. Juang, J. Nanopart. Res. **13,** 4411-4430 (2011).
[2] V. Dolgovskiy, V. Lebedev, S. Colombo et al., J. Mag. Mag. Mat. **379**, 137-150 (2015).
[3] I. Fescenko and A. Weis, J. Phys. D: Appl. Phys. **47**, 235001 (2014).
[4] V. Dolgovskiy, I. Fescenko, N. Sekiguchi et al., submitted to Appl. Phys. Lett. (2016).
[5] S. Colombo, V. Lebedev, Z. D. Grujic et al., IJMPI **2**, 1606002 (2016).
[6] S. Colombo, V. Lebedev, Z. D. Grujic et al., IJMPI **2**, 1604001 (2016).
[7] P.W. Goodwill, E. U. Saritas, L. R. Croft et al., Adv.Mater. **24**, 3870 (2012).
[8] B. Gleich and J. Weizenecker, Nature **435**, 1214 (2005).

Detection of physiological signals using FBG sensing techniques

D. Jia, H. Zhang, T. Liu
Tianjin University, China
E-mail: dagongjia@tju.edu.cn

We present the system that can be used to monitor the variation of physiological signals base on FBG sensor.

Fiber-optic pressure and temperature sensor

J. Jiang, S. Wang, K. Liu, J. Yin, F. Wu, W. Zhang and T. Liu
College of Precision Instrument & Optoelectronics Engineering, Institute of Optical Fiber Sensing of Tianjin University, Key Laboratory of Optoelectronics Information Technology, MEC, Tianjin 300072, China
E-mail: jiangjfjxu@tju.edu.cn

Pressure and temperature are important monitoring parameters for many industry fields, such as oil, petrochemical, civil engineering, ocean, aviation, space and so on. Fiber-optic sensor have advantage of compact structure, electromagnetism immunity, electrical passive, high sensitivity, long distance and multiplexing [1-3]. Thus they attract intensive study in recent years. In this presentation, we will introduce our recent development in pressure and temperature sensors [4-8].

We designed and demonstrated fiber-optic Fabry-Perot (FP) pressure sensor based on MEMS technology. A direct and non-destructive self-referenced residual pressure measurement method is developed for MEMS pressure sensor head chip, which solved the critical issue of residual pressure measurement inside a sealed cavity. Polarization low coherence interference is used for the high precision cavity length retrieving through the optical path scanning process and zero optical path difference matching. The multiplexing for fiber-optic FP pressure sensors is realized by wavelength-division-multiplexing of polarized low-coherence interferometry

We developed a FP temperature sensor based on differential pressure resulting from thermal expansion of sealed air. By using mechanical lever principle, we transformed temperature change into cavity length variation of FP interferometer. The temperature sensitivity can be designed flexibly and conveniently by choosing cavity radius, thickness of silicon diaphragm, and the original differential pressure between cavities. In addition, this kind of sensors can be multiplexed with pressure sensors.

We developed a cost-effective and batch producible fiber-optic dual-parameter sensor based on hybrid FP configuration, which can be used for simultaneous measurement of pressure and temperature. The silicon-glass-silicon sandwich bonding structure constructs serially connected silicon and air low-finesse FP cavities naturally, which will produce hybrid cavities interference for temperature and pressure sensing.

We investigated in-line miniature micro-Michelson temperature sensor, which is fabricated by directly polishing single-mode fiber end face. This simple sensor can achieve 950℃ high temperature measurement. For higher temperature measurement, a fiber-optic sensor using sapphire solid FP cavity is fabricated.

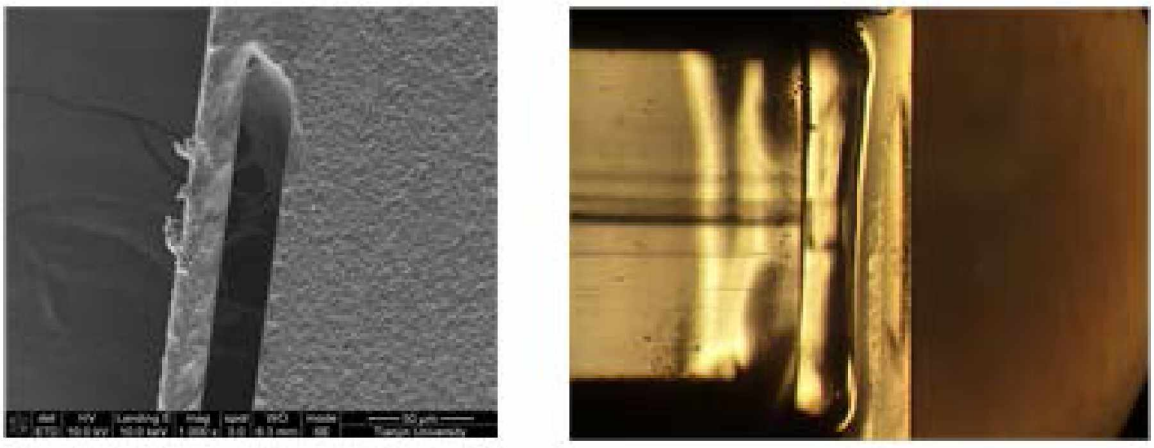

Fig. 1 (a) SEM of fiber-optic pressure sensor cross section. (b) Microscope photo of fiber-optic pressure sensor.

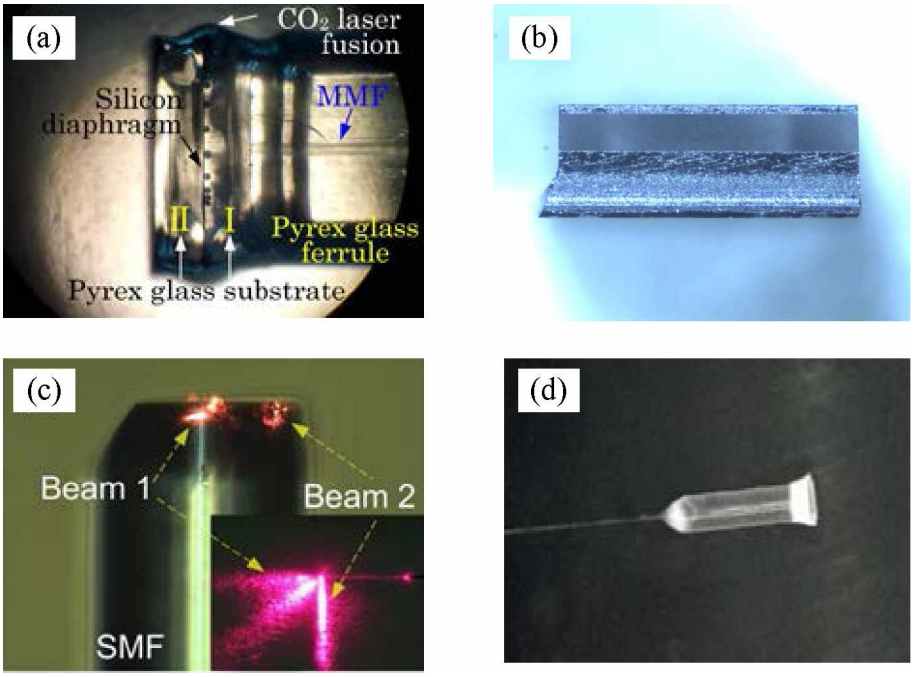

Fig. 2 (a) The temperature sensor based on differential pressure, (b) The pressure and temperature sensor with hybrid FP, (c)The temperature sensor based on micro Michelson interferometer, (d) Sapphire FP temperature sensor.

References

[1] M. Li and M. Wang, Opt. Exp. **14**, 1497 (2006).
[2] C. Wu, H. Y. Fu, K. K. Qureshi, et al., Opt. Lett. **36**, 412 (2011).
[3] J. Wang, B. Dong, E. Lally et al., Opt. Lett. **35**, 619 (2010).
[4] T.Liu, J. Yin, J. Jiang, et al., Opt. Lett. **40**, 1049 (2015).
[5] J. Yin, T. Liu, J.Jiang, et al., IEEE Photon. Technol. Lett. **28**, 625 (2016).
[6] J. Yin, T. Liu, J.Jiang, et al., Opt. Lett. **38**, 3751 (2013).
[7] J. Yin, T. Liu, J.Jiang, et al., IEEE Photon. Technol. Lett. **26**, 957 (2014).
[8] J. Yin, T. Liu, J.Jiang, et al., IEEE Photon. Technol. Lett. **26**, 2070 (2014).

Recent advances in the terahertz photonics and spectroscopy at Novosibirsk free electron laser

B.A. Knyazev[1,2], E.N. Chesnokov[3], Yu.Yu. Choporova[1,2], V.V. Gerasimov[1], Ya.V. Getmanov[1], B.G. Goldenberg[1], V.V. Kubarev[1,2], G.N. Kulipanov[1], A.K. Nikitin[4], V.S. Pavelyev[5], V.M. Popik[1], T.V. Salikova[1], M.A. Scheglov[1], S.S. Seredniakov[1], O.A. Shevchenko[1], A.N. Skrinsky[1], and N. A. Vinokurov[1,2]

[1] *Budker Institute of Nuclear Physics SB RAS, Novosibir2k, 630090 Russia*
[2] *Novosibirsk State University, Novosibirsk, 630090 Russia*
[3] *Institute of Chemical Kinetics and Combustion SB RAS, Novosibirsk, 630090 Russia*
[4] *Scientific and Technological Center for Unique Instrumentation RAS, 117342 Moscow, Russia*
[5] *Samara University, Samara, 443086 Russia*
E-mail: b.a.knyazev@inp.nsk.su

Novosibirsk free electron laser (NovoFEL) is a user facility [1] consisting of three laser systems emitting monochromatic high-power radiation in spectral ranges from 5 to 240 μm. The first THz laser system is in operation since 2003. It emits radiation as a continuous stream of 100-ps pulses with a repetition rate of 5.6 MHz in the spectral range from 90 μm to 240 μm with a line width less than 1%. In a routine regime, the average power of radiation at the user stations is 50-150 W at λ = 130 μm. A high power radiation, a relatively narrow linewidth and the tunability of the radiation enable performing a wide variety of experiments. In this paper, we survey selected experiments in photonics performed recently at workstations of the facility. Photonics is a rapidly developing field of optics, which is still obviously underdeveloped in the terahertz range. The NovoFEL opened new possibilities for the development of new methods and techniques in the area.

One of the main tasks in the photonics is the transformation of terahertz beams. Optical elements for terahertz waves are rather different comparing with the classical optical elements. A number of silicon diffractive optical elements, which enabled transforming NovoFEL Gaussian beam into the Laguerre-Gaussian and Hermite-Gaussian ones, have been designed and fabricated [2]. Other elements transformed the NovoFEL beam into determined volumes (*i. e.*, a pencil-like beam), or areas (*i. e.*, a uniformly illuminated square). A problem of strong Fresnel reflection was solved by the use of anti-reflection film covering [3].

Using binary phase spiral axicons [4], non-diffractive Bessel beams with angular orbital momentum (vortex beams) with different topological charges were formed. Since such beams have great potential for use in data transmission and remote sensing, we investigated both numerically an experimentally the techniques, which allow to increase a distance of beam propagation without beam divergence. It can be realized by reducing wavelength or expanding the beam with a telescopic system. Another experimentally verified feature of the Bessel beams, which is useful for beam transport, was the ability of these beams to reconstruct themselvs after passing randomly non-uniform media or obstacles blocking several central Bessel rings [5].

Surface plasmon polaritons (SPP) are a subject of special interest in the integrated optics, but SPPs in the mid-infrared and terahertz ranges are still investigated insufficiently. Experiments with the SPP launched using NovoFEL radiation showed that the propagation length of terahertz SPPs is about 10 cm. It appeared to be that the length at the gold-ZnS-air interface has a maximum, when ZnS thickness is about several hundreds of nanometers, which depended on surface quality. Such dependence has not been reported for the visible range. We have found also that THz SPPs can "jump" from one metal-dielectric interface to another one over the air gaps of up to 100-mm width [6]. A novel effect, the dependence of SPP generation efficiency on the direction of vortex beam rotation has been discovered, when the "end-fire coupling" technique was applied for SPP generation. This effect can be exploited for the development of a new type plasmonic key.

Large wavelength of terahertz radiation enabled performing the classical optics experiments when the ratio $\lambda / d \sim 1$, where λ is a wavelength and d is characteristic aperture size. We have studied diffraction of plane and vortex waves on different structures including periodic gratings and meshes (Talbot effect). The patterns observed in the case of vortex beams enables to detect characteristics of the beams.

High power of NovoFEL terahertz radiation enabled ignition of continuous optical discharge (COD) in gases at atmospheric pressure. It was found [7] that a sequence of 66-ps terahertz pulses strikes COD in Ar, He, N_2, Air and CO_2 at a specific power density of about 1 GW/cm^2. Tunability of NovoFEL radiation, enabled to carry out a number of experiments on absorption spectroscopy of molecular gases and flames. In paper [8], OH radicals and NO molecules were detected in flames. In this case, laser generation line width was practically the same as the molecule absorption line, and laser radiation may be assumed to be monochromatic. But, in fact, in some cases several vibrational-rotational transitions of a molecule can lie inside the laser line bandwidth. This feature was used in [9] for fast one-pulse spectroscopy of HBr molecule in the gas phase. Excitation of the molecule with a laser pulse excited $(J = 4) \leftarrow (J = 3)$ lines of $H^{79}Br$ and $H^{81}Br$ (66.70 μm and 66.72 μm) followed by a complicated free induced decay signal. Molecular spectrum can be reconstructed using a Fourier transform operation, but the induced decay signal for any molecular transition has a unique pattern, which can be used directly for detection of molecule.

The development and assembly of dedicated terahertz focusing system (beamline) was supported by Russian Science Foundation (grant 14-50-00080). The experiments were carried out with the application of equipment belonging to the Siberian Center for Synchrotron and Terahertz Radiation. The authors are grateful to the NovoFEL team for continuous support of the experiments. Binary axicons were designed and fabricated under support of the Ministry of Education and Science of Russian Federation (project 1879), the vortex beams were formed and investigated under support of RFBR grant 15-02-06444, and investigation of the optical discharge was performed under support of RFBR grant 14-22-02070.

References

[1] G.N. Kulipanov, E.G. Bagryanskaya E.N. Chesnokov et al., IEEE Trans. THz Sci. Technol. **5**, 798 (2015).
[2] A.N. Agafonov Yu.Yu. Choporova, A.K. Kaveevet al., Appl. Opt. **54**, 3635 (2015).
[3] A.N. Agafonov, B.O. Volodkin, A.K. Kaveev et al., Optoelectr. Instrum. Data Process. **49**, 189 (2013).
[4] B. Volodkin, Yu. Choporova, B. Knyazev et al, Opt Quant Electron. **48**, 223 (2016)
[5] Yu.Yu. Choporova, B.A. Knyazev, M.S. Mitkov et al., Phys. Rev. Lett. **115**, 163901 (2015).
[6] V.V. Gerasimov, B.A. Knyazev, A.K. Nikitin et al., Opt. Express **23**, 33448 (2015).
[7] V.V. Kubarev, O.A. Shevchenko, Ya.V. Getmanov et al., Proc. Intern. Conf. IRMMW-THz-2015, 23-28 August 2015, Hong Kong, China.
[8] E.N. Chesnokov, O.S. Aseev, O.P. Korobeinichev et al., Combustion Explosion and Shock Waves **46,** 149 (2010).
[9] E.N Chesnokov, V.V. Kubarev, P.V. Koshlyakov et al., Laser Phys. Lett. **10**, 055701 (2013).

Application of laser technologies in production of elements of cardiovascular bioprosthesis

A.P. Mayorov[1], I.Yu. Zhuravleva[2], A.M. Goncharenko[1], E.V. Kuznetsova[2], D.S. Bordzilovsky[1]
[1]*Institute of laser physics of the Siberian branch of the Russian Academy of Sciences, Novosibirsk*
[2] *Novosibirsk scientific research institute of a pathology of blood circulation of a name of academician E.N.Meshalkin of Ministry of Health of the Russian Federation*

Report describes the laser technologies used in the production of the elements of bioprosthesis. Authors describe existing problems, development of the technologies for their solution and create laser system for the production . The developed technology and instrumentation provide the upgrade of bioprosthesis and improve the long-term clinical results in their application.

Role of photonics in terahertz technologies for industrial applications

Kyung Hyun Park
Terahertz Basic Research Sectionr, ETRI Daejeon, 31429, KOREA
E-mail: khp@etri.re.kr

Terahertz (THz) technologies have attracted great interest in their possibilities over a wide range of industrial applications such as wireless communications, spectroscopy, and imaging. According to a recent forecast, terahertz components and systems market will continue to grow dramatically in the approaching decades [1]. Thanks to the last 10 years of efforts to develop cost-effective and easy-to-use systems, industrial applications of THz technologies are soon be open. Consequently, compact and low-cost THz devices are getting more important to the wide fields of applications.

Having our developed monolithically integrated single cavity dual-mode laser which ensures co-polarized and collinear dual-mode emission, significantly simplifies the optical alignment, and reduces the number of required components [2-4], we have also proposed several different types of photomixers including low-temperature grown (LTG) GaAs photomixers, evanescently coupled waveguide photodiodes (ECPDs) and uni-traveling-carrier photo-diodes (UTC-PDs). According to our research roadmap to open the industrial applications, we are currently developing arrayed type THz components.

Based on our continuous wave (CW) THz components, we have developed several systems including THz thickness measurement system, THz transmission or reflection type scanning imaging system, THz spectroscopic system, and their hybrid systems.

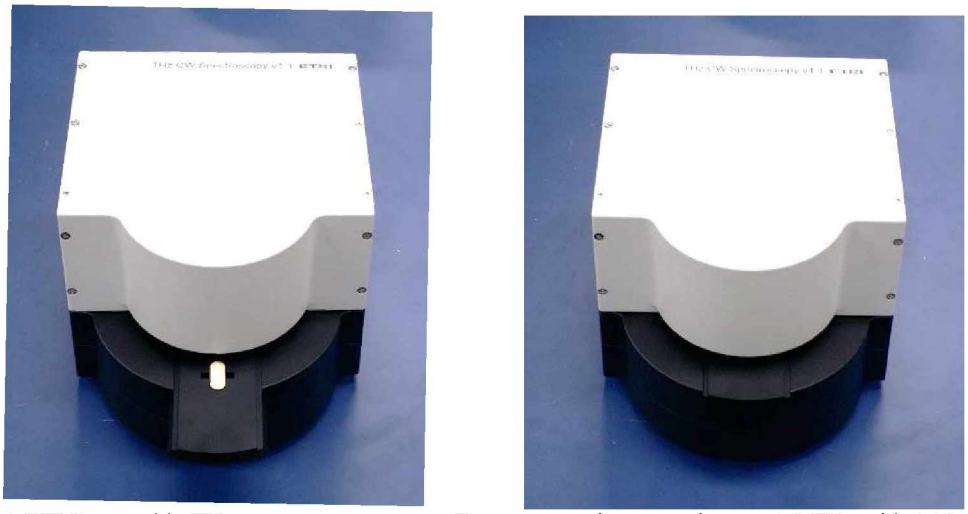

Fig. 1 ETRI's portable THz spectroscopy system. Frequency tuning range is over 1.5 THz with 0.25 GHz resolution. System size is 22×18×14 cm^3.

In this talk, our recent studies in the field of CW THz systems based on photonics technologies including beating sources, THz generating and detecting devices and their applications such as THz imaging and thickness measurements will be briefly reviewed [5-7].

References

[1] A. McWilliams, *Terahertz Radiation Systems: Techonologies and Global Markets*, BCC Research (2016).
[2] N. Kim, H.-C. Ryu, D. Lee et al., Laser Phys. Lett. **8**, 085805 (2013).
[3] E. S. Lee, N. Kim, S.-P. Han et al., ETRI Journal, will be published in 2016.
[4] K. Moon, I.-M. Lee, J.-H. Shin et al., Scientific Reports **5**, 13817 (2015).
[5] I.-M. Lee, N. Kim, E. S. Lee et al., Optics Express **23**, 846 (2015).
[6] S.-P. Han, H. Ko, N. Kim et al., Optics Express **22**, 28977 (2016).
[7] S.-P. Han, N. Kim, W.-H. Lee et al., Appl. Phys. Express **9**, 022501 (2016).

Pulsed UV laser technologies for ophthalmic surgery

A.M. Razhev
Institute of Laser Physics. Academician Lavrentyev Avenue 13/3, 630090, Novosibirsk, Russia
Novosibirsk State Technical University. Karl Marx Prospekt 20, 630073, Novosibirsk, Russia
E-mail: razhev@laser.nsc.ru

It is reported on the establishment of pulsed gas discharge excimer ArF, KrCl, KrF and XeCl lasers and the development of pulsed UV laser technology based on them for use in ophthalmic surgery. These lasers are characterized by high radiation energy, pulse power and total efficiency, allowing to be used for a variety of practical applications.

The results of the optimization of short-pulse UV laser radiation parameters and their successful use for the development of medical laser technologies for ophthalmic surgery and the creation of experimental excimer laser systems for excitation cheap gas mixtures by nanosecond transverse electric discharge without high-pressure neon or buffer-free gas mixtures are presented.

The results of the application of the developed medical UV laser systems for development of new laser technologies for ophthalmic surgery as joining efforts of Institute of laser physics research team with medical collaborators of the Novosibirsk city are presented.

For the application of pulsed UV radiation in ophthalmology laser radiation transmission curves by the human eye cornea in the UV region of the spectrum are studied. Based on these data the UV laser wavelengths for optimal corneal surface profiling without damage are defined. Special studies have shown the impact of the biological safety of a powerful UV laser radiation on human tissue, allowing going to clinical trials.

It is reported on the establishment of a method of treatment of herpetic keratitis, which is characterized by bactericidal, non-contact, painless influence on affected eye corneal tissue. After a long time of laser procedures relapse does not occur, typical of this disease.

As a result of joining efforts developed methods of excimer laser human eye cornea reshaping based on ArF and KrCl excimer laser. These methods based on the curvature of the cornea surface by changing its layer-evaporation on the rotating masks developed technology while preserving its transparency without thermal damage.

A safe, effective "ab-externo" open angle glaucoma surgery technology using XeCl laser is developed. It has been shown that this is the optimal wavelength for this technology.

Developed UV laser technology supported by the relevant patents of Russia, USA and Spain.

Cryogenic opto-acoustical gravitational wave antenna

V. Rudenko, S. Oreshkin, S. Popov, and I. Yudin
Sternberg Astronomical Institute of Moscow State University
119992 Moscow Universitetskii prospect 13, Russia
E-mail: rvn@sai.msu.ru

This Gravitational antenna OGRAN is the setup having a combination of acoustical and optical principles of gravitational wave detection. OGRAN was developed and constructed by collaboration of Moscow State University (Sternberg Astronomical Institute, SAI MSU) and Russian Academy of Sciences (Institute of Nuclear Research, INR RAS, and Institute of Laser Physics, ILP SB RAS). Detailed description of this antenna was given in [1, 2]. At present the antenna OGRAN is installed in underground facilities of the Baksan Neutrino Observatory of INR RAS and is going on through a commission stage. Using this instrument, a long time observation of the gravity gradient background is planned in parallel with neutrino events monitoring at the neutrino telescope setup (BUST) [3] having the goal of a joint search for collapsing stars – relativistic transient events in our Galaxy and close halo region with radius ~ 100 Kpc. Extension of the zone of detectable sources requires an instrument with enhanced sensitivity. For the OGRAN antenna construction (fig.1) [1, 2], it could be achieved in particular using its cryogenic version with cooled solid body GW detector. The unavoidable noise background for the OGRAN setup is composed by the two natural sources of fluctuations: thermal noise of the acoustical bar and photon noise of the optical read out. Effectiveness of these sources depends on the key parameters of the setup such as mechanical losses, temperature, optical power, cavity finesse. For calculation of optimal combination of variable parameters of the cooled antenna, we used the following (typical for OGRAN) constant values: length L=2 m, mass $M \cong$ 2000 kg, quality factor $Q_\mu=2\cdot10^6$, acoustical $\omega_\mu=10^4$ s, time of the signal $\tau=10^{-3}$ s. The temperature T in our calculation was considered as the variable argument inside the interval (3÷300) K. For the optical readout system, we supposed the following data: pump power P= 100 mW ÷ 1 W, number of reflection N =10^4÷10^5, photo efficiency η=0.7, λ_e =1 μm. Numerical calculation shown that at temperatures 50 – 100 K, the optical read out has the low noise factor, i.e., it is practically an "ideal registration system" without an additive noise. The receiver bandwidth is several tens of Hz, and the amplitude spectral noise density h_{min} is only few times larger than the level of potential sensitivity with ideal registration system $h_{min\,pot}$ ~10^{-21} Hz^{-1/2}

One of the large technological problems for the cryogenic version of the OGRAN setup is to keep mirror's optical characteristic invariable at low temperature under illumination of the 0.1-1 W laser power. At such power level, effect of the thermal induced lens of the mirror can have significant influence on the optical FP mode structure. At the present, CaF_2, sapphire and *Si* mono crystal are considered as promising materials for cryogenic mirror's substrates [4 (13)]. The *Sapphire* and CaF_2 have a broad transmission spectral range but the first is relatively expensive while the second has some problem with quality polishing. *Si* single crystals can be obtained in large volumes without structural defects having a very low impurity level. However the OGRAN setup uses Nd:YAG single frequency laser operating at 1064 nm. For this wavelength *Si* is not transparent and so it can't be a proper choice for OGRAN cryo-version. With this argumentation the CaF_2 substrates were selected in our test experiments to study of optical characteristics of cryogenic mirrors during the cooling process with the presence of optical pump. Two mirrors on CaF_2 substrate were attached with a good thermal contact to the ends of small model of the OGRAN detector of cylindrical shape with 14 cm diameter and 20 cm length made from aluminum alloy (total weight 8 kg). It was placed in the special cryostat [5 (12)] in the good thermal contact with walls of cryostat inner chamber. The only one optical window with 2 cm in diameter was foreseen at the end cover of the cryostat together with co-centric

holes in the inner envelopes. Through this window the light of pump laser can illuminate the FP resonator at the model detector (details of the cryostat and the model one can take in [5]). Reflected from FP resonator light might be picked up with outside photo detector. The goal of our experiments was consisted in the measuring FP cavity integral optical characteristics during the cooling process from room temperature up to liquid helium temperature The minimal temperature reached at the model body was about 5 K while the mirrors itself were cooled down up to 14-16 K. The two integral characteristics of the FP cavity were measured: finesse (sharpness) and the fraction of reflected light (contrast). It is known that a fraction of reflected light depends on the mode matching between the laser beam and the FP cavity. Thermal lens effect in mirrors destroys such matching and decrease the contrast. To check this effect for CaF_2 mirrors due to absorption light we have performed measurements of the part of reflected light at different laser powers, namely at 10, 20, 50, 100, 200 and 480 mW. For the low powers mirror's temperature measured by thermo sensor attached on the back side of the mirror and was practically the same as for the aluminum body. At the maximum power of 480 mW, the temperature difference between the mirrors and the aluminum body was about 14 - 15 K. The incident laser power was measured after reaching a quasi-stable point of thermal equilibrium, where the mirror's temperature was not changed during the measurement time. To control finesse evolution, we measured the width of FP cavity resonance peak by sweeping the laser frequency. We didn't find any significant changes of its value during cooling-heating cycles. It was close the same initial value of F=2300 for all available laser powers. The experimental data for the "contrast" are presented in (fig.2). At temperatures between 60 and 40 K, contrast value quickly decreases and becomes more flat below 40 K. This zone corresponds to the CaF_2 thermal conductivity increasing during cooling process from 1 W/cm K at 60 K up to 10 W/cm K at 30 K [6]. However the contrast variation was relatively small and does not exceed 20%. It should not produce a significant influence on the sensitivity of the OGRAN cryo-version. From our experiments we consider that CaF_2 substrate mirrors can be used in such cryo-setups. Nevertheless it should be noted that necessary to make more detailed experiments with the mirrors with CaF_2 substrates as well as mirrors with sapphire substrates.

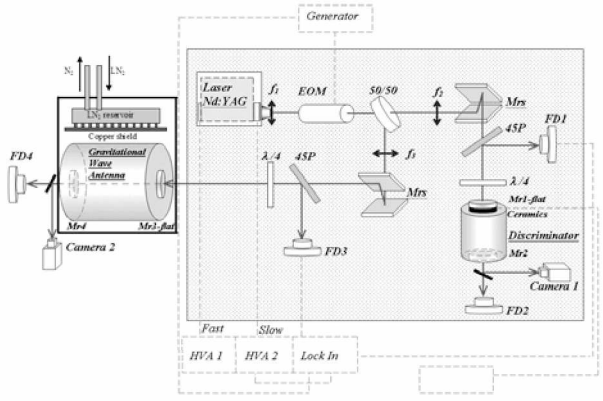

Fig. 1 Scheme of the Cryo-OGRAN detector.

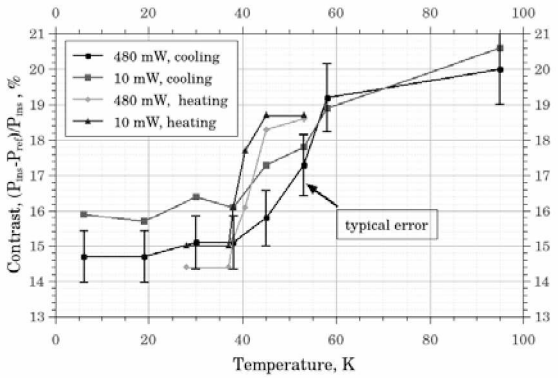

Fig. 2 Contrast temperature variation for CaF2 mirrors.

References

[1] S.N. Bagaev, L.B. Bezrukov, N.L. Kvashnin et.al. Rev. Sci. Instrum. **85**, 065114 (2014).
[2] S.N. Bagaev, L.B. Bezrukov, N.L. Kvashnin, et.al. Instrum. and Experim. Techn., **58**, № 2, 257 (2015).
[3] R.V. Novoseltseva, M.M. Boliev, I.M. Dzaparova et al., Bull. Russ. Acad. Sci., Phys. **75**, 419 (2011).
[4] C.Schwarz, D.Hainert, P.Seidel at al. Phys.Status Solidi A, **208,** №12. 2719. (2011).
[5] V.A.Krysanov, A.M.Motylev, S.I.Oreshkin et.al. Measurement Technique **57**, №12. 1416 (2015).
[6] G.A. Slack. Phys.Rev.**122**, №.5, 1451 (1961).

Electrically controllable terahertz loop-shape metamaterial based on vanadium dioxide thin film

H.-C. Ryu[1], J.-H. Shin[2], and K. H. Park[3]
[1]*Affiliation, Address, Country Department of Car Mechatronics, Sahmyook University, Seoul 139-742, Korea*
[2]*Affiliation, Address, Country KU-KIST Graduate School of Converging Science and Technology, Korea University, Seoul 02841, Korea*
[3]*Terahertz Basic Research Section, Broadcasting-Media Basic Technology Research Group, Broadcasting-Media Research Laboratory, ETRI, Daejeon 305-700, Korea*
E-mail: hcryu@syu.ac.kr

We propose an electrically controllable terahertz wave modulator based on metamaterial and vanadium dioxide (VO2) thin film. Metamaterials have attracted great attentions owing to their unique responses for manipulating electromagnetic resonances that were mostly not founded in natural material. The controllable resonances of the artificially engineered metamaterials can offer the opportunities to realize the new and novel THz devices for a wide variety of THz applications [1]. Numerous researches on the realization of the tunable characteristics for the THz metamaterials have been reported by using semiconductors, graphene, and tunable functional-material [2, 3]. Tunable metamaterial based on vanadium dioxide (VO2) which has reversible switching properties caused by insulator-metal transition at a critical temperature at 340 K, is one of promising approach to spatially manipulate the THz wave thanks to easy fabrication and high tunability. There are several researches on the tunable THz metamaterials based on the phase transition of VO2 by applying temperature, THz-field, or light [4]. However, these methods need external devices such as a heater, a THz or a light source; the external devices make the THz tunable devices more expensive and bulky. Thus, the electrical control for the phase transition of VO_2 is preferred for the practical applications. A loop shape metamaterial is designed to play roles as a resonating metamaterial and a heater to electrically control a conductivity of VO_2 at the same time at shown in Fig. 1. These easily controllable THz metamaterials can be used as high-performance modulating filters or sensors.

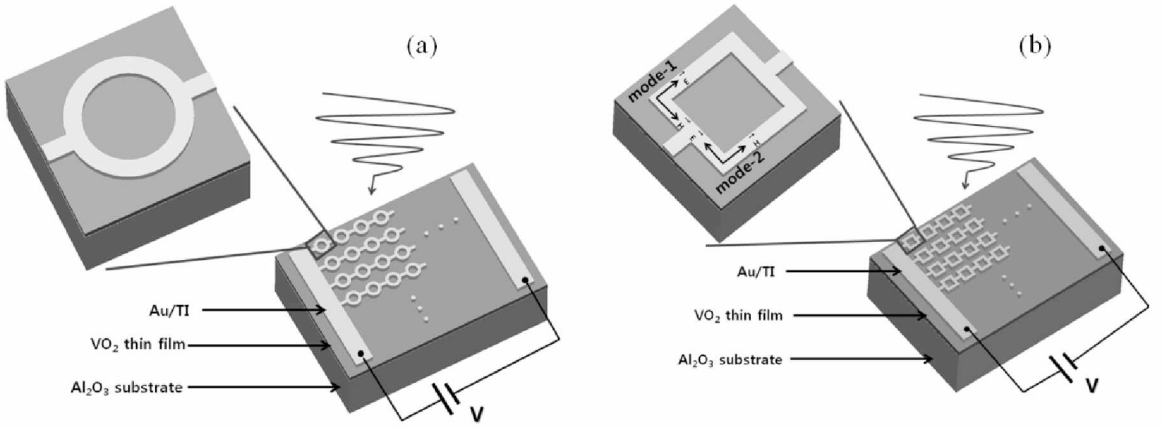

Fig. 1 Configuration of electrically controllable terahertz loop-shape metamaterial based on vanadium dioxide thin film. (a) ring (b) square

References

[1] H.-T. Chen, W. J. Padilla, J. M. O. Zide, A. C. Gossard, A. J. Taylor, and R. D. Averitt, Nature **444**, 597 (2006).
[2] L. Ju, B. Geng, J. Horng, C. Girit, M. Martin, Z. Hao, H. A. Bechtel, X. Liang, A. Zettl, Y. R. Shen, and F. Wang, Nat. Nanotech. **4**, 630 (2011).
[3] B. Sensale-Rodriguez, R. Yan, M. M. Kelly, T. Fang, K. Tahy, W. S. Hwang, D. Jena, L. Liu, and H. G. Xing, Nat. Comm. **3**, 1 (2012).
[4] M. Liu, H. Y. Hwang, H. Tao, A. C. Strikwerda, K. Fan, G. R. Keiser, A. J. Sternbach, K. G. West, S. Kittiwatanakul, J. Lu, S. A. Wolf, F. G. Omenetto, X. Zhang, K. A. Nelson, and R. D. Averitt, Nature **487**, 345 (2012).

Laboratory simulation of energetic flows of magnetospheric planetary plasma

I. F. Shaikhislamov, V. G. Posukh, A. V. Melekhov, E. L. Boyarintsev, Yu. P. Zakharov, P. A. Prokopov and A. G. Ponomarenko
Dep. of Laser Plasma, Institute of Laser Physics SB RAS, pr. Lavrentyeva 13/3, Novosibirsk, 630090, Russia
E-mail: ildars@ngs.ru

Laboratory modeling of space plasma processes is an important method of study of basic physics. Despite of significant progress in spacecraft measurements and numerical simulations a laboratory experiment remains a source of unique data inaccessible by other means. One of the fields where namely laboratory experiments with lasers have pushed the advances in theory and numerical simulation is interaction of counter-streaming plasma flows in presence of magnetic field. In 1970-s and 80-s a number of works with laser-produced plasma expanding with super-Alfvenic velocity into magnetized background have been carried out with the aim to model active near-Earth releases AMPTE, CRRES, Argus, Starfish. The other field which was extensively studied by means of laboratory experiment is magnetosphere. At KI-1 simulation Facility such studies are based on two sources of plasma – induction Θ-pinch and Laser Plasma (LP) – which interact with compact magnetic dipoles. Combination of energetically and spatially different plasma flows allowed modeling of extreme compression of the Earth's magnetosphere by super powerful CME or by artificial near-Earth releases [1]. Such complex systems as field-aligned currents connecting boundary layer with ionosphere has been studied in detail [2]. Namely laboratory experiments supplied necessary data to formulate and verify a Hall model of mini-magnetospheres [3] which explains its unusual features.

In the present experiment we investigate essentially new combination of interacting flows and magnetic field. Θ-pinch plasma fills the vacuum chamber and creates around magnetic dipole a magnetosphere with estimated size of about 30 cm. The novel feature is that laser plasma is generated inside of this magnetosphere at two targets symmetrically placed at dipole cover (fig 1). LP is directed opposite to the Θ-pinch flow and has kinetic energy large enough to sweep previously existing plasma and dipole magnetic field. We study the interaction at distances 40÷90 cm from the dipole beyond the previously existing magnetosphere. The specific case of plasma expansion from the inner region of magnetic dipole outward into the background flow has at least two possible applications. It directly relates to the concept of magnetosail. The other field is Hot Jupiters – close orbiting exoplanets heated by ionizing stellar radiation to a point of super-sonic expansion of upper atmosphere. The interaction of expanding planetary flow with counter-streaming stellar plasma in a case when such a planet possesses weak magnetic field [4, 5] was one of motivations of the present experiment.

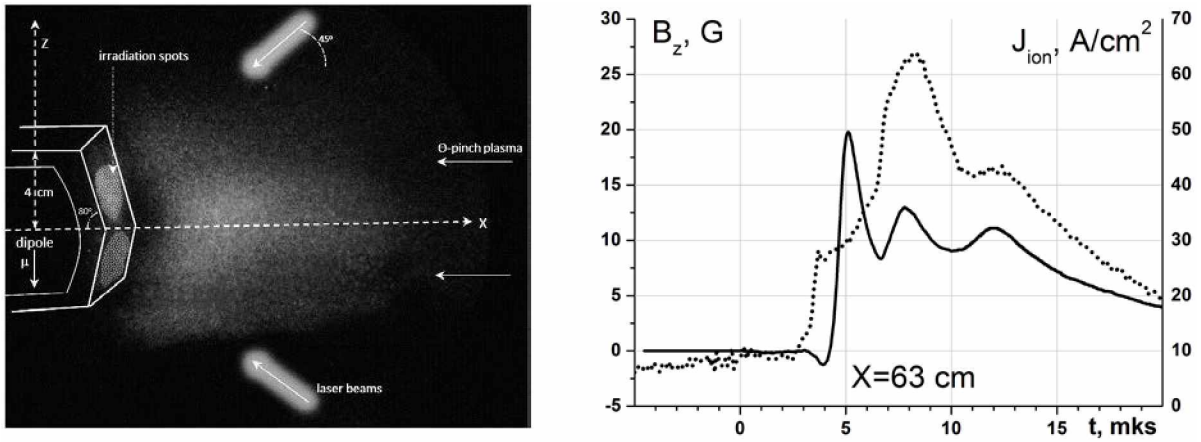

Fig. 1 Left - experimental set-up superimposed on snapshot of laser-produced plasma. Right - typical dynamic signals of ion current and magnetic field measured by probes at a distance of 63 cm.

Before the laser plasma is produced on the surface of the dipole, the flow of background plasma creates around it a magnetosphere with size of about 30 cm. Thus, LP, when created, expands at first in the dipole magnetic field of inner magnetosphere filled from about X=15 to X=30 cm by background plasma and after that across magnetopause into the background plasma proper where magnetic field is zero. Such scenario principally differs from the previous experiments on LP expansion in magnetized uniform background in that the magnetized background in the present case is a compact localized shell. The energy density of LP (total energy about 16 J in initial volume of about 8 cm^3) is comparable to that of dipole magnetic field already at the laser target and with further LP expansion quickly becomes dominant. It was found that the LP flowing through background plasma partially expels it due to Coulomb collisions. However, collisional interaction is rather weak and counter-streaming flows deeply penetrate into each other, so LP expansion isn't significantly affected at distances up to 100 cm.

The main finding of the experiment is that when background plasma pre-fills the vacuum chamber LP carries with itself across distances 40÷90 cm the magnetic field order of magnitude larger than in case without ambient plasma. This field is also much larger than the vacuum dipole field at these distances. Typical measurements are demonstrated in fig. 1. Obtained results impose a question of origin of such magnetic field carried by LP. They suggest a novel and unexpected feature that LP captures magnetospheric field rather than simply stretching it and that effectiveness of this capture is directly related to the density of background plasma which creates magnetosphere.

In previous experiments with uniform background the compression and strong increase of magnetic field at the LP front and its total expulsion inside of LP proper has been observed. Such behavior is explained in the frame of displaced electrons model. When the electron density of expanding plasma significantly exceeds that of background, which is true in our case at distances X<30 cm where magnetized shell exists, the electrons of background together with frozen-in magnetic field are displaced and strongly compressed at the front of LP. However, in present experiment no such compression is seen. Measured fields don't exceed the expected values of >50 G in the initial magnetized shell. Moreover, observed magnetic field is present in the whole LP flow.

On the base of the obtained experimental results a following conclusion was made. Plasma expanding outward from the inner region of magnetic dipole can interact with it by catching and dragging the magnetic field lines. The effectiveness of such process of transfer of magnetic field far from the dipole is directly related to the density of background plasma prefilling the magnetic field lines close to the dipole. Without pre-made plasma magnetized into dipole field lines the impulsive energetic plasma doesn't carry any significant field after crossing the dipole region. There can be two reasons why the LP catches and carries within itself the magnetized shell formed by background plasma. First, the dipole field lines loaded with plasma can't move faster than with the Alfven speed, and sufficiently fast impulsive flow can overcome the magnetized shell instead of displacing it. Second, the curvature of dipole field lines makes it possible for electrons of LP to mix with electrons of magnetized shell. Only by such mixing the LP might pick up the magnetic field instead of displacing it. The last feature is a main difference of the present work from previous studies of LP interaction with uniform magnetized background.

This work was supported by SB RAS Research Program (project II.10.1.4 N 01201374303), Presidium RAS program on fundamentals of double technologies and Russian Fund for Basic Research grants 14-29-06036, 16-52-14006.

References

[1] Ponomarenko A .G., Zakharov. Yu. P., Antonov V. M. et al., Plasma Phys. Control. Fusion **50**, 074015 (2008)
[2] Shaikhislamov I. F., Antonov V. M., Zakharov Yu. P. et al., Plasma Phys. Control. Fusion **51**, 105005 (2009)
[3] Shaikhislamov I. F., Antonov V. M., Zakharov Yu. P. et al., Adv. Space Res. **52**, 422 (2013)
[4] Antonov V. M., Boyarinsev E. L., Boyko A. A. et al., The Astrophysical Journal **769**, 28 (2013)
[5] Khodachenko M. L., Shaikhislamov I. F., Lammer H. & Prokopov P. A., The Astrophysical Journal **813**, 50 (2015)

Laser-driven plasma wakefield electron acceleration and coherent femtosecond pulse generation in X-ray and gamma ranges

V.I.Trunov[1], K.V.Lotov[2,3], K.V.Gubin[1], E.V.Pestryakov[1,2], S.N.Bagayev[1,2], P.V. Logachev[3]
[1]*Institute of Laser Physics SB RAS, Novosibirsk, Russia*
[2]*Novosibirsk State National Research University, Novosibirsk, Russia*
[3]*Budker Institute of Nuclear Physics SB RAS, 630090, Novosibirsk, Russia*
E-mail: trunov@laser.nsc.ru

At the present time, progress in laser wakefield acceleration (LWFA) of charged particles gives us possibilities to consider LWFA as a perspective method of electron beam production in the GeV energy range. LWFA-based installations can find future applications as advanced light sources. Combining the LWFA and Compton backscattering of a probe light beam on accelerated electrons opens a possibility to create a tabletop source of femtosecond (fs) light beam in the x-ray and gamma range. This kind of source can have high coherence and polarization, quasi-monochromatism, and possibility of tuning radiation parameters.

LWFA experiments are prepared in ILP SB RAS in collaboration with BINP SB RAS. The experiments will use a two-channel multi-terawatt femtosecond high contrast, high angular stability laser system with pulse repetition rate 10 Hz, which is developed in ILP SB RAS [1].

There are two basic schemes of LWFA, which are traditionally used (Fig.1). One scheme relies on plasma-filled dielectric capillaries. Best results are obtained for capillaries with a preformed plasma that has a density minimum on the axis. Another scheme uses supersonic gas jets.

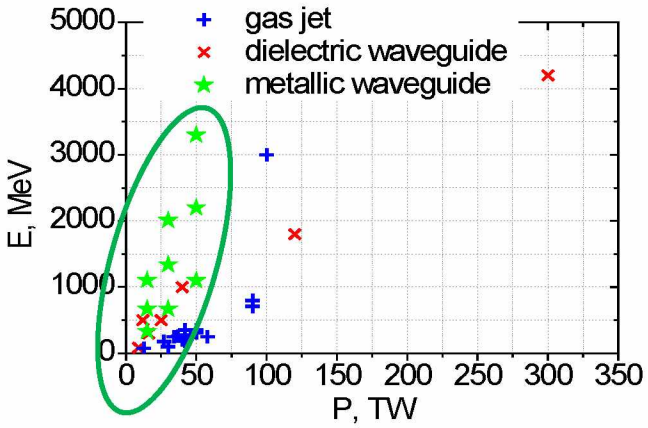

Fig. 1 The energy of laser wakefield accelerated electron versus the pump pulse power. For dielectric waveguides and gas jets, the points correspond to published experimental results. For metallic waveguides, the points are estimates made with the assumption of low attenuation of the drive laser pulse in the capillary.

The capillaries can also prevent laser beam diffraction by reflecting the pulse directly from the walls and extending acceleration length up to many Rayleigh lengths. We study narrow metal channels in this context. A metal channel can be considered as an extreme case of the plasma filled capillary. The metal walls act like a cold dense plasma with a sharp boundary. Propagation of high-intensity (up to 10^{17}W/cm^2), high-contrast (<10^{-8}), 50 fs laser pulse through the 20 mm long, 50 μm wide triangular copper channel was experimentally studied in vacuum and in helium at pressures 1÷10 mbar [2]. The main results are:

- Relative transmission 70% through the channel (15 Rayleigh lengths) is measured;
- Single mode regime of pulse propagation is demonstrated;
- No difference between propagation in vacuum and helium conditions is observed;
- Reduction of transmission to zero after hundreds or thousands of pulses is observed, which is caused by formation of local plugs in capillaries.

As a result, we can conclude that metal capillaries are a perspective and interesting direction, which deserves further studies. However, until the problem of fast capillary degradation is solved, another scheme has to be used as a long-lifetime source of accelerated electrons.

The first choice is a supersonic helium jet (Fig.2). In this case, gas ionization, formation of the plasma channel, driving wakefield oscillations, electron trapping an acceleration is provided by single sub-PW high-contrast fs laser pulse. Main parts of the facility (Laval nozzle with pulse valve, laser beam compressor and focuser, electron beam probes) will reside in three vacuum chambers. This layout is traditional for LWFA devices.

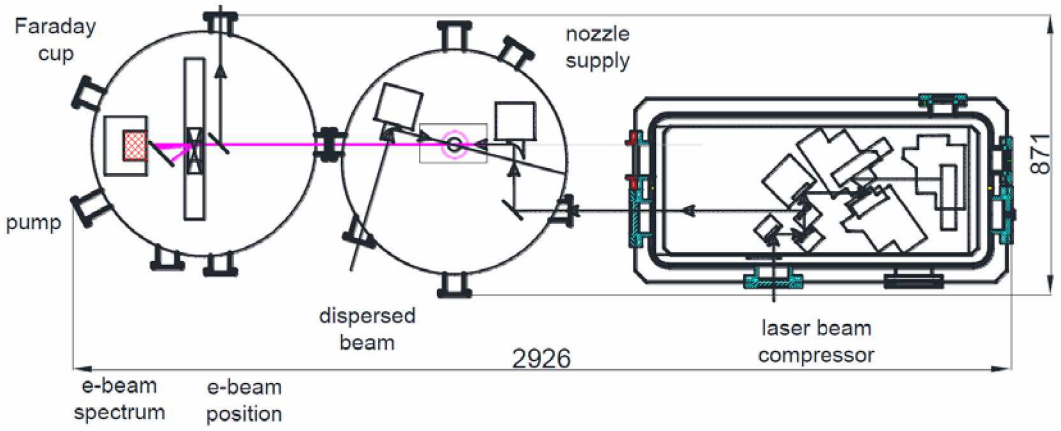

Fig. 2 The layout of the experimental facility.

Numerical analysis of electron acceleration shows the following:

- It is necessary to focus the laser beam down to diameter of about 10 μm. The Rayleigh length and effective length of acceleration is ~ 0.5 mm. The optimum plasma density is about $5 \cdot 10^{18}$ cm^{-3}.
- For the laser pulse energy of 0.3 J, the maximum electron energy can reach 100 MeV.
- Supersonic regime of the gas jet is necessary for achievement of small energy spread of electrons, because the supersonic jet has a spatially uniform gas density profile.

Numerical analysis of gas flow shows that we can use a simple conical Laval nozzle with the waist diameter 0.3÷0.4 mm, output diameter 1.5 mm, and cone angle 14°. In this case, we obtain the jet density up to 10^{19} cm^{-3} and Mach number 4 with the input gas pressure below 10 atm. Several nozzles are produced and being tested for gas density profiles. The gas system with the fast pulse valve is complete.

Faraday cup and magnetic spectrometer are chosen as a basic electron diagnostics. The Faraday cup measures the electron bunch charge in the range from 1 pC and, simultaneously, serves as the electron beam dump in the energy range 10÷100 MeV. It includes a capacitor with a tungsten part 6 cm thick and 1 cm thick aluminum cover plate. The Faraday cup is designed for full stopping of 100 MeV electrons with minimized backscattering and, from other hand, has a minimized capacity of 14 pF. The spectrometer is based on permanent magnets and has the deflecting field 0.75 T. The deflected beam is detected by the Renex luminophor and a CCD camera. Both devices are created and now being tested under a real high-energy electron beam at BINP.

The main immediate aim is production of laser beam-accelerated electrons with energy up to ~ 100 MeV. Production of high-energy Compton backscattered gamma-quanta with maximum energy up to ~ 200 keV is planned as the next stage.

This work is supported in part by RAS Program "Extreme laser radiation: physics and fundamental applications", project number 115113010008, and by SB RAS Project II.15.4.3.

References

[1]V E Leshchenko, V I Trunov, S A Frolov, E V Pestryakov, V A Vasiliev, N L Kvashnin, S N Bagayev. Coherent combining of multimillijoule parametric-amplified femtosecond pulses. Laser Phys. Lett. **11,** 095301, 2014

[2] K.V.Lotov, K.V.Gubin, V.E.Leshchenko, V.I.Trunov, and E.V.Pestryakov, "Guiding femtosecond high-intensity high-contrast laser pulses by copper capillaries," Phys. Plasmas **22**, 103111 (2015).

LECTURE
Lasers and infrared thermography: harmony, mutual assistance and reciprocal gain

Boris G. Vainer
Rzhanov Institute of Semiconductor Physics SB RAS, Novosibirsk State University
13 Lavrentyev av, Novosibirsk, 630090, Russia
E-mail: boris-stmt@yandex.ru

In this review, the beneficial outcomes arisen from a simultaneous use of the laser- and infrared thermography (IRT)-based techniques are demonstrated and comprehensively analyzed. The newest literary and original experimental results collected from different research areas are presented.

Probably, biomedicine is the most advantageous application domain where IRT and lasers are usefully employed in common. Several following examples confirm this statement.

IRT in cooperation with laser Doppler flowmetry (LDF) [1], laser Doppler perfusion imaging (LDPI) [2] and laser speckle contrast imaging (LSCI) [2, 3] are used for microvascular investigations. It is shown in [3] and [4] that the IRT results correlate well with LSCI and LDPI ones, respectively. In [5], IRT and dual-wavelength laser Doppler imaging (LDI) are applied to the investigation of a circulation within the morphoea in humans. Here the fact is taken into consideration that the LDI red wavelength (633 nm) represents the blood flow through large, thermoregulatory vessels, but a green one (532 nm) represents the nutritive capillary blood flow. IRT in turn reflects the circulation intensity predominantly in the thermoregulatory vessels. IRT and LDF are also used as mutually complementary means in the latent myofascial trigger points irritation combined with breath holding studies [6]. A joint use of the IRT and 780-nm LDF diagnostic means for a severe acute respiratory syndrome (SARS) or pandemic influenza fast screening at a quarantine depot is described in [7].

In [8], the extent of the living tissue thermal injuries emerged in the course of a surgical (laryngeal) operation instrumented with microsecond Er:YAG and superpulsed CO_2 lasers is visualized and quantitatively analyzed with the help of IRT. IRT was also used to monitor the laser ablation overheating during the operation realized with a picosecond infrared laser (PIRL) [9]. Using a porcine (*ex vivo*) eye model, an IRT-based analysis of the peak corneal temperature change during excimer laser ablation is performed in [10]. The ablation parameters were local frequency, system repetition rate, pulse energy, optical zone size, and refractive correction.

A laser and IRT were simultaneously used in the studies [11] devoted to a heating-arisen pain syndrome in the rat: CO_2 laser – to deliver the heat stimulus, and IRT – to monitor the temperature changes. A similar IRT and laser co-operation is described in [12], where the laser-enhanced transdermal drug delivery was studied. There, the effects of 1064 nm-Nd:YAG lasers with long-pulsed 15 J /cm^2 and Q-switched 0.5 J /cm^2 output modes on the rat skin stratum corneum were investigated. IRT was applied here to monitor the skin surface dynamical temperature distribution around the laser beam influence point.

A net clinical result of a low-level laser therapy (LLLT) procedure in the patients suffered from venous leg ulcers was unbiasedly monitored using the IRT method in [13]. A possible influence of a low-level semiconductor laser irradiation on a human face was also recorded by infrared camera and reported in [14].

IRT may serve as unprecedented measuring instrument when information about a cross-sectional pattern in the electromagnetic radiation directional diagram, including that of a laser radiation, is required. A simple IRT-based method proposed for this purpose [15, 16] is practically indifferent to radiation source wavelengths. In particular, it is applicable to both infrared [15, 16] (Fig. 1) and terahertz [17] lasers. A simple linear relation between the thin indicator (screen) local temperature $T(X,Y)$ measured by the IR camera and the irradiance $I(X,Y)$ of the screen heated by radiation at the point (X,Y) is derived in [16]:

$$I(X,Y) = 2(h + 4\sigma T_a^3)[T(X,Y) - T_a] \quad .$$

Here T_a is the ambient temperature, h – the convective heat transfer coefficient depending on the experimental conditions, and σ – the Stefan-Boltzmann constant.

A laser and IRT joint use in physics was recently demonstrated in [18]. The laser here served as part of an ellipsometric system, which, in its turn, served as independent additional measurement instrument in the adsorption/desorption physical-chemical experiments. As an unexpected side effect revealed by IRT in those measurements, a heating of the sample caused by a He-Ne low-power laser that can influence the sorptive power of the investigated adsorbent surface is recorded.

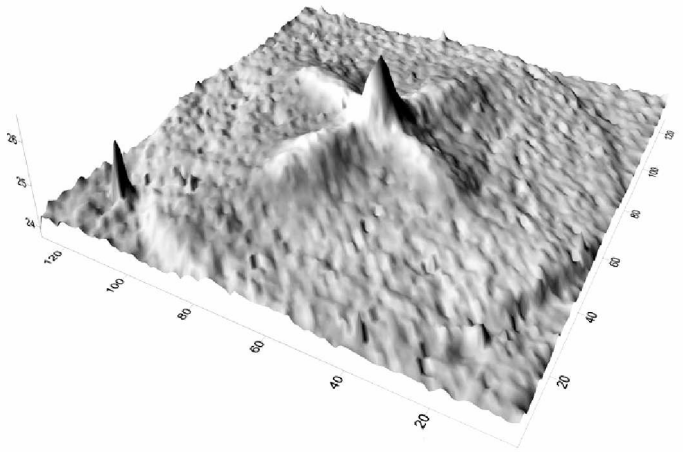

Fig. 1 Energy directional diagram 3D-thermogram of the electromagnetic radiation emitted by a low-power combined source containing four infrared diodes and pulsed semiconductor laser (at the centre of the radiant).

In summary, it is demonstrated that a modern IRT-based technique successfully supports a lot of laser-based technologies in biomedical, physical, chemical and other scientific spheres. When combined into an inseparable tandem, an infrared camera and a laser allow obtaining a much more profit than it can be achieved with a separate use of these modalities.

This work was supported by the Russian Foundation for Basic Research under Grant No. 15-02-07680.

References

[1] D. Zhang, L. Li, H.-M. Ma, C.-F. Ye, S.-Y. Wang, D.-S. Chen, J. Tradit. Chin. Med. **30**, 243–248 (2010).
[2] J. Allen, K. Howell, Physiol. Meas. **35** R91–R141 (2014).
[3] J. D. Pauling, J. A. Shipley, S. Raper, M. L. Watson, S. G. Ward, N. D. Harris, N. J. McHugh, Microvasc. Res. **83** 162–167 (2012).
[4] O. Schlager, M. E. Gschwandtner, K. Herberg, T. Frohner, M. Schillinger, R. Koppensteiner, W. Mlekusch, Microvasc. Res. **80** 54–57 (2010).
[5] T. L. Moore, S. Vij, A. K. Murray, M. Bhushan, C. E. M. Griffiths, A. L. Herrick, Br. J. Dermatol. **160** 864–867 (2009).
[6] Y. Kimura, H.-Y. Ge, Y. Zhang, M. Kimura, H. Sumikura, L. Arendt-Nielsen, Acta Physiol. **196** 411–417 (2009).
[7] T. Matsui, S. Suzuki, K. Ujikawa, T. Usui, S. Gotoh, M. Sugamata, Z. Badarch, S. Abe, J. Med. Eng. Technol. **33** 403–409 (2009).
[8] A. Böttcher, N. Jowett, S. Kucher, R. Reimer, U. Schumacher, R. Knecht, W. Wöllmer, A. Münscher, C. V. Dalchow, Eur. Arch. Otorhinolaryngol. **271** 1121–1128 (2014).
[9] A. Böttcher, S. Kucher, R. Knecht, N. Jowett, P. Krötz, R. Reimer, U. Schumacher, S. Anders, A. Münscher, C. V. Dalchow, R. J. D. Miller, Eur. Arch. Otorhinolaryngol. **272** 941–948 (2015).
[10] S. A. Mosquera, S. Verma, J. Biomed. Opt. **20** 078001 (2015).
[11] P. Carrive, M. Churyukanov, D. Le Bars, Pain **152** 676–686 (2011).
[12] C. Liu, J. Zhang, Y. Yue, Q. Luo, D. Zhu, J. Biomed. Opt. **18** 061228 (2013).
[13] J. Taradaj, A. Franek, E. Blaszczak, A. Polak, D. Chmielewska, P. Krol, P. Dolibog, Wounds **24** 138–145 (2012).
[14] B. G. Vainer, Proc. SPIE **4360** 470–481 (2001).
[15] B. G. Vainer, In: Quantitative InfraRed Thermography 5, Eurotherm Seminar 64, QIRT'2000, Reims, France, July 18–21, 2000. Proceedings. Ed. by D.Balageas, J.-L.Beaudoin, G.Busse, and G.M.Carlomagno. UTAP URCA (2000) pp. 84–91.
[16] B. G. Vainer, J. Phys. D: Appl. Phys. **41** 065102 (2008).
[17] N. A. Vinokurov, B. A. Knyazev, G. N. Kulipanov, A. N. Matveenko, V. M. Popik, V. S. Cherkassky, M. A. Shcheglov, Tech. Phys. **52** 911–919 (2007).
[18] B. G. Vainer, A. A. Guzev, K. P. Mogilnikov, S. I. Romanov, V. A. Shvets, Proc. QIRT 2014 Conf., 7-11 July 2014, Bordeaux, France – Available at QIRT Open Archives: http://qirt.gel.ulaval.ca/archives/qirt2014/QIRT2014.html, Paper QIRT-2014-167 (7 pp).

High-efficiency lasing and spectroscopy of domestic Nd:YAG and Ho:YAG ceramics

S.M. Vatnik, I.A. Vedin, V.V. Osipov, K.E. Luk'yashin, R.N. Maksimov, V.I. Solomonov, Yu.L. Kopylov, I.Sh. Steinberg, P.E. Tverdokhleb, A.A. Pavlyuk
Institute of Laser Physics SB RAS, Novosibirsk, Russia
E-mail: vatnik@laser.nsc.ru

We report on spectroscopy and high-efficiency lasing of YAG ceramics synthesized at IREE (Fryazino) and IEP (Ekaterinburg). The best slope efficiency is to be 36% for 1%Nd:YAG ceramics and 40% for 1%Ho:YAG ceramics, in the latter case the emission was centered at 2090 nm. Internal losses in domestic ceramics was estimated as well.

Speed meter based on dissipative coupling

S. Vyatchanin, A. Matsko
Faculty of Physics, M.V. Lomonosov Moscow State University, Russia
E-mail: svyatchanin@phys.msu.ru

We show that generalized dissipative optomechanical coupling enables a direct quantum measurement of speed of a free test mass. An optical detection of a weak classical mechanical force based on this interaction is proposed with sensitivity better than the standard quantum limit. The realization of dissipative coupling is discussed.

Distributed polarization coupling measurement in polarization-maintaining fibers

Hongxia Zhang, Wang Feng, Dagong Jia, Tiegen Liu
College of Precision Instrument & Opto-electronics Engineering, Tianjin University, Tianjin 300072, China
Key Laboratory of Opto-electronics Information Technology (Tianjin University), Ministry of Education 300072, Tianjin, China
E-mail: hxzhang@tju.edu.cn

Owing to wide spectrum of light source, low coherence interferometry (LCI) possesses a lot of merits (e.g., high spatial resolution, wide dynamic range) and is widely used in many high-resolution measuring and sensing systems. Distributed fiber optics sensors, which employ WLI based on polarization mode coupling detection in polarization maintaining fibers(PMFs), are widely used in the measurement of strain, twist, temperture and many other physical parameters. The intensity and position of the coupling points can be effectively detected in the polarization coupling measurement.

However, the signal noise ratio (SNR) and the detection sensitivity of polarization coupling measurement will decrease due to the nonlinear error caused by the vibration of the step motor and the movable mirror in the scanning Michelson interferometer. To detect the weak coupling point, an EMD-based method is preposed. The experimental results illustrate that the EMD-based method can suppress the noise and improve the SNR effectively. The results show that the EMD-based method is effectively and applicable for PCM and the coupling point can still be detected when the intensity is as weak as -70 dB.

The interference term generated from LCI usually contains useful information. However, due to the effect of noise, interference term retrieval (ITR) is challenging. A conventional approach to ITR from interferometry uses Fourier transform to map the spectral domain interferogram to the temporal pulse, with the peak of the pulse corresponding to the interference term then being artificially extracted by setting the appropriate filter window. After extraction, a fast Fourier transform (FFT) operation back in the spectral domain allows the interference term to be recovered. An obvious disadvantage of this technique is that the filter must be precisely set to exclude the noise.

Empirical mode decomposition (EMD) is usually applied to nonlinear and nonstationary signals that can be adaptively decomposed into several intrinsic mode functions (IMFs) in a decreasing frequency order. EMD is effective in suppressing continuous noise, such as Gaussian noise and noise caused by mechanical vibration. However, the noise found in the spectral domain interferogram tends to contain intermittent noise so that EMD creates a mode-mixing problem, wherein local oscillations with different frequencies or scales are mixed in one IMF. The IMF then has no physical meaning. Ensemble empirical mode decomposition (EEMD) has been introduced as a way to solve the mode-mixing problem.

We proposed a novel technique based on EEMD-EMD to achieve automatic ITR from the spectral domain LCI. In EEMD, the correlation coefficient (CC) of each IMF is calculated and a characteristic parameter (CP) is introduced to recognize and remove the IMFs of noisy components. The remaining IMFs are used to reconstruct a new signal followed by EMD to extract the interference term. An experiment based on distributed polarization coupling detection in polarization-maintaining fibers (PMFs) was conducted; the PMFs having different lengths and coupling intensities were investigated. It was shown that by setting an appropriate CP, the interference term could be automatically extracted. The relative errors of the extracted coupling intensity were less than 2 %. This suggests that our method may have potential applications in interferometric measurement.

Raman spectra combined with PSO-LSSVM algorithm to detect the content of edible harmonic oil in three groups

Yanjun Zhang, Baodan He, Xinghu Fu, Jinrui Xu, and Kunpeng Zhou
The Key Laboratory for Special Fiber and Fiber Sensor of Hebei Province, School of Information Science and Engineering, Yanshan University, Qinhuangdao, Hebei 066004, P. R. China
E-mail: yjzhang@ysu.edu.cn

The paper presents a method of combining the Raman spectrum and the least square support vector machine based on particle swarm optimization to detect the content of three components of edible blend oil rapidly and quantitatively. In the course of the quantitative detection of cooking oil, three components of edible oil were used as the research object. The mathematical models of LSSVM and PSO-LSSVM were established after different pretreatment. The predictive ability of the model is analyzed by the correlation coefficient and mean square error. LSSVM kernel parameter σ and γ are optimized by particle swarm optimization ability and fast convergence speed. It overcomes the shortcomings of LSSVM model parameter selection method. The validation set correlation coefficient of the model for the quantitative analysis of the three components of the edible blend oil, soybean oil, peanut oil and sunflower kernel oil was 0.9677, 0.9972, 0.9953 and mean square error was 0.0549, 0.0092, 0.0471. The experimental results show that compared with the LSSVM algorithm, the prediction accuracy of PSO-LSSVM model is higher and the convergence rate is faster. Thus the method can detect the content of three components of edible oil accurately.

References

[1] Huijuan Wu, Yunjiang Rao, Cheng Tang, et al. Sensors and Actuators A: Physical **167**, 548(2011).
[2] Zhengxian Zhou, Songlin Zhuang. Optics Communications **33**, 1(2014).
[3] Pu Wei, Xuekang Shan, Xiaohan Sun. Optical Fiber Technology **19**, 47(2013).
[4] Mahmoud S S, Visagathilagar Y, Katsifolis J. Photonic Sensors **2**, 225(2012).
[5] Rao Yunjiang, Wu min, Ran Zenglin, et al. Chinese Journal of Sensors and Actuators **20**, 45(2007).
[6] David Looney, Danilo P. IEEE Transactions on Signal Processing **57**, 1626(2009).
[7] Renping Shao, Wentao Hu, Yayun Wang et al. Measurement **54**, 118(2014).
[8] Qiao Hu, Zhengjia He, Zhousuo Zhang et al. Mechanical Systems and Signal Processing **21**, 688(2007).
[9] Liu Heng bing, Han Shiqin, Liu Jing. Computer Engineering and Applications **43**, 72(2007).
[10] Xiaoning Jia, HangYang, Siliang Ma et al. Optics and Lasers in Engineering **57**, 28(2014).
[11] Kuang Chua Chuaa, Vinod Chandran, U. Rajendra Acharyaa et al. Medical Engineering & Physics **32**, 679(2010).
[12] B. Liang, S.D.Iwnicki, Y.Zhao. Mechanical Systems and Signal Processing **39**, 342(2013).

Probing the rotational dynamics of polar molecules using laser-induced THz wave generation

L. Alexandrov, M. Emelin, and M. Ryabikin
Institute of Applied Physics of the Russian Academy of Sciences, 603950 Nizhny Novgorod, Russia
E-mail: Alekvlis@gmail.com

Laser-assisted molecular alignment and orientation have become useful tools for molecular frame studies in physics and chemistry [1]. The ability to create an ensemble of polar molecules oriented in one direction in the absence of external influences has a great importance for applications in the attosecond and collisional physics, such as a molecular orbital tomography with high harmonic generation [2]. Several methods for nonadiabatic field-free orientation of asymmetric molecules have been demonstrated recently [3, 4]. In these methods, an ultrashort laser pulse gives a kick to the molecules, thereby creating the rotational wave packets whose dynamics exhibits a set of rotational revivals. An important problem is to measure the degree of order of the resulting ensemble. Currently, there are two main methods for probing the rotational dynamics of a molecular sample: Coulomb explosion [5] and high-order harmonic generation [6]. However, the search for new methods is still a topical issue.

In this contribution, we propose a novel all-optical method for probing the molecular orientation. This method is based on the measurement of the terahertz (THz) signal produced in ionization of oriented asymmetric molecules by an intense femtosecond laser pulse.

The ionization-induced optical-to-THz frequency conversion is closely related to the excitation of macroscopic quasi-dc currents whose excitation efficiency determines to a large degree an efficiency of the generation of THz waves [7]. Recently, we have examined the possibility of exploiting the asymmetry of the medium, rather than the properties of the laser field acting on it, to facilitate the generation of directional photocurrents [8]. We showed that the subcycle asymmetry of the ionization process in combination with the effect of the Coulomb potential on the escaping electron is a mechanism responsible for a high-efficiency generation of residual current in tunneling ionization of oriented asymmetric molecules.

The idea of the proposed method is based on the assumption that for molecules with nonzero dipole moment one can expect a strong dependence of the generated residual current on the angle between the direction of the dipole moment of a molecule and the electric field vector of the laser pulse. Theoretical study in this work is based on a single-active-electron quantum mechanical simulation for a two-dimensional model of a diatomic molecule in a strong laser field. The variable parameters of the model are the nuclear charge ratio and the internuclear distance.

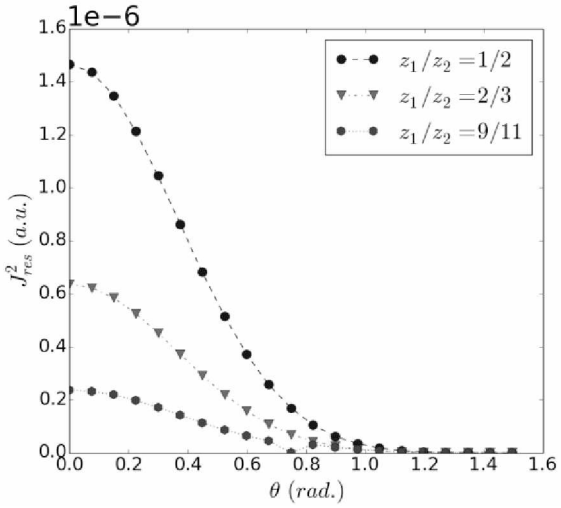

Fig. 1 Dependence of the residual current on the angle between the electric field vector and the molecular axis for different ratios of nuclear charges of a single-electron diatomic molecular system.

Figure 1 shows the orientation angle dependence of the generated residual current obtained for internuclear distance equal to 1.5 a.u. and probe laser pulse with wavelength $\lambda = 800$ nm and intensity $I = 5*10^{13}$ W/cm^2. Results for several nuclear charge ratios are presented. As follows from Fig. 1, the magnitude of the current depends strongly on the molecular orientation angle θ.

The experimental study of molecular rotational dynamics is usually based on the "pump-probe" scheme. The free rotational dynamics of molecules proceeds on a time scale much longer than the time scale of residual current generation process initiated by a femtosecond probe laser pulse. Therefore, the calculations of residual current as a function of the time delay between the pump and probe pulses can be performed in approximation of a fixed angular distribution of molecules during the probe pulse. We use the approach proposed in [9] for the simulations of rotational dynamics of a molecular ensemble after the kick acquired from the pump pulse. The calculations of the nonlinear response of the medium to the probe pulse were carried out by averaging of a single particle response calculated for various orientations of the molecule over the molecular rotational wave packet at the probing time.

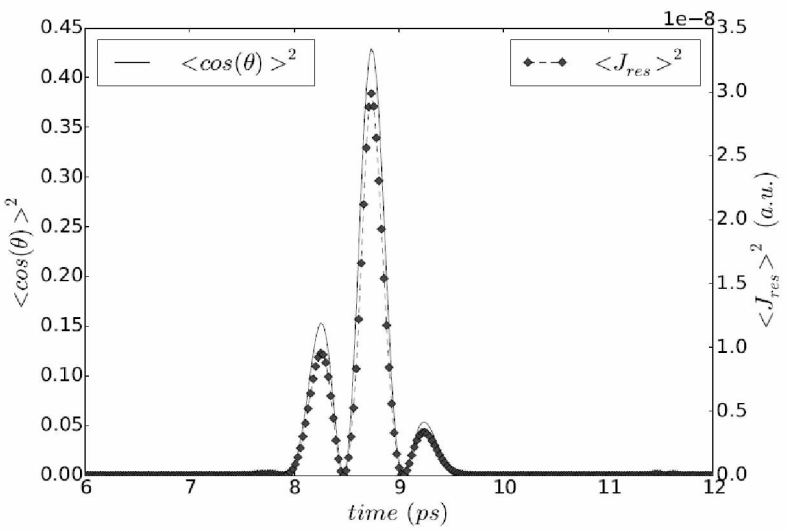

Fig. 2 The expected values of the residual current generated in a gas of CO molecules and the cosine of molecular orientation angle θ as functions of the time delay between the pump and probe pulses.

Figure 2 shows the dependencies of the expected values of the residual current generated in a gas of CO molecules and the cosine of molecular orientation angle on the time delay between the pump and probe pulses. The pump pulse intensity was $1.5*10^{14}$ W/cm^2, the probe pulse intensity was $5*10^{14}$ W/cm^2, and the initial gas temperature was T = 50K. From Fig. 2 it follows that the generated macroscopic current is directly proportional to the expected value of $\cos(\theta)$. Given the proportionality between the magnitudes of THz signal and residual current, the results in Fig. 2 demonstrate the possibility of probing the rotational dynamics of an ensemble of polar molecules using the THz signal generated therein. Because of the relative simplicity of the proposed measurements, this method can be quite competitive with the more complex methods based on the use of the Coulomb explosion or high-order harmonic generation.

References

[1] H. Stapelfeldt and T. Seideman, Rev. Mod. Phys. **75**, 543 (2003).
[2] C. Vozzi, M. Negro, F. Calegari et al., Nature Phys. **7**, 822 (2011).
[3] H. Sakai, S. Minemoto, H. Nanjo et al., Phys. Rev. Lett. **90**, 083001 (2003).
[4] S. De, I. Znakovskaya, D. Ray et al., Phys. Rev. Lett. **103**, 153002 (2009).
[5] L. Holmegaard, J. H. Nielsen, I. Nevo et al., Phys. Rev. Lett. **102**, 023001 (2009).
[6] E. Frumker, C. T. Hebeisen, N. Kajumba et al., Phys. Rev. Lett. **109**, 113901 (2012).
[7] V. B. Gildenburg and N. V. Vvedenskii, Phys. Rev. Lett. **98**, 245002 (2007).
[8] L. N. Alexandrov, M. Yu. Emelin, and M. Yu. Ryabikin, Phys. Rev. A **87**, 013414 (2013).
[9] M. Spanner, S. Patchkovskii, E. Frumker et al., Phys. Rev. Lett. **109**, 113001 (2012).

Attosecond x-ray plasma laser via modulation of active medium by IR laser field

V. A. Antonov[1], T. R. Akhmedzhanov[2], Y. V. Radeonychev[1], A. Morozov[3], A. Goltsov[3], M. O. Scully[2], S. Suckewer[3] and O. A. Kocharovskaya[2]

[1]*Institute of Applied Physics of the Russian Academy of Sciences, Nizhny Novgorod 603950, Russia*
[2]*Texas A&M University, College Station, TX 77843-4242, USA*
[3]*Princeton University, Princeton, NJ 08540-5621, USA*
E-mail: antonov@appl.sci-nnov.ru

The resonant interaction of a quasi-monochromatic extreme ultraviolet (XUV) or x-ray radiation with an atomic or nuclear transition with modulated parameters (a transition frequency, a decoherence rate, and a dipole moment) results in generation of a broadband spectrum of coherent sidebands. Such interaction can be used for an efficient control of the spectral content and the temporal shape of the output field by means of (i) a deep high frequency modulation of the nuclear transition frequency in 10-100 keV spectral range via the Doppler effect caused by the nuclear target vibrations up to 10 GHz modulation frequency [1-4], as well as (ii) modulation of the parameters of atomic transitions (the frequency, the dipole moment and the decoherence rate) in the XUV spectral range under the action of a strong infrared (IR) laser field with THz - PHz frequency, in particularly, due to the sub-laser-cycle linear Stark effect (or via formation of the Floquet states, in general), as well as the quasi-static ionization from the excited states [5-8]. The last processes can be alternatively viewed as a highly nonlinear mixing of the XUV and IR fields.

Such a dynamical-modulation control has various applications, ranging from production of few-cycle pulses with a carrier photon energy below atomic ionization potential and isolated attosecond pulse formation in the soft-XUV spectral range [5-8], to shaping of individual hard x-ray photons into the time-bin qubits [1, 2] and ultrashort pulse trains [3, 4].

The main focus of this talk is on the possibility of efficient transformation of modern x-ray plasma laser radiation into the trains of sub-fs pulses [6, 8], as well as sub-fs pulse generation directly in the active media of x-ray plasma lasers. The sub-femtosecond x-ray pulses provide a unique combination of high spatial and temporal resolution. Currently, the only source of such pulses is high harmonic generation (HHG) of laser fields, which dictates relatively low energy of the pulses (typically, in the range 1-100 nJ) because of the low efficiency of HHG process. At the same time, modern table-top plasma lasers are able to generate soft x-ray pulses in 4-100 nm wavelength range with much higher energy (from μJ up to several mJ), but with rather long picosecond or sub-ps duration. Thus, a highly efficient method for transformation of an output radiation of x-ray plasma laser into an attosecond pulse train is very desirable.

In this contribution we show, in particular, that picosecond pulses with a carrier wavelength 13.5 nm (generated by H-like LiIII recombination x-ray laser [9]) may be efficiently converted into the train of sub-femtosecond pulses in a thermally equilibrium plasma of Li^{2+} ions dressed by the properly chosen IR field, see Fig.1(a). Moreover, using of an IR field of the same frequency and intensity directly applied to the active medium of recombination LiIII x-ray laser (with ion density $10^{17}cm^{-3}$ and total length 1mm) with fully inverted 2P-1S transition can result in formation and strong (by a factor of 50) amplification of 0.9 fs pulses.

Even shorter pulses can be generated in a "water window", the range of wavelengths between K absorption edges of carbon and oxygen (2.3-4.4nm), which is of particular interest for applications in biology and medicine due to the potentially high contrast and high resolution dynamical imaging of proteins in live cells. We show that applying of an IR field of a properly chosen wavelength and

intensity directly to the inverted media of a recombination CVI x-ray laser [10] may lead to formation of strongly amplified attosecond pulses in this particular spectral range, Fig.1(b).

In such a way, both an efficient conversion of x-ray laser radiation into the trains of sub-fs pulses in resonantly absorbing plasma medium, as well as formation and amplification of sub-fs pulses directly in the active media of x-ray lasers in the presence of a moderately strong IR laser field modulating the parameters of the resonant transition look promising.

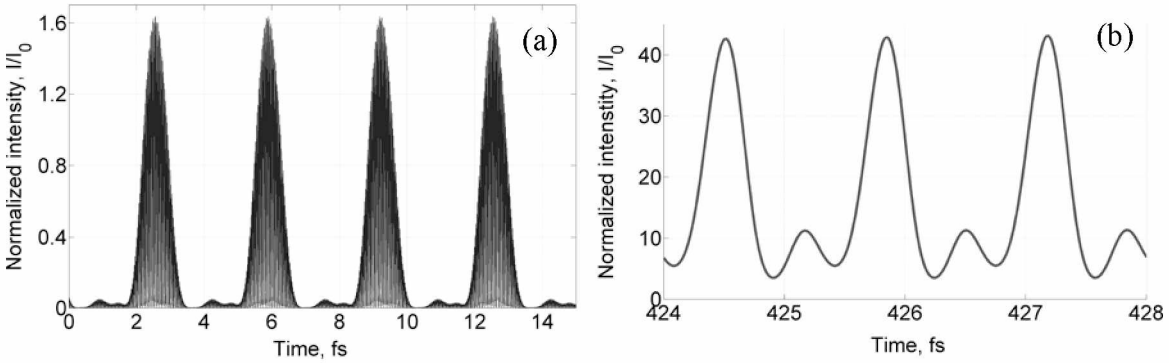

Fig. 1. (a) - Efficient transformation of the quasi-continues (ps) 13.5 nm radiation of H-like LiIII x-ray laser into a train of 0.9fs pulses after passing of 2 mm long thermally equilibrium (resonantly absorbing) Li^{2+} plasma with ion density $10^{17}cm^{-3}$ in the presence of 2μm IR field with intensity $3.6x10^{14}W/cm^2$. The peak intensity of the produced pulses is 1.6 times higher than the intensity of the incident XUV radiation. **(b)** - Formation and amplification of 330 as pulses at 3.38nm carrier wavelength (in a "water window") in the active medium of recombination CVI x-ray laser with ion density $10^{17}cm^{-3}$ and total length 1.8mm in the presence of IR field with the wavelength 2μm and intensity $9x10^{15}W/cm^2$. The peak pulse intensity is 42.6 times higher than the intensity of the incident x-ray field.

References

[1] F. Vagizov, V. Antonov, Y. V. Radeonychev, R. N. Shakhmuratov, and O. Kocharovskaya, Nature **508**, 80 (2014).
[2] R. N. Shakhmuratov, F. G. Vagizov, V. A. Antonov, Y. V. Radeonychev, M. O. Scully, and O. Kocharovskaya, Phys. Rev. A **92**, 023836 (2015).
[3] V. A. Antonov, Y. V. Radeonychev, and O. Kocharovskaya, Phys. Rev. A **92**, 023841 (2015).
[4] Y. V. Radeonychev, V. A. Antonov, F. G. Vagizov, R. N. Shakhmuratov, and O. Kocharovskaya, Phys. Rev. A **92**, 043808 (2015).
[5] V. A. Antonov, Y. V. Radeonychev, and O. Kocharovskaya, Phys. Rev. Lett. **110**, 213903 (2013).
[6] V. A. Antonov, Y. V. Radeonychev, and O. Kocharovskaya, Phys. Rev. A **88**, 053849 (2013).
[7] V. A. Antonov, T. R. Akhmedzhanov, Y. V. Radeonychev, and O. Kocharovskaya, Phys. Rev. A **91**, 023830 (2013).
[8] T. Akhmedzhanov, V. A. Antonov, O .Kocharovskaya, Phys. Rev A, submitted.
[9] D.V. Korobkin, C.H. Nam, S. Suckewer, A. Goltsov, Phys. Rev. Lett. **77**, 5206 (1996).
[10] Y. Luo, A. Morozov, D. Gordon, P. Sprangle, A. Svidzinsky, H. Xia, M. Scully, S. Suckewer, Proceedings of the14th International Conference on X-Ray lasers, Springer Proceedings in Physics, **169**, Eds. J. Rocca, C. Menoni, M. Marconi, 21 (2014).

Multiple filamentation of terawatts laser pulses with different diameters at the atmospheric path

D.V. Apeksimov[1], A.A. Zemlyanov[1], A.N. Iglakova[1], A.M. Kabanov[1], O.I. Kuchinskaya[2], G.G. Matvienko[1], V.K. Oshlakov[1], A.V. Petrov[1]

[1] *Institute of Atmospheric Optics V.E. Zuev SB RAS, Tomsk, 634021, sq. Academician Zuev 1, Russia,*

[2] *National Research Tomsk State University, Tomsk, 634050, Lenin Avenue 36, Russia*

E-mail: kam@iao.ru

The results of experiments on the position control filamentation zone terawatt pulses of the first harmonic of Ti:Sapphire-laser are resented. Pulse duration was τ = 50 fs, pulse energy is 80 mJ beam diameter is d_0 = 5, 2.5 and 1.25 cm (the level of e^{-2}), a pulse repetition rate is of 10 Hz on the path length of 110 m. Experiments were carried out on the stand of IAO SB RAS. The spatial focus (defocus) of the laser beam with the telescope (5) consisting of a focusing (f_1 = 1000 mm) and defocusing (f_2 = -500 mm) mirrors, by varying the base (distance between the mirrors) of the telescope. The base of 500 mm corresponds to a collimated beam. Reducing the base defocused beam, increase the base focused. Sequence arrangement of mirrors leads to a decrease of the beam diameter is 2 times ($f_1 \rightarrow f_2$), either to the same increase it ($f_2 \rightarrow f_1$). The experiments were recorded beginning filamentation region, its end and the distribution of filaments within the region filamentation by a movable screen (13). The number of filaments was determined by the burns on photo paper. Figure 1 shows the number of filaments along the area at different initial filamentation focusing (defocusing). With an increase in the base of the telescope (fig. 2a-c) start and end of filamentation shifted towards the radiation source. Reduced base results in a displacement of the source region filamentation.

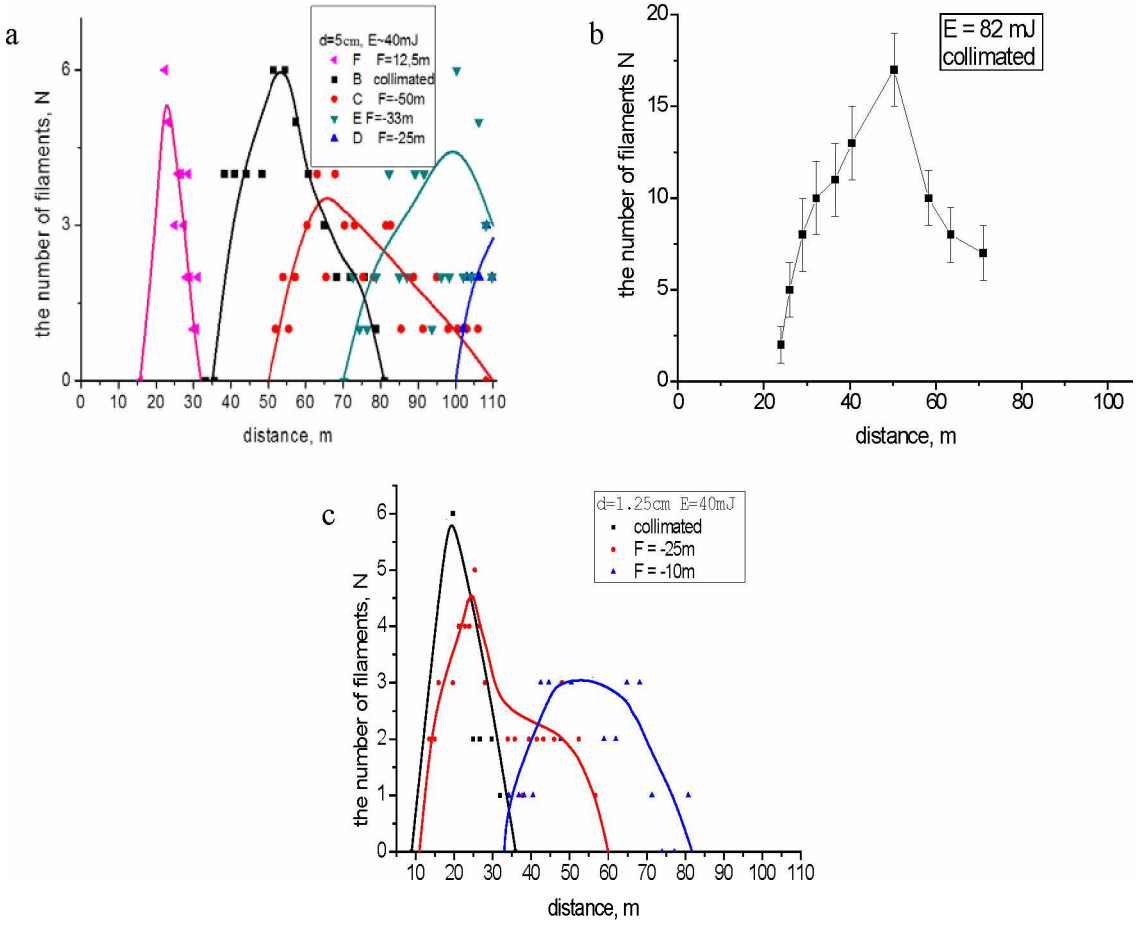

Fig. 1 Distribution of the number of filaments inside area filamentation at different focusing (defocusing) beam diameter: a) 5 cm, b) 2.5 cm, and c) 1.25 cm.

Figure 2a shows the dependence of the length of the field for different initial filamentation focusing (defocusing) for different beam diameters. It is seen that increasing the value of the numerical aperture leads to a decrease in the length field filamentation relative power increase and a decrease in the numerical aperture to increase the path length of the region filled with filaments (Fig 2b).

Experiments were performed on remote induction plasma on target in the zone of the beam filamentation and identification of the elemental composition of the emission spectra. The measured emission spectra of the samples of metals (Al, Cu, Fe, Na) at a distance of 50m from leser to a collimated beam with energy of 40 mJ. In experiments on filamentation of laser beams in air shows that the variation of the beam diameter and its initial focus is to efficiently manage the situation in the field of multiple filamentation tracks scale of hundreds of meters. This defocusing the beam has limits. These levels depend on the diameter of the beam and its power, above which filamentation of the beam stops. Managed filamentation of the laser beam allows to form a predetermined distance from the source of the intensities of the optical field sufficient to induce the plasma on the targets for the analysis of the elemental composition.

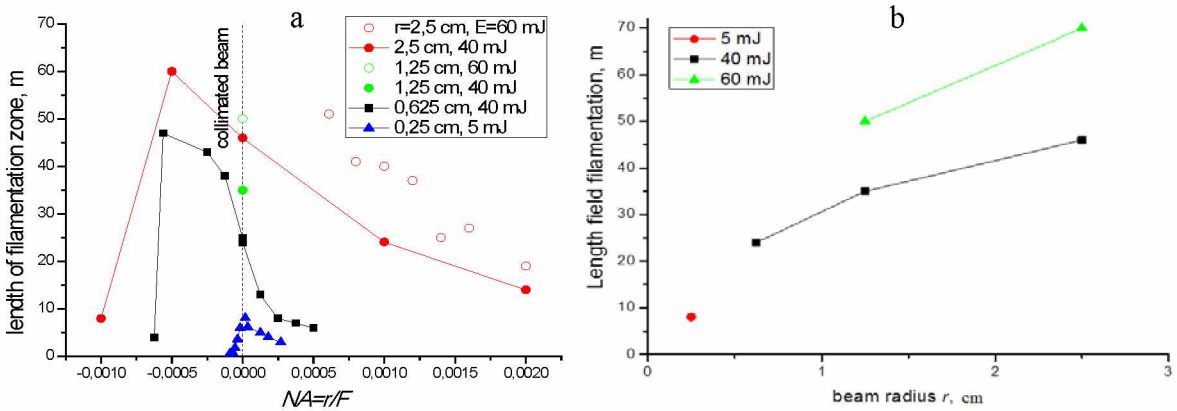

Fig. 2 a) Length field filamentation of numerical aperture for different pulse energies. b) Length field filamentation of initial radius of the collimated beam for different pulse energies.

This work was financially supported by the Russian Science Foundation (agreement № 15-17-10001).

References

[1] Apeksimov D. V., Bukin O. A., Golik S. S., Zemlyanov A. A., Iglakova A. N., Kabanov A. M., Kuchinskaya O. A., Matvienko G. G., Oshlakov V. K., Petrov A. V., Sokolova E. B., Khoroshaeva E. E., "Spatial characteristics of the filamentation region of gigawatt laser pulses at their various focusing along an atmospheric path," Atmospheric and oceanic optics **27**, 1042 (2014).

[2] Apeksimov D. V., Zemlyanov A. A., Iglakova A. N., Kabanov A. M., Kuchinskaya O. A., Matvienko G. G., Oshlakov V. K., "Filamentation of terawatt laser pulses on a hundred-meter atmospheric path," Atmospheric and oceanic optics **28**, 274 (2015).

Post-filament light channels

D.V. Apeksimov[1], A.A. Zemlyanov[1], A.N. Iglakova[1], A.M. Kabanov[1], O.I. Kuchinskaya[2], G.G. Matvienko[1], V.K. Oshlakov[1], A.V. Petrov[1]
[1]Institute of Atmospheric Optics V.E. Zuev SB RAS, Tomsk, 634021, sq. Academician Zuev 1, Russia
[2]Research Tomsk State University, Tomsk, 634050, Lenin Avenue 36, Russia
E-mail: kam@iao.ru

Self-focusing and filamentation of laser pulses in atmospheric optics tasks can be used for the sensing of the atmosphere, creating extended ionized channels forming in a given coordinate route high intensity laser radiation field [1-3]. At the same time after the "disintegration" filamentation region as after the termination of plasma formation and disappearance of visible glowing filaments (filaments), each of them is formed by a narrow, weakly divergent light channel. Properties data channels - wide spectral composition (Figure 3d), high intensity, continuing at great distances, are of interest for the above-mentioned problems of atmospheric optics. Earlier properties postfilamentation channels (PFC) have been studied by us and by other authors for the focused beams [4,5]. This PFC research work carried out for collimated beams of different diameters on the road about 150 m. The experimental procedure is described in detail in [2,3,5]. Examples of imaging energy density distribution in the cross section of the beam at different distances from the end of the field of multiple filamentation (FMF) for one of the primary beam diameter (d_0 = 2,5 cm) are shown in Fig. 1

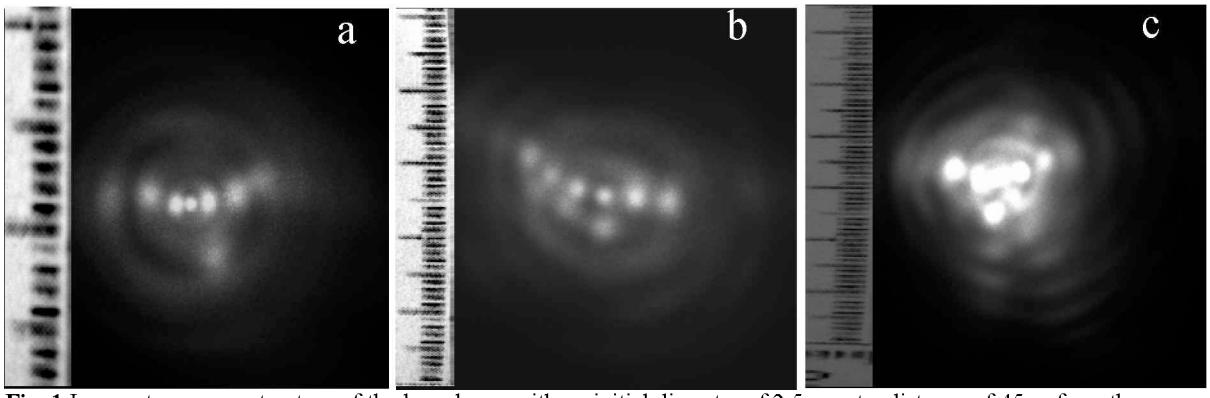

Fig. 1 Images transverse structure of the laser beam with an initial diameter of 2.5 cm at a distance of 45 m from the source (3 m from the end FMF) (a), 105 m from the source (65 m from the end FMF), (b), 138 m from the source (98 m from the end FMF) (c).

The images show that the central part of the beam provides bright, so-called "hot" point - postfilamentation channels surround system less bright rings that may interfere with the divergence of PFC. Dependence of the radius of the beam and the spread distance from the PFC are shown in Fig. 2.

Depending obtained indicate that the PFC is tens divergence micro radians, while the divergence of the beam after passing through all the global focus (not including the area of the conical feed filamentation - rings color system) is ~ micro radians, that is. two orders of magnitude greater. It was found that when exposed postfilamentation channels to sample optical glass away from FMF in tens times exceeding its length, resulting in the formation of multiple filamentation in it, having the structure of a hollow cone, observed earlier in [6].

Thus, the results of experimental studies and filamentation postfilamentation channels controlled by the path length of 150 meters for collimated beams of various diameters showed that: the divergence of the laser beam after the filamentation area is much greater than the divergence postfilamentation channels; at distances from the end of the field much larger than the length of the filamentation area filamentation of postfilamentation channels contain sufficient intensity to generate multiple filamentation in the optical elements and enables us to provide a functional effect on the optical elements of the matrix; wide range and high intensity slightly divergent postflamentation channels allows their use for the remote sensing of the atmosphere.

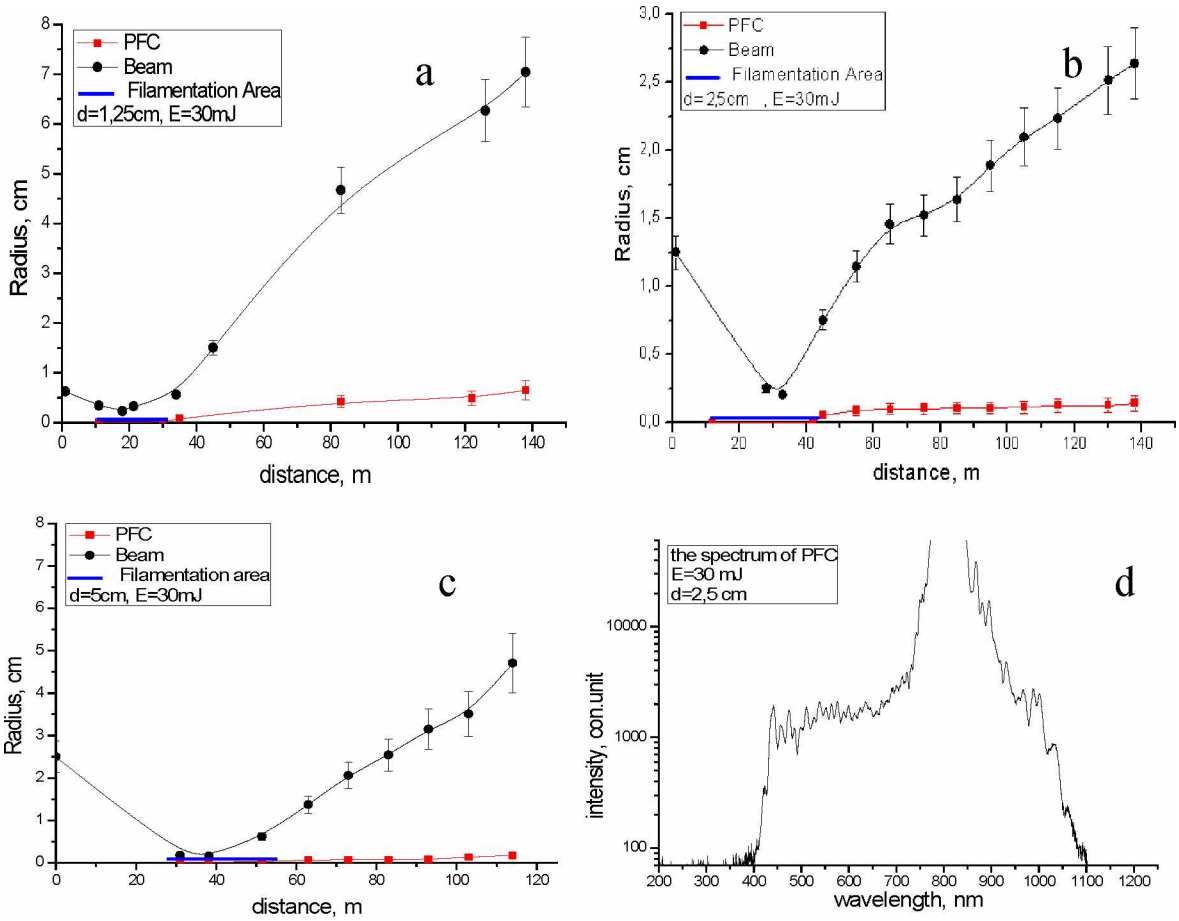

Fig. 2 Changes in the beam radius and postfilamentation channels with different initial diameters a) 1.25 cm; b) 2.5 cm;c) 5 cm of distance from the laser pulse. d) - The spectrum of PFC.

Fig. 3 Snapshot multiple filamentation in glass K8 when exposed PFC at a distance of 90 m from the end of FMF.

Work performed with financial assistance of the Russian Science Foundation (agreement №16-17-10128).

References

[1] Geints J.E., Zemlyanov A.A., Kabanov A.M., Matvienko G.G. "Nonlinear optics femtosecond atmosphere" Tomsk: Publishing House of the Institute of Atmospheric Optics, 212 (2010).

[2] Apeksimov D. V., Zemlyanov A. A., Iglakova A. N., Kabanov A. M., Kuchinskaya O.I., Matvienko G. G., Oshlakov V. K., "Filamentation of terawatt laser pulses on a hundred-meter atmospheric path," Atmospheric and oceanic optics **28**, 274 (2015)

[3] Apeksimov D.V., Zemlyanov A.A., Iglakova A.N., Kabanov A.M., Kuchinskaya O.I., Matvienko G.G., Oshlakov V.K., Petrov A.V. "Multiple filamentation of laser beams with different diameters in the air at a 100-meter path" Atmospheric and oceanic optics **29**, 51 (2016).

[4] Hui Gao, Weiwei Liu and See Leang Chin. "Post-filamentation multiple light channel formation in air" Laser Physics **24**, 1 (2014).

[5] Apeksimov D.V., Zemlyanov A.A., Kabanov A.A. "Post-filamentation light channel in air" Atmospheric and oceanic optics **29**, will be published soon (2016).

[6] Apeksimov D.V., Golik S.S., Zemlyanov A.A., Iglakova A.N., Kabanov A.M., Kuchinskaya O.A., Matvienko G.G., Oshlakov V.K., Petrov A.V., Sokolova E.B. "Multiple filamentation of collimated laser radiation in water and glass" Atmospheric and oceanic optics **28**, 972 (2015).

Control of light-pulse propagation in electromagnetically induced grating using additional driving field

V.G. Arkhipkin, S.A. Myslivets, P.S. Pankin
L.V.Kirensky Institute of Physics, Krasnoyarsk, Russia
E-mail:*avg@iph.krasn.ru*

Electromagnetically induced grating (EIG) [1] is created in a three-level quantum system whena weak probe field and a strong-pumpstanding wave satisfy the conditions for electromagnetically induced transparency (EIT) [2]. EIG is formed owing to periodicspatially modulated absorption, where transparency occurs at the antinodes (peaks) of the standing-wave field and absorption is high at the nodes. EIG transmission behavior is significantly different from that of the typical EIT. Under certain conditions EIG may have a photonic band gap structure that has potential applications for manipulation of light propagation.The EIG has been explored to achieve tunable band gap [3, 4], to generate stationary light pulses [5], to implement optical routing [7], as the diffraction grating [1]and etc.J.-H. Wu et al [8] have proposed a possibility to control the spectral properties EIG using additional driving field with frequency ω_3 in the four-level scheme N-type (Fig. 1), where the coupling field with frequency ω_2 is the standingwave, and field with frequency ω_1 is the weak probe field.

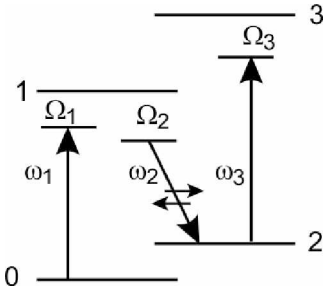

Fig. 1 Schematic diagram of a four-level N-type atomic system interacting with a weak probe field ω_1 and a strong-pump standing field ω_2 and a strong drive field ω_3. $\Omega_{1,2,3}$ are the single-photon detuning from the respective transitions.

In this paper we theoretically studied propagation of a weak light pulse in such system (Fig.1). Here the transitions |0>-|1>, |1>-|2> and |2>-|3> are electric dipole allowed while the transitions |0>-|2> and |0>-|3> are electric dipole forbidden. The weak probe (the frequencyω_1,and the wave vector k_1) and strong drive (ω_3, k_3) fields with a Rabi frequency G_1 and G_3propagate in z direction. A coupling field(ω_2, k_2) is the standing-wave with spatial dependent Rabi frequency $G_2(z)=G_{2+}e^{ik_2z}+G_{2-}e^{-ik_2z}$ is formed by the forward and backward waves that propagate toward one another.

Susceptibilityof a weak probe field propagating in a four-level medium (Fig.1)may be presented as [9,10]

$$\chi(\omega_1,z)=i\chi_p\frac{(\Delta_{20}\Delta_{30}+|G_3|^2)\gamma_{10}}{\Delta_1\Delta_{20}\Delta_{30}+\Delta_{10}|G_3|^2+\Delta_{30}|G_2(z)|^2},\quad \chi_p=\frac{|d_{10}|^2N}{2\hbar\gamma_{10}} \tag{1}$$

$$\Delta_1=\gamma_{10}-i\Omega_1,\ \Delta_2=\gamma_{12}-i\Omega_2,\ \Omega_1=\omega_1-\omega_{10},\ \Omega_2=\omega_2-\omega_{12},\ \Delta_{20}=\gamma_{20}-i\Omega_{20},$$
$$\Delta_{30}=\gamma_{30}-i\Omega_{30},\ \Omega_{20}=\omega_1-\omega_2-\omega_{20},\ \Omega_{30}=\omega_1-\omega_2+\omega_3-\omega_{30}.$$

γ_{ij} are the half-width transitions, d_{10} is the matrix element of the dipole moment of the transition, N is the concentration of atoms.

Deriving Eq. (1) we assume that the medium is linear with respect to the probe field. The coupling field is strong enough that EIT well-established within the whole sample. The susceptibility (1) is even function of z, which is convenient to expand in a cosine Fourier series $\chi(z,\omega_1)\simeq\chi_0+\chi_1\cos(2k_2z)$. For simplicity, we took into account only two spatial harmonicswhich approximate $\chi(\omega_1,z)$ enough well.

$$\chi_0=(k_2/\pi)\int_0^{\pi/k_2}\chi(z,\omega_1)dz,\quad \chi_1=(2k_2/\pi)\int_0^{\pi/k_2}\chi(z,\omega_1)\cos(2k_2z)dz.$$

Due to spatial periodic modulation of the susceptibility (1) induced by coupling standing-wavethe probe field propagate as in a multilayer periodic structure with periodicity $a=\pi/k_2=\lambda_2/2$. So it can propagate not only in the forward direction (a transmitted wave), but also in backward one (a reflected wave).

By using the method of coupled waves [11], we find the transmission t and the reflection $r$amplitude coefficients for probe wave propagating in periodic structure with length L,

$$t(\omega_1)=\frac{A(L)}{A_0}=\frac{s\cos(sL)\exp(ik_2L)}{s\cos(sL)+i(\Delta k-\alpha)\sin(sL)},\quad r(\omega_1)=\frac{B(L=0)}{A_0}=\frac{\sigma\sin(sL)}{s\cos(sL)+i(\Delta k-\alpha)\sin(sL)} \tag{2}$$

$$s=\pm\sqrt{(\Delta k-\alpha)^2-\sigma^2},\quad \Delta k=k_2-k_1,\quad \alpha=2\pi\chi_0k_1,\quad \sigma=\pi\chi_1k_1.$$

Here L is the length of sample, $A_0$is the amplitude of incident probe wave, A(L) is the amplitude of probe field on the output of sample (forward wave), andB(L=0) is the amplitude of the reflected probe field (backward wave).

By utilizing Eq. (2) and the Fourier transform method, one can study the propagation dynamics of an incident probe pulse. We assume that the input probe pulse is the Gaussian pulse $E_{1i}(t)=E_0\exp(-t^2/\tau^2)\exp(i\omega_1t)$, where$E_0$ is the amplitude, $2\tau=T_p$is the pulse length at the e^{-1} level, and ω_1 is the central (carrier) frequency. The pump and the drive fields are the continuous monochromatic waves. The spectrum of the input probe pulse is the Fourier transform of the given pulse:$E_{1i}(\omega)=2^{-1/2}\tau E_0\exp[-\tau^2(\omega-\omega_1)^2/4$. The reflected and the transmitted Fourier components of the probe pulse can be derived as $E_{1r}=r(\omega)\,E_{1i}(\omega)$ and $E_{1t}=t(\omega)\,E_{1i}(\omega)$. The reflected and the transmitted pulse in the time domain are derived via inverse Fourier transform.

For numerical simulation, we used Rb atomic parameters asEIT medium. The probe transition wavelenght is λ_{10} =780.792 nm while for the coupling field is λ_{12} =780.778 nm. Fig.2a shows the transmission and reflection spectra of a probe fieldfor different the Rabi frequencies of a drive fieldG_3.In the absence of the control field (G_3=0), the Rabi frequencies$G_{2+}$and G_{2-} are selected such that a bandgapand a passband arose.When a drive field is swiched on bandgap and passband are destroyed with increasing G_3.Fig.2b illustrates transmittedandreflected Gaussian probe pulse for different Rabi frequencies of a drive field. It is seen that using the drive field can control the transmission and reflection of EIG.

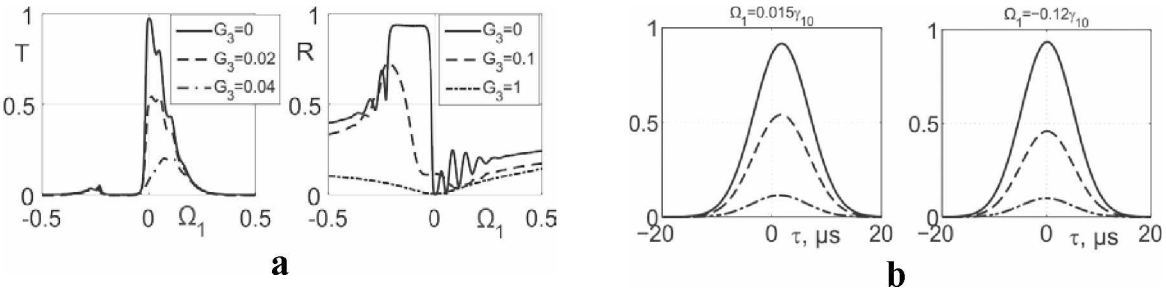

Fig. 2a) Transmission (left) and reflection (right) spectra as a function of the probe detuning Ω_1(in units γ_{10}) for different different the Rabi frequencies G_3(in units γ_{10}).**b).**The transmitted (left) and reflected (right) probe pulse for different Rabi frequencies of a drive field indicated in Fig. 2. Other parameters are $G_{2+}=5\gamma_{10}$, $G_{2-}=(5/6)\,G_{2+}$, $\gamma_{10}=\gamma_{12}=\gamma_{32}=2\pi$ 6 MHz, $\gamma_{20}=2\pi$ 1kHz, $N=10^{12}$ cm^{-3}, L=2 cm.

In conclusion, we are shown howthetransmissionand reflection of probe pulse in EIG can becontrolledusing additional drive field. All-optical switching of the reflected and transmitted pulse aredemonstrated.

References

[1] H.Y. Ling, Y.Q. Li, M. Xiao, Phys. Rev. A **57**, 1338 (1998).
[2] M.Fleischhauer, M.D. Lukin, A. Marangos, Rev. Mod.Phys. **77**, 633 (2005).
[3] A. Andre, M.D. Lukin, Phys. Rev. Lett. **89**, 143602 (2002).
[4] M. Artoni, G.La Rocca, Phys. Rev. Lett. **96**, 073905 (2006).
[5] M. Bajcsy, A.S. Zibrov, M.D. Lukin, Nature **426**, 638 (2003).
[6] Y.W. Lin, W.T. Liao et al, Phys. Rev. Lett. **102**, 213601 (2009).
[7] A.W. Brown, M. Xiao, Opt. Lett. **30**, 699 (2005).
[8] J.-H. Wu, A. Raczynski, J. Zaremba et al., J. Mod. Optics **56**, 768 (2009).
[9] V.G. Arkhipkin, Quantum Electron. **27**, 341 (1997).
[10] S.E. Harris and Y. Yamamoto, Phys. Rev. Lett. **81**, 3611 (1998).
[11] S.Y. Karpov and S.N. Stolyarov, Physics-Uspekhi **36**, 63 (1993).

Laser fluorescent polarization defects microscopy in optical materials

M. Arsenteva[1], V. Dresvyansky[1], S. Zilov[1], A. Rakevich[1], O. Buhtsooge[2] and E. Martynovich[1]
[1]*Irkutsk Branch of the Institute of Laser Physics SB RAS, 664033, Irkutsk, Lermontov street, 130A, Russia*
[2]*Institute of Physics and Technology Mongolian Academy of Science, 210651, Ulaanbaatar, Enkhtaivan av., 54B, Mongolia*
E-mail: sasha.moiseeva@mail.ru

The efficiency of the interaction of optical radiation with matter is largely determined by the type (multipolarity) and the orientation of the elementary oscillators, describing the quantum systems interacting with radiation. For example, in case of electric dipole interaction the energy of interaction of optical radiation with luminescence centers depends on the orientation of the electric field vector and the vector of the electric dipole moment of the elementary oscillator associated with the quantum transitions responsible for the absorption and emission of light in the luminescence centers [1].

The luminescence centers in crystals usually have pronounced anisotropic properties. Thus, the transition from the ground state of the center to the excited state and vice versa, i.e. absorption and emission of light by the color centers in crystals, are simulated by linear electric dipole oscillator or by rotator oriented along one of the crystallographic axes. Therefore, the light emitted by the center will be polarized in a certain way and the degree of polarization of the total luminescence of these centers summarized for all possible orientations of the center will be different from zero and will be dependent upon the crystal orientation relative to the direction and polarization of the exciting light and luminescence observation direction [2]. This fact can be used to build a spatial pattern of luminescence centers distribution according to the degree of polarization and constitutes the basis of our proposed method of determining the size of grain in optical ceramics containing emission centers of known origin.

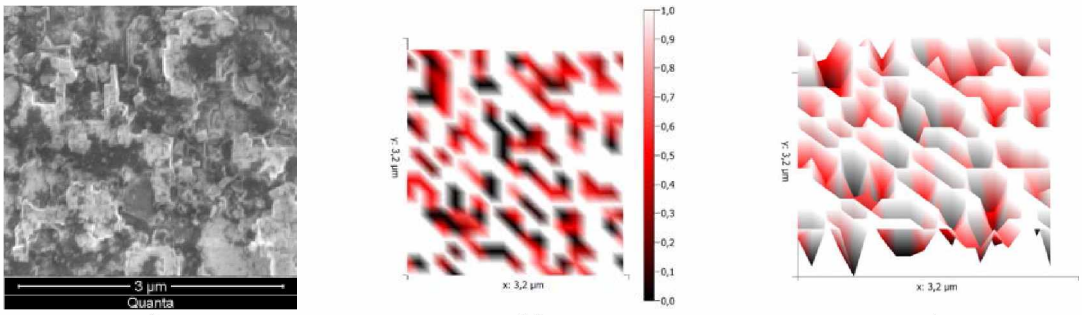

a) b) c)

Fig. 1 Images of the optical ceramics surface a) – the SEM data, b) and c) – the data of laser luminescent polarization microscope with 2D and 3D scanning respectively.

To extract information from the observation of polarized luminescence it is necessary to be able to examine the degree of radiation polarization depending on the relative orientation of the electric vector of the exciting light wave, the crystal axes and the direction of observation. The degree of polarization $P = (I_{II} - I_{\perp})/(I_{II} + I_{\perp})$ is a measure of the luminescence polarization when the exciting light is linearly polarized, $I_{\parallel}$ — the intensity of the luminescence component polarized in the same plane as the excitation light, and $I_{\perp}$ — the intensity of the luminescence component polarized in the orthogonal plane as the excitation light. Since the orientation of the luminescence centers does not change in a single grain and the grains themselves in ceramics have a random distribution, we can assume that the abrupt change in the value of the polarization degree will occur at the grain

boundaries. Thus, knowing the scanning step, it is possible to determine the size of a single grain with a certain probability.

Given that the proposed method is new, we have approbation it at centers with known properties to assess its adequacy. We carried out experiments with F_2 color centers in lithium fluoride ceramics. It is known that these centers are oriented along the diagonals of the cube faces (C_2). The experiments were carried out on a laser confocal scanning microscope MicroTime 200 with implemented two-channel scheme of registration of the luminescence intensity I_{II} and $I_{\perp}$.

The mathematical tool developed on the analysis of the polarization component of luminescence allows us to consider arbitrary multipolarity transitions oriented on arbitrary axes of symmetry. Calculation of the degree of polarization of the luminescence P, excited and observed for a given type centers shows that the degree of polarization of luminescence varies from 0.33 to 0.66, and depends on the crystal orientation. The obtained dependence has been confirmed experimentally.

Map of the spatial distribution of the polarization degree was built as a result of the measurements. On this map different values of P correspond to specific colors: the places where this velue converges to maximum – the map has red color, where it converges to a minimum - white color, the place where the glow is absent (zero) - black color. The brightness indicates the total intensity for both channels. As an example, in Figure 1 we present the comparative images of the optical ceramics surface according to data from scanning electron microscope (SEM), and laser luminescent polarizing microscope. As one can see our map of the spatial distribution of polarization degree adequately reflects the results of SEM. Further analysis consists of determining of the boundaries and size of grains displayed on the map with taking into account the step of scan.

The work was performed as part of the SB RAS project II.10.1.6., and with the financial support of RFBR project № 16-52-44056.

References

[1] P. Feofilov, 88 (1959).
[2] E. Martynovich and V. Dresvyansky, Opt. Communications, V. **224**. 263 (2003).

Two-photon absorption at the $2^1S–2^3S$ Forbidden Transition of Helium

E. Baklanov[1] and P. Pokasov[2]
[1]*Institute of Laser Physics, Siberian Branch, Russian Academy of Sciences, prosp. Lavrent'eva 13/3, 630090 Novosibirsk, Russia*
[2]*Novosibirsk State University, ul. Pirogova 2, 630090 Novosibirsk, Russia*
E-mail:baklanov.ev@gmail.com

The 2^1S-2^3S transition between the triplet and singlet parts of the helium spectrum is of interest for spectroscopy because of its small radiative width (8 Hz), which is determined by the 2^1S level decay to the 1^1S ground state. The possibility of a precise measurement of the 2^1S-2^3S transition frequency was studied in [3,4,5].We study two-photon absorption at the $2^1S–2^3S$ transition of helium, when the pumping field (1083 nm) is in resonance with the $2^3S–2^3P_1$ transition and the stimulated field (3561 nm) is in resonance with the $2^1S–2^3P_1$ transition.

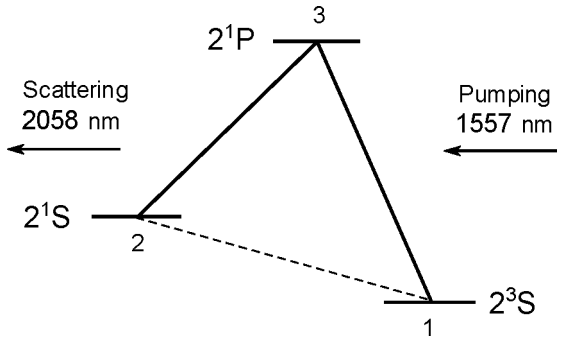

We consider the problem of the interaction of two waves propagating in the same direction in a gas of three-level atoms. Our estimates show that the gain for the scattered wave is rather highThe density of particles detected at the 2^1Slevel in one second for pumping wave 1 mW/cm^2 can be

$$R(2^1S) = 10^8 cm^{-2} s^{-1}.$$

To detect atoms in the excited 2^1Sstate, we will consider a technique based on the detection of spontaneous vacuum-ultraviolet 58-nm photons.We are interested in the signal-to-noise ratio in the detection of VUV photons with a wavelength of 58 nm. The number of photons absorbed within the detection time t is equal to $N = Rt$, where R is the number of atoms excited to the 2^1Sstate per unit time. In the absence of a background, the fluctuation of the photon number is equal to $\sqrt{N}$. To detect a line shape with an accuracy of 10^{-3}, we should ensure that

$$\frac{Signal}{Nose} = \frac{N}{\sqrt{N}} = 10^3.$$

The results obtained show the way to observe of two-photon absorption at the $2^1S–2^3S$ transition of helium.

References

[1] E. Baklanov and A. Denisov, Laser Phys. **8**, 567 (1998).
[2] E.V. Baklanov, P.V. Pokasov, D.Yu. Primakov, V.A. Tykilin, Laser Physics **15**, 1068 (2005).
[3] K.A.H. van Leeuwen and W. Vassen, Europhys. Lett.**76**, 409 (2006).

Control the propagation of radiation spectrum and correlations in optically dense gas by the microwave field

K. Barantsev, A. Litvinov, and E. Popov
Peter the Great St. Petersburg Polytechnic University, St. Petersburg, Politechnicheskaya, 29, Russia
E-mail: kostmann@yandex.ru

It is known that, because of quantum interference, interaction of a three-level system with a two-frequency laser field in the Λ configuration gives rise to a superposition state that does not interact with the laser radiation. This phenomenon is referred to as the coherent population trapping (CPT) effect [1,2]. In the presence of the closed excitation contour density matrix of an atom depends on the relative phase of radiation [3]. In this manner the CPT effect can be either fully destroyed or restored. The possibility to control the superposition state parameters was investigated for both the atomic [4] and solid-state systems [5].

New interesting feature of three-level atoms that form an optically dense medium and are excited by a three-frequency laser radiation (Δ-scheme, Fig.1(a)) is the presence of spatial quasiperiodic refractive index oscillations [6]. This nontrivial phenomenon can be used as a basis for development of materials with a controlled photon band that can be changed by manipulating the laser fields affecting the atomic ensemble.

In this work we have developed the theory of propagation of the laser radiation with finite width of spectrum in optically dense gas, consists of Δ-atoms, in the presence of closed excitation contour (Fig.1(a)). This theory takes into account fluctuations of optical fields with Rabi frequencies Ω_1 and Ω_2 and correlations between them. It is based on the set of quantum kinetic equations for the atomic density matrix $\tilde{\rho}_{mn}(z,t)$ and transport equations for the field correlation functions:

$$\left(\frac{\partial}{\partial t}+\upsilon\frac{\partial}{\partial z}\right)\tilde{\rho}_{mn}=-\frac{i}{\hbar}\sum_{j}^{3}[H_{mj}\tilde{\rho}_{jn}-\tilde{\rho}_{mj}H_{jn}]+R_{mn}+S_{mn}, \qquad (1)$$

$$\frac{\partial}{\partial z}\left\langle\Omega_n^*(z,t)\Omega_m(z,t')\right\rangle=i\left(q_m\left\langle\Omega_n^*(z,t)\rho_{3m}(z,t')\right\rangle-q_n\left\langle\Omega_m(z,t')\rho_{n3}(z,t)\right\rangle\right), \qquad (2)$$

where H is the Hamiltonian, R is the relaxation matrix, S is the collision integral, z is the axis along wave vector of radiation, υ is the projection of atom velocity on the z axis, $\rho_{mn}(z,t)$ is the slow amplitude of density matrix, q_m is the dimensional coefficients, m, n = 1,2,3. Equation (2) is obtained from the wave equations for the complex amplitudes of the field after averaging over the field fluctuations.

On the Fig.1 (b) one can see the intensity I_1 of the field with Rabi frequency Ω_1 depending on coordinate z for different shapes and width Γ_{las} of the input laser spectrum. There are the spatial quasiperiodic intensity oscillations, the period of which depends on overlapping integral of the laser spectrum and the absorption line of the gas. In the case of $\Gamma_{las}=1\gamma$ overlapping integral takes a maximum value, therefore the period of oscillations is minimal. And vice versa, in the case of $\Gamma_{las}=40\gamma$ and Gaussian profile of spectrum overlapping integral takes a minimum value and oscillations become extended.

Also, in this work we have calculated the propagation of field correlations in the optically dense gas. It was found that the correlation in the field can be increased under certain conditions. This fact can be used to create the filter of coherent part of radiation.

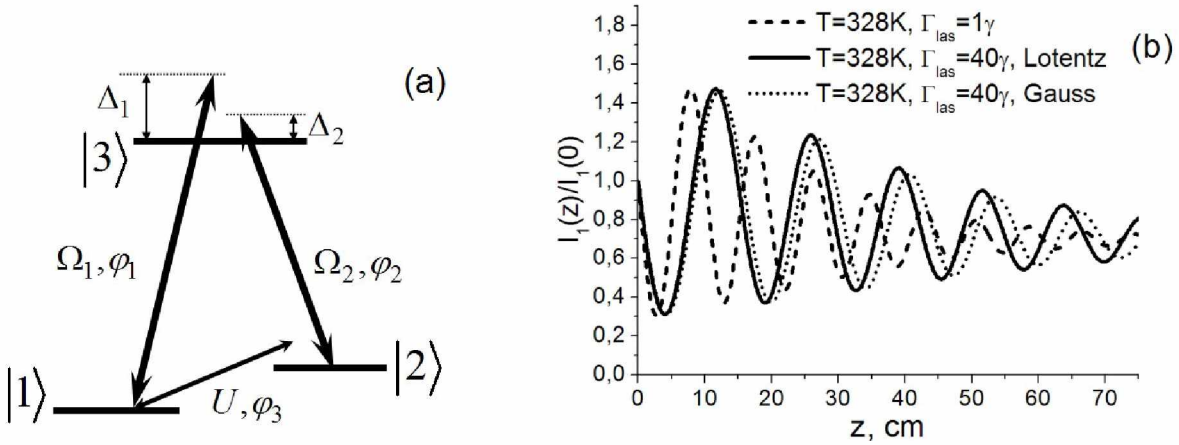

Fig. 1 (a) - Scheme of atomic levels in closed excitation contour (- scheme). Ω_1 and Ω_2 are the Rabi frequencies of optical fields, U is the Rabi frequency of microwave field, Δ_1 and Δ_2 are one-photon detuning, φ_n are the relative phases of the fields. (b) - Normalized intensity I_1 of the frequency component Ω_1 depending on the coordinate z along propagation of radiation for different spectrum widths Γ_{las} for Lorentzian and Gaussian shapes of the laser spectrum. γ is decay rate of excited level.

References

[1] B.D. Agapiev, M.B. Gorniy, B.G. Matisov, Yu.V. Rozhdestvensky, UFN **163**, 1 (1993).
[2] E. Arimondo, Progress in optics **35**, p.257-354 (1996).
[3] D.V. Kosachiov, B.G. Matisov, Yu.V. Rozhdestvensky, J. Phys. B **25**, 2473 (1992).
[4] S.J. Buckle, S.M. Barnett, P.L. Knight et. al., Optica Acta **33**, 1129 (1986).
[5] A.N. Litvinov, K.A. Barantsev, B.G. Matisov et. al., Optics Communications 305, 155 (2013).
[6] K. A. Barantsev, A. N. Litvinov, JETP **118**, №4, pp. 569-579 (2014).

Atomic spectroscopy in periodic fields

M.Yu. Basalaev[1,2], V.I. Yudin[1-3], A.V. Taichenachev[1,2]
[1]*Novosibirsk State University, ul. Pirogova 2, Novosibirsk, 630090 Russia*
[2]*Institute of Laser Physics SB RAS, pr. Akademika Lavrent'eva 13/3, Novosibirsk, 630090 Russia*
[3]*Novosibirsk State Technical University, pr. Karla Marksa 20, Novosibirsk, 630073 Russia*
E-mail: mbasalaev@mail.com

For the last several decades rapid scientific and technological progress has been substantially connected with an expansion of the lasers and laser technologies at different areas of the science, engineering, and industry. Many impressive successes in these directions are due to the theoretical support, motivation, and interpretation of experimental researches. In this context, of paramount importance is the formulation of mathematical models (equations) and finding of their solutions, which adequately describe the physical picture of investigated problems. During long time, steady states (which arises under the interaction of a quantum system with stationary external fields) play a key role in the theoretical description of the basic problems in laser physics and spectroscopy (for example, see [1–3]). However, in the last few years the devices in which different parameters of electromagnetic fields are periodically modulated have gained a greater importance. First of all, the so-called frequency comb generators use the periodic pulse modulation of a laser field. Such sources of pulse radiation are actively used now in modern atomic clocks for frequency measurements, and they have promising perspectives for direct frequency comb spectroscopy. Also, the phase (frequency) and/or amplitude periodic modulation of the laser field is now widely used for different tasks and applications (including atomic clocks and magnetometers). In all these examples the standard concept of steady state based on the time-independent equation is inapplicable.

We generalize the steady-state concept for an arbitrary quantum system under arbitrary periodic external influence. In this way we prove the following existence theorem: if the coefficients of density matrix dynamic equation

$$\frac{\partial}{\partial t}\hat{\rho}(t) = -\frac{i}{\hbar}[\hat{H}, \hat{\rho}(t)] + \hat{\Gamma}\{\hat{\rho}(t)\}, \qquad \mathrm{Tr}\{\hat{\rho}(t)\} = 1 \tag{1}$$

have the period T, then the periodic solution with the same period T exists always. A completely unexpected result is that so universal and fundamental a statement is based only on the normalization condition for the density matrix. Due to the relaxation processes this solution is realized as an asymptotics ($t \to +\infty$) and, therefore, can be characterized as a periodic steady state. The developed simple algorithm allows us to directly construct this solution independently of initial conditions and without the use of either Floquet or Fourier formalisms. Our approach considerably simplifies the analysis regardless of the periodic modulation character: from smoothly harmonic type to ultrashort pulses.

Some authors supposed (without proof) the existence of the periodic steady-state solution for some certain problems. In this case they usually used the Fourier analysis for numerical calculations). However, an intuitive assumption about the periodic steady state is now rigorously substantiated [4]. At the same time, of special interest is the direct and simple method, which allows us to construct the periodic solution without Fourier expansion.

Let us describe one possible numerical algorithm allowing to construct the periodic solution of equation (1). First, rewrite the differential equation (1) for the density matrix in the vector form:

$$\frac{\partial}{\partial t}\vec{\rho}(t) = \hat{L}(t)\vec{\rho}(t), \qquad \mathrm{Tr}\{\hat{\rho}(t)\} = 1, \tag{2}$$

where the column vector $\vec{\rho}(t)$ is formed by the matrix elements $\rho_{ab}(t)$ using some definite rule, the linear operator $\hat{L}(t)$ corresponds to the right-hand member of Eq. (1). In accordance with Eq. (2), for other instant of time t_2 we can write

$$\vec{\rho}(t_2) = \hat{A}(t_2, t_1)\vec{\rho}(t_1), \tag{3}$$

where the two-time evolution operator $\hat{A}(t_2,t_1)$ is determined by the matrix $\hat{L}(t)$. Consider $\vec{\rho}(t)$ at arbitrary instant of time t. In conformity with Eq. (3), the vector $\vec{\rho}(t+T)$ is determined as

$$\vec{\rho}(t+T) = A(t+T,t)\vec{\rho}(t)\,, \tag{4}$$

where T is time period in the operator $\hat{L}(t)$, i.e. $\hat{L}(t+T) = \hat{L}(t)$. Supposing the existence of the periodic solution $\vec{\rho}(t+T) = \vec{\rho}(t)$, it follows from Eq. (4) that this solution satisfies the equation

$$\vec{\rho}(t) = A(t+T,t)\vec{\rho}(t)\,, \qquad \mathrm{Tr}\{\hat{\rho}(t)\} = 1\,, \tag{5}$$

which always has a nonzero solution as it has been proven in our work [4]. We consider an arbitrary periodic dependence of the operator $\hat{L}(t)$. For instance, under an atom-field interaction such a dependence can be produced by the modulation of the field parameters (amplitude, phase, polarization, etc.).

The selected time interval $[t_0,\ t_0 + T]$ is divided into N small subintervals, where $t_N = t_0 + T$. The character of partition (uniform or nonuniform discrete mesh) and number of subintervals are determined in conformity with the studied problem. The dependence $\hat{L}(t)$ we will approximate by step function where the matrix $\hat{L}(t)$ has the constant value $\hat{L}(t_{m-1})$ inside of subinterval $(t_{m-1},t_m]$. In this case the vector $\vec{\rho}(t_0)$ in initial point t_0 is determined by Eq. (5), where the evolution operator $\hat{A}(t_0+T,t_0)$ has the form of a chronologically ordered product of the matrix exponents:

$$A(t_0+T,t_0) \approx \prod_{m=1}^{m=N} e^{(t_m-t_{m-1})\hat{L}(t_{m-1})} = e^{(t_N-t_{N-1})\hat{L}(t_{N-1})} \times \ldots \times e^{(t_1-t_0)\hat{L}(t_0)}\,. \tag{6}$$

The vectors $\vec{\rho}(t_m)$ in other points of the interval $[t_0,\ t_0 + T]$ are determined by the recurrence relation

$$\vec{\rho}(t_m) = e^{(t_m-t_{m-1})\hat{L}(t_{m-1})}\vec{\rho}(t_{m-1})\,. \tag{7}$$

In summary, in the framework of density matrix formalism we have rigorously proven the existence theorem of the periodic steady state for an arbitrary periodically driven system. Due to the relaxation processes this state is realized as an asymptotics ($t \to +\infty$) independently of initial conditions, i.e., periodicity is the main attribute of steady state. The proof simultaneously contains a computational algorithm, which uses neither Floquet nor Fourier theories. Our method radically simplifies the calculations for arbitrary types of periodic modulation (including the ultrashort pulses) and opens up great possibilities for analysis and development of new methods in laser physics, nonlinear optics, and spectroscopy.

The work was supported by the Ministry of Education and Science of the Russian Federation (State Assignment No. 2014/139, Project No. 825), by the Russian Foundation for Basic Research (Grants No. 16-32-60050, 16-32-00127, 15-32-20330, 15-02-08377, 14-02-00712, 14-02-00939), and by Russian Presidential Grant (NSh-6689.2016.2)

References

[1] W. Demtroder, "Laser Spectroscopy" (Springer-Verlag, Berlin, 2003).
[2] V.S. Letokhov and V.P. Chebotaev, "Nonlinear Laser Spectroscopy" (Springer-Verlag, Berlin, 1977).
[3] S.G. Rautian and A.M. Shalagin, "Kinetic Problems of Nonlinear Spectroscopy" (North-Holland, Amsterdam, 1991).
[4] V I. Yudin, A.V. Taichenachev, and M.Yu. Basalaev, Phys. Rev. A **93**, 013820 (2016).

Tunable multicolored generation using silicon nanopillars

L.S. Basalaeva[1], Yu.V. Nastaushev[1], F.N. Dultsev[1], N. V. Kryzhanovskaya[2]
[1]*A.V. Rzhanov Institute of Semiconductor Physics SB RAS, Lavrentieva, 13, Novosibirsk 630090, Russia*
[2]*St. Petersburg Academic University - Nanotechnology Research and Education Centre of the Russian Academy of Sciences, Khlopina str. 8, St. Petersburg 194021, Russia*
E-mail: GolobokovaLS@isp.nsc.ru

Silicon nanopillars (Si NPs) have a unique capability of manipulating and controlling light on a nanoscale. The new mechanism to generate structural color through the tall Si NPs has been demonstrated in [1-2]. Structural color generation has aroused considerable interest with its promising applications in various fields including imaging sensors, optical filters, and displays. Si NPs exhibit intense Mie resonances in the visible spectral region [3]. An important advantage of the structures is that the properties of the entire system can be controlled by changing geometrical dimensions of the Si NPs [4-5]. A decrease in the coefficient of the reflection of light from structures with Si NPs is related to a considerable increase in the area of the surface with Si NP arrays in comparison with a flat surface. It is important that the profile of the refractive index is modulated by an ordered array of NPs (medium–pillar–medium) while scattering occurs at an individual Si NP.

The present study focuses on the optical properties of Si NPs with diameter 60 nm÷250 nm and height 100 nm÷800 nm (pitch 400 nm÷1700 nm). We measure the reflectance spectra of square arrays of Si NPs. Si NPs arrays viewed under the bright-field illumination can demonstrate the vivid color generation. We investigate how the resonances in the Si NPs can be tuned by tuning geometrical dimensions of the nanopillars. The passivation of Si NPs was performed. Si NWs were treated in boiling nitric acid. Then, Si NWs were chemically and electrically passivated through the deposition of TiONx nanolayer at 8 nm thickness. Scanning Electron Microscope (SEM) and Atomic Force Microscopy (AFM) were used to characterize the Si NPs. Reflectance spectra from arrays of Si NPs were measured at wavelengths ranging from 500 nm to 1150 nm. Spectra were normalized with the spectrum taken from a gold wafer. The light was normally incident toward the sample and focused through an objective. We found some peaks and dips in the measured spectra. The position of the dips varied with Si NPs diameter. The wavelength of minimum reflectance shifts to longer wavelength region with an increase in Si NP diameter. Tunable color generation from vertical silicon Si NPs is demonstrated. Si NP arrays (after nitric acid) exhibit similar color but lower intensity. It is worth noting that Si NP annealing lead to a decrease in the intensity of the reflected signal at the resonance wavelengths, with almost unchanged wavelength of reflection minimum. The spectrum can be modified by varying the geometrical parameters of Si NPs (diameters, pitch, and height).

The work was supported by RFBR via grant 16-32-00269 mol_a.

References

[1] K. Seo, M. Wober, P. Steinvurzel et al., Nano Lett. **11**, 1851 (2011).
[2] M. Khorasaninejad, N. Abedzadeh et al., Nano Lett. **12**, 4228 (2012).
[3] F. J. Bezares, J. P. Long et al., Optics Express **21**, 27587 (2013).
[4] K. T. Fountaine, W. S. Whitney et al., J. Appl. Phys. **116**, 153106 (2014).
[5] S. Tsoi, F.J. Bezares, et al., Appl. Phys. Lett. **108**, 111101 (2016).

Experimental realization of surface plasmon laser

F.A. Benimetskiy[1], A.I. Plekhanov[1], A.S. Kuchyanov[1], R.G. Parkhomenko[2], T.V. Basova[2]
[1]*Institute of Automation and Electrometry, 1 Acad. Koptug Ave., Novosibirsk, Russia*
[2]*Institute of Inorganic Chemistry, 3 Acad. Lavrentiev Ave., Novosibirsk, Russia*
E-mail: benimetskiy@gmail.com

Over the last decade, nanophotonics is undergoing rapid development. One of the interesting devices that has been theoretically predicted [1] and realized [2] is spaser. Spaser is an acronym for surface plasmon amplification by stimulated emission of radiation. Surface plasmon lasers have many potential practical applications such as ultrasensitive detection, spectroscopy of chemical. They are potentially able to provide ultra-fast (fs-scale or faster) optical processes [3] and useful as a novel versatile biomedical tool [4], etc.

The spaser is analogous to the conventional laser. A spaser consists of a metal nanoparticle as the resonator surrounded by a nanoshell of the gain medium. In contrast, the spaser as a nanoscopic quantum generator of localized surface plasmons is a promising candidate for a wide range of applications because it allows beating the diffraction limit and focusing electromagnetic energy on spots much smaller than a wavelength.

We have fabricated spherical and cylindrical spasers with gold core and silica dye-embedded shell and characterized them with the use of transmission electron microscopy, confocal microscopy (Fig.1). We have studied the stimulated emission of spherical and cylindrical spasers with the different aspect ratio, which allowed to significantly expand the spectral range of the spasing. We have shown that the stimulated emission threshold was about 250 kW/cm^2 for spherical spasers and some less for cylindrical ones. The spasing signature can be also seen from the concurrent onset of the line width narrowing plateau and the nonlinear kink of the "S"-shape L-L plot shows the output power of the spasing mode as a function of pump power. In addition, emission dynamics obtained for spherical spasers at a wavelength of 526 nm showed that the pulse is shortened at excess pumped critical threshold.

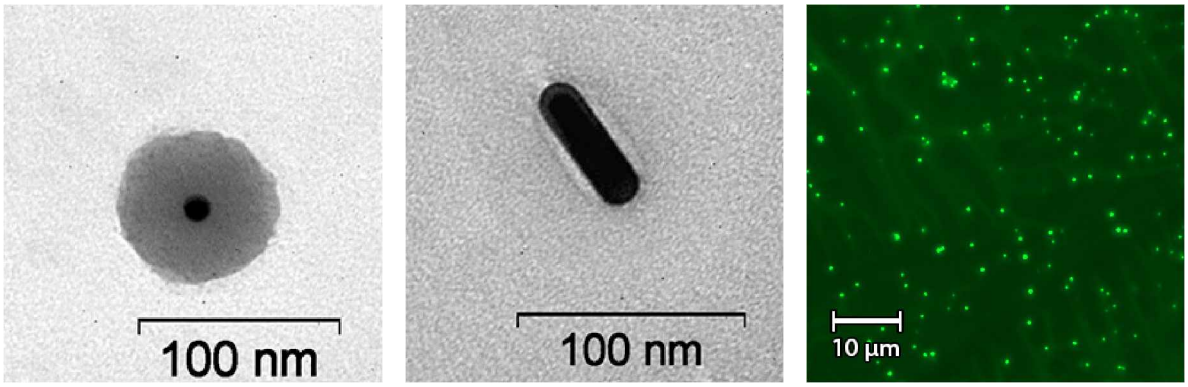

(a) (b) (c)

Fig. 1 Schematic of a spherical spaser made from a gold core and surrounded by silica shell with doped dye molecules. Schematic of a (a) spherical and (b) cylindrical spaser made from a gold core and surrounded by silica shell with doped dye molecules. (c) Confocal microscopy image of the spherical spasers.

This work was supported by RFBR 15-03-03833 and 16-32-00710 mol_a.

References

[1] Bergman, D., Stockman, M. Rev. Lett., **90**, 027402 (2003).
[2] Noginov, M., Zhu, G.; Belgrave, A; Bakker, R., Shalaev, V., Narimanov, E., Stout, S., Herz, E., Suteewong, T., Wiesner, U., Nature, **460**, 1110 (2009).
[3] Stockman M., J. Opt. **12**,024013 (2010).
[4] Galanzh E.I., Weingold R., Nedosekin D.A., Sarimollaoglu M, Kuchyanov A.S., Parkhomenko R.G., Plekhanov A.I., Stockman V.I., Zharov V.P. Spaser as Novel Versatile Biomedical Tool., arXiv 1501.00342 (2015).

Laser cooling and trapping of strontium atoms

O.I. Berdasov[1,2], S.A. Strelkin[1,2], A.Yu. Gribov[1,2], A.A. Galyshev[1,2], K. Yu. Khabarova[1,3], N.N. Kolachevsky[1,2,3], S.N. Slyusarev[1]

[1]*Federal State Unitary Enterprise "AllRussia Research Institute for Physicotechnical and Radio Engineering Measurements" (VNIIFTRI), Mendeleevo, Moscow oblast, 141570 Russia*

[2]*National Research Nuclear University "MEPhI," Kashirskoe sh. 31, Moscow, 115409 Russia*

[3]*Lebedev Physical Institute, Russian Academy of Sciences, Leninskii pr. 53, Moscow, 119991 Russia*

E-mail: berd_7@mail.ru

Deep laser cooling of strontium atoms allows to decrease Doppler effect, to localize atoms and to increase interaction time between clock laser and atoms, which is important for precision spectroscopy. We present our work on cooling and trapping strontium atoms to the optical lattice within high performance optical atomic clocks creation.

Förster resonances in rubidium and cesium atoms for Rydberg blockade, entanglement and quantum gates

I.I. Beterov[1,2,3], M. Saffman[4], E.A. Yakshina[1,2], D.B. Tretyakov[1,2], V.M. Entin[1,2], S. Bergamini[5], E.A. Kuznetsova[6], I.I. Ryabtsev[1,2]

[1]*Rzhanov Institute of Semiconductor Physics SB RAS, 630090 Novosibirsk, Russia*
[2]*Novosibirsk State University, 630090 Novosibirsk, Russia*
[3]*Novosibirsk State Technical University, 630073 Novosibirsk, Russia*
[4]*University of Wisconsin-Madison, Madison, Wisconsin, 53706, USA*
[5]*The Open University, Walton Hall, MK7 6AA, Milton Keynes, UK*
[6]*Institute of Applied Physics RAS, 603950, Nizhny Novgorod, Russia*
E-mail: beterov@isp.nsc.ru

Two-qubit quantum gates are the key element of a quantum computer. In general, any quantum algorithm can be implemented using a two-qubit controlled-NOT (CNOT) or controlled-Z (CZ) gate and single-qubit rotations. Arrays of optical dipole traps with ultracold neutral atoms can be used as quantum registers of arbitrary dimensions, and the interaction of the atom qubits to perform two-qubit gates can be controlled by their temporary excitation to Rydberg states, which experience strong long-range interactions [1].

At the same time, high-fidelity two-qubit gates with Rydberg atoms have not been demonstrated yet. Our approach to building a two-qubit gate is based on controlled phase shifts of collective states of two qubits during double adiabatic passage across the Stark-tuned Förster resonance. The interaction strength should be adjusted to provide a certain phase shift (for example, π), during the interaction time. This can be easily done with Stark-tuned Förster resonances that provide fast and flexible control by manipulating the energies of Rydberg levels with an electric field. The Rydberg levels are adjusted in such a way that one Rydberg level lies midway between two other Rydberg states of the opposite parity. Then a resonant energy transfer between Rydberg atoms initially excited to the middle state becomes possible via resonant dipole-dipole interaction.

If two Rydberg atoms are frozen in space, dipole-dipole interaction at a Förster resonance induces the Rabi-like coherent population oscillations between collective states of these atoms. The frequency of these collective oscillations is sensitive to variations of the interaction energy due to fluctuations of the spatial position of the atoms within the optical dipole traps. This can substantially increase the phase gate error. We propose to overcome this difficulty by using a double adiabatic rapid passage across Stark-tuned Förster resonances with a deterministic phase accumulation [2].

The scheme of the CZ gate is shown in Fig.1(a). Two optical dipole traps with one atom in each trap are located at a distance R between them. Scheme of the CZ gate is shown in the left-hand panel of Fig.1. The two atoms are simultaneously excited to Rydberg state $|\mathrm{r}\rangle$ by a π laser pulse labeled as 1. The distance between the traps must be sufficiently large to avoid the effect of Rydberg blockade. A time-dependent external electric field shifts the collective energy levels so that the Förster resonance $|\mathrm{rr}\rangle \rightarrow |\mathrm{r'r''}\rangle$ is passed adiabatically two times. This results in a deterministic phase shift of state $|\mathrm{rr}\rangle$ in the case when both atoms are initially prepared in state $|11\rangle$.

We have calculated the time dependence of population and phase of the collective $|90S_{1/2}, 96S_{1/2}\rangle$ state of two Cs atoms at $|90S_{1/2}, 96S_{1/2}\rangle \rightarrow |90P_{1/2}, 95P_{1/2}\rangle$ Förster resonance for slightly different interatomic distances R=24, 25 and 26 μm [see Fig.1(b)-(h)]. Our calculations have shown that this variation of the interatomic distance leads to small phase changes at the end of the adiabatic passage, thus evidencing that our method to perform two-qubit quantum gates is insensitive to the atom position uncertainty.

In the scalable quantum register with neutral atoms one of the possible error sources is absorption of the photons which are emitted by the atoms when the qubit state is measured using resonance fluorescence. The absorption of these photons by the qubits in the neighboring sites of the array of optical dipole traps may lead to the decoherence of the quantum state of the qubits. This effect can be suppressed by using the resonance fluorescence of the auxiliary qubits for quantum state

measurement. The atoms of different chemical elements with different emission wavelength can be used as auxiliary qubits, as shown in Fig.1(h). This is also valuable for quantum simulators with Rydberg atoms. We have studied theoretically the interaction of Rb and Cs Rydberg atoms [3]. We have found numerous Förster resonances which can be used to increase the strength of the interspecies interaction [Fig.1 (i)]. We have calculated the constants of the van der Waals interaction taking into account the degeneracy of the Rydberg energy levels.

This work was supported by the Russian Science Foundation Grant No. 16-12-00028 in the part of numeric simulation of the two-qubit gates and Bell states, by RFBR Grants No. 14-02-00680 and 16-02-00383, by Novosibirsk State University and Russian Academy of Sciences. MS was supported by NSF award 1521374, the AFOSR MURI on Quantum Memories and Light-Matter Interfaces, and the ARL-CDQI through cooperative agreement W911NF-15-2-0061. S.B. was supported by EPSRC grant no EP/K022938/1.

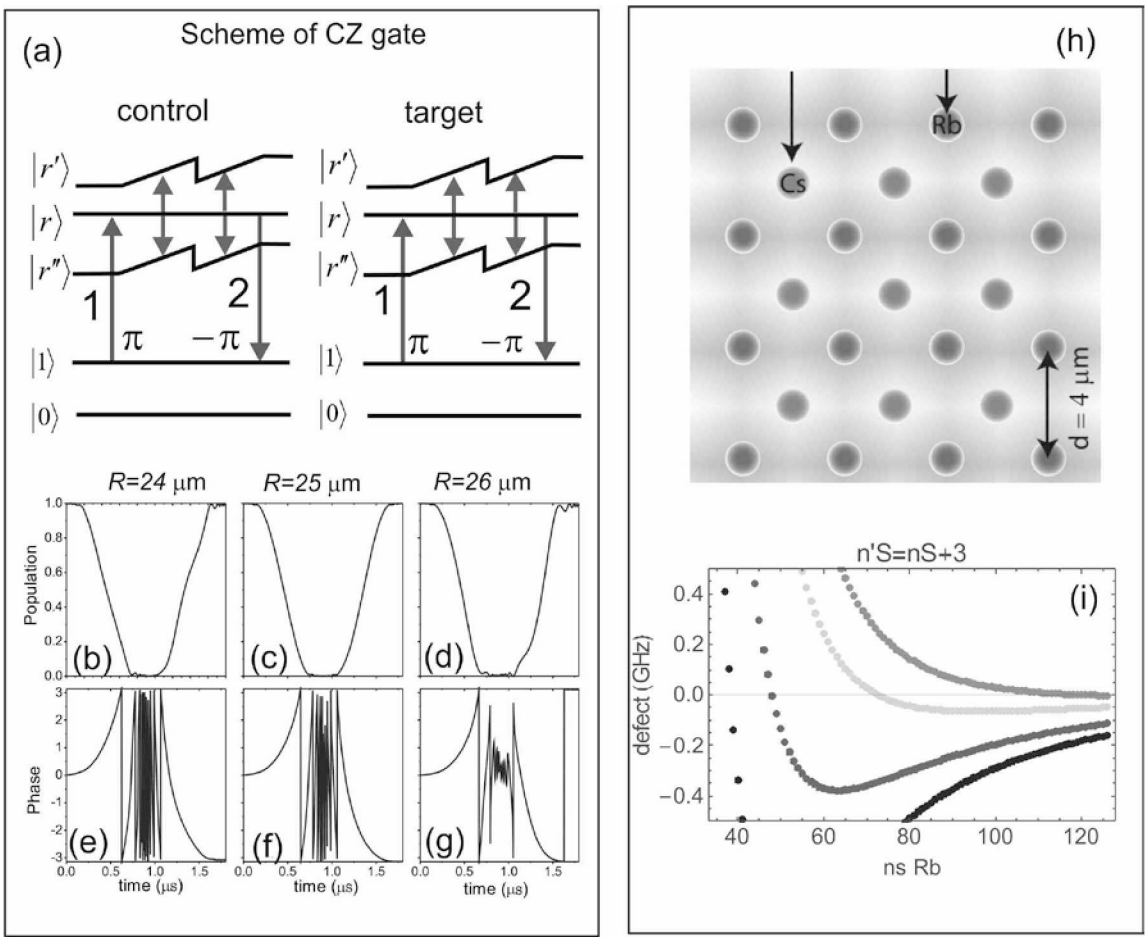

Fig. 1 (a) Scheme of a CZ gate using double adiabatic rapid passage across Stark-tuned Förster resonance; (b)-(g) Double adiabatic passage of the Stark-tuned Förster resonance for different interatomic distances R. (b),(c),(d) Time dependences of population of the collective state $|90S_{1/2}, 96S_{1/2}\rangle$ of two Cs atoms calculated for R=24, 25 and 26 μm, respectively; (e),(f),(g) Time dependences of phase of the collective state $|90S_{1/2}, 96S_{1/2}\rangle$ of two Cs atoms calculated for R=24, 25 and 26 μm, respectively. (h) Scheme of the quantum register with Cs atoms used as main qubits and Rb atoms used as auxiliary qubits. (i) Dependence of the Förster energy defect for $Rb(nS)+Cs(n'S)\rightarrow Rb(nP)+Cs(n''P)$ Förster resonance with $n'=n+3$ and $n''=n'-1$ on the principal quantum number n.

References

[1] D. Jaksch et al., Phys. Rev. Lett **85**, 2208 (2000).
[2] I.I. Beterov et al., arXiv:1606.08198
[3] I.I. Beterov and M.Saffman, Phys. Rev. A **92**, 042710 (2015).

Study of theoretical model and spectrum characteristics of photonic crystal fiber superimposed grating

Weihong Bi, Peng Jiang, Yuefeng Qi , Yang Wu, Xinghu Fu, and Guangwei Fu
The Key Laboratory for Special Fiber and Fiber Sensor of Hebei Province, School of Information Science and Engineering, Yanshan University, Qinhuangdao, Hebei 066004, P. R. China
E-mail: bwhong@ysu.edu.cn

The spectra and characteristics of superimposed photonic crystal fiber (PCF) grating are researched in theory and experiment. Theoretically, the analysis model of superimposed PCF grating is proposed based on the V-I transfer matrix method, the reflection spectrum and time-delay characteristic of superimposed Bragg grating and superimposed chirped grating are simulated and studied. Experimentally, a quadruple superimposed Bragg grating with equidifferent wavelength spacing and a superimposed chirped grating with wavelength spacing of 0.82nm are fabricated through 193nm ultraviolet laser in a single mode photosensitive PCF. The results show that the spectrum of superimposed Bragg grating can be flexibly customized by the parameters of each sub grating. Superimposed chirped grating has the characteristics of periodic wide band resonance whose period can be adjusted by the grating period offset, and flat resonant amplitudes and good linear group delays are observed. The grating spectra obtained from experiments are in good agreement with the theoretical analysis. The research results in this paper can be helpful to the design, fabrication and application of superimposed PCF grating.

References

[1] Y C Ma, H Y Liu et al.. , Meas. Sci. Technol., **24**,055201(2013).
[2] D. M. Meghavoryan, A. V. Daryan, IEEE Photon. Technol. Lett., **15**,1546(2003).
[3] M. Sumetsky, S. Ramachandran, Opt. Express, **16**,402(2008).
[4] J. L. Zheng, R. Wang, T. Pu, L. Lu, T. Fang, Y. Su, L. Li, and X. F.,Opt. Express, **19,**8580(2011).
[5] C. L. Tien, H. W. Chen, W. F. Liu, S. S. Jyu, S. W. Lin, and Y. S. Lin.,Thin Solid Films, **516,**5360(2008).
[6] S. Triollet, L. Robert, E. Marin, Y. Ouerdane, Meas. Sci. Tech, **22**,015202(2011).
[7] T. Li, X. Dong, C. C. Chan, C. L. Zhao and S. Jin., IEEE Photon. Technol. Lett., **23**,1706(2011).
[8] John Canning, Optical Fiber Technology, **6**,275(2000).
[9] P.E.D et al.,Opt. Communications, **115,**327(1995).
[10] M. Lancry, P. Niay, M. Douay, C. Depecker, P. Cordier, and B. Poumellec, Lightwave Technol, **24**,1376(2006).
[11] M. Lancry and B. Poumellec, Phys. Rep, **523**,207(2013).

Mechanism and experimental study on the detection of diesel oil in the mixture of kerosene and diesel oil with long period fiber grating

Weihong Bi, Yunhai Xing, Xinghu Fu, and Guangwei Fu
The Key Laboratory for Special Fiber and Fiber Sensor of Hebei Province, School of Information Science and Engineering, Yanshan University, Qinhuangdao, Hebei 066004, P. R. China
E-mail: bwhong@ysu.edu.cn

Using the coupled-mode theory, this paper analyses the sensitive features of refractive index of long period fiber grating, and gets the relationship between long period fiber grating's resonant wavelength or transmitted intensity and the environmental refractive index. Also this paper uses this relationship to detect the content of diesel oil in the mixed solution of kerosene and diesel, gets the relationship between the content of diesel oil of the mixed solution and the long period fiber grating's resonant wavelength or transmitted intensity. The result shows that when the kerosene of the mixed solution increases, the long period fiber grating resonance wavelength shifts. When the concentration of diesel oil reaches a certain concentration that the refractive index of the solution is equal to the cladding index, the resonance wavelength shifts to the maximum. Beyond this concentration, the transmission peak back to the original location of the resonant wavelength, but the shape changes greatly, the peak loss diminishes, bandwidth increases, and with the concentration of diesel oil continues to increase, the peak loss increase and bandwidth diminishes. This paper proves that the feasibility of detecting the concentration of diesel oil in mixed solution of kerosene and diesel oil with the long period fiber grating and that long period fiber grating has a good application prospect in the detection of mixed fuel concentration.

References

[1]Costa R C, Sodré J R, Fuel, **89**,287(2010).
[2]Hsieh W D, Chen R H, Wu T L, et al. , Atmospheric Environment,**36**,403(2002).
[3]Opekar F, Čabala R, Kadlecova T., Analytica Chimica Acta, **694**,57(2011).
[4]Falate R, Kamikawachi R C, Müller M, et al., Sensors and Actuators B: Chemical, **105**,430(2005).
[5]Puckett S D, Pacey G E.,Talanta, **78**, 300(2009).
[6]Erdogan,T.,J. Lightwave Technol., **15**,1277(1997).
[7]Kaler R S, Tiwari U, Mishra V, et al.,Optik, **123**,1071(2012).
[8]Lee B H,Liu Y,Lee S B,et al.,Optics Letters,**22**,1769(1997).
[9]Stegall D B,Erdogan T.,IEEE Photonics Tech Lett,**11**,343(1999).

Ultrahigh-quality enhanced absorption resonance based on the coherent population trapping in a vapour cell with antirelaxation coating of walls

D.V. Brazhnikov[1,2], A.S. Novokreshchenov [1], A.V. Taichenachev[1,2], V.I. Yudin[1–3], Ch. Andreeva[4], V.M. Entin[2,5], I.I. Ryabtsev[2,5], S.M. Ignatovich[1], N.L. Kvashnin[1], V.I. Vishniakov[1] and M.N. Skvortsov[1]

[1] *Institute of Laser Physics SB RAS, pr. Lavrentieva 13/3, Novosibirsk 630090, Russia*

[2] *Novosibirsk State University, ul. Pirogova 2, Novosibirsk 630090, Russia*

[3] *Novosibirsk State Technical University, pr. K. Marksa 20, Novosibirsk 630073, Russia*

[4] *Institute of Electronics, Tzarigradsko chaussee blvd 72, Sofia 1784, Bulgaria*

[5] *Rzhanov Institute of Semiconductor Physics SB RAS, pr. Lavrentieva 13, Novosibirsk 630090, Russia*

Email: brazhnikov@laser.nsc.ru

Electromagnetically induced transparency (EIT) resonances caused by coherent population trapping (CPT) have been found to be useful in many directions of laser physics, nonlinear optics, optical communications, quantum informatics, laser cooling of atoms and, especially, quantum metrology. Resonances of opposite sign (electromagnetically induced absorption – EIA) have far less applications due to some problems. Indeed, buffer-gas-filled or antirelaxation-coated cells are exploited everywhere for improving the properties of EIT. Unfortunately, these methods are useless in the case of EIA in standard observation schemes [1,2] due to collisional depolarization of excited state. There are several "non-standard" methods for observing EIA signals, but it is still very hard to get simultaneously narrow (~kHz) and high-contrast (> 50%) EIA resonances.

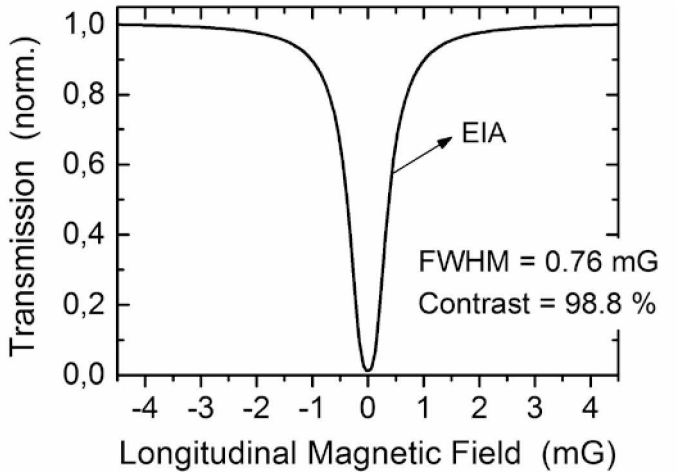

Fig. 1 Numerically calculated EIA resonance in the probe-wave transmission of a buffer-gas-filled cell.

We study EIA in the Hanle configuration with the help of a new scheme proposed previously [3]. This resonance usually appears as a subnatural-width dip in the laser-wave transmission signal from a vapour cell, when the magnetic field is being scanned. The new scheme allows us using a buffer gas for improving properties of the nonlinear resonance. The method implies using pump and probe counterpropagating waves with the same frequency and orthogonal linear polarizations. We considered optical transition $F_g=1\rightarrow F_e=1$ in the D_1 line of ^{87}Rb (λ=795 nm, $\gamma=2\pi\times5.57$ MHz). This transition is open, i.e. its branching ratio differs from unity. It should be emphasize that usually the openness of an atomic transition suppresses amplitudes of the EIT as well as EIA resonances in standard schemes of observation. In our scheme the openness played crucial and quite positive role and led to the great increase of the contrast of the nonlinear resonance. In particular, the theory

showed that the contrast can reach values up to 100% at kHz or even sub-kHz width (see Fig.1 as an example).

We have also carried out some preliminary experiments. A buffer-gas-filled cell with the natural mixture of rubidium isotopes was used (Ar pressure ≈ 5 Tor). The cell was placed in a two-layer magnetic shield (without the end caps) that suppressed the inhomogenity of the stray magnetic field down to approximately 8 mG. The cell dimensions were 60 × 30 mm. The diameter of the laser beams was 0.9 mm. We observed the contrast of about 30-40%, depending on the atomic transition, pump beam power and temperature of the cell. The EIA resonance had the width of about 20 mG (≈15 kHz), which was determined mainly by the power broadening and inhomogeneous stray magnetic field. We expect that further improvements of the setup (adding the third magnetic layer with the end caps, increasing the diameter of the pump beam) will bring better results. We are also going to test the proposed method using an antirelaxation-coated vapour cell.

The work was supported by the RFBR (15-02-08377, 15-32-20330, 14-02-00712, 14-02-00939), the RF Ministry of Education and Science (order no. 2014/139, project no. 825), the Presidium of SB RAS, and the EU project FP7-PEOPLE-2011-IRSES №295264 "COSMA".

References

[1] A.M. Akulshin, S. Barreiro, A. Lezama, Phys. Rev. A **57**, 2996 (1998).
[2] Y. Dancheva, G. Alzetta, S. Cartaleva, M. Taslakov, Ch. Andreeva, Opt. Commun. **178**, 103 (2000).
[3] D.V. Brazhnikov, A.V. Taichenachev, A.M. Tumaikin, V.I. Yudin, Laser Phys. Lett. **11**, 125702 (2014).

Emission amplification on the transitions $B \rightarrow X$ (λ = 353 nm) of XeF* molecules in pulsed inductive discharge

D. Churkin[1, 2], A. Razhev[1, 3], E. Kargapol'tsev[1]
[1]*Institute of Laser Physics SB RAS, Ac. Lavrentyev's prosp., 13/3, Novosibirsk 630090, Russia*
[2]*Novosibirsk State University, Pirogova st., 2, Novosibirsk 630090, Russia*
[3] *Novosibirsk State Technical University, K. Marx prosp., 20, 630073, Novosibirsk, Russia*
E-mail: churkin@laser.nsc.ru

The results of experimental studies of dependence on the spectral characteristics of the radiation XeF* molecules on the composition and level of energy input into the active medium in a pulsed inductive discharge are presented.

Pulsed inductive discharge is a promising method for pulsed gas lasers excitation [1–5], including UV excimer lasers. The aim of this study was to search for the conditions of gas mixtures excitation and lasing on transitions B → X of excimer XeF* achievement in a pulsed inductive discharge. To generate a pulsed inductive discharge in gases used high-voltage excitation system similar to [4]. Inductive laser oscillator consists of a ceramic tube 800 mm long and 40 mm diameter with wounded 26 inductor sections made of the core wire PV6-Z, and connected in parallel. The optical cavity was formed by dense rear mirror (R = ∞) and the front output window of MgF_2. The active medium used in the composition of the gas mixture Xe-F_2 and He-Xe-F_2.

In experiments carried out the registration and comparison of emission intensity corresponding to transitions $B \rightarrow X$ molecule XeF* (in the area of 351 – 355 nm) for different ratios of Xe–F_2 and at different charging voltages are performed. Analysis of the results showed that the maximum intensity of the radiation in the 351 – 355 nm is achieved at a ratio of Xe:F_2 – 7:1. Dilution of this mixture by He buffer gas can significantly increase the emission intensity of XeF* molecules. The optimum composition of a three component mixture of He: Xe: F_2 was 248:7:1.

General view of the emission spectrum of a Xe-F_2 and He-Xe-F_2 mixtures in the 180 – 1100 nm is shown in Figures 1 and 2.

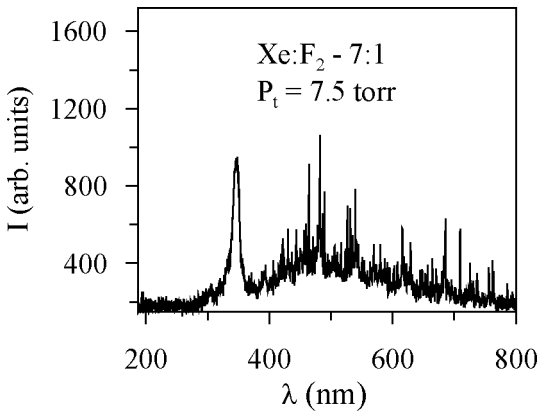

Fig.1 The emission spectrum of a mixture of Xe: F_2 – 7:1 in a pulsed inductive discharge. U_{ch} = 26 kV.

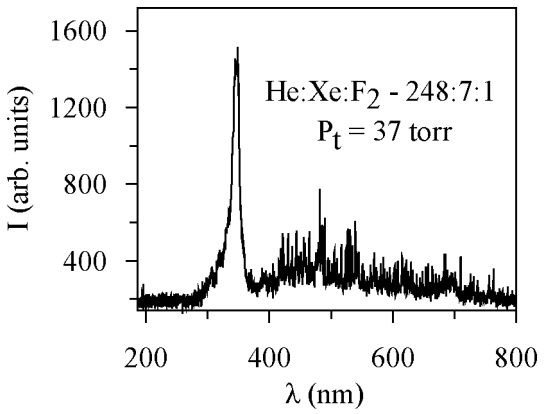

Fig. 2 The emission spectrum of a mixture of He:Xe: F_2 – 248:7:1 in a pulsed inductive discharge. U_{ch} = 26 kV.

We see that when pumping a two-component mixture of a large proportion of the energy is used to excite the different states of atoms and ions Xe, H, Cl (radiation in the visible spectrum). Adding a buffer gas resulted in a reduction of radiation in the visible range and a simultaneous increase in the

intensity of luminescence molecules XeF*. We believe that such a redistribution of the intensities indicates the changes in the kinetics of processes occurring in the plasma of pulsed inductive discharge.

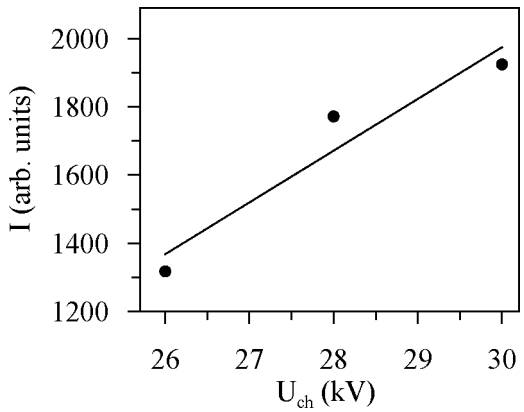

Fig. 3 The dependence of the intensity of the XeF* molecules radiation on charging voltage.

When closing the rear mirror the intensity of the radiation XeF* molecules reduced by 2–2.5 times, indicating the presence of the gain in the active medium. The gain is dependent on the composition and total pressure of the gaseous medium, and the charging voltage. In experiments, an increase in the charging voltage leads to a continuous increase of the radiation intensity molecules XeF* (Fig. 3). Since the possibility of pumping system were limited to the value of 30 kV to determine the optimal level of energy input was not possible.

In our experiments, the laser oscillation mode in the transition B→X molecule XeF* was not achieved. However, this does not mean that lasing in the inductive discharge to Xe*F excimer molecules not possible. In order to achieve the ultimate goal, namely, the lasing transitions excimer XeF*, necessary to develop a new generation circuit pulsed inductive discharge and laser occillator structures, providing a higher level of energy input into the active medium. One of the directions of further research is to develop a system of formation of the inductive discharge of transformer type, similar to that used in [6, 7].

This work was supported by RFBR grant №16-02-00316.

References

[1] A.M. Razhev, V.M. Mkhitaryan, D.S.Churkin, JETP Lett. **82(5)**, 259 (2005).
[2] A.M. Razhev, D.S. Churkin, JETP Lett. **86(6)**, 420 (2007).
[3] A.M. Razhev, D.S. Churkin, A.S. Zavyalov, Vestnik NSU, Seria Fizika **4(3)**, 12 (2009) (in Russian).
[4] A.M. Razhev, D.S. Churkin, Opt. Communications **282(7)**, 1354 (2009).
[5] A.M. Razhev, D.S. Churkin, E.S. Kargapol'tsev, Laser Phys. Lett., **10**, 075002 (4pp) (2013).
[6] W.E. Bell, Appl. Phys. Lett., **7(7)**, 190, (1965).
[7] J.P. Goldborough, E.B. Hodges, and W.E. Bell. Appl. Phys. Lett., **8(6)**, 137, (1966).

UV excimer laser system for ab-externo surgery open-angle glaucoma

D. Churkin[1, 2], A. Razhev[1, 3], E. Kargapol'tsev[1], O. Ermakova[4], I. Iskakov[4], V. Chernykh[4]
[1]*Institute of Laser Physics SB RAS, Ac. Lavrentyev's prosp., 13/3, Novosibirsk 630090, Russia*
[2]*Novosibirsk State University, Pirogova st., 2, Novosibirsk 630090, Russia*
[3] *Novosibirsk State Technical University, K. Marx prosp., 20, 630073, Novosibirsk, Russia*
[4] *Novosibirsk branch of the Federal State Institution "Intersectoral Research and Technology Complex" Eye Microsurgery "named after academician SN Fyodorov Ministry of Health of the Russian Federation." St. Colchis, 10, 630071, Novosibirsk, Russia.*
E-mail: churkin@laser.nsc.ru

Open-angle glaucoma is one of the most common eye diseases. Today there are several different methods [1-6] of laser treatments for this disease. However, they all have certain disadvantages associated, including the necessity of opening the eye, or the necessity of the operation of the optical near field of the eye. Consequently, the actual problem is the development of new, more effective treatments for open-angle glaucoma. The aim of this work was to develop such a method, and a laser medical device for its implementation.

The development of the new method was based on the results of experimental investigations on the effects of a powerful short-pulse UV laser radiation on human scleral tissue. Details of these investigations are described in [7, 8]. It was shown that in terms of the maximum rate of ablation and minimal trauma, the XeCl (308 nm) laser radiation is the most acceptable for practical use. As a result, the basis for the establishment of a medical device for the treatment of open-angle glaucoma was chosen XeCl excimer laser.

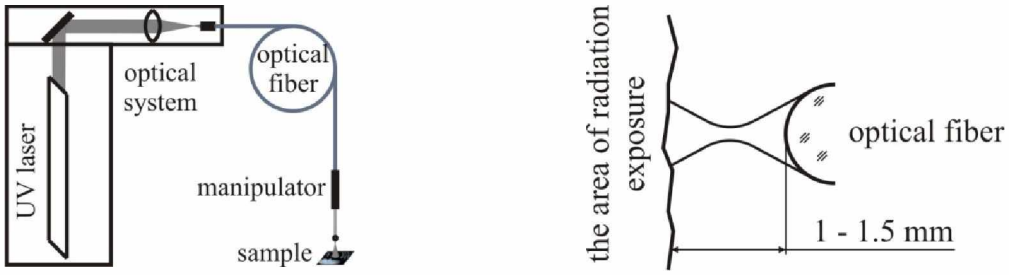

Fig. 1 Scheme of laboratory model ophthalmic laser system based on XeCl laser optical system (a). Schematic view of the light rays travel at the output of the fiber with spherical tip (b).

To carry out further tests laboratory model on the basis of an ophthalmic system Medilex™ has been developed. To deliver 308 nm to the surgical field, flexible fiber light guide with easy-to-use handle was used (Fig 1 (a)). At the other end of the fiber was mounted crane consisting of a handle and a limit switch, enclosed in a stainless steel tube. The light guide has a spherical tip of about 900 microns in diameter, operated as a microlens. Figure 2 shows the mold cavities resulting from the effects of radiation on the end flap of the sclera of the human eye (a), (b) and on its surface (c). In the latter case, the experiment was stopped immediately after the time the tissue perforation.

As can be seen from Fig. 2(a) and (b), the UV laser light into the tissue initially forms a conical recess, further, as the evaporation material characteristic constriction is formed, after which the beam begins to diverge. Thus, the shape of the cavities analysis it can be concluded that the spherical tip acts as a lens, and the measurement of the value allows to evaluate the recess focal length which was about 1 mm. As a result, the beam profile and the general appearance of the rays at the output of the fiber obtained are close to that shown in Fig. 1 (b).

(a) (b) (c)

Fig. 2 The shape of the cavity, formed by the UV laser light at the end of (a), (b) and sclera surface (c) at the output of the fiber with spherical tip.

By analyzing the diameters of the holes resulting from perforation of the tissue (Fig. 2(c)) can conclude that the waist diameter of about 80 microns. Because of diffraction effects and other features of the propagation of radiation (including laser) beam through an optical fiber cannot be focused to a spot size of the infinitely small, the size of the waist is in this case to determine the minimum spot size which allows you to create a spherical tip of the optical fiber. In this case, the energy density at the tissue surface may theoretically reach 40 J/cm^2. In real conditions of operations on living eyes, this value will be less because of the absorption of UV radiation intraocular fluid. At the same time, the operation required to significantly lower (a few J/cm^2), the amount of energy density, so the surgeon during the operation is to vary the distance from the fiber tip to the working surface, and hence the energy density.

16 eyes of 16 patients with open angle glaucoma were operated. Follow up term is 3-12 months. Intraocular fluid does not block ablation of sclera under exposure of 308 nm. The exposures of studied excimer laser wavelengths to morphological structure of sclera have no any coagulate damage and other pathological changes. After surgery all patients reached stable decrease of intraocular pressure. Outflow tract is completely functioning, which results in stable visual functions in all treated eyes.

A new method for ab-externo excimer laser surgical treatment of open angle glaucoma is developed. For the first time, the technology allows for the operation incisions and scleral ablation trabeculae and Descemet's membrane UV laser radiation with a small footprint and traumatic surgery. As a consequence, informed choice of laser wavelength is noted that the procedure for thinning of trabeculae does not stop even when a filtering aqueous humor. The result is a higher clinical effect – a significant reduction in postoperative complications related to inflammation and scarring.

References

[1] D. Aron-Rosa, A. Maden, S. Ganem, B. Aron, M. Gross, J.Cataract Refract. Surg., **16(5)**, 617 (1990).
[2] S.V. Antonyuk, Synopsis of a thesis of PhD-medicine, 23 (1999).
[3] N.N. Ereskin, D.A. Magaramov, Actual problems of clinical ophthalmology: Proc. rep. Regional scientific-practical. Conf. of Ural. – Chelyabinsk, 247 (1999).
[4] N.N. Ereskin, A.V. Doga, D.A. Magaramov, V.A. Sugrobov, Patent of the Russian Federation № 2192230. Classes: A61F9 / 007 A61F9 / 008. Publ. 10.11.2002.
[5] V.V. Lantukh, I.A. Iskakov, O.G. Gusarevich, A.M. Razhev, Zh. V. Vasiliev, M.M. Pyatin, Patent of the Russian Federation 2072817. Classes: A61F9 / 007, A61N5 / 06. Publ. 02.10.97.
[6] N.N. Ereskin, A.V. Doga, D.A. Magaramov, V.A. Sugrobov, Patent of the Russian Federation 2192230. Classes: A61F9 / 007, A61F9 / 008. Publ. 10.11.2002
[7] O.V. Ermakova, I.A. Iskakov, V.V. Chernykh, A.N. Trunov, A.M. Razhev, D.S. Churkin, E.S. Kargapol'tsev, Ophthalmosurgery, **4**, 98 (2013).
[8] O.V. Ermakova, I.A. Iskakov, V.V. Chernykh, A.M. Razhev, D.S. Churkin, E.S. Kargapol'tsev, Patent of the Russian Federation № 2535079. Priority on 11/14/2013 Registered: 08/10/2014.

Synthesis and characterization of carbon nitride films produced in plasma powerful optical pulsating discharge

V. Demin[1], T. Smirnova[1], V. Borisov[1], G. Grachev[2], A. Smirnov[2], M. Chomyakov[2]
[1]*Institute of Laser Physics Russion Academy of Science, Lavrent'ev pr. 13/3,Novosibirsk 630090, Russia*
[2]*Nikolaev Institute of Inorganic Chemistry Russion Academy of Sciences, Lavrent'ev pr.3, Novosibirsk 630090, Russia*
E-mail: demin@niic.nsc.ru

Carbon nitrides have been discussed as a potential material for many tribological applications because of their particular mechanical properties. Although the synthesis of single-phase crystal coatings remains an open challenge, the films (CNx) with low nitrogen concentration have been used in industry. To-day, a lot technologies for hard carbon nitride coatings obtaining exist (RF and DC sputtering, ion beam deposition, laser ablation).

The aim of this work is the development of a new laser-plasma process of obtaining carbon nitride coatings from acetonitrile (CH3-CN), the study of their chemical composition, structure and properties.

A new process of laser-plasma chemical vapor deposition had been developed for the synthesis of the coatings by the joint work of the Institute of Laser Physics SB RAS and the Institute of Inorganic Chemistry SB RAS [1-2]. The advantage of the process consists in using a powerful laser plasma of optical discharge which characterized by unique combination of properties unavailable for other modes (gas thermal, microwave, glow and arc discharge, a continuous laser plasma, pyrolysis, burning, etc.).

Carbon nitride films deposition was carried out at atmospheric pressure in absence of camera for substrate. A zone of substrate was protected from air by gas stream between nozzle and substrate surface [2].

Fig.1. Process of laser-plasma deposition

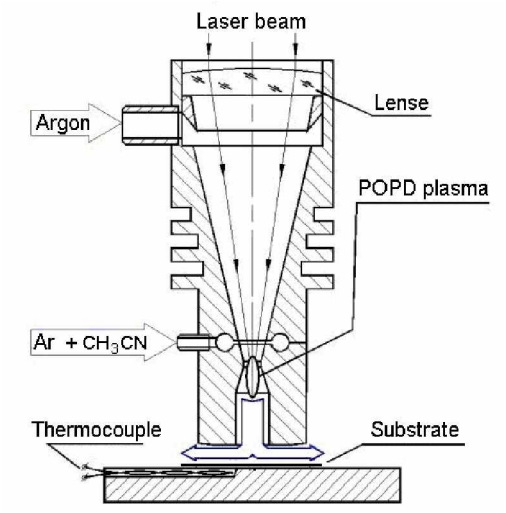

Fig.2. Scheme of laser-plasma deposition

The films characterization was carried out by IR-spectroscopy, Raman spectroscopy, AFM, X-ray phase analysis. It was found that properties of the films depend on input energy laser irradiation, substrate temperature, precursor concentration. As showed X-ray phase analysis the CNx films were nanocrystalline with x ≤25 at%. It was shown from IR and Raman spectroscopy that carbon nitride films comprise Csp^3-N bonds and nanocrystalline carbon including diamond-like carbon nanoclusters.

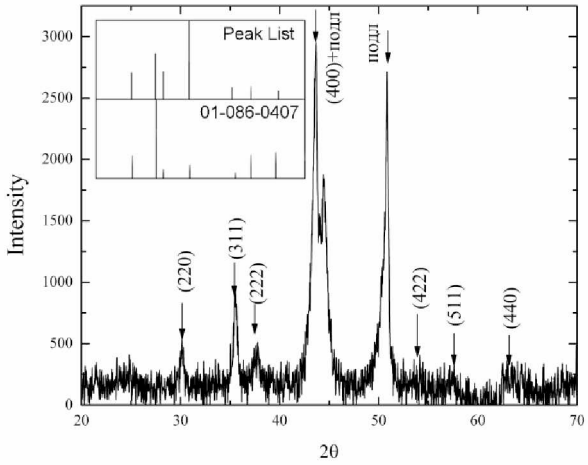

Fig. 3 Diffraction pattern of the film.

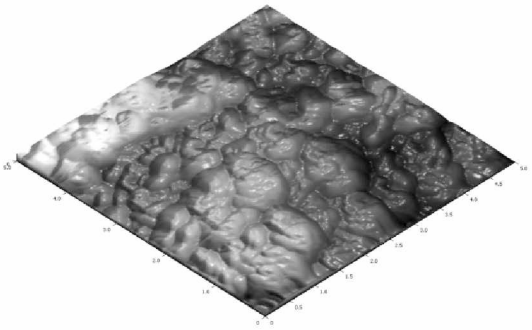

Fig. 4 AFM image of the film with structure has been shown in Fig. 3

Diffraction pattern of the film is shown in the Fig.3. The observed reflections in diffraction pattern evidence on the crystalline phase formation. Analysis of diffraction pattern showed that the set of reflections are not consistent with the data for the known structural forms of carbon nitride. The crystalline nature of this film was confirmed by AFM data (Fig.4). The results of the diffraction pattern analysis with PANanalytical X'Pert HighScore Plus program showed that the resulting crystalline phase has a spinel structure, and can be attributed to a cubic system (sp. Gr.-Fd-3m), a = 8.3342. The possibility of formation of a new modification of the cubic carbon nitride with a spinel structure was predicted in the theoretical work published in 1999 year. According to theoretical calculation, this structural type may be formed at high pressure and temperature. Availability of this structural modification of high-pressure carbon nitride in our system is provided by a high laser plasma power density of the energy in the volume of the gas phase and formation of shock waves on the surface of the substrate.

A scanning nano-hardness tester (NanoScan) was used to determine the films micro-hardness. To define the real hardness of the coating (excluding a softer substrate influence), the results of nano-identification were treated taking into account a substrate hardness according to the techniques suggested in [4].The measured so produced carbon nitride films on stain steel substrate was 46±7 GPa for nanocristalline films and 22±2 GPa for amorphous films produced.

In conclusion. A new process of chemical vapor deposition of the carbon nitride coatings by using powerful laser plasma of optical discharge was developed. A new modification of the cubic carbon nitride with a spinel structure was synthesized.

References

[1] S.N. Bagayev, G.N. Grachev, A.G. Ponomarenko, A.L. Smirnov, V.N. Demin, A.V. Okotrub, A.M. Baklanov., SPIE, 6732 (2007)
[2] V.N. Demin, T.P. Smirnova, V.O. Borisov, G.N. Grachev, A.L. Smirnov, M.N. Khomyakov, Surface Engineering **31**(8), 628 (2015).
[3] Ralf Riedel, Phys. Rev. Lett. **83**(4), 5046 (1999).
[4] B.Jönsson , S.Hogmark, Thin Solid Films **114**, 257 (1984).

Distributed strain and temperature discrimination using two types of fiber in OFDR

Zhenyang Ding, Di Yang, Tiegen Liu, Yang Du, Kun Liu, Yonghan Zhou, Zhexi Xu and Junfeng Jiang
College of Precision Instrument and Opto-Electronics Engineering, Tianjin University, Tianjin China and Key Laboratory of Opto-Electronics Information Technical (Tianjin University), Ministry of Education, Tianjin 300072, China
E-mail: zyding@tju.edu.cn

The main objective of this work is present a simple and effective method to achieve a distributed strain and temperature discrimination using two types of fiber by Rayleigh backscattering spectra (RBS) shift in optical frequency domain reflectometry (OFDR). We use two types single mode fiber (SMF) of a reduced-cladding (RC) SMF and a standard SMF placed side by side as the sensing fiber. Since the RC SMF and the standard SMF have different sensitivity responses to strain and temperature variation, which can measure strain and temperature variation simultaneously by simply monitoring the optical frequency shifts of RBS.

In the previous method, M. Froggatt et al. [1,2] use a polarization maintaining fiber (PMF) to sense strain and temperature variation simultaneously by measuring autocorrelation and cross-correlation RBS shifts. However, this method requires an external polarization controller to adjust the state of polarization of input light coupled to PMF, which will make the sensor system complicated. Even worse, the strain sensitivity response of using the autocorrelation RBS shift is 111 times less than that of using the cross-correlation. The temperature sensitivity response of using the autocorrelation RBS shift is 40 times less than that of using the cross-correlation[3], which will seriously deteriorate the performance of this method comparing with only using cross-correlation RBS shift. In addition, Da-Peng Zhou et al. [4] combine Brillouin optical time-domain analysis (B-OTDA) and OFDR to distinguish between strain and temperature. However, this method is so expressive and complex that two complicated systems need to be implemented.

In our presented method, the sensitivity responses to strain and temperature of using the RC SMF are higher than using the standard SMF, so the performance of our proposed method will not be deteriorated obviously comparing with the single parameter measurement (strain or temperature) only using a standard SMF as the sensing fiber. A 50 m measurable range and the spatial resolution of 18 cm are demonstrated experimentally with error of 0.31 °C in temperature and 7.97 με in strain.

References

[1] M. E. Froggatt, D. K. Gifford, S. T. Kreger et al., Optical Society of America: Cancún, Mexico, 23 October 2006; paper ThC5.
[2] M. E. Froggatt, US patent, US 7, 538, 883 B2, 2009.
[3] W. Li, L. Chen, and X. Bao, Optics Communications **311**, 26 (2013).
[4] Z. Da-Peng, L. Wenhai, C. Liang et al., Sensors **13**, 1836 (2013).

Stabilisation of a femtosecond frequency standard using a Michelson interferometer

A. Dmitriev[1], E. Baklanov[2], N. Golovin[3], and S. Grigoryva[4]
[1]*Institute of Laser Physics, Siberian Branch, Russian Academy of Sciences, prosp. Lavrent'eva 13/3, 630090 Novosibirsk, Russia*
[2]*Novosibirsk State University, ul. Pirogova 2, 630090 Novosibirsk, Russia*
[3]*Novosibirsk State Technical University, prosp. Marksa 20, 630073 Novosibirsk, Russia*
[4]*D.Serikbayev East Kazakhstan State Technical University, Serikbaev str. 19, 070010, Republic of Kazakhstan*
E-mail: alexander_dmitriev@ngs.ru

At present many frequency standards make use of femtosecond lasers that generate a periodic train of short pulses in the mode-locking regime. Since the pulse repetition rate is mastered by an etalon microwave oscillator, the optical frequencies of the laser appear to be precisely calibrated in the units of its frequency. One of the main problems in the implementation of an optical scale is to remove the offset common for all frequencies, which is often referred to as the CEO (carrier-envelope offset). Commonly this problem is solved by means of an optical frequency synthesiser using a f–$2f$ interferometer [1]. Another method of controlling the frequency comb is based on using an external high-Q resonator [2, 3]. In the case [3], the repetition rate and the CEO are stabilised simultaneously. In the present, the control of the frequency comb offset is implemented using a Michelson interferometer that detects the phase difference between the pulses and, therefore, determines the CEO.

Elimination of the CEO. The origin of the CEO is related to the difference between the phase velocity and the group velocity of the pulse during the laser cavity roundtrip. Then the shape of each pulse will be conserved, but the carrier frequency will acquire the phase shift with respect to the pulse peak, proportional to the CEO. When we measure the interference signal produced by two pulses by means of the Michelson interferometer. For recording the signal, one can make use of the scheme, analogous to the scheme of the Hänsch – Couillaud detector [7], which is widely used in highly sensitive polarisation methods of laser frequency stabilisation [8].

Scheme of the standard. Consider the frequency standard in which the COE is eliminated using the above method. The scheme includes two control loops. The first loop is fast and keeps the repetition rate of the femtosecond laser pulses constant. The second control loop is slow as compared to the first one and intended to eliminate the CEO.

Conclusions. At present the high-precision measurement of frequency is implemented using the femtosecond laser with the f–$2f$ interferometer [1]. However, for the operation of this interferometer it is necessary to have a spectral width greater than an octave. However, there are many commercial nanosecond and picosecond self-mode-locked lasers, in which the f–$2f$ interferometer cannot be used because of a small spectral width. The simple scheme of a frequency standard proposed here is applicable for different, which allows the extension of the considered method over the nano- and picosecond-range self-mode-locked lasers.

References

[1] R.Holzwarth, Th. Udem, T.W. Hänsch, J.C. Knight, W.J.Wadsworth, P. Russell, Phys. Rev. Lett. **85**, 2264 (2000).
[2] R.J.Jones, T. Ido, T.Loftus, M. Boyd, A. Ludlow, K., M. Thorpe, K. Moll, J. Ye, Laser Phys. **15**, 1010 (2005).
[3] D. Basnak, K. Bikmukhametov, A. Dmitriev, A. Dychkov, S. Kuznetsov, A. Lugovoy, P. Mitsziti Quantum Electron. **42**, 71 (2012).
[4] T.W. Hänsch, B. Couillaud, Opt. Commun. **35**, 441 (1980).
[5] F. Riehle, Frequency Standards: Basics and Applications (Weinheim: Wiley-VCH, 2004).

The error of meter standard due to diffraction divergence and wavefront curvature

A.K. Dmitriev[1,2], N.N. Golovin[1], N.Zh. Altynbekov[1], A.A. Isakova[1]
[1]*Novosibirsk State Technical Universiy, 630073, Novosibirsk, prosp. K.Marksa, 20, Russia*
[2]*2Institute of Laser Physics of SB RAS, 630090, Novosibirsk, Ac. Lavrentyev's prosp., 13/3, Russia*
E-mail: alexander_dmitriev@ngs.ru

At the present time the wavelength of optical optical frequency standards is accepted as a reference length [2]. To link the wavelength of the standard to the geometric length a Michelson interferometer is most widely used. Measurement error when using such a "ruler" is influenced by a number of factors, which can be divided into four groups [4, 5]: adjustment of the interferometer (inaccuracy 10-8 - 10-9), environmental conditions (10-6 - 10-8), frequency (wavelength) stability of a laser, the error of detecting apparatus, geometry of the laser beam (divergence, wavefront curvature).

Previously one attempts to theoretically investigate the influence of the wavefront distortion and beam divergence on the interference pattern in the Michelson interferometer [6-8]. In these works, usually the effect of only one of these parameters was taken into account. Besides, studies were carried out for beams with relatively large waist diameters to minimize the influence of the diffraction divergence of the beam on the error of linear measurements. However, for some tasks it may be that the order of accuracy of measurement $10^{-2}\lambda$ is quite sufficient. This would eliminate the large dimensions of the beam and use small-size optics. In the present study we investigated the error of measurement meters, caused by the diffraction divergence and wavefront curvature of the Gaussian light beam for the small radii of the beam waist (ω_0= 0.5 … 3 mm) and its position in the reference arm of the interferometer (ω_0= 0.5 … 1.5 mm) relative to photodetector.

The calculations of the diffraction pattern and fringe maximum displacement regarding the case of a plane light wave were carried for the various cross sections of the light beam and various positions of the beam waist in the reference arm relative to the photodetector.

When Gaussian beam pass through the Michelson interferometer fringes at the interferometer output will not be equidistant in contrast to the case of the plane wave. Fig. 1 illustrates for comparison general shifts of fringes for different values of ω_0 ($\omega_0/\lambda=5\times10^2$ (a) $\omega_0/\lambda = 10^3$ (b)) and z_1 (z_1=0 (solid curves), z_1 = 3 m (dashed curves) and z_1 = 5m. (dotted curves)).

As we can see, the shifts are zero when $z_2 = z_1$. In this case, beams passing through the reference and measuring arms of interferometer have the same diffraction divergence and their phase fronts coincide.

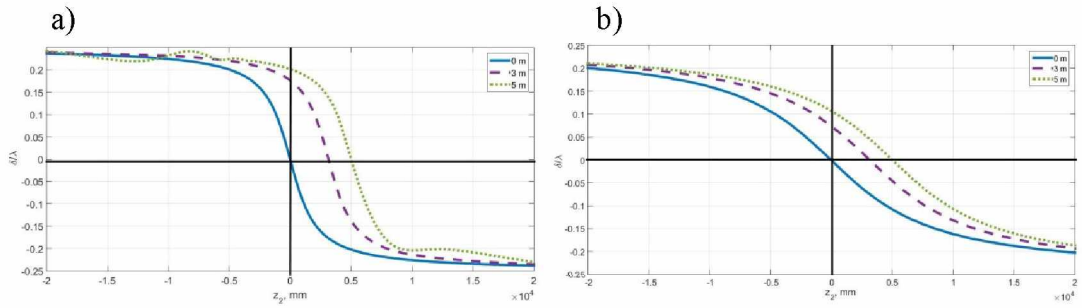

Fig. 1 General shifts of fringes: a) $\omega_0/\lambda=5\times10^2$, b) $\omega_0/\lambda=10^3$.

Also it is seen that with increasing ω_0 phase shift rate is reduced, and therefore the error of length measurement will decrease. Since the interval length is determined by the number of bands when moving the measuring mirror between two selected points z_2' and z_2'' then $\Delta l=(z_2''+ z_2')/2$. The systematic error when using a Gaussian beam Δ is equal to the difference of shifts of transition bands: $\Delta=\delta(z_2'')-\delta(z_2')$. In other words, the error Δ is qualitatively proportional to the derivative of the total shift.

Fig. 2 shows the errors in units of wavelengths Δ / λ, constructed depending on $Z = (z_2'' + z_2')/2$, with Δl = 1m. Errors are given for different values of of ω_0 ($\omega_0/\lambda = 5\times10^2$ (a), $\omega_0/\lambda = 10^3$ (b)) and z_1 (z_1=0 (solid curves), z_1 = 3 m (dashed curves) and z_1 = 5m. (dotted curves)).

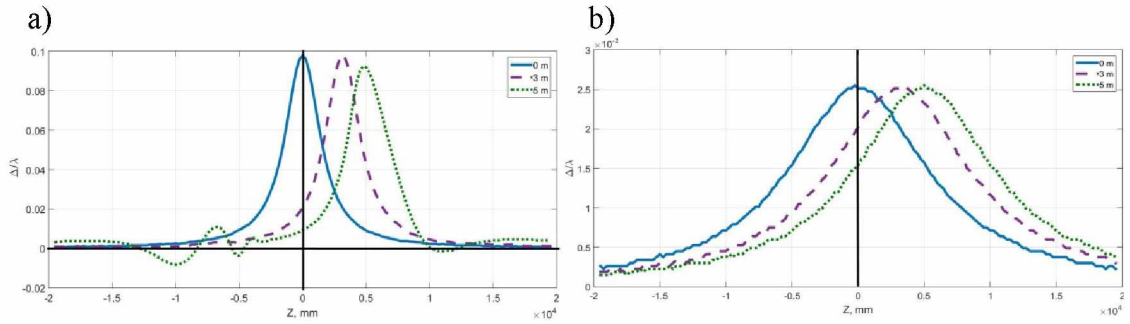

Fig. 2 General shifts of fringes: a) $\omega_0/\lambda = 5\times10^2$, b) $\omega_0/\lambda = 10^3$.

The errors in all cases have the maximum at $z_2 = z_1$, since at this point there is maximal rate of change of the fringes shift (see Fig. 1). It is seen that the maximum error decreases with increasing radius of the beam waist. With increasing beams path difference error decrease, but contrast of the interference fringes which is maximum at $z_2 = z_1$ is reduced too.

As noted above, the maximal error decreases with increasing radius of the beam waist. Below the dependence of maximal error of the meter definition from the waist size, expressed in wavelength units is shown.

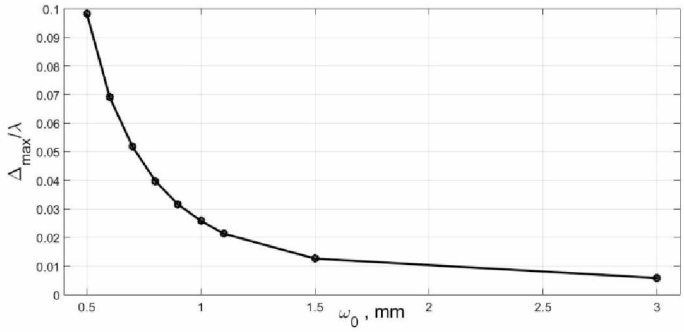

Fig. 3 The dependence of the maximal error in the meter definition from the radius of the Gaussian beam waist.

It is seen that the maximum of error is inversely proportional to ω_0. Already at ω_0 = 3 mm its value (5×10^{-9}) is already comparable with the error associated with the alignment of the interferometer (10^{-8} – 10^{-9}), and below error related to environmental conditions (10^{-6} – 10^{-8}) [4].

The work was supported by grants from the Ministry of Education and Science of the Russian Federation in the framework of the project of the state task (project 1316) and RFBR № 15-02-02557.

References

[1] Comptes Rendus de la 17e CGPM (1983), 1984, p.97.
[2] Quinn T.J., Metrologia **40**, 103 (2003).
[3] Udem Th., Reichert J., Haensch T.W., Phys. Rev. Lett. **82**, 3568 (1999).
[4] Beers J.S. and Penzes W.B. J., Res. Natl. Inst. Stand. Technol. **104**, 225 (1999)
[5] Bobroff N., Meas. Sci. Technol. **4**, 907(1993).
[6] K . Dorenwendt und G. Bönsch, Metrologia **12**, 57 (1976).
[7] G. Mana, Metrologia **26**, 87 (1989).
[8] Andrew John Lewis, "Absolute length measurement using multiple-wavelength phase-stepping interferometry", London: University of London (2002).

Measuring the carrier envelope offset frequency of the self-mode-locked laser

A.K. Dmitriev, N.I. Dmitrieva, N.N. Golovin, A.A. Isakova, A.A. Lugovoy
Novosibirsk State Technical University, Novosibirsk, Russia
E-mail: alexander_dmitriev@ngs.ru

A new method for measuring the carrier envelope offset frequency of the self-mode-locked laser is suggested. These measurements allow to eliminate the influence of the dispersion of a Fabry-Perot interferometer and noncoincidence of its mirrors surface with phase front of the laser radiation.

High harmonic generation in gases with two-color crossed laser fields: theory and experiment

A. S. Emelina[1], M. Yu. Emelin[1], R. A. Ganeev[2], M. Suzuki[2], H. Kuroda[2], and V. V. Strelkov[3]
[1]*Federal State Budgetary Institution of Science «Federal Research Centre Institute of Applied Physics of the Russian Academy of Sciences», 46 Ulyanov Str., Nizhny Novgorod 603950, Russia*
[2]*Ophthalmology and Advanced Laser Medical Center, Saitama Medical University, Saitama 350-0495, Japan*
[3]*Federal State Budgetary Institution of Science A. M. Prokhorov General Physics Institute of the Russian Academy of Sciences, 38 Vavilova Street, Moscow 119991, Russia*
E-mail: emelin@ufp.appl.sci-nnov.ru

Laser sources of mid-IR radiation open up new perspectives for the creation of compact sources of coherent X-ray radiation with photon energies of the order of several keV through the high harmonic generation (HHG) in gases. However, there are several factors that lead to a significant decrease in the efficiency of HHG with increasing laser wavelength. Thus, increasing the efficiency of the HHG with the mid-IR sources is an actual problem. The use of a driving field consisting of the laser field and its second harmonic is one of the reliable methods for enhancing the harmonic yield [1–3].

In this contribution, the high-order harmonic generation in silver, gold and zinc plasma plumes irradiated by orthogonally polarized two-color field is studied theoretically and experimentally [4].

A significant enhancement of the harmonic yield in the case of two-color pump (TCP) was observed experimentally in all the metal plasmas used, see Fig. 1. The enhancement factor in the case of TCP compared with single-color pump (SCP) significantly varied in different ranges of harmonic spectra and also depended on the plasma species. In the case of Ag plasma, the enhancement factor for H21–H23 was in the range of 3 to 5. For higher orders, introduction of BBO in the path of the driving beam led to at least approximately 50-times growth of harmonic emission of orders of the thirties to forties. We observed similar behavior of the enhancement factor in the case of gold and zinc plasmas, though the value of this parameter was smaller.

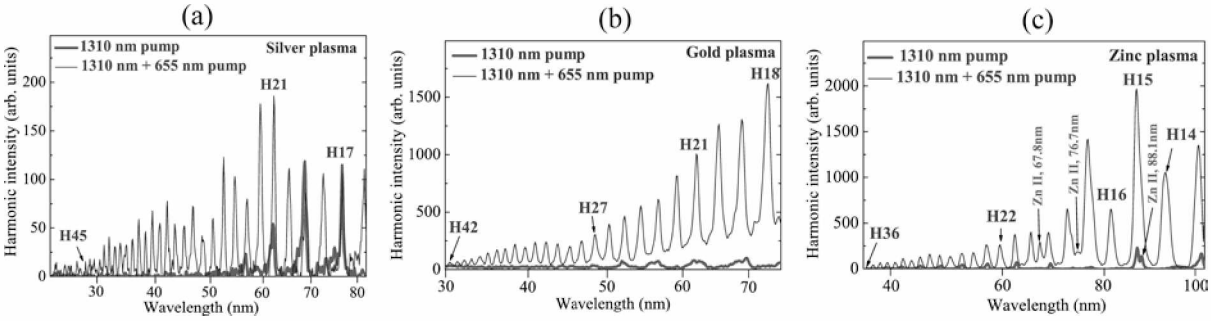

Fig. 1 HHG in (a) Ag, (b) Au, and (c) Zn plasmas using 1310 nm and 1310 nm + 655 nm pumps.

Our theoretical study based on the approach proposed in [5] show that the widely-used theoretical approach assuming the 1*s* ground state of the generating particle fails to reproduce the experimental results. We have derived a general expression for the dipole matrix element **d(p)** corresponding to the transition from an arbitrary nonmagnetic bound state of the hydrogen-like atom to the continuum plane wave. Figure 2(a) shows spectra of silver ion response obtained with the same ionization potential $I_p = 21.48$ eV and various quantum numbers of the outer electron used. Note that the HHG spectrum obtained with the widely used expression for **d(p)** with $n = 1$ and $l = 0$ differs essentially from the experimental one, see Fig. 1(a), thin line. In contrast to that, the shape of the spectrum obtained with the actual quantum numbers of the outer electron in Ag^+ ($n = 4$ and $l = 2$) is quite close to the shape of the experimental one. Thus, the proper choice of the expression for **d(p)** is crucial for the correct reproduction of the HHG spectrum in theoretical calculations.

Figures 2(b) and 2(c) show the spectra of the silver ion response for several intensity ratios (α) and phase shifts between field components (φ). Figure 2(b) shows the worst case ($\varphi = 0$) and Fig. 2(c) shows the best one ($\varphi = \pi/2$). The harmonic spectra obtained with other values of φ are in between of

these two cases. It is clear that the effect of the second field depends strongly on α and φ, and under the optimal conditions the gain can achieve almost 3 orders of magnitude in terms of harmonic intensity. Results for gold and zinc ions are qualitatively similar, but the gain is lower.

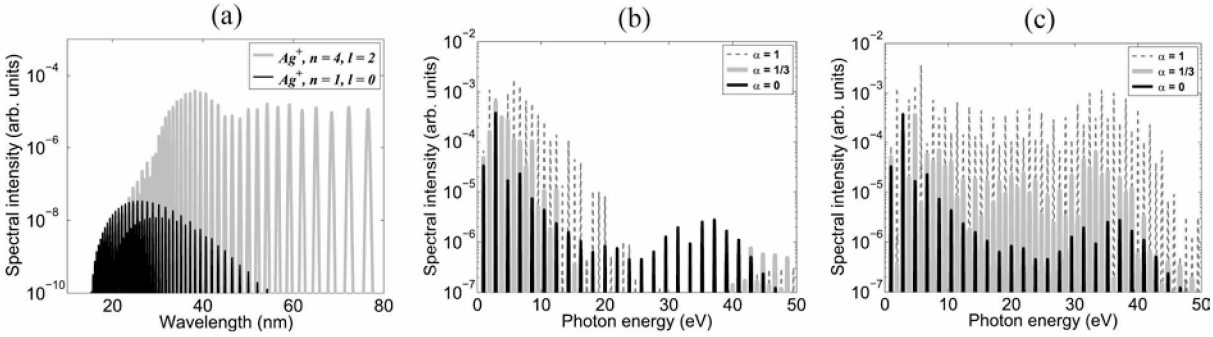

Fig. 2 Spectra of a silver ion response: (a) with $\alpha = 1/3$, $\varphi = \pi/2$ and various **d**(**p**) (see legend); (b) with $\varphi = 0$ and various α (see legend); (c) with $\varphi = \pi/2$ and various α (see legend). Results in (b) and (c) are obtained with the actual quantum numbers.

Our theoretical studies allow clarifying an important aspect of the HHG enhancement in the two-color field which was not discussed earlier. Namely, according to the simple-man HHG model, in the SCP case the majority of the ionized electrons do not come back to the parent ion or come back with low energy. We show that in the two-color field with comparable intensities of the components the majority of the electrons can come back with high energy corresponding to the close-to-the-cutoff harmonics. Though deflected in the orthogonal direction by the second field, the returning electron wave packets are large enough to recombine nearly as efficiently as in the single-color case.

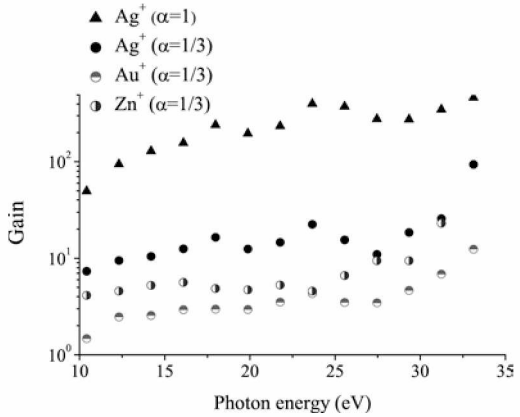

Fig. 3 The gain in harmonic intensity in the TCP case compared to the SCP one for different plasmas.

As it follows from Fig. 2, the microscopic response is very sensitive to the relative phase φ. This phase changes during the fields' propagation in the medium. Therefore, we have performed a complete study of the HHG phase matching in a two-color field. The gain due to the two-color field obtained in our theoretical calculations is presented in Fig. 3. One can see that for given α the highest gain is achieved for silver, in agreement with the experiment. For $\alpha = 1/3$ (close to our experimental conditions) the typical gain obtained in the calculations for silver is 10-30, which is in reasonable agreement with the experimental value (about 50). Moreover, Fig. 3 shows that the gain grows with harmonic order as it was observed in experiment, see Fig. 1(a). For gold and zinc the enhancement more weakly depends on the harmonic order, also in agreement with experimental results.

References

[1] T. T. Liu, T. Kanai, T. Sekikawa, and S. Watanabe, Phys. Rev. A **73**, 063823 (2006).
[2] I. J. Kim, C. M. Kim, H. T. Kim et al., Phys. Rev. Lett. **94**, 243901 (2005).
[3] R. A. Ganeev, H. Singhal, P. A. Naik et al., Phys. Rev. A **80**, 033845 (2009).
[4] A. S. Emelina, M. Yu. Emelin, R. A. Ganeev et al., Opt. Express **24**, 13971 (2016).
[5] M. Lewenstein, Ph. Balcou, M. Yu. Ivanov et al., Phys. Rev. A **49**, 2117 (1994).

Effect of magnetic field of mid-IR laser pulse on the spectral shape of high harmonics produced in gases

A. S. Emelina, M. Yu. Emelin, M. Yu. Ryabikin
Federal State Budgetary Institution of Science «Federal Research Centre Institute of Applied Physics of the Russian Academy of Sciences», 46 Ulyanov Str., Nizhny Novgorod 603950, Russia
E-mail: ana_b@rambler.ru

The use of mid-IR driving laser pulses has been demonstrated experimentally to produce high-harmonic x-ray emission spanning keV bandwidth [1] that, in the Fourier limit, is capable of supporting few-attosecond pulses. However, with increasing laser wavelength, the role of nondipole effects grows. The magnetic component of the Lorentz force is known to lead to the deflection of the electron trajectory from the straight path. As a result, it reduces the probability of electron recombination with the parent ion, thereby reducing the efficiency of optical frequency conversion into the X-ray range. With increasing laser wavelength, the above-mentioned effect increases due to the increase of both the electron velocity and the time interval of its free motion. That is why the nondipole effects are typically crucial for high harmonic generation driven by mid-IR laser sources.

In this contribution it is shown that the magnetic field of mid-IR laser pulse affects not only the amplitude, but also the shape of the spectrum of generated radiation. It is also demonstrated that the electron magnetic drift does not play a negative role only; in some cases it has a positive effect.

We use the single-active-electron approximation to describe the interaction of an atom with a strong electromagnetic field. Our theoretical study is based on an analytical approach. We use the quantum-mechanical treatment of high harmonic generation (HHG) within the strong-field approximation [2] modified properly to take into account the atomic bound-state depletion and the effect of the magnetic field of a laser pulse on the dynamics of the released electron [3, 4].

A very peculiar feature of magnetic-drift limited HHG [3, 4] is the shape of the photon emission spectrum, which now loses a familiar plateau-like (or multi-plateau) structure. This can be seen from a comparison of the spectra obtained in the dipole approximation and beyond it (cf. corresponding lines in figure 1). In the nondipole case, even at moderate laser intensities, along with an overall reduction of the harmonic output compared to the dipole approximation, distinct minima are observed in both the low-energy and near-cutoff parts of the plateau (figure 1(a)). With increasing intensity of the laser, this effect becomes more and more pronounced and eventually, the cutoff disappears and the spectrum becomes arcuate rather than plateau-like (figure 1(b)). This kind of modification of the plateau structure of the photon emission spectra can be quite easily explained by analyzing the weights of classical electron trajectories that returns exactly to the nucleus at the time of recombination. The maximum in the harmonic emission spectrum corresponds to the kinetic energy at the time of recombination of the electron that follows the optimal trajectory.

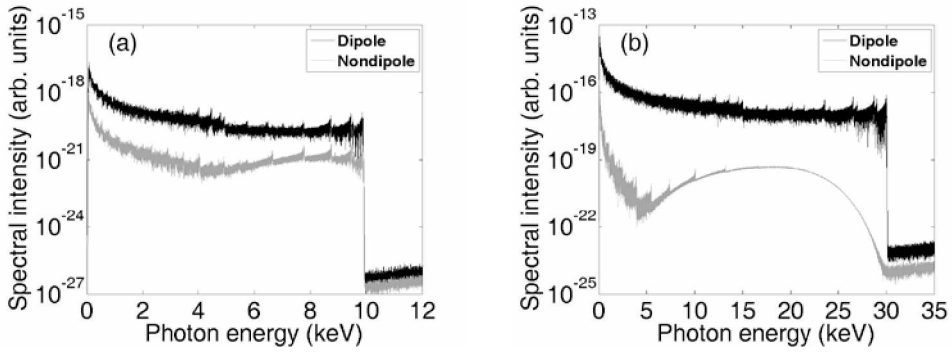

Fig. 1 HHG spectra for the He^+ ion driven by a 6-cycle laser pulse with $I = 2\times10^{15}$ W cm^{-2} at a wavelength of 3.9 μm and peak intensity of (a) 2.2×10^{15} W/cm^2 and (b) 6.7×10^{15} W/cm^2. Different lines represent the spectra obtained in the dipole approximation and beyond it (see legends).

From Fig. 1 one can see also that even in the magnetic-drift limited case, the width of the generated harmonic spectrum can be wide enough for few-attosecond and even subattosecond pulse production. However, it is extremely challenging to achieve this limit because of the need to compensate across this enormous bandwidth for the attosecond chirp inherent to the HHG process. An alternative and relatively simple route for breaking the attosecond barrier has been proposed recently [5], which relies on the interference of high-harmonic emission from multiple reencounters of the electron wave packet with the ion. We examine the impact of the electron magnetic drift caused by a strong mid-infrared laser field on the feasibility and ultimate limitations of this method.

Figure 2 shows the spectral content of the x-ray burst generated in helium on the trailing part of a 1.5-cycle laser pulse. Black line represents the spectrum calculated in the dipole approximation. This spectrum exhibits two pronounced peaks at photon energies near 0.6 keV and 3.05 keV originating from two different reencounters. Such two-peak structure of the spectrum leads to the modulation of the fs x-ray harmonic burst into a waveform of ultrashort beats. Obviously, the beating contrast of the resulting waveform is highest when the two spectral peaks are of comparable weights. In Fig. 2, the relative weight between the lower- and higher-energy peaks in the spectrum calculated for the dipole case is substantially different. However, by attenuating the first peak using the spectral filter (the transmission through the Al filter can be used [5]) the two peaks can be equalized. As a result, a perfectly contrasted waveform can be obtained with the width of each beat of about 1 as.

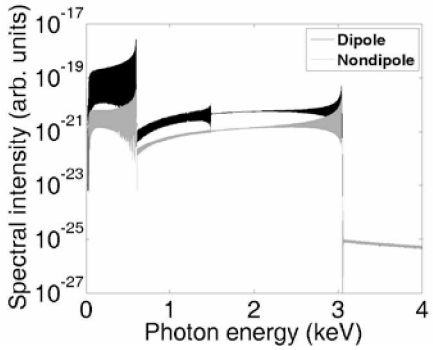

Fig. 2 Spectrum of the selected x-ray burst generated on the trailing part of a 1.5-cycle laser pulse with I=3.3×10^{14} W/cm^2 and λ_0=9 μm; the results obtained in the dipole approximation and beyond it are shown.

The spectrum of the same x-ray burst calculated beyond the dipole approximation is represented by gray line in Fig. 2. Importantly, it turns out that the effect of the magnetic field, which is typically detrimental to HHG, does not lead to fatal consequences in the case under consideration. Indeed, the emission spectrum in this case still exhibits two distinct peaks. Moreover, the magnetic field of the laser pulse serves here as a spectral filter, which in certain cases may favorably alter the relative weights of the peaks in the HHG spectrum. Just such a case can be seen in Fig. 2. In the nondipole spectrum, the low-energy peak is significantly reduced, whereas its high-energy counterpart is only slightly attenuated. As a result, only a small additional spectral filtering is required to equalize the two peaks.

We also examine what happens to the HHG spectra at laser wavelengths longer than 9 μm [6]. It has been shown that, up to driving wavelengths of 16 μm, the electron magnetic drift does not destroy completely the mechanism of the formation of subattosecond keV beats but rather alters the relative weights between different reencounter contributions to the HHG spectrum. Eventually, intense high-contrast keV beats of durations shorter than 0.8 as are shown to be attainable using few-cycle mid-IR laser pulses with the central wavelength of about 12 μm.

References

[1] T. Popmintchev, M. Chen, D. Popmintchev et al., Science **336**, 1287 (2012).
[2] M. Lewenstein, Ph. Balcou, M. Yu. Ivanov et al., Phys. Rev. A **49**, 2117 (1994).
[3] A. S. Emelina, M. Yu. Emelin, and M. Yu. Ryabikin, Quantum Electron. **44**, 470 (2014).
[4] A.S. Emelina, M.Yu. Emelin, and M.Yu. Ryabikin, JOSA B **32**, 2478 (2015).
[5] C. Hernández-García, J. A. Pérez-Hernández, T. Popmintchev et al., Phys. Rev. Lett. **111**, 033002 (2013).
[6] A.S. Emelina, M.Yu. Emelin, and M.Yu. Ryabikin, Phys. Rev. A **93**, 043802 (2016).

Bioeffects of terahertz radiation is base for new application in medicine

V. Fedorov
Institute of Laser Physics SB RAS, prospekt Lavrentyeva 13/3, Novosibirsk, 630090 Russia
E-mail: vif41@mail.ru

Terahertz radiation induces conformation transitions in biomolecules and effects on membrane state and gene activity in cells. For details, see reviews [1–6]. This influences genetic, biochemical, morphological and physiological characteristics in organism and induces the alterations in the state of control physiological systems [7]. This can be used for ilness diagnostics and treatment.

The study at organismic level and treatment of diseases

The investigation of terahertz effects on organism level lets to use the terahertz radiation as treatment factor. It was demonstrated the dose-dependent influence of terahertz radiation on rat spleen cell production of antibodies to sheep red blood cells and on migration ability of B-lymphocytes in antigen presence. In addition it was demonstrated the dose-dependent influence of THz radiation on stage of bone regeneration in rats with experimental defect of femur. These results allowed to use the gas-discharge HCN laser (0,89 THz) for treatment traumatic and degenerative disorders in bone and cartilage tissues. Treatment of rats with experimental mechanical damage to the skin demonstrates the decrease in wound area from 170 to 17 mm^2 during 8 days after exposition 400 $\mu W/cm^2$ x 15 min.

Terahertz irradiation of patients with post-operative and post-traumatic mechanical skin lesions (7 exposures on 400 $\mu W/cm^2$ x 15 min per day demonstrates the next results of treatment: the acceleration of wound healing, the prevention of post-operative and post-traumatic suppuration of wounds, the increase in contraction of wound surface, the stimulation of regenerative ability and optimization of cellular composition of wound exudate. Terahertz irradiation of 2 acupuncture points G1.4 (on hand) and E36 (on foot) in volunteers with spinal osteochondrosis (3 exposures on 1 mW/cm^2 x 15 min on day) induces positive dynamics of metabolism indices in the cartilage (normalization of chondroitin sulfate and glycosaminoglycans serum levels). Experimental treatment of grafted Guerin carcinoma by terahertz radiation (2 sessions on 1,44 J/cm^2) demonstrates the reduction of tumor growth during 20 days after two sessions of irradiation. Degree of tumor growth reduction after terahertz treatment and x-rays treatment are identical [8].

The study at cellular level and diagnostics

Modern medicine requires new methodological principles, which will allow to create a preventive approach to health , based on preclinical detection of risk factors. The study of terahertz biologic effects on cellular level provides a background to the creation of principally new methods of diagnostics. The results of a preliminary study of biological effects has allowed to develop the principle of detection by terahertz radiation of apparently healthy individuals who are carriers of risk factors for immune deficiency. It was demonstrated that terahertz radiation causes more pronounced increase of mitogen-induced proliferation of lymphocytes. It was found that among healthy persons there are the individuals with initially low proliferative activity of lymphocytes. Responses of lymphocytes to terahertz irradiation were different. There is the absence of proliferous potential ability or pronounced proliferous potential ability. In the first case there is an insufficiency of immune system, in the second case – the lesion of regulation of immune system. It may be used at asymptomatic and early stages of different diseases, which induced by immune insufficiency: all diseases of internal organs, oncologic diseases, autoimmune diseases etc. It can be a base for creating the diagnostic test to evaluate the ability of lymphocytes to proliferation and apply it to identify

individuals at the early stages of different diseases, which induced by immune insufficiency: all diseases of internal organs, different hematological diseases, oncologic diseases, autoimmune diseases etc. This may facilitate the identification of trends to failure of the immune system in healthy individuals.

It was demonstrated that terahertz radiation results in a viability reduction in part of irradiated lymphocytes. This is tested by the appearance in cytoplasm the colorant penetrating only nonviable cells. Based on this result it is possible to create the diagnostic test for identifying of potentially nonviable lymphocytes and used it to identify healthy individuals which have the early stages of various hematological disorders, different variations of immune system disturbance and other diseases that lead to such violations. Terahertz radiation induces a specific state, which in combination with provoking factor reveals to morphological or functional abnormalities which are undiagnosable by traditional methods. The study of terahertz radiation influence on membrane stability of red blood cells demonstrates that terahertz radiation does not influence spontaneous hemoglobin output, but increases the hemoglobin output induced by water adding to isotonic buffer solution (hypoosmotic hemolysis). This effect is increased if the concentration of sodium chloride solution is decreased. Terahertz radiation causes pronounced shorting of duration of full hypoosmotic hemolysis. Results of these experiments can be a premise for creating the diagnostic test for identifying a tendency to disturbance of red blood cell membrane resistance in healthy individuals for recognition of early stage of various hematological, nephrological, endocrinological and other diseases which are associated with impaired membrane status of these cells.

Molecular level. Treatment and diagnostics

The results of terahertz effects on moleclar level study demonstrates that terahertz radiation induces conformation transitions in biopolymer molecules [9-11]. These results open up the prospect of obtaining substances with the desired properties: inhibitors of enzyme activity, selective blockers of receptors, components for hybrid nanotechnology, targeted cancer drugs for blocking the growth and spread of cancer. It is possible the creation of components for principal new diagnostic kits.

References

[1] V. I. Fedorov, S. S. Popova, A. N. Pisarchik, Int J Infrared and Millimeter Waves **24**, 1235 (2003).
[2] A. Ramundo Orlando, G.-P. Gallerano, J. Infrared, Millimeter and Terahertz Waves **30**, 1308 (2009).
[3] G. J. Wilmink, J. E. Grundt, J.Infrared, Millimeter and Terahertz Waves **32**, 1074 (2011).
[4] H. Hintzsche, H. Stopper, Critical Reviews in Environmental Science and Technology **42**, 2408 (2012).
[5] P. Weightman, Phys. Biol. **9**, 053001 (2012).
[6] Li Zhao, Yan-Hui Hao, Rui-Yun Peng, Mil Med Res. **1**, 26 (2014).
[7] V. I. Fedorov, Biomeditsinskaya Radioelectronika, N 2, 17 (2011).
[8] V. K. Kiseliov, V. I. Makolinets, N. A. Mitryaeva et al., 2-nd International Conference "Terahertz and Microwave radiation: Generation, Detection and Applications" Moscow, 2012, p. 133.
[9] O. P. Cherkasova, V. I. Fedorov, E. F. Nemova et al., Optics and Spectroscopy **107**, 536 (2009).
[10] I. V. Lundholm, H. Rodilla, W. Y. Wahlgren et al., Structural Dynamics **2**, 054702 (2015).
[11] B. S. Alexandrov, V. Gelev, A. R. Bishop et al., Phys. Lett. A **374**, 1214 (2010).

Terahertz radiation influence on dynamics of achieving the adult state in offspring of irradiated parent Drosophila

V. Fedorov[1], N. Weisman[2], E. Nemova[1]
[1]*Institute of Laser Physics SB RAS, Prospekt Lavrentyeva 13/3, Novosibirsk, 630090, Russia*
[2]*Institute of Cytology and Genetics SB RAS, Prospekt Lavrentyeva 10, Novosibirsk, 630090, Russia*
E-mail: vif41@mail.ru

It was demonstrated that terahertz radiation influences genetic system of plants and animals. A maturation of organism is the process of sequential switching of more and increasingly complex gene systems. In present study we investigated terahertz radiation influence on development dynamics of offspring obtained from irradiated or non-irradiated females mating with irradiated or non-irradiated males.

Methods. Fruit flies of both sexes subjected to 30-minute exposure of broadband terahertz radiation (0.1 - 2.2 THz) with a pulse power of 8.5 mW, a pulse duration of 1 ps and a repetition rate of 76 MHz. After the irradiation was carried out mating of exposed (E) and intact (I) individuals in various combinations. As a control (K) used flies that were near terahertz source during irradiation, but do not fall into the irradiation zone. We used clutch of eggs in the first two days after irradiation, which corresponds to mature eggs at the time of irradiation. the adult stage of offspring individuals. , It was recorded the number of reaching the adult stage of offspring individuals and their gender (daily from the first case of reaching). To determine the significance of differences between the curves of the maturation dynamics the $\chi 2$ test was used.

Results. The progenies derived from mating of unexposed females with non-irradiated (♀♀K x ♂♂K) or intact (♀♀K x ♂♂I) males. The first case of reaching of adult state in individuals of both sexes is registered on the 11th day from the beginning of mating. The number of individuals is small. The following day, the maturing of males and females is increased significantly and reaches a maximum value on the 13th day from the beginning of mating. Then, the number of ripe specimens of both sexes is decreased consistently (Fig.1,2).

The progeny derived from mating of intact females and unexposed males (♀♀I x ♂♂K). The first case of reaching of adult state in individuals of both sexes is registered on the 12th day from the start of mating. The following day, the maximum number of ripe individuals of both sexes is recorded. After that, it is indicated a consistent decrease in the number of ripe individuals. The total duration of the ripening period varies from 8 to 10 days at different variants of mating (Fig.1,2). The curves of development dynamics of males and females do not differ significantly. Sex ratio was 1:1.

The progenies derived from mating of irradiated females with irradiated (♀♀E x ♂♂E) or intact (♀♀E x ♂♂ I) males. The first case of reaching of adult state in individuals of both sexes is registered on the 11th day from the beginning of mating. The number of individuals is small. The following day, the maximum number of ripe individuals of both sexes is recorded compared to other days. Third day of maturing is characterized by a decrease in the number of individuals, reaching the adult stage. Then, the relative number of ripe individuals sharply decreased. The total duration of the ripening period was within 5 - 6 days (Fig.1,2). The curves of development dynamics of males and females do not differ significantly. Sex ratio was 1:1.

The progenies derived from mating of intact females and irradiated males (♀♀I x ♂♂E). The first case of reaching of adult state in individuals of both sexes is registered on the 11th day from the start of mating, but the maximum number of ripe individuals of both sexes is registered on the 13th day from the beginning of the mating. The total duration of the ripening period was 7 days in males and females. Total number of ripe males was higher than females. Sex ratio was 1:0.83. The curves of

development dynamics of males and females are different significantly ($\chi 2$=4,86). Another difference was the dynamics of subsequent reduction in the relative abundance of mature flies. In males, it was almost as good as in the control group. Females have been a sharp decrease in the relative number of ripe individuals (Fig.1,2). This curve of development dynamics significantly different from the control ($\chi 2$=8.41).

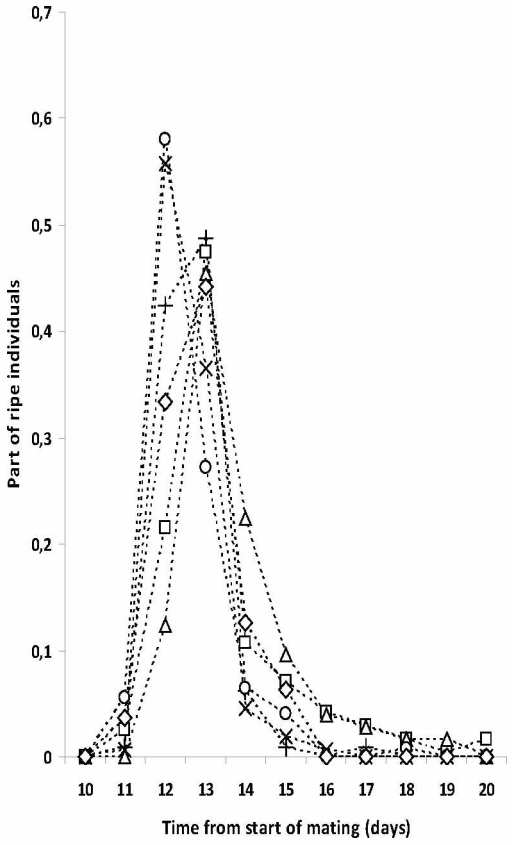

Fig. 1. Dynamics of maturation of male individuals. Oblique cross – ♀♀E x ♂♂E, circle – ♀♀E x ♂♂I, rectangular cross – ♀♀I x ♂♂ E, rhombus – ♀♀K x ♂♂K, square – ♀♀K x ♂♂I, triangle – ♀♀I x ♂♂K.

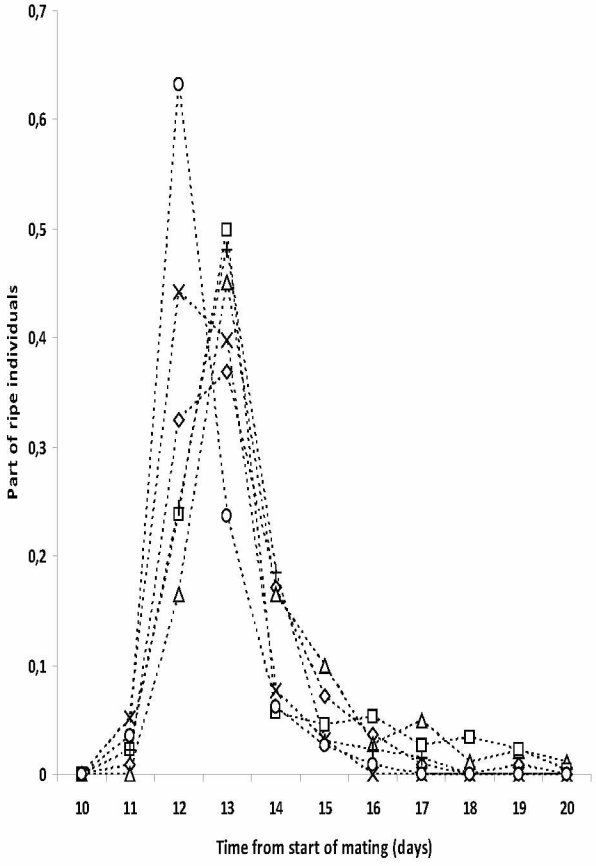

Fig. 2. Dynamics of maturation of female individuals.

Thus, terahertz radiation causes a shortening of development period to adulthood in offspring obtained by mating irradiated females with both irradiated and non-irradiated males. In the case of progeny derived from mating of irradiated males and intact females, the effect of THz radiation depends on the sex of offspring.

Extremely broadband femtosecond laser source based on parametric amplification in the mid-infrared

S. A. Frolov, V. I. Trunov, and E. V. Pestryakov
Institute of Laser Physics SB RAS, 13 Lavren'tyev prosp., Novosibirsk, Russia
E-mail: stanislav.a.frolov@gmail.com

We present the results of numerical studies on the development of methods for the generation of powerful IR radiation of ultrashort duration using the dual channel femtosecond laser system based on parametric amplification, working at 10 Hz repetition rate, created in Institute of Laser Physics (ILP) SB RAS.

In order to achieve longer wavelengths we use the femtosecond signal and idler radiation of our laser system. To move further to IR at each step we parametrically amplify the idler from previous step with the signal wave. Having the signal at the central wavelength of 0.86 μm and idler at 1.4 μm we successively obtain new wavelengths of 2.24, 3.7, 5.7, and 10.4 μm. Compared to difference frequency generation, such approach enables to retain high energy in IR pulses at cost of higher complexity. The scheme presented by us enables generation of IR pulses with higher efficiency at wider wavelength range compared to previous one of ours [1].

Although large number of nonlinear optical crystals are suitable for the mid-IR range, their practical use is limited either by low damage threshold, low available aperture or degradation due to two-photon absorption. We decrease the influence of the latter effect by subsequent idler wavelength increase, which allows using more optimal crystals. We chose $AgGaSe_2$ (AGSe) crystal due to its high nonlinearity, high damage threshold, high available aperture up to several cm and transparency range up to 18 μm [2]. In our scheme of nonlinear conversion we use LBO crystals for near- to mid-IR (up to 2.24 μm) and AGSe for mid- to far-IR as shown in Fig. 1a. The generated spectra is shown in Fig. 1b. With optimizations of various parameters the optimum energy and pulse duration of generated pulses were computed to be 130 mJ and 35 fs for 2.24 μm, 40 mJ and 60 fs for 3.7 μm, 15 mJ and 90 fs for 5.7 μm, and 7 mJ and 150 fs for 10.4 μm central wavelength.

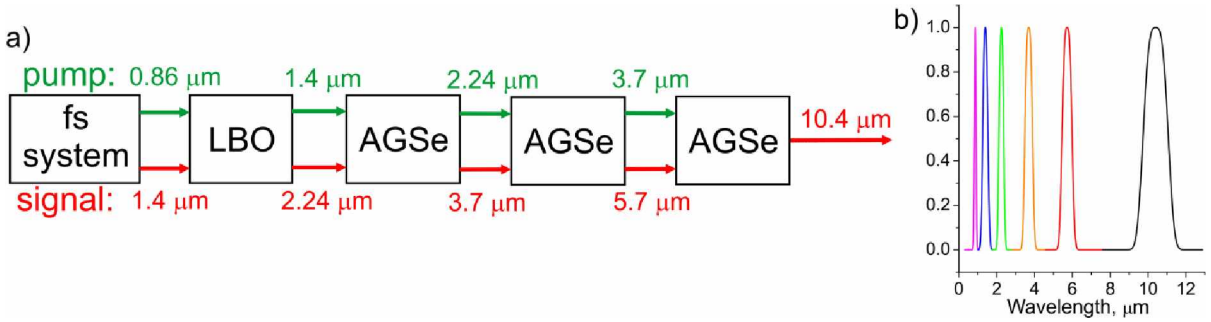

Fig. 1 a) scheme of nonlinear frequency conversion and b) generated IR-spectra of all conversion steps

A method of generation of terawatt femtosecond pulses in IR range with use of high-power laser system developed at ILP SB RAS has been proposed. Its advantages are possibility to use crystals suitable for relatively narrow wavelength range and ability to provide high pulse energy. The peak power of femtosecond IR-pulses that can be generated with our scheme is high enough for enhancing the experimental research on the development of new approaches to the atmosphere diagnostics, generation of powerful femtosecond, attosecond pulses in X-ray and so on.

References

[1] V.I.Trunov, S.A. Frolov, E.V.Pestryakov, Proceeding of SPIE, **9680**, 96803N-1 (2015).
[2] P.G. Schunemann, K.L. Schepler, P.A. Budni. Mrs Bulletin, **23**, 45 (1998).

Research on cladding mode resonance sensing characteristics based on triple cladding quartz specialty fiber

Xinghu Fu, Haiyang Xie, Guangwei Fu, and Weihong Bi
The Key Laboratory for Special Fiber and Fiber Sensor of Hebei Province, School of Information Science and Engineering, Yanshan University, Qinhuangdao, Hebei 066004, P. R. China
E-mail: fuxinghu@ysu.edu.cn

In recent years, fiber optic sensor has received extensive attention and research due to its unique advantages, and it has been successfully used in many areas, such as aerospace, construction engineering, biomedicine, etc. However, the balance between the simple structure and the superiority performance of these sensor is becoming a "bottleneck" which has already restricted the development of this field. Utilizing the structure characteristics of multi-cladding fiber, the cladding mode resonance fiber sensor makes the light transmitted from core and cladding couple with each other, so as to realize the detection of the measurement physical quantity. This sensor has the advantages of simple structure, controllable mode excitation, high sensitivity, no-cross sensitivities and so on, which opens up a new way for the research and application of the special fiber optic sensor. Thus, it is of great significance to carry out the relevant theoretical and experimental research around its characteristics. In this paper, the cladding mode resonance phenomenon of the triple cladding quartz specialty fiber (TCQSF) and the characteristics of this sensor have been analyzed specifically based on coupled mode theory. Utilizing the coupled mode theory, the effective model of the TCQSF is established. The relationship between the length and transmission spectrum of the sensor is established. A straight forward experiment is performed to study the temperature sensing properties of this cladding mode resonance sensor. The relationship between different temperature and wavelength drift is studied experimentally. Moreover, the curvature sensing characteristics of this sensor is studied. The relationship between different curvature and wavelength drift is studied experimentally. Finally, the characteristics of the sensor based on TCQSF which is dislocation welding with the single mode fibers is studied. The relationship between the size of the dislocation and refractive index sensitivity is analyzed. The refractive index and temperature characteristics of the sensor are tested and discussed.

References

[1] Y. F. Lu, C. Y. Shen, C. Zhong, et al, IEEE Photonics Technology Letters **26**, 1124(2014).
[2] M. R. Mokhtar, K. Owens, J. Kwasny, et al. , IEEE Sensors Journal **12**, 1470(2012).
[3] G. A. Cardenas-Sevilla, D. Monzon-Hernandez, I. Torres-Gomez, et al., Optics & Laser Technology **44**, 1516(2012).
[4] M. M. Luo, Y. G. Liu, Z. Wang, et al. , Optics Express **21**, 30911(2013).
[5] F. Zou, Y. Q. Liu, C. L. Deng, et al. , Optics Express **23**,1114(2015).
[6] S. Pevec and D. Donlagic,Optics Letters **39**, 6221(2014).
[7] J. T. Zhou, Y. P. Wang, C. R. Liao, et al., Sensor and Actuators B: Chemical **208**, 315(2015).
[8] S. M. Tripathi, A. Kumar, M. Kumar, et al., Optics Letters **37**,4570(2012).
[9] H. Qu, G. F. Yan and M. Skorobogatiy, Optics Letters **39**, 4835(2014).
[10] Xinghu Fu, Haiyang Xie, Xianglong Zeng, Guangwei Fu, Weihong Bi, Optics Express **23,** 2320(2015).

Impulse photoconductivity of diamond at low temperature

D. Genin[1], E. Lipatov[1], and D. Grigor'ev[2]
[1]*Institute of High Current Electronics, Tomsk, Akademicheskiy av. 2/3, Russian Federation*
[2]*National Research Tomsk State University, Tomsk, Lenina av. 36, Russian Federation*
E-mail: dm_genin@vtomske.ru

In 1968 academician LV Keldysh predicted the existence of the electron-hole liquid (EHL) in semiconductors [1]. EHL is a condensed state of the electron-hole plasma, which occurs at low temperatures and high concentrations of electron-hole pairs (EHP). At low temperatures, the EHP form a hydrogen-quasiparticles - free excitons (FE). At low concentrations free excitons in the semiconductor can be regarded as an ideal gas, consisting of virtually interacting particles. At high concentration of excitons they form the exciton complexes (EC) - trions and biexcitons which act as condensation nuclei of EHL drops. This EHL is not molecular fluid, as carriers are free to migrate through the drop, which is typical for liquid metal (analogy, liquid alkali metals).

If the EHL is formed in the semiconductor sample, it increases the sample's conductivity. Our idea was to try to use the EHL effect in diamond photo-electronic switches. EHL was experimentally found in many semiconductors in the form of droplets surrounded by exciton gas. EHL was observed in semiconductors that have indirect-like structure (Ge, Si, SiC and C) and the direct-gap structure (GaAs, CdS, CdTe, etc.).

The phase transition EHP - EHL occurs at concentrations above the EAF and the temperature below the critical point of the sample. For germanium concentration and temperature of the phase transition is $8.9 \cdot 10^{16}$ cm^{-3} and 6.7 K, respectively. For silicon - $1.2 \cdot 10^{18}$ cm^{-3} and 28 K, respectively. The typical size of the EHL drops in Ge and Si is 10-100 microns.

The third simple semiconductor with indirect-many-valley structure and nature of the conduction band is diamond. It's band gap is 5.49 eV, the dielectric constant is 5.7. Calculations showed that the EHL should be formed in diamond at the EHP concentration of 10^{20} cm^{-3} and a temperature below 138 K.

Natural diamond is heavily contaminated with nitrogen impurity that forms the variety of defects, including polyols containing vacancies, interstitial sites, and other impurity atoms. Such defects can act as centers of exciton recombination. That's why the first results in the field of EHL formation in diamonds were obtained only in 2000.

In our work we investigated the formation of EHL in diamond samples and their conductivity in such conditions. There were 5 samples: one natural diamond and 4 artificial samples. The scheme of experimental setup is shown on the Fig. 1. The samples were irradiated by KrCl*-laser (λ=222 nm) and cooled by liquid nitrogen. EHL was detected by the appearing of the wide band near 240 nm in the spectrum of the sample photoluminescence and the temperature dynamic of this band. Two samples out of five showed this band, both were made by CVD (chemical vapor deposition) method. The threshold values of laser radiation intensity for EHL formation were 3 and 10 MW/cm^2 for these samples. The difference can be explained by different level on impurities contained.

The sample with lowest EHL formation threshold was used in the research of impulse conductivity. It had the electrode system on it's surfaces and was switched in the electric circuit like it is shown on the Fig. 1c. When the laser pulse intensity was about 3 MW/cm^2 the amplitude of voltage pulse through the sample was 2-3 times higher at 90 K than at 300 K. On the other hand, at 90 K the photoconductivity was 10 times higher at 3.4 MW/cm2 intensity than at 0.55 MW/cm2 intensity (Fig. 2).

Preliminary we can conclude that the presence of EHL in diamond sample can drastically increase it's conductivity. It can be used in photo-electronic switches based on diamonds.

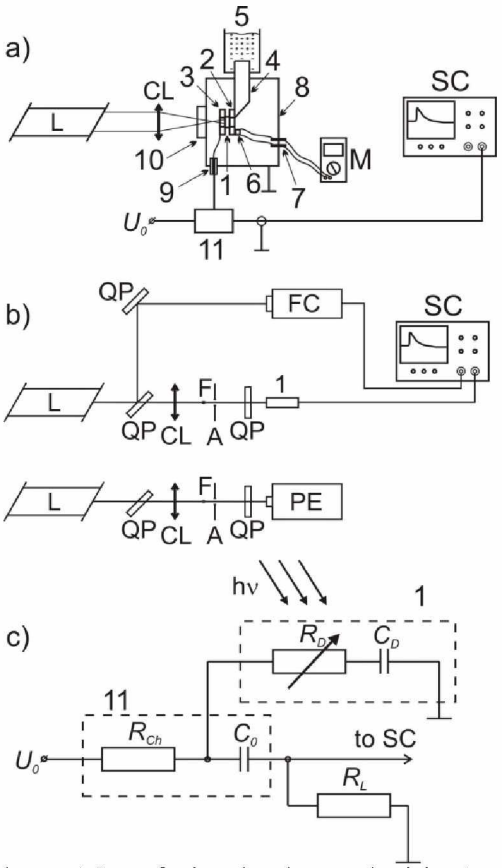

Fig. 1 Experimental setup scheme. a) Setup for impulse photoconductivity. 1 – diamond sample, 2 – ground copper electrode, 3 – potential copper electrode, 4 – heat sink, 5 – volume with liquid nitrogen, 6 – thermoresistor, 7 – low-voltage contacts, 8 – chamber, 9 – high-voltage contact, 10 – silica window. b) Experimental scheme. L – KrCl*-laser, QP – silica plates, CL – cylindrical lense, F – focus spot of CL lense, A – pinhole, 1 – diamond sample, FC – photocathode, SC – oscilloscope, PE – pyroelectrical detector. c) Electric cirquit for pulsed photoconductivity measurement and equivalent scheme of diamond sample. 1 – 1 – diamond sample, 11 – shielded box, hν – laser radiation, RD – resistance of «low-resistant» layer, CD – capacity of high-resistant layer, C0 – storage capacitor, R_{Ch} - charging resistor, RL – resistance of oscilloscope.

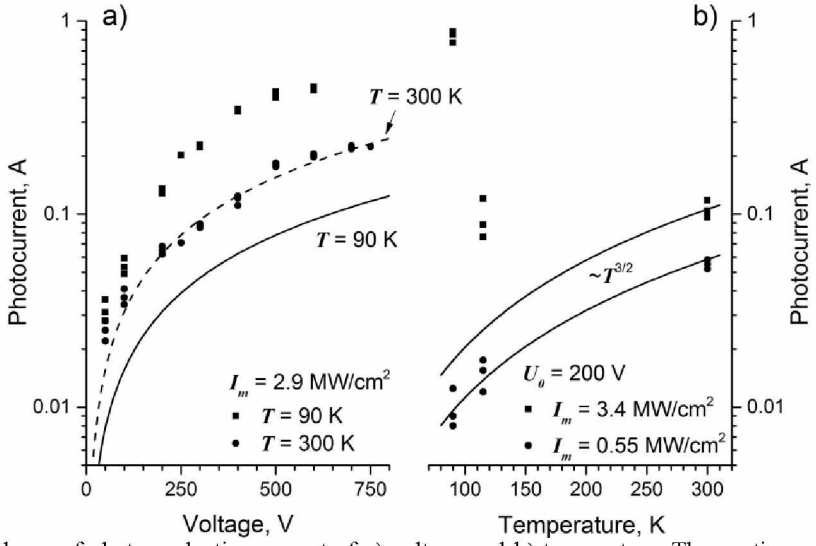

Fig. 2 Dependence of photoconductive current of a) voltage and b) temperature. The continuous curve on a) is the result of theoretical calculations that don't take into account the presence of EHL.

References

[1] L. Keldysh. Electron-hole droplets in semiconductors. «Nauka», 468 (1988)

Shifts and broadening of Rydberg states in ions of the group IIb elements

I.L. Glukhov, E.A. Nikitina, and V.D. Ovsiannikov
Voronezh State University,Faculty of Physics
394018 Voronezh, University square 1, Russia
E-mail: GlukhovOfficial@mail.ru

Blackbody-radiation(BBR)-induced shifts and rates of induced transitions from Rydberg s-,p-, d-states in ZnII, CdII and HgII ions of the group IIb elements were calculated on the basis of the quantum defect method (QDM), similar to the case of the group IIa ions [1,2], which ensures correct asymptotic behavior for wavefunctions with large principal quantum number n.

For concise presentation of the obtained results approximation formulae were used for relative BBR-induced decays and excitations:

$$R_{nlj}^{dec(exc)}(T)=\frac{a_0^{dec(exc)}(T)+a_1^{dec(exc)}(T)x+a_2^{dec(exc)}(T)x^2}{n^2\left[\exp\left(\frac{Z^2T_a}{n^3T}\right)-1\right]},\quad x=\frac{100}{nT^{1/3}} \tag{1}$$

and the shifts

$$\varepsilon_{nlj}^{BBR}(T)=2416.6\left(\frac{T}{300}\right)^2\left(a_0^{\varepsilon}(T)+a_1^{\varepsilon}(T)z+a_2^{\varepsilon}(T)z^2\right), \tag{2}$$

where the fraction x is the cubic root of the fraction of the transition energy $1/n^3$ to the nearby states and the thermal energy of environment T/T_a (both in atomic units, where $T_a=315776$ K is the atomic unit of temperature), n is the Rydberg-state principal quantum number and T is the temperature of environment. The rates of the BBR-induced decays and excitations are $\Gamma_{nlj}^{dec(exc)}(T)=R_{nlj}^{dec(exc)}(T)\Gamma_{nlj}^{sp}$.

The rate of spontaneous decays Γ_{nlj}^{sp} of the Rydberg state $|nlj\rangle$ into the lower-energy states is inverse of the natural lifetime τ_{nlj}^{sp} ($\Gamma_{nlj}^{sp}=1/\tau_{nlj}^{sp}$). The factor n^3 is characteristic of the asymptotic (at $n\to\infty$) dependence of τ_{nlj}^{sp} on the principal quantum number. The rest of the n-dependence may be well approximated by a polynomial, as follows

$$\tau_{nlj}^{sp}=a_0^{sp}n^3\left(1+\frac{a_1^{sp}}{n}+\frac{a_2^{sp}}{n^2}+\frac{a_3^{sp}}{n^3}\right) \tag{3}$$

Coefficients $a_i^{dec(exc)}(T)$ and $a_i^{\varepsilon}(T)$ may be fitted by simple polynomials in powers of temperature with a good accuracy in a range of T=200 to 1000 K, as follows

$$a_i(T)=\sum_{k=0}^{2}b_{ik}\left(\frac{100}{T}\right)^{k/3} \tag{4}$$

The standard curve fitting polynomial procedures were used for determining all polynomial coefficients of equations (1)-(4).

References

[1] I.L. Glukhov, S.N. Mokhnenko, E.A. Nikitina, and V.D. Ovsiannikov, Eur. Phys J. D **69**, 1 (2015).
[2] I.L. Glukhov, E.A. Nikitina, and V.D. Ovsiannikov, J.Phys. B **49**, 035003 (2016).

Metal – dielectric interferometer for sensor applications by frustrated total internal reflection

N.D. Goldina
Institute of Laser Physics of SB RAS, Ac. Lavrentyev'sprosp. 13/3, Novosibirsk, 630090 Russia
E-mail: ngold@laser.nsc.ru

Shifting the minimum reflectance of p-polarized light R_p in the angular and spectral measurements by FTIR scheme is typically used to determine the refractive index of the medium (the analyte). In conventional schemes with a metal film on the hypotenuse plane of the prism surface plasmon resonance (SPR) is observed, with the addition of the dielectric layer is called plasmon resonance waveguide (PWR).

A two-layer structure (the scheme is shown in the inset of Fig. 1) can be considered as two-mirror multibeam reflection interferometer upon oblique incidence. The first mirror is a metal film, the second mirror of the interferometer is a TIR interface and has a high reflection. The calculated maximum reflection coefficient of this interferometer is close to unity. The interferometer resonant effects occur with additional capabilities for scheme tuning. Furthermore, it is possible to use orthogonal s-polarization. Thin layer dielectric-metal structure composed of aluminum (thickness << wavelength) and a dielectric layer on the quartz prism is considered. We study the angular and spectral characteristics of the reflected light at angles of incidence exceed the critical angle.

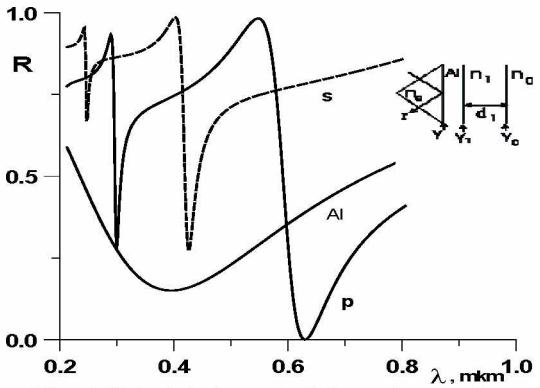

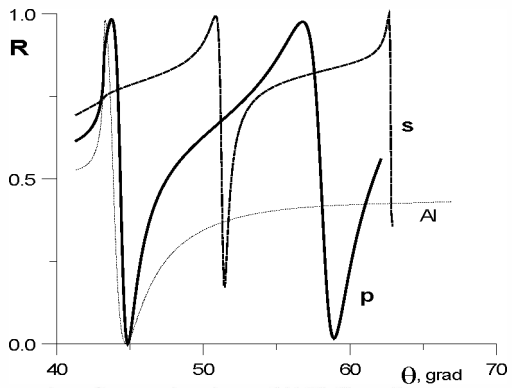

Fig. 1 Calculated spectral dependences R_s and R_p for a two-layer structure Al+ZnS and a one-layer Al for comparison. Angle is 44°.
Fig. 2 Calculated angular dependences R_s and $R_p$forAl+Na_3AlF_6, λ=0.63 mkm.

As shown in Figure 1, the asymmetric dependence observed in the interference spectrum of the structure Al + ZnS (wavelength 0.63 mkm). The operating range is narrowed in order compared to the pure Al. The curve shift R_p, when changing the refractive index of air (1.00-1.01), is 37 nm.

Note,that in the two-layer structure can be observed angular dependence of the interference for both polarizations. This is shown in Fig. 2, where the computation of the two-layer structure Al + cryolite (wavelength 0.63 mkm) is presented. The angular shift is the same for two- and one-layer and equal to 0.5°.

The difficulty in creating the sensor structure (calculation and experimental making) is the need to take into consideration a number of independent parameters characterizing the properties of the metal and dielectric.

References

[1] H. A. Macleod, *Thin-Film Optical Filters* (CRC, Taylor Francis, Boca Raton, FL, 2010).
[2] N. D. Goldina, V.S. Terent'ev, V.A. Simonov. Opt. Spectrosc. **120**(5), 796 (2016).

Cold Thulium atoms spectroscopy in optical dipole trap

A. Golovizin[1,2,3], E. Kalganova[1,2,3], D.Tregubov[1,2,3], G. Vishnyakova[1,2,3], D. Sukachev[1,3], K. Khabarova[1,3], V. Sorokin[1,3], N. Kolachevsky[1,2,3]

[1]*P.N. Lebedev Physical Instititue, Leninsky prospekt 53, 119991 Moscow, Russia*
[2]*Moscow Institute of Physics and Technology, 141700 Dolgoprudny, Moscow region, Russia*
[3]*Russian Quantum Center, Skolkovo, Moscow Region, Russia*
E-mail: artem.golovizin@gmail.com

The field of laser cooling of rare-earth elements is being rapidly developed in the last decade. Nowadays lanthanides find their application from world leading optical clocks [1] to novel experiments on dipole-dipole interaction in ultracold fermionic and bosonic gases [2,3].

Thulium atom has a large magnetic moment $4\mu_B$, that makes it a promising object for study dipole-dipole interaction and for quantum simulations. Besides that Tm has narrow magnetic dipole transition $4f^{13}(^2F_o)6s^2(J=7/2)\rightarrow 4f^{13}(^2F_o)6s^2(J=5/2)$ between the fine components of Tm ground state at wavelength λ = 1.14 μm, which we consider as a candidate for a 2D optical lattice clock.

In our group we've demonstrated deep laser cooling of Tm atoms down to 9 μK in two stage magneto-optical trap [4]. Such a low temperature leads up to 50% reload efficiency to optical dipole trap produced by 4 W 532 nm Verdi laser, and about 5% efficiency to 1D optical lattice at 807 nm with 1W Ti:sapphire laser. To confirm theoretically calculated γ=1.2 Hz natural linewidth of considered clock transition we have measured upper clock level lifetime in dipole trap. The measurement procedure is shown on Fig.1. After cooling and reloading, some fraction of Tm atoms was excited by 1.14 μm resonant pulse of 30 ms duration; then atoms remained in the ground state were removed by 1ms 410 nm resonant pulse. Number of atoms decayed back to the ground state vs. waiting time was measured and from exponential fit to the experimental data upper clock level lifetime was estimated to be τ = 112±4 ms, that gives upper bound on natural transition linewidth 1.4 Hz, what is in the excellent agreement with the theoretical value.

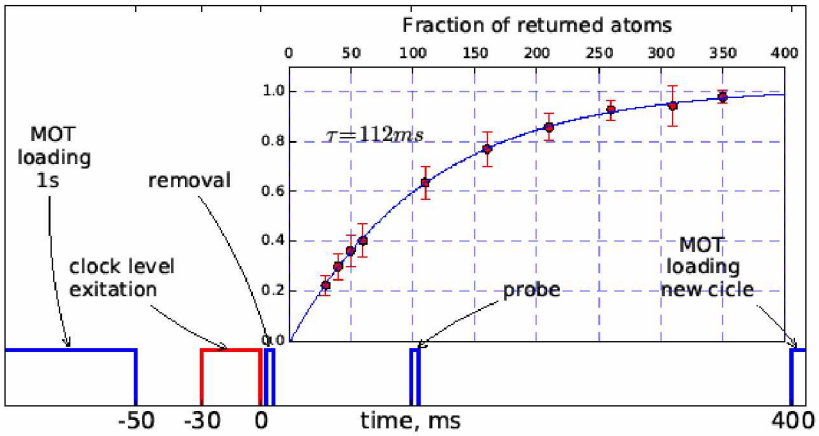

Fig. 1 Measurement of the lifetime of the upper clock level. The normalized number of atoms decayed to the ground level (circles with errorbars) vs. waiting time and exponential fit (blue line) in the insert.

References

[1] Hinkley, N., et al. "An atomic clock with 10–18 instability." Science 341.6151 (2013): 1215-1218.
[2] Aikawa, K., et al. "Bose-Einstein condensation of erbium." Physical review letters 108.21 (2012): 210401.
[3] Aikawa, K., et al. "Anisotropic relaxation dynamics in a dipolar Fermi gas driven out of equilibrium." Physical review letters 113.26 (2014): 263201.
[4] Vishnyakova, Gulnara Aleksandrovna, et al. "Ultracold lanthanides: from optical clock to a quantum simulator." Physics-Uspekhi 59.2 (2016): 168.

Spectrum and localization radius of intense sound produced by a powerful repetitively pulsed laser radiation

G. Grachev, A. Dmitriev, I. Miroshnichenko, A. Smirnov, V. Tischenko
[1]*Institute of Laser Physics SB RAS, Ac. Lavrentyev's prosp., 13/3, Novosibirsk, 630090, Russia*
E-mail: mib383@gmail.com

An optical pulsating discharge (OPD) generated by powerful high frequency (~100 kHz) pulsed laser radiation is a unique acoustic source of wide range (from infrasound to ultrasonic) sound [1]. Infrasound is generated due to shock wave merging mechanism [2]. The method is probably only possible way for remote (from hundreds meters to kilometers) generation of intense infra and ultrasound due to wide directional pattern of infrasound source and high attenuation of ultrasonic in atmosphere. As shown by previous studies, the proposed method is relatively efficient – about 20% of the laser energy is converted into sound [3].

We have considered the spectrum and localization radius of acoustic field generated by optical pulsating discharge.

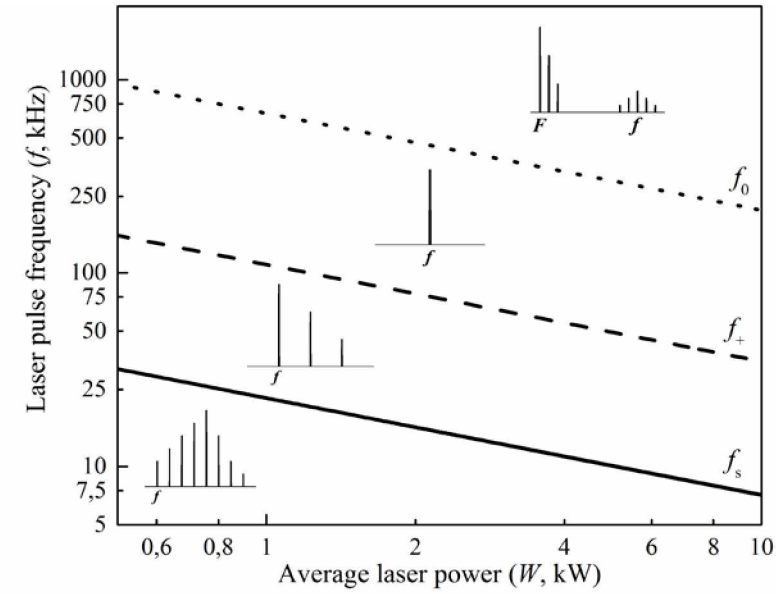

Fig. 1 The dependence of bound frequencies from average laser power. Inserts corresponds schematic spectrum structure for each field of laser parameters.

The spectrum was studied experimentally and by calculations. In the experiments we used pulse periodic CO_2-laser LOK-3MF, the average power of ~1 kW, pulse repetition rate f varied from about 3 kHz to about 180 kHz. OPD was generated in an argon stream or on the surface of the thin metal disk. We were obtained laser pulse frequencies (bound frequencies: f_s, f_+, f_0) corresponding to various spectrum. The spectrum may contain many lines in a wide frequency range or a few lines (may be only one) in ultrasonic region. Under the influence of pulse trains with repetition rate $F<<f$ it is possible to generate low frequency sound due to mechanism of shock wave merging. Fig. 1 shows the dependence of the bound frequencies from the average laser power W. Chart is divided by 4 fields. Each field corresponding laser parameters for every spectrum structure as it shown on the figure inserts.

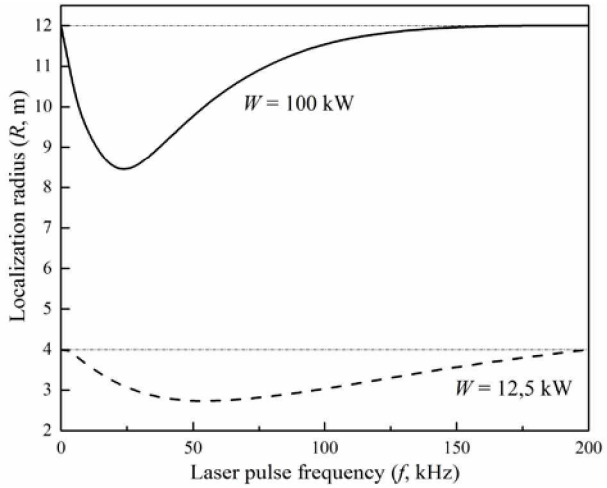

Fig. 2 The dependence of localization radius R of OPD sound from laser pulse frequency f for different average powers.

Localization radius R of OPD sound is distance from OPD corresponding to130 dB acoustic intensity level (pain threshold). The dependence of R from laser pulse frequency f has been calculated. It takes into account atmospheric absorption of sound. We varied the pulse repetition rate, and the average power of the laser radiation. Fig. 2 shows the dependence of R from f for two different average powers. By increasing the average laser power, localization radius, of course, is increasing, as it increases the total power of sound. With frequency increasing, localization radius decreases due to the fact that more and more of the sound power is concentrated in the ultrasonic frequency range. Starting with a certain frequency localization radius begin to grow back to the original due to the shock wave merging mechanism – the power of ultrasonic frequency "pumped" into the low frequency range, for which the absorption is insignificant.

Thus, optical pulsating discharge generated by repetitively pulsed laser radiation is an intense sound source with tunable spectrum and localization radius. The tuning is performed by changing the laser pulse repetition frequency.

References

[1] G. Grachev, A. Dmitriev, I. Miroshnichenko et al, Quantum Electron. **46**, 169 (2016).
[2] V. Tishchenko, V. Apollonov, G. Grachev et al, Quantum Electron. **34**, 941 (2004).
[3] V. Tishchenko, V. Posukh, A. Gulidov et al, Quantum Electron. **41**, 895 (2011).

Polarimetric imaging in complex environments

Haofeng Hu, Tiegen Liu, and Bingjing Huang
College of Precision Instrument & Opto-electronics Engineering, Tianjin University, Tianjin 300072, China
Key Laboratory of Opto-electronics Information Technology, Ministry of Education, Tianjin 300072, China
E-mail: tgliu@tju.edu.cn

The complex environments (dust, fog, haze, underwater, uneven illumination, low light illumination, etc.) significantly influence the detection effect, the identification ability and the application scope of the optical imaging detection technique. Polarimetric imaging, which based on the measurement of the polarization information, can effectively decrease the influence of the environment on the detection effect. Therefore, polarimetric imaging has unique advantage for the detection in complex environments. This work focuses on two types of complex environments including scattering medium (underwater imaging scenarios) and uneven illumination.

In underwater imaging scenarios, the scattering media could cause severe image degradation due to the backscatter veiling as well as signal attenuation. We consider the polarization effect of the object, and propose a method of retrieving the objects radiance based on estimating the polarized-difference image of the target signal. We show with a real-world experiment that by taking into account the polarized-difference image of the target signal additionally, the quality of the underwater image can be effectively enhanced [1], which is particularly effective in the cases where both the object radiance and the backscatter contribute to the polarization, such as underwater detection of the artifact objects.

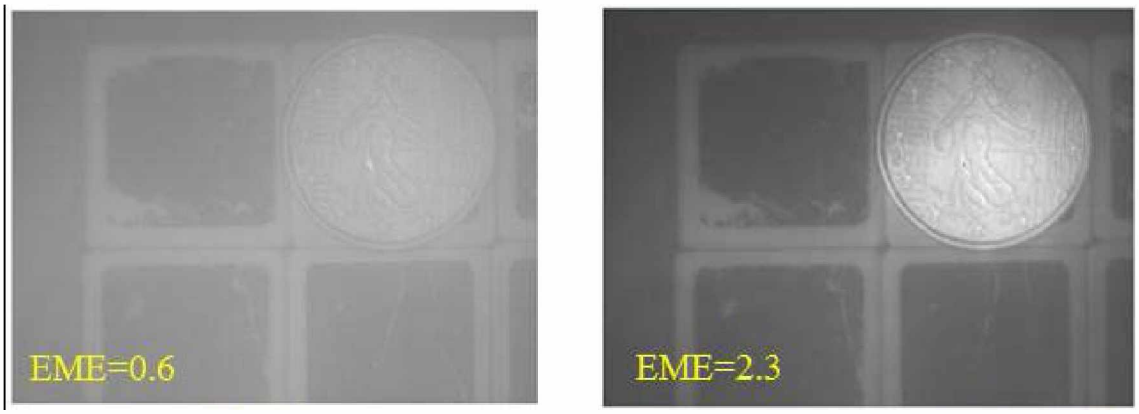

Fig. 1 Intensity image and the recovered image by our method in underwater imaging scenarios.

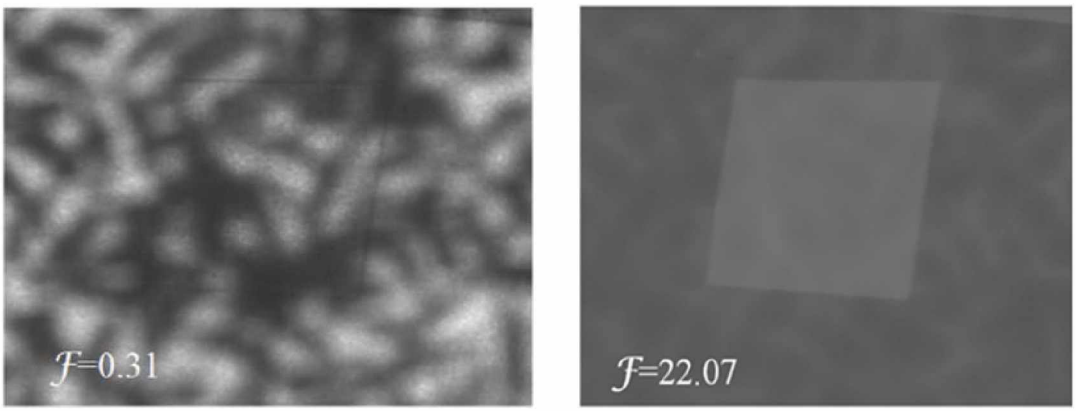

Fig. 2 Intensity image and the recovered image under uneven illumination scenarios.

In polarimetric imaging, the uneven illumination could cause the significant spatial intensity fluctuations in the scene, and thus hampers the target detection. We propose a method of illumination compensation and contrast optimization for Stokes polarimetric imaging, which allows significantly increasing the performance of target detection under uneven illumination. We show with numerical simulation and real-world experiment that, based on the intensity information contained in the polarization information, the contrast can be effectively enhanced by proper approach [2], which is of particular importance in practical applications with spatial illumination fluctuations, such as remote sensing.

References

[1] B. Huang, T. Liu, H. Hu, J. Han, and M. Yu, Optics Express **24**, 9826 (2016).
[2] B. Huang, T. Liu, J. Han, and H. Hu, Optics Express **23,** 23603 (2015).

The method of estimating the time of laser cooling of atoms in a standing wave

R.Y. Ilenkov[1,2], O.N. Prudnikov[1,2], A.V. Taichenachev[1,2], V.I. Yudin[1-3]
[1]*Institute of Laser Physics SB RAS Ac. Lavrentyev's prosp., 13/3, Novosibirsk, 630090 Russia*
[2]*Novosibirsk State University, ul. Pirogova 2, Novosibirsk, 630090 Russia*
[3]*Novosibirsk State Technical University, pr. Karla Marksa 20, Novosibirsk, 630073 Russia*
E-mail: ilenkov.roman@gmail.com

The invention of the laser allowed scientists to control both internal and external degrees of freedom of atoms and molecules with high accuracy. Now you can speed up, slow down, capture a single atoms and collimated atomic beams. Currently, laser cooling has become an area of science at the crossroads of laser physics and atom optics [1-3]. Initially, the theory of translational motion of atoms in laser fields developed in the framework of a simple model of the atom, the internal degrees of which are described by two states corresponding to non-degenerate energy levels [4-6]. It was believed that the use of this model is quite adequate to describe the main experimental results. It seemed that taking into account the actual structure of the atomic levels degenerated in the projection of the total angular momentum, will only lead to a small number corrections. Applied to laser cooling the main result of the following two-level model [1,2], is the existence of a theoretical limit on the minimum temperature cooling, the so-called Doppler limit, which is a typical value for the alkali metal atoms is about one microkelvin.

The main difficulty of the theoretical description of the interaction of atoms with the field consists in that the kinetics of neutral atoms in coherent light fields is described by quantum kinetic equations for the two-point atomic density matrix that includes all atomic levels and coherence between them, as well as take into account the recoil effects that occur in the processes of absorption and emission of photons. For a qualitative description of kinetic effects was originally developed semiclassical approach [1,2], where the equation for the quantum density matrix reduces to the Fokker-Planck equation for the distribution function in the phase space. The main condition for the applicability of the semiclassical approach is the smallness of the recoil parameter $w_r / \gamma << 1$. This approach was used to obtain expressions for the force and diffusion coefficients which allow a qualitative description of the dynamics of atoms in optical fields and the effects of Doppler and sub-Doppler cooling of atoms. Later quantum methods were development to describe the kinetics of atoms that goes beyond the semiclassical approximation [7-9]. It should be noted that the quantum approaches also have limitations. For example, to describe the cooling atoms and localization in the optical potential approach is used based on the quantum secular approximation [7,10-13]. This approach assumes that the distance between the energy bands in the optical potential greater than their width, due to optical pumping and tunneling, and the depth of the optical potential is determined by the light shifts. Then, at a fixed depth of the optical potential, this approximation is valid in the limit of large detuning. Conversely, it fails a given detuning in an optical deep potential. Moreover, even if these conditions are good secular approximation is valid only for the lower vibrational levels of the optical potential and breaks for higher where the distance between the vibrational levels becomes smaller due to the effects of anharmonicity. In addition, a completely secular approach is not applicable for atomic commit above-barrier motion. Previously, we have developed a fast and efficient method of calculation [14] steady momentum and spatial distributions of atoms in the field of a standing light wave with a full account of the effects of recoil and localization.

However, for practical applications, it is important to know how much time atoms will be cooled to the desired temperature and located in the optical potential. Direct dynamic solution of the problem of cooling of atoms in a resonant monochromatic radiation, including full account of recoil effects and localization of atoms, such as the Monte-Carlo method, has a number of drawbacks. Firstly, the addition time grid leads to a significant increase of the required computational resources and CPU time spent. Secondly, any numerical calculation error inevitably accumulates, moreover, it increases more and more with increasing time required to reach a steady mode. Consequently, the accuracy of the solution will be limited by this error.

The presence of statistical methods in the field of laser cooling has been shown in [15]. However, in [15] considered a limiting case of strong localization, when the recoil effect is suppressed by the Lamb-Dicke effect. Therefore, it is important to develop a more general approach, applicable to a wide range of problems of laser cooling, which is the main objective of this work.

Was developed by the statistical method which allows to quickly and with high efficiency to obtain information for the time of laser cooling [16]. It was implemented for the quantum problem, taking into full account recoil effects, and for the quasi-classical Fokker-Planck equation. We investigated the dependence of the cooling rate of the two-level atom in a standing wave field on the intensity of the light field, the detuning from the atomic resonance, the frequency of single photon recoil and width of the initial distribution of the atoms. The initial distribution of thermal atoms and has a width Δq_{start} in q-space.

Dependence of the average time required to establish the average kinetic energy of the recoil frequency is shown in Fig. 1a. In classical regime, all methods give the same result, but with an increase recoil frequency appears more striking differences. It can be seen that a simple estimation for slow atoms gives clearly incorrect results. The cooling time for the quantum problem, taking into full account recoil effects, is less then the cooling time for the quasi-classical Fokker-Planck equation.

In addition, there is an optimum in terms of minimizing the cooling time of the light field frequency detuning from the atomic resonance (Fig 1b). The position of the optimal detuning depends on the recoil frequency and intensity of the light field.

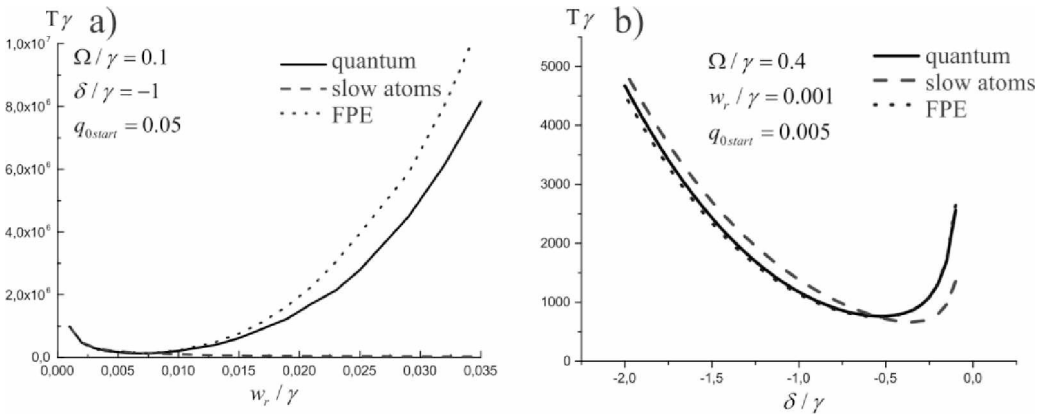

Fig. 1 Dependence of the average time required to establish the average kinetic energy of a) recoil frequency, b) detuning field from atom transition.

The work was supported by the Ministry of Education and Science of the Russian Federation (State Assignment No. 2014/139, Project No. 825), by the Russian Foundation for Basic Research (Grants No. 14-02-00712, 14-02-00939, 15-02-08377, 15-32-20330).

References

[1] V.G. Minogin, V.S. Letokhov "Laser Light Pressure on Atoms" (Gordon and Breach, New York 1987).
[2] A. P. Kazantsev, G. I. Surdutovich, and V. P. Yakovlev, "Mechanical Action of Light on Atoms" (World Scientific, Singapore, 1990).
[3] Cohen-Tannoudji C. "Atomic motion in laser light." Paris, 1992. 164 P.
[4] A. P. Kazantsev, Sov. Phys. Usp. **21**, 58 (1978).
[5] R.J. Cook, Phys. Rev. A **22**, 1078 (1980).
[6] V.G. Minogin, JEPT **52**, 1032 (1980).
[7] A. Aspect, E. Arimondo, R. Kaiser, N. Vansteenkiste, and C. Cohen-Tannoudji, Phys. Rev. Lett. **61**, 826 (1988).
[8] J. Hack, L. Liu, M. Olshanii, H. Metcalf, Phys. Rev. A **62**, 013405 (2000).
[9] S. M. Yoo, J. Javanainen, J. Opt. Soc. Am. B **8**, 1341 (1991).
[10] Y. Castin and J. Dalibard Europhys. Lett. **14**, 761 (1991).
[11] K. Berg-Sorensen, Y. Castin, K. Molmer and J. Dalibard Europhys. Lett. **22**, 663 (1993).
[12] J.Guo and P.Berman, Phys. Rev. A **48**, 3225 (1993).
[13] Y. Castin, K. Berg-Sorensen, J. Dalibard, and K. Molmer, , Phys. Rev. A **50**, 5092 (1994).
[14] Prudnikov O.N., Ilenkov R.Y., Taichenachev A.V., Tumaikin A.M., Yudin V.I. JEPT **122**, 939 (2011)
[15] Taichenachev A. V., Tumaikin A. M., Yudyn V. I., Hollberg L. Phys. Rev. A **63**, 033402 (2001)
[16] Ilenkov R.Y., Prudnikov O.N., Taichenachev A.V., Tumaikin A.M., Yudin V.I. JETP, **150**, 5 (2016).

Laser cooling of atoms on weak optical transitions

R.Y. Ilenkov[1,2], O.N. Prudnikov[1,2], A.V. Taichenachev[1,2], V.I. Yudin[1-3],
[1]*Institute of Laser Physics SB RAS Ac. Lavrentyev's prosp., 13/3, Novosibirsk, 630090 Russia*
[2]*Novosibirsk State University, ul. Pirogova 2, Novosibirsk, 630090 Russia*
[3]*Novosibirsk State Technical University, pr. Karla Marksa 20, Novosibirsk, 630073 Russia*
E-mail: ilenkov.roman@gmail.com

Invention such precise and powerful tool as a laser has opened before scientists a wide range of capabilities for atom manipulation: acceleration, deceleration, localization, deflection, and focusing. So laser cooling has become an integral part of both fundamental science and many practical applications (high-precision frequency and time standards, nanolithography, quantum information etc.)

The theoretical description of the kinetics of neutral atoms in the polarized light fields with all the atomic levels, the coherence, the recoil effect is both important and challenging problem. The first step toward understanding mechanisms of interaction between atoms and light was called quasi-classical approach. [1,2] It lies in the fact that the equations for the density matrix can be reduced to the Fokker-Planck equation for the Wigner function in the phase space. Simplicity of this approach has allowed to understand many of cooling mechanisms in the usual and ordinary terms of force and diffusion. However, this approach can only be applied in certain cases. First, the small recoil frequency parameter compared to the rate of spontaneous decay, and secondly, the momentum of a light field photon should be much smaller than the width of the momentum distribution of the atoms. Later quantum methods were developed [3,4], for example, the secular approach which describes cooling and localization of atoms in the optical potential. In this approximation distance between the energy bands in the optical potential is greater than their broadening caused by optical pumping. At a fixed depth of the optical potential this approximation is valid in the limit of large detuning, and thus, for a given configuration is disrupted in a deep optical potential. Moreover, even when this condition, the secular approximation is valid only for the lower vibrational levels, and fails for the higher, where the distance between the levels becomes smaller due to the effects of anharmonicity. The more secular approximation is not applicable to atoms undergo above-barrier motion.

We have developed an own quantum method [5] to obtaining the stationary distribution of two-level atoms in a standing wave of arbitrary intensity, allowing full account the recoil effect. The method used is to decompose the density matrix elements in the Fourier series for the spatial harmonics, which is possible due to periodicity of the light wave. Thus we obtain a system recursively coupled equations, where each harmonic is expressed through the previous one, and starting from free selected one (in our calculations, usually twenty or more) all the harmonics are equal to zero. Using this method kinetics of atoms in light fields of varying intensity was investigated. The new and most important result was mode which we called the anomalous localization. In strong standing wave (Rabi frequency greater than the constant spontaneous relaxation) was detected a anomalous behavior of atoms, namely, the concentration at the peaks of the optical potential.

The next important step was to study the quantum modes for different parameters of the problem. It is known that the quasi-classical approach gives Gaussian shape momentum distributions of and is completely inapplicable to the quantum regimes. The results of quantum calculation are shown in Fig.1. There is a bimodal distribution - the narrow central peak and a broad substrate. If we put atoms with bimodal distributions into the small depth optical trap it will lead to cutting off the hot atoms and we get the final momentum distribution of atoms below the Doppler limit, maintaining a significant number of atoms. Such a clearly expressed bimodal structure with high accuracy can be approximated by two Gaussian functions corresponding to the two-speed groups of atoms. Atoms are essentially

non-equilibrium momentum distribution, which is a good approximation can be described by two Gaussian functions. The possibility of obtaining the temperature of cold fraction below $\hbar\gamma$. The proportion of the fraction of cold atoms is sufficiently high and may reach 60%.

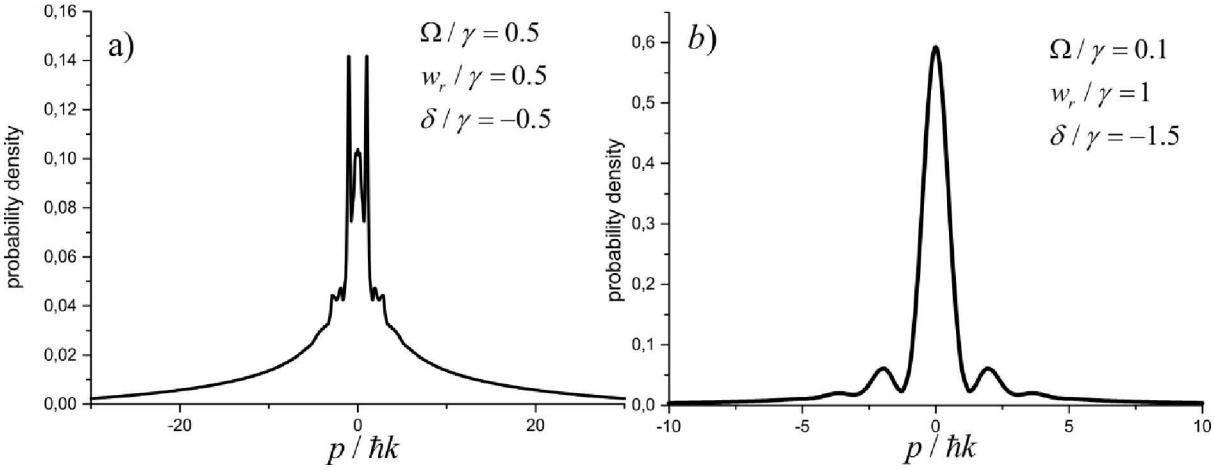

Fig. 1 Bimodal momentum distributions of cold atoms in quantum regimes: a) The distribution has a clearly expressed narrow peaks which width of order a single photon momentum. b) The distribution has narrow structure of cold atoms and wide wings. Parameters of the problem are located on graphs.

The work was supported by the Ministry of Education and Science of the Russian Federation (State Assignment No. 2014/139, Project No. 825), by the Russian Foundation for Basic Research (Grants No. 14-02-00712, 14-02-00939, 15-02-08377, 15-32-20330).

References

[1] V.G. Minogin, V.S. Letokhov, "Laser Light Pressure on Atom"s, Gordon and Breach, New York, 1987.
[2] A.P. Kazantsev, G.I. Surdutovich, and V.P. Yakovlev, "Mechanical Action of Light on Atoms", World Scientific, Singapore, 1990.
[3] A. Aspect, E. Arimondo, R. Kaiser, N. Vansteenkiste, and C. Cohen-Tannoudji, Phys. Rev. Lett. **61**, 826 (1988).
[4] S.M. Yoo and J. Javanainen, J. Opt. Soc. Amer. B **8**, 1341 (1991).
[5] O.N. Prudnikov, R. Ya. Il'enkov, A. V. Taichenachev, A. M. Tumaikin, V. I. Yudin, "Steady state of a low-density ensemble of atoms in a monochromatic field taking into account recoil effects", JETP **112**, 939 (2011).

The laser pumping rubidium frequency standard

A. Isakova, N. Golovin, K. Savinov, A. Dmitriev
Novosibirsk State Technical University, Russia
E-mail: alina_isakova@ngs.ru

Currently, a special place is the problem is improve the accuracy of frequency standards. For some of the tasks necessary to create a relatively cheap and small compact standards. In 1993, it was proposed to use the effect of coherent population trapping (CPT) to create a microwave frequency standard which would be lack the microwave resonator [1]. In recent years, widely used creation of standards based on this effect.

CPT resonance phenomenon manifests itself in the cell by pumping two interacting light waves with difference of frequency equal to the frequency of the hyperfine transition.

To create a combined frequency standard in the optical and microwave ranges is preferable to use the classic laser diode. Necessary to realize laser radiation at a wavelength of 795 nm with a modulations at a frequency equal to half the value of the frequency of the clock transition. As has been demonstrated previously [2], efficient modulation occurs at a frequency equal intermode interval of laser.

In this work, a detailed study of the dependence of the transformation coefficients of the microwave pumps current modulation in the lateral components of the frequency amplitude.

The studies were conducted on the semiconductor laser (wavelength 795 nm), which is manufactured by VitaWave. To be able to configure laser the desired frequency and line narrowing of the laser has to work with an external resonator. The resonator length was chosen specifically to implement Rb frequency standard value when intermode frequency is in the $F_0/2$.

In our experiments, the dependence of the amplitudes of the lateral components of the frequency of the microwave generator was also a resonance character. The spectrum of the laser radiation was observed using a Fabry-Perot interferometer with a free spectral range of 18 GHz. The maximum value of the amplitudes of the lateral components has occurred at a frequency of f = 3.54 GHz (Fig. 1), which corresponds to a cavity length l = 42 mm. Difference lateral components amplitudes may be related to the fact that when the pump current modulation takes place simultaneously both amplitude and frequency modulation.

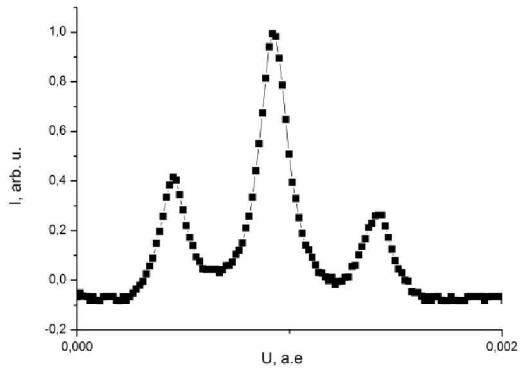

Fig. 1 The spectrum of the laser radiation at a frequency of 3.54 GHz swap

When the microwave modulation current pumping diode laser at a frequency near 3.54 GHz, resonance dependence of the conversion factor in the side of the microwave modulation amplitude of the frequency components was observed (Fig. 2). Declines depending side components of the amplitude can be explained by inaccuracies in the measurement of the length of the laser cavity.

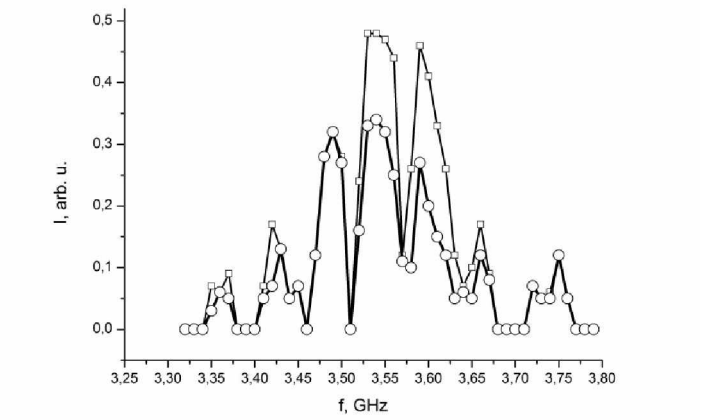

Fig 2 Dependence of the amplitude of the side components of the microwave frequency swap (square- left lateral component, circle-right).

References

[1] N. Cyr M. Tetu, M. Breton, All-optical microwave frequency standard: A proposal IEEE Trans. Instrum Meas. **42**, 640 (1993).

[2] Yu A Matyugin, D Yu Ivashko, N V Fateev, S N Bagayev, V G Volkov, Generation of equidistant frequencies in a semiconductor laser with an external cavity, Quantum Electronics **29** (1999).

Gas-discharge pumped excimer lasers on binary gas mixtures as a powerful UV source

E.S. Kargapoltsev[1], A.M. Razhev [1,2], D.S. Churkin [1,3]
[1] *Institute of Laser Physics. Academician Lavrentyev Avenue 13/3, 630090, Novosibirsk, Russia*
[2] *Novosibirsk State Technical University. Karl Marx Prospekt 20, 630073, Novosibirsk, Russia*
[3] *Novosibirsk State University. St. Pirogov Str. 2, 630090, Novosibirsk, Russia*
E-mail: djohn797@mail.ru

Laser performance with high-voltage excitation system in order to obtain a powerful laser radiation of electronic transitions of excimer molecules in two-component gas active media without any conventional buffer gas was designed.

Investigation of spectral, energy and temporal characteristics of the laser discharge excimer ArF (193 nm), KrCl (222 nm), KrF (248 nm) and XeCl (308 nm) lasers in the inert-gas halides are presented.

The maximum laser energy realized by excitation of gas mixtures (working inert gas and a halogen molecule) such as: Ar:F2, Kr:BCl3, Kr:F2 and Xe:BCl3.

ArF laser output energy varied from 40 to 160 mJ depending on laser excitation condition such as discharge voltage (15-26 kV) and total working pressure (0.7-1.2 atm).

The pulse power of the ArF-laser was ~ 19 MW with the pulse duration 8±1 ns (FWHM).

KrCl laser output energy varied from 70 to 110 mJ depending on laser excitation condition such as discharge voltage (20-26 kV) and total working pressure (1.1-1.3 atm).

The pulse power of the KrCl-laser was ~ 14 MW with the pulse duration 8±1 ns (FWHM).

KrF laser output energy varied from 60 to 170 mJ depending on laser excitation condition such as discharge voltage (10-26 kV) and total working pressure (0.4-1.1 atm).

The pulse power of the KrF-laser was ~ 24 MW with the pulse duration 7±1 ns (FWHM).

XeCl laser output energy varied from 50 to 130 mJ depending on laser excitation condition such as discharge voltage (10-26 kV) and total working pressure (0.45-0.65 atm).

The pulse power of the XeCl-laser was ~ 9 MW with the pulse duration 14±1 ns (FWHM).

For the ArF, KrCl, KrF and XeCl lasers the maximum laser efficiency (from stored energy) equal to 0.4%, 0.25%, 0.8% and 0.7% respectively.

Also, KrF laser output energy 115 mJ was obtained on laser excitation condition such as discharge voltage (15-26 kV) and total working pressure (0.6-0.8 atm) at the gas mixture Kr:NF3.

The results are promising in terms of experimental laser physics, and from the standpoint of theoretical calculations. They will make more advanced kinetic model excimer laser compared to traditional.

New near-infrared laser lines of the gas-discharge pumped atomic Xe I-, Ar I- and Kr I-lasers

E.S. Kargapoltsev [1], A.M. Razhev [1,2], , D.S. Churkin [1,3]
[1] *Institute of Laser Physics. Academician Lavrentyev Avenue 13/3, 630090, Novosibirsk, Russia*
[2] *Novosibirsk State Technical University. Karl Marx Prospekt 20, 630073, Novosibirsk, Russia*
[3] *Novosibirsk State University. St. Pirogov Str. 2, 630090, Novosibirsk, Russia*
E-mail: djohn797@mail.ru

The results of an experimental study of spectral, energy and temporal characteristics of the pulsed discharge multi-wavelength Ar I-, Kr I- and Xe I- high-pressure lasers are presented.

Twelve new near-infrared atom transition laser lines at Ar I, Xe I and Kr I ranging from 1,48 to 4,06 μm are reported for the first time.

The previously known experimental Ar I-laser spectral lines contains: 0.91, 0.96, 1.41, 1.69, 1.79 μm, and five new: 1.55, 1.75, 1.84, 2.02, 3.59 μm. The most intense of the presented spectral line is 1.79 μm, while the minimum intensity has a line of 1.41 μm, which is 0.6 relative units of the maximum.

The previously known experimental Kr I-laser spectral lines contains: 2.19, 2.48, 2.52, 2.57, 3.07 μm, and new one: 2.29 μm. The most intense of the presented spectral line is 2.52 μm, while the minimum intensity has a line of 2.29 μm, which is 0.1 relative units of the maximum.

The previously known experimental Xe I-laser spectral lines contains: 0.979, 1.06, 1.6, 1.73, 2.026, 2.48, 2.63, 2.65, 3.47 μm, and six new: 1.48, 1.63, 1.91, 1.98, 2.69, 4.06 μm. The most intense of the presented spectral line is 2.026 μm, while the minimum intensity has a line of 0.979 μm, which is 0.2 relative units of the maximum.

The maximum laser energy was realized by transverse high-voltage excitation of high-pressure gas mixtures (buffer gas and working gas): He:Ar=96.3:3.7 %, He:Kr=97.5:2.5 % and Ar:Xe=96.7:3.3 %.

Ar I-laser maximum output energy 10 mJ was obtained at the discharge voltage 14.5 kV and total working pressure 4.8 atm.

Kr I-laser maximum output energy was 1 mJ discharge voltage 14 kV and total working pressure 4.1 atm.

Xe I-laser maximum output energy 30 mJ was obtained at the discharge voltage 23 kV and total working pressure 4 atm.

The pulse power of the Ar I-laser was ~ 0.2 MW with the pulse duration 50±1 ns (FWHM).

The pulse power of the Kr I-laser was ~ 0.03 MW with the pulse duration 40±1 ns (FWHM).

The pulse power of the Xe I-laser was ~ 0.8 MW with the pulse duration 40±1 ns (FWHM)

Microstructures with negative radius of curvature obtained by laser ablation in ethanol method with follow chemical etching

V.S. Kazakevich[1], P.V. Kazakevich[1], P.S. Yaresko[1], D.A. Kamynina[1,2]
[1]*Samara branch of P.N. Lebedev Physical Institute of the Russian Academy of Sciences, Samara, 443011, Novo-Sadovaya 221, Russia*
[2] *Samara University, Samara, 443086, Moskovskoyeshosse 34, Russia*
E-mail: Kamyninada@gmail.com

Introduction

Micro and nano structuring of metal surfaces allows to expand the properties of initial materials and as a result, the range of their use [1]. Structuring of the sample surface can be carried out by different ways:chemical etching, lithography, mechanical impact, laser technology, etc. A combination of several techniques may lead to new results. The aim of this work was to obtain developed microstructures on the titanium surface by laser ablation in ethanolwith followed chemical etching.

Experimental technique

Creating of the initial relief on the titanium surface by laser ablation method in ethanol (95%) was performed [2]. Radiation parameters of Nd: YAG laser: λ = 1064 nm, τ = 250 ps, ν = 20 Hz, Q = 0.3 mJ, Q_S = 0.1 ÷ 0.6 J/cm^2. Target surface treatment was carried out in two modes: dynamic and stationary. In the case of a dynamic mode cell with the sample moved by motorized tables Standarelatively to the focal spot. Move options: speed of 500 μm/s, step offset by the other coordinate - 16 microns. In case of a stationary mode cell with the target remain fixed relatively to the focal spot. The thickness of liquid above the sample surface was 5 mm.

The following treatment of the laser-induced structures surface carried out by chemical etching. As the reagent was used the blend of acids withpercentage ratio: HNO_3 -98%, HF - 2%.

Analysis of the titanium surface at various stages of processing was carried out by a scanning electron microscope Carl Zeiss Evo 50 with nitrogen-freeenergy dispersivedetectorX-Max 80(EDX, error of measurements is about 1%). Visualization of the obtained structures also was carried out by 3D-modelingsoftware ImageJ.

Resultsanddiscussion

As a result of one hundred pulses subnanosecond IR laser radiation in the range of fluences from 0.1 to 0.6 J/cm^2 impact on the titanium surface in ethanol media in the dynamic and stationary modes, the cracking of the sample surface layer on a lot ofirregular polygons with an average size of 2 mm was observed (Figure 1a). That roughly 2 times smaller than grains sizeof the used titanium sample. Energy-dispersive analysis shows an inhomogeneous oxygen distribution on the sample surface (Figure 1b).

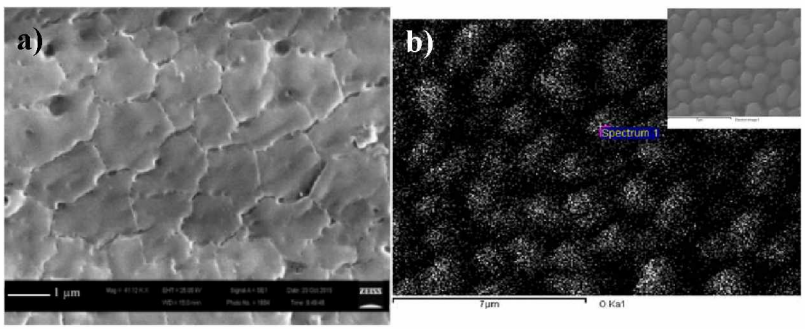

Fig. 1 a) SEM image of theTi target irradiated in ethanol at dynamic mode; **b)** Oxygen surface distribution EDX map on the Ti target irradiated in ethanol, which presented on inset;

These data allows to reveal the dependence of the oxygen percentage ratio in the surface layer on the laser fluence (Figure 2).

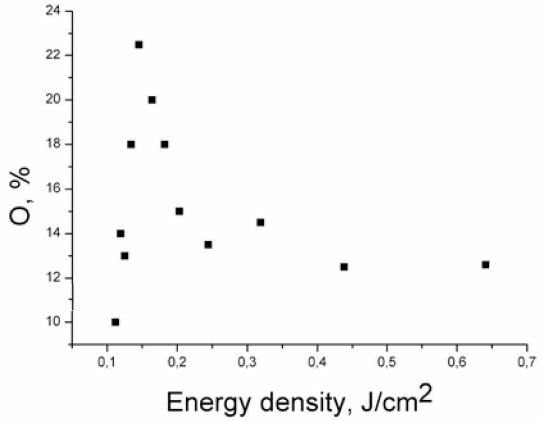

Fig. 2 Oxygen percentage ratio in the Ti target surface layer dependence on the laser fluence.

The discovered dependence can be explain by the fact that during the laser ablation of titanium in ethanol, containing water, oxidative reactions can take place. Furthermore, a change in fluence at the surface of the titanium target, as in [1,3,4], lead to a color change of the sample surface, which can be directly associated with different thickness of the oxide layer [4].

With the increase of the number of laser pulses acting on the titanium surface up to 20000 structure depicted in Figure 3awas observed, with characteristic dimensions: the average diameter of the foundation – 2 microns, average height – 3 μm. The dynamics of changes in the sample surface morphology in the pulses range from 100 to 20000 showed that the initial cracking of the oxide layer (Fig. 1a) effecting on the further growth of the microstructures as the physicochemical properties of titanium and titanium oxide are different.

Removal of the oxide layer by chemical etching from the structures surface obtained by laser ablation in ethanol lead to the identification of titanium structures with characteristic dimensions: the average diameter of the foundation – 1.5 μm, the average height – 0.7 μm, presented in Figure 3b.

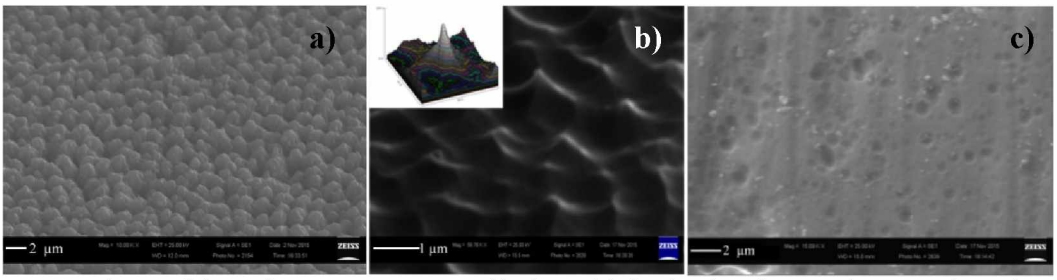

Fig. 3 SEM image of the surface structures prepared by laser ablation in ethanol at a stationary mode on the Ti target. 20000 pulses **a)** before chemical etching;**b)** after chemical etching, with the result of 3D-modeling the individual surface element in the inset; **c)** SEM image of the Ti surface after a chemical etching.

These structures have a "negative radius of curvature", which may be associated with the formation of the oxide layer with an inhomogeneous morphology on the sample surface after laser processing.

Chemical etching of the not subjected to laser treatment titanium surface, does not lead to the formation of structures, its result is shown in Figure 3c.

References

[1] Makarov S.V., Nano and microstructuring of the surface of metals and semiconductors in the air by femtosecond laser pulses (Moscow: P.N. Lebedev Physical Institute of the Russian Academy of Sciences), p. 149 (2014).

[2] Zijie Y., Douglas B. Chrisey, J. of Photochemistry and Photobiology C: Photochemistry Reviews **13**, 204 (2012).

[3] Barmina E.V., Stratacis E., Fotacis K., Shafeev G.A., J. Quantum Electronics **40**, 1012 (2010).

[4] Stepanov A.Y., Sotnikova L.V., Vladimirov A.A., Khaneft A.V., Prosvirkina E.V., Titov F.V., Diaghilev D.V., J. Polzunovsky messenger **3**, 53 (2014).

High-power femtosecond all-fiber oscillators: limitations and new possibilities

D.S. Kharenko[1,2], A. E. Bednyakova[2,3], E. V. Podivilov[2,3], M. P. Fedoruk[1,2], S. A. Babin[1,2]
[1]*Institute of Automation and Electrometry, SB RAS, Novosibirsk 630090, Russia*
[2]*Novosibirsk State University, Novosibirsk 630090, Russia*
[3]*Institute of Computational Technologies, SB RAS, Novosibirsk 630090, Russia*
E-mail: kharenko@iae.nsk.su

Generation of highly-chirped dissipative solitons (HCDS) is one of the most advanced ways to obtain high-energy femtosecond pulses in mode-locked lasers. Implementation of the combined cavity consisting of short single-mode fiber (SMF) for NPE mode-locking and long polarization maintaining (PM) fiber for pulse energy scaling [1] results in the sufficient increase of the cavity length and pulse energy as a consequence. However, this way is limited by the stimulated Raman scattering (SRS) threshold. There are two opportunities for further developments. First one is the scaling by increasing the fiber mode field diameter (MFD) at a maximum cavity length below the SRS threshold [2]. Second one is using the SRS effect for a coherent highly-chirped Raman dissipative solitons (RDS) [3] generation.

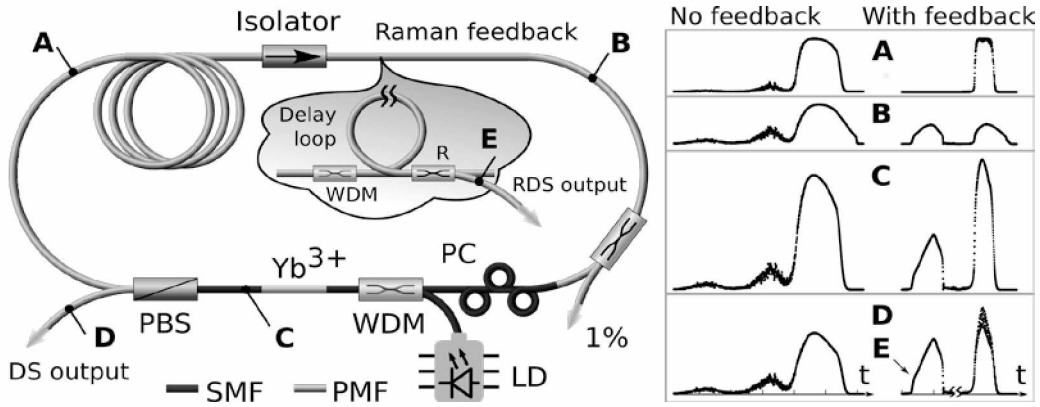

Fig. 1 Combined experimental setup of an all-fiber highly-chirped DS–RDS fiber oscillator (with feedback shown in the cloud). Calculated pulse shapes at the different points of cavity is presented at the right.

The scheme presented in Fig. 1 can be used as a base for both ways. For the first case (MFD scaling) we try LMA fibers with 10 μm core for building the all-fiber laser cavity in the hybrid SM–PM fiber configuration. We add a spectral filter into the cavity that strongly influences the parameters of the output pulses. In the second case the formation of RDS is possible with intracavity feedback loop provided by re-injection of the Raman pulse into the laser cavity with proper timing (cloudy inset in Fig. 1). The influence of the feedback loop on the first-order Raman pulse is shown in Fig. 1 (right part). Further investigations have shown that the second-order RDS can be generated, see Fig.2, in a similar way as the first-order RDS – by adding a second loop of intracavity feedback [4].

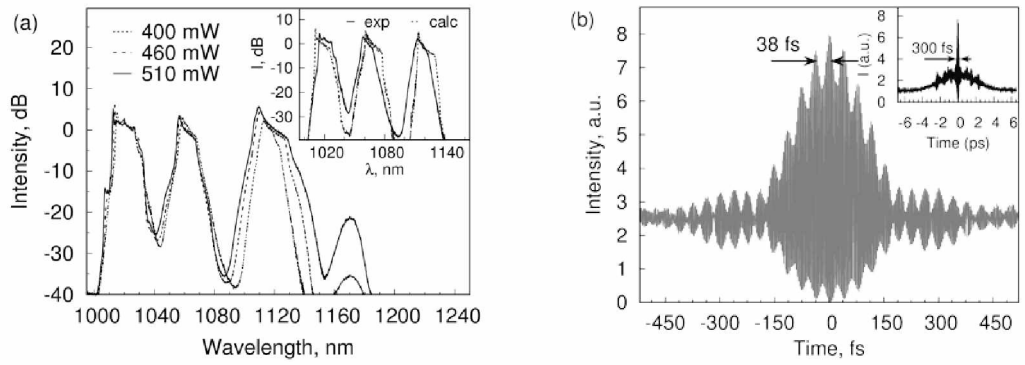

Fig. 2 (a) Experimental spectrum of three-color bound solitons at different pumping and its comparison with numerical simulations (inset): DS (1020 nm), 1st-order RDS (1065 nm) and 2nd-order RDS (1120 nm); (b) ACF of the combined pulse, with a wide range ACF in the inset.

It turned out that all the pulses (DS, 1st- and 2nd-order RDS) have a chirp parameter of >100 and can be externally compressed to 200-300 fs duration. Together, DS, RDS and second-order RDS form a three-color complex. The experimental spectra of such complex agree well with the calculation results presented in Fig. 2 (a). The important feature is a mutually coherence that has been confirmed by efficient coherent combining exhibiting <40 fs interference fringes within the combined pulse envelope Fig. 2 (b).

To demonstrate a possibility of simultaneous cavity length and MFD increase, the HCDS regime was obtained at five different lengths of PM-part of cavity. As a result, the repetition rate was reduced from ~20 MHz to ~5 MHz [5]. The spectral shapes are shown in Fig. 3 (a) for the 10 μm core and the PF period of 15 nm. The spectra of the generated DS pulses are centered near 1050 nm. A small portion of the signal goes out of the PF bandwidth, which slightly reduces the DS pulse quality. The comparison of the DS energy in fiber cavities with different core diameters and with different PF periods in 10-μm fiber cavity is presented in Fig. 3 (b). The maximum energy of the Raman-free DS in 10-μm fiber cavity with the 17-nm PF is 32 nJ at L~20 m (rhombs in Fig. 3 (b)). The critical length can be increased to ~40 m by decreasing the PF bandwidth down to 15 nm that results in the pulse energy increase up to 53 nJ (squares in Fig. 3 (b)). This value is in agreement with the theoretical estimation [1] of the SRS threshold, which is proportional to the mode field area. The output pulse was compressed down to 250 fs. The duration of the chirped pulse was estimated as 14 ps. Consequently, the compression factor was quite large, amounting to about 60.

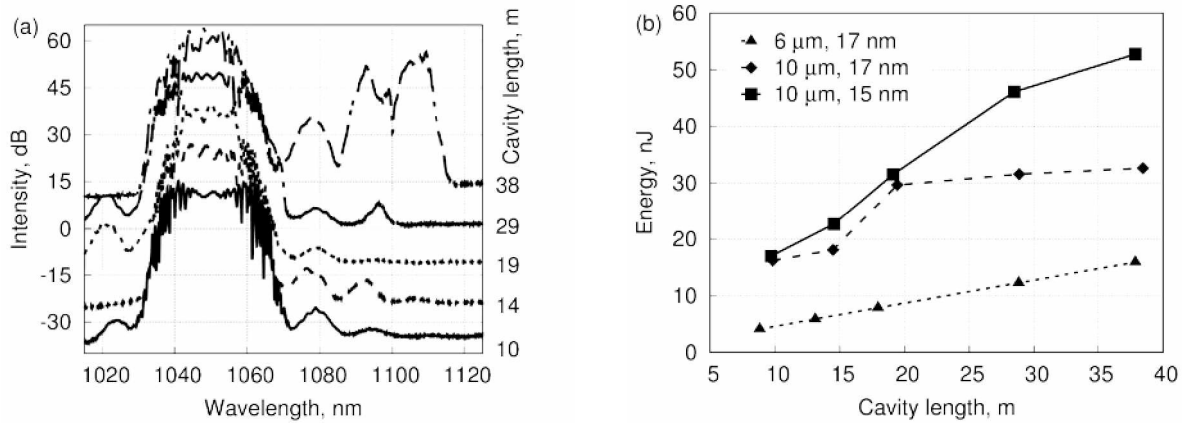

Fig. 3 (a) Generated output spectrum as dependent on cavity length for PF period of 15 nm; (b) Output energy of the DS as dependent on cavity length for different PF periods and fiber cores.

In conclusion, we studied the possibility of a complex approach to the optimization of output pulse energy for an highly-chirped all-fiber oscillator, that involves the enlargement of the cavity length (by PM fiber) and its mode area simultaneously. By suppressing Raman effect via the intra-cavity filtering, highly-chirped pulses with energy as high as 53 nJ at 250 fs compressed duration are generated in 40-m long 10-μm core fiber cavity. An alternative approach of Raman dissipative solitons opens the door towards cascaded generation of coherent dissipative solitons in a broad spectral range (so-called dissipative soliton comb) that can improve areas such as frequency comb generation, pulse synthesis, biomedical imaging and also emerge new applications.

References

[1] D. S. Kharenko, E. V. Podivilov, A. A. Apolonski and S. A. Babin, Opt. Lett. **37**, 4104 (2012)
[2] S. Lefrançois, K. Kieu, Y. Deng, J. D. Kafka and F. W. Wise, Opt. Lett. **35**, 1569 (2010)
[3] S. A. Babin, E. V. Podivilov, D. S. Kharenko, et al, Nat. Comm. **5**, 4653 (2014)
[4] D. S. Kharenko, A. E. Bednykova, E. V. Podivilov et al, Opt. Lett. **41**, 175 (2016)
[5] D. S. Kharenko, V. A. Gonta, S. A. Babin, Las. Phys. Lett. **13**, 025107 (2016)

Compression of waveform of Mössbauer γ-ray photon in optically deep vibrating recoilless resonant absorber

I. R. Khayrulin[1], V. A. Antonov[2], Y. V. Radeonychev[2], and O. A. Kocharovskaya[3]
[1]*Lobachevsky State University of Nizhny Novgorod, Nizhny Novgorod 603950, Russia,*
[2]*Institute of Applied Physics of the Russian Academy of Sciences, Nizhny Novgorod 603950, Russia*
3*Department of Physics of Texas A&M University, College Station, TX 77843-4242, USA*
E-mail: antonov@appl.sci-nnov.ru

The concepts and ideas of coherent, nonlinear, and quantum optics have begun to penetrate into the range of 10-100 kiloelectronvolt (keV) photon energies, corresponding to soft γ-ray or, equivalently, hard X-ray radiation. Some of the recent experimental achievements in this frequency range include the demonstration of parametric down-conversion in the Langevin regime [1], cavity electromagnetically induced transparency [2], collective Lamb shift [3], vacuum-assisted generation of atomic coherences [4], and single-photon revival in nuclear absorbing sandwiches [5]. Also, realization of a single photon coherent storage [6] and stimulated Raman adiabatic passage [7] were recently proposed in this regime. More related works can be found in the review [8].

Recently, transformation of 14.4 keV photons spontaneously emitted by a radioactive ^{57}Co source, into a periodic sequence of pulses of duration shorter than the lifetime of the emitting state of the nuclei was realized [9]. The ability to control the shape, duration, and repetition period of the produced pulses was shown. The spectral-temporal conversion of radiation occurred as a result of radiation passage through a foil with resonantly absorbing nuclei of ^{57}Fe which harmonically oscillate along the propagation direction. Uniquely large ratio of resonance energy of the nuclei to the resonance bandwidth (3×10^{12} for 14.4 keV transition of ^{57}Fe) makes effective the use of the Doppler effect in the photon-nuclei interaction for generating the well-separated phase-locked γ-radiation sidebands and producing the pulse train. The same technique in a combination with time-delayed coincidence measurement [10] allowed one to demonstrate the possibility to control the waveform (time-dependence of the detection probability) of a single γ-ray photon, which is an important contribution into the fast developing quantum γ-ray optics and its applications for quantum information processing [8]. In that experiment, the nuclear absorber with moderate optical depth, $T_M \sim 5$, and natural abundance, ~2%, of the resonant isotope ^{57}Fe was used.

In the present contribution, we consider the possibilities to extend the potential of this technique using the Mössbauer absorber, 100% enriched by ^{57}Fe nuclei with optical depth up to 100. In such a deep resonant medium, the influence of the resonant dispersion [11] and dynamical beats [10] on the waveform of the γ-ray photon become important. In the reference frame of the oscillating absorber the electric field of the incoming photon is frequency modulated, corresponding to a comb of "in-phase" and "anti-phase" spectral components. If the amplitude of the absorber vibration, R, satisfies condition $kR=1.84$, where $k=2\pi/\lambda$, and λ is the wavelength of the photon, the incident spectrum contains only the one "anti-phase" component of appreciable amplitude. As shown in [9], suppression of this component via tuning it to the absorber resonance allows transforming the exponentially decaying waveform of the incident γ-ray photon into decaying pulse train. In an optically deep absorber, instead of suppression of the "anti-phase" spectral component, its initial phase can be inverted (changed by π) via the resonant dispersion. In other words, the "anti-phase" spectral component can be transformed into "in-phase" one resulting in its constructive interference with the other spectral components and formation of pulses with higher amplitude. We analyzed both these possibilities in detail.

Based on the accurate numerical solution [9] for the waveform of the γ-ray photon propagating through the vibrating absorber, we numerically found the optimal parameters of the system which allow producing pulses with the highest amplitude, and achieve the highest peak detection probability of the output photon (per unit time). The result of such an optimization for the case of suppression of the "anti-phase" spectral component and the same frequency of vibration as in [9], $\Omega/2\pi=10.2$MHz, is shown in Fig. 1(a). The waveform of the outgoing photon corresponding to the optimal set of parameters in Fig.1(a), that is the resonant optical depth of absorber $T_M=17.5$, and the initial phase of absorber vibration $\theta_0=1.35\pi$, is shown in Fig. 1(b) along with the waveform, plotted for the

parameters of experiment [9], i.e. T_M=5.2 and θ_0=0, but for 100% enriched by ^{57}Fe resonant absorber. As seen from the figure, the optimization has allowed increasing the peak detection probability of the photon by approximately 60% and enhancing the contrast of the pulses. Since in experiment [9] the resonant absorber with natural abundance, ~2%, of ^{57}Fe nuclei was used, the detected waveform was approximately 4 times weaker, as compared to that shown in Fig. 1(b), because of the large photoabsorption.

Besides, we have shown the possibility to produce the pulses via π phase shift of the "anti-phase" spectral component due to the resonant dispersion of the medium. It was shown that use of the resonant dispersion allows achieving higher average amplitude of the pulses in the pulse train as compared to suppression of the "anti-phase" component via its resonant absorption. At the same time, the peak detection probability of the photon does not reach the limit, corresponding to constructive interference of all the spectral components of the output field. The reasons for this discrepancy are: partial absorption of the (quasi)resonant spectral component and nonuniformity of the resonant phase incursion of the different frequencies within the bandwidth of this component.

In a summary, in this contribution we have analyzed the opportunities to extend the capabilities of the method for γ-ray photon shaping in a vibrating recoilless resonant absorber [9] using the optically deep absorber, enriched by the resonant nuclei. The produced single-photon pulse trains can be applied for the time-resolved resonant nuclear spectroscopy [11], as well as for the quantum information transfer and processing [12].

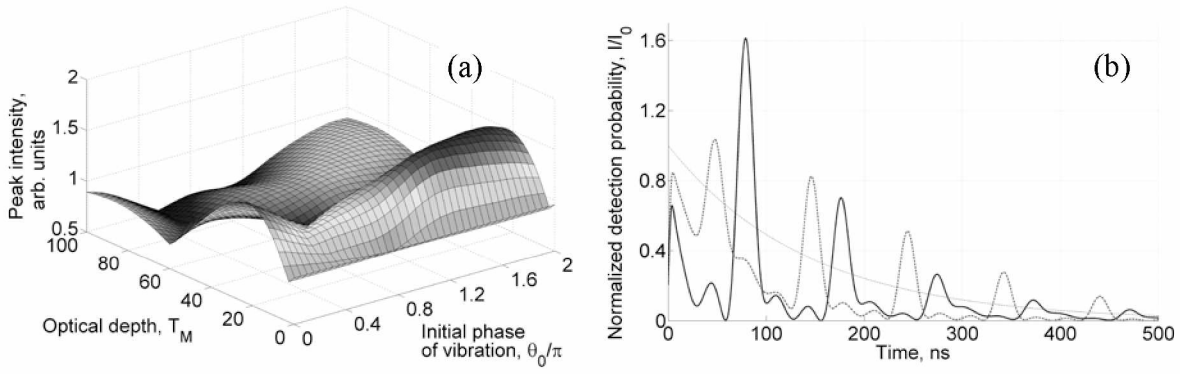

Fig. 1 (a) - Dependence of the peak detection probability of the outgoing photon, normalized to the peak detection probability without absorber, on the optical depth of absorber, T_M, and initial phase of absorber vibration, θ_0. The frequency of vibration is $\Omega/2\pi$=10.2MHz. The central frequency of the source, ω_r, exceeds the resonance frequency of the absorber, ω_a, by the frequency of absorber vibration, Ω, that is ω_r- ω_a= Ω. **(b)** - Time dependence of the detection probability of the photon at the exit of the vibrating resonant absorber, normalized to the peak detection probability without absorber. The relevant parameters are: kR=1.84, $\Omega/2\pi$=10.2MHz, ω_r- ω_a= Ω. The absorber is 100% enriched by the resonant ^{57}Fe nuclei. The bold blue curve corresponds to the optimal parameters in (a): T_M=17.5, θ_0=1.35π. The dashed red curve corresponds to the parameters from [9]: T_M=5.2 and θ_0=0. The thin light grey curve is the exponential waveform without absorber.

References

[11] S. Shwartz, R. N. Coffee, J. M. Feldkamp, Y. Feng, J. B. Hastings, G. Y. Ying, and S. E. Harris., Phys. Rev. Lett. **109**, 013602 (2012).
[12] R. Röhlsberger, H-C. Wille, K. Schlage, and B. Sahoo, Nature **482**, 199 (2012).
[13] R. Röhlsberger, K. Schlage, B. Sahoo, S. Couet, and R. Rüffer, Science **328**, 1248 (2010).
[14] K. P. Heeg, et al., Phys. Rev. Lett. **111**, 073601 (2013).
[15] R. Shakhmuratov, F. Vagizov, and O. Kocharovskaya, Phys. Rev. A **87**, 013807 (2013).
[16] W.-T. Liao, A. Pálffy, and C. H. Keitel, Phys. Rev. Lett. **109**, 197403 (2012).
[17] W.-T. Liao, A. Pálffy, and C. H. Keitel, Phys. Lett. B **705**, 134 (2011).
[18] B. W. Adams, et al., J. Mod. Opt. **60**, 2 (2013).
[19] F. Vagizov, V. Antonov, Y. V. Radeonychev, R. N. Shakhmuratov, and O. Kocharovskaya, Nature **508**, 80 (2014).
[20] F.J. Lynch, R.E. Holland, and M. Hamermesh, Phys. Rev. **120**, 513 (1960).
[21] V. A. Antonov, Y. V. Radeonychev, and O. Kocharovskaya, Phys. Rev. A **92**, 023841 (2015).
[22] R. N. Shakhmuratov, F. G. Vagizov, V. A. Antonov, Y. V. Radeonychev, M. O. Scully, and O. Kocharovskaya, Phys. Rev. A **92**, 023836 (2015).

Stabilization of kilohertz solid-state laser system parameters for high harmonic generation experiments

A.V. Kirpichnikov[1], V.V. Petrov[1,2,3], G.V. Kuptsov[1,3], A.V. Laptev[1], V.A. Petrov[1,2], V.I. Trunov[1], and E.V. Pestryakov[1]

[1]*Institute of Laser Physics SB RAS, Novosibirsk,630090, Russia*
[2]*Novosibirsk State Technical University, Novosibirsk, 630073, Russia*
[3]*Novosibirsk State National Research University, Novosibirsk, 630090, Russia*
E-mail: kirp@laser.nsc.ru

The design and creation of femtosecond laser systems with high intensities are one of the most important trends in laser physics. Laser facilities with the intensity reaching the level of 10^{25} W/cm^2 or higher open a way to the experimental research of the wide range problems in fundamental physics, chemistry, biology and their applications [1].

Obtaining one or more of attosecond light pulses opens the possibility of coherent control of electronic processes in the attosecond time scale [2]. Although attosecond pulses train is obtained relatively easy through high harmonic generation process, the generation of a single attosecond pulse requires more complex laser systems with either polarization gating, dual-frequency mixing or spatial filtering. Common to all these methods is the stabilization of the carrier-envelope offset phase, which allows optimizing the electric field shape of the radiation to generate one or two pulses [3].

Our all solid-state femtosecond laser system consists of a master oscillator and a multi-pass amplifier. A mirror-dispersion controlled oscillator generates broadband (~100 nm), ultrashort (~10 fs) pulses at ~75 MHz repetition rate. The pulses are stretched by traversing a suitable amount of optical glass to decrease intensity for amplification. Third-order dispersion pre-compensation is achieved by a certain number of reflections from TOD-dispersion compensating mirrors. Then the pulses are amplified by 9- passes through a -pumped amplifier up to ~ 0.6 mJ. After the first four passes pulses with 1 kHz repetition rate are selected from the MHz-pulse train to be further amplified in another five passes. After amplification the pulses are recompressed to less than 30 fs with central wavelength – 800 nm by a double-prism compressor.

The spectral components of radiation emitted from the femtosecond laser cavity have non-zero offset. To measure the offset, spectrum is generated broader than an octave in a nonlinear fiber, and then red spectral components are frequency doubled and are beaten with blue components. The beat signal is rectified by a photodetector. An electronic unit selects the beat frequency and provides feedback to stabilize the frequency shift, which is calculated by the beat frequency. The control element of feedback loop is the acousto-optic modulator, which reduces the pump power of the master femtosecond oscillator.

Phase perturbations during the amplification are registered in a nonlinear f-2f interferometer. The emission spectrum is broadened in the sapphire plate. The red part of the spectrum is frequency doubled in a nonlinear crystal and is beaten with a blue part of the spectrum at the input of the spectrometer. Perturbation phase is calculated by computer using the spectral beats. A signal proportional to phase deviations in the amplifier is mixed with the carrier phase drift signal of the master oscillator and used to control acousto-optic modulator's power. The stabilization system implemented has allowed one to achieve phase residual instability ~0.17 radian (rms) for 30 fs-pulse, which is sufficient to forthcoming high harmonic generation experiments efficiently.

This work is supported in part by RAS Program "Extreme laser radiation: physics and fundamental applications", registration number AAAA-A15-115113010002-9 and Government program, registration number 01201374306.

References

[1] V.V. Petrov, E.V. Pestryakov, A.V. Laptev, V.A. Petrov, G.V. Kuptsov, V.I. Trunov, S.A. Frolov, QUANTUM ELECTRONICS **44**, 452–457 (2014).
[2] M. Schultze, A. Wirth, I. Grguras, M. Uiberacker, T. Uphues, A.J. Verhoef, J. Gagnon, M. Hofstetter, U. Kleineberg, E. Goulielmakis, F. Krausz, Journal of Electron Spectroscopy and Related Phenomena **184**, 68–77 (2011).
[3] Pengfei Lan, Eiji J. Takahashi, and Katsumi Midorikawa, PHYSICAL REVIEW A **82**, 053413 (2010).

A new nonlinear optical crystal $Nd_kY_lLa_mSc_n(BO_3)_4$ (k+l+m+n=4)

A.E. Kokh[1], N.G. Kononova[1], A.B. Kuznetsov[1,2], K.A. Kokh[1], A. Maillard[3], R. Maillard[3], E. Pestryakov[2,4]
[1]*IGM SB RAS, 630090, Novosibirsk, Russia*
[2]*Novosibirsk State University, Novosibirsk, Russia*
[3]*LMOPS Lorraine University, Supelec 57070 Metz, France*
[4]*ILP SB RAS, 630090, Novosibirsk, Russia*
E-mail: pefvic@laser.nsc.ru

A new noncentrosymmetric $Nd_kY_lLa_mSc_n(BO_3)_4$ (NYLSB) crystal with huntite-like structure was grown by the high-temperature top-seeded solution (TSSG) method using $LiBO_2$–LiF solvent. Linear and nonlinear optical parameters of crystal material and spectroscopic properties of Nd-ion in the NYLSB were investigated and compared with that of Nd:$YAl_3(BO_3)_4$ crystal.

The composition of the mixture in molar parts for $Nd_kY_lLa_mSc_n(BO_3)_4$ crystal growth was as follows: $0.08Nd_2O_3$-$0.3Sc_2O_3$-$0.06Y_2O_3$-$2B_2O_3$-2.1LiF-$1.5Li_2O$ and the chemical composition of $Nd_{1.03}Y_{0.19}Sc_{2.78}(BO_3)_4$ is similar to LYSB ($La_{0.72}Y_{0.57}Sc_{2.71}(BO_3)_4$)-crystal [1]. Fig. 1 shows the X-ray powder diffraction patterns of NYSB (a) and LYSB (b) crystals. It may be concluded that the structures of both crystals is the same with noncentro-symmetric R32 space group.

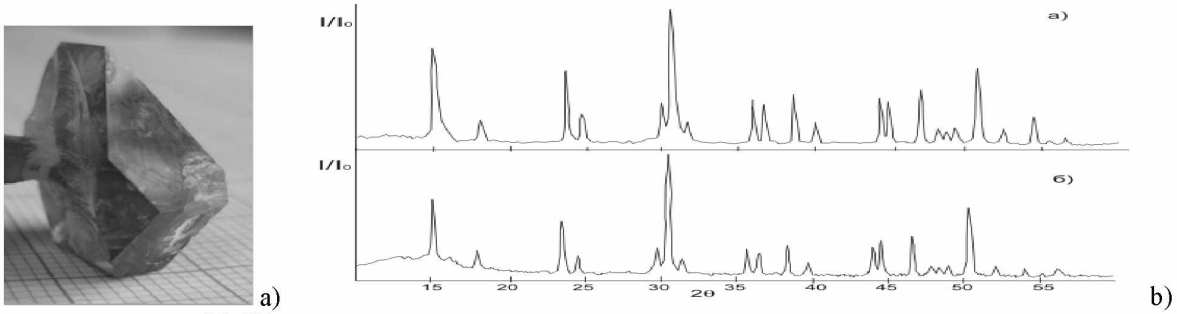

a) b)

Fig. 1 a) NYSB-crystal, b) X-ray powder diffraction patterns of NYSB (a) and LYSB (б) crystals.

Also we observe the regular shift of the NYSB x-ray diffraction pattern to higher diffraction angles because Nd^{3+} ionic radius is less than La^{3+} one. The calculated cell parameters of NYSB crystal are as follows:

Cell parameters	$La_{0.72}Y_{0.57}Sc_{2.71}(BO_3)_4$ LYSB [2]	$Nd_{1.03}Y_{0.19}Sc_{2.78}(BO_3)_4$ NYSB [this work]
a, Å	9.774(1)	9.761(3)
c, Å	7.946(2)	7.905(5)

The transmittance spectrum of 400 μm thick NYSB-optical element was recorded at room temperature using Shimadzu 3010 spectrophotometer in the range 300 - 3000 nm. A typical Nd^{3+} spectrum with a lot of absorption peaks in spectra range 300-900 nm with transmission coefficient about 0.06 at 532 nm was observed. Calculation of refraction index of NYSB in transmission range has shown that ordinary and extraordinary indexes of NYSB and LYSB-crystals are quite close in values.

Second harmonic generation (SHG) of Nd:YAG laser (λ=1064 nm) experiments were performed on the 2.5 mm thick plate with orientation θ_{PM} =31 deg to the optical axis. The assumption was done that the type I phase matching angle must be close to those of LYSB (for which the phase matching angle-θ_{PM} is equal to 33.48 deg) [3]. As the expression of the effective nonlinear coefficient for this symmetry and for this phase matching type is $d_{eff}(I) = d_{11}\cos\theta\cos3\varphi$ (φ being the angle between the projection of wave vector in the ***xy*** plan and the ***x***), the crystal is cut so that the incident wave propagated in the ***xz*** plane (φ =0°) in order to obtain a maximum efficiency. The plate has transparent windows big enough for analyzing the optical quality and efficiency of SHG.

A maximum SHG efficiency is obtained by turning the sample around the normal incidence, which corresponds to a variation of θ for type I phase matching at θ_{PM} = 34.8 deg. This result is in good

agreement with a similar value of phase matching θ_{PM} angle and consequently of refractive indexes of LYSB and NYSB.

In continuous mode with a focused Gaussian beam we obtained $P(\omega)/P(2\omega)$ = 2.75W/3.42 μW for 43 μm beam waist size. That corresponds to calculated d_{eff} (I) = 0.91 pm/V without taking into account its absorption [3]. This value increases up to 2.3 pm/V if one takes into account the optical losses in NYSB samples: 21 cm^{-1} at 532 nm and 0.2 cm^{-1} at 1064 nm. And as a result, the value of ratio d_{eff}(NYSB)/ d_{eff}(NYAB) is equal to 0.5 for calculation without and 1.28 with optical losses.

Measurements also have been performed in a pulsed mode. For the maximum incident power 0.82W corresponding to the density of 156 MW/cm^2 we have obtained about 0.5% efficiency.

In order to decrease the concentration of Nd and in turn to lower the absorption at around 532 nm, we have grown another crystals with partial substitution of Nd by La. In selected crystal we managed to decrease the concentration of Nd from $3.5\cdot10^{21}$ to $1.5\cdot10^{21}$ cm^{-3} in new mixed crystal - $Nd_kY_lLa_mSc_n(BO_3)_4$ with (k+l+m+n=4) or NYLSB [4].

Since the magnitude of NLO-coefficient d_{eff}(NYLSB) has been obtained by the microscopic component of hyperpolarizability tensor of BO_3-group of crystal with β_{111} susceptibility [5], the isomorphous replacement of rare earth cation should not change NLO-properties of the mixed crystal. On the other hand the spectroscopic properties were changed.

The UV-VIS-NIR absorption spectra of NYLSB-crystals were measured and investigated at room temperature. The features corresponding to the main absorption transitions of Nd-ion from fundamental level -$^4I_{9/2}$ to excited levels: $^4F_{3/2}$, $^4F_{5/2}$ +$^4S_{3/2}$, $^4F_{9/2}$ and other have been identified and analyzed within the framework of Judd-Ofelt theory.

Typical NIR fluorescence spectra of NYLSB-crystal were obtained with excitation at 532 nm within the absorption band -$^2K_{13/2}$ +$^4G_{9/2}$+$^4G_{7/2}$. The fluorescence spectra consists of four band emissions peaking at 898 nm ($^4F_{3/2}\rightarrow{}^4I_{9/2}$), 1061.5 nm ($^4F_{3/2}\rightarrow{}^4I_{11/2}$), 1330- nm ($^4F_{3/2}\rightarrow{}^4I_{13/2}$) and 1800nm ($^4F_{3/2}\rightarrow{}^4I_{15/2}$, not measured), the first two bands are presented in fig. 2.

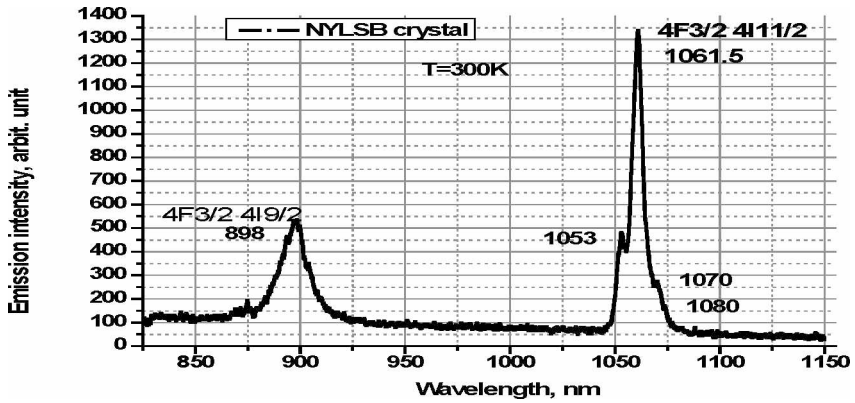

Fig. 2 NIR fluorescence spectrum of NYLSB-crystal at room temperature.

The fluorescence lifetime of excited level $^4F_{3/2}$ was measured at room temperature in NYLSB sample with concentration of Nd ions - $4\cdot10^{21}$ cm^{-3}, it is equal to $53\cdot10^{-6}$ s. The decays were found to be single exponential.

The major conclusion drawn from these studies is that the new NYLSB-crystal could be suitable for microchip SFD laser applications.

The work was partly supported by the Program RAS "Extreme laser fields and fundamental applications" and Program of Basic Researches NANB-SB RAS, project 115-29.

References

[1] N. Ye, J.L. Stone-Sundberg, M.A. Hruschka, G. Aka, W. Kong, D.A. Keszler, Chem. Mater., **17**(10), 2687–2692 (2005).
[2] N. Ye, Y. Zhang, W. Chen, D.A. Keszler, G. Aka, J. Cryst. Growth, **292** (2), 464–467 (2006).
[3] R.S. Klein, G.E. Kugel, A. Maillard, A. Sifi and K. Polgar, Opt. Mater. **22,** 163 (2003).
[4] A.E. Kokh, N.G. Kononova, M.V. Fedorova, P.P. Fedorov, M.N. Mayakova, Doklady Physics, **57**, 148-150 (2012).
[5] V.V. Atuchin, B.I. Kidyarov, E.V. Pestryakov, MPLP'2008, Novosibirsk, Russia, Technical Digest, 229-230 (2008).

Wide aperture PPLN structures for cascade MID-IR OPO intravavity pumping

D. Kolker, N. Kostyukova, A. Boyko, A. Pronyushkina, B. Nyushkov, S. Trashkeev, V. Shur
Novosibirsk State University, Novosibirsk, Russia
Institute of Laser Physics SB RAS, Novosibirsk, Russia
E-mail: dkolker@mail.ru

We are reporting about investigation of 3 mm aperture periodically polled lithium niobate (PPLN) structures for intracavity MID-IR pumping. Exclusive PPNL structures at multigrating, fan-out and multi fan-out configuration were prepared at "Labfer LTD". The cascade MID-IR OPO was demonstrated recently by our group with MBI collaboration.

Fiber laser with hybridization of passive mode locking and undamped regular spikes

A. Komarov[1], A. Dmitriev[2], K. Komarov[1], F. Sanchez[3]
[1] *Institute of Automation and Electrometry, Russian Academy of Sciences, Acad. Koptyug Pr. 1, 630090 Novosibirsk, Russia*
[2] *Novosibirsk State Technical University, K. Marx Pr. 20, 630073 Novosibirsk, Russia*
[3] *Laboratoire de Photonique d'Angers, Université d'Angers, 2 Bd Lavoisier, 49045 Angers, France*
E-mail: komarov@iae.nsk.su

At the present time, the development of lasers of high-energy pulses is one of the most important problems [1-4]. These lasers are widely used in various areas of science, technology, and engineering. We put forward a way to realize such pulse sources based on fiber lasers with hybridization of passive mode locking and the regime of undamped regular spikes. We present results of a numerical simulation of a formation of reproducible stable high-energy pulses in these lasers.

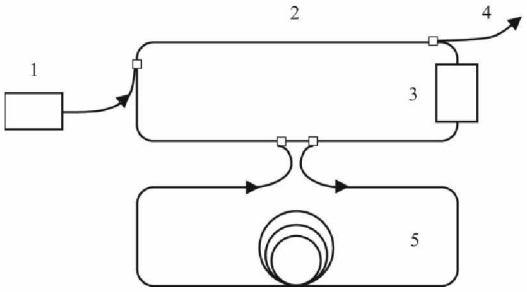

Fig. 1 Schematic representation of laser setup.

The investigated laser is schematically represented in Fig. 1. It contains a continuous pumping source 1, a gain fiber 2 (~ 10 m), a device of nonlinear losses 3, a long passive fiber 5 (~ 1.7 km). Without the long passive fiber 5, owing to the device of nonlinear losses 3, the laser operates in the regime of regular undamped spikes [2]. Each spike is formed from intracavity spontaneous emission. As result, pulses coming out from the laser cavity through the coupler 4 have random irreproducible space-time structure. In the well-known scheme of a fiber laser operating in the regime of regular undamped spikes, we add the long passive fiber 5. As a result, a part of the radiation goes out from the laser cavity through the fiber 5, and then it enters again in the laser cavity. We are investigating the case when the time of a pulse passage through the fiber 5 is approximately equal to the temporal interval between the adjacent spikes. This determines the length of the fiber 5. In this case, each spike is formed from radiation of previous spike. As result, all pulses in output radiation are reproducible. In this case, the laser operates in a hybrid regime of passive mode locking and regular undamped spikes.

We have investigated this lasing regime using a numerical simulation. Figures 2-4 present results of our investigation. Figure 2 shows the dependence of the radiation energy $J(\zeta)$ in the active ring cavity on a number of passes through the cavity.

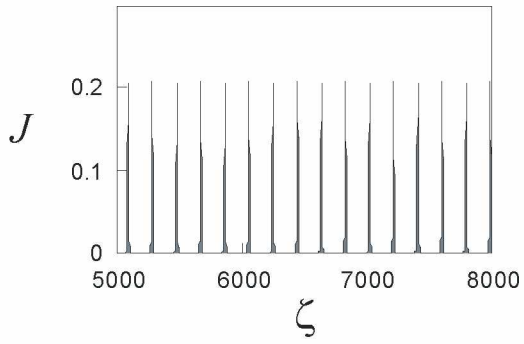

Fig. 2 Dependence of the radiation energy J in the active ring cavity on a number of passes ζ of radiation through the cavity.

Figure 3 shows a propagation of a pulse in the long passive fiber 5. Decrease of the pulse is due to linear losses in the fiber. Figure 4 demonstrates the distribution of radiation I_p in the fiber 5 for $\zeta = 630$. The small pulse induces a generation of the large pulse.

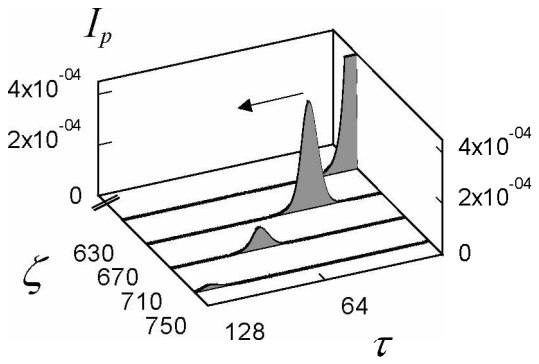

Fig. 3 Distribution of radiation in the long passive fiber $I_p(\tau)$ for various numbers of passes ζ.

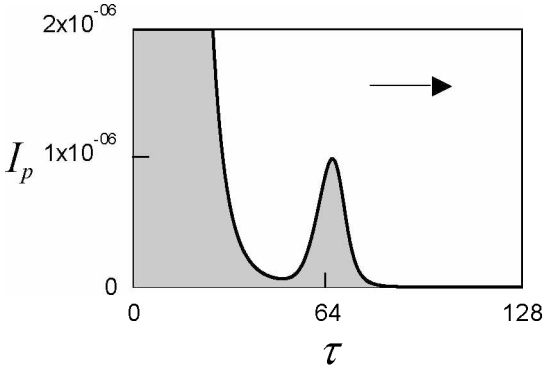

Fig. 4 Distribution of radiation in the long passive fiber $I_p(\tau)$ for $\zeta = 630$.

A duration of pulses in output radiation is ~ 1 μs. Energy of pulses is several μJ. In the case of regime of regular undamped giant pulses, energy of the generated pulses can be considerably increased.

The suggested scheme of a laser mode-locking opens up fresh opportunities to design high-energy pulse lasers.

The work was supported by a grant of Ministry of Education and Science of the Russian Federation in the framework of the project of the state task (project 1316).

References

[1] A. Komarov, F. Armani, A. Dmitriev, K. Komarov, F. Sanchez, *Phys. Rev. A* **87,** 023838 (2013).
[2] A. Hideur, T. Chartier, M. Brunel, M. Salhi, C. Ozkul, F. Sanchez, *Optics. Commun.* **198,** 141 (2001).
[3] V.I. Denisov, B.N. Nyushkov, V.S. Pivtsov, *Quant. Electron.* **40**, 25 (2010).
[4] S.M. Kobtsev, S.V. Kukarin, S.V. Smirnov, Y.S. Fedotov, *Laser Physics* **20,** 351 (2010).

Terahertz and mid-infrared radiation from gas ionized by two-color laser pulses

V. A. Kostin, I. D. Laryushin, A. A. Silaev, N. V. Vvedenskii
University of Nizhny Novgorod, Nizhny Novgorod, Russia
Institute of Applied Physics, Russian Academy of Sciences, Nizhny Novgorod, Russia
E-mail: silaev@appl.sci-nnov.ru

The ionization-induced generation of broadband intense terahertz (THz) radiation by ultrashort (femtosecond) laser pulses attracts considerable interest due to various applications. The most of the experimental and theoretical studies of such laser-plasma generation are now concentrated on the so-called two-color method providing strong THz pulses with very broad spectrum when an ultrashort two-color pulse with frequency ratio of two ionizes a gas [1-3]. In this method, the main contribution to the low-frequency THz radiation is defined by the free-electron current in the formed laser plasma [2, 3]. Detuning the frequencies of two-color laser pulses away from frequency ratio of two results in a very wide tunability of the THz radiation emitted by the laser-produced plasma and in the possibility for generation of short mid-infrared pulses [4].

In this work, we show that the generation of low-frequency THz and mid-infrared radiation can be understood as the ionization-induced multiwave mixing (or, in other words, generation of combination frequencies) [5]. We show that the main features of this wavemixing are defined by the intrinsic nonlinear properties of the ionized particles. Particularly, the number of mixed waves, which is typically large, is determined by the effective exponent of the ionization rate as a function of ionizing field strength. The dependences of maximum (over the phase shift between one-color components of the two-color pulse) amplitude of low-frequency current density on frequency ratio consist of resonant-like peaks at frequency ratios located near rational fractions with not so big odd sum of numerator and denominator (fractions such as 1 : 2, 2 : 3, 3 : 4, 2 : 5, etc.). The magnitudes of different peaks can be comparable when the two laser components have close intensities, and the laser-plasma generation of low-frequency radiation with the two-color pulses of uncommon frequency ratios may be effective enough.

Our closed-form analytical formula supports the above conclusions and reveals similarities and differences between the ionization-induced wavemixing under consideration and the common wavemixing associated with Kerr-like nonlinear response of bound charges. These differences originate mainly from the essentially high-order character of nonlinear ionization and the associated strong nonlinear dispersion: (i) the number of mixed waves drastically depends on the laser intensity; (ii) the effect is strongly modified at high enough intensities due to the neutral depletion; (iii) there is an asymmetry with the respect to the sign of the detuning from the exact synchronism. The identification of these similarities and differences should promote the sensible and targeted design of methods for radiation generation in the THz, mid-infrared, and other frequency ranges.

This work was supported by the Government of the Russian Federation (Agreement No. 14.B25.31.0008) and Russian Foundation for Basic Research (Grants No. 14-02-00847, 16-32-60166, and 16-32-60200).

References

[1] D. Kuk, Y. J. Yoo, E. W. Rosenthal et al., Appl. Phys. Lett. **108**, 121106 (2016).
[2] N.V. Vvedenskii, A.I. Korytin, V.A. Kostin et al., Phys. Rev. Lett. **112**, 055004 (2014).
[3] V.A. Andreeva, O.G. Kosareva, N.A. Panov et al., Phys. Rev. Lett. **116**, 063902 (2016).
[4] T. Balčiūnas, D. Lorenc, M. Ivanov, Opt. Expr. **23**, 15278 (2015).
[5] V. A. Kostin, I. D. Laryushin, A. A. Silaev, N. V. Vvedenskii, Phys. Rev. Lett., accepted (2016).

Optimization of stabilization regimes of the optical frequency standards based on resonant two-level atoms

D. Kovalenko[1], M. Basalaev[2,3], V.I. Yudin[1-3]
[1]*Novosibirsk State Technical University, pr. Karla Marksa 20, Novosibirsk, 630073, Russia*
[2]*Institute of Laser Physics SB RAS, pr. Akademika Lavrent'eva 13/3, Novosibirsk, 630090, Russia*
[3]*Novosibirsk State University, ul. Pirogova 2, Novosibirsk, 630090, Russia*
E-mail: dvk.laser@yandex.ru

The important issue by development of frequency standards is increase of their stability. Stabilization of the oscillator frequency$\nu_L$neara reference frequency $\nu_0$can be performed by means of a modulation of the frequency difference $\delta = \nu_L - \nu_0$. Harmonic type of themodulationoflaser frequency near a resonance frequency of an atomic transition is widely used in optical frequency standards. By stabilization it is necessary to gain the maximal slope of linear part of theasymmetric discriminant curve of the error signal near ν_0, because this slope is one of the parameters determining frequency standards stability [1].

In this work weinvestigate the case when modulationlawof the laser frequencyωhas following form: $\omega(t) = \omega + \Delta\omega\sin(\omega_m t)$, where $\Delta\omega$ is depth of modulation, ω_m is modulation frequency. The first-harmonic signal of transmitted powerwas chosen as the error signal. On the basis of theoretical method developed in our work [2] thedependence of the slope of the first-harmonicsignalon modulation parameters ($\Delta\omega$, ω_m), Rabi frequency Ω and the reference signal phaseφ for two-level atomic system in spontaneous relaxation model was optimized by use of the density matrix formalism. Optimal modulation parameters were found where the maximal slope is reachedat fixed values of Ω and φ (see fig.1(a,b)).

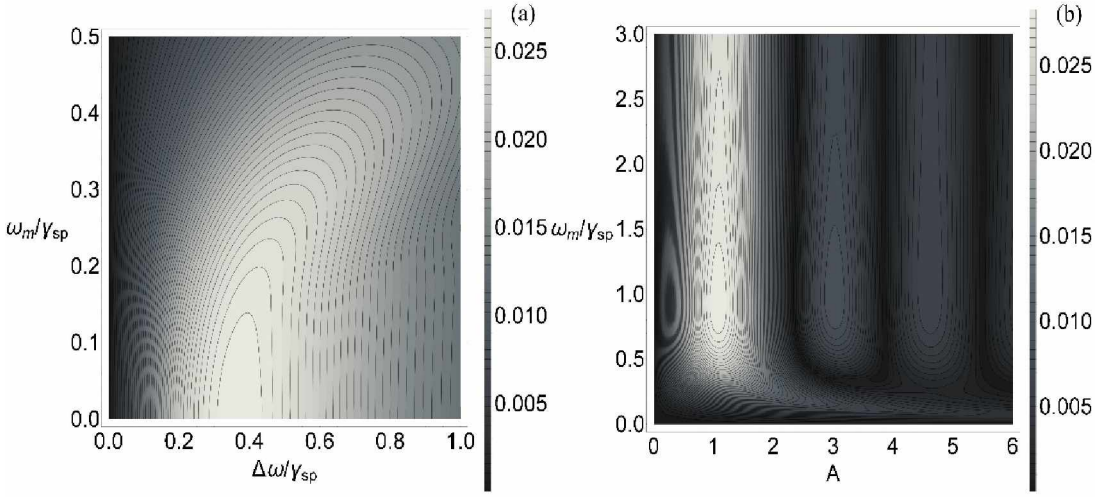

Fig. 1 (a) Counter plot of the dependence of the slope ofthe first-harmonic signal (in relative units) on modulation parameters ($\Delta\omega$, ω_m) for$\varphi = 0$ and $\Omega = 0.1\gamma_{sp}$. (b) Counter plot of the dependence of the slope ofthe first-harmonic signal(in relative units) on modulation parameters (A, ω_m), where $A = \Delta\omega/\omega_m$ is modulation index, for$\varphi = \pi/2$ and $\Omega = 0.1\gamma_{sp}$. γ_{sp} is the decay rate of excited level.

Two special cases in relation to modulation law$\omega(t)$of the laser frequencyωwere also considered separately: 1) the in-phase component of the first-harmonic signal ($\varphi = 0$) and 2) the quadrature component of the first-harmonic signal ($\varphi = \pi/2$). It was shownthat the maximal slope of the quadraturecomponent is significantly more than the maximal slope of the in-phase component at Rabi frequencies $\Omega \geq \gamma_{sp}$(see fig.2 (a)). Also the quadraturecomponentis reached at higher modulation

frequencies (see fig. 2(b)) (at higher frequencies technical noises are lower). It makes the quadraturecomponent more usable in stabilization systems.

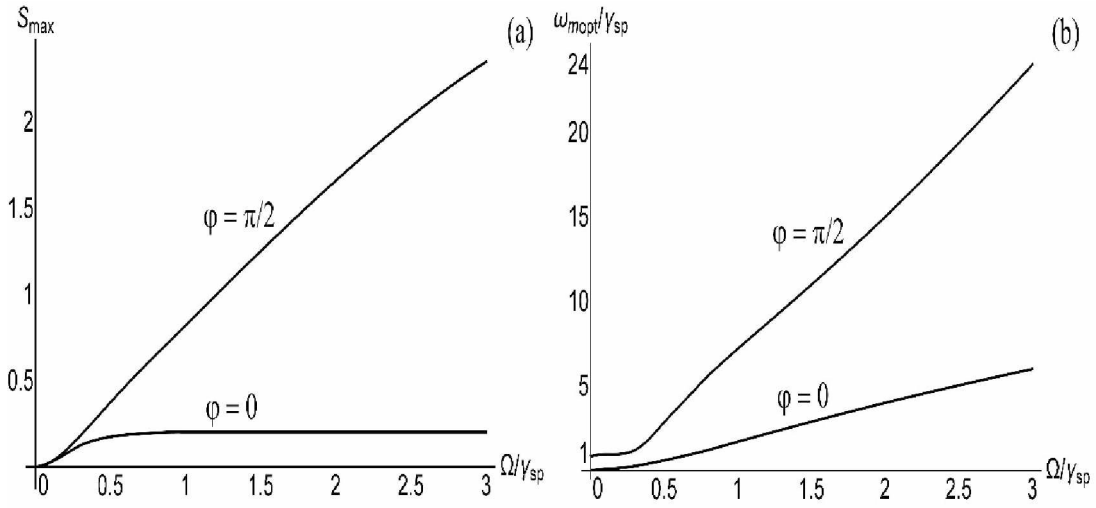

Fig. 2 (a) The dependence of the maximal slope S_{max} on Rabi frequency Ω for the in-phase component ($\varphi == 0$) and the quadrature component ($\varphi = \pi/2$). (b) The dependence of the optimal modulationfrequency $\omega_{m\,opt}$ on Rabi frequency Ω for the in-phase component ($\varphi = 0$)and the quadraturecomponent ($\varphi = \pi/2$).

The work was supported by the Ministry of Education and Science of the Russian Federation (State Assignment No. 2014/139, Project No. 825), by the Russian Foundation for Basic Research (Grants No. 16-32-00127, 16-32-60050).

References

[1] F. Riehle, "Frequency Standarts: Basics and Applications", Wiley-VCH Verlag GmbH& Co. KGaA, Weinheim (2004).
[2] V. I. Yudin, A. V. Taichenachev, and M. Yu. Basalaev, "Dynamic steady state of periodically driven quantum systems", Phys. Rev. A **93**, 013820 (2016).

Highly sensitive and fast response ammonia sensor

A. Kuchyanov
Institute of Automation and Electrometry SB RAS, Novosibirsk, Russia
E-mail: aleks@iae.nsk.su

We have implemented a highly sensitive and fast response (100 ms) ammonia sensor based on Fabry-Perot interferometer and total internal reflection of a light in opal like silica film.

The design of ultrabroadband parametric amplifier for multiterawatt femtosecond laser system with 1 kHz repetition rate

G.V. Kuptsov[1,2], V.V. Petrov[1,2,3], V.A. Petrov[1,3], A.V. Kirpichnikov[1], A.V. Laptev[1], and E.V. Pestryakov[1]
[1]*Institute of Laser Physics SB RAS, Novosibirsk, Russia*
[2]*Novosibirsk State National Research University, Novosibirsk, Russia*
[3]*Novosibirsk State Technical University, Novosibirsk, Russia*
E-mail: kuptsov.gleb@gmail.com

At the Institute of Laser Physics of SB RAS a multiterawatt femtosecond diode-pumped system with pulse repetition rate up to 1 kHz based on all diode-pumped Yb^{3+}-doped media is developed. It consists of two optically synchronized channels: parametric amplification channel and laser amplification channel. Pulses from the laser amplification channel are used as pump for the parametric amplification channel.

In the parametric amplification channel supercontinuum pulse (~150 nm FWHM) is produced [1] and temporally stretched to ~400 ps to prevent optical breakdown during the amplification process and to match it with pump duration (~1 ns). Also, we have simulated the pulse propagation through 10 m long highly nonlinear photonic crystal fibre [2]. The experimental results and modeling data are in good agreement. Our simulations show that the supercontinuum can be used as a seed signal for amplification in the parametric amplification channel. Then the radiation is to be amplified to 10 mJ which corresponds to 1 TW power at the output of the system. The system can be scaled straightforwardly using additional laser amplification channels to obtain multi-TW level.

We were to estimate ultrabroadband parametric amplifier parameters to obtain the desired 10 mJ. So, we chose the BBO crystal, and the acceptance bandwidth, peak gain dependencies over phase-matching angle, noncollinear angle, temperature and crystal length were investigated. Two crystals scheme was proposed, pump divided unevenly between two crystals. For each stage optimal parameters were established: crystal lengths 1,1 and 1,5 cm, phase-matching angles 23,32° and 23,30°, noncollinear angles 0.4° and 0.8°, resulting in a gain profile with a ~30% dip near the center. Such approach tailors the amplified signal spectral shape suppressing the central peak.

However, the laser amplification channel is expected to produce 1 ns, 150 mJ pulses centered at 515 nm with 1 kHz repetition rate to achieve the possibility of described amplification of supercontinuum up to 10 mJ. The laser amplification channel consists of two consequent all-diode-pumped Yb:YAG multipass amplifiers and a second harmonic generation unit. Inside the second multipass cryogenic (120 K) amplifier the beam travels about 30 m. This leads to extreme sensitivity to angular displacements and drifts. There were ~mrad in long term and ~tens urad short term beam pointing fluctuations at the output of the amplifier. This leads to the necessity of cooling system optimization to allow using the output beam as pump for parametric amplifier.

The experiments were carried out to determine the sources of instabilities. Using the experimental data, the cooling system has been optimized, drastically reducing the short-term and long-term angular stability. Also, the cooling cycle-to-cycle repeatability of the system parameters increased significantly. Our calculation shows that achieved beam stability is acceptable to be used as the pump for the parametric amplifier.

All the data, both simulated and experimental, are used in the development of the channels of the all-diode-pumped high intensity cryogenic laser system working with 1 kHz repetition rate.

This work is supported in part by RAS Program "Extreme laser radiation: physics and fundamental applications", registration number AAAA-A15-115113010002-9 and Government program, registration number 01201374306.

References

[1] G.V. Kuptsov, V.A. Petrov, A.V. Laptev, V.V. Petrov, E.V. Pestryakov, Laser Optics, 2014 International Conference, vol: IEEE Conference Publications (2014).
[2] G.V. Kuptsov, V.V. Petrov, V.A. Petrov, A.V. Laptev, E.V. Pestryakov, Proc. of SPIE, 9810, 98101S-1 (2015).

Quantum key distribution between two buildings in Moscow via telecom fiber

V. Kurochkin, A. Miller, A. Sokolov, A. Kanapin and Y. Kurochkin
Russian Quantum Center, 100, Novaya st. Skolkovo, Moscow reg., 143025, Russia
E-mail: v.kurochkin@rqc.ru

In this work we present first in Russia demonstration of city based quantum key distribution in telecom optical fiber. The quantum key distribution setup was built on the base of autocompensation plug&play optical scheme [1]. Autocompensation optical scheme stabilizes single photon properties propagating in the optical fiber in the city environment. Id Quantique ID230 single photon detector was used to detect single photon signal. This detector works in the free-running mode with quantum efficiency 10% and 10-20 dark counts per second [2].

Quantum key distribution was implemented on the base of phase coding of the quantum states of single photons, emitted from a pulsed semiconductor laser, in the two alternative non-orthogonal bases. All the optical elements including laser, phase modulators and high speed attenuators are integrated to the single mode fiber. Before each experiment start the procedure of setup adjustment have been conducted in the multi photon mode. Bob emitted multi photon laser pulses and measured the time of signal forth and back propagation through the quantum channel. Using the measurement result Bob set all corresponding time delays for the optoelectronic elements guidance, single photon detectors synchronization and quantum key distribution BB84 protocol execution. On the next stage Alice attenuated laser pulse to the 0.2 photon/pulse on its way back with the use of fast attenuators. Frequency of the pulse repetition was 10 MHz. Key was distributed with the use of BB84 protocol [3].

The optical fiber length is 30,6 km. Sifted key generation rate is 1.8 kbit/s and QBER is 4.5-5.5%. We take into account the neighbor fiber lines effect on the QBER and methods of increase of the signal/noise ratio.

The support from the Ministry of Education and Science of the Russian Federation in the framework of the Federal Program (Agreement 14.582.21.0009) is greatly acknowledged.

References

[1] N. Gisin, G. Ribordy, W. Tittel, and H. Zbinden, "Quantum cryptography," Rev. Mod. Phys. 74, 145–195 (2002).
[2] http://www.idquantique.com/photon-counting/photon-counting-modules/id230/.
[3] C.H. Bennet and G. Brassard, in Proceedings of IEEE International Conference on Computers, Systems and Signal Processing (Bangalore, India, December 9-12, 1984), p. 175.

Optical properties of quasi-organized bimetallic clusters obtained by laser-assisted colloidal deposition

S. Kutrovskaya[1], A. Kucherik[1], S. Arakelian[1], A. Osipov[1], T. Vartanyan[2], T. Itina[3]
[1]*Stoletov Vladimir State University, Vladimir, Russia*
[2]*St.Petersburg National Research University of Information Technologies, Mechanics and Optics, St. Petersburg, Russia*
[3] *Université de Lyon, UJM-Saint-Etienne, CNRS, Laboratoire Hubert Curien, Saint-Etienne, France*
E-mail: 11stella@mail.ru

Nanoparticles of noble metals are widely used for various applications in many areas such as nanophotonics, nano- and microelectronics, photochemistry, etc. The development of these applications relies on the properties of the generated structures that start deviating from those of massive samples when particle size drops below around 100 nm. Such dimensional effects change characteristic parameters of various processes (the frequency of plasmon resonance, electron free path length and others) and define physicochemical properties of nanosystems.

Nanostructured noble-metallic clusters demonstrate nonlinear optical effects in visible spectral range because of their plasmonic properties. In addition, optical characteristics of these structures strongly depend on the period. If the distance between the particles is close to their sizes, the optical properties of the randomly deposited structures may considerably differ from these of periodical structures. Thus, sintering of the bimetallic gold and silver complexes results in pronounced changes of the optical properties. In this case, both morphology and shape of the particles influence the final optical properties. One of the challenging issues in the demonstration of the scale-effect for metallic cluster is the control over particles size.

Laser ablation is considered to be one of the versatile methods of nanoparticle generation that allows a reliable control over particle sizes. In particular, the presence of nanoparticles was demonstrated in pulsed laser deposition performed both in vacuum and in inert gases. Laser ablation in liquid media, furthermore, was shown to be a promising approach for a wide range of applications. In contrast to nanoparticles synthesized by chemical techniques, nanoparticles generated by laser ablation in liquids can be free of surface active substances and irrelevant ions, thus providing a possibility of generating chemical "pure" colloids.

The properties of nanoparticles generated by laser ablation in liquids depend on many parameters, such as laser wavelength, laser pulse duration, laser fluence, material absorption, choice of the liquid, etc. One of the main difficulties in the application of high intensity laser sources is high plasma energy and droplet formation, which are really hard to avoid. When pulsed lasers are used, furthermore, laser intensity is typically sufficiently high for laser-induced nanoparticle fragmentation to occur during nanoparticle formation in colloids, considerably complicating the prediction of the experimental results. In fact, strong shock waves, phase transitions, and cavitation bubbles are known to be generated by both nanosecond and femtosecond pulse durations. Under such conditions, not only target is affected by laser action, but also particles, if they are present in the surrounding liquid. In addition, such effects as optical breakdown and liquid decomposition were reported to occur at high laser intensities. These effects can result in uncontrollable changes in both particle size and size distribution.

When a continuous-wave laser is used for nanoparticle production, its intensity is typically orders of magnitude smaller than the one in pulse-periodic regime. The role of laser is mostly thermal in this case. For a particular range of laser intensities, melting of the target is expected leading to a molten bath/layer formation, whose thickness is defined by the coefficient of thermal diffusion of the target material. However, liquid is typically heated too, and its convective movement can prevent the formation of shock waves, of a cavitation bubble or a gas cavity with a high gas pressure. Therefore,

both the mechanisms and sizes of nanoparticle formed by continuous-wave laser are different from the ones in pulsed-periodic regime and are not yet completely understood.

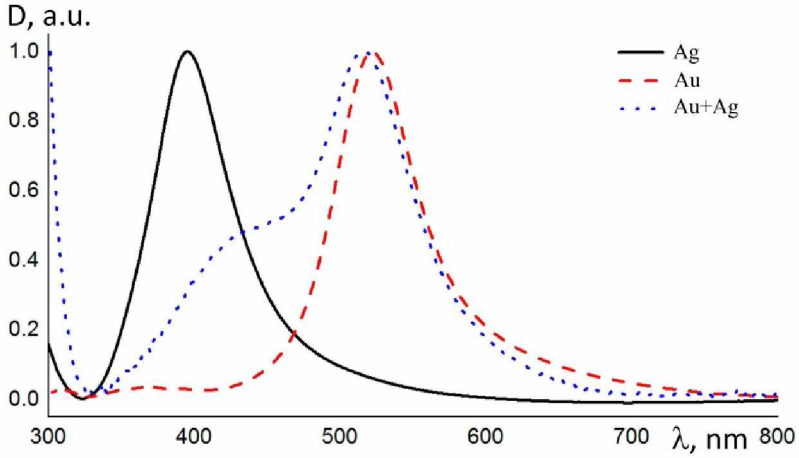

Fig. 1 Optical spectra of colloidal particles before and after laser irradiation. Demonstrated the formation of a bimetallic clusters.

We report the results of continuous wave laser interactions with both gold and silver targets in the presence of different liquids (deionized water, ethanol, and glycerol) [1]. Upon moderate laser irradiation at wavelength of 1.06 nm during 30 min, nanoparticle colloids are shown to be formed with surprisingly narrow size distributions and average dispersion as small as 15-20 nm. The average particle sizes range between 8 and 52 nm for gold and between 20 to 107 nm for silver. This parameter is shown to be stable and well-controlled by such laser parameters as intensity and effective irradiation time, as well as by the choice of the liquid phase. The possibilities of an efficient control over the proposed synthesis techniques are discussed and the results of a bimetallic Au-Ag structure deposition from the obtained colloids are presented [2]. The formation of the extended arrays of gold and silver nanoparticles with controlled morphology is examined. The changes in the optical properties of the obtained thin films are found to depend on their morphology, in particular, on the particle size and distance between them.

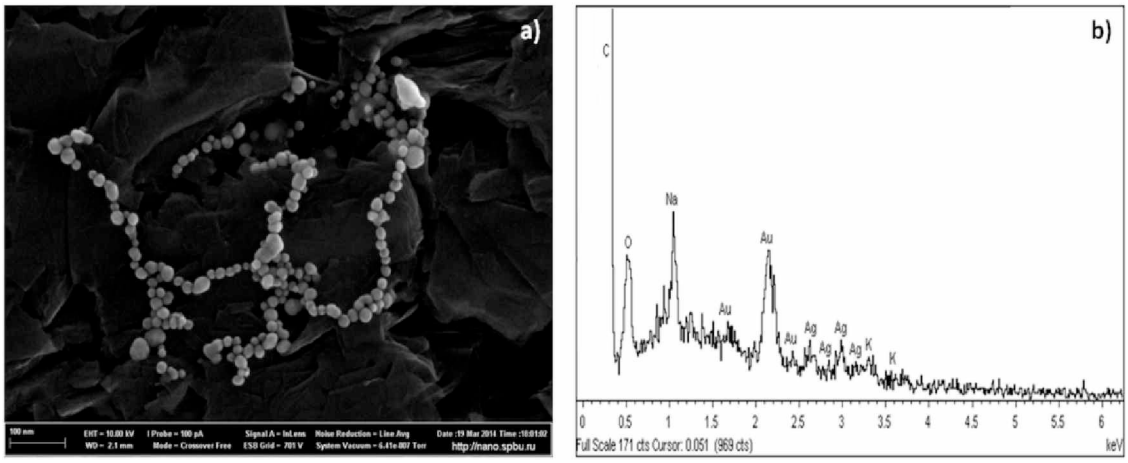

Fig. 2 SEM-images of synthesis bimetallic cluster (a) and it elements analyze (b).

References

[1] S.M. Arakelyan, V.P. Veiko, S.V. Kutrovskaya, A.O. Kucherik, A.V. Osipov, T.A Vartanyan., T.E. Itina, "Reliable and well-controlled synthesis of noble metal nanoparticles by continuous wave laser ablation in different liquids for deposition of thin films with variable optical properties", J Nanopart Res (2016) 18:155.

[2] A. A.Antipov, S.M. Arakelyan, T. A. Vartanyan, T.E. Itina, S.V. Kutrovskaya, A.O. Kucherik, I.V. Sapegina: Optical properties of nanostructured gold–silver films formed by precipitation of small colloid drops. Optics and Spectroscopy (2015).

The software package for simulating the characteristics of photoluminescence anisotropic crystals

A. V. Kuznetsov, N. L. Lazareva, and E. F. Martynovich
Irkutsk Branch of the Institute of Laser Physics SB RAS, Irkutsk State University Lermontov, 130A, Irkutsk, 664033, Russia
E-mail: filial@ilph.irk.ru

The process of carrying out the research of the luminescence characteristics of anisotropic media and analyzing of their spatial distributions requires a large number of different parameters. It is necessary to take into account the changes in the crystal luminescence intensity depending on the distance as much as the changes in the luminescence exciting optical radiation state of polarization. The characteristics of crystals are the magnitude and orientation of the electric dipole moments of quantum transitions in the luminescence centers and their permittivity tensors. The main characteristics of the exciting optical fields in the electric dipole approximation are the ordinary and extraordinary waves wave and electric vectors. The characteristics of crystals are their permittivity tensors as much as the magnitude and orientation of the electric dipole moments of quantum transitions in the luminescence centers. The number of possible orientations of the luminescence centers and related orientations of the transitions dipole moments depends on the symmetry of the crystal recognized as the category and the type of the syngony. It is also strictly necessary to specify the direction of the luminescence observation and to take into account the emission diagram of the luminescence of each of the dipole radiators used. Any vector is defined by three different coordinates. Therefore the total number of critical parameters is significant. Facts named within necessitated the special program writing for the research accelerating and the better understanding of the processes occurring in anisotropic crystals at interaction with optical radiation. The program also removes difficulties of the fluorescent characteristics detection and description. Semiclassical electric-version of the interaction of light with an anisotropic crystalline medium containing luminescence centers with different orientations permitted by the laws of symmetry [1], became the theoretical basis for the program development.

The program is written in C ++ in the environment Borland C ++ Builder development. The main objectives of the program are the calculation and plotting different values and displaying numerical values needed for further research.

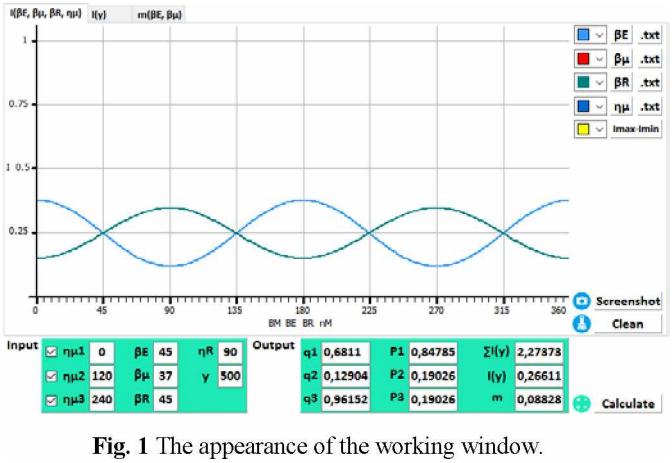

Fig. 1 The appearance of the working window.

View desktop window is shown in the Fig. 1. The program contains three tabs, each is a field for building specific dependency graphs. A window to enter the numerical values of physical quantities derived from calculations is situated below. Centers of different orientations permitted by the laws of

symmetry of the crystals contribute to the overall intensity of the luminescence. These centers correspond to the specific orientation of the electric dipole moment of the quantum transitions responsible for the absorption and the luminescence. The program feature is the ability to enable and disable each of the individual dipole center for a more detailed consideration of the contribution of the others.

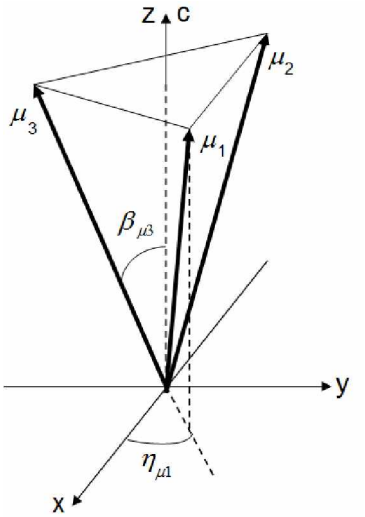

Fig. 2 A possible variant of the orientation of the dipole moments of the transitions in the crystal with a point symmetry group D_{3d}.

Fig. 2 shows a possible variant of the orientation of the three dipole moments in the luminescence centers responsible for transitions in the crystal medium category with the point group symmetry D_{3d} [2]. The crystal was used as an object of study for demonstration of the the written program capabilities. You can specify two angles to orientate each of the transitions dipole moment in these crystals: the angle between the dipole moment and the optical axis - β_μ, and the angle between the projection of the dipole moment in the XY plane and the X axis – η_μ.

The following relationships can be calculated using the program:

• the luminescence intensity dependence from the angle of rotation of the electric vector of about the optical axis;

• dependence of the luminescence intensity from angles which determine the direction of the transition dipole moments of about the optical axis and about the axis X;

• dependence of the luminescence intensity from angles defining direction of observation of the luminescence;

• the luminescence intensity dependence from the crystal distance;

• the dependence of the spatial modulation of the luminescence intensity of the depth from different angles which determine the direction of the field vectors and luminescence centers orientation.

References

[1] Martynovich E.F. color centers in laser crystals / E.F. Martynovich. - Irkutsk: Izd Irkut. University Press, 2004. - 227 p.

[2] Sirotin Y.I. Fundamentals of crystal. / Y.I. Sirotin, M.P. Shaskol'skaya. - M .: Science, Heads. Ed. Sci. lit-ry, 1979. - 640 p.

[3] Martynovich E.F. Luminescence, intrinsic photoeffect, and color-center conversion in anisotropic crystals under femtosecond laser excitation / E.F. Martynovich // Russian Physics Journal. – 2000. - Vol. 43, № 3. – pp. 193-204.

[4] Martynovich E.F. The effect of dispersion on the spatial distribution of the intensity of the luminescence excited by colliding laser pulses / E.F. Martynovich, G.V. Rudenko, S.I. Polityko // Optics and Spectroscopy. - 2009. - T. 106. - №1. - S. 128-133.

Highly efficient tapered diode-pumped Yb:KYW laser

S.A. Kuznetsov, V.S. Pivtsov
Institute of Laser Physics SB RAS, 630090, Novosibirsk, Ac. Lavrentyev's prosp., 13/3, Russian Federation
E-mail: clock@laser.nsc.ru

Optical frequency synthesizers based on femtosecond lasers are most important blocks of precision laser systems for measurement of absolute optical frequencies and their stability. They are also used to solve the problem of transferring the frequency characteristics of optical frequency standards to the radio frequency range. At present, synthesizers on the basis of ytterbium-doped crystals are becoming more popular. The absorption bands of ytterbium crystals coincide with the generation range of high-power semiconductor diode lasers (940 nm and 980 nm). Among ytterbium-doped media, the potassium tungstates Yb:KYW and Yb:KGW are most promising owing to large absorption cross-sections and induced radiation, wide luminescence band, and rather high heat conduction. In this paper, various schemes of small cavities of a Yb:KYW laser with high-power multimode diode pumping are investigated.

As an active medium, we used Yb:KYW crystal with 5 at. % Yb^{3+} ions and a thickness of 1.5 mm. The crystals were cut in the direction of axis c (E || a, b). The temperature of the crystal was stabilized at 9°C using a Peltier element. The source of pumping was a LIMO25-F100-DL980 laser with a multimode fiber output. The central radiation wavelength was 981 nm, the maximum output power was 25 W, and the fiber core diameter was 105 μm. The pump laser radiation had circular polarization.

Earlier studies [1-2] showed the possibility of creation of a high-efficiency Yb:KYW laser with a differential efficiency of 40% and a full optical efficiency of 35%. In this paper, investigations of the V-shaped cavity have been performed. The pump laser radiation was focused by two lenses with a focal length of 25 mm. The cavity contained a Yb:KYW crystal, a flat dichroic mirror, a mirror with a curvature radius of 50 mm, a GTI-mirror, and an output mirror with different transmission coefficients. The intermode frequency was about 2.5 GHz.

The generation power versus the incident pump power for the free generation regime has been determined. Measurements for output mirrors with various transmission coefficients (1%, 2.2%, 3%, and 4%) have been made. The differential efficiency was 53.2%, the optical efficiency was 48%, and the maximal output power was 3.94 W at a pump power of 8.2 W. This is a record result when using a multimode pump source. Since the pumping radiation was unpolarized, its part with S-polarization was used inefficiently due to smaller absorption in the crystal (E||b) and small mirror transmission. This decreased the overall efficiency and increased the generation threshold.

Maximum efficiency can be achieved by using single-mode diode pumping for this scheme when the pump and generation waists fully overlap. The pump source is a distributed Bragg reflector tapered diode laser [3]. The pump diode consists of a 4-mm-long gain-guided tapered section and a 2-mm-long 4-μm-wide index-guided straight ridge-waveguide section containing a 1-mm-long surface Bragg grating. The DBR TDL emits at 981 nm with a spectral linewidth of less than 20 pm (FWHM). In addition, the device has a nearly diffraction limited output beam with a lateral beam propagation factor $M^2 1/e^2 = 1.2$ containing more than 72% of the power in the central lobe. The maximum output power is 7 W, and the light is collimated by an aspheric lens with a focal length of 3 mm and a cylindrical lens with f= 30 mm. Preliminary results of investigations of the Yb:KYW laser using the DBR TDL for pumping are presented.

This work was performed at the support of the Russian Foundation for Basic Research (project no. 16-02-00639-a) and RAS Presidium Program "Extreme Light Fields and Their Applications".

References

[1] S.A. Kuznetsov, V.S. Pivtsov, Quantum Electronics **44**, 444 (2014).
[2] A. A. Kirpichnikova, S. A. Kuznetsov, V. S. Pivtsov, Bulletin of the Russian Academy of Sciences. Physics **79**, 169 (2015).
[3] C. Fiebig, G. Blume, M. Uebernickel, et al., IEEE J. of SELECTED TOPICS IN QUANTUM ELECTRONICS **15**(3), 978 (2009).

The investigation of thermal effects in Yb:YAG multipass amplifier of high power femtosecond laser system

A.V. Laptev[1], E.V. Pestryakov[1], V.V. Petrov[1,2,3], G.V. Kuptsov[1,2], V.A. Petrov[1,3], A.V. Kirpichnikov[1]
[1]*Institute of Laser Physics SB RAS, Novosibirsk, Russia*
[2]*Novosibirsk State National Research University, Novosibirsk, Russia*
[3]*Novosibirsk State Technical University, Novosibirsk, Russia*
E-mail: alex_laptev@ngs.ru

For Chirped Pulse Amplification (CPA) high power laser systems, optical pumping in multipass or regenerative amplifiers induces a thermal load that becomes especially critical as repetition rate of the laser increases. The thermal load causes a refractive index gradient and leads to thermal lensing in the amplifier medium. This thermal lensing induces different kinds of optical aberrations, birefringence, besides a reduction in the amplified beam size causes optical damage. One of the ways to decrease thermal lensing is to perform cooling of the amplified medium [1]. Cryogenic cooling results in decrease of the thermal loading and is commonly used to reduce the thermal lensing effect.

At the Institute of Laser Physics of SB RAS a high power femtosecond laser system with pulse repetition rate 1 kHz based on diode-pumped Yb^{3+}-doped media has been developing. One of the major features of this system is based on the parametric and laser method [2] of the amplification of pulses generated by master oscillator in the two optically synchronized channels. Temporally stretched pulse of master oscillator based on Yb:Y_2O_3 ceramics is amplified in regenerative amplifier to energy up to 0.5 mJ. Then radiation is divided to a parametric amplification channel and a laser amplification channel. In parametric amplification channel there are photonic-crystal fibre for spectrum broadening, parametric amplifier and compressor. In amplification channel there are two multipass amplifiers and SHG crystal. The first is 6-pass amplifier based on Yb:YAG water-cooled crystal that increases pulse energy up to 10 mJ. The second amplifier consists of 8 cryogenically cooled Yb:YAG bonded crystals and is used to amplify pulse energy up to 300 mJ. The cooling system of the second amplifier is based on four closed-loop helium cooler operating in vacuum chambers. Each chamber contains two Yb-YAG crystals which are mounted to a heatsink block that is in contact with closed-loop cryocooler. The expected output pulse parameters of the laser system are duration 10 fs and energy 10 mJ with 1 kHz repetition rate.

In this work we numerically solved the thermal conductivity equation to get temperature distribution in amplifier elements of the laser system as well as parameters of thermal lenses. The results of modeling show that the value of the temperature difference is about 100-140 C between the axis and the edge of the crystal using the water-cooling and in the pump power range 100-200 W. The dioptric power slope of the thermal lenses for water-cooled Yb:YAG amplifier is about 5 $m^{-1}W^{-1}$.

Such as all path length of the cryogenic amplifier is about 25 m, therefore for efficient amplification it is very crucially to minimize the short and long time angular stability of the beam. To reduce the mechanical vibrations the cooling system has been optimized. The results of the experiments show that short time angular stability is increased in three times and is about 5 μrad (RMS) with maximal deviation 10 μrad. Also, long time angular stability is increased to one order and two orders of magnitude for horizontal and vertical directions and equals about 11 μrad and 0.1 μrad, respectively.

This work is supported in part by RAS Program "Extreme laser radiation: physics and fundamental applications", registration number AAAA-A15-115113010002-9 and Government program, registration number 01201374306.

References

[1] M. Pittmat, S. Ferre, J.-P. Rousseau et al, Appl.Phys. B **74**, 529 (2002).
[2] V. Petrov, E. Pestryakov, A. Laptev et al, Quantum Electronics **44**, 452 (2014).

Spatial-modulation method for studying of quantum systems orientation in crystalline media

N. Lazareva, A. Kuznetsov, and E. Martynovich
Irkutsk Branch of the Institute of Laser Physics SB RAS, 130A Lermontov str, Irkutsk, 664033, Russia
Irkutsk State University, 20 Gagarin blvd, Irkutsk, 664033, Russia
E-mail: filial@ilph.irk.ru

Important properties of crystalline optical materials depends on the orientation of contained in them quantum systems interacting with the radiation. Therefore, the development of crystalline optical elements for different purposes need to have data on their orientation. Therefore, some methods for determining the orientation of the centers in crystals have been developed already [1-3].

In this paper we develop a theory of the spatial modulation of photoluminescence intensity of anisotropic crystals under laser excitation [4]. The proposed new method allows to determine the orientation of the quantum systems in anisotropic crystals of different crystallographic point group. The method was tested on the example of one of the color centers in the crystal of neutron-irradiated sapphire. Sapphire is optically uniaxial crystal. It has the formula of symmetry $L_3 3L_2 2PC$ refers to the axial central class D_{3d} trigonal system, the middle category. Any possible orientation of the dipole moment of transition in these crystals will be repeated up to 3 orientations (fig.1.a) due to the symmetry axis of the third order of L_3.

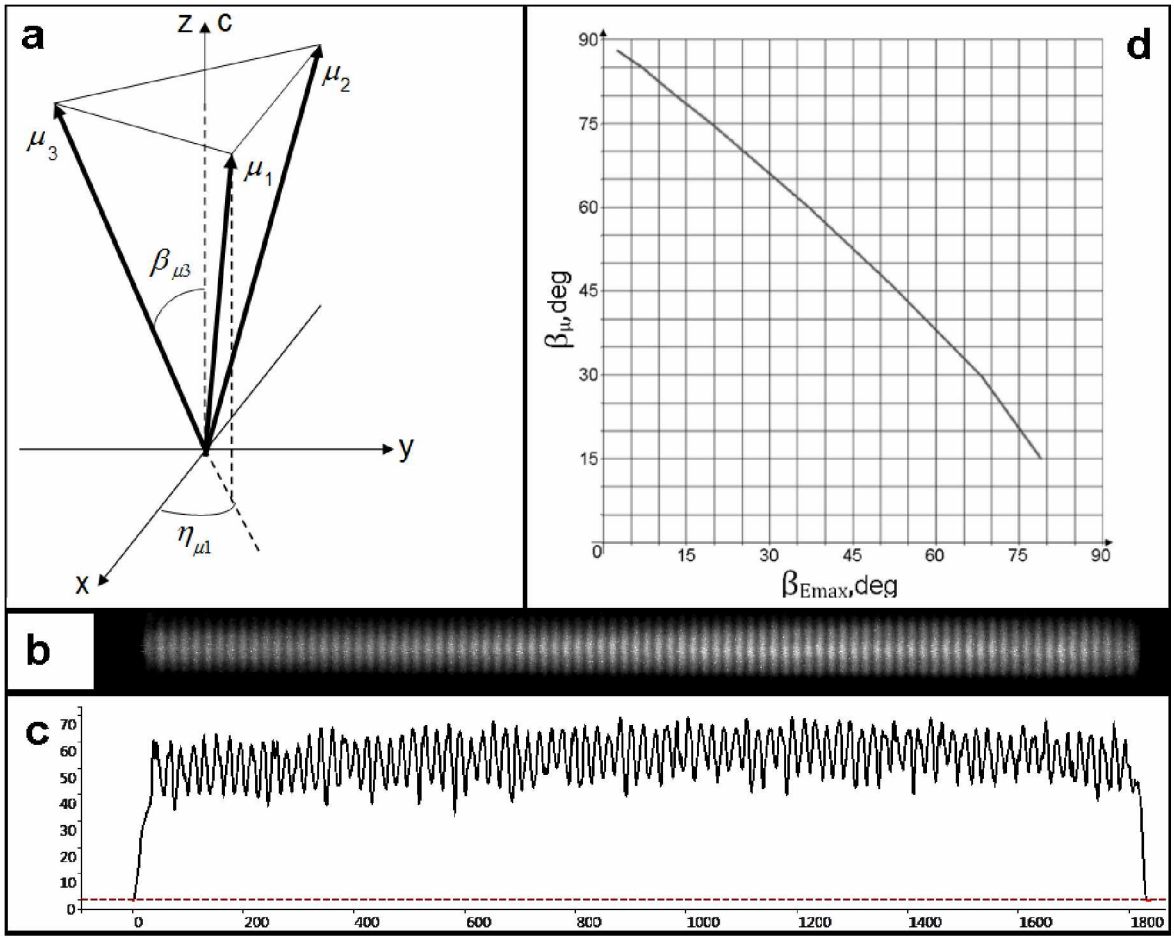

Fig. 1 a - A possible variant of the orientation of the dipole moments of the transitions in the crystal with a point symmetry group D_{3d}; b - photo of a spatially periodic distribution of the luminescence intensity of the sample were obtained; c - section of the luminescence intensity; d - plot of the angle β_{Emax} versus β_μ.

In the experiment, the luminescence excitation is perpendicular to the optical axis of the crystal. Monitoring was carried out perpendicular to the laser beam at an angle of 45° to the optical axis of the crystal. Photographs of a spatially periodic distribution of the luminescence intensity of the sample were obtained (fig.1.b) at different orientations of the electric vector β_E about the optical axis of the crystal. To determine the depth of the luminescence intensity modulation by means of the program «MultiVox DICOM Viewer» section of the luminescence intensity is obtained for each photo received (fig.1.c). By simple mathematical calculations defined angle β_{Emax} - the angle of rotation of the electric vector with respect to the optical axis of the crystal, corresponding to the maximum value of the depth of the luminescence intensity modulation.

On fig.1.d shows a plot of the angle β_{Emax} versus β_μ (fig.1.a). This graph is obtained by mathematical modeling. Comparing the experimentally obtained value β_{Emax} with this plot, we get the value of the orientation angle of the test color centers in the crystal matrix.

Thus, in this paper, the correspondence between the luminescence intensity modulation depth and orientation of the dipole moments of quantum transitions were defined by theoretical methods. The new method of measuring the orientation of the quantum systems in crystalline media was developed and experimentally tested.

This work was supported by the project II.10.1.6 of Programs FNI of State Russian Academies, project number 3833 of ISU State Assignment and RFBR grant № 16-52-44056 Mong_a.

References

[1] P.P. Feofilov «Polyarizovannaya lyuminestsentsiya atomov, molekul i kristallov», M: Gos. izd-vo fiz.-mat. lit-ry, str. 198 (1959).

[2] M.Ye. Springis «Primeneniye metoda polyarizatsionnykh otnosheniy dlya issledovaniya tochechnykh defektov v kristallakh a-Al_2O_3» - Izvestiya AN Latv. SSR, Seriya fiz. i tekh. nauk, **№4**, str. 38 (1980).

[3] E.F. Martynovich «Tsentry okraski v lazernykh kristallakh», - Irkutsk: Izd-vo Irkut. un-ta - str. 150 (2004).

[4] Martynovich E.F., G. Petite, V.P. Dresvianskiy, A.A. Starchenko, Appl. Phys. Lett. **84**, p 4550 (2004).

Polarizational dependence of recoil-induced resonances

David Lazebny[1,2], Denis Brazhnikov[1], Alexey Taichenachev[1,2], Valery Yudin[1,2,3]
[1] *Institut of Laser Physics SB RAS, Lavrent'eva 13/3, Novosibirsk 630090, Russia*
[2] *Novosibirsk State University, Pirogova 2, Novosibirsk 630090, Russia*
[3] *Novosibirsk State Technical University, Karla Marksa 20, Novosibirsk 630073, Russia*
E-mail: becks.ddf@gmail.com

Laser cooling of atoms using magneto-optical trap is an essential part of modern atomic physics [1,2]. In order to measure temperature of cold atoms and their function of distribution methods of nonlinear spectroscopy are widely used. One of such methods is based on the so-called recoil-induced resonances which were predicted in the work [3] for the first time and were observed in this work [4]. In our work we described theoretically the most general case of recoil-induced resonances for arbitrary polarization of fields forming recoil-induced resonances and for arbitrary dipole allowed transition, since in previous works all analysis was down to either simplified two-level models or transition for certain values of momenta for ground and excited states or for concrete polarizations of fields.All calculations were provided for two different cases. In the first case cold atoms were supposed to be free and in the second one they were considered in the working magneto-optical trap which definitely had a significant impact on polarization dependence of recoil-induced resonances.

The main results of the work are:

1. For any closed dipole transition we got explicit analytical expressions for polarization dependence of magnitude of recoil-induced resonances as for the case of free atoms and for atoms in the magneto-optical trap. Max and min values were gotten.
2. In working trap contributions associated with orientation and alignment are suppressed because of averaging over parameters of local polarization vector of field of trap. One can easily retrieve information about an average value of multipole momenta of atom in magneto-optical trap from polarization measurements.
3. Theory can be generalized subject to real hyperfine structure.

The work was supported by the Ministry of Education and Science of the Russian Federation (State Assignment No. 2014/139, Project No. 825), by the grant of President of the Russian Federation (NSh- 6689.2016.2), by the Russian Foundation for Basic Research (grant nos. 14-02-00712, 14-02-00939, 15-32-20330, 15-02-08377, 16-32-00127).

References

[1] H. J. Metcalf and P. Straten, J. Opt. Soc. Am. B 20, 887 (2003).
[2] V.I. Balykin, V.G. Minogin, and V.S. Letokhov, Rep. Progr. Phys. **63**, 1429 (2000).
[3] J. Guo, P. R. Berman, B. Dubetsky, and G. Grynberg, Phys. Rev. A **46**, 1426 (1992).
[4] J. Courtois, G. Grynberg, B. Lounis, and P. Verkerk, Phys. Rev. Lett. **72**, 3017 (1994).

Laser pumped ^{4}He magnetometer with light shift suppression

S. Li, X. Peng*, Z. Lin, H. Wang, and H. Guo†

State Key Laboratory of Advanced Optical Communication Systems and Networks, School of Electronics Engineering and Computer Science, and Center for Quantum Information Technology, Peking University, Beijing 100871, P. R. China

*E-mail: xiangpeng@pku.edu.cn

†E-mail: hongguo@pku.edu.cn

Laser-pumped atomic magnetometer has been well developed and exhibits higher sensitivity compared with the lamp-pumped type. As light shift transfers the laser frequency or intensity fluctuations to the magnetic-field measurement results, high-sensitivity atomic magnetometer requires the optical frequency stabilized to suppress the light shift. Commonly, those schemes need additional atomic reference cells and experimental setup, which makes the atomic magnetometer system less compact. More importantly, since the parameters of reference cells[1] are inconsistent with those of atomic sensor the laser center frequency is difficult to be locked to the desired point automatically, which essentially causes systematic errors. Light shift can induce the atomic alignment to orientation conversion (AOC) effect[2]. This effect can deviated the left-circularly MODR signal I_L and right-circularly MODR signal I_R. We use the different signal to control the laser frequency.

The experimental setup of our laser pumped ^{4}He magnetometer is illustrated schematically in Figure1, which is under the conventional MODR configuration. A linearly polarized light derived from a DFB (Distributed Feedback) fiber laser, is used for optically pumping and aligning the metastable state of ^{4}He excited by a 33 MHz radio frequency discharge in a 45 mm long and 30 mm diameter atomic vapor cell (at room temperature, 0.3 Torr). The cell is placed in the center of a five-layer μ-metal magnetic shield. A constant magnetic field B_0 is generated by a solenoid. The magnetic field is set around the geomagnetic field value. The MODR signals are driven by a weak oscillating magnetic field B_1, which is generated by a pair of Helmholtz coils.

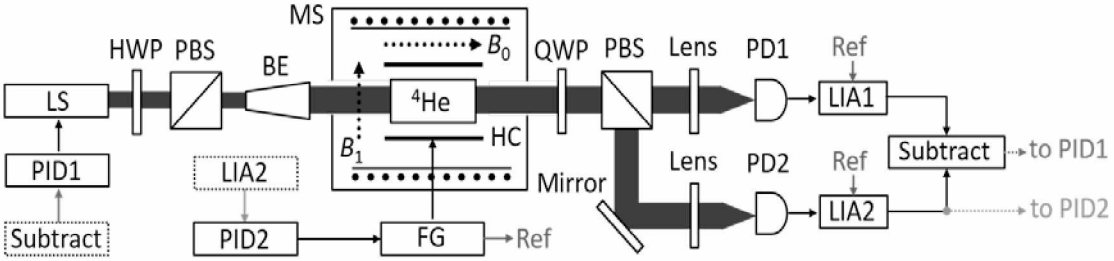

Fig. 1 The Experimental setup of the laser-pumped magnetometer with light shift suppression. LS, laser source; HWP, half-wave plate; PBS, polarization beam splitter; BE, beam expander; MS, magnetic shield; HC, Helmholtz coil; QWP, quarter wave plate; PD, photodiode; PID, Proportion-Integration-Differentiation; LIA, lock-in amplifier. FG, function generator; Ref, demodulation reference frequency.

In order to observe the two signals (I_L and I_R) simultaneously, a circular analyzer which consists of the QWP and the PBS is used in the experiment. The fast axis of the QWP is set at 45° with respect to thepolarization axis of the PBS. With this structure, the two circular components of the linearly polarized laser light can be transformed into two orthogonally linearly polarized light fields after passing the QWP, which can be exactly reflected or transmitted by the PBS and detected independently.

We then adopt the magnetometer system with stabilized laser frequency to monitor the magnetic field variations inside the magnetic shield over more than 300 s. Fig. 2 shows the sensitivity of the

magnetometer, which reaches a noise floor of about 3 pT/Hz$^{1/2}$ above 10 Hz. There exists a noise peak at 50 Hz due to the magnetic field noise in the lab.

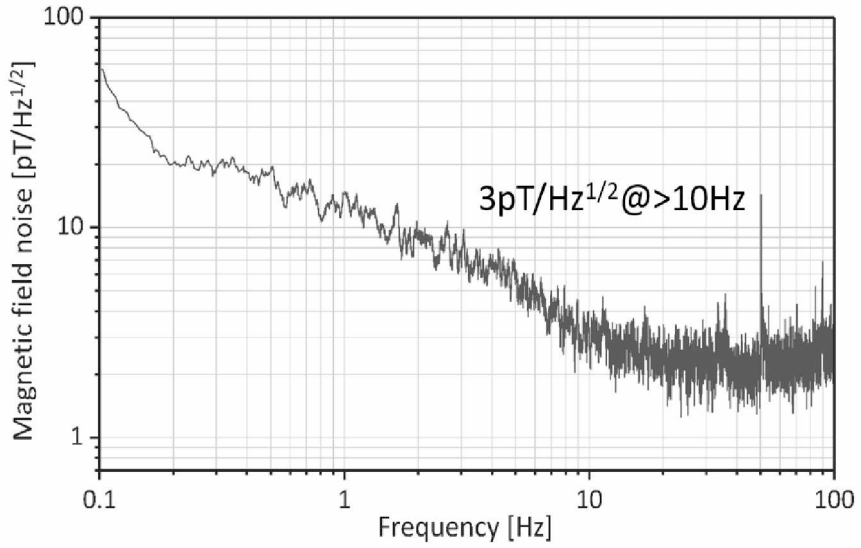

Fig. 2 The measured magnetic field sensitivity of the laser-pumped magnetometer, of which the laser frequency is stabilized.

References

[1] T. Zelevinsky, D. Farkas, and G. Gabrielse, Phys. Rev. Lett. **95**, 203001 (2005).
[2] M. Auzinsh, D. Budker, S. M. Rochester, Oxford University Press, Oxford, 2010.

Investigation of mixed gas sensing based on fiber ring intracavity absorption laser

Kun Liu, Lin Yu, Junfeng Jiang, Tao Wang, Meng Xue, Tiegen Liu
[1]*College of Precision Instrument and Opto-Electronics Engineering, Tianjin University, Tianjin China and Key Laboratory of Opto-Electronics Information Technical (Tianjin University), Ministry of Education, Tianjin 300072, China*
E-mail: beiyangkl@tju.edu.cn

Aiming at the requirement of monitoring gas pollutants in real time in the fields of industrial production and environmental protection, we investigate the gas sensing technique based on fiber laser intracavity absorption spectroscopy. After conducting the theoretical analysis of intracavity gas sensing, we construct the mixed gas sensing system which has a ring cavity structure and operates in C+L band. By combining intracavity absorption with wavelength sweep and modulation, we realize the sensitive detection of the mixed gases of C_2H_2, CO and CO_2. In order to solve the problem of spectral overlap in mixed gas sensing, we proposed a method to separate the overlapping absorption lines rapidly, then their respective absorbance distribution can be retrieved. Considering the nonlinear and creeping characteristics occurred in the wavelength tuning process using the scanning laser source in our sensing system, we use the wavelength reference gas cell for laser wavelength calibration. The gas cell is filled with multiple gases and the absorption lines of each gas locate in one band of the laser source. The absorption wavelengths of different gases are used as the real-time wavelength reference and have good temperature stability. As a result, the accurate wavelength calibration of scanning laser source is realized in the wide tuning range and temperature range. The minimum detectable concentrations are 0.6 ppm，17.4 ppm and 19.2 ppm respectively, and the maximum errors of CO and CO_2 are reduced to 35% and 42% of the errors without using the method.

Hybrid structures with InAs/AlGaAs quantum dots strongly coupled to plasmonic bowtie nanoantennas

A.A. Lyamkina[1], K. Schraml[2], A.K. Bakarov[1], M. Kaniber[2], S.P. Moshchenko[1]
[1]*A.V. Rzhanov Institute of Semiconductor Physics SB RAS, Lavrentieva, 13, Novosibirsk 630090, Russia*
[2]*Walter Schottky Institut, Technische Universit¨at M¨unchen, Am Coulombwall 4,Garching 85748, Germany*
E-mail: lyamkina@isp.nsc.ru

Deterministically integrating semiconductor quantum emitters with plasmonic nano-devices paves the way towards chip-scale integrable, true nanoscale quantum photonics technologies. For this purpose, stable and bright semiconductor emitters are needed, which moreover allow for CMOS-compatibility and optical activity in the telecommunication band. Here, we demonstrate strongly enhanced light-matter coupling of single near-surface (< 10nm) InAs quantum dots monolithically integrated into electromagnetic hot-spots of sub-wavelength sized metal nanoantennas.

In this work structures with proximal InAs/AlGaAs QDs (distance to surface of 10 nm) grown in Stranski-Krastanov mode were studied. On the structure surface a periodical array of gold bowtie antennas was formed by electron lithography. Bowtie parameters were chosen to provide a spectral overlap of plasmon resonance and QD emission band [1,2]. Bowtie triangle size of 100 nm and the gap of 5 nm were verified by scanning electron microscopy (SEM) measurements. Microphotolumenescence (micro-PL) measurements were conducted with the excitation laser wavelength of 850 nm. As self-assembled QDs are randomly distributed, the part of QDs that strongly interact with antennas is low. On the map of integral intensity of micro-PL of 15x15 μm three QDs with an optical signal that exceeds average by an order of magnitude were observed. Laser reflection scan demonstrates a periodic structure with parameters corresponding to SEM image of antennas. The correlation of positions of high intensity QDs with maximums of laser reflection indicates that that QDs are located directly under nanoantennas.

Micro-PL spectra were measured for different polarizations in the detection channel relative to bowtie main axis. Spectra of a QD with high intensity were measured in co-polarization and cross-polarization that are parallel and perpendicular to the bowtie axis respectively. The maximum PL intensity for these polarizations was differed by a factor of 16 compared to a reference QD located out of the bowtie field. The proximity to a bowtie antenna dramatically changes the QD emission pattern from an isotropic one to a dipole pattern with the degree of polarization of 86%.

The micro-PL dynamics reveals a decrease of the exciton life-time for the QDs interacting with antennas by a factor of 3.5 that was limited by the setup resolution. Therefore the increase of micro-PL intensity, strong polarization dependence and the decrease of the life-time confirm that there is strong exciton-plasmon interaction between proximal QDs and nanoantennas.

In summary, we demonstrated pronounced light-matter-coupling of bright (16x enhanced) and fast (< 200 ps), monolithically integrated, semiconductor InAs quantum dots positioned 10nm below small feed-gap (25nm) lithographically defined Au bowtie nanoantennas, resulting in Purcell-factors > 3.5.The obtained results open the door to the control over emitter properties in hybrid metal-semiconductor nanostructures.

The work was supported by RFBR via grant 16-37-60075. AAL acknowledges the financial support via RF president scholarship (SP-3014.2016.3).

References

[1] K. Schraml, M. Spiegl, M. Kammerlocher et al, Phys. Rev. B **90**, 035435 (2014)
[2] A. Regler, K. Schraml, A.A. Lyamkina et al., J. Nanophoton. **10(3)**, 033509 (2016)
[3] A.A. Lyamkina, S.P. Moshchenko, D.V. Dmitriev et al, JETP Letters, **99(4)**, 219 (2014).

Coupling of monolithically integrated quantum dots to V-groove based plasmonic nanostructures

A.A. Lyamkina, L.S. Basalaeva, S.P. Moshchenko
A.V. Rzhanov Institute of Semiconductor Physics SB RAS, Lavrentieva, 13, Novosibirsk 630090, Russia
E-mail: lyamkina@isp.nsc.ru

Plasmonic waveguides are commonly considered as promising candidates for integral photonic nanostructures as they allow to concentrate electric field on a scale below the light wavelength and therefore significantly reduce geometrical size of these structures. A possible scheme of plasmonic waveguides is based on fabrication of a narrow V-groove channel in a metal substrate [1]. Recently this concept was successfully transferred to silicon wafers and V-groove channels with crystallographic planes (111) were formed by UV-photolithography followed by chemical etching [2]. Thin gold film was then deposited by means of electron beam evaporation. Obvious advantages of this technique are technological simplicity that enables producing highly reproducible channels and possible implementation for integral hybrid structures. On the other hand, fabrication of a channel that is faceted with crystallographic planes limits the waveguide geometry including bending to an arbitrary angle.

This geometrical limitation to a waveguide configuration can be overcome with chains of metal nanoparticles. When chain parameters are optimized, plasmonic modes can propagate over large distances with extremely low losses [3]. In this work plasmonic waveguides based on nanopyramids formed in nanoholes chemically etched in silicon and GaAs are theoretically investigated. Such geometry also allows to form pyramid-like nanoantennas and highly efficient plasmonic waveguides in a close proximity to monolithically integrated quantum dots (QDs) and other quantum emitters for integral photonic chips.

Numerical simulations of plasmonic waveguides were carried out within the discrete dipole approximation [4]. Parameters of metal particles were set regarding realistic geometry of nanoholes that were formed in silicon substrates by electronic beam lithography with subsequent selective chemical etching. An important feature of this work is modification of individual particle geometry by turning a lithographical pattern relative to crystallographic axes. Dependence of chain waveguide transmission on a particle geometry and interparticle distance is studied. It is shown that chains of elongated pyramids enable highly efficient transmission of a signal from a point dipole source. Due to localized plasmon resonance nature these waveguide are essentially frequency selective and varying particle parameters the waveguide band can be designed to increase signal to noise ratio. Dependence on QD position is studied and the hybrid structure is optimized to perform strong exciton-plasmon interaction. Results obtained could be used for integral hybrid schemes based on semiconductor substrates with monolithically integrated quantum emitters.

The work was supported by RFBR via grant 16-37-60075 and 16-32-00269. AAL acknowledges the financial support via RF president scholarship (SP-3014.2016.3).

References

[1] S.I. Bozhevolnyi et al., Nature **440**, 508 (2006).
[2] C.L.C. Smith et al., Nano Lett. **14**, 1659 (2014).
[3] I.L. Rasskazov, S.V. Karpov, V.A. Markel, Opt. Lett. **38**, 4743 (2013).
[4] M.A. Yurkin and A.G. Hoekstra, J. Quant. Spectrosc. Radiat. **112**, 2234 (2011).

Generation of a laser-plasma ion flow in a microwave cavity

A.E. Medvedev, G.N. Grachev
Institute of Laser Physics SB RAS, Russia
E-mail: medvedev@laser.nsc.ru

Atmospheric-pressure gas discharges occupy an ever greater place in practical applications. Some of their obvious properties make it possible to consider atmospheric glow discharge plasma as a platform of the 21st century technologies [1]. To increase the specific energy contribution and homogeneity of plasma, high-frequency power supply sources are used. Magnetron microwave generators are highly efficient and have no competitors in simplicity and reliability. In this paper, a possibility of using microwave-range electric energy to accelerate ions of optical pulsating discharge (OPD) laser plasma for non-vacuum surface-treatment technologies is considered [2].

The electric field does not penetrate into dense laser-plasma, and all voltage applied to the gap (U) drops across the screening layer $l \approx r_D (1+U/T)^{1/2}$ formed by positive ions (where r_D is the Debye length and T is the plasma temperature). The thickness of the screening layer at atmospheric pressure does not exceed the free path length. For a not too high frequency of the external source, when the oscillation amplitude of electrons (a) is greater than l, the electrons will reach the electrode. Then, owing to the semiconductor properties of the plasma-conducting body interface, at the screening layer there will be direct voltage needed for ion acceleration, in addition to alternating voltage. It is well-known that in high-frequency discharge plasma as the gas pressure and field frequency rise, the direct voltage at near-electrode layers drops, and interaction with the surface in the microwave frequency range is not observed. However, for plasma density more than 10^{13} cm^{-3} at an external generator frequency not higher than 10 GHz the condition $a>l$ is satisfied. It follows from our estimates that in the microwave field the OPD plasma ($10^{13}\div10^{18}$ cm^{-3}) ions will interact with the surface with energy of up to several hundred eV.

An analysis was made to test experimentally the possibility of obtaining, on the basis of OPD, an ion flow at atmospheric pressure and using it in the surface treatment technology. The motion of particles was simulated. The plasma was considered as an electrode under a floating potential located in the gap with an alternating field. On the basis of the analysis results, calculation and design of a toroidal cavity resonator were made. The cavity was located on a technological head forming a laser beam and a gas flow. Laser plasma is initiated in the gap of the toroidal resonator capacitor. The gap is formed by a conducting plate and the resonator head. This allows free motion of the plasma with the microwave field along the surface being treated. The energy input to the cavity from the pulsed microwave generator of a frequency of 2,47 GHz and a power of up to 3 kW is synchronous with the laser pulsed radiation.

The results of measurements of microwave characteristics of the technological head are described. Preliminary experiments on the action of OPD plasma in the electric field on the surface being treated are presented.

References

[1] Roth J.R., Nourgostar S., Bonds T.A., IEEE Trans. Plasma Sci. 2007. V. 37, P. 233.
[2] Bagaev S.N., Grachev G.N., Ponomarenko A.G. et al., Russian-French-German Laser Symposium 2009, P. 65.

Characterization of Er^{3+}/Yb^{3+}- and Yb^{3+}- doped tungsten tellurite glasses

M. Merzliakov[1,2], V. Kouhar[3], G. Malashkevich[3], and E. Pestryakov[1,2]
[1] *Institute of Laser Physics SB RAS, Novosibirsk 630090, Russia*
[2] *Novosibirsk State University, Novosibirsk 630090, Russia*
[3] *B.I. Stepanov Institute of Physics of the National Academy of Sciences of Belarus, Minsk* 220072, *Belarus*
E-mail: mm@laser.nsc.ru

Tungsten tellurite glass (TW-glass) is caused a growing interest because of unique combination of properties [1-3]. Glasses of the TeO_2-WO_3-$(Er, Yb)_2O_3$ system had been synthesized and their spectral-luminescent properties were investigated to evaluate the prospects for lasing. Judd-Ofelt intensity parameters have been determined from measured and calculated absorption transitions of Er^{3+} from the ground state to ($^4F_{5/2}$ & $^4F_{3/2}$) band, ($^4F_{7/2}$ & $^2H_{11/2}$ & $^4S_{3/2}$), $^4F_{9/2}$, and $^4I_{9/2}$. This made it possible to determine the radiative lifetime of $^4I_{13/2}$ level, absorption, emission, and gain cross section in the 1.53 μm band. The minimum value of inversion parameter was found to be 0.2. We model the population of the energy levels to determine the minimum pump intensity to the inversion parameter becomes equal to 0.2.

Partial Er^{3+}:Yb^{3+} energy level system as well as the relevant energy transfer between the Yb^{3+} and Er^{3+} ions are presented in Fig. 1. The resonant energy transfer corresponds to a de-excitation of an Yb^{3+} ion from its excited state $^2F_{5/2}$ to the ground state $^2F_{7/2}$ and an excitation of a neighboring Er^{3+} ion from its ground state $^4I_{15/2}$ to the upper state $^4I_{11/2}$. Due to the very short lifetime of the upper state (W_{32} ~150000 s^{-1} is typical for $^4I_{11/2}$ ~~> $^4I_{13/2}$ in Er^{3+} doped glass) a quick relaxation to the metastable Er^{3+} state $^4I_{13/2}$ takes place and, thus, any back-transfer of energy is suppressed.

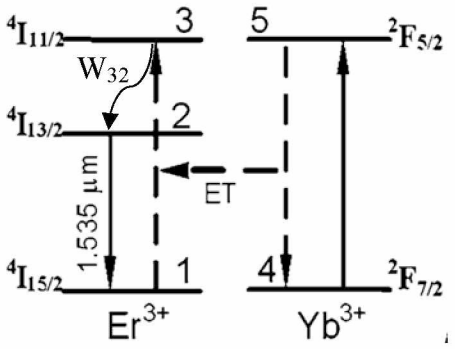

Fig. 1 Simplified energy level diagram of the co-doped Er^{3+}:Yb^{3+} TW-glass system.

The corresponding rate equations without any upconversion processes, energy back-transfer, without absorption of pump light by the Er^{3+} ions, and for low pump intensity can be expressed as

$$\partial N_2/\partial t = W_{32} N_3 - W_{21} N_2 \quad (1a)$$

$$\partial N_3/\partial t = \sigma_{13} \varphi_p N_1 + K_{tr} N_5 N_1 - W_{32} N_3 \quad (1b)$$

$$\partial N_5/\partial t = \sigma_{45} \varphi_p N_4 - K_{tr} N_5 N_1 - W_{54} N_5 \quad (1c)$$

$$N_1 + N_2 + N_3 = N_{Er} \quad (1d)$$

$$N_5 + N_4 = N_{Yb} \quad (1e)$$

where t represents the time, N_i is the concentration of ions in the *i-th* state, N_{Er}, N_{Yb} - concentration of Er and Yb ions, W_{ij} represents the rate transition from *i-th* to *j-th* state, σ_{ij} – cross section of $i \rightarrow j$ transition, K_{tr} – cross-relaxation from Yb^{3+} to Er^{3+} coefficient, $\varphi_p = I_p/h\nu$, I_p pump intensity, $h\nu$ –energy of pump photon.

Using this model and experimental spectroscopic data, we have determined the minimum pump intensity and cross-relaxation coefficient K_{tr} for the sample of Er^{3+}:Yb^{3+} TW-glass consisting of $60TeO_2$-$25WO_3$-$14Yb_2O_3$-Er_2O_3 (mol.%).

References

[1] E. Anashkina, A. Andrianov, V. Dorofeev et al., Applied Optics **55**, 4522 (2016).
[2] V. Dorofeev, A. Moiseev, M. Churbanov et al., Optical Materials **33**, 1811 (2011).
[3] G. Malashkevich, N. Ovcharenko, T. Smirnova et al., *Fizika i Khimiya Stekla*. **13**, 866 (1987).

Control of the electron dynamics in atomic ionization by an ultrashort two-color laser pulse for enhanced ultrahigh-order harmonic generation

O. Meshkov[1,2], M. Emelin[2], and M. Ryabikin[2]
[1]*Lobachevsky State University of Nizhny Novgorod, 603950 Nizhny Novgorod, Russia*
[2]*Institute of Applied Physics of the Russian Academy of Sciences, Nizhny Novgorod 603950, Russia*
E-mail: mike@ufp.appl.sci-nnov.ru

The advent of high-power midinfrared femtosecond laser sources has opened up new perspectives in the research of strong-field laser-matter interactions. One of the most impressive benefits of using mid-IR sources to drive the processes associated with laser-induced ionization is a dramatic extension of the plateau in the spectrum of photons produced via high-order harmonic generation (HHG) in gases [1]. The extension of the plateau produced with longer-wavelength driving lasers is due to the proportionality of the electron ponderomotive energy to the square of the laser wavelength. However, the efficiency of harmonic generation by individual atoms is known to scale unfavorably (as λ^{-5-6} [2]) with the laser wavelength; this is caused to a large degree by a decrease in the probability of electron recollision with the parent ion due to the larger free-electron wave-packet spreading in a lower-frequency laser field. It was demonstrated that this loss of efficiency can be substantially compensated for by implementing phase-matched HHG at high gas pressures and large interaction lengths using gas-filled waveguides [1]; the capability of this approach is, however, limited by the requirement of very low ionization level of a gas leading to limitations on the laser intensity to be used. A search for alternative approaches to increase harmonic yields is therefore a topical issue. One of the most promising approaches is to use multifrequency laser fields to facilitate favorable phase-matching conditions and/or to maximize harmonic emission from each particle of a gas. Recently, different schemes were proposed to achieve these goals using two- or three-color driving fields [3–6]. Most of these approaches relied on the use of many-cycle laser pulses; the physical origin of the yield enhancement on a single-atom level was usually explained in terms of the peculiarities of the free-electron behavior in a multicolor field.

In this contribution, we studied the possibility to enhance the efficiency of HHG using few-cycle optical waveforms obtained by superposing two laser pulses of different color delayed optimally relative to each other. A wide range of laser intensities has been addressed. Special attention was paid to the dynamics of the depopulation of atomic states, which, one the one hand, promotes electrons to the continuum to take part in the high-energy photon emission, but, on the other hand, depletes the nonlinear medium. The use of above-mentioned waveforms gives extra flexibility compared to the single-color case to control the bound-state depopulation and the electron acceleration in the continuum. The study was carried out using the quantum-mechanical treatment of HHG within the strong-field approximation [7] modified properly to adequately take into account the depletion of atomic states. Both frequency components of the laser pulse were considered linearly polarized along the same axis, whereas the total electric field of the synthesized waveform was taken as

$$E(t) = E_1 \cos[\omega_1 (t+\tau) + \phi] \exp\left[-2\ln 2 \frac{(t+\tau)^2}{\tau_1^2} \right] + E_2 \cos(\omega_2 t) \exp\left(-2\ln 2 \frac{t^2}{\tau_2^2} \right),$$

where E_1, ω_1, τ_1 and E_2, ω_2, τ_2 are the field amplitude, frequency, and duration of the 1st and 2nd pulse, respectively; τ is the delay between two pulses and ϕ is an additional phase shift of the 1st pulse. Both strong- and moderate-intensity regimes have been explored, which correspond to strong and weak ionization cases, respectively; the latter case is more favorable in terms of phase matching. The parameters of the laser pulses were optimized to provide the maximal harmonic yield within a given range of harmonic photon energies. Typical results for the above two cases are shown in Fig. 1 (left and right panels, respectively). These results demonstrate usability of the approach proposed here to increase by up to order of magnitude the efficiency of optical frequency conversion into sub-keV or few-keV photon energy ranges.

High efficiency of HHG in optimal conditions presented in Fig. 1 is explained by the peculiarities of the photoelectron dynamics, which are in these cases characterized by a combination of high-probability release of the electron responsible for highest-order harmonic production and its subsequent strong acceleration accompanied by a relatively low probability of the bound-state depletion during the time interval between ionization and recollision. Similar results were reported by us earlier for the case of HHG driven by nonlinearly chirped few-cycle laser pulses [8].

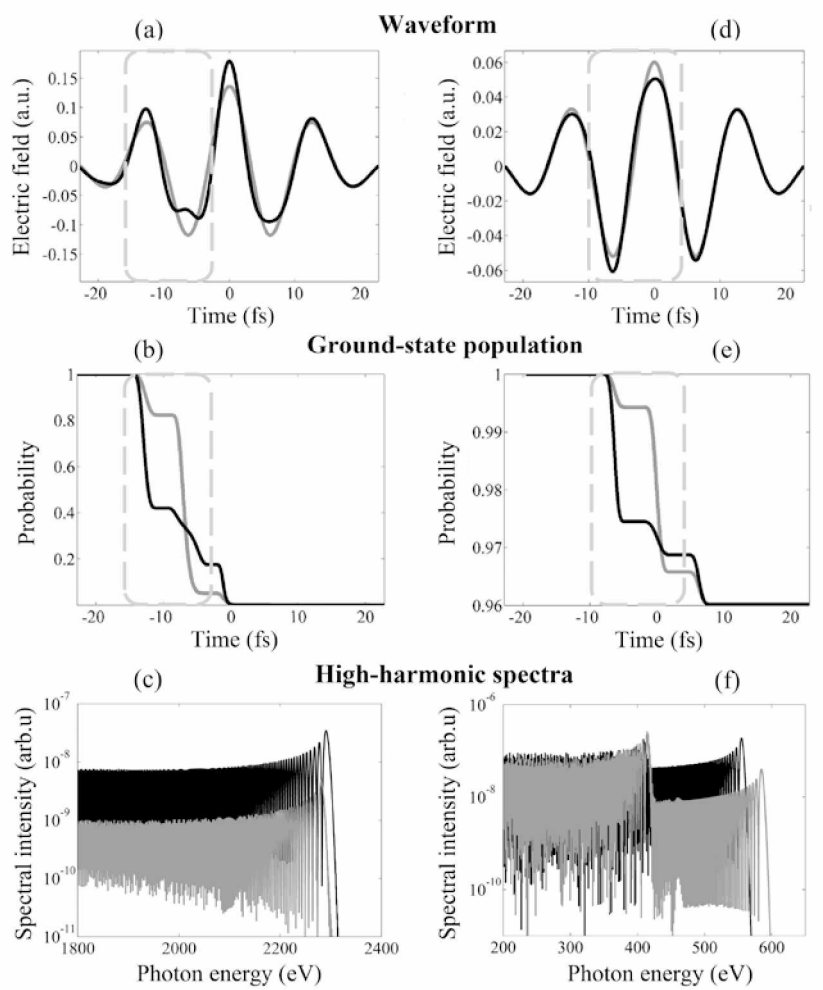

Fig. 1 (a) Time profile of the laser electric field, (b) time dependence of the atomic ground-state population, and (c) high-energy part of the HHG spectrum for a hydrogen atom driven by a single-color (λ=3,9 μm, grey line) and two-color (λ_2=3,9 μm, λ_1=1,95 μm, black line) few-cycle laser pulse. FWHM of the 3,9 μm pulse is 1,5 cycles; the values of other parameters (see text) are chosen to maximize the harmonic yield between 2100 and 2300 eV: I=6,5×10^{14} W/cm^2 (single-color field), I_2=6,5×10^{14} W/cm^2, I_1=7,5×10^{13} W/cm^2, τ_1=2,1 T_1, τ=0,25 T_2, ϕ=0 (two-color field); $T_{1,2}=\lambda_{1,2}/c$. Dashed line outlines the region responsible for the formation of the spectra shown. (d-f) Same as (a-c) but with the constrain imposed on the ionization level to not exceed 4%; the laser parameters are chosen to maximize the harmonic yield between 500 and 600 eV: I=1,27×10^{14} W/cm^2 (single-color field), I_2=1,25×10^{14} W/cm^2, I_1=4,0×10^{12} W/cm^2, τ_1=1,5 T_1, τ=0,25 T_2, ϕ=0 (two-color field).

References

[1] T. Popmintchev, M. Chen, D. Popmintchev et al., Science **336**, 1287 (2012).
[2] J. Tate, T. Auguste, H. G. Muller et al., Phys. Rev. Lett. **98**, 013901 (2007).
[3] E. J. Takahashi, P. Lan, O. D. Mücke et al., Nat. Commun. **4**, 2691 (2013).
[4] C. Jin, G. Wang, H. Wei1et al., Nat. Commun. **5**, 4003 (2014).
[5] S. Haessler, T. Balčiunas, G. Fan et al., Phys. Rev. X **4**, 021028 (2014).
[6] A. S. Emelina, M. Yu. Emelin, R. A. Ganeev et al., Opt. Express **24**, 13971 (2016).
[7] M. Lewenstein, Ph. Balcou, M. Yu. Ivanov et al., Phys. Rev. A **49**, 2117 (1994).
[8] A. A. Silaev, O. V. Meshkov, M. Yu. Emelin et al., Quantum Electron. **45**, 393 (2015).

Exitation of a broadband terahertz radiation by femtosecond laser pulses in poled nonlinear optical polymers

S.L. Mikerin, A.I. Plekhanov, A.E. Simanchuk, A.V. Yakimansky
Institution or Organization: Institute of Automation and Electrometry SB RAS, Novosibirsk, Russia
E-mail: mikerinsl@iae.sbras.ru

Reported on the use of new nonlinear optical polymer material based on polyimide with chromophore DR-13 for generating terahertz pulses. A short THz pulses (a few field oscillations) are excited through an optical rectification in 1-μm-film with amplitude per unit of thickness 200 times greater than in the ZnTe crystal with a thickness of 500 μm.

Continuous-wave fiber optic parametric oscillators: impact of dispersion inhomogeneities

V. Mishra[1], E. A. Zlobina[2], S. I. Kablukov[2], S.P. Singh[1], S. K. Varshney[1,3] and S. A. Babin[2,4]
[1]*Dept. of Physics, Indian Institute of Technology Kharagpur-721302, India*
[2]*Institute of Automation and Electrometry SB RAS, Novosibirsk, Russia*
[3]*Dept. of E&ECE, Indian Institute of Technology, Kharagpur-721302, India*
[4]*Novosibirsk State University, Novosibirsk, Russia*
E-mail: vishwatoshmihra34@gmail.com

Parametric four wave mixing (FWM) is an attractive process for nonlinear frequency conversion in optical fibers. Fiber optical parametric oscillators (FOPOs), utilizing the FWM principles, offer an opportunity to generate efficient tunable laser radiations in new spectral ranges, where the conventional fiber lasers are not available, in particular, in short-wavelength region, <1 μm. This region is particularly attractive for biological nonlinear microscopy - optical coherence tomography and coherent Raman scattering microscopy. All-fiber optical parametric oscillators operating below 1 μm usually comprise photonic crystal fiber (PCF) pumped by an Yb-doped fiber laser. Recently, we have demonstrated CW FOPO in such configuration with wavelength tuning from 923 to 1005 nm [1]. Shorter wavelengths generation was limited by greatly increasing FOPO threshold power at large parametric frequency shifts. This effect might be due to the influence of pump linewidth and fiber longitudinal dispersion inhomogeneity on the parametric gain which reduces the integral gain inside the FOPO cavity. Few approaches in the past have been reported to understand the effect of dispersion fluctuations on the net parametric gain in fiber parametric amplifiers [2, 3]. However, the impact of dispersion fluctuations on the CW FOPO parameters (threshold and output power, slope efficiency) has not been studied yet.

In the present work, a numerical simulation model of the oscillator according to FOPO theory [4] has been developed to account the impact of fiber inhomogenities on the performance of both polarization maintaining (PM) and non-PM FOPOs. The FOPOs were assembled using a 18-m long PM PCF (LMA-5-PM) from NKT photonics [1]. Ring cavity was formed by specially selected standard (for non-PM configuration) or PM (for PM configuration) wavelength division multiplexers (WDMs) used to launch the Stokes wave back into the cavity and remove the anti-Stokes wave outside it.

The pump power threshold of the FOPOs was calculated using the spectral variation of the cavity losses (see Fig. 1a). For the homogeneous fiber, the variation of P_{th} follows the analytical relation [4] given as,

$$P_{th} = (\gamma L)^{-1} \cosh^{-1}\left(1/\sqrt{T}\right) \quad , \tag{1}$$

where γ=10 (W.km)$^{-1}$ is the fiber nonlinear parameter, L = 18 m is the fiber length, T is the round trip cavity transmittance. Calculated P_{th} is shown in Fig. 1b along with the experimental data shown by points. One can see, that experimental P_{th} value is much higher at the shorter wavelengths than the theoretical one. We assume that it is due to the longitudinal dispersion fluctuations along the fiber.

The PM PCF supports two polarization modes and each mode has slightly different zero dispersion wavelength (ZDW). ZDWs for the fast- and slow-axis modes are 1052.95 and 1051.85 nm, respectively. The efficient parametric generation occurs when the phase matching condition is satisfied,

$$\beta_2(\omega_p)\Omega^2 + \beta_4(\omega_p)\Omega^4/12 + 2\gamma P = 0 \tag{2}$$

where the symbols have their usual meaning [1, 4]. The values $\beta_2(\omega_p)$ and $\beta_4(\omega_p)$ are expanded according to Taylor series, in terms of constants β_{03} and β_{04} at the ZDW:

$$\beta_2(\omega_p) = \beta_{03}(\omega_p - \omega_0) + \beta_{04}(\omega_p - \omega_0)^2/2 \qquad \text{and} \quad \beta_4(\omega_p) = \beta_{04} \tag{3}$$

In our calculations, we have considered β_{03} = 6.755×10^{-2} ps^3/km, β_{04} = -1.001×10^{-4} ps^4/km. In order to model the longitudinal dispersion fluctuations along the fiber, we divided the total fiber length (L) of 18 m into 100 equal segments and assumed that the ZDW in each segment takes a value which were randomly chosen from a standard normal distribution with mean equal to *ZDW* and

standard deviation equal to X. One random realization of longitudinal fluctuation in ZDW of the fiber at X = 0.34 nm is shown in Fig. 1c. Solid red line in Fig. 1c represents the ZDW of corresponding homogeneous fiber. We calculated the threshold pump powers for N random realizations of modified dispersion and averaged it in order to get the averaged threshold power (P_{th}). The variation of P_{th} with anti-Stokes wavelength (λ_i) for both types of FOPOs is given in Fig. 1d. The solid curves represent P_{th} variation calculated at the presence of dispersion fluctuations. Terms 'fast' and 'slow' in the curve legends indicate that in PM case, the pump is polarized along the fast and slow-axis of the fiber respectively. Corresponding experimental data are shown by points in Fig. 1d.

It is apparent that even a small variation in the fiber ZDW significantly affects the threshold power P_{th} of the CW FOPO for both the cases of PM and non-PM FOPO. Further from Fig. 1b and 1d it is clear that threshold is higher for PM FOPO than it is for non-PM FOPO because of the higher cavity losses (see Fig. 1a). Simulations also show an excellent agreement with the experimental results.

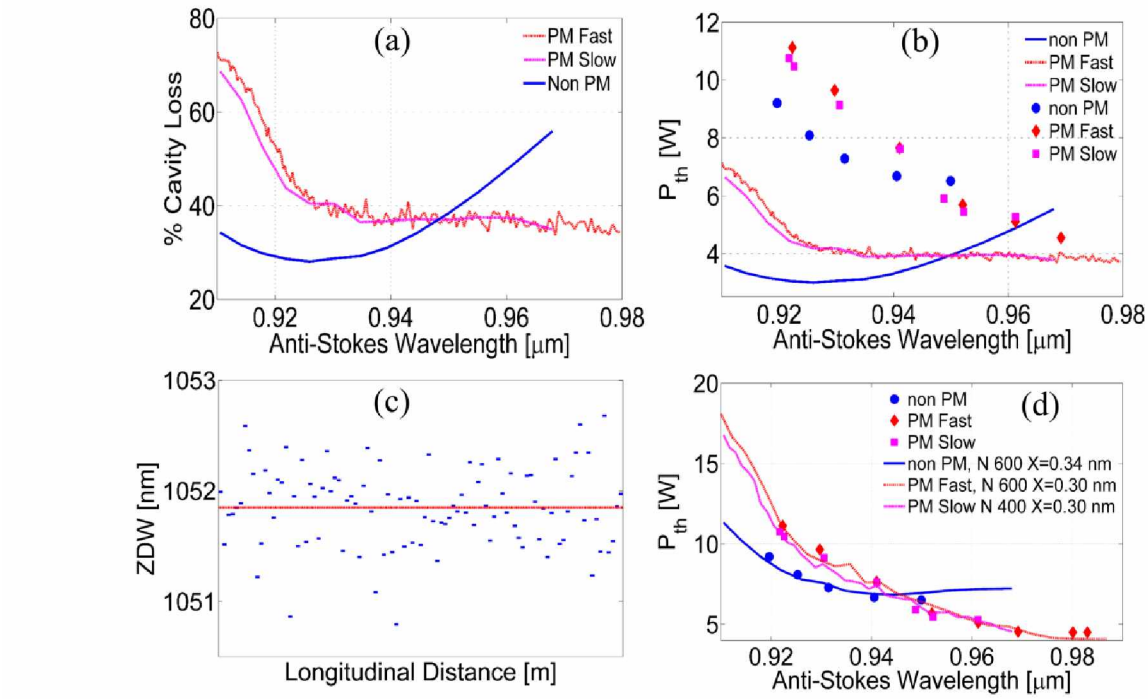

Fig. 1 (a) Variation of cavity losses for various type of FOPOs , (b) analytical threshold behavior without any ZDW fluctuation (solid lines) together with the experimental data, (c) A single realization of longitudinal ZDW fluctuation, and (d) variation of threshold according to our model (solid lines) together with the experimental data.

To conclude, we have studied the effect of fiber longitudinal dispersion fluctuation on the threshold pump power of a CW FOPO both in non-PM and PM configuration. The simulations show a significant increase in the threshold power at parametric wavelengths. It is observed that a slight variation of the fiber dispersion is capable of increasing the threshold tremendously, especially at short wavelengths. A good agreement between our experimental and numerically simulated data is observed.

This work was financially supported through Department of Science and Technology (DST), under Ref. No. INT/RUS/RFBR/P-184 and RFBR grant 15-52-45068_ind_a. The authors would like to convey their sincere thanks to both of the sponsoring agencies.

References

[1] E.A. Zlobina, S.I. Kablukov, S.A. Babin, Opt. Exp. **18**, 833 (2015).
[2] M. Farahmand, M. Sterke, Opt. Exp. **12**, 136 (2004).
[3] J. S. Y. Chen et al., Opt. Exp. **14**, 9491 (2006).
[4] M.E. Marhic. Fiber Optical Parametric Amplifiers, Oscillators and Related Devices (Cambridge University, 2008).

Paradox of photons discontinuous trajectories being located by means of "weak measurements" in the nested Max-Zehnder interferometer

G.N. Nikolaev
Institute of Automation and Electrometry of SB RAS, pr. Koptyuga 1, Novosibirsk, 630090, Russia
Novosibirsk State University, Pirogova str. 2, Novosibirsk, 630090, Russia
E-mail: nikolaev@iae.nsk.su

In a recent letter A. Danan et al. have experimentally demonstrated an intriguing behavior of photons in an interferometer [1]. This experiment was inspired by recent discussion about the past of a quantum particle in an interferometer [2]. Simplified layout of the experimental setup is a nested Max-Zehnder interferometer (MZI) depicted in Fig. 1. Ordinary beam splitters BS1 and BS2, and mirrors A and B form an inner MZI. Polarized beam splitters PBS1 and PBS2, and mirrors C, E and F form an outer MZI. Various mirrors inside the MZI vibrate with different frequencies. The rotation of a mirror causes a vertical shift of the light beam reflected off that mirror. The shift is measured by a quad-cell photodetector QCD. When the vibration frequency of a certain mirror appears in the power spectrum, authors conclude that photons have been near that particular mirror. When both the inner MZI and the large one are adjusted to produce constructive interference of the light beams propagated toward mirror F and QCD respectively, the power spectrum shows peaks at all frequencies.

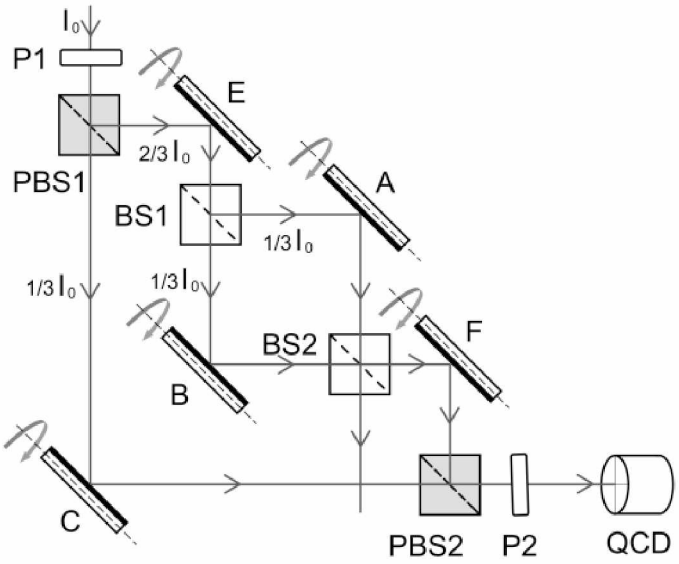

Fig. 1 Simplified experimental setup with two nested Mach-Zehnder interferometers. A, B, C, E, and F stands for mirrors; P1 and P2 stands for polarizers; BS1 and BS2, and PBS1 and PBS2 stands for ordinary and polarized beam splitters respectively. The elements BS1, A, B, and BS2 form an inner MZI whereas the elements P1, PBS1, C, E, F, PBS2, and P2 form an outer MZI.

The surprising result is obtained when the inner MZI is tuned to destructive interference of the light propagating toward mirror F. In that case the power spectrum shows not only peak at the frequency of mirror C but two more peaks at the frequencies of mirrors A and B, and no peaks at the frequencies of mirrors E and F. From these results authors conclude that the past of the photons is not represented by continuous trajectories, because the photons are registered inside the inner MZI and not registered outside it. The authors provide an explanation using the two-state vector formalism of quantum theory [3, 4] and claim that this would be the most intuitive explanation of the phenomenon. They also discuss that an explanation in terms of classical electromagnetic waves is certainly possible and provide a partial classical description of their results but consider there is no simple interpretation of the results within the framework of the approach.

These unusual results raised a spirited discussion [5–11]. The most thorough analysis of the experiment both analytical and numerical was made in [9] on the base of the optical paraxial approach. Nevertheless, until now there was no comprehensive and clear analysis of the experiment within the framework of the classical electromagnetic waves approach. In particular, it was unclear if the nature of the absence of peaks at the frequencies of mirrors E and F is the same or different.

In this paper, we present a physically clear and comprehensive analysis of the paradoxical results [1] based on traditional concepts of the classical electromagnetic waves (or quantum mechanics). These concepts imply the continuity of the wave (photon) trajectories.

We show that taking into account a) smallness of the optical beams deflection due to the mirrors vibrations, and b) axial symmetry of the beams, the light power difference absorbed by the upper ($y \geq 0$) and the lower ($y \leq 0$) cells of QCD may be represented as follows

$$D = \frac{2}{9} I_0 \{[\delta_A + \delta_C + \delta_E + \delta_F] cos(\varphi_{AC}) + [\delta_B + \delta_C + \delta_E + \delta_F] cos(\varphi_{BC}) + \delta_C + [\delta_A + \delta_B + 2(\delta_E + \delta_F)][1 + cos(\varphi_{AB})]\} \int_{-\infty}^{\infty} f^2(x, 0)\, dx$$

where I_0 is the light intensity at the entrance of MZI, $f(x, y)$ is normalized amplitude distribution ($\iint_{-\infty}^{\infty} f^2(x, y)\, dxdy = 1$), δ_i is the vertical displacement of the light beam at QCD caused by the mirror i vibration, $\varphi_{ij} \equiv \varphi_i - \varphi_j$, φ_i is the phase change of the light beam due to its propagation from the compound MZI entrance toward mirror i and, finally, to QCD.

In the case of constructive interference both inner and outer IMZ ($\varphi_A = \varphi_B = \varphi_C$), the expression in braces for the difference D becomes as follows $\{\cdots\} = \{3[\delta_A + \delta_B + \delta_C + 2(\delta_E + \delta_F)]\}$. The signal power spectrum consists of peaks at frequencies of all the mirrors. Multiplier 2 at δ_E and δ_F caused by constructive interference of light beams in upper and lower arms of inner IMZ. Moreover, the power spectrum at the vibration frequencies of mirrors E and F has a peak that is four times more the peaks at the vibration frequencies of mirrors A, B, and C, because the power spectrum is proportional to the square of the oscillation amplitude at each frequency.

In the case of destructive interference of inner IMZ ($\varphi_A = \varphi_C = \varphi_B \pm \pi$) the expression in braces for difference D becomes as follows $\{\cdots\} = \{\delta_A - \delta_B + \delta_C\}$. Nature of the peaks absence at the vibration frequencies of mirrors E and F is different. Deflection of mirror E equally shifts beams in upper and lower arms of inner IMZ, and that is why it doesn't change its destructive interference. Deflection of mirror A (or B) results in perturbation of destructive interference of inner IMZ proportional to δ_A (δ_B). Moreover, output beam from inner IMZ is antisymmetrical about the y axis caused by axial symmetry of incident light beam and smallness of mirror deflection. In turn, the change of the output due to deflection of mirror F is symmetrical and is not measured, consequently, by QCD.

It should be noted that measured signal D is entirely caused by the interference of modulated and unmodulated parts of light beams of IMZ. So, in the case of destructive interference of inner IMZ ($\varphi_A = \varphi_C = \varphi_B \pm \pi$) the only unmodulated part is the one propagating along the lower arm of the outer IMZ. When this light beam moving from the mirror C is blocked then all peaks disappear.

So, there is clear explanation of paradoxical results [1] based on traditional concepts of the classical electromagnetic waves. Thus, there is no necessity for a new concept of discontinuous trajectories.

References

[1] A. Danan, D. Farfurnik, S. Bar-Ad et al., Phys. Rev. Lett. **111**, 240402 (2013).
[2] L. Vaidman, Phys. Rev. A **87**, 052104 (2013).
[3] Y. Aharonov and L. Vaidman, Phys. Rev. A **41**, 11 (1990).
[4] Y. Aharonov, P. G. Bergmann and J. L. Lebowitz, Phys. Rev. **134**, B1410 (1964).
[5] M. Wiesniak, arXiv: quant-ph/1407.1739 (2014).
[6] H. Salih, arXiv: quant-ph/2015.03.05 (2014).
[7] B. E. Y. Svensson, arXiv: quant-ph/1402.4315 (2014).
[8] J.-H. Huang, L.-Y. Hu, X.-X. Xu et al., arXiv: quant-ph/1402.4581 (2014).
[9] P. L. Saldanha, Phys. Rev. A **89**(3), 033825 (2014).
[10] F. Li, F. A. Hashmi, J.-X. Zhang et al., Chinese Phys. Lett. **32**(5), 050303 (2015).
[11] K. Bartkiewicz, A. Cernoch, D. Javurek et al., Phys. Rev. A **91**, 012103 (2015).

Detailed theoretical study of the new resonance in the saturated-absorption spectroscopy of atomic vapours

Aleksey Novokreshchenov[1], Denis Brazhnikov[1,2]
[1]*Institute of Laser Physics, 630090 Novosibirsk, Russia*
[2]*Novosibirsk State University, 630090 Novosibirsk, Russia*
E-mail: Aleksey-box@mail.ru

One of the most important fundamental phenomena in nonlinear laser spectroscopy of gases is saturated-absorption resonance (SAR) in the field of counterpropagating light waves [1]. Usually, SAR is observed as a single structure (dip or peak, it depends on the waves' polarizations and the structure of atomic energy levels). However the new effect was discovered several years ago [2], which consisted in observing of double structure of SAR: a narrow peak was formed in the middle of conventional saturated-absorption dip. In the work [2] the effect was explained using the simple spectroscopic model of a two-level atom, i.e. without taking into account degeneracy of energy levels. It was noted that the effect could not be caused by previously known phenomena. However, that simple model did not consider effects that can affect the form of the resonance in real experiments. In particular, it is well known that the higher-order spatial harmonics (HSH) of atomic polarization as well as changes in the parameters of light waves polarizations can have significant influence on the shape of SAR [1].

In this research we theoretically investigate the influence of HSH and parameters of light wave polarizations on the double structure of the saturated-absorption resonance taking into account the real (degenerate) structure of atomic energy levels. The results obtained demonstrate the significant influence of considered effects on the shape and contrast of the central peak (see Fig. 1a as an example of the resonance curve). Moreover, numerical calculations show that variation of the polarization parameters can result in disappearance of the double-structure effect (Fig. 1b). It is associated with the peculiarities of optical pumping in atomic gas. The optimal values of light wave polarizations and intensities to obtain a high-contrast central peak have been defined.

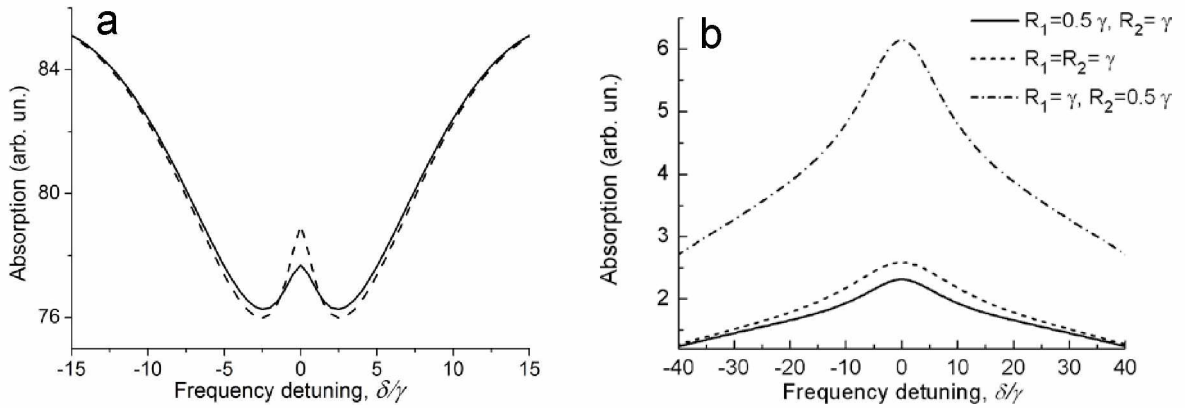

Fig. 1. Saturated-absorption resonance: (a) Influence of HSH on the contrast of central peak (solid line takes into account the higher spatial harmonics); (b) variation of light-field polarization parameters results in disappearance of the double-structure effect (lin || lin configuration, R_1, R_2 are the Rabi frequencies).

The results have essentially complemented the knowledge about the new nonlinear effect that was discovered in [2] and can be used, for example, in quantum metrology for laser stabilization. This work was partially supported by RFBR (grant nos. 15-02-08377, 15-32-20330) and by Russian Presidential Grant (NSh-6689.2016.2).

References

[1] V.S. Letokhov, V.P. Chebotayev, Nonlinear laser spectroscopy (2013).
[2] V.V. Vasil'ev, V.L. Velichanskii, S.A. Zibrov, A.V. Sivak, D.V. Brazhnikov, A.V. Taichenachev, and V.I. Yudin, "Dual structure of saturated absorption resonance at an open atomic transition", J. Exp. Theor. Phys. **112**(5), 770 (2011).

Light guiding in a fiber-coupled liquid crystal

B. Nyushkov[1,2], S. Trashkeev[1,2], P. Purtov[3], D. Kolker[1,2], A. Ivanenko[1]
[1] *Institute of laser physics, SB RAS, 13/3 pr. Lavrentyeva, 630090 Novosibirsk, Russia*
[2] *Novosibirsk State University, 2 ul. Pirogova, 630090 Novosibirsk, Russia*
[3] *Voevodsky Institute of Chemical Kinetics and Combustion, SB RAS, 630090 Novosibirsk, Russia*
E-mail: clock@laser.nsc.ru

Among various soft matters, liquid crystals (LCs) have perhaps the most interesting and promising optical properties. LCs feature very high nonlinear optical susceptibility of complex orientation-electronic nature [1, 2]. Orientation order and anisotropy of LCs can be easily modified by applying relatively weak electro-magnetic fields and inducing thermal gradients [3]. Good quality optical contact between LCs and glass substrates is normally achievable. It makes LCs attractive optic media for research into nonlinear photonics and development of novel optic devices, including fiber-coupled ones. Thus a miniature fiber-coupled LC-based laser frequency converter was demonstrated recently [4]. It has a fiber input and a free-space output. An important task for further elaboration of such LC-based nonlinear photonic devices is transition to the in-line (fully fiber-coupled) design. In-line LC-based fiber-optic elements may be in demand for various applications ranging from ultra-compact laser systems to telecom technologies.

On the basis of the above, we studied experimentally feasibility of nonlinear fiber-to-fiber coupling via nematic liquid crystal (NLC). The experimental approach is illustrated in Fig.1. Two identical telecom single-mode optical fibers (core diameter ~ 8 μm) were terminated coaxially in a cylindrical sleeve filled with NLC. A room-temperature cyanobiphenyl-based (nCB) nematic mixture was used. The spacing *S* between the fiber end faces was adjustable from ~ 10 to 500 μm by means of a translation stage with a micrometer. To monitor the gap a CCD camera with microimage optics was used. A lengthwise slit in the mating sleeve enabled adjustment of the NLC capacity. A fiber-coupled laser diode at 1480 nm with output power tunable from few to 400 mW was used as a light source.

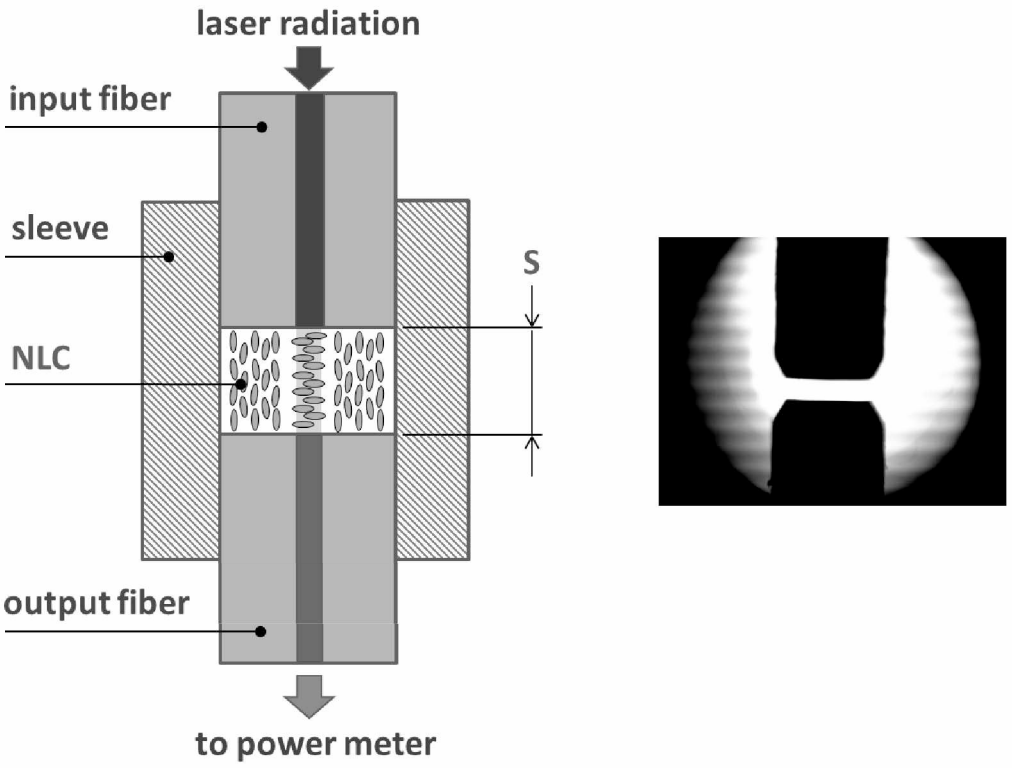

Fig. 1 Experimental fiber coupling arrangement: NLC – nematic liquid crystal, S – fiber spacing value (varied ~10 ÷500 μm). The right inset is a microimage of the gap (obtained by a monitoring CCD camera).

We discovered that strong optical coupling (loss ~ 1 dB) of two single-mode optical fibers separated coaxially by NLC can be achieved through a self-induced light guide despite a relatively large fiber-to-fiber spacing and a low optical power. This effect is due to light-induced reorientation of NLC molecules, which causes self-confinement of a propagating laser beam. Self-confinement of light in NLCs was already observed and explained earlier [2]. In our work this effect was for the first time exploited to achieve and study nonlinear fiber-to-fiber coupling and to demonstrate feasibility of development of NLC-based in-line fiber-optic elements and devices. Fig. 2 represents the measured transmission curve for fiber-to-fiber coupling via a 320-μm NLC-filled gap.

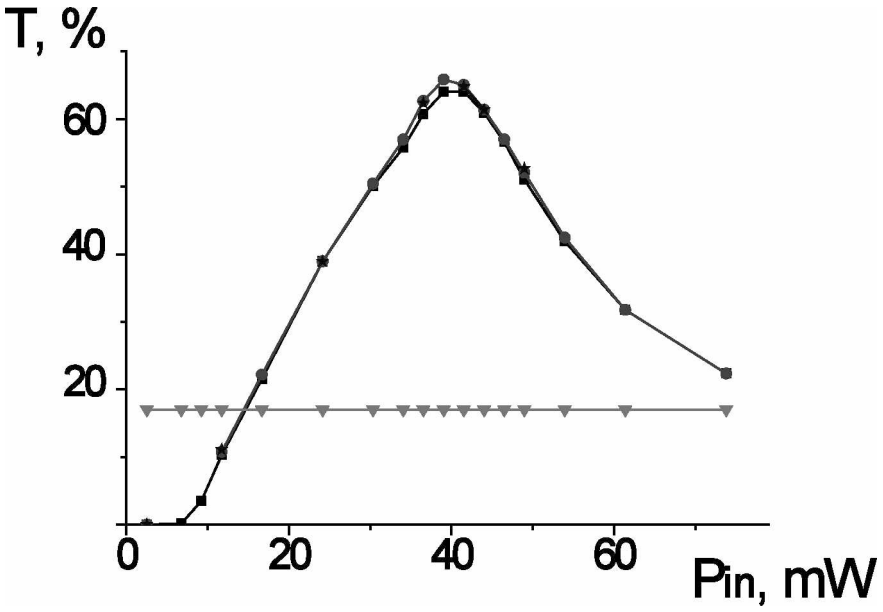

Fig. 2 Experimental transmission curve (dependence of fiber-to-fiber coupling coefficient on the input optical power) traced 3 times for reproducibility proof at $S \approx 320$ μm. The horizontal line marked by triangles is measured transmission of the same gap but filled with a refractive-index matching gel instead NLC.

Despite the huge fiber spacing equal to ~4 diffraction lengths, the transmission reached nearly 70% at a certain optical power level (~ 40 mW). The self-induced light guiding was enough stable over time and quite reproducible. The largest fiber spacing which still allowed strong optical coupling was estimated experimentally as nearly 450 μm.

The physics of self-triggered light guiding in NLC is supposed to be based on the balance between diffraction and self-focusing. However it differs from nonlinear light propagation in solids because of highly nonlocal response of NLC. Thus the critical power for the above balance in NLC is defined by an equation different from the Kerr case typical for solids [2]. In NLC the critical power varies with the beam waist. Self-focusing weakens (the critical power increases) as the spot-size reduces, thereby preventing collapse and stabilizing the self-trapped wavepacket in NLC.

The obtained results prove feasibility of strong nonlinear fiber-to-fiber optical coupling via nematic liquid crystals. It opens up possibilities for development of novel NLC-based in-line fiber-optic elements with such functionalities as laser frequency conversion, power limitation, and polarization control.

The work was partially supported by government programs (projects: NSh-6689.2016.2, 030720140005, and 030720140007).

References

[1] S.I. Trashkeev, V.M. Klement'ev, G.A. Pozdnyakov Quantum Electron. **38**, 373 (2008).
[2] M. Peccianti, G. Assanto Phys. Rep.**516**, 147 (2012).
[3] S.N. Bagayev, V.M. Klementyev, B.N. Nyushkov et al, J. Phys.: Conf. Series **345**, 012018 (2012).
[4] B.N. Nyushkov, S.I. Trashkeev, V.M. Klement'ev et al, Quantum Electron. **43**, 107 (2013).

Laser synthesis of a silicon nanoparticle in liquid

A. Osipov[1], S. Arakelian[1], A. Evlukhin[2], S. Kutrovskaya[1], A. Kucherik[1]
[1]*Stoletov Vladimir State University, Vladimir, Russia*
[2]*Laser Zentrum Hannover e.V., Hannover, Germany*
E-mail: osipov@vlsu.ru

Silicon nanoparticles are wildly used in different photonic applications [1, 2]. Its optical properties, including resonant responses, are considerably dependent on the sizes, shape, and crystallization degree. The methods of laser ablation in liquid allow to control the average size and spherical shape of the fabricated particles choosing suitable irradiation conditions (pulse duration, energy density etc.).

In this paper we present results of the silicon nanoparticle synthesis (with average nanoparticle size control) by the continuous laser irradiation of the thin silicon target placed in ethanol. Porous and monolithic silicon targets are considered. The generated colloidal solutions are used for formation of the one-layered covering composed of silicon nanoparticles with resonant optical response in the visible spectral range.

For fabrication of silicon nanoparticles the method of CW-laser ablation was used [3]. Application of the CW-laser radiation source with moderate intensity provided the possibility to obtain nanoparticle with a small deviation of the average value. To avoid the oxidation of nanoparticles we realized the laser ablation experiment in the 99% ethanol.

The laser beam (diameter 100 μm) was focused on the surface of the target (using the long focal-length lens with the focal length of 100 mm) and scanned it. The power variation was in the diapason of 10 – 100 W, which was resulted in the radiation intensity of 10^5 – 10^6 W/cm^2. The whole irradiation time was 60 minutes.

The laser irradiation of the porous target resulted in a wider distribution function of nanoparticle sizes as compared with crystalline target (fig.1). In the both cases spherical nanoparticles with average diameter of 100 nm were obtained (fig.2).

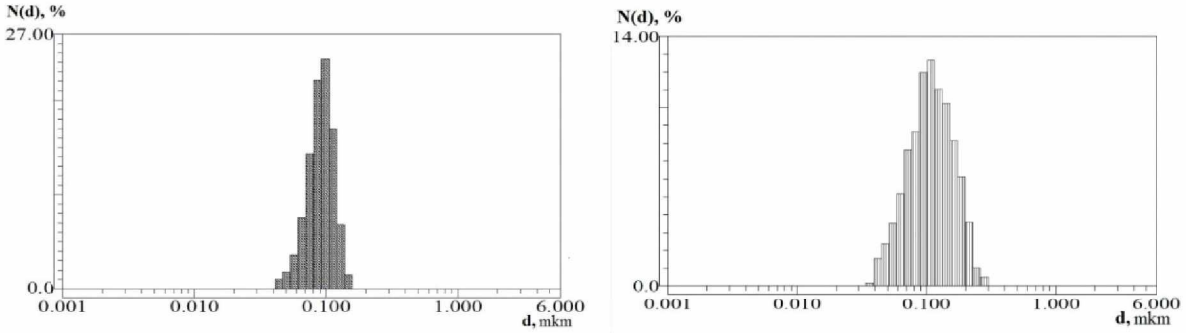

Fig. 1 The histogram of the particle diameters distribution in colloidal system, which was obtained using laser irradiation (intensity 10^6 W/cm^2, scanning speed 100 μm/s) of the monolithic target (a) and porous (b).

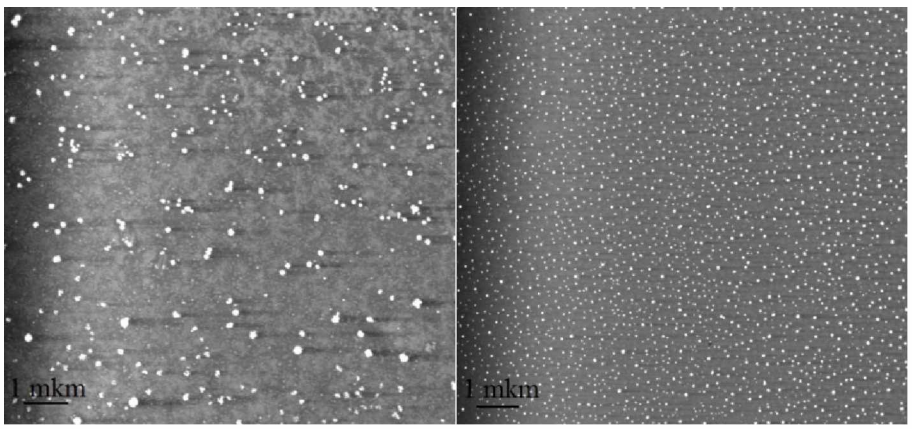

Fig. 2 REM-images of colloidal particles, obtained during the ablation of the monolithic (a) and porous (b) targets.

Images of the particles shown in fig.2 correspond to the evaporation process of the ethanol colloidal drop with nanoparticles inside. The experiment was carried out in a temperature controlled chamber with the temperature of 20 °C. As it can be seen from fig.2 there are uniformly deposited particles on the base area of the drop after its evaporation.

To control the deposition of the nanoparticles from a small colloidal drop we have used the methods described in [3]. The results of silicon nanoparticle depositions under different temperature conditions is shown in fig.3.

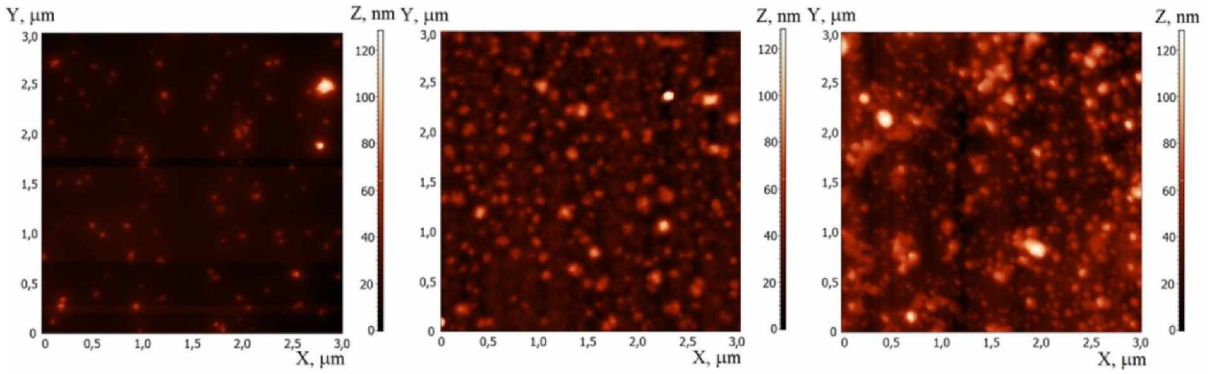

Fig. 3 AFM-images if the deposition of the silicon colloidal particles in controlled temperature chamber with temperature conditions 15 oC, 10 oC, 5 oC accordingly (left to right).

It is necessary to note that due to the thermostabilization and vapor saturation the evaporation process in the temperature controlled chamber differs from the evaporation at the natural conditions.

The measurements of nanoparticle optical properties were carried out using a microscope with x100 lens. As we can see from fig.4 nanoparticles can resonantly scatter light of different frequencies.

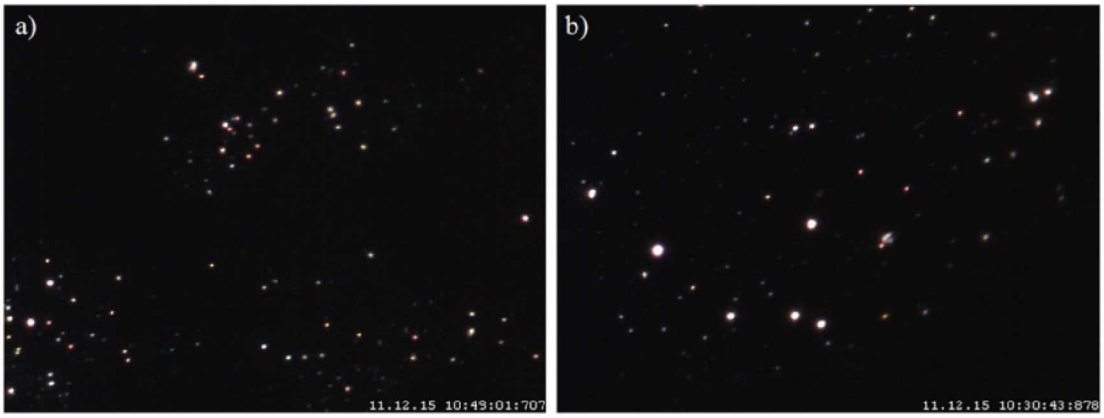

Fig. 4 A dark-field (scattered light) image of the deposited colloidal systems of monolithic (a) and porous (b) silicon

It could be with the different sizes and crystallization degree of the nanoparticles [1]. It is also important that in the case of the irradiation of the porous silicon target a large amount of nanoparticles does not support the resonant optical response in the visible range, because of their low refractive index.

References

[1] Zywietz U., Evlyukhin A. B., Reinhardt C., Chichkov B. N. "Laser printing of silicon nanoparticles with resonant optical electric and magnetic responses", Nature Commun. **5**, 3402 (2014).

[2] A.I. Kuznetsov, A.E. Miroshnichenko, Y.H. Fu, J. Zhang and B. Luk'yanchuk, "Magnetic light", Scientific Reports **2**, 492 (2012).

[3] A.A. Antipov, S.M. Arakelyan, T.A. Vartanyan, T.E. Itina, S.V. Kutrovskaya, A.O. Kucherik, I..V. Sapegina, "Optical properties of nanostructured gold–silver films formed by precipitation of small colloid drops", Optics and Spectr.oscopy **119**, 119 (2015).

Efficient lasing in the IR, UV and VUV in run-away electron preionized discharges

A.N. Panchenko, N.A. Panchenko, D.A. Sorokin, M.I. Lomaev
AInstitute of High Current Electronics SB RAS, Academichesky Av., 2/3, Tomsk, 634055, Russia
E-mail: alexei@loi.hcei.tsc.ru

It is known that main parameters of gas discharge lasers such as pulse duration, output and efficiency are substantially determined by uniformity and stability of self-sustained volume discharge in active mixtures. Currently it is generally recognized that necessary conditions for volume discharge development are the use of properly shaped electrodes with no strong edge effects, preionization from different sources (VUV radiation, x-rays, electron beam and so on) producing certain electron number density, over-voltage pulse applied to a laser gap [1–3].

Nevertheless, formation of quite uniform discharge in various gases at high pressure and efficient lasing are possible even without any preionization if voltage pulses with amplitude over 100 kV and sub-ns rise-time are applied to needle or blade electrodes [4]. In this case volume discharge is formed due to preionization by beam of run-away electrons. This discharge form is called run-away electron preionized diffuse discharge (REP DD) [5].

Below laser parameters in different spectral ranges under REP DD excitation are presented. REP in various gas mixtures was formed by a RADAN-220 generator producing voltage pulses with amplitude of 250–300 kV and rise-time about 1 ns. Laser gap was formed by two blade electrodes 30 cm in length. The discharge gap d between the electrodes was d=1.8 cm. The optical cavity comprised plane mirrors. Mixtures of rare gases, nitrogen, hydrogen, deuterium with SF_6 and F_2 were used in experiments.

Two operation modes of N_2 laser in N_2-SF_6 mixtures under REP DD excitation were obtained in experiments. Maximal electric efficiency of N_2 laser is characteristic of the first operating mode. In this the case main part of energy stored in the generator is deposited into discharge plasma during 10 ns. The maximal energy of the UV radiation at 337 nm was 4.2 mJ, the peak radiation power reached 1.4 MW. The electrical efficiency was as high as 0.2 %. Such efficiency is close to the ultimate theoretical value and to maximal efficiencies obtained experimentally for discharge nitrogen laser emitting at 337 nm.

Characteristic feature of the second operation mode of N_2 laser is two or three radiation peaks during successive current oscillations. This operation mode was achieved for the first time in the gas mixtures at pressure below ≈100 Torr.

Ultimate efficiency of non-chain chemical HF(DF) laser was demonstrated under REP DD excitation. Duration of REP DD current in SF_6-$H_2(D_2)$ mixtures was about 10 ns. Input electric power was as high as 15 MW·cm^{-3}. Laser pulses have one peak with about 75 ns in duration (FWHM) followed by an exponentially decaying tail. Maximal output on HF and DF molecules reached 110 mJ and 75 mJ, respectively, with peak radiation power over 1.2 MW.

Intense cascade transitions prove the high uniformity of REP DD which provides uniform energy deposition into the discharge plasma. Cascade transitions increase the extraction efficiency from the active medium of non-chain chemical lasers, because one HF or DF excited molecule may emit up to 3–4 photons. Besides due to high REP DD power, the lasing on separate lines started within 15–20 ns after the gap breakdown which decreases the energy loss for attainment of the lasing threshold. These factors provide ultimate efficiency of the REP DD pumped non-chain laser.

Efficient UV and VUV laser action on excimer molecules in rare gases–F_2 mixtures was obtained for the first time. Therewith an oscillatory character of REP DD with duration over 50 ns was evident. Laser action was observed during 2–3 current periods (see Fig. 1). This means maintaining the REP DD diffuse burning phase even after repeated change of the current direction. Maximal output of XeF* laser in 30 ns pulse was as high as 10 mJ, corresponding to electrical efficiency of 0.65%.

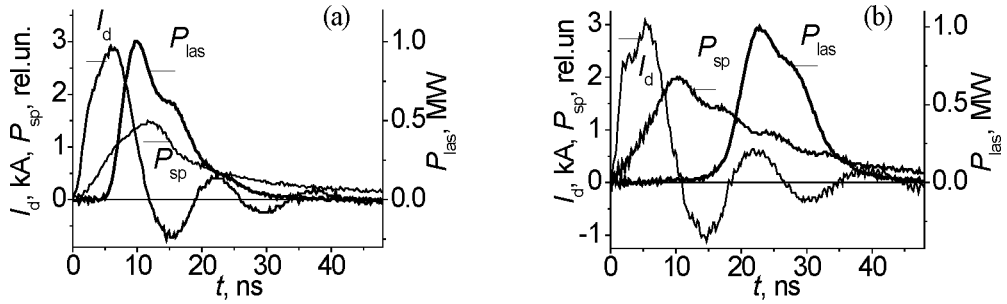

Fig. 1 Waveforms of REP DD current (I_d), spontaneous emission (P_{sp}) and laser pulses (P_{las}) on KrF* (a) and XeF* (b) molecules. Gas mixtures of the He : Kr : F_2 = 3 atm :100 : 5 Tor (a) and He : Xe : F_2 = 3 atm :10 : 5 Torr (b) compositions are used.

Lasing on KrF* molecules starts within 10 ns and lasted during two current half-cycles, while total duration of the laser pulse was as long as 30 ns. This also indicates the high homogeneity and stability of the REP DD in He-Kr-F_2 mixtures. The laser output increases linearly with He pressure and reached Q=20 mJ, the electrical efficiency was as high as 1.3%.

Thus, the results obtained demonstrate that parameters of REP DD pumped XeF* and KrF* lasers are comparable with the parameters of lasers pumped by a transverse discharge with preionization.

Simultaneous laser action on red FI lines and VUV transition of F_2 molecules at 157 nm was obtained in He-F_2 mixtures (see Fig.2, a). VUV laser pulse on F_2 molecules had two distinct peaks and one weak peak during three half-periods of the REP DD current, lasing duration was as long as 25 ns. The VUV radiation power in the peaks increased exponentially with He pressure. Maximal VUV energy of 2 mJ was achieved at He pressure of 5 atm. Therewith electrical efficiency of F_2 laser was as high as 0.1%, which, similarly to XeF* and KrF* lasers, is comparable with the parameters of F_2 lasers pumped by a transverse discharge with preionization

REP DD in binary and ternary Ar-Xe-(He) and Ar-Kr-(He) mixtures intensively emits at wavelength close to 147 nm. Parameters of VUV emission in REP DD in these mixtures was studied (see Fig.2, b). Increase of helium pressure results in dramatic increase of the VUV radiation intensity while its duration at half-maximum decreased. Radiation at 147 nm appears within 5–10 ns after REP DD formation which may be a sign of laser action. Additional experiments for obtaining the VUF laser emission in rare gas mixtures with increased cavity resonator Q-factor are necessary.

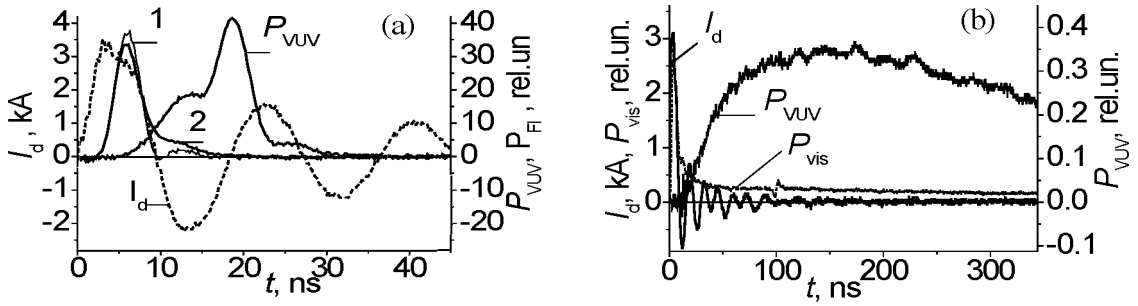

Fig. 2 Waveforms of REP DD current I_d and laser radiation on FI (curves 1, 2) and F_2 (P_{VUV}) in the He:F_2=3 atm:5 Torr mixture, output coupler with reflectivity of 7% (1, P_{VUV}) and 90% (2) are used (a) and waveforms of REP DD current I_d and visible (P_{vis}) and VUV (P_{VUV}) emission in He:Ar:Xe=3 Atm:400:0.4 Torr mixture (b).

This work was made under the support of the Russian Foundation for Basic Research, project No. 14-08-00074.

References

[1] A. J. Palmer, ‚Appl. Phys. Lett. **25**, 138 (1974).
[2] J. I. Levatter, S. C. Lin, J. Appl. Phys. **51**, 210 (1980).
[3] E. A. Stappaerts, Appl. Phys. Lett. **40**, 1018 (1982).
[4] P. O. Vil'tovskii, M. I. Lomaev, A. N. Panchenko, et.al., Quantum Electron. **43**, 605 (2013).
[5] E. H. Baksht, A. G. Burachenko, I. D. Kostyrya, et.al. J. Phys. D. **42**, 185201 (2009).

Localized eigenmodes in mesh synthetic photonic lattices

A.Pankov[1], I. Vatnik[1,2], D. Churkin[1], A. Sukhorukov[3]
[1]*Novosibirsk State University, Pirogova str. 2, Novosibirsk 630090, Russia*
[2]*Institute of Automation and Electrometry, Novosibirsk 630090, Russia*
[3]*Nonlinear Physics Centre, Research School of Physics and Engineering, The Australian National University, Canberra ACT 2601, Australia*
E-mail: ilya.vatnik@gmail.com

Photonic lattices are a versatile platform for realizing and observing numerous optical phenomena. This platform can provide such properties and possibilities, which no other system can offer. One of representatives of this class is a discrete mesh lattice1. Such systems are composed of an array of waveguides with each one being discretely and periodically coupled to its adjacent neighbors (Fig.1, : (a,c)). Unlike ordinary waveguide arrays, light propagation in such mesh systems is discretized in two dimensions (transverse and longitudinal). Though such systems are quite complex and expensive in manufacturing, therefore another type of photonic lattices was designed – synthetic photonic lattices (SPL) (Fig1, left, (b,d)). These lattices are analogous to discrete mesh lattices with one important difference – signal evolution in synthetic photonic lattices takes place in time domain instead of spatial domain evolution of mesh lattices. As indicated in several studies, SPL can be used to observe a number of processes, like discrete quantum walk, PT – symmetry[1-2], discrete solitons and optical diametric drive acceleration through action-reaction symmetry breaking.

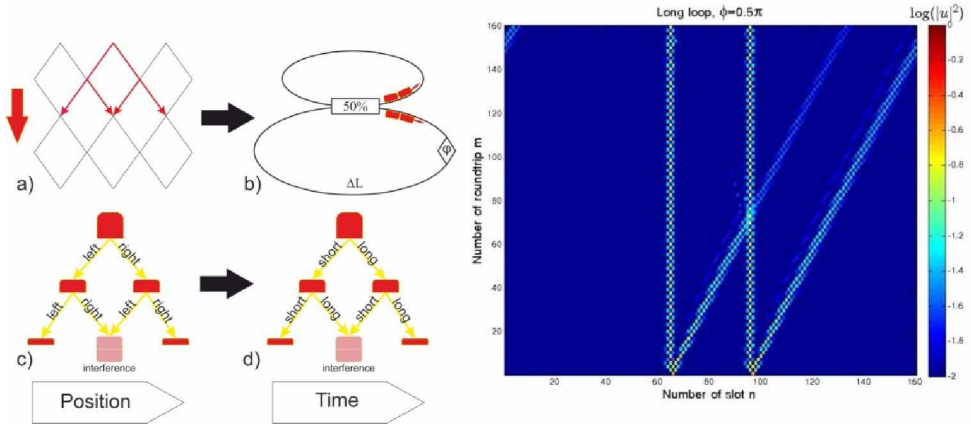

Fig. 1 Left: (a,c) mesh photonic lattice, (b,d) synthetic photonic lattice. Right: evolution of localized modes excited at m=0.

An SPL consists of two coupled fiber loops that are coupled via a central 50:50 directional coupler. These two fiber loops differ in length by ΔL. Here, the equivalent transverse coupling to the left and right sites is enabled by this length difference between the two loops. An independent discretization in time is then obtained by monitoring the round-trip number m in these loops. Hence, the system is essentially discretized in two dimensions (Fig. 1, right). As we will see, the propagation dynamics of light pulses, launched in such discrete temporal lattices is exactly identical to those expected in the spatial configurations. Evolution of impulse chain depends on phase of each impulse and can be altered by phase modulators. Phase modulation plays role of an optical potential in the system. Different configuration of this potential leads to different eigenmodes, that is the pulse chains with stable number of pulses within. We show analytically and numerically that controlling phase shift of light pulses by means of phase modulator it's possible to construct an analogue of a waveguide in SPL with the eigenmodes localized inside the waveguide. It is found that modes corresponding to surface waves on borders of potential wells may emerge. We investigate the evolution of these localized waves in SPL.

This work was supported by Russian Ministry of Education and Science (14.584.21.0014)

References

[1] M. Miri, A. Regensburger, U. Peschel, D. Christodoulides, Physical Review A **86**(2), 023807 (2014).
[2] A. Schreiber, K. Cassemiro, V. Potoček et. al., Physical review letters **104**(5), 050502 (2010)

Laser deformography and earthquake precursors

S. Panov[1], M. Parushkin[1], V. Semibalamut[2], Yu. Fomin[2], Yu. Rybushkin[2]
[1]*Institute of Laser Physics SB RAS, 630090 Novosibirsk, ak.Lavrent'ev 13/3, Russia*
[2]*Siberian Branch of the Federal Research Center unified geophysical service of the RAS, 630090 Novosibirsk, ak.Lavrent'ev 13/3, Russia*
E-mail: lss@laser.nsc.ru

For more than 20 years in the Baikal region Institute of Laser Physics is carried out continuous monitoring of the deformation processes of Earth's crust in the underground mine of geophysical test site "Talaya" observations using the laser strainmeter developed in the Institute. As a result of processing large amounts of data, new information about the impact of the process of preparing regional strong earthquakes on the deformation processes at the observation point was obtained.
The report describes systematic recurring features in the deformation process, pointing to the preparation of a regional earthquake.

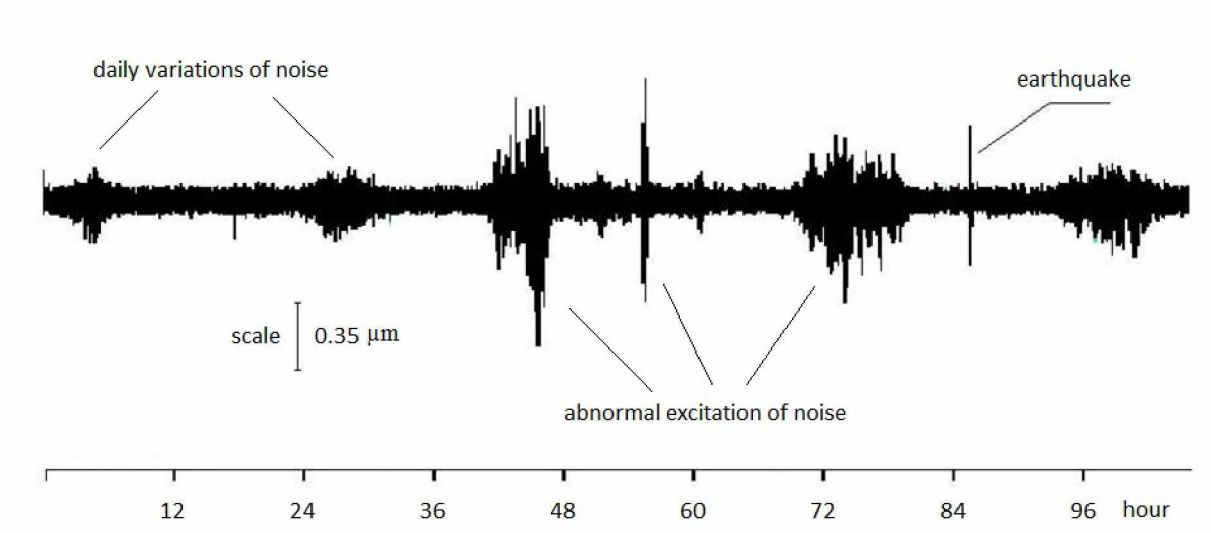

Fig. 1 Excitation of microdeformation noise before the earthquake of energy class K = 13.5.

Identified features lie in different ranges of the oscillation periods: days-long monotonic strain drift, disturbances in the course of semidiurnal tidal fluctuations, super long-period oscillations excited in the lithosphere and the atmosphere on the eve of seismic events, generation of the micro deformation noise with periods ranging from 20 to 40 s Fig.1. Data of rather rare and unique case of the deformation process during the preparation of the earthquake of the 14th energy class located at a distance of 30 km from the observation point are described.

The three-channel laser strainmeter for geophysical research

S. Panov[1], M. Parushkin[1], V. Semibalamut[2], Yu. Fomin[2], A. Rybushkin[2], S. Tokmoldin[3], V. Klimenov[3]
[1]*Institute of Laser Physics SB RAS, 630090 Novosibirsk, ak.Lavrent'ev 13/3, Russia*
[2]*Siberian Branch of the Federal Research Center unified geophysical service of the RAS, 630090 Novosibirsk, ak.Lavrent'ev 13/3, Russia*
[3]*LLP Physical-Technical Institute, 040907 Almaty, pos. Alatau, st. Ibragimova, 11, Kazakhstan*
E-mail: lss@laser.nsc.ru

Laser strainmeter designed in Institute of Laser Physics for geodynamic monitoring of stressedly-deformed state of rock and study features of the deformation process on the eve of regional earthquakes is described. Strainmeter is built under the scheme of unequal-path Michelson interferometer with a transfer of phase information from optical range to radio-frequency range by optical heterodyne. Acousto-optic modulators are used to obtain heterodyne and measuring radiations with fixed optical frequency difference (1 MHz). The main advantage of the laser strainmeter is that it does not require the use of shielding of laser beams on the measuring base. The original method of eliminating the influence of the atmosphere on the strain measurement is used. This method consists in the direct measurement of the variations of the wavelength in the atmosphere using a short fixed length measuring arm (standard) and provides a relative sensitivity about 10^{-14} in a band of recorded frequencies up to 1 kHz and a measurement base up to 300 m. Strainmeter can be used in the mining industries for the prediction and prevention of emergency situations caused by rock bumps and other manifestations of rock pressure.

Blue rubidium fluorescence in an extremely thin cell

A. Pazgalev[1], P. Petrov[2], and T. Vartanyan[2]
[1]*Division of Plasma Physics, Atomic Physics and Astrophysics, Ioffe Phys.-Technical Institute, St.Petersburg, Russia*
[2]*Laboratory of Surface Photophysics, Center of Information Optical Technologies, ITMO University, St.Petersburg, Russia*
E-mail: pazgalev@gmail.com

An interaction of excited states of alkali atoms with transparent dielectric surfaces such as glass and sapphire are not fully understood. It is known that the excited atom loses its energy almost completely in a collision with sapphire (Al_2O_3) surface. It happens notwithstanding that sapphire has a wide transparency window stretching up to vacuum ultraviolet range, which means that sapphire has no energy levels/energy zones corresponding to alkali excited state energy (~ 1.5–3 eV). The question arises: what process is responsible for energy exchange and quenching of alkali excited states?

Besides, an atom approaching the surface experiences attraction due to induced mirror image resulting in van-der-Waals (vdW) or Casimer-Polder interaction [1]. VdW interaction scales as $V(r)/h \sim C_3/r^3$, where r is the atom-to-surface distance, with $C_3 \sim 1.1$ kHz·μm^3 for Rb $5S_{1/2} \rightarrow 5P_{3/2}$ transition [1]. An estimated frequency shift due to vdW interaction is about 1 GHz at the distance $r \sim 10$ nm. The frequency shifts may be different for different states causing level crossing, states mixing and nonadiabatic transitions.

The main goal of our research is to investigate the Rubidium excited states (primarily $5P_{3/2}$ and $5D_{5/2}$) fluorescence in close proximity to sapphire surface. We are looking for energy shifts and optical line asymmetry produced by excited atoms moving to and from the surface. The main difficulty in such measurements originates from the fact that the number of atoms near the surface is very low. Hence, the major part of the fluorescence or absorption signal comes from the atoms that are far away from the surface.

We use an Extremely Thin Cell (ETC) with variable thickness of 250–400 nm filled with natural mixture Rubidium isotopes made by Armenian group, see *e.g.* [2]. The cell has two round flat surfaces; its interior has a wedge shape with the dimensions specified above. We have ability to choose a desired thickness by illuminating the cell at the defined wedge height. We expect that with cell size of 400 nm about 2–3 per cent of atoms would be surface-influenced to provide us some insight.

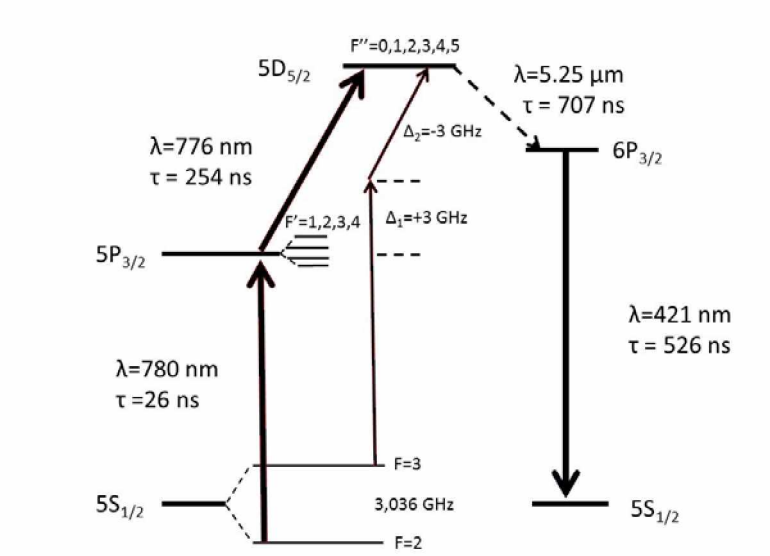

Fig. 1 Levels of ^{85}Rb: two-step excitation populates $5D_{5/2}$ level, fluorescence from $6P_{3/2}$ level is detected.

The relevant Rubidium levels are presented in Fig.1. We populate the level $5D_{5/2}$ by two-step excitation by means of two cw-diode lasers (ECDL TOPTICA DL-100) adjusted to resonant transitions $5S_{1/2} \rightarrow 5P_{3/2}$ and $5P_{3/2} \rightarrow 5D_{5/2}$ with wavelength of 780 and 775 nm. An intense blue light with λ=421 nm is observed from $6P_{3/2}$ level. The luminescence is unidirectional in contrast with four-

wave-mixing case [3]. It should be noted that thermal time-of-flight is only ~1 ns, very short in comparison with 707 ns, the $5D_{5/2}$-level spontaneous decay time.

The set-up is shown in Fig.2. First, stabilized by Rb reference cell 780 nm-laser excites the one of ^{85}Rb hyperfine $5S_{1/2} \rightarrow 5P_{3/2}$ transition. Second laser with λ=775 nm is scanned by piezo. Two laser beams are focused in the cell with spot size of ~85 μm. Diffraction grating monochromator M266 (Solar LS) is used for detection of blue light by means of CCD or PM Tube (Hamamatsu H11890).

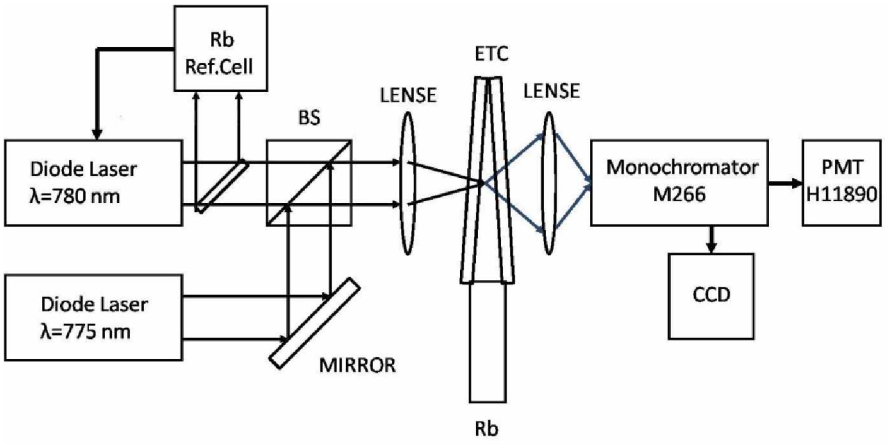

Fig. 2 Set-up. Beam-splitter BS combines two laser beams into one, the first lense condenses light into Extremely Thin Cell (ETC), 421 nm blue fluorescence is detected by photo-multiplier tube PMT or CCD.

Fig. 3 presents an example of the excitation spectrum of $6P_{3/2}$-level blue fluorescence when second laser was scanned around $5P_{3/2} \rightarrow 5D_{5/2}$ resonance line. The power of the second laser was minimized to suppress power broadening. Blue fluorescence intensity in dependence on the cell thickness, Rb number density and lasers light power were investigated and will be reported. Some line shape distortion could be explained taking into account unresolved hyperfine structure of $5P_{3/2}$ excited state. The observed minor lines originate from non-resonant two-photon excitations from ground state hyperfine sublevels of ^{87}Rb (two lines) and ^{85}Rb (one line). Note, also, that the measured line width is almost twice less than the Doppler width.

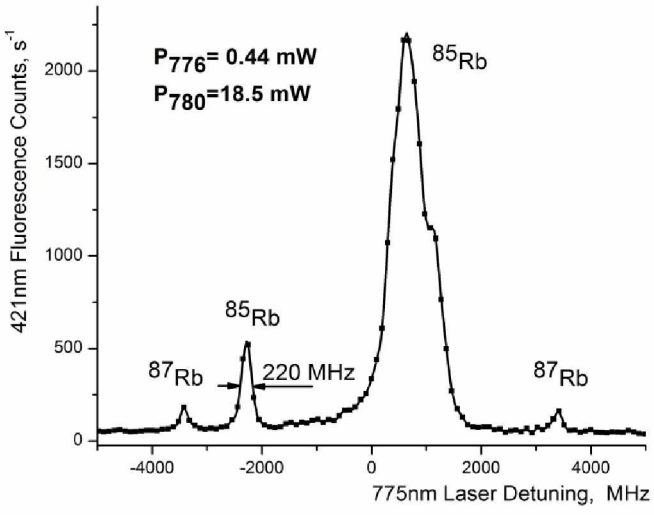

Fig. 3 Blue fluorescence line shape versus 775nm-laser detuning.

References

[1] K. A. Whittaker, J. Keaveney, I. G. Hughes, et al., Phys. Rev. A **92**, 052706 (2015).
[2] D. Sarkisyan, D. Bloch, A. Papoyan, M. Ducloy, Opt. Commun., **200**, 201 (2001).
[3] A. Akulshin, D. Budker, R. McLean, Opt. Lett., **4,** 845 (2014).

Numerical investigation of laser amplification of near transform-limited broadband pulses

V.A. Petrov[1,2], G.V. Kuptsov[1,3], V.V. Petrov[1,2,3], A.V. Laptev[1], A.V. Kirpichnikov[1] and E.V. Pestryakov[1]
[1]*Institute of Laser Physics SB RAS, Novosibirsk, Russia*
[2]*Novosibirsk State Technical University, Novosibirsk, Russia*
[3]*Novosibirsk State National Research University, Novosibirsk, Russia*
E-mail: petrov.nstu@gmail.com

Transform-limited pulses with energy level under hundreds of uJ and high repetition rates are necessary and essential tool for femtochemistry study and laser spectroscopy [1]. To satisfy requirements of these researches, the pulses should produce excellent pulse-to-pulse stability and broad bandwidth. There are lots of oscillators that generate transform-limited pulses with durations of a few hundreds of femtoseconds and nJ order of energy level. One of the ways of creation of a laser system that produces pulses such as described above could be amplification of the pulses without temporal stretching.

There are a few models describing the laser amplification process for significantly chirped pulses or an inhomogeneously broadened medium. These models are based on the iterative algorithm using Frantz-Nodvik equations for each independent frequency or solving the system of equations in accordance for instantaneous frequency independently, but all these models cannot be applied to the transform-limited pulses amplification in homogeneously broadened medium. Furthermore, the less pulse is chirped the less accuracy these models have, providing not correct results [2] for weakly chirped broadband or transform-limited pulses.

In this paper we present the model describing the laser amplification process of near transform-limited broadband pulses in homogeneously broadened medium. The model based on the system of rate equation coupled with photon-transport equation and written in the moving frame coordinates:

$$\begin{aligned}\frac{\partial I(z,t)}{\partial z} &= \sigma(\omega) I(z,t) N(z,t) \\ \frac{\partial N(z,t)}{\partial t} &= -\frac{\sigma(\omega)}{\hbar\omega} I(z,t) N(z,t)\end{aligned} \tag{1}$$

where I(z, t) – an intesity of laser pulse, c – the velocity of light, σ – emission cross-section, ω – the frequency of pulse, N(z, t) – an inversion population density. In our model $\sigma(\omega)$ is a function that represents the spectral distribution of emission cross-section. According with our assumption the production $\sigma(\omega)I(z,t)$ corresponds to the interaction of laser pulse with a medium and should be done in frequency domain:

$$\begin{aligned}\frac{\partial I(z,t)}{\partial z} &= N(z,t)\int_{-\infty}^{\infty}\left(\int_{-\infty}^{\infty} I(z,\tau)e^{-i\omega\tau}d\tau\right)\sigma(\omega)e^{i\omega t}d\omega = \\ &= N(z,t)\int_{-\infty}^{\infty} I(z,\tau)d\tau\int_{-\infty}^{\infty}\left(\sigma(\omega)e^{i\omega(t-\tau)}d\omega\right) = \\ &= N(z,t)\int_{-\infty}^{\infty} I(z,\tau)G(t-\tau)d\tau = N(z,t)S(z,t)\end{aligned} \tag{2}$$

In the equation (2) the function S(z,t) represents a convolution a laser pulse with a medium in time domain. For the second equation in the system (2) the same transformations should be done with $h\omega \approx h\omega_0$, where $\omega 0$ is a central frequency of laser pulse. Then system (2) is rewritten as:

$$\frac{\partial I(z,t)}{\partial z} = S(z,t)N(z,t)$$
$$\frac{\partial N(z,t)}{\partial t} = -\frac{1}{\hbar\omega_0}S(z,t)N(z,t) \quad (3)$$

The system (3) describes simultaneous interaction of all frequencies of the propagating pulse at each step along propagation axis, thus providing valid approach for the laser amplification of an unchirped pulse.

This system of equations was analyzed and we come to the conclusion that the proposed system provides information about the output characteristics of an unchirped pulse after passing through an active homogeneously broadened medium and about the population inversion inside the medium at any moment of time.

Investigation of amplification of 1 ps transform-limited laser pulse at 1030 nm central wavelength was done for Yb-doped media [4] (Yb:Y_2O_3, Yb:YAG) by using both of models and compared. We analyzed the evolution of spectral and temporal profiles of the pulse during propagation through the active medium. The dependencies of output intensity from the input pulse temporal profile and energy, the pump wavelength and power, length of active medium and its gain cross-section. We observed that increasing pulse spectral bandwidth leads to the lesser accuracy while using well-known models, but in our simulations we get the reliable results without dependency on the bandwidth.

This model could be used for simulations of laser amplification of weakly chirped broadband or transform-limited pulses in homogeneously broadened medium.

This work is supported in part by RAS Program "Extreme laser radiation: physics and fundamental applications", registration number AAAA-A15-115113010002-9 and Government program, registration number 01201374306.

References

[1] R. Guichard, J. Caillat, S. Haessler et al., Springer Series in Optical Sciences **177**, 191-206 (2013)
[2] P. Raybaut, F. Balembois, F. Druon et al., IEEE journal of quantum electronics **41**, 415-425 (2005).
[3] Sh. Matsuoka and K. Yamakawa, Jpn. J. Appl. Phys. **37**, 5997-6000 (1998).
[4] **V.** V. Petrov, E. V. Pestryakov, V. A. Petrov et al., Laser Phys. **24**, 074014 (2014).

Experimental characteristics of polymer terahertz photonic crystal fiber for laser control

B.V. Poller[1], A.V. Britvin [1], A.V. Povazhaev[1], A.B. Poller[2], E.N. Chesnokov[3]
[1]*Institute of Laser Physics of SB RAS, Pr. Lavrentyeva 13/3, Novosibirsk, 630090, Russia*
[2]*ZAO«SKB», st. Plotinnaya 7, Novosibirsk, 630058 Russia*
[3]*Voevodsky Institute of Chemical Kinetics and Combustion SB RAS, Institutskaya 3, Novosibirsk, 630090, Russia*
E-mail: lablis@mail.ru

Laser Terahertz (THz) control systems require waveguide and selective elements. Currently waveguides for the transmission of terahertz radiation [1-2] are studied. Creating a photonic crystal fibers (PCF) with a hollow core reduces losses and allows to select the THz signals.

We have proposed the formation variant of periodic structures using the assembly of polymer waveguides [2] to generate PCF. In order to generate a hollow core PCF we have proposed the method of forming a waveguide of the folded film with fibers attached to it Fig. 1 (b-c).

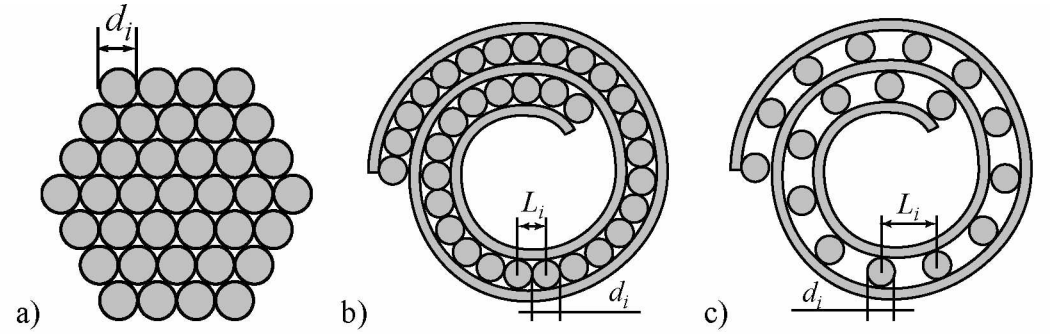

Fig. 1 Formation of the photonic crystal fiber with set of fibers: a) tight assembly; b) dense spiral convolution; c) sparse spiral convolution.

Fibers with diameter of 350 ± 25 microns is used in the manufacturing of PCF samples. PCF formation iscarried out in a polypropylene tube of 10 mm inner diameter and a wall thickness of 1.5 mm. The measurement of waveguides spectral transmittance characteristics is taken with BRUKER IFS 66v/S spectrometer in the synchrotron radiation center at the ICKC, Russian Academy of Sciences.

Fig. 2 shows the transmission spectra of the polypropylene rod, PCF with a dense arrangement of fibers based on the self-organization and PCF formed by spiral convolution of fibers on the film (film thickness of 9 and 18 microns). The sample length is 10 mm.

The transmission spectra of PCF with a spiral periodic structure arouse the greatest interest. Fig. 3 shows the transmission spectra of PCF with a spiral structure with a different film thickness and length of the samples. For comparison, the figure shows the range of polypropylene rod transmission.

The greater transmission compared with other samples is primarily due to the appearance of air cavities. The graph clearly shows the frequency changes of the transmission spectrum. It should also be noted the diminution of waveguides transmission above 50 microns, taking into account that the transmission of the polypropylene is increased in this range.

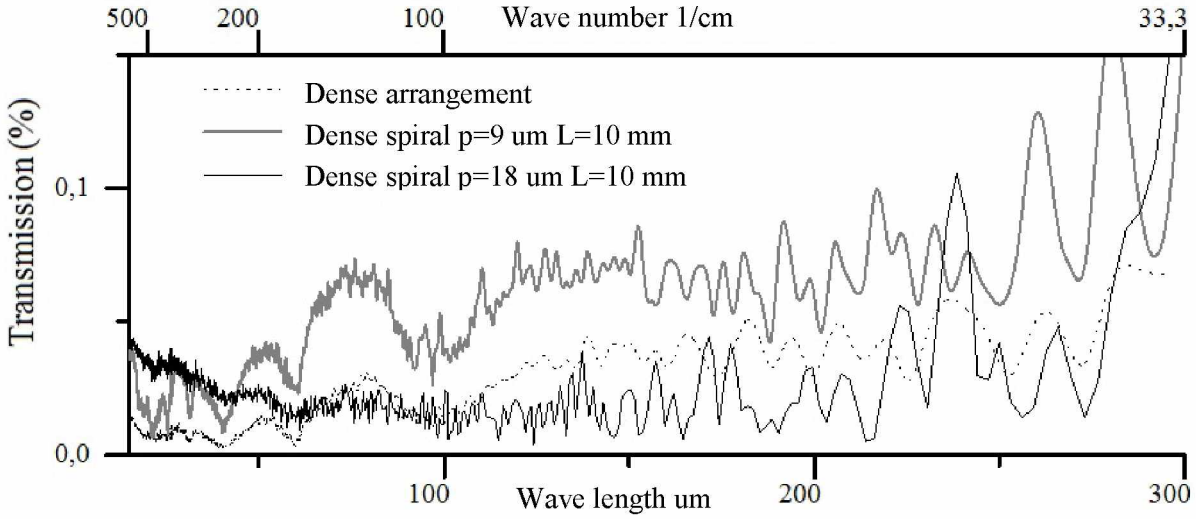

Fig. 2 The waveguide samples transmission range.

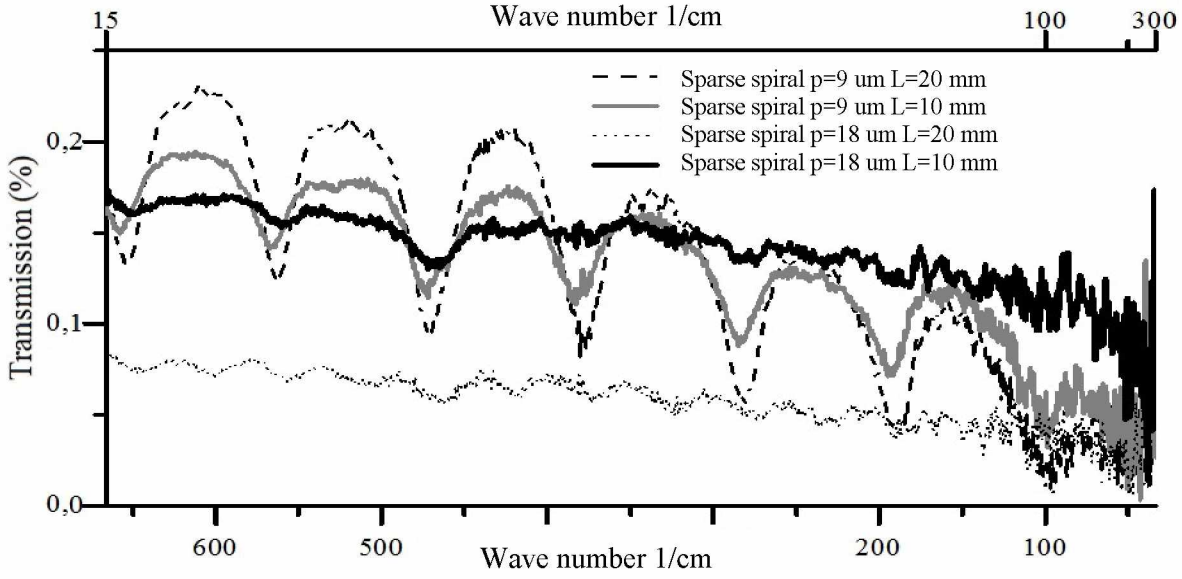

Fig. 3 PCF transmission spectrum with a sparse spiral convolution.

It should be noted that the observed periodic changes of the THz radiation transmission that are more than 2 times on the interval 15-100 microns with a period of the wave number of 110 cm^{-1} indicates that the reflection angle of Thz radiation is changed due to the periodic variation of the waveguide wall material refraction index and respectively the transmittion factor of the photonic crystal fiber is also changed.

This type of photonic crystal waveguide can be used as a comb filter of THz radiation.

References

[1] Bora Ung, Anna Mazhorova, Alexandre Dupuis, Mathieu Rozé, and Maksim Skorobogatiy, "Polymer microstructured optical fibers for terahertz wave guiding", Optics Express **19**, B848–B861 (2011).

[2] B.V. Poller, V.M. Klementyev, Y.D. Kolomnikov, S.I. Konyaev, S.I. Trashkeev, A.B. Poller, O.A. Wanda, The characteristics of the polymer terahertz photonic crystal fiber models of and nanocomposite liquid crystal transducers of laser and thermal radiation // GEO-Siberia-2011. T. 5. Specialized instrumentation, metrology, thermal physics, microengineering. Part 2: Mater. IV International. Scien. congress "GEO-Siberia 2011", 19-29 April 2011, Novosibirsk. - Novosibirsk: SSUGT 2011 [in Russian]

Effect of temporal delay in formation of coherent population trapping resonance in ^{87}Rb under dynamic excitation

I. Popkov[1], S. Khripunov[1], D. Radnatarov[1], S. Kobtsev[1], V. Andryushkov[1], M. Basalaev[1] and M. Balabas[2]
[1]*Novosibirsk State University, Novosibirsk, Pirogova st., 2, Russia*
[2]*Saint Petersburg University, St. Petersburg, Lt. Shmidt Embarkment, 11, Russia*
E-mail: ivan.popkov@yahoo.com

The present work reports the results of studies of a new effect, which manifests itself as a temporal delay of electromagnetically induced transparency on the atomic D_1 line of rubidium under dynamic excitation of its Λ-system of levels by bi-chromatic pump field. It was found out that as the system excitation frequency rises, the maximum of the coherent population trapping (CPT) resonance is reached at progressively later phase of the periodic signal controlling the system excitation.

CPT resonance in this three-level system was created by scanning the frequency difference of the bi-chromatic pump field around the ground-state hyperfine-splitting frequency (6.834 GHz) of ^{87}Rb. At relatively slow scan rates (~1 Hz) of the frequency difference, the maximum of the CPT resonance was met at the moment when the frequency difference of the bi-chromatic pumping field became equal to the value of the ground-state hyperfine-splitting frequency. At higher scan rates (>100 Hz), the CPT resonance maximum occurred at a later moment.

We studied this effect of CPT resonance formation in rubidium cells of two different types: one with buffer gas and the other with anti-relaxation wall coating. To quantify the effect, we measured the phase delay, or phase incursion of the periodical signal controlling the frequency difference of the bi-chromatic pumping field, at which the CPT resonance maximum occurred. Fig. 1 demonstrates both experimental and theoretical dependencies of the phase delay upon the scan frequency of the frequency difference of the bi-chromatic pump field. There is a clear correlation between the theoretical and experimental curves, which both reach saturation at comparatively high scan frequencies.

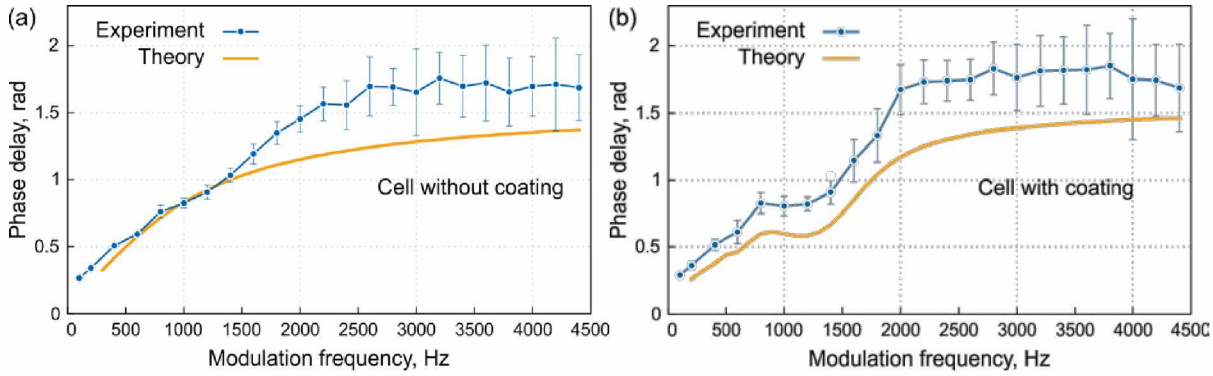

Fig. 1 Dependence of the phase delay upon the scan frequency of the frequency difference of the bi-chromatic pumping field: a) optical cell with buffer gas, b) optical cell with anti-relaxation coating of the inside wall surface.

The present work provides details of the conducted experiments and modelling methods, discusses the influence of the discovered effect on stability of atomic clocks relying on dynamically excited CPT resonances.

The present work was carried out with support from Russian Science Foundation Grant №16-12-10147.

Terahertz vibrations in intracellular media

S.S. Popova
Institute of Laser Physics SB RAS, Ac.Lavrentyev's prosp., 13/3, Novosibirsk 630090, Russia
Novosibirsk State University, Pirogova Str., 2, Novosibirsk 630090, Russia
E-mail: svt9ppv@gmail.com

Terahertz vibration properties in biological material are still not entire clear. Strong coupling between electromagnetic and acoustic vibrations led to enhanced nonlinearity. The properties studies are a valuable type of basic science research because they serve to enhance our fundamental understanding of the biological activity nature.

The key question consists of the energy distribution in biological media. Most of authors implicitly presume equilibrium distribution in homogenous media for biological condition. This model is not feasible for intracellular media due to two factors: (1) processes in live material occur far from thermodynamic equilibrium, and (2) living cells inner media is ordered by a network of tubules forming the cytoskeleton that dramatically differ from homogeneity.

Except thermodynamic equilibrium there are two possibilities for energy distribution. First of it connect with inhomogeneous distribution of thermal energy in sample. In this case there is local thermal equilibrium without remarkable features in energy levels distribution. More sophisticated and interesting case is non-equilibrium energy level distribution like in laser active media population inversion.

Several researchers have proposed that nearly all of energy can concentrated in just one of vibrational mode. These theories were initially hypothesized by Frohlich in series seminal papers published between 1960 and 1980 years [e.g. 1, 2]. On the basis of the general principles Frohlich derived a rate equation using a special type of interaction of a vibration system with its surroundings. Remarkable implication of the rate equation is the possibility of process like Bose-condensation in biological media under room temperature. The coherent endogenous electric field of oscillating nature is assumed to be the key factor of biological order.

Living cells inner media is ordered by a cytoskeleton that can affect non-equilibrium distribution of energy in intermolecular vibrations. The landscape of almost all biological macromolecules and kinetics of biochemical process are influences by spatial characteristics. The cytoskeleton organizes the cell, mediates transport of molecules, structures, organelles, and other cell components. Microtubules structuring cytoskeleton possess interesting properties [3, 4]. It is unique ordering differ from both the homogenous media and the crystalline structures with translation symmetry.

Knowledge of the terahertz vibration properties is critical for general understanding the life nature and requires explicit treatment.

References

[1] H. Frohlich, Phys. Lett. A **26**, 402 (1968).
[2] H. Frohlich, Phys Lett. A **39**, 153 (1972).
[3] M. Caplow, R.L. Ruhlen, J. Shanks, J. Cell Biol. **127**, 779 (1994).
[4] M.V. Sataric, J. Pokorny, J. Fiala et al., Bioelectrochem. Bioenergetics **41,** 53 (1996).

Absorptive optical bistability in an active interferometer

D. Primakov, P. Pokasov and S. Bagayev
Institute of Laser Physics SB RAS, Lavrentyev avenue 13/3, Novosibirsk, 630090, Russia
E-mail: dima@laser.nsc.ru

The paper is dedicated to investigations of transmission regimes of an interferometer of Fabry-Perot type with saturated amplifying and absorbing media inside. We call such interferometer as an active one. The influence of saturation type of the absorbing medium on forming nonlinear transmission regimes of the active interferometer is considered in details.

Bistable regimes of transmission of an active interferometer are of great interest for an amplification of weak optical signals, for use in optical logic schemes and for investigations of such processes as fluctuations, optical turbulence etc [1].

It is known that an interferometer with a saturated absorber inside can demonstrate bistable regimes of transmission in the one case only when saturation of absorption has a homogeneous type [2]. For the first time it is shown that the presence of a saturated amplifying medium inside the interferometer allows one to obtain optical bistability at any saturation type of both absorbing and amplifying media.

The principles of an amplification of weak optical signals and the use of an active interferometer for this purpose are described. It is shown that the contrast of bistable transition and the efficiency of weak signal amplification correspondently depend on the ratio of saturation parameters in amplification and absorption media. Results of some experiments with an active interferometer both on the basis He-Ne/CH_4 and on the basis of CO_2/SF_6 (nonlinear amplifier/absorber) are provided. At the last case an enhanced contrast of bistable transition at a level of 10^4 was observed [3].

References

[1] H. Gibbs. Optical Bistability: Controlling light with light, (New York: Academic Press), 1985.
[2] S. Bagayev and P. Pokasov, Laser Physics **10**, 894 (2000).
[3] S. Bagayev, V. Chebotayev, M. Ostromensky, P. Pokasov, Laser Physics **4**, 299 (1994).

Laboratory simulations of Alfven waves via collisionless interaction of laser plasma injected in magnetized background plasma

P. Prokopov, Yu. Zakharov, V. Tishchenko, I. Shaikhislamov, V. Posukh, A. Melekhov, A. Ponomarenko, E. Boyarintsev
Institute of Laser Physic, SB RAS, Novosibirsk, Av. Lavrentyeva 13/3, 630090, Russia
E-mail: paprok312@gmail.com

Collisionless interaction of interpenetrating plasma flows was studied in this work. Cloud of explosive Laser-produced Plasma (LP) expanding in magnetized Background Plasma (BP) generates plasma perturbations propagating along the external magnetic field. Here we consider perturbations with signs of Alfven Wave (AW), and high-frequency whistler precursor.

Experiments were carried out at KI-1 facility [1]. Large scale high-vacuum chamber 5 m long and 1.2 m diameter kept a vacuum of ~ 10^{-6} Torr can be filled by means of θ-pinch with the background plasma (H^+ or He^+). LP-clouds can be generated by two independent microsecond-pulse CO2-laser systems with similar parameters of radiation focused on a flat (or convex) polyethylene target (focal size of laser spot ∅2.5 cm). External magnetic field up to 500 Gs along the chamber axis is created by quasi-stationary current in a solenoid covering the entire outer surface of the vacuum chamber. Diagnostic of plasma is performed using double Langmuir probes, magnetic probes and Rogowski coil for direct detection of current J_Z related to AW [2–4].

In this experiment LP is injected along the chamber axis and along the external magnetic field lines. BP and LP are sufficiently collisionless and interaction takes place due to a so-called magnetic laminar mechanism (MLM) or Larmor coupling [5–7]. LP, propagating with velocity V_0, forms a so-called magnetic cavity (area of displaced external magnetic field), the curl electric field E_φ is generated at its boundary. BP-ions accelerate along to this field, while ions of LP are decelerated in their Larmor rotation (opposite to E_φ). Effectiveness of this mechanism depends mainly on a MLM-parameter $\delta = R_*^2 / R_L R_{L*} \geq 1$, where $R_* = \left(3N_e / 4\pi n_*\right)^{1/3}$ – the radius of diamagnetic cavity (N_e – total number of electrons, n_* – concentration of BP-ions), R_L, R_{L*} – Larmor radii of LP-ions and BP-ions respectively. Axial current J_Z and corresponding circular magnetic fields are generated as a result of this interaction, which could generate AW propagating along external magnetic field lines.

Registered signs of AW are longitudinal current J_Z and corresponding transverse component of magnetic field, which propagates along the chamber axis with the speed close to Alfven speed (calculated value of Alfven speed ≈ $6.96*10^6$ cm/s, with plasma parameters B_0 = 100 Gs, BP density $n^* = 10^{13}$ cm^{-3}, BP ions – H_+). Fig. 1 illustrates, that perturbations of current and magnetic field are time correlated. Experimental speed of AW, calculated as ratio of distance from target to probe and time of arriving of front of J_Z perturbation, is 106 cm / 15 μs = $7.07*10^6$ cm/s with considering the own speed of BP.

Derivatives of variation of magnetic fields transverse components are presented at fig 2(a). They more clearly illustrate that there is high-frequency precursor in front of a maximum of magnetic field perturbation. This so-called whistler precursor [8] propagates at a speed ~300 km/s, has right-hand circular polarization. The direction of polarization changes from right-handed to left-handed when AW arrives at the probe. This moment can be clearly seen at the fig. 2(b), which illustrates the hodograph of transverse component of magnetic field.

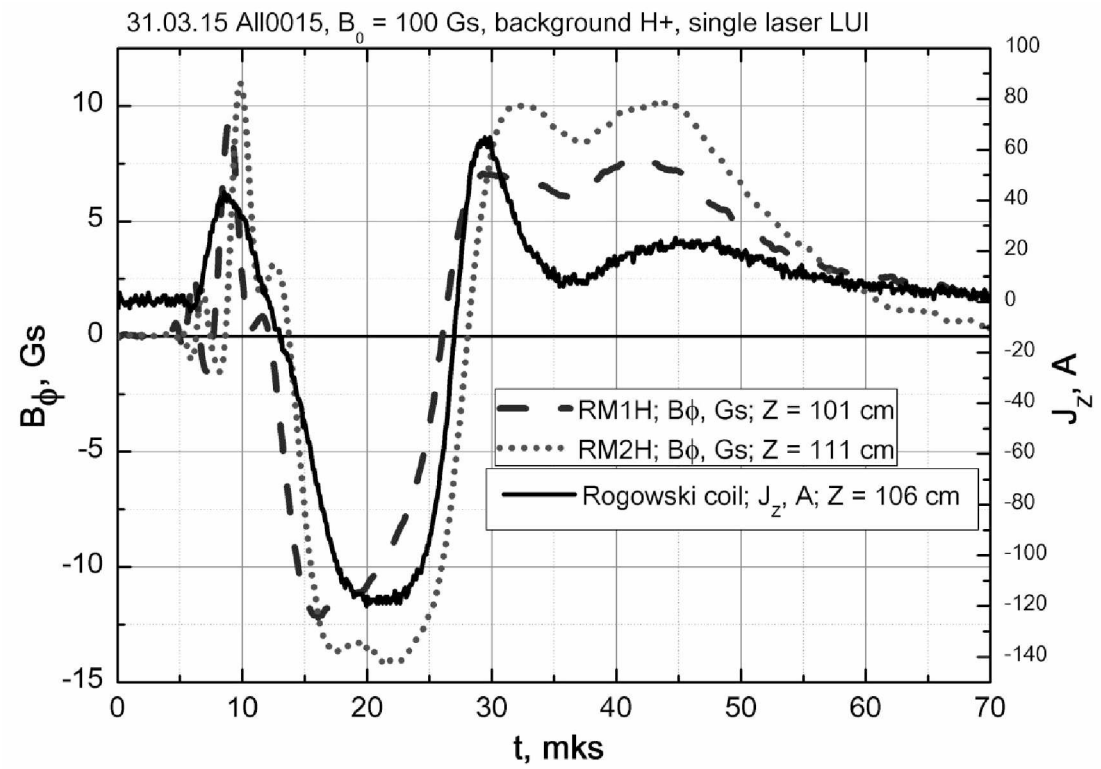

Fig. 1 Perturbations of longitudinal current J_Z and corresponding magnetic field Bφ.

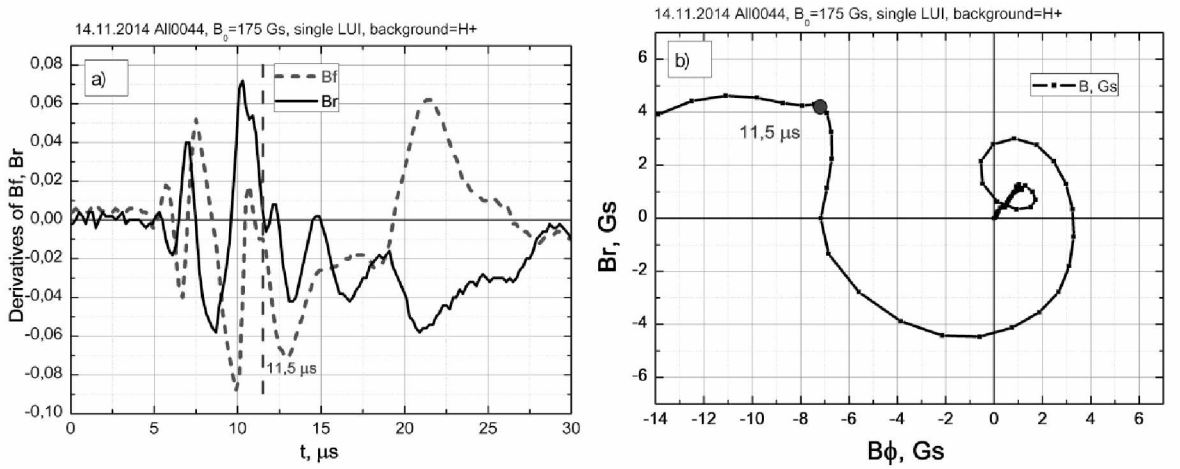

Fig. 2 a) Derivatives of Bφ and Br variations have high frequency oscillations on the front of perturbations; b) hodograph of transverse component of magnetic field, polarization changes its direction at the moment 11.5 μs.

This work was carried out in the framework of the research ILP SB RAS II.10.1.4 (01201374303); RAS Presidium Program "Fundamental principles of dual-use technologies…"; RAS Presidium Program #21 "Extreme laser radiation: Physics and fundamental applications".

References

[1] Yu. Zakharov, IEEE Transactions on Plasma Sc. **31**, 1243 (2003).
[2] W. Gekelman et al., J. of Geophys. Res.: Space Phys. **108**, A7 (2003).
[3] C. Niemann, W. Gekelman, C. Constantin et al., Phys. of Plasmas **20**, 012108 (2013).
[4] V. Oraevsky, Y. Ruzhin, V. Badin et al., Advance in Space Res. **29**, 1327 (2002).
[5] V. Terekhin, A. Golubev, V. Bashurin, J. of Appl. Mech. and Tech. Phys. **5**, 10 (1983).
[6] Yu. Zakharov, V. Antonov, V. Bashurin, et al., J. of Appl. Mech. and Tech. Phys. **6**, 3 (1985).
[7] I. Shaikhislamov, Yu. Zakharov, V. Posukh et al., Plasma Phys. and Controlled Fusion **41**, 1 (2015).
[8] G. Dudnikova et al., Plasma Astrophys. ESA SP-V**311**, 191 (1990).

Self-saturation of two-and three-level nondegenerate transitions in spectroscopy of the unidirectional waves

E.G. Saprykin [1], A.A. Chernenko[2], A.M. Shalagin[1,3]
[1]*Institute of Automation and Electrometry of SB RAS, Pr. Koptuga 1, Novosibirsk, 630090 Russia, tel. 330 68 69*
[2] *Insitute of Semiconductor Physics of SB RAS, Pr. Lavrentyeva 13, Novosibirsk, 630090 Russia, tel. 333 24 08*
[3] *Novosibirsk state university, Pirogova st.2, Novosibirsk, 630090 Russia, tel. 330 68 69*
E-mail: chernen@isp.nsc.ru

Results of development of theory of the nonlinear optical phenomena caused by self-saturation of transitions under action of the spontaneous radiation of extended system in a method of the probe field [1-4] on a case of strong and probe waves of one direction of propagation are submitted. Within developed model of the self-saturation transition effect [1], using analytical and numerical methods, spectroscopic manifestations of this effect in system of two- and three- nondegenerate atom levels (Λ- and V-type of transitions) are investigated.

It is shown that in case of the unidirectional waves in action of effect of self-saturation are displayed both the regularities, observed at opposite directed waves [2-4], and specific properties are found. The general property is formation of the uniform strip of saturation in the probe field work leading to reduction of amplitude of the absorption line counter of the probe field, and also to reduction of amplitude and saturated width of populational part of the nonlinear resonance.

Specifics of manifestation of self-saturation effect in the unidirectional waves are caused by existence in spectra of the saturated absorption resonances of two and three level systems the narrow structures in the form of enlightenment peak, or absorption peak, an essential contribution to which make nonlinear interferential effects.

Influence of the self-saturation effect on parameters of the nonlinear resonance narrow structures carries other character than in case of opposite directed waves: effect reduces amplitudes of narrow structures on the considered transitions, but differently influences on widths of these structures. In two-level system self-saturation leads to broadening of structure in the form of a dip and to narrowing of the peak form structures. In three-level system self-saturation isn't shown in widths of narrow structures of nonlinear resonances.

References

[1] S.G. Rautian, E.G. Saprykin, A.A. Chernenko, Opt. Spectrosc. **98**, №2, 292 (2005).
[2] S.G. Rautian, E.G. Saprykin, A.A. Chernenko, Opt. Spectrosc. **98**, №3, 476 (2005).
[3] S.G. Rautian, E.G. Saprykin, A.A. Chernenko, Opt. Spectrosc. **99**, №6, 1014 (2005).
[4] S.G. Rautian, E.G. Saprykin, A.A. Chernenko, Opt. Spectrosc. **104**, №4, 647 (2008).

Influence of spontaneous emission on working transition to the sign and structure of the nonlinear absorption resonance of two-level system in spectroscopy of the unidirectional waves

E.G. Saprykin [1], A.A. Chernenko[2], A.M. Shalagin[1,3]
[1]*Institute of Automation and Electrometry of SB RAS, Pr. Koptuga 1, Novosibirsk, 630090 Russia, tel. 330 68 69*
[2] *Insitute of Semiconductor Physics of SB RAS, Pr. Lavrentyeva 13, Novosibirsk, 630090 Russia, tel. 333 24 08*
[3] *Novosibirsk State University, Pirogova st.2, Novosibirsk, 630090 Russia, tel. 330 68 69*
E-mail: chernen@isp.nsc.ru

Analytical and numerical researches of the saturated absorption resonance line shape of two-level gas environment in the field of two unidirectional waves are conducted. It is shown that, both at motionless, and at moving atoms, the nonlinear resonance line shape can considerably change at modification of a ratio between values of the level relaxation constants Γ_m , Γ_n and the first Einstein coefficient of A_{mn} , determining a share of spontaneous disintegration of the upper level by working transition (branching parameter of radiation). At the same time the narrow nonlinear resonance arising in work of the probe field on transitions with the long-living lower level ($\Gamma_m >> \Gamma_n$) depending on a sign of the value $\Gamma_m - A_{mn} - \Gamma_n$ can be shown as in the form of a traditional dip (at $\Gamma_m - A_{mn} > \Gamma_n$), and in the form of peak (at $\Gamma_m - A_{mn} < \Gamma_n$). The possibility of peak structure of a nonlinear resonance is found for the first time. In case of transitions with the long-living upper level ($\Gamma_n >> \Gamma_m$) the narrow resonance shape is shown only in the form of a dip. Transformation of the resonance shape from a dip in peak is caused by specifics of a relaxation of the lower level population beats on the closed or almost closed transition when disintegration of the upper level completely or almost completely happens on working transition. Features of the saturated absorption line spectrum at transition $^1S_0$ - $^1P_1$ in the counter and unidirectional waves are discussed.

Resonances of electromagnetically induced transparency and electromagnetically induced absorption in spectra of magnetic scanning on transition with J=1

E.G. Saprykin [1], A.A. Chernenko[2], A.M. Shalagin[1,3]
[1]*Institute of Automation and Electrometry of SB RAS, Pr. Koptuga 1, Novosibirsk, 630090 Russia, tel. 330 68 69*
[2] *Insitute of Semiconductor Physics of SB RAS, Pr. Lavrentyeva 13, Novosibirsk, 630090 Russia, tel. 333 24 08*
[3] *Novosibirsk State University, Pirogova st.2, Novosibirsk, 630090 Russia, tel. 330 68 69*
E-mail: chernen@isp.nsc.ru

Results of the theoretical analysis of the physical processes leading in experiments [1-4] to essential distinction of the magnetic scanning spectra at change of mutual orientation of the polarization planes of laser waves are submitted.

In model of atomic transition with full level moments J=1 stationary and non-stationary numerical solutions of equations for density matrix in the gas environment resonantly interacting with two counter and unidirectional light waves are received. Behavior of the saturated absorption resonance shapes and spectra of magnetic scanning depending on relaxation characteristics of transitions (widths of levels and transitions, branching parameter of radiation), directions of propagation and mutual orientation of polarization, and also intensities probe and strong wave are investigated.

It is shown that for a long-living lower state both at opposite directed [5], and at the unidirectional waves the main process defining features of the magnetic scanning spectra from mutual orientation of the polarization planes of light waves (resonances of EIT and EIA [1-4]) is the magnetic coherence induced by the linear polarized strong field between levels at the lower state of atomic transition. The maximum contribution due to the transfer process of magnetic coherence from the upper levels on lower state doesn't exceed 10% of amplitude of a nonlinear resonance, and the contribution of nonlinear polarization at a combinational frequency makes still smaller value. Features of the magnetic scanning spectra on closed and almost closed transitions in the unidirectional waves are found.

It is established that the shape of a nonlinear resonance in case of counter waves at orthogonally polarized fields depends essentially on openness degree of atomic transition, and at parallel polarization this dependence is expressed poorly. In case of the unidirectional waves qualitative dependence of the nonlinear resonance shape on orientation of the polarization planes of waves is found, at the same time influence of the transition openness degree is shown only quantitatively in amplitudes of resonance structures.

Researches of the more complex models of atomic transition (J=2-J=1, J=2-J=2) in a stationary case give qualitative consent with results of calculations for transition with J=1 both on spectra of nonlinear resonances, and on spectra of magnetic scanning.

References

[1] F.M. Akulshin, S. Barreiro, and A. Lesama, Phys.Rev. A **57**, 2996 (1998).
[2] Y.J. Lee, H.J. Lee, I.-H, Bae et.al., Phys.Rev. A **81**, 023416 (2010).
[3] S.K. Kim, B.S. Moon, K. Kim et.al., Phys.Rev. A **68**, 063813 (2003).
[4] D.V. Brazhnikov, A.V. Taichenachev, A.M. Tumaikin, et.al., *JETP Lett* **91**, 625 (2010).
[5] E.G. Saprykin, A.A. Chernenko, A.M. Shalagin, *JETP*, **140**, 229 (2014).

Many-particle losses in a linear Paul trap

I. Semerikov[1,2], I. Zalivako[1,2,4], A. Borisenko[1,2,4], T. Shpakovky[1,2], V. Sorokin[1] , K. Khabarova[1,2,3] and N. Kolachevskiy [1,2,3]

[1]*P.N. Lebedev Physical Institute, 119991 Moscow, Leninsky prospekt 53, Russia*

[2]*Russian Quantum Center, 143025 ul. Novaya 100, Skolkovo, Moscow region, Russia*

[3]*VSUE VNIIFTRI, 141570 Mendeleevo, Moscow Region, Russia*

[4]*Moscow Institute of Physics and Technology (State University), 141700 Dolgoprudny, Moscow Region, 9 Institutskiy per., Russia*

E-mail: ilia179@mail.ru

Single ions and their ensembles trapped in ion trap are widely used for many scientific applications ranging from frequency standards [1] to quantum computing and simulations [2]. Some key benefits of such systems include very low achievable temperatures of the ions in a trap, long coherent time and lifetime up to several months. One of the interesting objects for quantum computing appears to be the ion Coulomb crystals that can be observed when trapped ions are cooled below a certain critical temperature. To create an ion crystal several tens of ions should be trapped, stored and cooled. Losses mechanisms of different nature may limit the number of stored ions.

In our setup in LPI ions are created by means of electron irradiation of the neutral magnesium atoms in the center of the linear Paul trap. Thus the temperature of the trapped Mg^+ ions before laser cooling is high and the lifetime is measured to be 1.7 s . To study the loss process at high temperatures the numerical simulation of the ion dynamic in the trap was performed. It was shown that for number of ions from 10 to 15 the main loss mechanism is similar to evaporation and should not play significant role at lower temperatures. Indeed, after applying laser cooling the lifetime was measured to be 120 s which is in good agreement with our calculations. Simulations also demonstrated that collision events with the residual background gas molecules are rare and cannot influence the lifetime at high temperatures.

References

[1] C. W. Chou, D. B. Hume, Koelemeij, J. C. J. et al., Phys. Rev. Lett. **104**, 070802 (2010)

[2] J. I. Cirac, P. Zoller, Phys. Rev. Lett.**74**, 4091 (1995)

Nonlinear optical properties of poled chromophore-doped polyimides and electro-optical devices based on them

A.E. Simanchuk[1], S.N. Atutov[1], S. L. Mikerin[1], A.I. Plekhanov[1], V.A. Sorokin[1], A.V. Yakimansky[2], N.A. Valisheva[3]

[1]*Institute of Automation and Electrometry of the Siberian Branch of the Russian Academy of Sciences, pr. Koptyuga 1, 630090 Novosibirsk, Russia*

[2]*Institute of Macromolecular Compounds of the Russian Academy of Sciences, Bolshoi pr. 31, 199004 St. Petersburg, Russia*

[3]*Institute of Semiconductor Physics of the Siberian Branch of the Russian Academy of Sciences, pr. Lavrentieva 13, Novosibirsk, Russia, 630090*

E-mail: simmk@yandex.ru

Chmophore-doped polymers ordered by an external electric field possesses unique electro-optical (EO) response, which is more an order of magnitude higher than analogous solid state crystalline structures (for example lithium niobate). Such high nonlinearity allows to reduce the operating voltage of the modulators based on these materials by an order of magnitude. Moreover, the frequency dispersion of refractive index of the polymer structures is much less than crystalline counterparts and allows optical and radio waves propagate in-phase over long distances, ensuring a high conversion efficiency at microwave frequencies modulating. Besides high nonlinearity, material working at high modulating frequencies, and therefore in conditions of high heat for a long time, must possess the thermal stability of these nonlinear optical properties. The use of polyimide as a polymeric backbone for the merging of optically active chromophores opens up new possibilities for electro-optic materials with high temperature and temporal stability of the nonlinear response[1,2].

Here we present the results of experimental investigation the dispersion of nonlinear optical response and EO properties of the original chromophore-containing polyimides with covalently attached commercial chromophores DR1 and DR13. These investigations were performed by the method of second harmonic generation and Teng-Man technique.

The maximum values of the d_{33} were founded to be from 25 to 120 pm/V, depends on the samples. It is shown that the nonlinear response remains stable at temperatures up to 120 °C.

We have experimentally demonstrated the electro-optic modulation properties of the phase modulator based on the studied materials.

This work was supported by RFBR 14-29-08134 grant.

References

[1] Larry R. Dalton, William H. Steier, Bruce H. Robinson et. al., J. Mater. Chem., 1999, 9, 1905-1920.

[2] Larry R. Dalton, Philip A. Sullivan, and Denise H. Bale, Chem. Rev., 2010, 110, 25–55.

Vibration measurement based on modulation of laser radiation

V. Sobolev, E. Utkin, G. Kashcheeva and A. Shcherbachenko
Institute of Automation and Electrometry, Siberian Branch of the Russian Academy of Sciences (IAiE SB RAS), Novosibirsk, 630090, RUSSIA
E-mail: sobolev@iae.nsk.su

Most modern laser systems for contactless measurement of vibration are based on the Doppler effect and differ by complexity and very high cost. It is mainly caused by the fact that for extraction the Doppler signal's frequency proportional to the vibration velocity they use interference of laser radiation scattered by the vibrating object and the reference radiation. The report suggests ways to simplify and reduce the cost of these systems through the use of power or amplitude modulation of the probe laser field. At the same time such complex and capricious node as an interferometer is excluded from the Doppler system, and on the output, in contrast to existing systems, a signal proportional to vibrodisplacement is generated.

We shall consider a case of laser power modulation. Let modulating function has the form $P(t) = \left[1 + m \cdot \cos(\Omega t)\right]$, where m is the modulation index, and Ω - the modulation function angular frequency. Analysis showed that the spectrum of the modulated field corresponds to Fig. 1a. During the motion of the object spectrum of the scattered field has the form shown in Fig 1b. It is seen that each harmonic is Doppler shifted on the frequency and the distance between them remained equal, but increased by a certain amount.

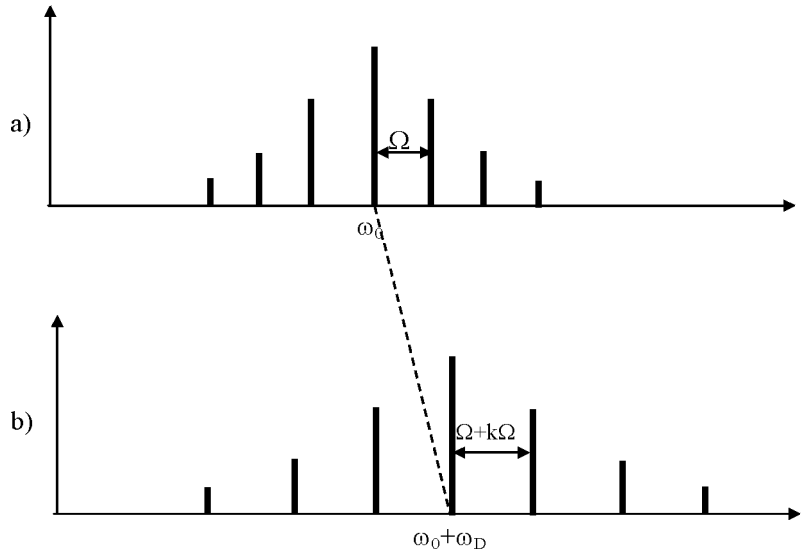

Fig. 1 Signals spectra: a) probing radiation b) reflected field, ω_0 -carrier frequency.

The signal at the output of the photodetector as authors shown becomes $I_d(t) = \left\{1 + \cos\left[\Omega(1+K)t\right]\right\}$. We see that it is similar to the modulating function P(t), but shifted to a new Doppler frequency proportional to the velocity and equal ΩK. Coefficient K = 2V/C, where C is the light velocity.

To select the new Doppler shifted signal frequency the spectrum of the signal $I_d(t)$ is transferred to area zero frequencies and multiplying by the quadrature signals of modulating function we receive two complex signal components with new Doppler frequency Ω_D equal to $K\Omega$:

$$Z_C(t) = \cos(K\Omega t); \quad Z_S(t) = \sin(K\Omega t)$$

The phase of this complex signal is proportional to the instantaneous value of the vibrodisplacement, and the following algorithm is used to evaluate it: $\varphi_n = \arg(Z_n^* Z_{n+1})$, where Z_n and Z_{n+1} are the complex signal discrete counts at the moments t_n, t_{n+1}.

It follows from the foregoing that the proposed method and the corresponding measurement system design does not need the interferometer of optical fields. This is a very important advantage of the proposed principle, as it allows the use not only coherent, but any light source to form a probe beam. For the experimental verification of the proposed principle the setup has been designed which functional diagram is presented in Fig. 2. Output signal oscillogram at vibration amplitude of 6 mm and frequency 2 Hz is presented in Fig. 3.

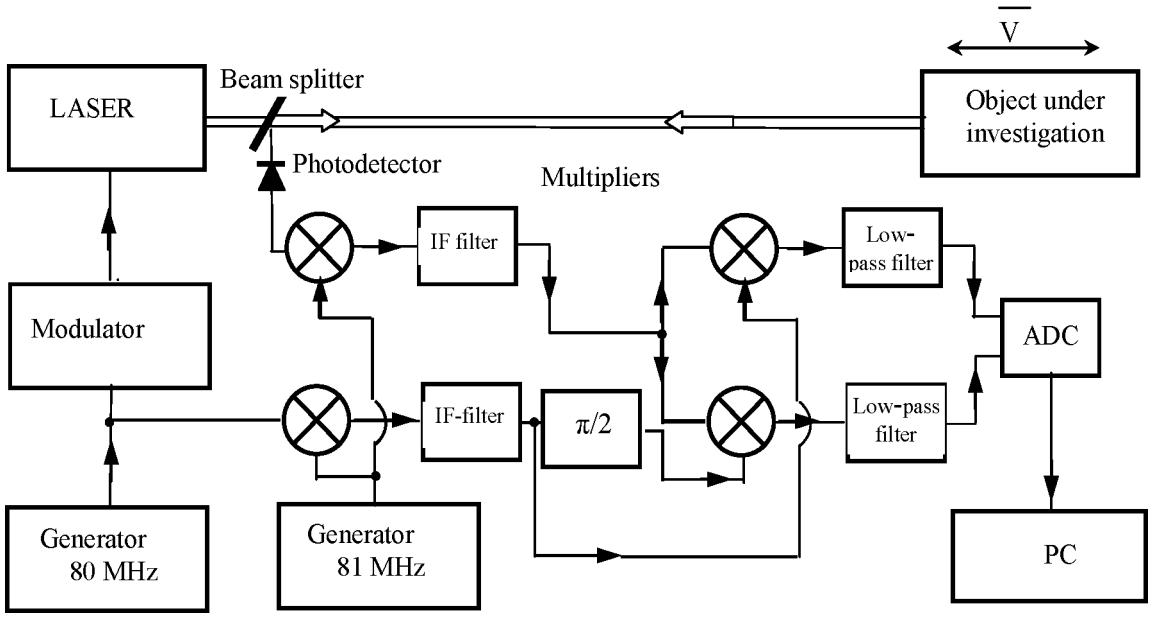

Fig. 2 Functional diagram of the setup for vibration measurements.

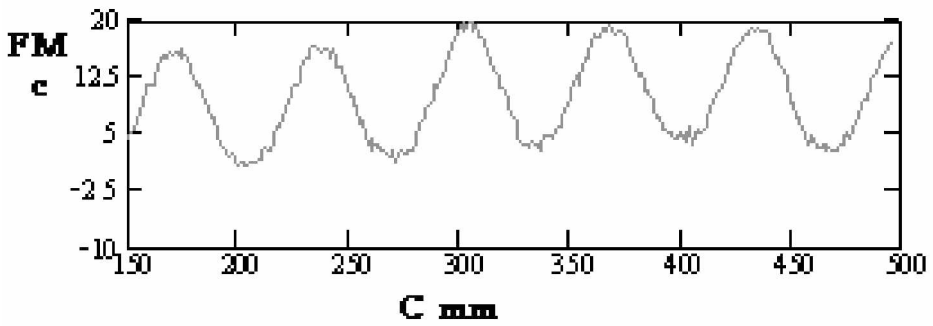

Fig. 3 Output signal waveform at vibration amplitude of 6 mm and frequency 2 Hz.

Passive synchronization of erbium and ytterbium doped fiber Q-switching lasers induced by 1530 nm laser pulses in common graphene saturable absorber

F. Song [1], Y.Y. Ren [2], M. Feng[3]

[1]*The Key Laboratory of Weak-Light Nonlinear Photonics, Ministry of Education, School of Physics and TEDA Applied Physics School, Nankai University, Tianjin 300071, China*

[2]*Key laboratory of Optical Information and Technology, Ministry of Education and Institute of Modern Optics, Nankai University, Tianjin, 300071, China*

E-mail: fsong@nankai.edu.cn

We have fabricated a passively synchronized Q-switched fiber laser working at 1060/1530 nm by a common GSA Fig.1. The process of synchronized pulses formation and the impact of 1530 nm laser pulses on 1060 nm continue wave laser in GSA are investigated. The experimental results show that the 1530 nm laser pulses induce the 1060 nm Q-switched laser pulses, and cause the formation of the pulsed laser synchronization through the XAM effect in GSA[1]. With the increasing pumping power, the repetition rate of synchronized pules could be tuned from 24.51 kHz to 39.85 kHz. This laser may have potential applications in the field of nonlinear frequency conversion, multi-color pump probe spectroscopy, Raman scattering spectroscopy and so on [2-7].

When pump power is increased to 46mW, continuous wave laser light of 1530 nm is observed firstly. With the PC appropriately adjusted, stable passive Q-switched pluses of 1530 nm is observed at pump power of 181 mW. The pulse width is 6.02 μs and the repetition rate is 19.99 kHz, with the output power of 0.79 mW. Keep the PC state fixed and increase the pump power gradually, the repetition rate and output power of the pulses are increased, and the pulse width is decreased as is shown in Fig.2. When pump power is tuned to 267 mW, laser light of 1060 nm emerged as Q-switched operation state whose pulse width is 18.79 μs. The repetition rate of the 1060 nm pulses is 23.96 kHz which is equal to the repetition rate of the 1530 nm pulses.

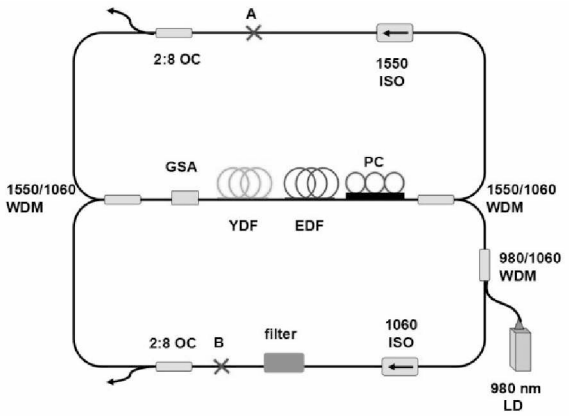

Fig. 1 The experimental setup of the passive Q-switched laser.

Continue increase the pump power, both of the two pulses width decrease gradually and the repetition rate increase consistently as is shown in Fig.2(c) and Fig.2(d). It is clear that the Q-switched pulses of two wavelengths are always synchronized with the pump power increased gradually from 267 mW to 430 mW. With the increasing pump power, the 1060 nm pulse width decreases continuously, because the peak power of 1530 nm laser increases with the pump power and induces strengthening XAM effect. But the variation of 1060 nm pulses width experiences two processes, while the peak power of 1530 nm laser increases almost linearly. The two processes type decrease of 1060 nm laser pulse width is consistent with the saturable absorption property and XAM effect of graphene. When pump power reaches 430 mW, both of the two pulses widths are the narrowest and the difference value between the two pulse widths are the smallest. Owing to the narrowest pulse width and the highest peak power, 1530 nm laser pulses induce the highest XAM effect in graphene, and result in the narrowest pulse width of 1060 nm laser light. The corresponding pulses train is

shown in Fig.3(a) and the output spectrum of the laser is shown in Fig.3(b) and Fig.3(c). During the pump power increased from 267 mW to 430 mW, the 1060 nm pulse width is always greater than the 1530 nm pulse width.

To further prove the 1530 nm Q-switched pulses induced XAM effect in graphene is the dominant factor to format synchronized Q-switched pulses, the 1530 nm path at the position A between the ISO and OC is cut off as is shown in the Fig. 3. Though the PC state and pump power are carefully adjusted, 1060 nm Q-switched pulses cannot be obtained. But when the position B in the 1060 nm path is cut off, stable Q-switched pulse of 1530 nm can be easily obtained at proper pump power and PC state. This phenomenon illustrate that the 1060 nm Q-switched laser pulses are induced by 1530 nm Q-switched pulses, and confirm that the 1530 nm Q-switched pulses caused XAM effect in graphene is the dominant factor to realize the passive synchronization of Q-switched laser pulses.

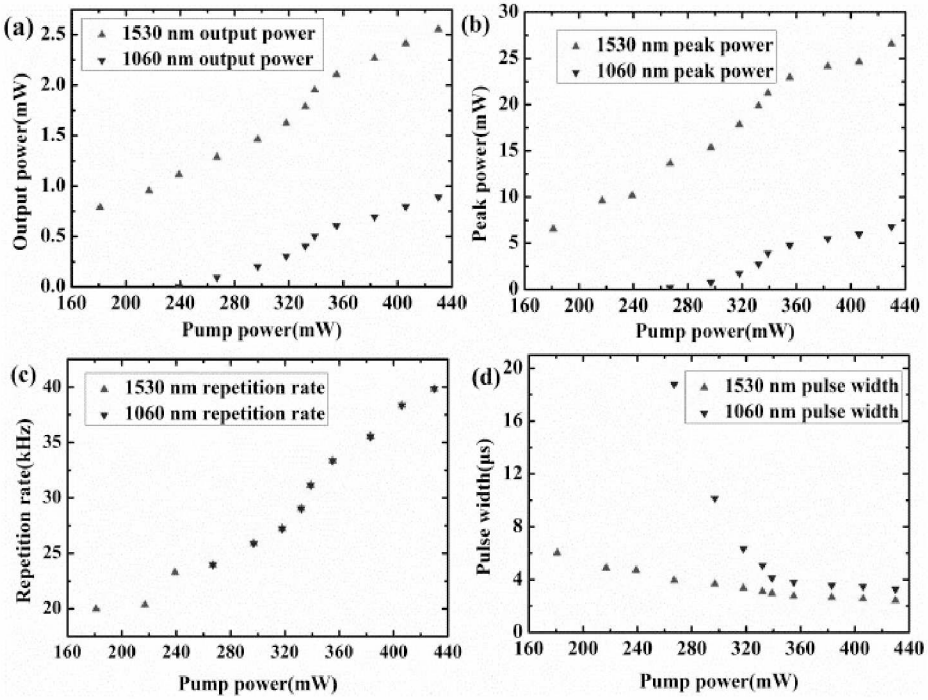

Fig. 2 (a) Output power, (b) peak power, (c) repetition rate and (d) pulse width of Er-laser and Yb-laser as a function of pump power.

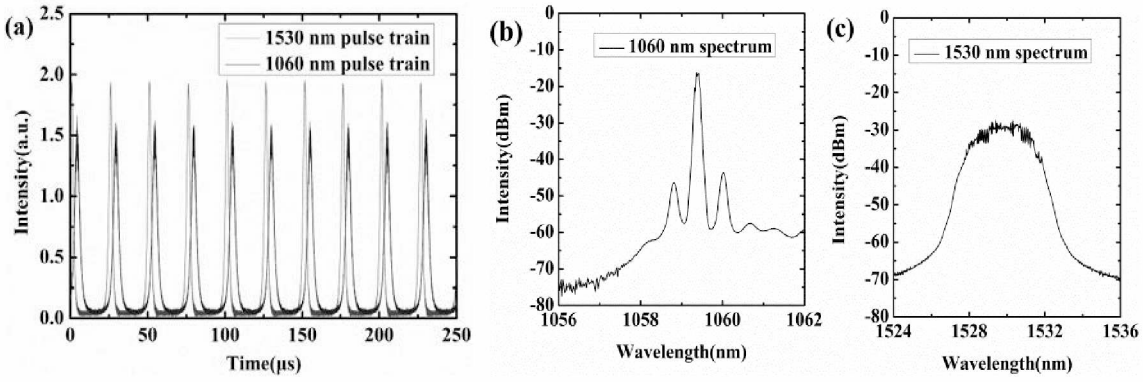

Fig. 3 (a) The pules train when pump power is 430 mW, the corresponding output spectra of (b) Yb-laser and (c) Er-laser.

References

[1] Q. Sheng, M. Feng, W. Xin et al., Appl. Phys. Lett. **105**, 041901 (2014).
[2] J. Liu, S. Wu, Q. Yang et al., Opt. Lett. **36**, 4008 (2011).
[3] Q. Sheng, M. Feng , W. Xin et al., Opt. Express, **21**, 14859 (2013).
[4] Q. Bao, H. Zhang, Y. Wang et al., Adv. Funct. Mater, **19**, 3077 (2009).
[5] Q. Wang, T. Chen, B. Zhang et al., Appl. Phys. Lett. **102**, 131117 (2013).
[6] W. B. Cho, J. W. Kim, H. W. Lee et al., Opt. Lett. **36**, 4089 (2011).
[7] M. Zhang, E. J. R. Kelleher, F. Torrisi et al., Opt. Lett. **20**, 25077 (2012).

Measurement of eigenmode excitation spectrum in synthetic photonic lattices

A.Tikan[1], I. Vatnik[1,2], D. Churkin[1], A. Sukhorukov[3]
[1]*Novosibirsk State University, Pirogova str. 2, Novosibirsk 630090, Russia*
[2]*Institute of Automation and Electrometry, Novosibirsk 630090, Russia*
[3]*Nonlinear Physics Centre, Research School of Physics and Engineering, The Australian National University, Canberra ACT 2601, Australia*
E-mail: ilya.vatnik@gmail.com

Light propagation in periodic structures is the object of everyone's attention over the years1.This area of research is exploring the dynamics of light, which cannot be observed in a continuous medium. An example of such systems are Bragg grating structures or structures consisting of optical waveguides. The latter are a special class of periodic systems, opening are range of possibilities for controlling light. Recently more and more attention is given to photonic lattices implemented by means of optical fibers. The main representatives of this class are mesh and synthetic photonic lattices (SPL). The first one is a network of a number of optical couplers, and has some practical limitations. The first one is a network of a number of optical couplers, and has some practical limitations. The second one consists of two fiber rings of different lengths, connected through the 50/50 fiber coupler. Optical losses are vanished due to optical amplifiers inserted into the system. A sequence of light pulses circulates through the system, with the number of pulse, phase and amplitude of each pulse varying. Phase of the pulses can be altered by means of phase modulator, inserted into one of the loops. It can be shown that pulse evolution in both systems is governed by the same equation set. Though, use of SPL opens new fields for research because of huge experimental possibilities. For example, in the work an evolution of pulses in a system with the introduction of various kinds of local inhomogeneities was studied. It was shown that the controlled phase shift of each pulse plays a role of quantum potential, while the envelope of the pulse chain plays a role of a wave function of the quantum particle. For example, in the absence of phase shifts train of the pulses circulates in the two rings, with the number of pulses gradually increasing. This can be considered as spreading of the wave function.

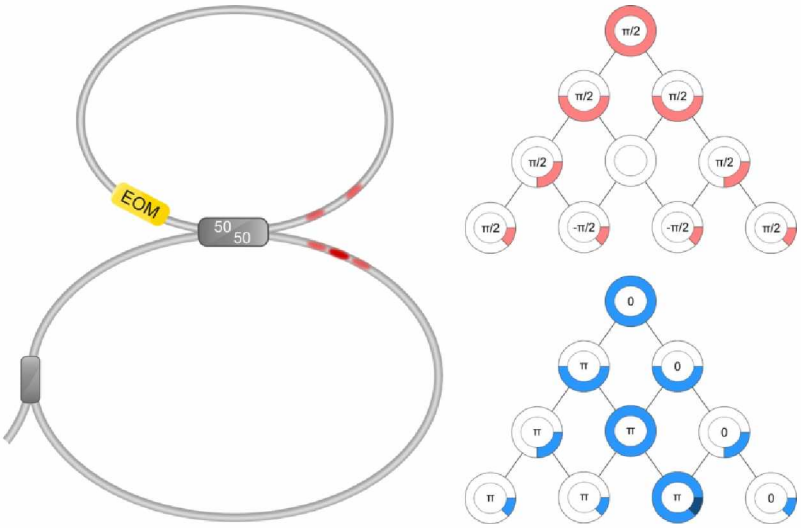

Fig. 1 Scheme of a synthetic photonic lattice and basics of an operation

Knowledge of both phase and intensity of the pulse train means the SPL becomes completely described. We have found an easy way to qualitatively reconstruct the eigenmode excitation spectrum using this knowledge. We propose a technique of measuring relative optical phases of pulses circulating in synthetic photonic lattices. The technique is based on optical heterodyning and makes it possible to obtain complete knowledge about light evolution in the synthetic photonic lattices. One of the sequences is the possibility of reconstructing the eigenmode excitation spectrum, using

measurements of output pulse train phases and intensities only. We demonstrate that the Fourier transform intensity of the complex amplitude over roundtrip number m has a shape similar to that of eigenmode excitation spectrum.

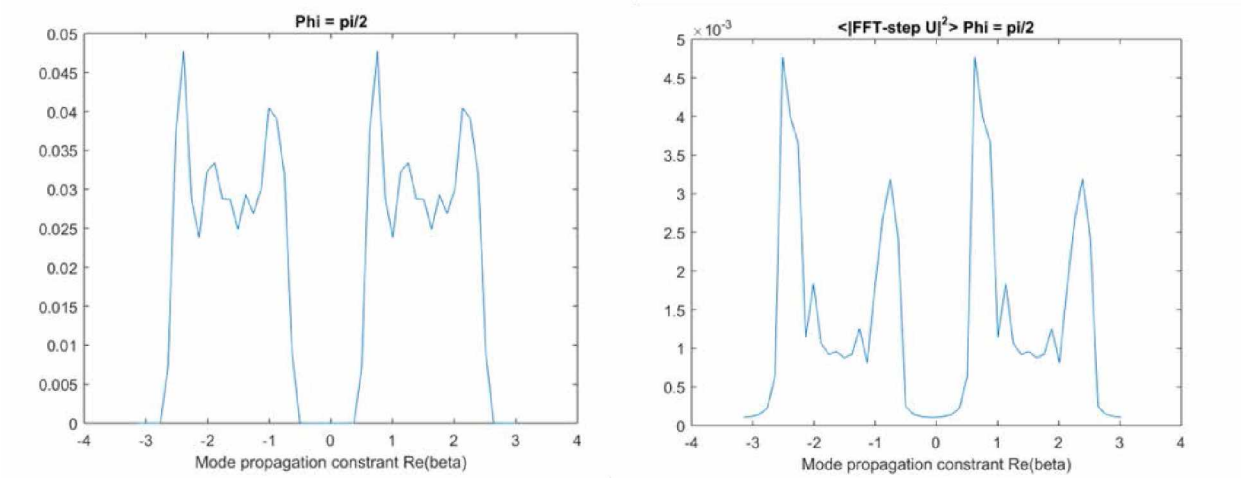

Fig. 2. Comparing mode excitation spectrum (left) and result of Fourier transform of complex pulse amplitude over m (right) with random distribution of potential with value of pi/2.

This work was supported by Russian Science Foundation (project no. 16-12-10402).

References

[1] A. Regensburger, C. Bersch, B. Hinrichs, et. al., Phys. Rev. Lett. **107**(23), 233902 (2011).
[2] A. Schreiber, K. Cassemiro, V. Potoček et. al., Phys. Rev. Lett. **106**(18), 180403 (2011).

Mechanism merging of waves produced by laser plasma pulses in magnetic tube

V.N. Tishchenko, Y.P. Zakharov, I.F. Shaikhislamov, A.G. Berezutski, E.L. Boyarintsev, A.V. Melekhov, A.G. Ponomarenko, V.G. Posukh, P.A. Prokopov
Institute of laser physics SB RAS AC. Lavrentyev's prosp., 13/3, Novosibirsk, 630090 Russia
E-mail: a.berezuckiy@yandex.ru

It was shown that mechanism of merging of waves acts not only in magnetized gases and plasmas [1] but in vacuum magnetic field as well. At the KI-1 Facility the plasma was produced by successive irradiation of the target by a train of laser pulses in a vacuum in magnetic field of about 350 Gauss. When delay between pulses was less than ~ 10 ms the laser plasma formed unbroken stream containing torsional Alfvén and slow magnetosonic waves. The waves are combined in space and contained in a narrow magnetic tube.

The experiment was performed with the aim to justify the applicability of the mechanism of merging of waves (MMW) in various media. The essence of the MMW is that the shock waves created by a train of plasma explosive pulses partially merge in space and form a low-frequency wave whose length is much greater than the radius. The length is linearly dependent on energy input. In magnetized collisionless plasma MMW generates a quasi-stationary wave (QW) consisting of torsional Alfvén (AQW) and the slow magnetic (MQW) waves. QW is located in a narrow magnetic tube. MQW is a compression wave which carries energy and momentum while AQW carries angular momentum (the rotation of plasma), the longitudinal current, azimuthal magnetic and radial electric field.

The experiment revealed a new effect, confirming the applicability of the MMW in the vacuum magnetic field. Namely, in vacuum magnetic field the source generates plasma stream in which the localized field currents and compressions jumps of plasma are the same as in magnetized background. Conditions and manifestations of MMW forming QW in vacuum magnetic field is the same as in the presence of background plasma [2]. With a two-component laser plasma ($2H^{+} + C^{++}$) a torsional Alfvén wave was generated even by a single plasma pulse. The radius of QW ~ 20 cm and its length ~ 2.5 m are limited by the size of the facility.

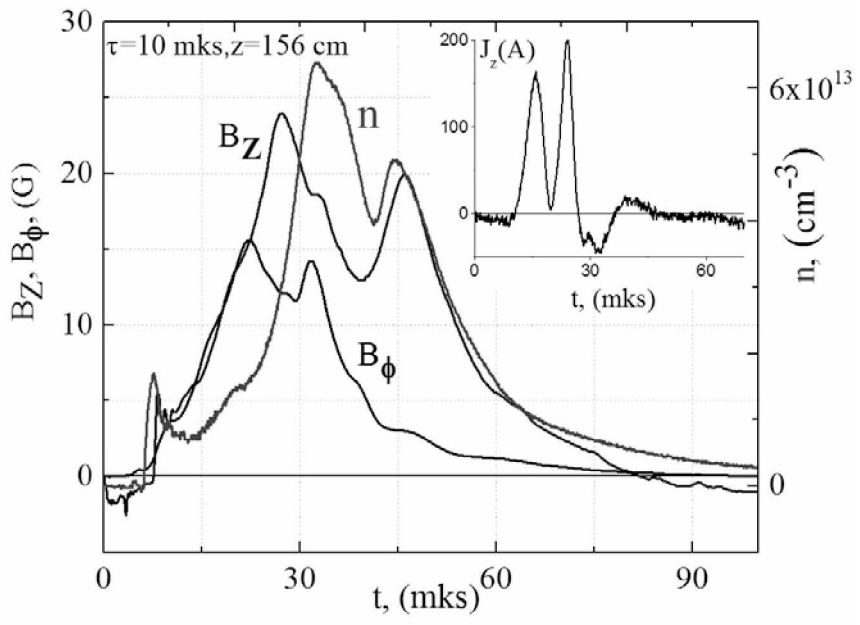

Fig.1

Fig. 1 shows the concentration of plasma n, longitudinal B_Z and azimuthal Bφ magnetic field, the longitudinal current J_Z and radial electric field *Er*. At a delay of the second laser pulse relative to the first T <15 ms the plasma pulse creates a joint stream that contains azimuthal magnetic field $B\varphi$, electric field *Er* and J_Z current along the external magnetic field. These values are the main feature of the torsional Alfvén wave. Features of MQW are a jump of the plasma density and the displacement of the longitudinal magnetic field B_Z. Maximums on the signals of *Bz* and n correspond to the passage of plasma flows from the first and second pulses.

The following features are additional confirmation of the applicability of the MMW in the vacuum magnetic field. Pulses have created joint plasma flow, as well as the AQW and MQW, only when the criteria proposed for the MMW in the magnetized background plasma have been fulfilled. The dimensionless repetition frequency of pulses based on dimension frequency $f \sim 1/\tau$ given by

$$\omega \approx f \cdot R_d / C_J$$

should be equal to $\omega = \omega_r \sim 0.3 - 0.5$. When $\omega << \omega_r$ a separate plasma streams form containing $B\varphi$, *Er*, J_Z and B_Z. At $\omega >> \omega_p$ the length of QW weakly depends on the number of pulses. C_J is the Alfven speed in the magnetic tube, *Rd* - dynamic radius of a single pulse.

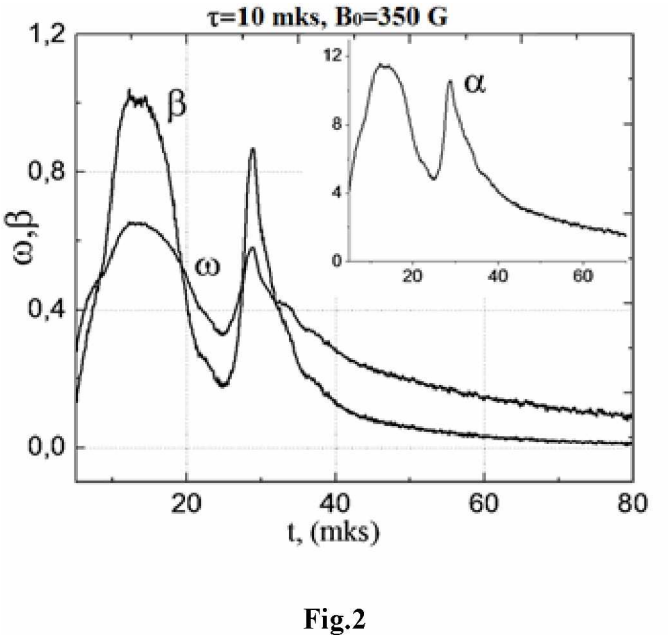

Fig.2

Applicability of MMW in a tube at any number of pulses illustrates Fig.2, which shows $\omega(t)$, $\alpha(t)$ and $\beta(t)$ in the tube after the two pulses. Here $\alpha(t)$ is the ratio of the Larmor radius to the length of the ion-inertia length, $\beta(t)$ - the ratio of plasma pressure to magnetic pressure in the tube. When the third pulse delay relative to the second is less than the lower limit ($\tau < 10$ *ms*) the conditions for the formation of a joint plasma stream containing the combined current, electric and magnetic fields are fulfilled. Disturbances from the third pulse, as well as the second should propagate in the tube as the AQW and MQW.

Thus, periodic plasma pulses together with MMW create in vacuum magnetic field the rotating plasma stream containing the torsional Alfvén and slow magnetic waves localized in the magnetic tube.

This work was supported by the Program of the Presidium of RAS "Fundamental principles of dual-use technologies in the interests of national security"

References

[1] V.N. Tishchenko, I.F. Shaikhislamov, Quantum electronics **44**, 98 (2014)

[2] V.N. Tishchenko, I.F. Shaikhislamov, A.G. Berezutski "The mechanism merging of waves in space plasma with magnetic field: transport the momentum and angular momentum." Almanac of the Moscow State University. "Supercomputer technologies in science, education and industry", 2015, p. 65.

Elementary spectroscopic effects in a cat-state field

V.A. Tomilin, L.V. Il'ichov
Institute of Automation and Electrometry SB RAS, Novosibirsk 630090, Russia
Novosibirsk State University, Novosibirsk 630090, Russia
E-mail: 8342tomilin@mail.ru

Fundamental phenomena of non-linear spectroscopy were observed in the fields of classical nature [1], lasers being the sources of these fields (thus one may call it non-linear laser spectroscopy with equal right). As it is well known, the state of laser radiation in a regime of well-established generation is close to the Glauber coherent state $|\alpha\rangle_G$ (G-states) [2]. The latter is the most accurate quantum analogue to a classical monochromatic wave with definite amplitude and phase. However, it is still a quantum object, and hence the radiation mode is allowed to be in superposition of different G-states. Of certain interest is to study how the familiar spectroscopic effects change when the field is prepared in such an exotic quantum state.

In this work we investigate theoretically the resonance fluorescence of a two-level atom placed in non-classical (cat-state) field which is a superposition of Glauber coherent states (G-states), and the bichromatic spectroscopic scheme for a Λ-type system with one transition exposed to the same type of field, and the one interacting with the field in G-state. We choose the important sub-class of the cat-states, known as the Yurke-Stoler (YS) states [3]. YS-state with parameter α is can be expressed through G-states as follows: $|\alpha\rangle_{YS} = \frac{1}{\sqrt{2}}(|i\alpha\rangle_G + i|-i\alpha\rangle_G)$.

This type of state is extremely vulnerable to decoherence. To counteract it, we include the source of the field explicitly into the theoretical model. Exact details of the preparation of YS-state are not relevant for this study as soon as the desired state is achieved. Due to that, we choose the simplest possible model that allows the existence of stationary YS-state. The similarity between G-states and YS-states allows us to choose the source of the field as harmonically oscillating dipole and the random photon loss process acting together.

Inserting the two-level atom in the field initiates fluorescence. Resulting quantum master equation for the atom-field state includes the atomic Hamiltonian, the interaction with the field and spontaneous decay of the excited atom state as well as the source and the damping terms for the field.

We have studied the case when the non-classical nature of the field is most pronounced, and this is at $|\alpha| \gg 1$. With additional condition of the field subsystem evolving much faster than the atom, the following ansatz for atom-field state can be used:

$$\hat{\varrho} = \hat{\varrho}^{(+)} \otimes |\alpha\rangle_{YS}\langle\alpha| + \hat{\varrho}^{(-)} \otimes |-\alpha\rangle_{YS}\langle-\alpha| + \hat{R} \otimes |\alpha\rangle_{YS}\langle-\alpha| + \hat{R}^{\dagger} \otimes |-\alpha\rangle_{YS}\langle\alpha| \quad (1)$$

Applying this ansatz to (3) gives the steady-state density matrix. Along with the Heisenberg version of the atomic raising operator (there are actually two of those, distinguished by the classical index $(\pm)$ referring to a certain sign of the field amplitude [4]), it allowed us to evaluate the spectrum of stationary resonance fluorescence (Fig. 1).

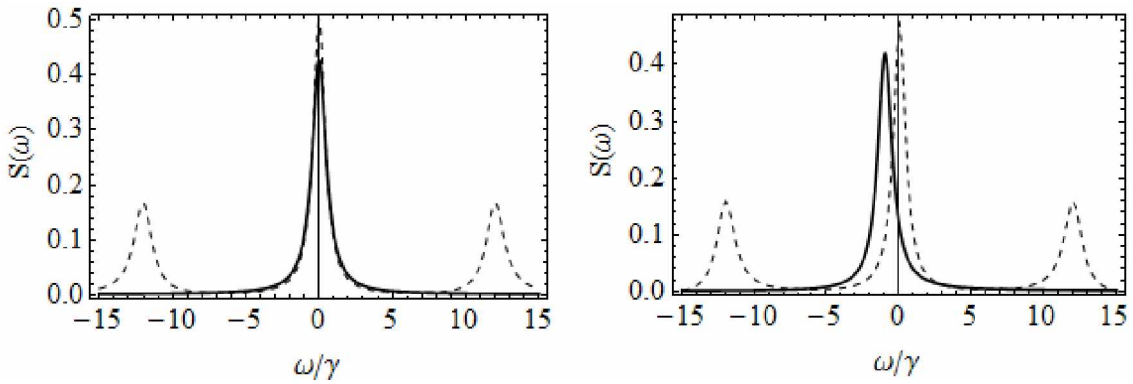

Fig. 1 Spectrum of resonance fluorescence from a two-level atom in a classical (dotted) and non-classical (solid) fields at zero (left) and non-zero detuning (right).

It was found that instead of the usual triplet, in the case of cat-state field the spectrum consists of a single peak centered at the atomic resonance frequency. The peak has the width $\sim \gamma$, i.e. the same one as in classical field. Because the peak's height is even smaller than that for a classical field of the same amplitude, the full fluorescence intensity in the non-classical field is significantly weaker than in the classical one. Also, at non-zero detuning a slight asymmetry of the peak was observed. The absence of side peaks is stipulated by strong atom-field correlations which cause rapid decoherence of every subsystem.

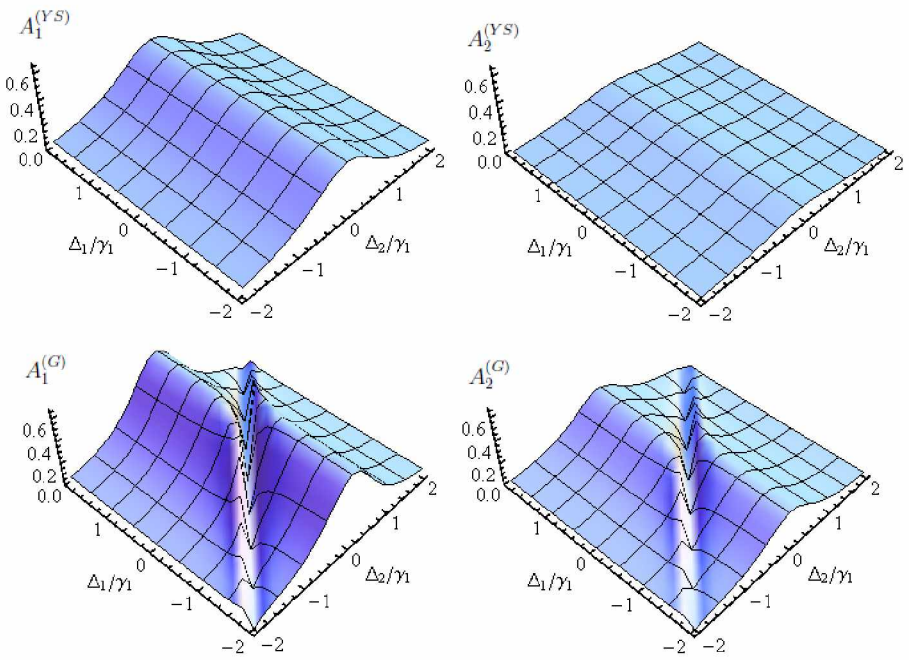

Fig. 2 Upper plots: field works (in a.u.) for both transitions in the case of YS-source versus field detunings. Lower plots: the same works in the case of G-source. Δ_i is the detuning of the field at $|0\rangle \rightarrow |i\rangle$ transition, γ_1 is the spontaneous emission rate from $|0\rangle$ to $|1\rangle$.

After evaluating the fluorescence spectrum, it is natural to extend the system to three levels, namely, to the Λ-type 3-level system with the upper state $|0\rangle$ and the lower states $|1\rangle$ and $|2\rangle$. The field on transition $|0\rangle \rightarrow |1\rangle$ is prepared in YS-state by the same mechanism as discussed above. The field on $|0\rangle \rightarrow |2\rangle$ is treated classically. Applying the same ansatz as in the two-level case, we were able to obtain the steady-state solution of the master equation. We have used it to evaluate the work per unit time done by each field in the stationary regime (Fig. 2). The striking difference from the case of two classical fields interacting with the system was the absence of the so-called "dark resonances" [5]. As is well-known, if the detuning of the fields are equal, the system appears in the so-called dark state – a certain superposition of the lower states, and does not interact with the field. However, in a cat-state field one can speak of two types of dark resonances, each one corresponding to a certain field amplitude. In case of YS-state, it happens that these resonances interfere destructively, thus cancelling the net dark resonance.

This work was supported by RFBR (grant 16-02-00329) and the Council of the President of the Russian Federation for Support of Young Scientists and Leading Scientific Schools (grant NSh-6898.2016.2).

References

[1] S.G. Rautian and A.M. Shalagin, Kinetic Problems of Nonlinear Spectroscopy (Elsevier, Amsterdam, 1991).
[2] C. DeWitt, A. Blandin, and C. Cohen-Tannoudji (eds.), Quantum Optics and Electronics (Gordon & Breach, New York, 1965).
[3] B. Yurke and D. Stoler, Phys. Rev. Lett. **57**, 13 (1986).
[4] V.A. Tomilin, L.V. Il'ichov, JETP Lett. **94**, 676 (2011).
[5] H.R. Gray, R.M. Whitley, and C.R. Stroud, Opt. Lett. **3**, 218 (1978).

Countermeasure to a time-shift attack in fiber-optic quantum key distribution systems

D.B. Tretyakov[1,2], A.S. Pleshkov[1,2,3], A.V. Kolyako[1,2,4], I.I. Ryabtsev[1,2], I.G. Neizvestny[1]
[1] *Rzhanov Institute of Semiconductor Physics SB RAS, 630090, Novosibirsk, Russia*
[2] *Novosibirsk State University, 630090, Novosibirsk, Russia*
[3] *Institute of Automation and Electrometry, 630090, Novosibirsk, Russia*
[4] *Institute of Laser Physics SB RAS, 630090, Novosibirsk, Russia*
E-mail: alexand.pleshkov@mail.ru

The main goal of quantum cryptography is to provide an absolutely secure transmission of a secret message between a sender and a recipient using single photons. The fundamental laws of quantum mechanics can guarantee the inability of undetectable interception of transmitted data by unauthorized persons.

Although quantum cryptographic protocol ensures an absolute security in theory, the practical implementation of it may have vulnerabilities. In 2008 it has been proposed and experimentally demonstrated a «time-shift attack», which enable to intercept the transmitted message undetectably [1]. This attack exploits the detection-efficiency mismatch in the time domain between two single-photon detectors of a quantum key distribution system due to the individual characteristics of the detectors themselves and the imperfections of the control electronics.

We have proposed and demonstrated a countermeasure to the time-shift attack based on the recipient independent decision which of the two single photons detectors will be a logic zero or one receiver for each clock pulse that neutralizes the effect of the time-shift attack. The method has been demonstrated on the quantum fiber-optic communication system (an autocompensated two-way scheme) [2], created by the Rzhanov Institute of Semiconductor Physics SB RAS.

This work was supported by the Russian Foundation for Basic Research (grants №14-07-00809), by the Siberian Branch of the Russian Academy of Sciences and by the Novosibirsk State University.

References

[1] Yi Zhao et al, Phys. Rev. A **78**, 042333 (2008).
[2] V.L. Kurochkin et al., Bulletin of RAS, Physics **80**, №1, 5 (2016).

Precision spectroscopy of cold magnesium atoms localized in a magneto-optical trap

M. Tropnikov[1], A. Bonert[1], D. Brazhnikov[1,2], and A. Goncharov[1,2,3]
[1]*Institute of Laser Physics SB RAS, pr. Acad. Lavrent'eva 13/3, 630090 Novosibirsk, Russia*
[2]*Novosibirsk National Research State University, Pirogova 2, 630090 Novosibirsk, Russia*
[3]*Novosibirsk State Technical University, pr. Karla Marksa 20, 630092 Novosibirsk, Russia*
E-mail: makstropnikov@gmail.com

Frequency standards play an important role in various fields of science and technology: in fundamental physical investigations, metrology, and navigation. The relative accuracy of a primary frequency standard based on a caesium fountain has probably reached its limit $\Delta\nu/\nu = 2*10^{-16}$ [1]. Further increase in the accuracy of frequency standards is associated with transition from the microwave range of the spectrum to the optical range and, hence, with the creation of optical frequency standards based on single ions or neutral atoms. Alkaline-earth and alkaline-earth-like atoms, such as Yb, Ca, Sr, Hg, and Mg, are among the main candidates for creating the optical frequency standards. However, ^{24}Mg has some advantages over the other candidates such as the narrowest intercombination transition, the simplest structure of the electron shells, and the smallest frequency shift of the "clock" transition due to black body radiation. The presence of strong closed $^1S_0$–$^1P_1$ transition allows effective cooling and trapping of magnesium atoms in a magneto-optical trap. Creation of a frequency standard based on Mg atoms is possible using $^1S_0$–$^3P_1$ transition with the natural linewidth of 36 Hz. Sub-Doppler cooling of magnesium atoms and their localization in an optical lattice will later allow one to employ strongly forbidden $^1S_0$–$^3P_0$ transition and realize the frequency standard with the relative inaccuracy of 10^{-16}–10^{-17} [2]. In this paper, the possibility of obtaining the narrow reference lines using $^1S_0$–$^3P_1$ transition in creating the optical frequency standard is shown and the progress achieved in the frequency stabilization by observed resonances studies is presented.

The source of radiation for clock $^1S_0$–$^3P_1$ transition spectroscopy is a system based on Ti:sapphire laser pumped by 15-wat solid-state Verdi V18 laser with a two-stage system of frequency stabilization and a frequency doubling in a $KNbO_3$ crystal in an external cavity.

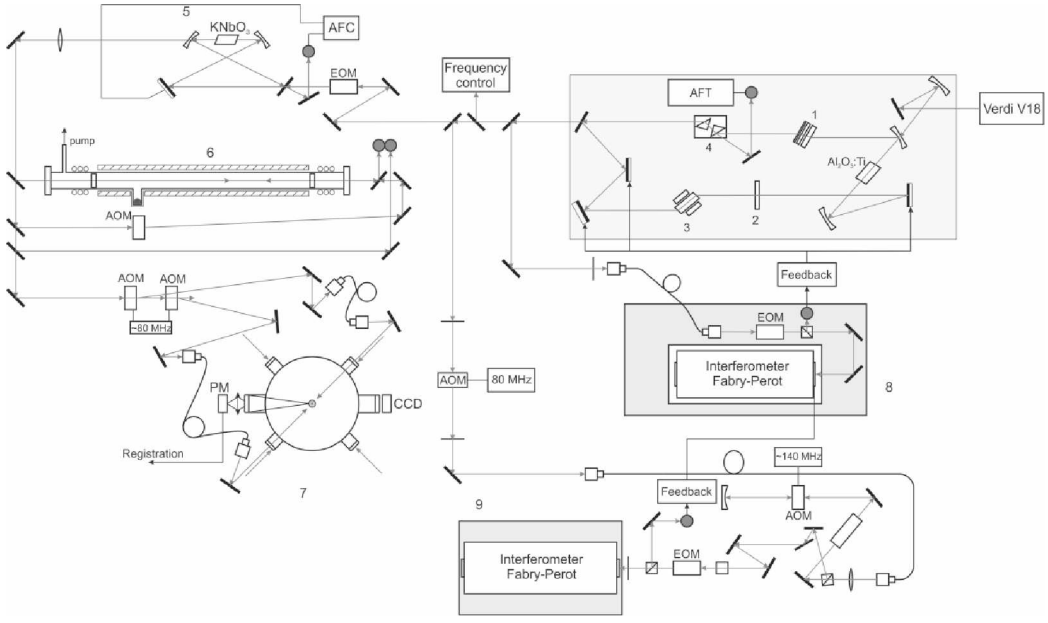

Fig.1. Schematic of the experimental setup used for spectroscopy of the clock transition. 1 – Lyot filter, 2 – etalon with FSR=100 GHz, 3 – Faraday rotator, 4 – etalon with FSR=20 GHz, AFT – automatic fine tuning, 5 – nonlinear crystal in an external cavity, AFC – automatic frequency control, 6 – Mg cell, 7 – magneto-optical trap, 8 – first stabilization system by the invar interferometer, 9 – second stabilization system by the glass-ceramic interferometer.

The frequency of the laser system radiation is stabilized by the two reference Fabry-Perot interferometers: with invar base and optical glass-ceramic base. The first interferometer provides the preliminary narrowing of the generation line of the Ti:sapphire laser, the second interferometer is used for correcting low-frequency perturbations of the first interferometer through automatic adjustment of its length by the piezoelectric actuator with an interferometer mirror installed on it.

The stabilized Ti:sapphire laser, which outputs about 1 W of power at 914 nm, is followed by cavity enhanced second harmonic generation inside a nonlinear $KNbO_3$ crystal that yields about 80 mW at 457 nm. Laser cooling and localization of magnesium atoms in a magneto-optical trap is carried out on the $^1S_0$–$^1P_1$ closed transition at 285 nm. Investigation of the $^1S_0$–$^3P_1$ transition of cold magnesium atoms localized in the MOT is performed by the method of fields separated in time (time-domain Ramsey–Borde atom interferometer) [3]. Two pairs of the light pulses formed from cw radiation of a highly stable laser system at 457 nm by acousto-optic modulators interact with a cloud of magnesium atoms. Pairs of pulses are transported into the magneto-optical trap through opposite windows via two single-mode fibers.

In recording narrow resonances, the radiation frequency of the laser system is tuned by a frequency synthesizer, the signal from which controls AOM in the frequency stabilizing system of the second interferometer. The fluorescence signal from a cloud of cold magnesium atoms on the resonance transition at 285 nm is detected by the photomultiplier. The Ramsey–Borde resonances in time-separated fields are shown in Fig. 2(a) for the delays between pulses T = 7.5, 58 μs.

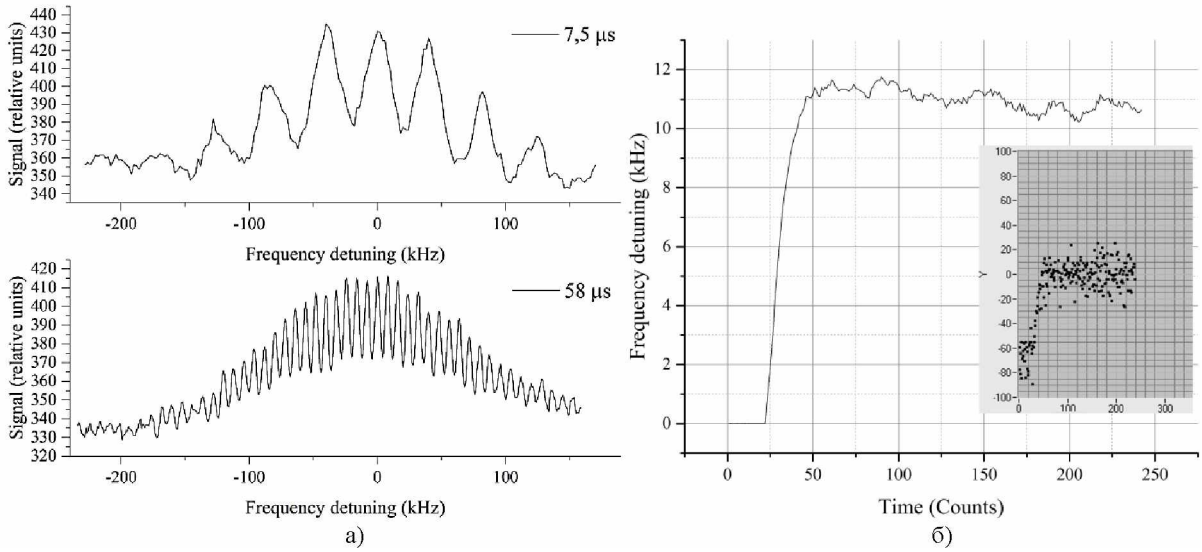

Fig. 2. (a) Resonances in time-separated fields for the delays between pulses T=7.5, 58 μs. (b) Detuning of the laser frequency from the central fringe of the resonances and stabilized third derivative (inset).

Frequency stabilization by the central fringe of observed resonances is performed. It is carried out by calculating the third derivative of the fluorescence signal at the central point of the periodic pattern of the resonances and automatic frequency control of the laser system so that the third derivative is equal to zero (see the inset in Fig. 2(b)). Preliminary study of dynamic characteristics of frequency stabilization by reference resonances is carried out. Laser system frequency detuning and the signal of the third derivative are shown in Fig. 2. The results obtained are preliminary and it is planned to obtain resonances with a higher resolution, perform laser frequency stabilization by them and improve stabilization characteristics.

References

[1] F. Levi, D. Calonico, C. E. Calosso, A. Godone, S. Micalizio and G. A. Costanzo, Metrologia, **51(3)**, 270 (2014).
[2] A. N. Goncharov, A. E. Bonert, D. V. Brazhnikov, A. M. Shilov and S. N. Bagayev, Quantum Electronics, **44(6)**, 521 (2014).
[3] K. Sengstock, U. Sterr, G. Hennig, D. Bettermann, J. H. Müller, W. Ertmer, Opt. Commun., **103**, 73 (1993).

CW laser performance of diode pumped 5%Tm:$KLu(WO_4)_2$ crystals

S.M. Vatnik[1], I.A. Vedin[1], P.F. Kurbatov[1], A.A. Pavlyuk[2]
[1] *Institute of Laser Physics Siberian Branch of Russian Academy of Sciences, Novosibirsk, Russia*
[2] *Institute of Inorganic Chemistry Siberian Branch of Russian Academy of Sciences, Novosibirsk, Russia*
E-mail: vatnik@laser.nsc.ru, vedin@laser.nsc.ru, pavlyuk@niic.nsc.ru

Lasers emitting at 2-μm spectral range are of particular interest for many scientific and technical applications including remote sensing, medicine and optically pumped midinfrared optical parametric oscillators. Monoclinic double tungstate crystals, due to their maximum absorption and emission cross sections and minimum concentration quenching, seem ideal as hosts for thin-disk lasers with simplified pump geometry (number of pump passes). The crystals of double potassium rare-earth tungstates doped with trivalent thulium ions are promising laser materials for compact highly efficient sources of coherent two-micron (1.8–2.0mm) radiation. The main advantages of these crystals are the large cross sections ($\sigma > 10^{-20}$cm^2) of stimulated transitions in the spectral regions of pumping (~0.8 mm) and lasing (~1.94mm) and a high slope efficiency (~50%) [1]. In this work, we present the results of investigation of the oscillation performance of thin-disk laser based on the 5%Tm:KLuW disks, epitaxial layers and composite structures 5%Tm:KLuW/KLuW. We report on the oscillation performance of various types thin-disk laser pumped by a laser diode bar with a maximum average CW optical power up to 50W at a wavelength of 808 nm at room temperature (T = 25°C). To design the laser head, high quality 5%Tm:KLuW crystal boule was grown by the modified Czochralski method at the Institute of Inorganic Chemistry, Russia. Epitaxial samples of 5%Tm-doped KLuW/KLuW was obtained by the Liquid Phase Epitaxy (LPE) method at the Fisica i Cristallografia de Materials i Nanomaterials (FiCMA-FiCNA), Spain [2]. The composite, analogy of epitaxial structure, consisting of 5%Tm-doped KLuW crystal layer and substrate of undoped KLuW was produced by the high-temperature diffusion bonding method at the Institute of Laser Physics, Russia [3]. Flat surfaces all of the samples were polished to high optical quality required for coating. The polished surfaces of active Tm-doped layers and disk were covered with a dielectric coating with a high reflectivity (R > 99.8%) at lasing (λ_g = 1950 nm) and pumping (λ_p = 808 nm) wavelengths. Then a metallic coating was added for mounting active elements to the copper heat sink with an indium solder. The front surface was AR-coated for these wavelengths, and the residual reflection was less ~0.2%. The laser experiments were performed using only 2 passes of the pump through the Tm-doped layer (i.e. there was no retroreflection of the pump beam) with nearly circular pump spot of 0.95 mm diameter on the sample. The shaped pump beam from the laser diode was polarized along the N_m principal optical axis for maximum absorption. The laser cavity with a length of L_c = 20mm was formed by a spherical output coupler (curvature radius r = -40 mm, transmittance T = 7.0% at λ_g = 1950 nm) and a rear mirror deposited on the end-face of crystal. We compared the slope efficiencies of 5%Tm:KLuW disk, epitaxial layer and composite structure 5%Tm:KLuW/KLuW (Tm-doped layer thickness 250 μm) in true CW pump mode, as seen in Table. 1.

Table 1 CW Output power, Slope and Optical efficiencies, Laser wavelength for 5%Tm:KLuW thin disk lasers with the active layer thickness 250μm, T=7.0%.

Type active element	Output power, W	Slope efficiency, %	Optical efficiency, %	Wavelength, nm
Epitaxy [1]	5.9	47	42	~1855
Composite [2]	4.6	40	43	~1846
Disk [2]	2.1	46	44	~1846

According to the measured data, the slope efficiency as much as 40% with respect to absorbed pump power was obtained for all thin-disk lasers. The corresponding fracture pump intensity was ~6.3 kW/cm^2 for composite structure and ~2.4 kW/cm^2 for disk active elements.

References

[1] X. Mateos, V. Petrov, J. Liu, et al., IEEE J. Quantum Electron. **42**, p. 1008 (2006).
[2] M. Segura, R.M. Solé, X. Mateos, et al., CrysEngComm. 14, No. 1 (2012).
[3] S.M. Vatnik, I.A. Vedin, P.F. Kurbatov, et al., Quantum Electronics 44, No. 11 (2014).

Non-collinear second harmonic generation in two-dimensional nonlinear optical superlattices

A. M. Vyunishev[1,2] and V. G. Arkhipkin[1,3]
[1]*L.V. Kirensky Institute of Physics, 660036, Krasnoyarsk, Russia*
[2]*Department of Photonics and Laser Technology, Siberian Federal University, Krasnoyarsk 660079, Russia*
[3]*Laboratory for Nonlinear Optics and Spectroscopy, Siberian Federal University, Krasnoyarsk 660079, Russia*
E-mail: vyunishev@iph.krasn.ru

Multiple non-collinear second harmonic generation (SHG) under Raman-Nath nonlinear diffraction (RNND) are of interest since the first experimental demonstration in 2008 [1]. RNND represents an nonlinear analogue of the most known phenomenon of Raman-Nath diffraction of light on standing ultrasonic wave in homogeneous optical media. Experimentally RNND appears as series of spatially ordered beams generated in the process of nonlinear optical scattering in the media with periodical modulation of quadratic nonlinear susceptibility as shown in Fig. 1. However, the phase mismatch of longitudinal wavevector components results in quite poor RNND efficiency, that prevents potential applications, such as multi-channel nonlinear optical converters and nonlinear multiplexors. This problem can be solved by using two-dimensional (2D) nonlinear photonic crystals (NPC's) [2], employing quasi-phase-matching (QPM).

Although some approaches have been developed to calculate SHG in 2D NPCs, such as the method based on Green's function formalism [3], the transfer-matrix method and the effective nonlinear coefficient model [4], it is desirable to have a simple approach adopted to transversely periodical rectangle 2D NPC's with arbitrary structured longitudinal modulation of nonlinearity. Developing this approach is essential for designing 2D NPC's with required nonlinear optical characteristics. Therefore, the subject of current work is to provide our theoretical and experimental study on Raman-Nath nonlinear diffraction in 2D NPC's.

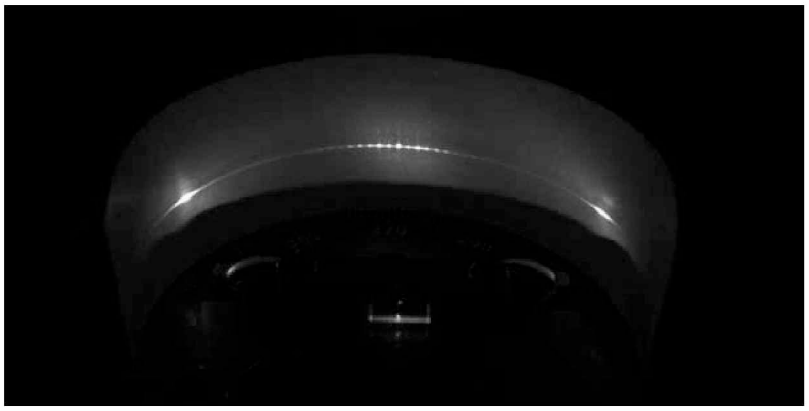

Fig. 1 Raman-Nath (central spots) and Cerenkov (side spots) nonlinear diffraction in NPC.

In this report, Raman-Nath nonlinear diffraction in the process of the second harmonic generation in different kinds of 2D NPC's is reviewed. Hereinafter, all mentions on structures are devoted with modulation of nonlinearity in longitudinal direction assuming periodical modulation in transverse direction. The following designs of 2D NPC's were considered: periodical, chirped and optimized one.

The most simple example of NPC is the periodical structure, which can be used for the most efficient quasi-phase-matched SHG. We experimentally studied SHG of femtosecond laser pulses in a rectangular 2D NPC in lithium niobate crystal. Multiple SH beams were observed in the vicinity of the propagation direction of the fundamental beam as shown in Fig. 1. It has been verified that the angular positions of these beams obey the conditions of RNND. Additionally, side beams corresponding Cerenkov nonlinear diffraction were observed. The measured SH spectra of specific RNND orders consist of narrow peaks that experience a high-frequency spectral shift as the order grows. This behavior is explained by dependence of phase mismatch on RNND order. We derive an

analytical expression for the process studied and find the theoretical results to be in good agreement with the experimental data. For the calculations, measured parameters of the fundamental pulses and the structure were used. We estimate the enhancement factor of Raman-Nath nonlinear diffraction in 2D structure to be 70. In our experiments, we used the structure with relatively large period, which corresponds 45^{th} QPM order. Therefore, the SHG efficiency can be significantly increased by using lower QPM orders.

In contrast, conversion of quasi-monochromatic radiation runs into difficulties because order-dependent phase mismatch. It is possible to satisfy the QPM condition for specific order, but interacting waves for other orders become non-phase-matched. Therefore, realization of multi-order RNND requires more complicated spatial modulations of nonlinearity. The most suitable structure of NPC can be synthesized by the method of superposition of a nonlinearity modulation [5]. This method makes it possible to design a NPC that provides a set of desired reciprocal lattice vectors for multiple SHG via RNND. In this case, specific phase mismatches corresponding to different RNND orders are compensated for by the appropriate reciprocal lattice vectors with the Fourier amplitudes as high as possible. For theoretical description of RNND in 2D NPC's, the model of nonlinear diffraction under Laue scheme was used [6]. Generalization of the model to the case of 2D structures is accomplished by using approach [7]. As the result, an analytical solution for angular distribution of spectral intensity was derived. It is shown that SH intensity for orders considered increases along the structure. The SHG efficiency can be a few orders of magnitude higher than in the case of non-phase-matched generation via RNND in 1D structure. The desired intensity distribution between separate orders can be achieved by varying parameters of the structure. Moreover, analytical expression obtained can be used for calculations other types of non-collinear interactions in 2D NPC's with arbitrary structures.

Conversion of broadband and widely tunable radiation represents a special interest for number applications. In this connection, we consider RNND in chirped 2D NPC's. The linear dependence of reciprocal lattice vector along the structure is expected to be useful for multiple SHG in wide spectral and angular ranges. We obtained exact analytical expressions for SH amplitude and for its spectral bandwidth as functions of the chirp parameter. As the spectral response of the structure is linearly distributed over the structure, different spectral components are consecutively involved in the process. When the SH intensity reaches its maximum at certain frequency, weak intensity oscillations appear. The scale of oscillations decreases in the propagation direction, which can be explained by spatial dependence of the phase mismatch in this direction. Increase of chirp parameter result in broadening of spectral range, where quasi-phase-matched SHG takes place. It is also accompanied by remarkable reductions of SHG efficiency. Therefore, the choice of the chirp parameter is a trade-off between a wide spectral (angular) bandwidth and high SHG efficiency. The results of analytical calculations are in excellent agreement with the numerical ones. We show that the process is robust to angular deviations of NPC's and it can be applied to enable tunable and broadband frequency conversion.

In summary, we have elaborated the theory of SHG under Raman-Nath nonlinear diffraction in 2D NPC's. Corresponding analytical solutions were obtained. The efficiency of these processes can be increased by several orders of magnitude compared to the case of non-phase-matched SHG in 1D NPC's. It is shown that 2D NPC's under study can be used for enhancement of the effect of Raman-Nath nonlinear diffraction in wide angular and spectral ranges. Theoretical results are in good agreement with numerical calculations and experimental data. These results may inspire a new family of multi-channel nonlinear optical converters for a wide range of applications.

References

[1] S.M. Saltiel et al., Phys. Rev. Lett. **100**, 103902 (2008).
[2] V. Berger, Phys. Rev. Lett. **81**, 4136 (1998).
[3]. X.-H. Wang and B.-Y. Gu, Eur. Phys. J. B **24**, 323 (2001).
[4]. A. Arie et al., Opt. Quantum Electron. **39**, 361 (2007).
[5]. A.A. Novikov, A.S. Chirkin, JETP **106**, 415, (2008).
[6]. I.V. Shutov et al., Opt. Spectr. **105**, 79 (2008).
[7]. M. Baudrier-Raybaut et al., Nature **432**, 374 (2004).

Synthetic frequency protocol in the Ramsey spectroscopy

V. I. Yudin[1-3], A. V. Taichenachev[1, 2], M. Yu. Basalaev[1, 2], T. Zanon-Willette[4]
[1]*Novosibirsk State University, ul. Pirogova 2, Novosibirsk, 630090 Russia*
[2]*Institute of Laser Physics SB RAS, pr. Akademika Lavrent'eva 13/3, Novosibirsk, 630090 Russia*
[3]*Novosibirsk State Technical University, pr. Karla Marksa 20, Novosibirsk, 630073 Russia*
[4]*LERMA, Observatoire de Paris, PSL Research University, CNRS, Sorbonne Universit'es, UPMC Univ. Paris 06, F-75005, Paris, France*
E-mail: viyudin@mail.ru

At the present time, huge progress occurs for high-precision optical atomic clocks based on both neutral atoms in optical lattices and trapped ions. Exceptional accuracy and stability at the 10^{-17}–10^{-18} level are achieved. Potential possibilities to achieve the level of 10^{-19} become clearer for nuclear clocks and for highly charged ions On the way to these remarkable achievements, different barriers arise, which require the development of new unconventional approaches. As an example, for some of the promising clock systems, one of the key problems is the frequency shift of the clock transition due to the excitation pulses themselves. For the case of magnetically induced spectroscopy these shifts (quadratic Zeeman and ac-Stark shifts) could ultimately limit the achievable performance. Moreover, for ultranarrow transitions (e.g., electric octupole and twophoton transitions) the ac-Stark shift can be so large in some cases to rule out high accuracy clock performance at all.

Unconventional solution to this important problem was proposed in the paper [1], in which so-called hyper-Ramsey method has been developed. Soon this approach was successfully realized in [2], where the huge suppression (by four orders of magnitude) of probe-induced shifts was experimentally demonstrated. We develop new universal method to dramatically suppress probe-induced shifts and their fluctuations in any type of atomic clocks. Our approach is based on adaptation of so-called synthetic frequency concept [3] to the Ramsey spectroscopy with the use of interrogations for different durations of free evaluation intervals. We show that this protocol in combination with the original hyper-Ramsey spectroscopy [1] makes most extremal results and is quite stable with respect to the decoherentization.

The essence of our approach consists in the following. Previously in the paper [3] the so-called synthetic frequency method, allowing to radically suppress thermal (BBR) shift in atomic clock, was proposed. However, an ideology of this method can be easy extended on cancelling of an arbitrary systematic shift. Indeed, let us consider two clock frequencies $\omega_1^{(0)}$ and $\omega_2^{(0)}$ (different in the general case). Assume that due to a certain physical cause we have the stabilized frequencies ω_1 and ω_2, which are shifted relative to the unperturbed frequencies at the values Δ_1 and Δ_2:

$$\omega_1 = \omega_1^{(0)} + \Delta_1; \qquad \omega_2 = \omega_2^{(0)} + \Delta_2. \tag{1}$$

Also assume that the ratio $\varepsilon_{12} = \Delta_1/\Delta_2 = const$ does not fluctuate, while the shifts $\Delta_{1,2}$ can be varied during experiment (i.e., $\Delta_{1,2} \neq const$). In this case, we can construct the following superposition:

$$\omega_{syn} = \frac{\omega_1 - \varepsilon_{12}\omega_2}{1-\varepsilon_{12}} = \frac{\omega_1^{(0)} - \varepsilon_{12}\omega_2^{(0)}}{1-\varepsilon_{12}}, \tag{2}$$

which is insensitive to the perturbations $\Delta_{1,2}$ and their fluctuations. This frequency we will call as "synthetic frequency". A key advantage of this concept consists in the following: to construct the shift-free frequency ω_{syn} we do not need to know the real values of shifts $\Delta_{1,2}$, because we need to know only their ratio ε_{12}, which can be exactly calculated (or measured) for many cases.

Consider an influence of probe-induced shift Δ_{sh}, which arises only during the Ramsey pulses, while this shift is absent during the dark time T. As a result, the stabilized frequency ω_T also becomes differing from unperturbed frequency ω_0:

$$\omega_T = \omega_0 + \overline{\delta}_T, \tag{3}$$

where the index T denotes the fixed time of the free evolution interval under frequency stabilization, and the resulting shift $\overline{\delta}_T$ exists due to the $\Delta_{sh} \neq 0$. On the basis of general principles, it can be shown that the dependence $\overline{\delta}_T$ on the value T can be expressed as the following decreasing series in terms of powers of $1/T$:

$$\overline{\delta}_T = \frac{A_1}{T} + \frac{A_2}{T^2} + \ldots + \frac{A_n}{T^n} + \ldots, \tag{4}$$

where the coefficients A_n depend on the pulse parameters (durations, amplitudes, phases, and the value Δ_{sh}).

Because the time T is precisely controlled in experiments, then we can set a goal to eliminate the main contribution $\propto A_1/T$ in Eq. (4) using the synthetic frequency protocol. To solve this task we will apply two different dark intervals T_1 and T_2 (but with the same Ramsey pulses), which will give us the corresponding stabilized frequencies ω_{T_1} and ω_{T_2}. Using Eqs. (2)-(4) we easy find the synthetic frequency $\omega_{syn}^{(1)}$ and its residual shift $\overline{\delta}_{syn}^{(1)}$:

$$\omega_{syn}^{(1)} = \frac{\omega_{T_1} - (T_2/T_1)\omega_{T_2}}{1-(T_2/T_1)}, \qquad \overline{\delta}_{syn}^{(1)} = \omega_{syn}^{(1)} - \omega_0 = \frac{\overline{\delta}_{T_1} - (T_2/T_1)\overline{\delta}_{T_2}}{1-(T_2/T_1)}, \tag{5}$$

where the expression for $\overline{\delta}_{syn}^{(1)}$ does not contain the term $\propto A_1$. In the particular case of $T_1 = \mathrm{T}$ and $T_2 = T/2$:

$$\omega_{syn}^{(1)} = 2\omega_T - \omega_{T/2}, \qquad \overline{\delta}_{syn}^{(1)} = 2\overline{\delta}_T - \overline{\delta}_{T/2}. \tag{6}$$

The value $\overline{\delta}_{syn}^{(1)}$ can be less than $\overline{\delta}_T$ [see Eq. (4)] by several orders of magnitude. Moreover, we can go further to define other synthetic frequency $\omega_{syn}^{(2)}$, for which both contributions A_1/T and A_2/T^2 will be simultaneously canceled. Here we need to use three different time intervals (T_1, T_2, T_3) with the corresponding stabilized frequencies (ω_{T1}, ω_{T2}, ω_{T3}). In particular, we consider the case of $T_1 = T$, $T_2 = T/2$ and $T_3 = \mathrm{T}/3$, for which the required superposition takes the form:

$$\omega_{syn}^{(2)} = 3\omega_T - 3\omega_{T/2} + \omega_{T/3}, \qquad \overline{\delta}_{syn}^{(2)} = 3\overline{\delta}_T - 3\overline{\delta}_{T/2} + \overline{\delta}_{T/3}, \tag{7}$$

where the value $\overline{\delta}_{syn}^{(2)}$ can be less than $\overline{\delta}_{syn}^{(1)}$ by several orders of magnitude.

To conclude, the synthetic frequency protocol in the Ramsey spectroscopy is a novel technique that offers a spectroscopic signal that is virtually free from probe-induced frequency shifts and their fluctuations. Most extremal results are obtained in combination with so-called hyper-Ramsey spectroscopy [1]. In the latter case, the probe-induced frequency shifts can be suppressed considerably below a fractional level of 10^{-18} practically for any optical atomic clocks, where this shift previously was metrologically significant.

The work was supported by the Ministry of Education and Science of the Russian Federation (State Assignment No. 2014/139, Project No. 825), by the Russian Foundation for Basic Research (Grants No. 16-32-60050, 16-32-00127, 15-32-20330, 15-02-08377, 14-02-00712, 14-02-00939).

References

[1] V.I. Yudin, A.V. Taichenachev, C.W. Oates et al., "Hyper-Ramsey spectroscopy of optical clock transitions", Phys. Rev. A **82**, 011804(R) (2010).

[2] N. Huntemann, B. Lipphardt, M. Okhapkin et al., "Generalized Ramsey Excitation Scheme with Suppressed Light Shift", Phys. Rev. Lett. **109**, 213002 (2012).

[3] V.I. Yudin, A.V. Taichenachev, M.V. Okhapkin et al., "Atomic Clocks with Suppressed Blackbody Radiation Shift", Phys. Rev. Lett. **107**, 030801 (2011).

Simulation by laser plasma blobs of the coronal mass ejection impact onto Earth's magnetosphere at presence of interplanetary quasi-perpendicular shock

Yu.P. Zakharov[1], A.G. Ponomarenko[1], V.A. Terekhin[2], E.L. Boyarintsev[1], A.V. Melekhov[1], V.G. Posukh[1], P.A. Prokopov[1], K.V. Vchivkov[1]

[1]*Institute of Laser Physics(ILP) Russian Academy of Sciences, Av. Lavrentyeva 13/3, 630090, Novosibirsk, Russia*
[2]*All-Russian Research Institute of Experimental Physics (ARRIEP), Av, Mira, 37, 607188, Sarov, Russia*
E-mail: ki1z@mail.ru

Due to our complex approach, by both laboratory (in ILP) and numerical (ARRIEP) simulations, we could study for the first time [1,2] a main generation processes of the Collisionless Shock Waves (CSW) by exploding plasma clouds (or blobs) in magnetized Background Plasma (BP). It was done for the most appropriate case of Laser Plasma (LP) expansion transverse to uniform magnetic field B_0, but in a more general case of CSW generation in space by plasma blobs (like a Coronal Mass Ejection – CME at Sun), a Quasi-Perpendicular (QP) CSW could be formed with angle $\theta \leq 45^0$ between a shock normal and B_0. Therefore for the dangerus impact of giant CME onto Earth magnetosphere and relevant strong compression of its Magneto Pause (MP) size from the usual value $R_m \approx 10\ R_e$ to new one $R_m^* \sim 5 \div 6\ R_e$ (R_e is radius of the Earth), we need take into account a presence of CSW in front of CME. Recently we had conducted a first HERMEX experiment [3] on the simulation of such two-fold compression of the Earth's MP in BP flow, but without CSW, since a corresponding θ was ~ 0 under conditions of LP blob ejection along to field B_0 (without any interactions between them and BP).

Here we are discussing the setting of new LP-experiment for the QP-Shock generation (on the base of Magnetic Laminar Mechanism-MLM [2,4,5]) and present its first results together with the main features of general experimental scheme to simulate a super-extreme MP-compression up to 6 times. Recent numerical simulations of NASA [6] show that in such extreme case (probable at the early stage of solar activity), Solar Wind and CME plasmas could penetrate up to upper ionosphere, resulting in a lot of various chemical reactions and even possible origin of prebiotic life chemistry [7].

General scheme of experiment MPS (MP and Shock) is the same as HERMEX [3] one, but instead of placing both a dipole and laser target at the central Z-axis of KI-1 chamber of ILP (∅120 cm × 5 m), they were shifted horizontally into opposite directions – to the left (Y = 15 cm) and to the right (45 cm), respectively. Since a shift along to Z between them is 83 cm and Direct Distance (DD) between them is $R_0 \approx 103$ cm, a normal to flat target was almost matched with **DD**-vector and was directed at the desired angle $\theta \approx 45^0$ to the field $B_0 = 80$ G. The vector μ of magnetic dipole (up to the 10^6 G*cm^3) lies near in horizontal plane and was oriented also at angle $\theta = 45^0$ (to the B_0-field and BP-flow), i.e. near perpendicular to **DD**-vector. A hydrogen BP with a density n_* up to $3{,}5*10^{13}$ 1/cc, temperature $T_e^* \approx 10$ eV and velocity $V_* \leq 30$ km/s filled a high-vacuum chamber (and has a radius of 1 m-column up to ~ 45 cm). Here we present a data with BP after maxima, with $n_* = (1 \div 2)*10^{13}$ 1/cc. Polyethylene target was irradiated (in a spot ∅2 cm) by 2 CO_2-laser beams with total energy up to 400 J of pulse with 100 ns peak (and μs-"tail"). Generated LP-blob (H^+, C^{+3}, C^{+4} ions) has a front velocity $V_0 \approx 200$ km/s, effective energy E_0 up to 1 kJ (into 4π sr) and expansion into angle $\Delta\Omega \sim \pi$ [1,2,5].

For the given parameters of MPS-experiment, its important part on the QP-Shock generation was preliminary simulated here in ILP (see Fig. 1a,b) for energy $E_0 \approx 1000$ J by hybrid code "Cloud" (used earlier [8] for KI-1 researches) and tested recently [2] on the results of ARRIEP numerical hybrid simulations for MLM [4] and ILP data [1,2] on laboratory CSW. "Cloud" results show that along to $\theta = 45^0$, a strong disturbances could be generated, propagating with its own Alfven-Mach number $M_A^* = V_d/C_A \approx 2 \div 3$ after the point of "equal mass radius" $R_m \approx 80$ cm for $n_* = 2*10^{13}$ 1/cc (here the $V_d \approx 100$ km/s is disturbance front velocity and $C_A \approx 40$ km/s is Alfven velocity in BP). For the value of ion-acoustic velocity $C_S \approx 32$ km/s we could determined magnetosonic Mach number $M_f = V_d/C_f$, where $C_f(\theta)$ is phase velocity of fast magnetosonic wave [9], that is $C_{fl} = 1{,}15C_A \approx 45$ km/s for our angle. Therefore, according to both calculated and observed (Fig 2a) numbers $M_f \approx 2{,}2$ of disturbances, they are a super-magnetosonic shock-like structures with the compression of BP density n_* and the parallel (to shock front) component of magnetic field, nearly corresponding to Shock Adiabatic Equation [9].

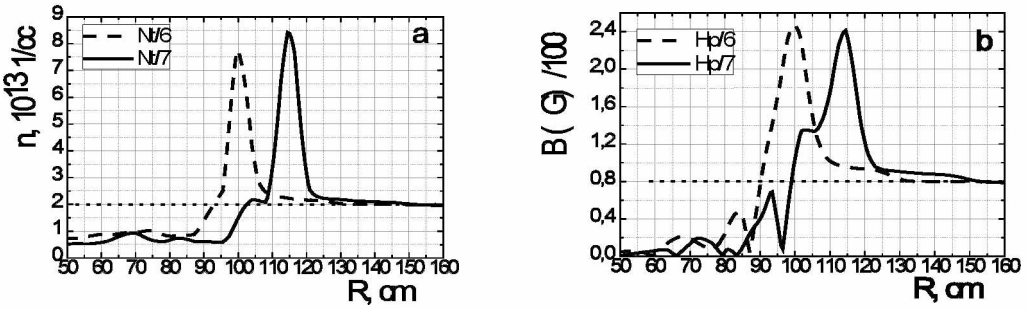

Fig. 1a Distributions of total (LP+BP) plasma density n_T for the moments t = 6 μs and 7 μs. Data for $\theta = 45^0$ on quasi-perpendicular (QP) Collisionless Shocks Wave (CSW) formation by hybrid simulation "Cloud").
Fig. 1b Corresponding strong disturbances of magnetic field (H_p), parallel to CSW-plane, calculted as a total $(H_r^2 + H_z^2)^{1/2}$. All n and B-fronts have a relevant scale ~ C/ω_{pi} (ion inertial length).

Now only experimental features of KI-1 facility ILP could supply the opportunity to generate both transverse [1,2] and QP Shocks (Fig. 2a) in laboratory, first of all, due to unique method [2] of producing Laser Plasma Blob (LPB) with effective kinetic energy up to $E_0 \sim 1000$ J. Namely such large values of E_0 and effective number electrons $N_{e0} \geq 10^{19}$ in LPB are need to supply effective MLM-interaction of LPB with BP and generate quasi-perpendicular CSW in it at the angle up to $\theta \approx 45^0$ due to the enough large value of MLM-parameter $\delta_0 \approx 1,5$ [4], determined as $\delta_0 = R_*^2/R_L R_L^*$.

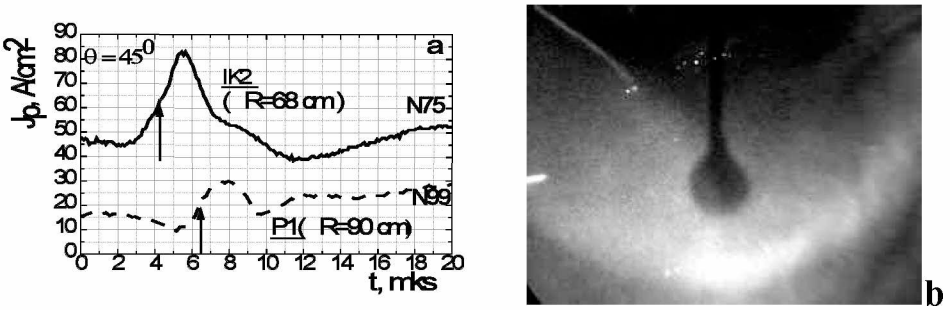

Fig. 2a. Dynamics of QP-disturbances in Background Plasma (BP) at two distances R (68 and 90 cm) from laser target by data of two Langmuir probes: P1 (close to dipole) and IK2. The fronts of signals are marked by arrows to determine disturbance velocity V_d. BP- Hydrogen ($1 \div 2 * 10^{13}$ 1/cc), B_0=80 G, initial LP' M_{a0} =5.
Fig. 2b. A model of magnetosphere around Dipole ($\mu = 0,75 * 10^6$ G*cm^3) in a flow (from Bottom to Top) of Laser Plasma under conditions of HERMEX [3] experiment. Diameter of Dipole 5,5 cm, with a moment μ directed vertically (out of paper), while at the right magnetopause boundary a flutes are seen.

Here $R_* = (3N_{e0}/4\pi n_*)^{1/3}$ is maximal size of diamagnetic cavity of LPB in BP [4] and R_L, R_L^* are Larmor radii of both LPB' and BP' ions determined by V_0 and B_0. So, the effective MLM-interaction for CSW generation could be [4] at angles $\theta \geq 90^0 - \arcsin(2/3\delta_0)$, that means essential effect only near "equator" (where $\theta = 90^0$) of expanding sphere with magnetic field directed from its pole to pole. For the main goal of whole experiment – maximal compression [3] of Magnetosphere Model (MM), we could expect that kJ-LPB from its distance $R_0 \approx 100$ cm (to dipole) with the energetic criterion $K = 3E_0 R_0^3/\mu^3 \approx 10^5$ should compress MM up to size $R_m^* \approx 0,75 R_0/K^{1/6} \approx 11$ cm (from the initial $R_m \approx 30$ cm).

This work was supported by ILP SB RAS Research Program II.10.1.4 (01201374303), the RAS Presidium Programs: "Extreme laser radiation: Physics and fundamental applications" and "Fundamental principles of innovative technologies…".

References

[1] Yu.P. Zakharov, et al., Digest Int. Conf. "Modern Problems of Laser Physics" (Novosibirsk, 25-31 August), 193 (2013).
[2] Yu.P. Zakharov, A.G. Ponomarenko, V.A. Terekhin, et al., Quantum Electronics **46**, 399 (2016).
[3] Yu.P. Zakharov, A.G. Ponomarenko, V.M. Antonov et al., J. Phys.: Conf. Ser. **688**, 012129 (2016).
[4] V.A. Terekhin, et al., Prikl. Mekh. Tekh. Fiz., N5, 10 (1983); Yu.P. Zakharov, et al., Ibid, N6, 3 (1985).
[5] I.F. Shaikhislamov, Yu.P. Zakharov, V.G. Posukh, et al., Plasma Physics Reports **41**, 399 (2015).
[6] V.S. Airapetian, et al., in Proc. 18th Cambridge Workshop on "Cool Stars, Stellar Systems, and the Sun" p. 257 (2015).
[7] V.S. Airapetian, A. Glocer, G. Gronoff, et al., Nature – Geoscience **9**, 452 (23 May 2016).
[8] G.I. Dudnikova, V.A. Vshivkov, Yu.P. Zakharov et al., in "Plasma Astrophysics" ESA **SP-311**, 191 (1990).
[9] J.D. Huba (Ed.), NRL Plasma Formulary, 26 (2016).

Ablation of optical transparent materials using picosecond laser pulses

M. Zavyalova, A. G. Verkhogliad, M. F. Stupak
Technological Design Institute of Scientific Instrument Engineering SB RAS, Novosibirsk, Russia
E-mail: mzav@tdisie.nsc.ru

We present experimental results of the different processes that can give from focusing an ultrafast laser light in the picosecond regime on a host of transparent materials, e.g., a silica, a silica glass and dielectric films.

Near-infrared quantum cutting in Tb^{3+} and Yb^{3+} co-doped glass containing Ag nanoparticles

A. H. Zhou[1,2], F. Song[1,2], Y. D. Han[1,2], W. J. Zhao[1], D. D. Ju[1,2]
[1]*School of Physics, Nankai University, Tianjin, 300071*
[2]*The Key Laboratory of Weak Light Nonlinear Photonics , Ministry of Education, Nankai University, Tianjin 300457, China*
E-mail: fsong@nankai.edu.cn

Tb^{3+}, Y^{b3+} and Ag co-doped glass were synthesized by a melt-quench technique. Ag nanoparticles (NPs) were formed in the glass matrix and confirmed by transmission electron microscopy (TEM). The effect of Ag NPs on visible and near-infrared luminescence were investigated. The electric field distributions of Ag NPs are emulated by FDTD solutions software. Local field enhancement (LFE) induced by localized surface plasmon resonance (LSPR) was found to be responsible for the fluorescence enhancement [1, 2].

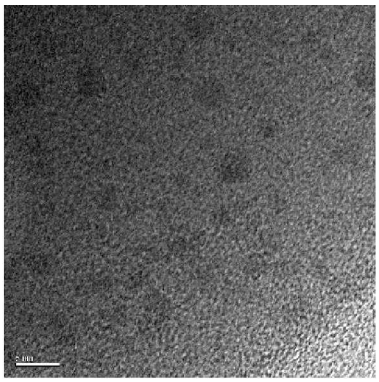

Fig. 1 TEM image of the 2% of Ag_2O in the glass.

Phosphate glasses with compositions $75P_2O_5$-$5Li_2O$-$20CaF_2$-$1Tb_2O_3$-$1Yb_2O_3$ were prepared using melt quenching technique. Silver was added in the form of oxides such an Ag_2O in concentrations ranging from 0 to 4 additive mol.%. Fig. 1 shows the TEM image of 2% which clearly displays homogeneous distribution and the average particle size is found to be approximately 4nm.

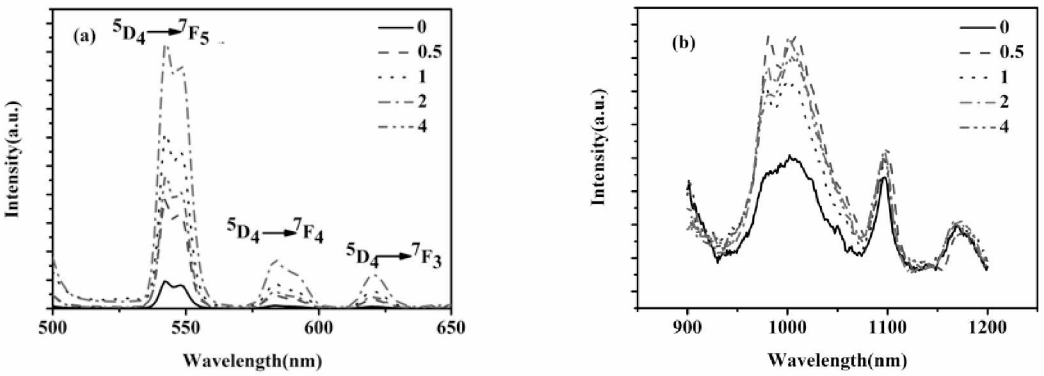

Fig. 2 Visible emission spectra (a) and Near-infrared emission spectra (b) of Tb^{3+} , Yb^{3+} co-doped phosphate glass for different concentration of Ag NPs under an excitation of 483nm.

Fig.2(a). and (b). show the visible emission spectra and near-infrared emission spectra for Tb^{3+}, Yb^{3+} co-doped phosphate glass without silver NPs and with silver NPs of varying concentration of 0.5 mol%，1 mol%，2 mol% and 4 mol%, respectively. The results show that visible luminescence intensity first increase, then decreases with the increase of the Ag NPs concentration. The maximum enhancement factor is about 8.7 when the concentration of Ag NPs is 2%. At the same time, near-infrared luminescence was also enhanced, which put forward the convenience of the present glass as a possible luminescent layer to enhance the sufficiency of silicon solar cells [3].

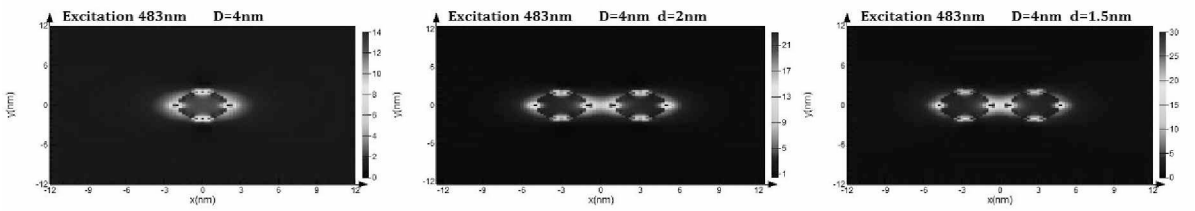

Fig. 3 Electric fields near silver: (a) D=4nm, (b) D=4nm, d=2nm, and (c) D=4nm, d=1.5nm.

The electric field distributions of Ag NPs are emulated by FDTD solutions software. Local field enhancement (LFE) induced by localized surface plasmon resonance (LSPR) [4] was found to be responsible for the fluorescence enhancement.

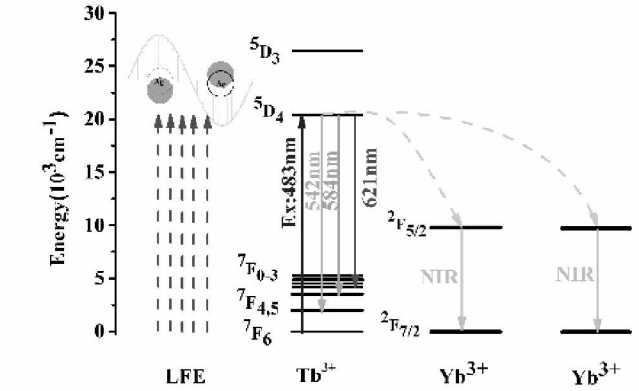

Fig. 4 Energy levels diagram of Tb^{3+}, Yb^{3+} ions in the QC energy transfers.

Due to the above mentioned reasons, the mechanism of fluorescence enhancemenet is the increase of local electric field primarily generated by LSPR (Fig.4). Mechanism of luminescence enhancement by Ag NPs is extremely complicated. In spite of size of NPs, distance between NPs and luminophore, the shape and quantity of NP and dielectric constant of glass are all important factors which cannot be neglected. So, it is very difficult to accurately determine the contribution of each of these parameters to the emission processes within disordered matrices. This part study will be gradually improved in the future work.

References

[1] A. D. Sontakke, J. Ueda, Y. Katayama et al, Journal of Applied Physics. **117**, 013105 (2015).
[2] B. M. Ende, L. Aarts, A. Meijerink, Adv. Mater. **21**, 3073 (2009).
[3]Q. Sun, S. C. Zhan, E. Z. Liu, Ceramics international. **41**, 12644 (2015).
[4]B. Zheng, S. Y. Xu, L. Lin, OPTICS LETTERS **40**, 2630 (2015).

SCIENTIFIC EQUIPMENT
COMPANY GROUP

WWW.SPEGROUP.RU
Novosibirsk, Inzhenernaya str., 4a, office 212
+7 (383) 330-82-95, sales@spegroup.ru

MANUFACTURING, RESEARCH & DEVELOPMENT EQUIPMENT

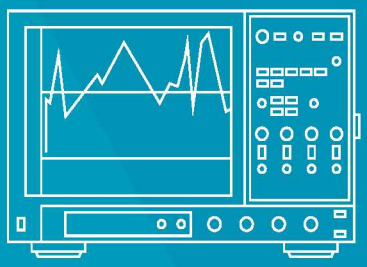

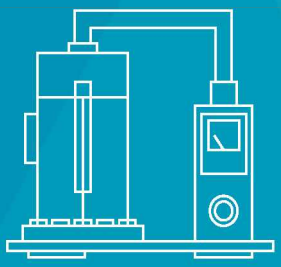

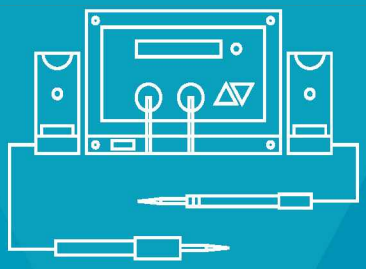

MAJOR ACTIVITIES:

- Radiophysics and Electronics
- Electricity and Magnetics
- Environmental monitoring
- Testing and Quality Control
- Microscopy
- Sample Preparation
- Furnaces and Drying Ovens
- Soldering and assembly components
- Laboratory furniture and supplies
- Vacuum equipment
- Systems for frame-by-frame and video recording of processes
- Microelectronics
- Photonics
- Chemical and structural analysis
- Water and Gas Preparation
- Chemical Reagents
- Spectrometry
- Particle size measuring
- Chromatography
- 3D scanning and printing
- Analytical equipment for geology
- Biotechnology

The *Nauchnoe Oborudovanie* group of companies was founded in 1999. It is one of the biggest suppliers of scientific and industrial equipment in Siberia and in the Far East with core activities covering provision of research institutes and industrial enterprises with high-tech equipment.

We analyze the customer's problem and select appropriate equipment to deal with a specific challenge. We supply instruments, provide technological and methodological support as well as warranty and post-warranty service. From delivering a single product to fulfilling complete enterprise supply programs, *Nauchnoe Oborudovanie* always meets its commitments and has gained the reputation of so reliable partner that some customers entrust us with complete equipping of their laboratories including both instruments and consumables.

Highly skilled technical specialists with their own research experience who constantly improve their professional level make our team. We regularly get acquainted with the new equipment and approaches in instrument engineering, and attend international exhibitions and training seminars organized by the manufacturers. We can offer the most advanced solutions for any customers' task. The existing working relationship with many laboratories of SB RAS allows inviting field experts to satisfy the customer's unique needs. Moreover, we conduct workshops providing our customers with an opportunity to try the latest equipment.

We have established partnership relations with many the world's leading manufacturers of scientific and technological equipment, both in Russia and abroad. Besides, we have our own engineering department; if necessary, we can develop and produce an instrument to solve the customer's problem.

The institutes of the Siberian Branch of the Russian Academy of Sciences focused on the fundamental research, many industrial enterprises, engineering companies, higher education institutions of the Siberian and Far Eastern regions are among our customers.

In addition to supply and production of equipment, we are engaged in the promotion of the scientific developments with commercial potential of institutes of the Russian Academy of Sciences in the foreign markets, and organize joint projects of the SB RAS institutes with different organizations to develop specific technological and knowledge-based solutions.

We see our goal to create and maintain long-standing mutually beneficial relationships with each customer.

Contact us:

Russia, Novosibirsk, Inzhenernaya str., 4a, office 212

Tel./fax: +7 (383) 330-82-95

E-mail: sales@spegroup.ru

www.spegroup.ru

The Novosibirsk Regional Fund for the Support of Science and Innovation http://fondnid.ru (hereinafter the Fund) was established by the Government of the Novosibirsk Region to implement the science, technology and innovation policy of the Novosibirsk Region and achieve high performance from scientific, technical and human resources to ensure socio-economic development of the region. Founded in 1996.

FOUNDATION FOR THE SUPPORT OF SCIENCE AND INNOVATION

The Fund carries out the following activities according to the legislation of the Russian Federation:

- Scientific and technical activities regarding the generation and application of new knowledge to solve technological, engineering, economic, social, humanitarian and other issues, as well as the functioning of science, technology and production as an integrated system;
- Participation in the creation and development of innovation infrastructure in the Novosibirsk Region;
- Organises and conducts expert examination and audit of innovative projects and programmes with the assistance of experts; provides advice and assistance in the implementation of innovative projects and programmes;
- Supports technology transfer into the production and service sectors; participates in international programmes and projects for the benefit of the Novosibirsk region;
- Develops and implements a set of mechanisms that promote the development of small and medium enterprises in the fields of science, technology and innovation;
- Participates in the development of venture capitalism and attracts investment and other resources for the implementation of promising projects.

As part of its activities, the Fund operates in the following areas:

- Has been annually organising and conducting the Siberian Venture Fair (hereinafter the Fair) www.svfair.ru since 2007 – one of the key innovative events of the Novosibirsk Regional Government, aimed at forming partnerships between entrepreneurs in the scientific and technical sphere and the investment and expert community with the purpose of forming and developing innovative business in the Novosibirsk Region;
- Prepares innovative projects for competitions held by federal authorities, public corporations, foundations, and others, including international organisations, as well as participating in fairs and exhibitions, including venture capital events (expert analysis, assistance in developing a basic business plan);
- Organises and conducts training seminars, including providing consulting and training to projects that help to form innovative infrastructure, in addition to innovative scientific and technical projects that are implemented with the participation of the Novosibirsk Region;
- Conducts analysis, including market research and monitoring in the fields of science, technology and innovation;
- Organises and conducts the examination of innovative investment projects;
- Organises and conducts activities to promote scientific, technical and innovation activity in the Novosibirsk Region.

Please consider possible areas of cooperation for the implementation of mutually beneficial joint activities.

+7-383-223-63-60, +7-383-223-20-04,
fond.nid@mail.ru; vif.nsk@mail.ru.

Office 301 and 605, 2 Sibrevkoma Street,
Novosibirsk 630007.